Kent C. Condie

EARTH

as an Evolving Planetary System

Second Edition

Earth as an Evolving Planetary System

Earth as an Evolving Planetary System

Second Edition

Kent C. Condie

AMSTERDAM • BOSTON • HEIDELBERG • LONDON • NEW YORK
OXFORD • PARIS • SAN DIEGO • SAN FRANCISCO • SYDNEY • TOKYO

Academic Press is an imprint of Elsevier

Academic Press is an imprint of Elsevier
The Boulevard, Langford Lane, Kidlington, Oxford OX5 1GB, UK
Radarweg 29, PO Box 211, 1000 AE Amsterdam, The Netherlands
225 Wyman Street, Waltham, MA 02451, USA
525 B Street, Suite 1900, San Diego, CA 92101-4495, USA

Second edition

British Library Cataloguing in Publication Data
A catalogue record for this book is available from the British Library

Library of Congress Cataloging-in-Publication Data
A catalog record for this book is available from the Library of Congress

For information on all **Academic Press** publications
visit our web site at elsevierdirect.com

Printed and bound in Great Britain
11 12 13 14 10 9 8 7 6 5 4 3 2 1

ISBN: 978-0-12-385227-4

Contents

Preface

Although this book began life in 1976 with the title *Plate Tectonics and Crustal Evolution*, the subject matter has gradually changed focus with subsequent editions, and especially since the third edition in 1989. In the past decade it has become increasingly clear that the various components of Earth act as a single, interrelated system, often referred to as the Earth System. One reviewer of the fourth edition pointed out that the title of the book was no longer appropriate, since plate tectonics was not a major focus. For this reason, for what would have been the fifth edition of the Plate Tectonics book, I have introduced a new title for the book, *Earth as an Evolving Planetary System*, which will be continued into still later editions.

Since the first edition in 1976, which appeared on the tail end of the plate tectonics revolution of the 1960s, our scientific database has grown exponentially and continues to grow—in fact, much faster than we can interpret it. If one compares the earlier editions of the book with this edition, a clear trend is apparent. Plate tectonics is no longer so exciting, but is now taken for granted. The changing emphasis during the past 30 years is from how one system in our planet works (plate tectonics) to how all systems in our planet work, how they are related, and how they have governed the evolution of the planet. As scientists continue to work together and share information from many disciplines, this trend should continue for many years into the future.

Today, more than any time in the past, we are beginning to appreciate the fact that to understand the history of our planet requires an understanding of the various interacting components and how they have changed with time. Although science is made up of specialties, to learn more about how Earth operates requires input from all of these specialties—geology alone cannot handle it. In this Earth System book, the various subsystems of the Earth are considered as vital components in the evolution of our planet. Subsystems include such components as the crust, mantle, core, atmosphere, oceans, and life.

As with previous editions, the Earth System book is written for advanced undergraduate and graduate students, and it assumes a basic knowledge of geology, biology, chemistry, and physics, which most students in the Earth Sciences acquire during their undergraduate education. It also may serve as a reference book for various specialists in the geologic sciences who want to keep abreast of scientific advances in this field. I have attempted to synthesize and digest data from the fields of oceanography, geophysics, paleoclimatology,

geology, planetology, and geochemistry and to present this information in a systematic manner to address problems related to the evolution of Earth during the last 4.6 billion years.

The second edition of the Earth System book includes some of the new and exciting topics in the Earth Sciences. Among these are results from increased resolution of seismic tomography by which plates can be tracked into the deep mantle and mantle plumes can be detected. High-resolution U/Pb zircon isotopic dating now permits us to better constrain the timing of important events in Earth's history. We have detrital zircons with ages up to 4.4 Ga, suggesting the presence of felsic crust and water on the planet by this time. New information on the core provides us with a better understanding of how the inner and outer core interact and how Earth's magnetic field is generated.

Two expanding areas of knowledge have also required two new chapters in the second edition: one on the supercontinent cycle and one on great events in Earth history. I appreciate Maya Elrick at the University of New Mexico who invited me to attend her graduate seminar on Great Events in Earth History during spring semester 2010. It was from this seminar that I decided the book really needed a "Great Events" chapter (Chapter 9). Really exciting work on the origin of life and the possibilities of life beyond Earth are discussed in the Great Events chapter. Also I include a section on when plate tectonics began and major changes at the end of the Archean. The continuing saga of mass extinctions and the role of impacts has required more coverage, and the Snowball Earth model is discussed in more detail. The episodic nature of crustal preservation, stable isotope anomalies, giant dyke swarms and other phenomena have been well documented in the past few years, so much so that new sections have been added to cover these subjects.

In addition, we have provided an updated interactive CD ROM by the author, titled *Plate Tectonics and How the Earth Works*, to accompany the new book. This CD, with animations and interactive exercises, can be obtained from Tasa Graphic Arts Inc., Taos, NM (www.tasagraphicarts.com).

Kent C. Condie
Department of Earth & Environmental Science
New Mexico Tech
Socorro, NM 87801 USA
kcondie@nmt.edu
http://www.ees.nmt.edu/condie

Chapter 1

Earth Systems

EARTH AS A PLANETARY SYSTEM

A **system** is an entity composed of diverse but interrelated parts that function as a whole (Kump et al., 1999). The individual parts, often called **components**, interact with each other as the system evolves with time. Components include reservoirs of matter or energy (described by mass or volume) and subsystems, which behave as systems *within* a system. Earth is considered to be a complex planetary system that has evolved over 4.6 Ga (46×10^9 years). It includes reservoirs, such as the crust, mantle, and core and subsystems, such as the atmosphere, hydrosphere, and biosphere. Because many of the reservoirs in Earth interact with each other and with subsystems, such as the atmosphere, there is an increasing tendency to consider most or all of Earth's reservoirs as subsystems.

The state of a system is characterized by a set of variables at any time during the evolution of the system. For Earth, temperature, pressure, and various compositional variables are most important. The same thing applies to subsystems within the Earth. A system is at equilibrium when nothing changes as it evolves. If, however, a system is perturbed by changing one or more variables, it responds and adjusts to a new equilibrium state. A **feedback loop** is a self-perpetuating change and response in a system to a change. If the response of a system amplifies the change, it is known as a **positive feedback loop**, whereas if it diminishes or reverses the effect of the disturbance, it is a **negative feedback loop**. As an example of positive feedback, if volcanism pumps more CO_2 into a CO_2-rich atmosphere of volcanic origin, this should promote greenhouse warming and the temperature of the atmosphere would rise. If the rise in temperature increases weathering rates on the continents, this would drain CO_2 from the atmosphere causing a drop in temperature, an example of negative feedback. Because a single subsystem in Earth affects other subsystems, many positive and negative feedbacks occur as Earth attempts to reach a new equilibrium state. These feedbacks may be short lived over hours or range to tens of thousands of years, such as short-term changes in climate, or they may be long lived over millions or tens of millions of years such as changes in climate related to the dispersal of a supercontinent.

The major driving force of planetary evolution is the thermal history of a planet, as discussed in Chapter 4. The methods and rates by which planets cool, either directly or indirectly, control many aspects of planetary evolution. In a silicate-metal planet like Earth, thermal history determines when and if a core will form (Figure 1.1). It determines if the core is molten, which in turn determines if the planet will have a global magnetic field (which is generated by dynamo-like action in the outer core; see Chapter 5). The magnetic field, in turn, interacts with the solar wind and with cosmic rays, and it traps high-energy particles in magnetic belts around the planet. This, of course, also affects life since life cannot exist in the presence of intense solar wind or cosmic radiation.

Planetary thermal history also strongly influences tectonic, crustal, and magmatic history (Figure 1.1). For instance, only planets that recycle lithosphere into the mantle by subduction, as Earth does, appear capable of generating continental crust, and thus having collisional orogens. Widespread felsic and andesitic magmas can only be produced in a plate tectonic regime. In contrast, planets that cool by mantle plumes and lithosphere delamination, as perhaps Venus does today, should have widespread mafic magmas, with little felsic to intermediate component. They also appear to have no continents.

So where does climate come into these interacting histories? Climate reflects complex interactions of the atmosphere–ocean system with tectonic and magmatic components, as well as interactions with the biosphere. In addition, solar energy and asteroid or cometary impacts can have severe effects on climatic evolution (Figure 1.1). The thermal history of a planet directly or indirectly affects all other systems in the planet, including life. Earth has two kinds of energy sources: those internal to the planet and those external to the

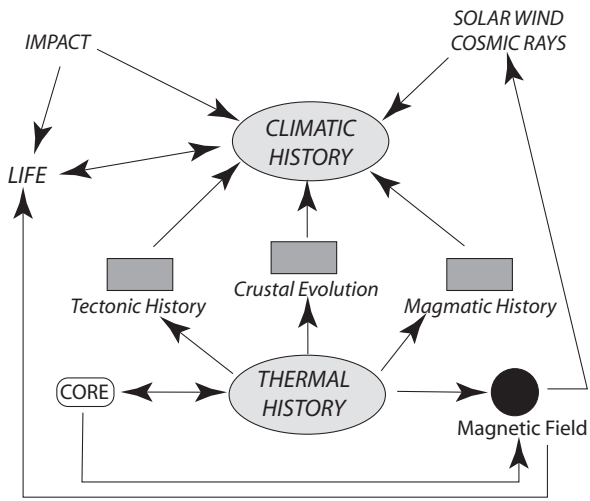

FIGURE 1.1 Major relationships between Earth's thermal and climatic histories.

planet. In general, internal energy sources have long-term ($>10^6$ y) effects on planetary evolution, whereas external energy sources have short-term ($<<0^6$ y) effects. Gradual increases in solar energy during the last 4.6 Ga have also influenced Earth's climate on a long timescale. Note that throughout the book the notations Ga (10^9 y), Ma (10^6 y), and ka (10^3 y) will refer either to datums in the past (e.g., millions of years ago) or time intervals (e.g., millions of years), depending on context of the sentence. The most important extraterrestrial effects on planetary evolution, and especially on climate and life, are asteroid and cometary impacts, the effects of which usually last for $<10^3$ y.

Many examples of interacting terrestrial systems are described in later chapters. However, before discussing these systems and their interactions, we first need to review the basic structure of Earth as determined primarily from seismology.

STRUCTURE OF EARTH

The internal structure of Earth is revealed primarily by compressional (P wave) and shear (S wave) waves that pass through the planet in response to earthquakes. Seismic wave velocities vary with pressure (depth), temperature, mineralogy, chemical composition, water content, and degree of partial melting. Although the overall features of seismic-wave velocity distributions have been known for some time, refinement of data has only been possible in the last 10 years. Seismic wave velocities and density increase rapidly in the region between 200 and 700 km deep. Three first-order seismic discontinuities divide Earth into crust, mantle, and core (Figure 1.2): the **Mohorovicic discontinuity** or **Moho** defining the base of the crust; the **core–mantle interface** at 2900 km; and at about 5200 km, the **inner-core/outer-core interface.** The core composes about 16% of Earth by volume and 32% by mass. The seismic discontinuities reflect changes in composition or phase or in both. Smaller, but very important velocity changes at 50–200 km, 410 km, and 660 km provide a basis for further subdivision of the mantle, as discussed in Chapter 4.

The major regions of Earth can be summarized as follows with reference to Figure 1.2.

1. The **crust** consists of the region above the Moho, and ranges in thickness from about 3 km at some oceanic ridges to about 70 km in collisional orogens.
2. The **lithosphere** (50–300 km thick) is the strong outer layer of Earth, including the crust, which reacts to many stresses as a brittle solid. The **asthenosphere,** extending from the base of the lithosphere to the 660-km discontinuity, is by comparison a weak layer that readily deforms by creep. A region of low seismic-wave velocity and high attenuation of seismic-wave energy, the **low-velocity zone (LVZ)**, occurs at the top of the asthenosphere

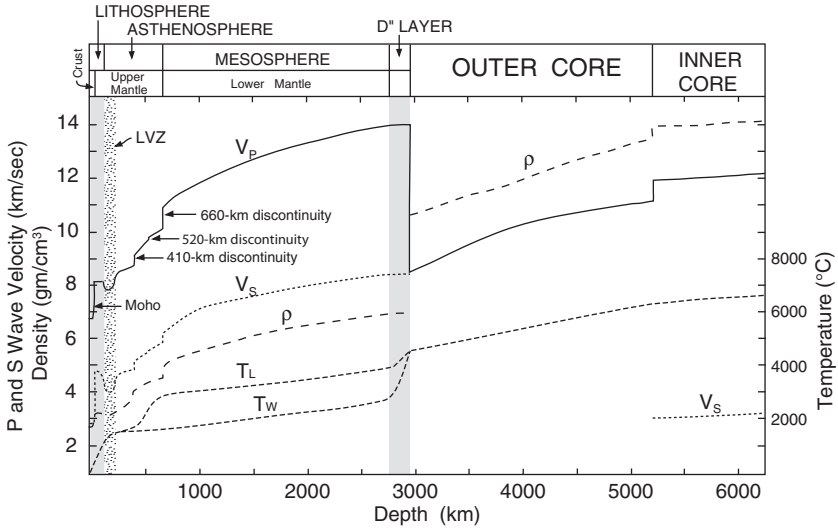

FIGURE 1.2 Distribution of average compressional (V_p) and shear wave (V_s) velocities and average calculated density (ρ) in Earth. Also shown are temperature distributions for whole-mantle convection (T_W) and layered mantle convection (T_L).

and is from 50 to 100 km thick. Significant lateral variations in density and in seismic-wave velocity are common at depths of less than 400 km.

3. The **upper mantle** extends from the Moho to the 660-km discontinuity, and includes the lower part of the lithosphere and the upper part of the asthenosphere. The region from the 410-km to the 660-km discontinuity is known as the **transition zone**. These two discontinuities, as further discussed in Chapter 4, are caused by two important solid-state transformations: from olivine to wadsleyite at 410 km and from ringwoodite to perovskite + magnesiowüstite at 660 km. In addition, a small discontinuity at 520 km is reported in some regions of the mantle.
4. The **lower mantle** extends from the 660-km discontinuity to the 2900-km discontinuity at the core–mantle boundary. For the most part, it is characterized by rather constant increases in velocity and density in response to increasing hydrostatic compression. Between 200 and 250 km above the core–mantle interface, a flattening of velocity and density gradients occurs, in a region known as the **D″ layer**, named after the seismic wave used to define the layer. The lower mantle is also referred to as the **mesosphere**, a region that is strong, but relatively passive in terms of deformational processes.
5. The **outer core** will not transmit S waves and is interpreted to be liquid. It extends from the 2900-km to the 5200-km discontinuity.
6. The **inner core**, which extends from 5200-km discontinuity to the center of Earth, transmits S waves, although at very low velocities, suggesting that it is a solid near the melting point.

There are only two layers in Earth with anomalously low seismic velocity gradients and steep thermal gradients: the lithosphere and the D″ layer just above the core (Figure 1.2). These layers are thermal boundary layers in the planet. Both layers play an important role in the cooling of Earth. Most cooling (>90%) occurs by plate tectonics as plates are subducted deep into the mantle. The D″ layer is important in that steep thermal gradients in this layer may generate mantle plumes, many of which rise to the base of the lithosphere, thus bringing heat to the surface (<10% of the total Earth cooling).

Uncertainty still exists regarding the temperature distribution in Earth. It is dependent on features of Earth's history as (1) the initial temperature distribution in the planet, (2) the amount of heat generated as a function of both depth and time, (3) the nature of mantle convection, and (4) the process of core formation. Most estimates of the temperature distribution in Earth are based on one or a combination of two approaches: Models of Earth's thermal history involving various mechanisms for core formation, and models involving redistribution of radioactive heat sources in the planet by melting and convection processes.

Estimates using various models seem to converge on a temperature at the core–mantle interface of about 4500 ± 500°C and the center of the core at 6700 to 7000°C. Two examples of calculated temperature distributions in Earth are shown in Figure 1.2. Both show significant gradients in temperature in the LVZ and the D″ layer. The layered convection model (T_L) also shows a large temperature change near the 660-km discontinuity, since this is the boundary between the shallow and deep convection systems in this model. The temperature distribution for whole-mantle convection (T_W), which is preferred by most investigators, shows a rather smooth decrease from the top of the D″ layer to the LVZ.

PLATE TECTONICS

Plate tectonics, which has so profoundly influenced geologic thinking since the early 1970s, provides valuable insight into the mechanisms by which Earth's crust and mantle have evolved as well as to how Earth has cooled. **Plate tectonics** is a unifying model that attempts to explain the origin of patterns of deformation in the crust, earthquake distribution, supercontinents, and midocean ridges, as well as providing a mechanism for Earth to cool. Two major premises of plate tectonics are that (1) the lithosphere (= plates) behaves as a strong, rigid substance resting on a weaker asthenosphere; and (2) the lithosphere is broken into numerous segments or plates that are in motion with respect to one another and are continually changing in shape and size (Figure 1.3). The parental theory of plate tectonics, *seafloor spreading*, states that new lithosphere is formed at ocean ridges and moves away from ridge axes with a motion like that of a conveyor belt, as new lithosphere fills in the resulting crack or rift. The mosaic of plates, which ranges from 50 to over 200 km thick, is bounded by ocean ridges, subduction zones (in part collisional boundaries), and transform faults (boundaries along which plates slide by each other) (Figure 1.3, cross sections).

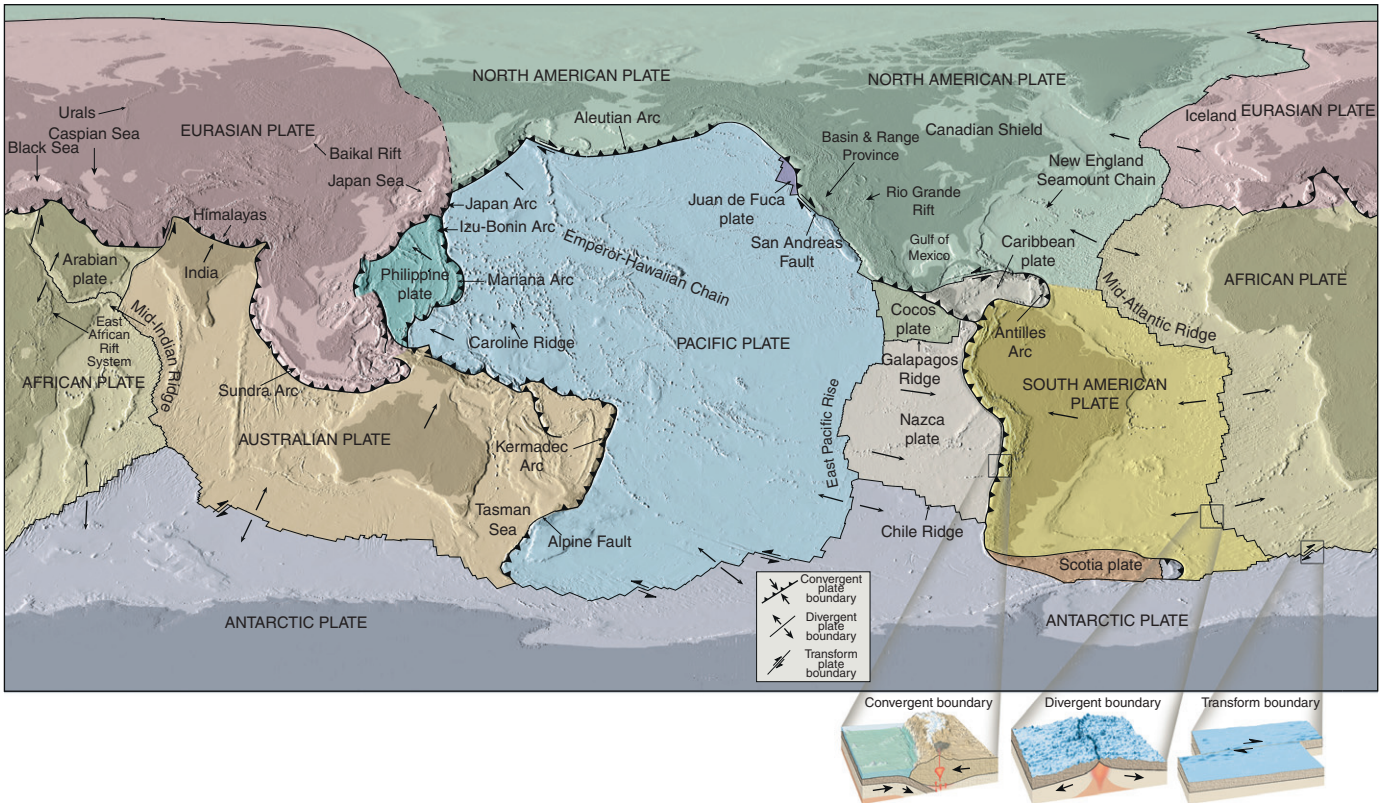

FIGURE 1.3 Map of the major lithospheric plates on Earth. Arrows are directions of plate motion. Filled barbs, convergent plate boundaries (subduction zones and collisional orogens); single lines, divergent plate boundaries (ocean ridges) and transform faults. Cross sections show details of typical plate boundaries. *Artwork by Dennis Tasa, courtesy of Tasa Graphic Arts, Inc.*

To accommodate the newly created lithosphere, oceanic plates return to the mantle at subduction zones such that the surface area of Earth remains constant.

Many scientists consider the widespread acceptance of the plate tectonic model as a "revolution" in the earth sciences. As pointed out by J. Tuzo Wilson in 1968, scientific disciplines tend to evolve from a stage primarily of data gathering, characterized by transient hypotheses, to a stage where a new unifying theory or theories are proposed that explain a great deal of the accumulated data. Physics and chemistry underwent such revolutions around the beginning of the 20th century, whereas the earth sciences entered such a revolution in the late 1960s. As with scientific revolutions in other fields, new ideas and interpretations do not invalidate earlier observations. On the contrary, the theories of seafloor spreading and plate tectonics offer for the first time a unified explanation for heretofore seemingly unrelated observations in the fields of geology, paleontology, geochemistry, and geophysics.

The origin and evolution of Earth's crust is a tantalizing question that has stimulated much speculation and debate dating from the early part of the 19th century. Some of the first problems recognized, such as how and when did the oceanic and continental crust form, remain a matter of considerable controversy even today. Results from the Moon and other planets indicate that Earth's continental crust may be a unique feature in the solar system. The rapid accumulation of data in the fields of geophysics, geochemistry, and geology since 1970 has added much to our understanding of the physical and chemical nature of Earth's crust and of the processes by which it evolved (see Chapter 10). Evidence favors a source for the materials composing the crust from within Earth. Partial melting of the mantle produces magma that moves to the surface and forms the crust. The continental crust, being less dense than the underlying mantle, rises isostatically above sea level and is subjected to weathering and erosion. Eroded materials are partly deposited on continental margins, and partly returned to the mantle by subduction to be recycled, and perhaps again become part of the crust at a later time.

IS THE EARTH UNIQUE?

Many features of our planet indicate that it is unique among other planets in the solar system and certainly among planets discovered so far around other stars. Consider, for instance, the following characteristics, sometimes referred to as the list of "Ifs" for Earth:

1. Earth's near-circular orbit results in a more or less constant amount of heat from the Sun. If the orbit were more elliptical, Earth would freeze over in the winter and roast in the summer. In such a case, higher forms of life could not survive.
2. If Earth were much larger, the force of gravity would be too strong for higher life-forms to exist.

3. If Earth was much smaller, water and oxygen would escape from the atmosphere and higher life forms could not survive.
4. If Earth was only 5% closer to the Sun, the oceans would evaporate and greenhouse gases would cause the surface temperature to rise too high for any life to exist (like on Venus today).
5. If Earth was only 5% farther from the Sun, the oceans would freeze over, photosynthesis would be greatly reduced leading to a decrease in atmospheric oxygen. Again, higher life-forms could not exist.
6. If Earth did not have plate tectonics, there would be no continents, and thus large numbers of terrestrial higher life-forms could not exist.
7. If Earth did not have a magnetic field of just the right strength, lethal cosmic rays would kill most or all life-forms (including humans) on the planet.
8. If Earth did not have an ozone layer in the atmosphere to filter out harmful ultraviolet radiation from the Sun, higher forms of life could not exist.
9. If Earth's axial tilt (23.4°) were greater or smaller, surface temperature differences would be too extreme to support life. Without the Moon, Earth's spin axis would wobble too much to support life.
10. Without the huge gravity field of Jupiter, Earth would be bombarded with meteorites and comets, such that higher life-forms could not survive on the planet.
11. The massive asteroid collision on Earth 65 Ma (65×10^6 years ago) led to the extinction of dinosaurs and cleared the way for the evolution and diversification of mammals and the eventual appearance of humans.

Are all of these features of planet Earth that make it suitable for higher life-forms simply a coincidence? Although lower life-forms, as discussed in Chapter 9, can survive over a wide range of physical and chemical conditions, higher life-forms cannot survive under such conditions. The fact that Earth has developed just the "right" conditions to support higher life-forms is sometimes referred to as the Goldilocks problem (Rampino & Caldeira, 1994). As in the Goldilocks story, while Venus is too hot (the papa bear's porridge) and Mars is too cold (the mama bear's porridge), Earth (the baby bear's porridge) is just right! Why is Earth just right? Although some scientists believe that these conditions came about by chance, others argue that the Earth's properties have developed in such a way as to *prepare* the planet for the origin, evolution, and survival of higher life-forms.

INTERACTING EARTH SYSTEMS

Earth subsystems are not static but have evolved with time, leading to the habitable planet on which we reside. Current and future interactions of these subsystems will have a direct impact on life, and for this reason it is important to understand how perturbation of one subsystem can affect other subsystems and how rapidly subsystems change with time. Short-term climatic cycles are superimposed on and

partly controlled by long-term processes in the atmosphere–ocean subsystem, which in turn are affected by even longer term processes in the mantle and core. Also affecting Earth's subsystems are asteroid and cometary impacts, both of which appear to have been frequent in the geologic past.

Some of the major pathways of interaction between Earth's subsystems and between the Earth and extraterrestrial systems are summarized in Figure 1.4.

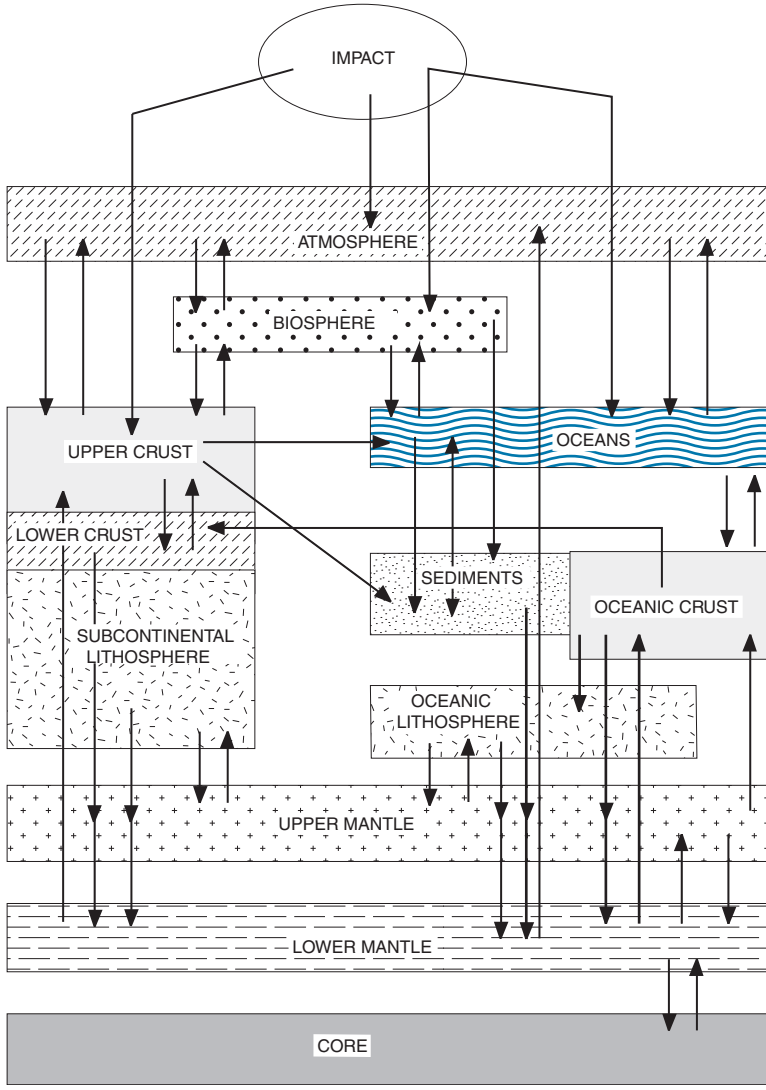

FIGURE 1.4 Box diagram showing the major subsystems of the Earth. Some of the major paths of interaction are noted with arrows.

Although we will consider some of these interactions in detail in later chapters, it is appropriate to preview some of them now. As an example, crystallization of metal onto the surface of the inner core may liberate enough heat to generate mantle plumes just above the core–mantle interface. As these plumes rise into the uppermost mantle, spread beneath the lithosphere, and begin to melt, large volumes of basalt may underplate the crust and also erupt at Earth's surface. Such eruptions may pump significant quantities of CO_2 into the atmosphere that, because it is a greenhouse gas, will warm the atmosphere leading to warmer climates. This, in turn, may affect the continents (by increasing weathering and erosion rates), the oceans (increasing the rate of limestone deposition), and life (leading to extinction of those forms not able to adapt to the changing climates). Thus, through a linked sequence of events, processes occurring in Earth's core could lead to extinction of life-forms at Earth's surface. Before such changes can affect life, however, negative feedback processes may return the atmosphere–ocean system to an equilibrium level, or even reverse these changes. For instance, increased weathering rates caused by increased CO_2 levels in the atmosphere may drain the atmosphere of its excess CO_2, which is then transported by streams to the oceans where it is deposited in limestone. If cooling is sufficient, this could lead to widespread glaciation, which in turn could cause extinction of some life-forms.

As an example of an interaction related to plate tectonics, consider the subduction of oceanic crust into the deep mantle. This crust produces distinct compositional domains in the mantle that, if incorporated into mantle plumes, can rise to the base of the lithosphere, partially melt, and produce basalts that erupt at Earth's surface. Again, greenhouse gases emitted during the eruptions can lead to climate warming.

To prepare for the continuing survival of living systems on planet Earth, it is important to understand the nature and causes of interactions between Earth subsystems and between Earth and extraterrestrial systems. How fast and how frequently do these interactions occur, and what are the relative rates of forward and reverse reactions? These are important questions that need to be addressed by the present and future generations of scientists.

FURTHER READING

Ernst, W. G. (2000). *Earth Systems, Processes and Issues* (576 pp). Cambridge, UK: Cambridge University Press.

Kump, L. R., Kasting, J. F., & Crane, R. G. (2010). *The Earth System* (3rd ed., 432 pp). Upper Saddle River, New Jersey: Prentice Hall.

Lillie, R. J. (1999). *Whole Earth Geophysics* (361 pp). Upper Saddle River, New Jersey: Prentice Hall.

Taylor, S. R. (1998). *Destiny or Chance, Our Solar System and Its Place in the Cosmos* (248 pp). Cambridge, UK: Cambridge University Press.

Chapter 2

The Crust

INTRODUCTION

Earth's crust is the upper rigid part of the lithosphere, the base of which is defined by a prominent seismic discontinuity, the Mohorovicic discontinuity or Moho. There are three crustal divisions—oceanic, transitional, and continental—of which oceanic and continental crust dominate (Table 2.1). Typically, oceanic crust ranges from 3 to 15 km thick and comprises 54% of the crust by area and 17% by volume. Islands, island arcs, and continental margins are examples of transitional crust that have thicknesses of 15–30 km. Continental crust ranges from 30–70 km thick and comprises 77% of the crust by volume but only 40% by area. Our knowledge of oceanic crust comes largely from ophiolites, which are thought to represent tectonic fragments of oceanic crust that are preserved in the continents, and from deep-sea drill cores. Our view of the lower continental crust is based chiefly on uplifted slices of this crust in collisional orogens and on xenoliths brought to the surface in young volcanics.

The crust can be further subdivided into **crustal types**, which are segments of the crust exhibiting similar geologic and geophysical characteristics. The 13 major crustal types are listed in Table 2.1 with some of their physical properties. The first two columns of the table summarize the area and volume abundances, and column 3 describes tectonic stability in terms of earthquake and volcanic activity and recent deformation.

To better understand the evolution of Earth, we must understand the origin and evolution of the crust. In this chapter we briefly summarize the physical and chemical properties of the crust and review characteristics of crustal provinces.

SEISMIC CRUSTAL STRUCTURE

The Moho

The **Mohorovicic discontinuity** or **Moho** is the outermost seismic discontinuity in the Earth and defines the base of the crust (see Figure 1.2 and Table 2.1) (Jarchow & Thompson, 1989). It ranges in depth from about 3 km at ocean

TABLE 2.1 Characteristics of Earth's Crust

Crustal type	Area %	Volume %	Stability	Heat flow (mW/m^2)	Bouguer anomaly (mgal)	Poisson's ratio
Continental						
1. Shield	6	11	S	40	−20 to −30	0.29
2. Platform	18	35	S, I	49	−10 to −50	0.27
3. Orogen						
PA	8	13	S	60	−100 to −200	0.26
MC	6	14	I, U	70	−200 to −300	0.26
4. Continental margin arc	2	4	I, U	50–70	−50 to −100	0.25
Transitional						
5. Rift	1	1	U	60–80	−200 to −300	0.30
6. Island arc	1	1	I, U	50–75	−50 to +100	0.25
7. Oceanic plateau	3	3	S, I	50–60	−100 to +50	0.30
8. Inland-sea basin	1	1	S	50	0 to +200	0.27
Oceanic						
9. Ocean ridge	10	2	U	100–200	+200 to +250	0.22
10. Ocean basin	38	12	S	50	+250 to +350	0.29
11. Marginal-sea basin	4	2	U, I	50–150	+50 to +100	0.25
12. Volcanic island	<1	<1	I, U	60–80	+250	0.25
13. Trench	2	1	U	45	−100 to −150	0.29
Average Continent	40	77		55	−100	0.27
Average Ocean	54	17		67 (95)[a]	+250	0.29

Stability key: S, stable; I, intermediate stability; U, unstable.
Poisson's ratio = $0.5\{1 - 1/[(Vp/Vs)^2 - 1]\}$.
PA, Paleozoic orogen; MC, Mesozoic-Cenozoic orogen.
[a]*Calculated oceanic heat flow.*

ridges to 70 km in collisional orogens and is marked by a rapid increase in seismic P-wave velocity from <7.6 km/s to ≥8 km/s. Because the crust is different in composition from the mantle, the Moho is striking evidence for a differentiated Earth. Detailed seismic refraction and reflection studies indicate that the Moho is not a simple boundary worldwide. In collisional orogens the Moho is often offset by complex thrust faults and in some places it is a complex transition zone rather than a distinct discontinuity. The Himalayan orogen is an example where a 20-km offset in the Moho occurs beneath the Indus suture and in some places it is a transition zone up to 10 km thick (Hirn et al., 1984; Spain & Hirn, 1997). This offset was produced as crustal slices were thrust on top of each other during the Himalayan collision. In crust undergoing extension, such as continental rifts, a sharp seismic discontinuity is often missing, and seismic velocities change gradually from crustal to mantle values. In some collisional orogens, the Moho may not always represent the base of the crust. In these orogens, thick mafic crustal roots may invert to **eclogite** (a high-density mafic rock composed of garnet and clinopyroxene) and seismic velocity increases to mantle values, yet the ecolgite protolith originally formed in the lower crust (Griffin & O'Reilly, 1987). The petrologic base of the crust where eclogite rests on ultramafic mantle rocks may not show a seismic discontinuity, since both rock types have similar velocities. This has given rise to two types of Mohos: the **seismic Moho** (defined by a jump in seismic velocities) and the **petrologic Moho** (defined by the base of eclogitic lower crust).

The origin of the Moho continues to be a subject of widespread interest (Jarchow & Thompson, 1989). Because the oceanic Moho is exposed in many ophiolites, it is better known than the continental Moho. From seismic velocity distributions and from ophiolite studies, the oceanic Moho is probably a complex transition zone from 0 to 3 km thick, between mixed mafic and ultramafic igneous cumulates in the crust and harzburgites (orthopyroxene-olivine rocks) in the upper mantle. It would appear that large tectonic lenses of differing lithologies occur at the oceanic Moho, which are products of ductile deformation along the boundary. The continental Moho is considerably more complex and varies with crustal type and age (Griffin & O'Reilly, 1987). Experimental, geophysical, and xenolith data, however, do not favor a simple gabbro-eclogite transition to explain the continental Moho. Beneath platforms and shields, the Moho is only weakly (or not at all) reflective, suggesting the existence of a relatively thick transition zone (>3 km) composed of mixed mafic granulites, eclogites, and lherzolites, with no strong reflecting surfaces.

Crustal Layers

Crustal models based on seismic data indicate that oceanic crust can broadly be divided into three layers, which are, in order of increasing depth, the **sediment layer** (0–1 km thick), the **basement layer** (0.7–2.0 km thick), and the **oceanic layer** (3–7 km thick) (Figure 2.1). Models for the continental crust have a greater

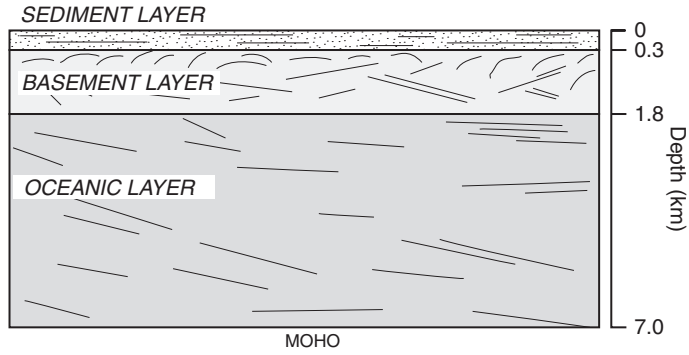

FIGURE 2.1 Standard cross section of oceanic crust based on seismic reflection data. Solid lines are examples of major reflectors.

range in both number and thicknesses of layers. Although two- or three-layer models for continental crust are most common, one-layer models and models with more than three layers are proposed in some regions (Christensen & Mooney, 1995; Mooney et al., 1998). With exception of continental borderlands and island arcs, continents range in thickness from about 35 to 40 km (mean = 41 km), while the average thickness of the oceanic crust is only 5–7 km.

P-wave velocities in crustal sediment layers range from 2 to 4 km/s, depending on degree of compaction, water content, and rock type. Velocities in the middle oceanic crustal layer are about 5 km/s, whereas those in the middle continental crustal layer are about 6.5 km/s (Table 2.2). Lower crustal layers in both oceans and continents are characterized by P-wave velocities of 6.5–6.9 km/s.

Seismic wave velocities increase with depth in the continental crust from 6.0 to 6.2 km/s at depths of <10 km to 6.6 km/s at depths of 25 km. Lower crustal velocities range from 6.8 to 7.2 km/s, and in some cases show a bimodal distribution. Some continental crust exhibits evidence of a small discontinuity at midcrustal depths, referred to as the **Conrad discontinuity** (Litak & Brown, 1989). When identified, the Conrad discontinuity varies in depth and character from region to region, suggesting that, unlike the Moho, it is not a fundamental property of the continental crust, and it is diverse in origin. Seismic reflections also occur at midcrustal depths in some extended crust like the Rio Grande rift in New Mexico.

Complexities in the Lower Continental Crust

Reflection seismology has provided a detailed view of the middle and lower continental crust. In some regions there are no Moho reflections, whereas in others Moho reflections are prominent and often show complex structure (Cook et al., 2010). These results have led to many interpretations of the Moho. As an example of a complex Moho, Figure 2.2 (upper section) shows a reflection

TABLE 2.2 Crustal Seismic Wave Velocities

Crustal type	V_{Pn} (km/s)	V_P upper crust (km/s)	V_P middle crust (km/s)	V_P lower crust (km/s)	Mean thickness (km)	Mean V_P (km/s)
Continental						
1. Shield	8.1	6.2 (13)	6.5 (13)	7.0 (14)	40	6.5
2. Platform	8.1	6.2 (15)	6.5 (13)	7.0 (14)	42	6.5
3. Orogen						
PA	8.1	6.1 (10)	6.4 (12)	6.8 (13)	35	6.4
MC	8.0	6.0 (16)	6.3 (11)	6.7 (25)	52	6.3
4. Continental margin arc	7.9	6.2 (18)	6.6 (10)	7.0 (10)	38	6.4
Transitional						
5. Rift	7.8	6.0 (11)	6.5 (6)	6.9 (11)	28	6.5
6. Island arc	7.8	6.2 (6)	6.6 (6)	7.2 (7)	19	6.4
7. Oceanic plateau	8.0	6.3 (5)	6.5 (10)	6.8 (10)	25	6.5
8. Inland-sea basin	8.1		2–5 (7)	6.8 (15)	22 [25]	6.0
Oceanic						
9. Ocean ridge	<7.5		5.0 (1)	6.5 (4)	5 [6]	6.4
10. Ocean basin	8.2	2–4 (0.5)	5.1 (1.5)	6.8 (5)	7 [11]	6.4
11. Marginal-sea basin	7.5–8.0	2–4 (1)	5.3 (3)	6.6 (5)	9 [13]	6.3
12. Volcanic island	7.5–8.0		6.6 (6)	7.0 (7)	13	6.5
13. Trench	8.0	2–4 (3)	5.1 (1.5)	6.8 (5)	8 [14]	6.4
Average Continent	8.1	6.2 (13)	6.5 (13)	7.0 (14)	41	6.5
Average Ocean	8.1	2–4 (0.5)	5.1 (1.5)	6.8 (5)	7 [10]	6.4

Crustal layer thicknesses (in km) given in parentheses.
PA, Paleozoic orogen; MC, Mesozoic-Cenozoic orogen.
Numbers in brackets [ ] are depths to the Moho below sea level.
Sources: Mooney et al. (1998) and references cited therein.

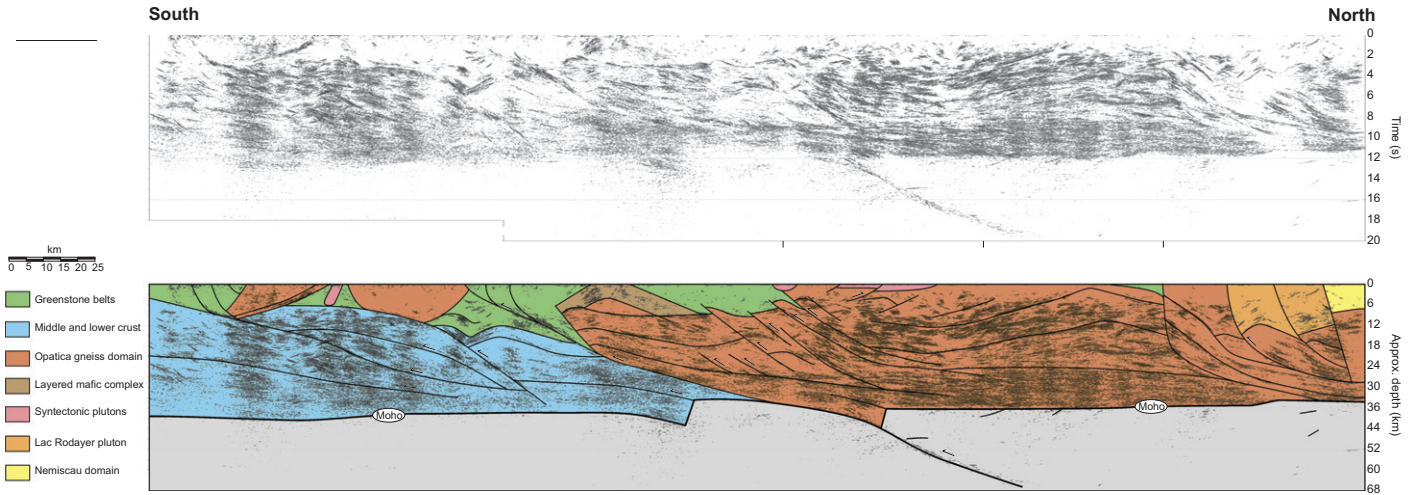

FIGURE 2.2 North-South seismic reflection profile from the Archean Superior craton, eastern Canada across the Opatica-Abitibi subprovinces (upper). Interpretative profile in color (lower). Note the prominent Moho reflections and the projections of reflections into the Mantle (M). *From LITHOPROBE, courtesy of Fred Cook and Canadian National Research Council (Cook et al., 2010, Fig. 13).*

profile in the eastern part of the Canadian shield. The interpretive cross section (lower section) shows the effects of underthrusting and tectonic underplating in response to compressive forces. This suggests that structures in the lower crust may be younger than those in the upper crust, and possibly decoupled from the upper crust. Two of the lower crustal slabs appear to be partially driven into the mantle by intense compressive forces.

It is not possible to directly date the age of the Moho in most sections, but approximate ages can sometimes be made from some combination of (1) ages of surface rocks and surface deformation, (2) the ages of lower crustal xenoliths, and (3) mapping of the geometric and cross-cutting relationships of layers whose age can be estimated at the surface. It is likely that no single origin can be assigned to the continental Moho. In some regions, tectonic underthrusting of oceanic crust beneath continental crust may account for younger rocks at depth, and the base of the underthrusted oceanic crust actually becomes the continental Moho. Alternatively, mafic and ultramafic magmas may intrude into the lower crust, spreading laterally underplating the crust, and thus the Moho relocates at the base of the igneous underplate. In addition, as discussed earlier, the mafic rocks in the deep crust may invert to eclogite, with corresponding relocation of the Moho to the top of the eclogite layer. In lower crust associated with subduction, fluids from the subducted plate may rise and alter the lower continental crust, reducing the seismic velocity contrast between the lower crust and mantle, thus rendering the Moho transparent to seismic waves. One thing is clear regarding the continental Moho: no single cause can explain this seismic boundary and the Moho may change with time in response to changing tectonic and thermal regimes.

CRUSTAL TYPES

Oceanic Crust

Seismic Features

Crustal structure in ocean basins is rather uniform, not deviating greatly in either velocity or layer thickness distribution from that shown in Figure 2.1 (Solomon & Toomey, 1992). Crustal thickness ranges from 6 to 8 km and, unlike the lithosphere, it does not thicken with age above spreading rates of about 20 mm/y (McClain & Atallah, 1986). Crustal thickness, however, drops rapidly at spreading rates less than this (Dick et al., 2003). The sediment layer averages about 0.3 km in thickness and exhibits strong seismic reflecting zones with variable orientations, some of which are probably produced by cherty layers, as suggested by cores retrieved by the Ocean Drilling Program. The thickness of the basement layer averages about 1.5 km, seismic wave velocity increases rapidly with depth, and significant seismic anisotropy has been described in some areas (Stephen, 1985). This layer also has numerous reflective horizons. In contrast, the oceanic layer is generally rather uniform in both thickness (4–6 km) and velocity (6.7–6.9 km/s).

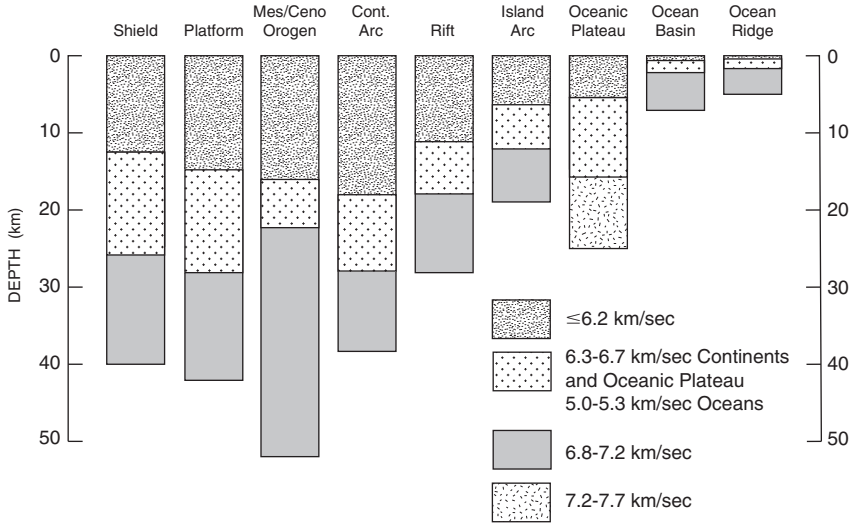

FIGURE 2.3 Seismic refraction sections of various crustal types. Ceno, Cenozoic; Mes, Mesozoic; cont., continental. Velocities are P-wave velocities.

Beneath ocean ridges, crustal thickness ranges from 3 to 6 km, most of which is accounted for by the oceanic layer (Figure 2.3) (Solomon & Toomey, 1992). Seismic reflections indicate magma chambers beneath ridges at depths of 1 to 3 km. Unlike other oceanic areas, the velocities in the oceanic layer are quite variable, ranging from 4.4 to 6.9 km/s. Anomalous mantle (Vp $<$ 7.8 km/s) occurs beneath ridge axes, reflecting high temperatures. Surface-wave data indicate that the lithosphere increases in thickness from $<$10 km beneath ocean ridges to 50 to 65 km at a crustal age of 50 Ma. Anisotropy in S-wave velocities in the oceanic mantle lithosphere is often pronounced with the fast wave traveling normal to ocean-ridge axes. Such anisotropy appears to be caused by alignment of olivine c axes in this direction (Raitt et al., 1969; Blackman et al., 2007).

The crust of back-arc basins is slightly thicker (10–15 km) than that of ocean basins, due principally to a thicker sediment layer in marginal seas. Crustal thickness in volcanic islands ranges from 10 to 20 km, with upper crustal velocities ranging from 4.7 to 5.3 km/s and lower crustal velocities from 6.4 to 7.2 km/s.

Ocean Ridges

Ocean ridges are linear rift systems in oceanic crust where new lithosphere is formed as the flanking oceanic plates move away from each other. They are topographic highs on the seafloor and are tectonically unstable. A medial rift

valley generally occurs near their crests in which new oceanic crust is produced by intrusion and extrusion of basaltic magmas. The worldwide ocean-ridge system is interconnected from ocean to ocean and is more than 70 000 km long (see Figure 1.3). Ridge crests are cut by numerous transform faults, which may offset ridge segments by thousands of kilometers.

From geophysical and geochemical studies of ocean ridges, it is clear that both structure and composition vary along ridge axes (Solomon & Tooney, 1992). In general, there is a good correlation between spreading rate and the supply of magma from the upwelling asthenosphere. Within each ridge segment, the characteristics of deformation, magma emplacement, and hydrothermal circulation vary with distance from the magma center. Also, both the forms of segmentation and the seismic crustal structure differ between fast ($\geq$80 mm/y half rate) and slow (12–50 mm/y) spreading ridges. Ultraslow spreading ridges ($\leq$12 mm/y) have the greatest topography, often with horsts of mantle rock exposed on the sea bottom (Dick et al., 2003).

From our geophysical and petrologic database, the following observations are important in understanding the evolution of slow- and fast-spreading ocean-ridge systems:

1. The lower crust (oceanic layer, Figure 2.1) is thin and poorly developed at slow-spreading ridges. The Moho is a sharp, tectonic boundary and may be a detachment surface (Dilek & Eddy, 1992). In contrast, at fast-spreading ridges the Moho is a transition zone up to 1 km thick.
2. In general, rough topography occurs on slow-spreading ridges, while smooth topography is more common on fast-spreading ridges. Fast-spreading ridges also commonly lack well-developed axial rifts.
3. Huge, long-lived axial magma chambers capable of producing a thick gabbroic lower crust are confined to fast-spreading ridges.
4. At slow-spreading ridges, like the Mid-Atlantic and SW Indian ridges, permanent magma chambers are often absent, and only ephemeral intrusions (chiefly dikes and sills) are emplaced in the medial rift (Dick et al., 2003). **Core complexes** at slow-spreading ridges may expose lower crustal gabbros by detachment faulting and they are often associated with serpentinized ultramafic rocks (Ildefonse et al., 2007).

Ocean Basins

Ocean basins comprise more of Earth's surface (38%) than any other crustal type (Table 2.1). Because the oceanic crust is thin, however, the basins make up only 12% by volume. They are tectonically stable and characterized by a thin sediment cover (approximately 0.3 km thick) and linear magnetic anomalies that are produced in erupted basalts at ocean ridges during reversed and normal polarity intervals. The sediment layer thickens near continents and arcs from which detrital sediments are supplied.

Volcanic Islands

Volcanic islands occur in ocean basins (such as the Hawaiian Islands) or on or near ocean ridges (e.g., St. Paul Rocks and Ascension Island in the Atlantic Ocean) (see Figure 1.3). They are large volcanoes that have erupted on the seafloor and whose tops have emerged above sea level. If they are below sea level, they are called seamounts. Volcanic islands and seamounts range in tectonic stability from intermediate or unstable in areas where volcanism is active (like Hawaii and Reunion) to stable in areas of extinct volcanism (such as Easter Island). Volcanic islands range in size from <1 to about $10^4 km^2$. Guyots are flat-topped seamounts produced by erosion at sea level followed by submersion, probably due to sinking of the seafloor. Coral reefs grow on some guyots as they sink, producing atolls. Some of the large volcanic islands may have developed over mantle plumes, which are the magma sources.

Trenches

Oceanic trenches mark the beginning of subduction zones and are associated with intense earthquake activity (see Figure 1.3). Trenches parallel arc systems and range in depth from 5 to 8 km, representing the deepest parts of the oceans. They contain relatively small amounts of sediment deposited chiefly by turbidity currents and derived from nearby arcs or continental areas.

Back-Arc Basins

Back-arc basins are segments of oceanic crust between island arcs (such as the Philippine Sea) or between island arcs and continents (such as the Japan Sea and Sea of Okhotsk). They are abundant in the Western Pacific and are characterized by a horst-graben topography (similar to the Basin and Range Province) with major faults subparalleling adjoining arc systems. The thickness of sediment cover is variable, and sediments are derived chiefly from continental or arc areas. Active basins, like the Lau-Havre and Mariana troughs in the Southwest Pacific, have thin sedimentary cover, rugged horst-graben topography, and high heat flow. Inactive basins, such as the Tasman and West Philippine basins, have variable sediment thicknesses and generally low heat flow.

Transitional Crust

Oceanic Plateaus

Oceanic plateaus are large flat-topped plateaus on the seafloor composed largely of mafic volcanic and intrusive rocks (Coffin & Eldholm, 1994). They are generally capped with a thin veneer of deep-sea sediments and typically rise 2 km or more above the seafloor. Next to basalts and associated intrusive rocks produced at ocean ridges, oceanic plateaus are the largest volumes of mafic igneous rocks at Earth's surface. The basaltic magmas giving rise to oceanic plateaus, together with their continental equivalents known as **flood basalts**,

are produced at hotspots which are probably caused by mantle plumes. Some of the largest oceanic plateaus, such as Ontong Java in the South Pacific and Kerguelen in the southern Indian Ocean (see Figure 3.8), which together cover an area nearly half the size of the conterminous United States, were erupted in the Mid-Cretaceous. Most oceanic plateaus are 15 to 30 km thick, although some exceed 30 km.

The seismic structure of oceanic plateaus is not well known. On the basis of existing seismic and gravity data, the largest plateaus such as Ontong Java and Kerguelen range from 20 to 33 km thick (Condie, 2001) (Figure 2.3). Midcrustal P-wave velocities are typically in the range of 6.5 to 6.7 km/s and lower crustal velocities are often very high (7.2–7.7 km/s), probably caused by underplated mafic layered intrusions related to plateau eruptions (Ridley & Richards, 2010).

Arcs

Arcs occur above active subduction zones where one plate dives beneath another. There are two types: **island arcs** develop on oceanic crust, and **continental-margin arcs** develop on continental or transitional crust. Island arcs commonly occur as arcuate chains of volcanic islands, such as the Mariana, Kermadec, and Lesser Antilles arcs (see Figure 1.3). Most large volcanic chains, such as the Andes, Cascades, and Japanese chains, are continental-margin arcs. Some arcs, such as the Aleutian Islands, continue from continental margins into oceanic crust. Modern arcs are characterized by variable, but often intense earthquake activity and volcanism, and by variable heat flow, gravity, crustal thickness, and other physical properties (Table 2.1). Arcs are composed dominantly of young volcanic and plutonic rocks and derivative sediments.

Resolution of seismic data is relatively poor in arc systems, and considerable uncertainty exists regarding arc crustal structure. Crustal thickness ranges from 5 km in the Lesser Antilles to 35 km in Japan, averaging about 22 km, and mantle velocities range from normal (8.0–8.2 km/s) to low (<7.8 km/s). All values given in Table 2.2 have large standard deviations and many arcs cannot be modeled as a simple two- or three-layer crust. Some evidence suggests that some island arcs have an intermediate-velocity layer (5.0–6.0 km/s) of varying thickness (Figure 2.3).

Seismic reflection profiles in arcs are extremely complex as shown by an interpretive profile across a typical forearc region (Figure 2.4) (von Huene & Scholl, 1991; Cawood et al., 2009). Although reflections are deformed by steep faults that dip toward the continent, they can be traced beneath the backstop in the forearc basin, where they appear to plunge into the continent. A strong continuous reflection near the base of the prism may be the upper contact of the subduction channel where sediments are recycled into the mantle. Underplated material includes both oceanic sediments and mafic igneous rocks that are part of dismembered ophiolites. Another important seismic feature of arcs is that S waves undergo splitting into fast and slow components beneath descending

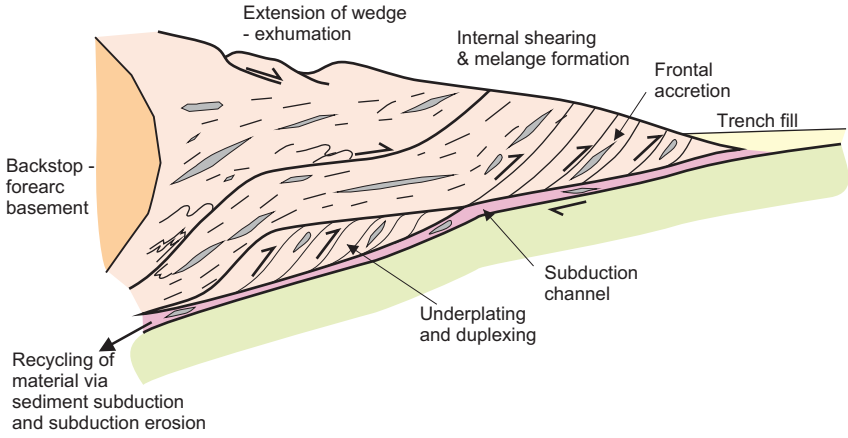

FIGURE 2.4 Diagrammatic cross section of an accretionary prism based on seismic reflection profiles and surface geology. *Courtesy of Peter Cawood and Geological Society of London.*

slabs, and the fast velocity direction generally parallels the trench. Seismic wave models suggest that three-dimensional flow beneath descending slabs is induced by trench migration. Long and Silver (2009) propose that the slab and subslab mantle are decoupled by shear heating from the asthenosphere.

Continental Rifts

Continental rifts are fault-bounded valleys ranging in width from 30 to 75 km and in length from hundreds to thousands of kilometers. They are characterized by a tensional tectonic setting in which the rate of extension is less than a few millimeters a year. Shallow magma bodies (<10 km deep) have been detected by seismic studies beneath some rifts such as the Rio Grande rift in New Mexico. The longest modern rift system is the East African system, which extends over 6500 km from the western part of Asia Minor to southeastern Africa (see Figure 1.3). The **Basin and Range Province** in western North America is a multiple rift system composed of a complex series of alternating grabens and horsts. **Aulacogens** are rifts that die out toward the interior of continents, and many appear to represent "failed arms" of triple junctions formed during fragmentation of supercontinents. Young rifts (<30 Ma) are tectonically unstable, and earthquakes, although quite frequent, are generally of low magnitude.

Continental rifts have thin crust (typically 20 to 30 km thick) and low mantle velocities (Vp < 7.8 km/s). Thinning of the crust in these regions is accomplished by thinning of the lower crustal layer (Figure 2.3), which ranges from only 4 to 14 km thick. This reflects the ductile behavior of the lower crust during extension. Although most earthquake foci in rifts are <20 km deep, some occur as deep as 25–30 km. In young crust that is being extended, such as the Basin and Range Province in the western United States, the lower crust is highly

reflective in contrast to a relatively transparent upper crust (Mooney & Meissner, 1992). Also, the reflection Moho is nearly flat, due presumably to removal of a crustal root during extension. Basin and Range normal faults cannot be traced through the lower crust and do not appear to offset the Moho.

Inland-Sea Basins

Inland-sea basins are partially to completely surrounded by tectonically stable continental crust. Examples include the Caspian and Black Seas in Asia and the Gulf of Mexico in North America (see Figure 1.3). Earthquake activity is negligible or absent. Inland-sea basins contain thick successions (10–20 km) of clastic sediments and both mud and salt diapirs are common. Some, such as the Caspian and Black Seas, are the remnants of large oceans that closed in the geologic past.

Inland-sea basins show a considerable range in crustal thickness and layer distributions. Crustal thickness ranges from about 15 km in the Gulf of Mexico to 45 km in the Caspian Sea basin. In general, the sedimentary layer or layers (Vp = 2–5 km/s) rest directly on the lower crust (Vp = 6.3–6.7 km/s), with little or no upper crust. Differences in crustal thickness among inland-sea basins are accounted for by differences in thickness of both sedimentary and lower crustal layers. Increasing velocities in sediment layers with depth, as shown for instance by the Gulf of Mexico, reflect an increasing degree of compaction and diagenesis of sediments.

Continental Crust

Shields and Platforms

Precambrian shields are stable parts of the continents composed of Precambrian rocks with little or no sediment cover. Rocks in shields may range in age from 0.5 to >3.5 Ga. Metamorphic and plutonic rocks dominate, and temperature-pressure regimes recorded in exposed rocks suggest burial depths ranging from as shallow as 5 km to as deep as 40 km or more. Shield areas, in general, exhibit very little relief and have remained tectonically stable for long periods of time. They comprise about 11% of the total crust by volume, with the largest shields occurring in Africa, Canada, and Antarctica.

Platforms are also stable parts of the crust with little relief. They are composed of Precambrian basement similar to that in shields overlain by 1 to 3 km of relatively undeformed sedimentary rocks. Sedimentary rocks on platforms range in age from Precambrian to Cenozoic and reach thicknesses up to 5 km, as is seen for instance in the Williston basin in the north-central United States. Platforms comprise most of the crust in terms of volume (35%) and most of the continental crust in terms of both area and volume. Shields and the Precambrian basement of platforms are collectively referred to as cratons. A **craton** is an isostatically positive portion of the continent that is tectonically stable

relative to adjacent orogens. For the most part, cratons are composed of uplifted, eroded ancient orogens.

Shields and platforms have similar upper- and lower-layer thicknesses and velocities (Figure 2.3). The difference in their mean thickness (Table 2.2) reflects primarily the presence of the sediment layer in platforms. Upper-layer thicknesses range from about 10 to 25 km and lower layers from 16 to 30 km. Velocities in both layers are rather uniform, generally ranging from 6.0 to 6.3 km/s in the upper layer and 6.8 to 7.0 km/s in the lower layer. Upper mantle velocities are typically in the range of 8.1 to 8.2 km/s, rarely reaching 8.6 km/s. Results suggest the existence of a high-velocity layer (~7.2 km/s) in lower crust of the Proterozoic age. Seismic reflection studies show an increase in the number of reflections with depth and generally weak, but laterally continuous Moho reflections (Mooney & Meissner, 1992).

Orogens

Orogens are long, curvilinear belts of compressive deformation produced by the collision of continents or of terranes and continents. Giant thrust sheets and nappes are found in many orogens. Collisional orogens range from several thousand to tens of thousands of kilometers in length, and are composed of a variety of rock types. They are expressed at Earth's surface as mountain ranges with varying degrees of relief, depending on their age. Older collisional orogens, such as the Appalachian orogen in eastern North America and the Variscan orogen in central Europe, are deeply eroded with only moderate relief, whereas young orogens such as the Alps and Himalayas, are among the highest mountain chains on Earth. Tectonic activity decreases with age of deformation in orogens. Orogens older than Paleozoic are deeply eroded and are now part of Precambrian cratons. Large plateaus, which are uplifted crustal blocks that have escaped major deformation, are associated with some orogens, such as the Tibet plateau in the Himalayan orogen.

Crustal thickness of orogens is extremely variable, ranging from about 30 km in some Precambrian orogens to 70 km beneath the Himalayas. In general, thickness decreases with age. Average layer thicknesses and velocities of the upper two layers of Phanerozoic orogens are similar to platforms (Table 2.2 and Figure 2.3), and average Phanerozoic collisional orogen crustal thickness is about 46 km. In areas with very thick crust, such as the Himalayas, the thickening occurs primarily in the lower crustal layer, which is expected since this layer behaves in a ductile manner during deformation. The velocity contrast between the lower crust and upper mantle is commonly less beneath young orogenic areas (0.5–1.5 km/s) than beneath platforms and shields (1–2 km/s).

Phanerozoic orogens show considerable heterogeneity in terms of seismic reflection profiles. The Caledonian and Variscan orogens in Europe appear to have lost their crustal roots and show well-developed, chiefly subhorizontal reflectors in the lower crust (Mooney & Meissner, 1992). This loss of crustal

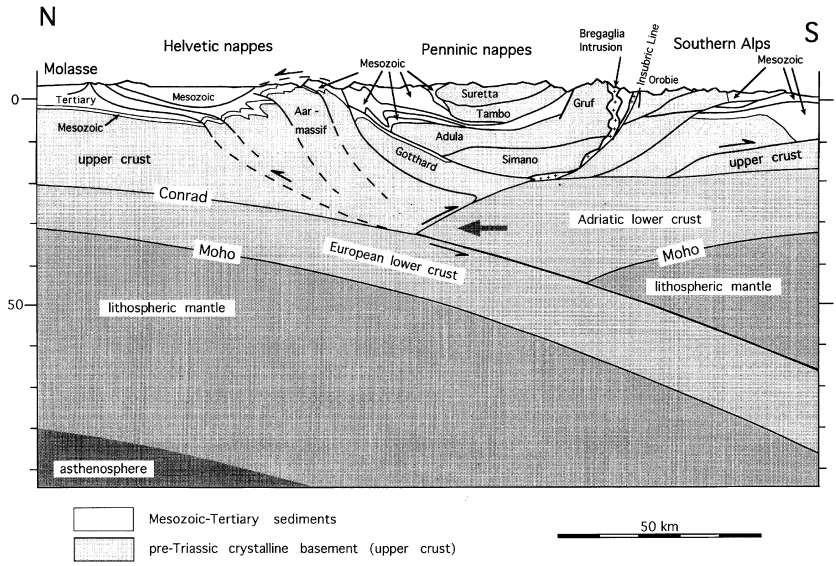

FIGURE 2.5 A tectonic north-south profile across the eastern Alps, an example of a typical collisional orogen. The subsurface features of the profile are from seismic reflection data. *Courtesy of Adrian Pfiffner.*

roots may have occurred during post-tectonic extensional collapse. Often, however, major thrust sheets, and in some instances sutures, are still preserved in the reflection profiles (Figure 2.2). In the southern Appalachians, the reflection data reveal a large décollement at midcrustal depths separating Precambrian basement from overlying allochthonous rocks of the Appalachian orogen (Cook et al., 1981). In very young orogens like the Alps, lower crustal reflectors dip to the center of a thick root, often with an irregular and offset Moho. At midcrustal depths, however, reflectors typically show a complex pattern that is suggestive of crustal wedging and interfingering of nappes (Figure 2.5).

CONTINENT SIZE

As has been known for some time, there is an overall positive correlation between the area of continents and microcontinents and their average elevation relative to sea level (Figure 2.6) (Cogley, 1984). Small continental fragments, such as Agulhas and Seychelles, lie two or more kilometers below sea level. The height of a continent depends on the uplift rate and the rates of erosion and subsidence. Collision between continents resulting in lithosphere thickening is probably the leading cause of continental uplift in response to isostasy. The anomalous heights of India and Arabia undoubtedly reflect the collision

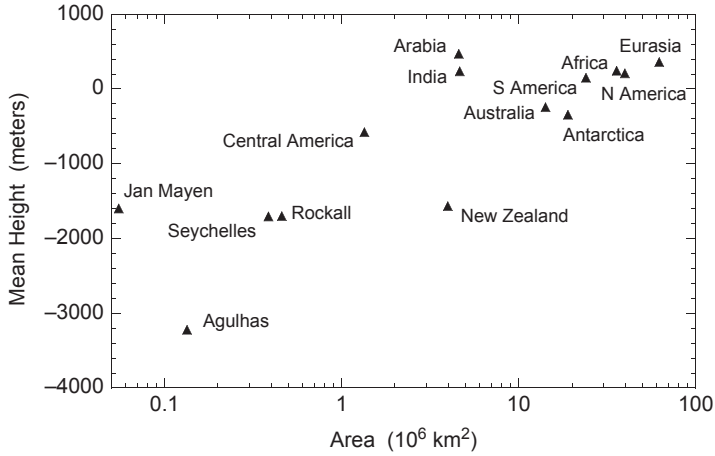

FIGURE 2.6 Mean continental heights as a function of continental area. *Data from Cogley (1984).*

of these microcontinents with Asia between 65 and 50 Ma, and in the case of India, this collision is continuing today. The six large continents have undergone numerous collisions in the last 1 Ga, each thickening the lithosphere in collisional zones leading to a greater average continent elevation. Hotspot activity can also elevate continents, and it is probable that the high elevation of Jan Mayen may be related to the Iceland hotspot. Also, Africa, which is higher than the other large continents by 200 m, may reflect the numerous hotspots beneath this continent.

The other five small continents in Figure 2.6 are mostly fragments that have been rifted from supercontinents. Since the breakup of supercontinents leads to a rise in sea level, it is not surprising that these microcontinents are completely flooded. Not until they collide with other continents will they emerge above sea level.

HEAT FLOW

Heat Flow Distribution

Surface heat flow in continental and oceanic crust is controlled by many factors, and for any given segment of crust it decreases with mean crustal age (Nyblade & Pollack, 1993). One of the most important sources of heat loss from the Earth is ocean ridges. Approximately 25% of total global heat flow can be accounted for by hydrothermal transport at ocean ridges (Davies, 1980). Heat flow on continents and islands varies as a function of the age of the last magmatic event, the distribution of heat-producing elements, and erosion level. Considering all sources of heat loss, the total heat loss from the Earth is about 42×10^{12} W,

12×10^{12} W from the continents, and 30×10^{12} W from the oceans (Sclater et al., 1980). The equivalent heat flows are 55 and 95 mW/m^2, respectively, for a worldwide average heat flow of 81 mW/ m^2 (Table 2.1). The difference between the average measured oceanic heat flow (67 mW/ m^2) and the calculated value (95 mW/ m^2) is due to heat losses at ocean ridges by hydrothermal circulation. Models indicate that 88% of the Earth's heat is lost from the mantle: 66% at ocean ridges and by subduction, 10% by conduction from the subcontinental lithosphere, and 12% from mantle plumes (Davies & Richards, 1992). This leaves 12% lost from the continents by radioactive decay of heat-producing elements.

Heat flows of major crustal types are tabulated in Table 2.1. Shield areas exhibit the lowest and least variable continental heat flow values, generally in the range of 35 to 42 mW/m^2, averaging about 40 mW/m^2. Platforms are more variable, usually falling between 35 and 60 mW/m^2 and averaging about 49 mW/m^2. Young orogens, arcs, continental rifts, and oceanic islands exhibit high and variable heat flow in the range of 50 to 80 mW/m^2. The high heat flow in some arcs and volcanic islands reflects recent volcanic activity in these areas. Heat flow in ocean basins generally falls between 35 and 60 mW/m^2, averaging about 50 mW/m^2. Ocean ridges, on the other hand, are characterized by extremely variable heat flow, ranging from less than 100 to greater than 200 mW/m^2, with heat flow decreasing with increasing distance from the ridge. Back-arc basins are also characterized by high heat flow (60–80 mW/m^2), whereas inland-sea basins exhibit variable heat flow (30–75 mW/m^2), reflecting, in part, variable Cenozoic sedimentation rates in the basins.

A **geotherm**, which is the conductive temperature distribution with depth beneath a given surface location, is dependent on surface and mantle heat flow and the distribution of thermal conductivity and radioactivity with depth. Geotherms in four crustal types are given in Figure 2.7. All of the geotherms have a nearly constant gradient in the upper crust, but diverge at depth resulting in up to 500°C difference in crustal types at Moho depths. Geotherms converge again at depths greater than 300 km where convective heat transfer in the mantle dominates.

Heat Production and Heat Flow in the Continents

Heat flow is significantly affected by the age and intensity of the last orogenic event, the distribution of radioactive elements in the crust, and the amount of heat coming from the mantle (Chapman & Furlong, 1992). Continental surface heat flow (q_0) is linearly related to average radiogenic heat production (A_0) of near-surface basement rocks by

$$q_0 = q_r + A_0 D \tag{2.1}$$

In this expression, q_r, commonly referred to as the reduced heat flow, is the intercept value for rocks with zero heat production; and D, the slope of the line relating q_0 to A_0, has units of depth and is commonly referred to as the

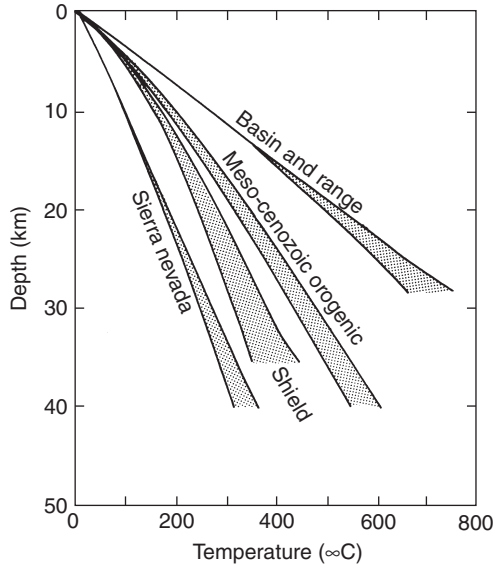

FIGURE 2.7 Geotherms in four continental crustal types. Shaded areas represent uncertainty ranges for each geotherm. *After Blackwell (1971) and Chapman (1986).*

characteristic depth. The **characteristic depth** is interpreted to reflect the thickness of the upper crustal layer enriched in heat-producing elements, and ranges from about 3 to 14 km. The **reduced heat flow** is the heat coming from below this layer and includes radiogenic heat from both the lower crust and mantle.

Examples of the linear relationship between q_0 and A_0 for several crustal types are given in Figure 2.8. The Appalachian orogen is typical of pre-Mesozoic orogens and most platform areas. Studies of elevated fragments of lower continental crust, such as the Pikwitonei province in Canada (Fountain et al., 1987), show that heat production and surface heat flow also yield a broadly linear relationship, indicating that the q–A relationship is independent of crustal level exposed at the surface (Mareschal et al., 1999). The chief factors distinguishing individual crustal types are the reduced heat flow values (q_r) and, to a lesser extent, the range of surface heat flow and heat productivity. On average, about 70% of heat flow at the surface is due to the reduced heat flow contribution (Artemieva & Mooney, 2001). Thermal modeling indicates that the q–A relationship can best be explained by a decrease in radiogenic heat production with depth in the crust. Uplifted blocks of middle crust have moderate levels of radiogenic elements (U, Th, K), so most of the drop in radiogenic heat production must occur in the lower crust, in agreement with a largely mafic composition as inferred from xenolith data (Rudnick & Fountain, 1995; Rudnick & Gao, 2004).

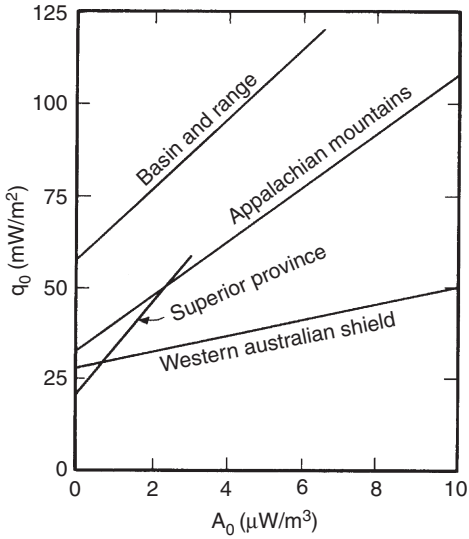

FIGURE 2.8 Surface heat flow (q_0) versus heat production of near-surface rocks (A_0) for several crustal types.

Reduced heat flow decreases with the average age of continental crust (Artemieva & Mooney, 2001) (Table 2.3). No relationship, however, appears to exist between the characteristic depth and mean crustal age, and neither heat flow nor reduced heat flow are related to lithosphere thickness (Jaupart et al., 1998). The reduced heat flow decays within 200–300 My to a value between 20 and

TABLE 2.3 Reduced Heat Flow Provinces

	Age (Ma)	q_0 (mW/m^2)	q_r (mW/m^2)	D (km)
1. Basin and Range (Nevada)	0–65	77	63	9.4
2. Eastern Australia	0.65	72	57	11
3. Appalachian mountains	400–100	56	34	7.5
4. United Kingdom	1000–300	69	24	16
5. Western Australian shield	2800	42	30	4.5
6. India shield	>1800	35	22	8
7. Superior Province (Canada)	2700	42	35	14
8. Baltic Shield	>1800	47	25	6.5

Note: q_0 and q_r, average surface and reduced heat flow, respectively; D, characteristic depth.

30 mW/m^2, which is about a factor of 3 faster than surface heat flow decays. It is probably related to variations in heat production in the mantle lithosphere (Lenardic, 1997). In contrast, equilibrium q values for oceans are 30–40 mW/m^2.

Two interpretations of the change in D between reduced heat flow provinces have been proposed (Jessop & Lewis, 1978): differences in crustal erosion level or differences in degree of chemical fractionation of the crust. Because the crustal level exposed at the surface as deduced from metamorphic mineral assemblages does not correlate with D, nor does D correlate with mean crustal age, the first interpretation seems unlikely. The alternative interpretation necessitates variable intensities of fractionation of U, Th, and K into the upper crust, which is not related to the age of the crust. This could occur by partial melting in the lower crust, producing granitoid magmas (in which U, Th, and K are concentrated), which rise to shallow levels. High-grade metamorphism in the lower crust also liberates fluids in which U, Th, and K can be dissolved, and thus transported to higher crustal levels.

A relatively low heat flow is observed in all Archean cratons (such as the Superior Province and Baltic Shield, Table 2.3) compared to post-Archean cratons (Rudnick et al., 1998). This may be caused by either (1) a greater concentration of U, Th, and K in post-Archean cratons, or (2) a thick lithospheric root beneath the Archean cratons that effectively insulates the crust from asthenospheric heat (Nyblade & Pollack, 1993; Rudnick et al., 1998). As we shall see in Chapter 4, the second factor is probably the principal cause of the low heat flow from Archean crust.

Age Dependence of Heat Flow

Average surface heat flow decreases with the average age of crustal rocks in both oceanic and continental areas (Sclater et al., 1980; Morgan, 1985). Continental heat flow drops with age to an approximately constant value of 40–50 mW/m^2 in about 1 Ga, and in oceanic areas, similar constant heat flow values are reached in only 50–100 Ma (Figure 2.9). Continental heat flow can be considered in terms of three components, all of which decay with time (Vitorello & Pollack, 1980; Michaut et al., 2007). Radiogenic heat in the upper crust contributes about 40% of the total heat flow in continental crust of all ages. The absolute amount of heat from this source decreases with time in response to erosion of the upper crust. A second component of heat, contributing about 30% to the heat flow in Cenozoic terranes, is residual heat of igneous activity associated with orogeny. These two components decay rapidly in a few hundred million years. The third and generally minor component comes from convective heat within the mantle. The age of the oceanic crust increases as a function of distance from ocean ridges and as a function of decreasing mean elevation as a consequence of seafloor spreading. The decrease in heat flow with distance to an active ocean ridge reflects cooling of new lithosphere that was formed at the ridge by injection of magma.

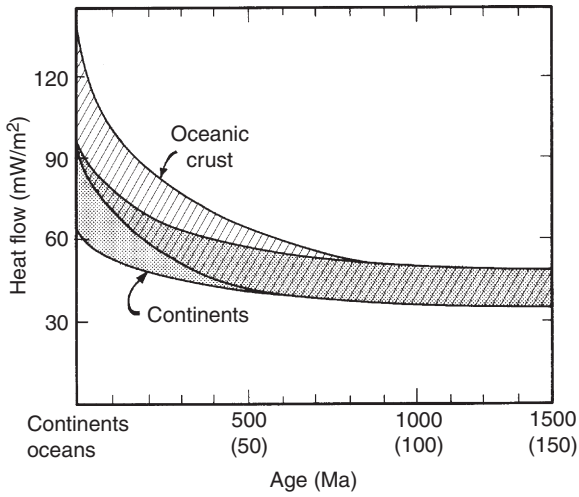

FIGURE 2.9 Age dependence of average heat flow for continental and oceanic crust. Numbers in parentheses on horizontal axis refer to ages in oceanic areas. *After Morgan (1985).*

Why should continental and oceanic heat flow decay to similar equilibrium values of 40–50 mW/m^2, when these two types of crust have had such different origins and histories? One possibility is summarized in Table 2.4. The model assumes a 10-km-thick oceanic crust and a 40-km-thick continental crust, with an exponential distribution of radiogenic heat sources in the continental crust. Equilibrium reduced heat flow values (q_r) are selected from the range of observed values in both crustal types. Both ocean basins and Precambrian shields have similar temperatures by depths of 100 km, the average thickness

TABLE 2.4 Heat Flow Model for Ocean Basin and Precambrian Shield

Ocean basin $q_0 = 50$ mW/m^2			Precambrian shield $q_0 = 38$ mW/m^2		
Thickness (km)	*A (mW/m^3)*	*q (mW/m^2)*	*Thickness (km)*	*A (mW/m^3)*	*q (mW/m^2)*
10	0.42	4	35	0.7*	25
90	0.02	2	65	0.02	1
Mantle	0.02	44	Mantle	0.02	12

$A = A_0 e^{-(x/D)}$ where $A_0 = 2.5$ mW/m^3 and $D = 10$ km.

of the lithosphere. The results clearly imply that more mantle heat is entering the base of the oceanic lithosphere (44 mW/m^2) than of the continental lithosphere (12 mW/m^2). Hence, when a plate carrying a Precambrian shield moves over oceanic mantle, the surface heat flow should rise until mantle convective systems readjust so they are again liberating most heat beneath oceanic areas.

EXHUMATION AND CRATONIZATION

To understand how continental crust evolves, we need to understand how orogens evolve, since continents comprise orogens of various ages. During continental collisions, large segments of continental crust are highly deformed and thickened and later they are uplifted and eroded and their roots evolve into cratons. The process of uplift and erosion is known as crustal **exhumation**. Crustal history is imprinted in rocks as pressure-temperature-time trajectories, generally referred to as crustal **P-T-t paths**. Not only orogens, but all crustal types record P-T-t paths, and to understand continental growth and development, it is important to reconstruct and understand the meanings of these P-T-t paths.

Burial of rocks in the crust results in progressive metamorphism as the rocks are subjected to increasing pressure and temperature. Given that metamorphic reactions are more rapid with rising than with falling temperature, metamorphic mineral assemblages may record the highest P-T regime to which rocks have been subjected. Later exhumation makes it possible to directly study rocks that were once buried at various depths in the crust, but are now exposed at the surface. Such rocks contain metamorphic mineral assemblages "arrested" at some burial depth or metamorphic grade. Minor changes in mineralogy known as retrograde metamorphism may occur during uplift, but such changes commonly can be identified without great difficulty by studying textural features of the rocks. Progressive metamorphism is accompanied by losses of H_2O and other volatile constituents, and some high-grade rocks are almost anhydrous.

Zones of increasing metamorphic grade can be classified into **metamorphic facies**, which represent limited ranges of burial depth, temperature, and water content in the crust. Five major facies of regional metamorphism are recognized (Figure 2.10). The *zeolite facies* is characterized by the development of zeolites in sediments and volcanics and reflects temperatures of generally less than 200°C and burial depths up to 5 km. The *greenschist facies* is characterized by the development of chlorite, actinolite, epidote, and albite in mafic volcanics and of muscovite and biotite in pelitic rocks. *Blueschist-facies* assemblages form at high pressures (>800 MPa) yet low temperatures (<400°C) in subduction zones, and typical minerals are glaucophane, lawsonite, and jadeite. The *amphibolite facies* is characterized by kyanite, staurolite, and sillimanite in metapelites and plagioclase and hornblende in mafic rocks. The highest grade rocks occur in the *granulite facies*, which is characterized by a sparsity or absence of hydrous minerals and the appearance of pyroxenes. Using experimental petrologic and oxygen isotope data, the temperature and pressure at

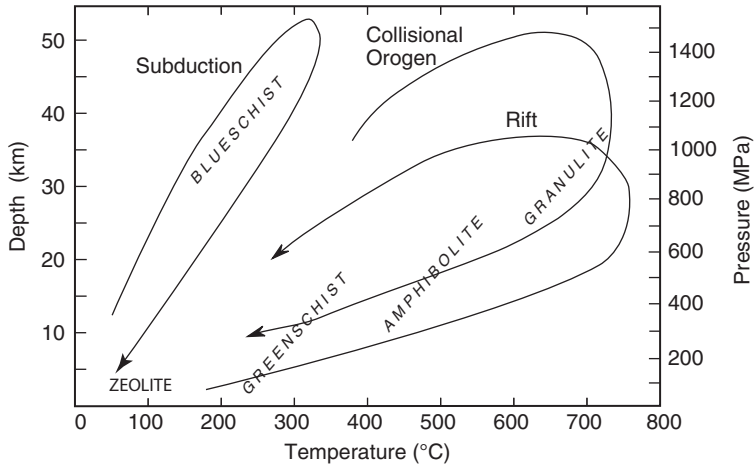

FIGURE 2.10 Pressure-temperature diagram showing the distribution of metamorphic facies and typical pressure-temperature-time paths.

which metamorphic mineral assemblages crystallize can be estimated, and from these results, burial depths of metamorphic terrains exposed at Earth's surface can be estimated.

Unraveling Pressure-Temperature-Time Histories

To begin to understand complex pressure-temperature-time (P-T-t) histories, many data sources must be used. It is important to know the sequence in which metamorphic minerals have grown and how their growth is related to deformation (Brown, 1993). This can be established from petrographic studies of metamorphic rocks in which textural relationships between mineral growth and deformational fabric are preserved. Particularly important are mineral inclusions in porphyroblasts, replacement textures of one mineral by another, and mineral zoning, all of which reflect changing conditions along the P-T-t path. By relating mineral growth relationships to experimentally determined P-T stability fields of metamorphic minerals, it is possible in some instances to pin down the pressure and temperature at which a given mineral assemblage grew. This is known as **geothermobarometry**. In turn, local P-T conditions may be related to broad regional fabrics in crustal rocks, thus relating microscopic growth data to orogenic development.

To add time to these events, it is necessary to isotopically date minerals that form along different segments of a P-T-t path and become isotopically closed at given temperatures. For instance, the $^{40}Ar/^{39}Ar$ method can be used to date hornblende, which closes to argon diffusion at about 500°C, muscovite that closes at 350 to 400°C, and K-feldspar that closes at 150–350°C. At lower

temperatures, fission tracks, which anneal in apatite at about 150°C are useful (McDougall & Harrison, 1988; Crowley & Kuhlman, 1988). To unravel P-T-t histories in the crust, it is necessary to combine results from field, petrographic, experimental, and isotopic studies. Even then it may not be possible to untangle a complex history in which a crustal segment has undergone multiple deformation and metamorphism.

Some Typical P-T-t Paths

Varying tectonic histories yield different P-T-t paths (Chapman & Furlong, 1992). P-T-t paths of collisional orogens are typically clockwise in P-T-t space and their general features are reasonably well understood from classic studies in the Appalachians, Caledonides, Alps, and Himalayas (Brown, 1993). This type of P-T-t path results from rapid crustal thickening so that maximum pressure is reached before maximum temperature (Figure 2.10). Hence, the metamorphic peak generally postdates early deformation in the orogen. This evolutionary path commonly leads to dehydration melting of the lower crust producing granitic magmas, which abound in collisional orogens.

During the development of a continental rift by crustal extension, the crust is heated from below by mantle upwelling before crustal thickening occurs, and the maximum temperature is reached before the maximum pressure. This produces a counterclockwise P-T-t path (Figure 2.10). The metamorphic peak usually predates or is synchronous with early deformation in these cases. Heating of the lower crust can lead to dehydration melting as a consequence of the metamorphism, producing felsic magmas. Any crustal environment in which heating precedes thickening of the crust results in counterclockwise P-T-t paths. In addition to rifts, extended margins of platforms and magmatically underplated crust, such as beneath continental flood basalts, have counterclockwise P-T-t paths. In some instances, such as the northern Appalachians, clockwise and counterclockwise P-T-t paths can occur in adjacent segments of the same orogen.

P-T-t paths of subduction zones are very steep, with pressure increasing rapidly as a slab descends into the mantle. Because the slab is relatively cool ($<$400°C), ultrahigh-pressure (UHP) metamorphic rocks, including blueschists and eclogites, are stabilized. The fact that the UHP rocks have returned to the surface from great depths is reflected by the occurrence of such high-pressure phases as coesite and diamond in some of these rocks. Just how these dense rocks are returned to the surface is not clear; perhaps they are housed in lower density rocks that rise buoyantly along the surface of descending slabs. These findings have provided compelling evidence that segments of the continental crust were subducted into the mantle at depths in excess of 100 km and returned to the surface during continental collisions. This disproves the idea that the continental crust cannot be subducted to mantle depths because it is less dense than that of the oceanic crust.

Cratonization

Although cratons have long been recognized as an important part of the continental crust, we still have much to learn about their origin and evolution. Most investigators agree that cratons are the end product of collisional orogenesis, and thus they are the building blocks of continents. Just how orogens evolve into cratons and how long it takes, however, are not well known. Although studies of collisional orogens show that most are characterized by clockwise P-T-t paths (Thompson & Ridley, 1987; Brown, 1993), the uplift/exhumation segments of the P-T paths are poorly constrained (Martignole, 1992). In terms of craton development, it is the <500°C portion of the P-T-t path that is most important.

Using a variety of radiogenic isotopic systems and estimated closure temperatures in various minerals, it is possible to track the cooling histories of crustal segments, and when coupled with thermobarometry, also the uplift/exhumation histories. Results suggest a wide variation in cooling and uplift rates with most orogens having cooling rates of <2°C/My, whereas a few (like Southern Brittany) cool at rates of >10°C/My (Figure 2.11). In most cases, it takes a minimum of 300 Ma to make a craton. Some terranes, such as Enderbyland in Antarctica, have had very long, exceedingly complex cooling

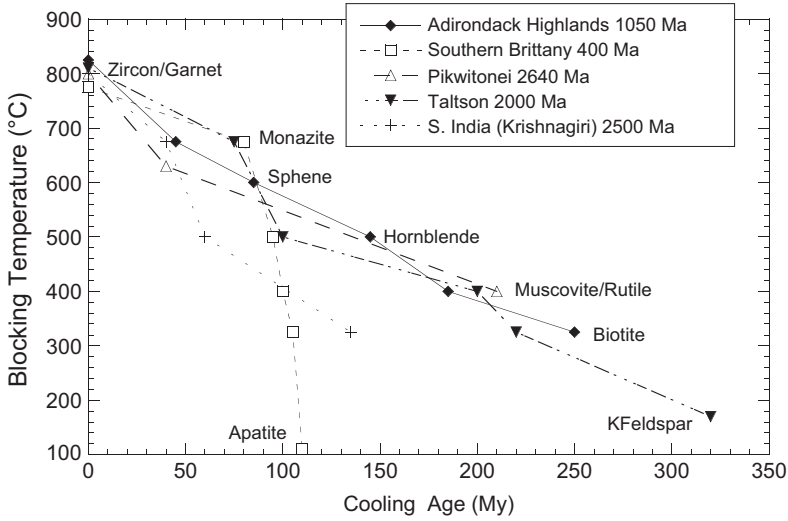

FIGURE 2.11 Cooling histories of several orogens. Ages of maximum temperatures given for each location and equated to zero age on the cooling age axis. Blocking temperature is the temperature at which the daughter isotope is trapped in a host mineral. *Data from Harley & Black (1987), Dallmeyer & Brown (1992), Mezger et al. (1991), Kontak and Reynolds (1994), and Plint & McDonough (1995).*

histories lasting for more the 2 Ga. Many orogens, such as the Grenville orogen in eastern Canada, have been exhumed as indicated by unconformably overlying sediments, and then reheated during subsequent burial and then re-exhumed (Heizler, 1993). In some instances, postorogenic thermal events such as plutonism and metamorphism have thermally overprinted earlier segments of an orogen's cooling history, such that only the very early high-temperature history (>500°C) and perhaps the latest exhumation record (<300°C) are preserved. Fission track ages suggest that final uplift and exhumation of some orogens, like the 1.9-Ga Trans-Hudson orogen in central Canada, may be related to the early stages of supercontinent fragmentation.

An important, yet poorly understood aspect of cratonization is that of how terranes that amalgamate during a continent–continent collision evolve into a craton. Does each terrane maintain its own identity and have its own cooling and uplift history? Or alternatively, do terranes anneal to each other at an early stage and the entire orogen cools and is elevated as a unit? What is the effect of widespread post-tectonic plutonism? Does it overprint and erase important segments of the orogen cooling history? It is well known that crustal cooling curves are not always equivalent to exhumation curves (Thompson & Ridley, 1987). In fact, some granulite-grade blocks appear to have undergone long periods of isobaric (constant depth) cooling before exhumation. Also, discrete thermal events can completely or partially reset thermochronometers without an obvious geologic rock record, and this can lead to erroneous conclusions regarding average cooling rates (Heizler, 1993).

Post-tectonic plutonism, which follows major deformation, or multiple deformation of an orogen can lead to a complex cooling history. Widespread post-tectonic plutonism can perturb the cooling curve of a crustal segment, prolonging the cooling history (Figure 2.12a). In an even more complex scenario, a crustal domain can be exhumed, reburied as sediments accumulate in an overlying basin, age for hundreds of millions of years at about the same

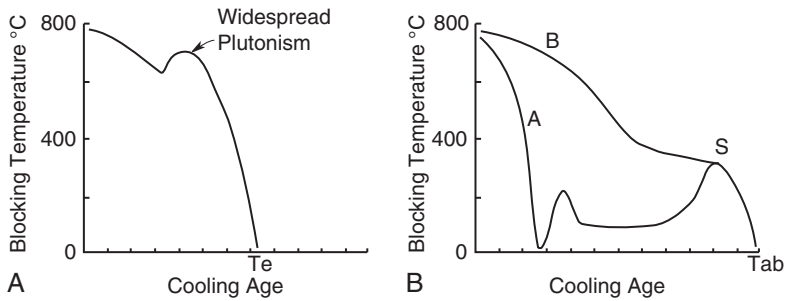

FIGURE 2.12 Two possible cooling scenarios in cratons: (A) overprinting of a post-tectonic granite intrusion event; (B) a complex, multiple-event cooling history. Te and Tab, final exhumation ages; S, suturing age of terranes A and B.

crustal level, and finally be re-exhumed (A in Figure 2.12b). In this example, all of the <400°C thermal history is lost by overprinting of the final thermal event. A second terrane B could be sutured to A during the first exhumation event (S in Figure 2.12b), and both domains are exhumed together during the final thermal event. It is clear from these examples that much or all of a complex thermal history can be erased by the last thermal event, producing an apparent gap in a cratonization cooling curve.

PROCESSES IN THE CONTINENTAL CRUST

Rheology

The behavior of the continental crust under stress depends chiefly on the temperature, the duration of the stresses, and the water content. The hotter the crust, the more it behaves like a ductile solid deforming by plastic flow, whereas if it is cool, it behaves as an elastic solid deforming by brittle fracture and frictional gliding (Ranalli, 1991; Rutter & Brodie, 1992). The distribution of strength with depth in the crust varies with tectonic setting, water content, strain rate, thickness and composition of the crust, and the geotherm. The **brittle–ductile transition** corresponding to an average surface heat flow of 50 mW/m^2 is at a 15- to 20-km depth, which also corresponds to the depth limit of most shallow earthquakes. Even in the lower crust, however, if stress is applied rapidly, it may deform by fracture; likewise, if pore fluids are present in the upper crust, weakening it, and stresses are applied slowly, the upper crust may deform plastically. In regions of low heat flow, such as shields and platforms, brittle fracture may extend into the lower crust or even into the upper mantle because mafic and ultramafic rocks can be very resistant to plastic failure at these depths, and thus faulting is the only way they can deform. Lithologic changes at these depths, the most important of which is at the Moho, also may be rheologic discontinuities.

The major factor controlling the strength of the continental lithosphere is the distribution of water in the crust and subcrustal lithosphere. The frequency of crustal earthquakes is generally thought to reflect water-rich regions that weaken the crust (Figure 2.13). In contrast, the lower continental crust, which has few earthquakes, is relatively dry and strong (Maggi et al., 2000). The coupling of strain and water content is illustrated in Figure 2.13, which shows strength–depth curves for wet and dry crust (Yardley, 2009). There is clearly a depth range in the midcrust in which there is a large strength difference between the wet and dry crust. As long as the deep crust is dry, it can sustain significant stresses, but if water is present even in small amounts, it will result in significant weakening with strain partitioned into the wet region. Thus, crustal earthquakes will be concentrated in this region as suggested in the figure.

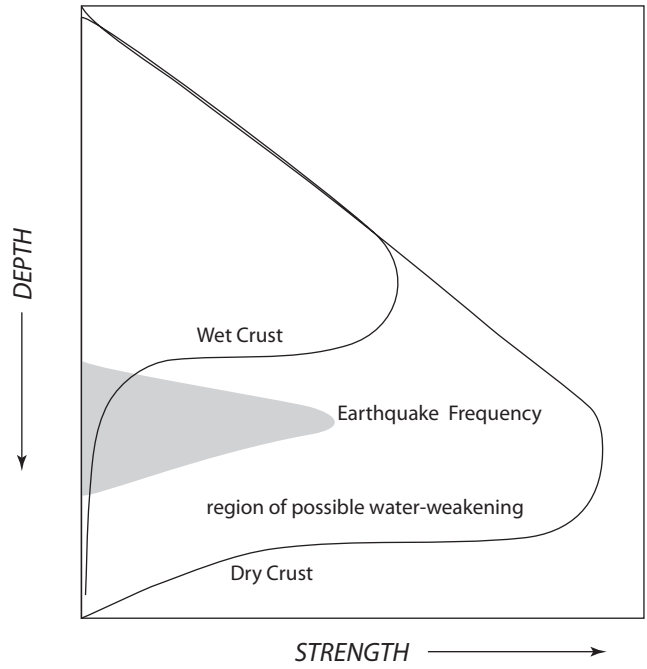

FIGURE 2.13 Schematic diagram showing the variation of crustal strength with depth for wet and dry crust. Also shown is a typical zone of crustal earthquakes. *Diagram modified after Yardley (2009).*

The Role of Fluids and Crustal Melts

Fluid transport in the crust is an important process affecting both rheology and chemical evolution. Because crustal fluids are mostly inaccessible for direct observation, this process is not well understood and difficult to study. Studies of fluid inclusions trapped in metamorphic and igneous minerals indicate that shallow crustal fluids are chiefly water, whereas deep crustal fluids are mixtures of H_2O and CO_2, and both contain various dissolved species (Bohlen, 1991; Wickham, 1992). Fluids are reactive with silicate melts and in the lower crust they can promote melting and also change the chemical and isotopic composition of rocks.

In the lower crust, only small amounts of fluid can be generated by the breakdown of hydrous minerals such as biotite and hornblende. Hence, the only major source of fluids in the lower crust is from the mantle. Studies of xenoliths suggest that the mantle lithosphere provides a potentially large source for CO_2 in the lower crust, and may be the principal source for CO_2 that is important in the production of deep crustal granulites.

The formation of granitic melts in the lower crust and their transfer to shallower depths is a fundamental process leading the chemical differentiation

of the continents. This is particularly important in arcs and collisional orogens. The melt-producing capacity of a source rock in the lower crust is determined chiefly by its chemical composition, temperature regime, and water content (Brown et al., 1995). Orogens that include a large volume of juvenile volcanics and sediments are more fertile (high melt-producing capacity) than those that include chiefly older basement rocks from which fluids and melts have been extracted (Vielzeuf et al., 1990). A fertile lower crust can generate a range of granitic melt compositions and leave behind a residue of granulites. Segregation of melt from source rocks can occur by several different processes, and just how much and how fast melt is segregated is not well known. It depends, however, on whether deformation occurs concurrently with melt segregation. Experiments indicate that melt segregation is enhanced by increased fluid pressures and fracturing of surrounding rocks. Modeling suggests that shear-induced compaction can drive melt into veins that transfer it rapidly to shallow crustal levels (Rutter & Neumann, 1995). Melt ascent is by ductile to brittle fracture. Ductile fractures propagate along foliation as sills or by dilation or shear bands as dykes (Brown, 2010). Emplacement of horizontal or tabular plutons occurs near the brittle–ductile transition, whereas vertical lozenge-shaped plutons characterize crystallization in ascent conduits.

CRUSTAL COMPOSITION

Approaches

Several approaches have been used to estimate the chemical and mineralogic composition of the crust. One of the earliest methods to estimate the composition of the upper continental crust is based on chemical analysis of glacial clays, which are assumed to be representative of the composition of large portions of the upper continental crust. Estimates of total continental composition are based on mixing average basalt and granite compositions in ratios generally ranging from 1:1 to 1:3 (Taylor & McLennan, 1985) or by weighting the compositions of various igneous, metamorphic, and sedimentary rocks according to their inferred abundances in the crust (Ronov & Yaroshevsky, 1969). Probably the most accurate estimates of the composition of the upper continental crust come from extensive sampling of rocks exhumed from varying depths in Precambrian shields and from the composition of Phanerozoic shales (Taylor & McLennan, 1985; Condie, 1993; Rudnick & Gao, 2004). Because the lower continental crust is not accessible for sampling, indirect approaches must be used. These include (1) measurement of seismic wave velocities of crustal rocks in the laboratory at appropriate temperatures and pressures, and comparing these to observed velocity distributions in the crust; (2) sampling and analyzing rocks from blocks of continental crust exhumed from middle to lower crustal depths; and (3) analyzing xenoliths of lower crustal rocks brought to the surface during volcanic eruptions. The composition of oceanic crust is estimated

from the composition of rocks in ophiolites and from shallow cores into the sediment and basement layers of oceanic crust retrieved by the Ocean Drilling Program. Results are again constrained by seismic velocity distributions in the oceanic crust.

Before discussing the chemical composition of the crust, we next review the major sources of data.

Seismic Wave Velocities

Because seismic wave velocities are related to rock density and density is related to rock composition, the measurement of these velocities provides an important constraint on the composition of both the oceanic and continental crust (Rudnick & Fountain, 1995; Ji et al., 2008). **Poisson's ratio**, which is the ratio of P-wave to S-wave velocity, is more diagnostic of crustal composition than either P-wave or S-wave data alone (Zandt & Ammon, 1995) (Table 2.1). Poisson's ratio increases both with density as rock composition changes from felsic to mafic, and with temperature, because S-wave velocity decreases more rapidly than P-wave velocity with rising temperature. This change is correlated with systematic variations in the quartz and feldspar content: the ratio increases with the feldspar content and decreases with quartz content.

Figure 2.14 shows average compressional wave velocities (at 600 MPa and 300°C) in a variety of crustal rocks. Velocities under 6 km/s are limited to

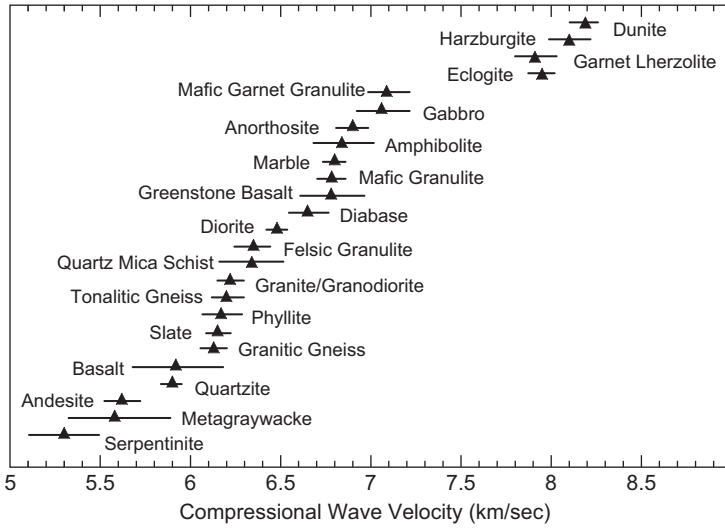

FIGURE 2.14 Average compressional (P) wave velocities and standard deviations at 600 MPa (20-km depth equivalent) and 300°C (assuming average heat flow) for major rock types. *Data from Christensen & Mooney (1995).*

serpentinite, metagraywacke, andesite, and basalt. Many rocks of diverse origins have velocities between 6 and 6.5 km/s, including slates, granites, altered basalts, and felsic granulites. With the exception of marble and anorthosite, which are minor components in the crust based on exposed blocks of lower crust and xenoliths, most rocks with velocities of 6.5–7.0 km/s are mafic in composition and include amphibolites and mafic granulites without garnet (Holbrook et al., 1992; Christensen & Mooney, 1995). Rocks with average velocities of 7.0–7.5 km/s include gabbro, hornblendite, and mafic garnet granulite, and velocities above 7.5 km/s are limited to nonserpentinized ultramafic rocks and eclogite (a very high-pressure mafic rock). It is important to note also that the order of increasing velocity in Figure 2.14 is not a simple function of increasing metamorphic grade. For instance, low-, medium-, and high-grade metamorphic rocks all fall in the range of 6.0 to 7.5 km/s.

Although rock types in the upper continental crust are reasonably well known, the distribution of rock types in the lower crust still remains uncertain. Platform lower crust, although having relatively high S-wave velocities, shows similar Poisson's ratios to collisional orogens (Figure 2.15a, Table 2.1, and Table 2.2). The lower crust of continental rifts, however, shows distinctly lower velocities, a feature that would appear to reflect hotter temperatures in the lower crust. Two observations are immediately apparent from the measured rock velocities as summarized in Figures 2.14 and 2.15b: (1) the velocity distribution in the lower crust indicates compositional heterogeneity, and (2) metapelitic rocks overlap in velocity with mafic and felsic igneous and metamorphic rocks. It is also interesting that, with the exception of rifts, mean lower crustal velocities are strikingly similar to mafic rock velocities. However, because of the overlap in velocities of rocks of different compositions and origins, it is not possible to assign unique rock compositions to the lower crust from seismic velocity data alone. When coupled with xenolith data, however, the seismic velocity distributions suggest that the lower continental crust is composed largely of mafic granulites, gabbros, and amphibolites (50–65%), with up to 10% metapelite, and the remainder of intermediate to felsic granulite (Rudnick & Fountain, 1995). Based on seismic data, however, the lower crust in the Archean Kaapvaal craton in southern Africa appears to be felsic to intermediate in composition (James et al., 2003).

In common rock types, Poisson's ratio (ν) varies from about 0.2 to 0.35 and is sensitive to composition. Increasing silica content lowers ν, whereas increasing Fe and Mg increases it (Zandt & Ammon, 1995). The average value of ν in the continental crust shows a good correlation with crustal type (Figure 2.16 and Table 2.1). Precambrian shield ν values are consistently high averaging 0.29, and platforms average about 0.27. The lower ν value in platforms and Paleozoic orogens reflects the silica-rich sediment layer that adds 4–5 km of crustal thickness to the average shield (Table 2.1). In Mesozoic-Cenozoic orogens, however, ν is still lower, but more variable, reflecting some combination of lithologic and thermal differences in the young orogenic crust. The high ratios

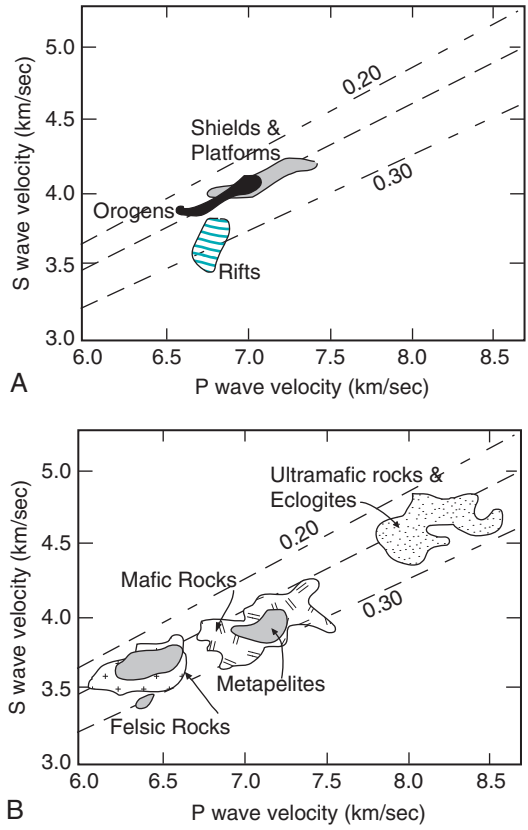

FIGURE 2.15 Compressional versus shear wave velocity diagrams showing (A) lower crust of various crustal types and (B) fields of various crustal and upper mantle rocks. Velocities normalized to 20-km depth and room temperature. Dashed lines are Poisson's ratio ($\nu = 0.5\{1 - 1/[(Vp/Vs)^2 - 1]\}$). *Modified after Rudnick & Fountain (1995).*

in continental-margin arcs may reflect and importance of mafic rocks in the root zones of these arcs, although again the variation in ν is significant.

Seismic Reflections in the Lower Continental Crust

Many explanations have been suggested for the strong seismic reflectors found in the lower continental crust (Figure 2.17) (Nelson, 1991; Mooney & Meissner, 1992). The most likely causes fall into one of three categories:

1. Layers in which fluids are concentrated,
2. Strain-banding developed from ductile deformation, and
3. Lithologic layering.

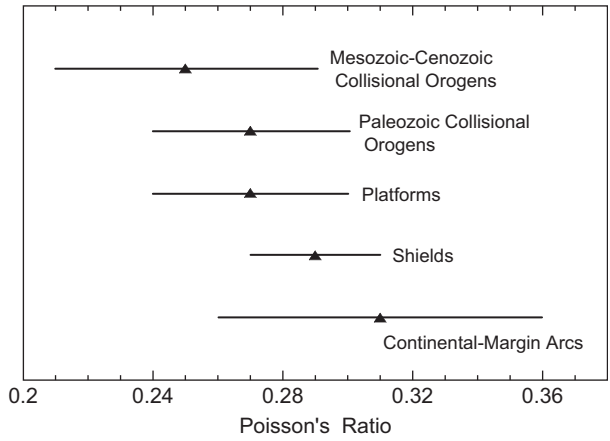

FIGURE 2.16 Mean values and one standard deviation of Poisson's ratio (ν) in various crustal types. *Data from Zandt & Ammon (1995).*

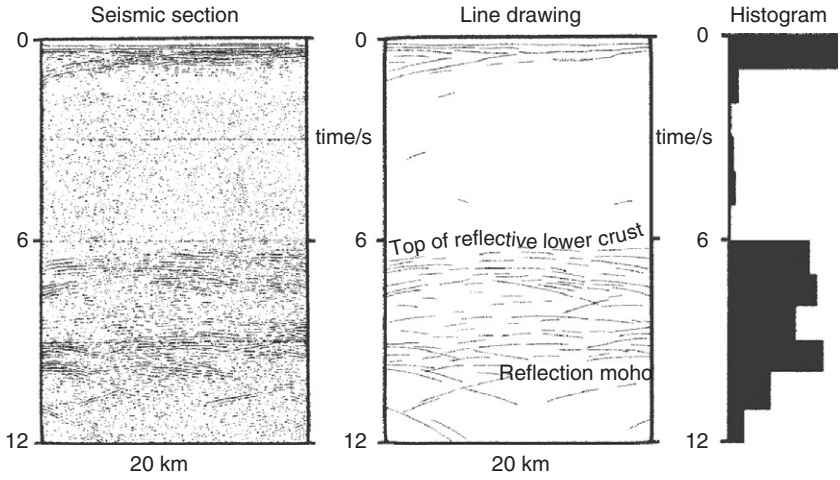

FIGURE 2.17 Seismic reflection profile in southwest England. Also shown is a line drawing of the data and a histogram of reflection depths summed over 1-sec travel-time intervals. *After Klemperer (1987).*

The jury is still out on the role of deep crustal fluids. Some investigators argue that physical conditions in the lower crust allow up to 4% of saline pore waters, and that the high electrical conductivity of the lower crust supports such a model. In this model, the seismic reflections are produced by layers with strong porosity contrasts. However, textural and mineralogic evidence from deep crustal rocks exposed at the surface and from xenoliths do not have high porosities, and thus contradict this idea.

Deformation bands hold more promise, at least for some of the lower crustal reflections, in that shear zones exposed at the surface can be traced to known seismic reflectors at depth in shallow crust (Mooney & Meissner, 1992). Some lower crustal reflection patterns in Precambrian cratons preserve structures that date from ancient collisional events, as seen, for instance, in the Trans-Hudson orogen of the Paleoproterozoic age in Canada. At least in these cases, it would appear that the reflections are caused by tectonic boundaries, or syntectonic igneous intrusions. In extended crust, like that found in rifts, ductile shearing in the lower crust may enhance metamorphic or igneous layering.

The probable cause of many lower crustal reflections is lithologic layering caused by mafic intrusions including compositional layering in these intrusions. Supporting this conclusion is the fact that some shallow reflectors in the crust that have been traced to the surface are caused by such features (Percival et al., 1989). Furthermore, a bimodal distribution of acoustic impedance in the lower crust favors layered sequences of rocks, especially interlayered mafic and felsic units (Goff et al., 1994). Also, models of reflectivity in the Ivrea zone (a fragment of mafic lower crust faulted to the surface in the Alps) show that lower crustal reflections are expected when mafic rocks are interlayered with felsic rocks (Holliger et al., 1993).

The fact that seismic reflectivity in the lower crust is widespread and occurs in crustal types with differing heat flow characteristics favors a single origin for most reflectors. From studies of exhumed lower crust and lower crustal xenoliths, it would seem that most lower crustal reflections are caused by mafic intrusions, and in some instances, the reflections have been enhanced by later ductile deformation.

Sampling of Precambrian Shields

Widespread sampling of metamorphic terrains exposed in Precambrian shields and especially in the Canadian shield has provided an extensive sampling base to estimate both the chemical and lithologic composition of the upper part of the Precambrian continental crust (Shaw et al., 1986; Condie, 1993; Rudnick & Gao, 2004). Both individual and composite samples have been analyzed. Results indicate that although the upper crust is heterogeneous, granitoids of granodiorite to tonalite composition dominate and the weighted average composition is that of granodiorite.

Use of Fine-Grained Detrital Sediments

Fine-grained detrital sediments may represent well-mixed samples of the upper continental crust, and thus provide a means of estimating upper crustal composition (Taylor & McLennan, 1985). However, to use sediments to estimate crustal composition, it is necessary to evaluate losses and gains of elements during weathering, erosion, deposition, and diagenesis. Elements,

such as rare earth elements (REE), Th, and Sc that are relatively insoluble in natural waters and have short residence times in seawater ($<10^3$ y) may be transferred almost totally into terrigenous detrital sediments. The remarkable uniformity of REE in pelites and loess compared to the great variability observed in igneous source rocks attests to the efficiency of mixing during erosion and deposition. Studies of REE and element ratios such as La/Sc, La/Yb, and Cr/Th indicate that they remain relatively unaffected by weathering and diagenesis. REE distributions are especially constant in shales and resemble REE distributions in weighted averages from Precambrian shields. With some notable exceptions (Condie, 1993), estimates of the average composition of the upper continental crust using the composition of shales are in remarkable agreement with the weighted chemical averages determined from rocks exposed in Precambrian shields.

Exhumed Crustal Blocks

Blocks of middle to lower continental crust are recognized in Precambrian shields or collisional orogens, the best known of which are the Kapuskasing uplift in southern Canada (Percival et al., 1992; Percival & West, 1994) and the Ivrea Complex in Italy (Sinigoi et al., 1994). Four different mechanisms have been suggested to bring these deep crustal sections to the surface: (1) large thrust sheets associated with continent–continent collisions, (2) transpressional faulting, (3) broad tilting of a large segment of crust, and (4) asteroid impacts. Common to all deep crustal exposures are high-grade metamorphic rocks that formed at depths of 20–25 km, with a few, like the Kohistan arc in Pakistan, coming from depths as great as 40–50 km. Metamorphic temperatures recorded in the blocks are typically in the range of 700–850°C. All blocks consist chiefly of felsic components at shallow structural levels and mixed mafic, intermediate, and felsic components at deeper levels. Commonly, lithologic and metamorphic features in uplifted blocks are persistent over lateral distances of more than 1000 km, as evidenced, for instance, by three deep crustal exposures in the Superior Province in southern Canada (Percival et al., 1992).

Examples of five sections of middle to lower continental crust are given in Figure 2.18. Each section is a schematic diagram illustrating the relative abundances of major rock types, and the base of each section is a major thrust fault. The greatest depths exposed in each section are on the order of 25–35 km. Each column has a lower granulite zone with mafic granulites dominating in three sections and felsic granulites in the other two. The sections show considerable compositional variation at all metamorphic grades, attesting to the heterogeneity of the continental crust at all depths. Mafic and ultramafic bodies and anorthosites occur at deep levels in some sections and probably represent layered igneous sheets intruded into the lower crust (Figures 2.18 and 2.19). Volcanic and sedimentary rocks are also buried to great depths in some sections.

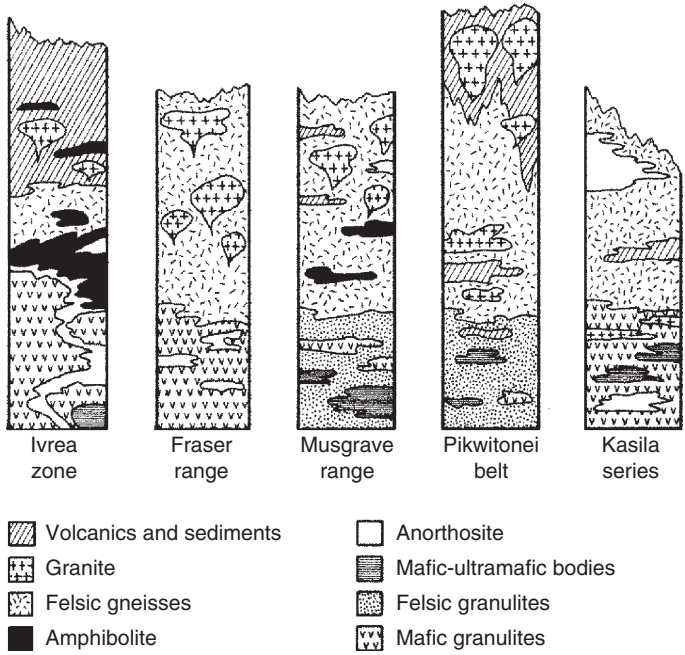

FIGURE 2.18 Schematic cross sections of continental crust based on exhumed sections of deep crustal rocks. *Modified after Fountain & Salisbury (1981).*

Intermediate and upper crustal levels are characterized by large volumes of granitoids.

More than anything else, the crustal sections indicate considerable variation in lithologic and chemical composition both laterally and vertically in the continental crust. The only large-scale progressive change in the crustal sections is an increase in metamorphic grade with depth. Although there is no evidence for a Conrad discontinuity in the sections, rapid changes in lithology may be responsible for seismic discontinuities of a more local extent. Again, it should be emphasized that many uplifted blocks probably do not sample the lower crust, but only the middle crust (~25 km). Today these blocks are underlain by 35–40 km of crust, probably composed in large part of mafic granulites. The crust in these areas may have thickened during continental collision (to 60–70 km), thus burying upper crustal rocks to granulite grade (35–40 km). Uplift and erosion of this crust brought felsic granulites to the surface with a possible mafic granulite root still intact. Thus, the differences between the generally felsic to intermediate compositions of uplifted crustal blocks and the mafic compositions of lower crustal xenolith suites (see below), may be due in part to different levels of sampling in the crust.

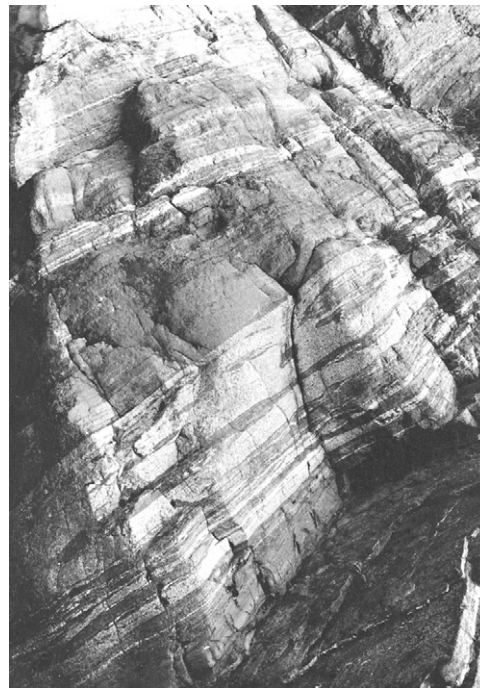

FIGURE 2.19 Layered mafic granulites from the Ivrea zone in the Alps. Similar rocks may comprise large volumes of the lower continental crust. *Courtesy of K. R. Mehnert.*

Crustal Xenoliths

Crustal xenoliths are fragments of the crust brought to the surface by volcanic eruptions. If one can determine the depth from which xenoliths come by thermobarometry, and estimate the relative abundances of various xenolith populations in the crust, it should be possible to reconstruct a crustal cross section (Kay & Kay, 1981). Although metamorphic xenoliths can be broadly ordered in terms of their crustal depths, metamorphic mineral assemblages in many lower crustal xenoliths are not definitive in determining precise depths (Rudnick, 1992; Rudnick & Gao, 2004). Even more difficult is the problem of estimating the relative abundances of xenolith types in the crust. Some lithologies may be oversampled and others undersampled by ascending volcanic magmas. Hence, it is generally not possible to come up with a unique crustal section from xenolith data alone.

Xenolith-bearing volcanics and kimberlites occur in many different tectonic settings, giving a wide lateral sampling of the continents. Lower crustal xenoliths from arc volcanics are chiefly mafic in composition and xenoliths of sediments are rare to absent. These results suggest that the root zones of

modern arcs are composed chiefly of mafic rocks (Condie, 1999). Xenoliths from volcanics erupted on continental crust are compositionally diverse and have complex thermal and deformational histories (Rudnick, 1992). Metasedimentary xenoliths, however, are minor compared to metaigneous xenoliths. In general, xenoliths of mafic granulite are more abundant than felsic granulite, suggesting that a mafic lower crust is also important in cratons (Rudnick & Taylor, 1987). Most of these xenoliths appear to be basaltic melts and their cumulates that were intruded into or underplated beneath the crust. Granulite-grade xenoliths reflect equilibration depths in the crust of more than 20 km and some more than 40 km. A smaller number of metasedimentary and gneissic xenoliths recording similar depths in many xenolith suites seem to require interlayering of felsic and mafic rocks in the lower crust. Where isotopic ages of xenoliths can be estimated, they range from the age of the host crust to either younger or older. For instance, mafic lower crustal xenoliths from the Four Corners volcanic field in the Colorado Plateau appear to be about 1.7 Ga, the same age as the Precambrian basement in this area (Wendlandt et al., 1993).

An Estimate of Crustal Composition

Continental Crust

The average chemical composition of the upper continental crust is reasonably well known from widespread sampling of Precambrian shields, geochemical studies of shales, and exposed crustal sections (Taylor & McLennan, 1985; Condie, 1993; Rudnick & Gao, 2004). An average composition is similar to granodiorite (Table 2.5), although differences exist that are related to the age of the crust, as discussed in Chapter 7. The composition of lower continental crust is much less well constrained. Uplifted crustal blocks, xenolith populations, and seismic velocity and Poisson's ratio distributions suggest that a large part of the lower crust is mafic in overall composition. If the upper continental crust is felsic in composition and the lower crust is mafic as most data suggest, how do these two layers form and how do they persist over geologic time? This intriguing question will be returned to in Chapter 7.

The estimate of total continental crust composition in Table 2.5 is a mixture of upper, middle, and lower crustal averages in equal amounts. The composition is similar to other published total crustal compositions, indicating an overall intermediate composition (Taylor & McLennan, 1985; Wedepohl, 1995). **Incompatible elements**, which are elements that are strongly partitioned into the liquid phase upon melting, are known to be concentrated chiefly in the continental crust. During melting in the mantle, these elements will be enriched in the magmas, and thus transferred upward into the crust as magmas rise. Relative to primitive mantle composition, 35–65% of the most incompatible elements (such as Rb, Th, U, K, and Ba) are contained in the

TABLE 2.5 Average Chemical Composition of Continental and Oceanic Crust

	Continental crust				Oceanic crust
	Upper	*Middle*	*Lower*	*Total*	
SiO_2	66.3	63.5	53.4	60.6	50.5
TiO_2	0.64	0.69	0.82	0.72	1.6
Al_2O_3	15.4	15.0	16.9	15.9	15.3
FeOT	5.04	6.02	8.57	6.71	10.4
MgO	2.48	3.59	7.24	4.66	7.58
MnO	0.10	0.10	0.10	0.10	0.19
CaO	3.59	5.25	9.59	6.41	11.3
Na_2O	3.27	3.39	2.65	3.07	2.68
K_2O	2.80	2.30	0.61	1.81	0.11
P_2O_5	0.15	0.15	0.10	0.13	0.2
Rb	82	65	11	49	1
Sr	320	282	348	320	113
Ba	628	532	259	456	7
Th	10.5	6.5	1.2	5.6	0.1
Pb	17	15.2	4.0	11	0.3
U	2.7	1.3	0.2	1.3	0.07
Zr	193	149	68	132	74
Hf	5.3	4.4	1.9	3.7	2.1
Nb	12	10	5	8.0	2.3
Ta	0.90	0.60	0.60	0.70	0.13
Y	21	20	16	19	28
La	31	24	8	20	2.5
Ce	63	53	20	43	7.5
Sm	4.7	4.6	2.8	3.9	2.6
Eu	1.0	1.4	1.1	1.1	1.0
Yb	2.0	2.2	1.5	1.9	3.1

Continued

TABLE 2.5 Average Chemical Composition of Continental and Oceanic Crust—Cont'd

	Continental crust				Oceanic crust
	Upper	*Middle*	*Lower*	*Total*	
V	97	107	196	138	275
Cr	92	76	215	135	250
Co	17.3	22	38	26.6	47
Ni	47	33.5	88	59	150

Major elements in weight percent of the oxide and trace elements in ppm.
Sources: Continental crust from Rudnick & Gao (2004, Table 11); oceanic crust (NMORB) from Sun & McDonough (1989) and miscellaneous sources.

continents, whereas continents contain <10% of the least incompatible elements (such as Y, Yb, and Ti).

Oceanic Crust

Because fragments of oceanic crust are preserved on the continents as ophiolites, we have direct access to sampling for chemical analysis. The chief problem with equating the composition of ophiolites to average oceanic crust, however, is that some or most ophiolites appear to have formed in back-arc or forearc basins and, in varying degrees, have geochemical signatures of arc systems. Other sources of data for estimating the composition of oceanic crust are dredge samples from the ocean floor and drill cores retrieved from the Ocean Drilling Program that have penetrated the basement layer. Studies of ophiolites and P-wave velocity measurements are consistent with the basement and oceanic layers composed largely of mafic rocks metamorphosed to the greenschist or amphibolite facies. The sediment layer is composed of pelagic sediments of variable composition and extent, and contributes <5% to the bulk composition of the oceanic crust.

An estimate of the composition of oceanic crust is also given in Table 2.5. It is based on the average composition of normal ocean ridge basalts, excluding data from back-arc basins, and pelagic sediments are ignored in the estimate. Although ophiolites contain minor amounts of ultramafic rock and felsic rock, they are much less variable in lithologic and chemical composition than crustal sections of continental crust, suggesting that the oceanic crust is rather uniform in composition. Because of the relatively small volume of oceanic crust compared to continental crust (Table 2.1) and because oceanic basalts come from a mantle source that is depleted in incompatible elements (Chapt. 4), the oceanic crust contains very little of Earth's inventory of these elements.

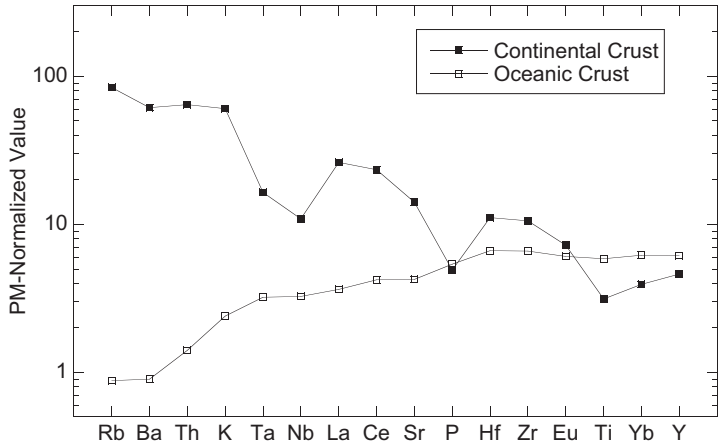

FIGURE 2.20 Primitive mantle normalized incompatible element distributions in continental and oceanic crust. *Data from Table 2.5; primitive mantle values from Sun and McDonough (1989).*

Complementary Compositions of Continental and Oceanic Crust

The average compositions of the continental and oceanic crusts relative to the primitive mantle composition show surprisingly complementary patterns (Figure 2.20). In continental crust the maximum concentrations, which reach values of 50–100 times primitive mantle values, are for the most incompatible elements K, Rb, Th, and Ba. These same elements reach less than 3 times the primitive mantle values in oceanic crust. The patterns cross at phosphorus (P), and the least incompatible elements (Ti, Yb, and Y) are more enriched in oceanic than in continental crust. The relative depletions in Ta-Nb, P, and Ti are important features of the continental crust and will be discussed more fully in Chapter 7. The complementary crustal element patterns can be explained if most of the continental crust is extracted from the upper 800 km of mantle, leaving an upper mantle depleted in very incompatible elements. The oceanic crust is then continuously produced from this depleted upper mantle throughout geologic time (Hofmann, 1988).

CRUSTAL PROVINCES AND TERRANES

Stockwell (1965) suggested that the Canadian Shield can be subdivided into structural provinces based on differences in structural trends and style of folding. Structural trends are defined by foliation, fold axes, bedding, and sometimes by geophysical anomalies. Boundaries between the provinces are drawn where one trend crosses another, along either unconformities or structural-metamorphic breaks. Large numbers of isotopic dates from the Canadian Shield indicate that structural provinces are broadly coincident with age provinces.

Similar relationships have been described on other continents and lead to the concept of a crustal province as discussed below.

Terranes are fault-bounded crustal blocks that have distinct lithologic and stratigraphic successions and that have geologic histories different from those of neighboring terranes (Schermer et al., 1984). Terranes have collided with continental crust or other terranes, either along transcurrent faults or at subduction zones, and eventually are sutured to continents (Maruyama, 1997; von Raumer et al., 2003). Many terranes contain faunal populations and paleomagnetic evidence indicating that they have been displaced great distances from their sources prior to continental collision. For instance, Wrangellia, an oceanic plateau that collided with western North America in the Late Cretaceous, traveled many thousands of kilometers from what is now the South Pacific. Results suggest that as much as 30% of North America formed by terrane accretion in the last 300 Ma and that terrane accretion has been an important process in the growth of continents.

Terranes form in a variety of tectonic settings including island arcs, oceanic plateaus, volcanic islands, and microcontinents (von Raumer et al., 2003). Numerous potential terranes exist in the oceans today and are particularly abundant in the Pacific Basin (Figure 2.21). Continental crust may be fragmented

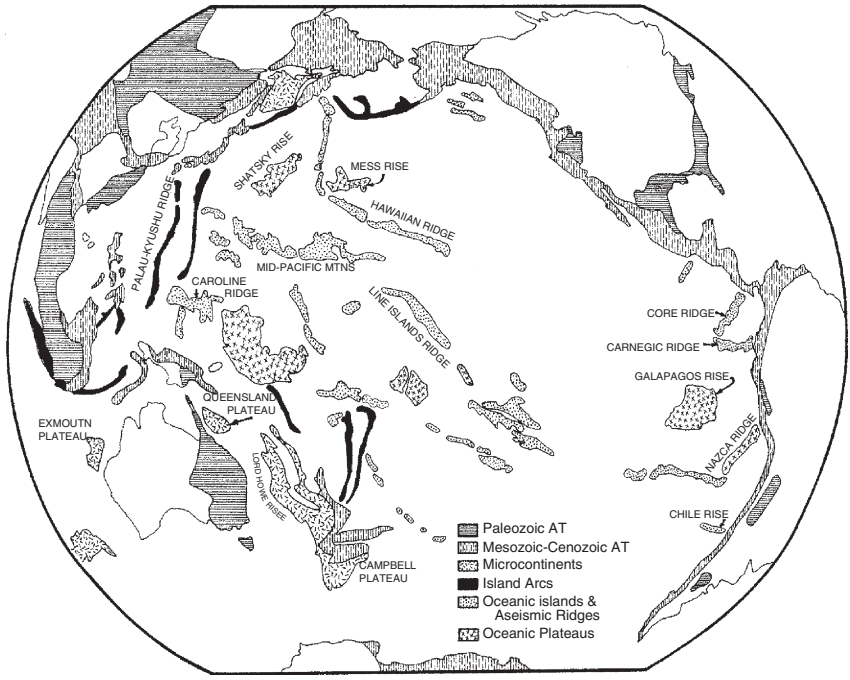

FIGURE 2.21 Map showing the distribution of accreted (AT) and potential terranes in the Pacific region. *Modified after Schermer et al. (1984).*

and dispersed by rifting or strike-slip faulting. In western North America, dispersion is occurring along transform faults such as the San Andreas and Fairweather faults, and in New Zealand movement along the Alpine transform fault is fragmenting the Campbell Plateau from the Lord Howe Rise (see Figure 1.3). Baja California and California west of the San Andreas fault were rifted from North America about 4 Ma, and today this region is a potential terrane moving northward, perhaps on a collision course with Alaska. Terranes may continue to fragment and disperse after collision with continents, as did Wrangellia, which is now distributed in pieces from Oregon to Alaska. The 1.9-Ga Trans-Hudson orogen in Canada and the 1.75–1.65 Yavapai orogen in the southwestern United States are examples of Proterozoic orogens composed of terranes (Karlstrom et al., 2001), and the Alps, Himalayas, and American Cordillera are Phanerozoic examples of orogens composed largely of terranes (Figure 2.21). Most crustal provinces and orogens are composed of terranes; in turn, cratons are composed of exhumed orogens. In fact, one might consider terranes to be the basic building blocks of continents, and terrane collision as a major means by which continents grow in size (Patchett & Gehrels, 1998).

A **crustal province** is an orogen, active or exhumed, composed of terranes, and it records the same isotopic ages and exhibits a uniform post amalgamation deformational history. Structural trends within provinces range from linear to exceedingly complex swirling patterns, reflecting polyphase deformation superimposed on differing terrane structural patterns. Exhumed crustal provinces that have undergone numerous episodes of deformation and metamorphism are old orogens, sometimes referred to as mobile belts. Isotopic dating using multiple isotopic systems is critical to defining and unraveling the complex, polydeformational histories of crustal provinces.

The identification of crustal provinces is not always obvious. Most crustal provinces contain rocks of a wide range in age and record more than one period of deformation, metamorphism, and plutonism. For instance, the Trans-Hudson orogen in North America (Figure 2.22) includes rocks ranging from about 3.0 to 1.7 Ga and records several periods of complex deformation and regional metamorphism. Likewise, the Grenville province records a polydeformational history with rocks ranging in age from 2.7 to 1.0 Ga. Some parts of crustal provinces are new mantle-derived crust, known as **juvenile crust**, whereas other parts represent reworked older crust. **Reworking**, also known as **overprinting** or **reactivation**, describes crust that has been deformed, metamorphosed, and partially melted more than once. It is possible, in some instances, to map reworked crust within crustal provinces, and these are sometimes referred to as relict-age subprovinces. There is increasing evidence that crustal reworking results from continental collisions, and large segments of Phanerozoic crust appear to have been reactivated by such collisions. For instance, much of central Asia at least as far north as the Baikal rift was affected by the India-Tibet collision beginning about 65 Ma. Widespread faulting and

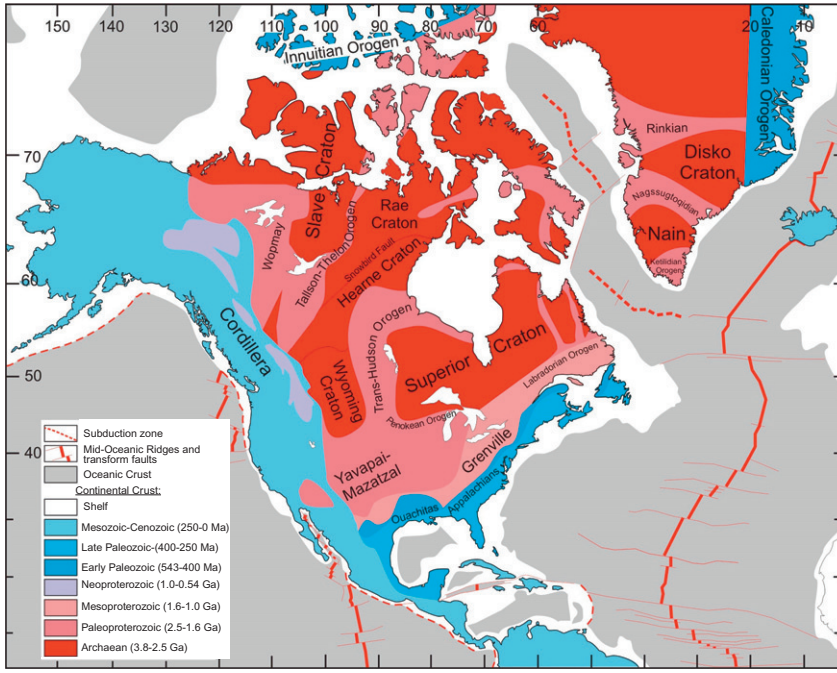

FIGURE 2.22 Distribution of North American crustal provinces. *Courtesy of Walter Mooney.*

magmatism at present crustal levels suggest that deeper crustal levels may be extensively reactivated. In Phanerozoic collisional orogens where deeper crustal levels are exposed, such as the Appalachian and Variscan orogens, there is isotopic evidence for widespread reactivation.

One of the most important approaches to extract multiple ages from crustal provinces is dating single zircons by the U-Pb method using an ion probe (such as SHRIMP, sensitive high-resolution ion microprobe) or a laser microprobe with an inductively coupled plasma mass spectrometer (LA-ICP-MS). Figure 2.23 shows an example of dating a felsic gneiss from southern Africa with SHRIMP. The scatter of data on the Concordia diagram shows complex Pb loss from the zircons, and even from within a single zircon. Note, for instance, the complex Pb loss from zircon grain 4. The most concordant domains can be fitted to a discordia line intersecting Concordia at 3505 $\pm$ 24 Ma, which is interpreted as the igneous crystallization age of this rock (Kroner et al., 1989). Three spots analyzed on the clear prismatic zircon grain 6 have a near concordant age of 3453 $\pm$ 8 Ma. This records a period of intense deformation and high-grade metamorphism in which new metamorphic zircons formed in the gneiss. Grain 20 has a slightly discordant age of 3166 $\pm$ 4 Ma and comes from a later granitic vein that crosses the rock. Other discordant data points in Figure 2.23

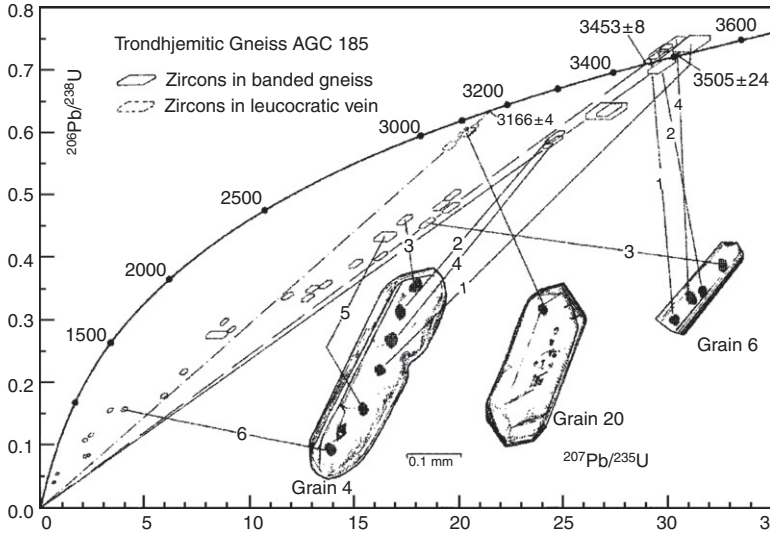

FIGURE 2.23 U-Pb Concordia diagram showing ion probe analyses of zircons from a trondhjemitic gneiss in NE Swaziland, southern Africa. Concordia is the bold solid line defined by concordant $^{206}Pb/^{238}U$ and $^{207}Pb/^{235}U$ ages. *From Kroner et al. (1989).*

cannot be fit to regression lines and reflect Pb loss at various times in the past, perhaps some as young as 3 Ga. When combined with other single zircon ages from surrounding gneisses, major orogenic-plutonic events are recorded at 3580, 3500, 3450, 3200, and 3000 Ma in this very small geographic area of Swaziland in southern Africa.

CRUSTAL PROVINCE AND TERRANE BOUNDARIES

Contacts between crustal provinces or between terranes are generally major shear zones, only some of which are the actual sutures between formerly colliding crustal blocks. Boundaries between terranes or provinces may be parallel or at steep angles to the structural trends within juxtaposed blocks. Some boundary shear zones exhibit transcurrent motions and others pass from flat-lying to steep structures and may have thrust or transcurrent offsets. Magnetic and gravity anomalies also generally occur at provincial boundaries, reflecting juxtaposition of rocks of differing densities, magnetic susceptibilities, and crustal thicknesses. The Grenville Front, which marks the boundary between the Proterozoic Grenville and Archean Superior Provinces in eastern Canada, is an example of a well-known crustal province boundary (Figure 2.24). Locally, the Grenville Front, which formed about 1 Ga, ranges in width from a few to nearly 100 km and includes a large amount of reworked Archean crust (Culotta et al., 1990). It also produces a major negative gravity anomaly. Seismic

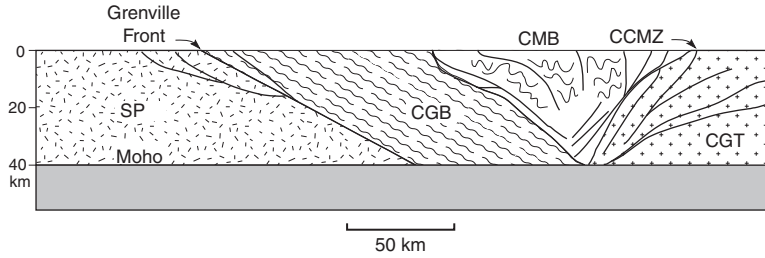

FIGURE 2.24 Diagrammatic cross section of the 1-Ga Grenville Province in eastern Canada. SP, Archean Superior Province; CGB, Central gneiss belt; CMB, Central metasedimentary belt; CGT, Central granulite terrane; CCMZ, Carthage-Colton shear zone.

reflection data show that the Grenville Front dips to the east and probably extends to the Moho. K-Ar biotite ages are reset at rather low temperatures (200°C) and gradually decrease from 2.7 Ga to about 1.0 Ga in an eastern direction across the Grenville Front. This front, however, is not a suture, but a major foreland thrust associated with the collision of crustal provinces. The actual suture has not been identified, but may be the Carthage-Colton shear zone some 250 km east of the Grenville Front (Figure 2.24).

Shear zones between crustal provinces range up to tens of kilometers in width, as illustrated by the Cheyenne Belt in the Medicine Bow Mountains in southeastern Wyoming (Figure 2.25). The Cheyenne Belt is a near vertical shear zone separating Archean gneisses of the Wyoming Province from Paleoproterozoic juvenile crust of the Yavapai Province on the south (Karlstrom & Houston, 1984). The timing of collision along this boundary is constrained by zircon ages from pre- and post-tectonic plutons at about

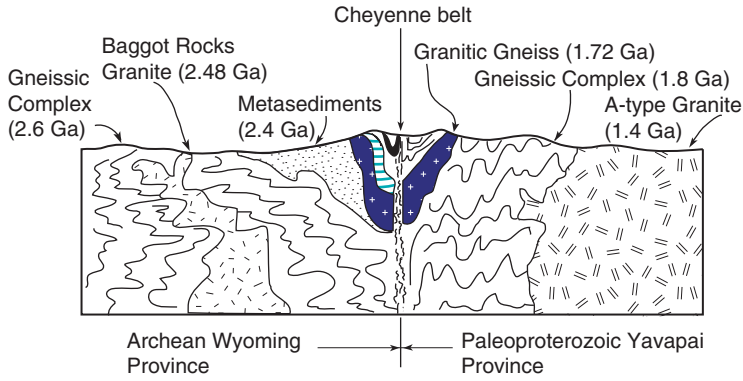

FIGURE 2.25 Schematic cross section of the Cheyenne Belt, a major shear zone separating the Archean Wyoming Province and the Paleoproterozoic Yavapai Province in southeastern Wyoming.

1.75 Ga (Condie, 1992). This boundary is complicated by the fact that deformed metasedimentary rocks (about 2.4 Ga) rest unconformably on the Archean gneisses and are also cut by the shear zone. The shear zone, which is up to several kilometers wide, is composed chiefly of mylonitized quartzofeldspathic gneisses.

THE UNITED PLATES OF AMERICA

North America provides an example of the birth and growth of a continent through geologic time. Field, geophysical, and Nd and U-Pb isotopic data from exposed Precambrian basement and from borehole basement samples indicate that North America is an amalgamation of plates, referred to by Paul Hoffman as the "United Plates of America" (Nelson & DePaolo, 1985; Patchett & Arndt, 1986; Hoffman, 1988). The Archean crust includes at least six separate provinces joined by Paleoproterozoic orogenic belts (Figure 2.22). The assembly of constituent Archean blocks took only about 100 My between 1900 and 1800 Ma. Apparent from the map is the large amount of crust formed in the Archean, comprising about 50% of the continent. Approximately 25% of the continent appears to have formed in the Paleoproterozoic, 10% in the Mesoproterozoic and Neoproterozoic, and about 15% in the Phanerozoic.

The systematic asymmetry of stratigraphic sections, structure, metamorphism, and igneous rocks in North American orogens is consistent with an origin by subduction and collision. Such asymmetry is particularly well displayed along the Trans-Hudson, Labradorian, and Penokean orogenic belts (Figure 2.22). In these belts, zones of foreland deformation are dominated by thrusts and recumbent folds, whereas hinterlands typically show transcurrent faults. Both features are characteristic of subduction zones. Some Proterozoic orogens have large accretionary prisms, whereas others do not. For instance, the Rae and Hearne cratons involve only suturing of Archean crust, whereas the Trans-Hudson Province is a collisional orogen up the 500 km wide. The Penokean, Yavapai, and Mazatzal Provinces are accretionary orogens added to North America at 1.9, 1.75, and 1.65 Ga, respectively, and the Grenville Province was added by one or more collisions at 1.2–1.0 Ga. The Cordilleran and Appalachian Provinces represent collages of accretionary terranes sutured along transform faults or large thrusts during the Phanerozoic.

FURTHER READING

Beardsmore, G. R., & Cull, J. P. (2001). *Crustal Heat Flow* (320 pp). Cambridge, UK: Cambridge University Press.

Brown, M., & Rushmer, T. (Eds.), (2006). *Evolution and Differentiation of the Continental Crust* (562 pp). Cambridge, UK: Cambridge University Press.

Juteau, T., & Maury, R. (1999). *The Oceanic Crust, from Accretion to Mantle Recycling* (390 pp). New York: Springer-Verlag.

Kleine, E. (2003). The Ocean Crust. In R. L. Rudnick (Ed.), *The Crust, Treatise on Geochemistry* (Vol. 3). Amsterdam: Elsevier.

Ries, A. C., Butler, R. W. H., & Graham, R. H. (2007). *Deformation of the Continental Crust: The Legacy of Mike Coward* (595 pp). Special Publication 272. Geological Society of London.

Rudnick, R. L., & Fountain, D. M. (1995). Nature and composition of the continental crust: A lower crustal perspective. *Reviews of Geophysics*, *33*, 267–309.

Rudnick, R. L., & Gao, S. (2004). Composition of continental crust. In *Treatise on Geochemistry* (Vol. 3.01, pp. 1–64). Amsterdam: Elsevier.

Taylor, S. R., & McLennan, S. M. (1985). *The Continental Crust: Its Composition and Evolution* (312 pp). Oxford: Blackwell Scientific Publishers.

Chapter 3

Tectonic Settings

INTRODUCTION

Rock assemblages that form in modern plate tectonic settings are known as **petrotectonic assemblages**. Such assemblages include both supracrustal rocks and intrusive igneous rocks. **Supracrustal rocks** are rocks that formed at or near the Earth's surface (sediments and volcanics) but lost many of their primary features during metamorphism and deformation. From studying modern plate settings, it is possible to learn more about what to look for in ancient rocks to be able to identify, or at least constrain, the tectonic setting in which they formed. From the results, it also may be possible to evaluate the intriguing question of just how far back in time plate tectonics has been operating.

Although we can sample and study sediments forming in modern plate settings, it is more difficult to study young plutonic and metamorphic rocks and deep-seated deformation. One approach is to examine deep canyons in mountain ranges where relatively young (<50 Ma) deep-seated rocks are exposed, to which a tectonic setting can be assigned with some degree of confidence. Seismic reflection profiles provide a means to study deep-seated deformation. These studies have been particularly useful in modern arc systems. As we saw in the previous chapter, it is also possible to study recently elevated blocks that expose lower crustal rocks as well as xenolith populations brought up in young volcanoes. Finally, it is possible to simulate P-T conditions that exist in modern plates in laboratory and computer models, from which constraints can be placed on geologic processes occurring at depth.

In this chapter we examine some of the processes that leave tectonic imprints in rocks and also review modern processes that are responsible for these imprints. It is only when results from a variety of studies converge on the same interpretation that ancient tectonic settings can be identified with confidence. Even then, one must use care in that one or more tectonic settings that no longer exist may have left imprints in the geologic record similar to those of modern plate settings. This is especially true for the Archean.

OCEAN RIDGES

Ocean Ridge Basalts

Experimental results indicate that **midocean ridge basalts (MORBs)** are produced by 10–20% partial melting of the upper mantle at depths of 50–85 km (Elthon & Scarfe, 1984; Kushiro, 2001). Melting at these depths produces olivine tholeiite magma. Seismic and geochemical results show that this magma collects in shallow chambers (<35 km) (Forsyth, 1996), where it undergoes fractional crystallization to produce tholeiites and minor amounts of more evolved liquids including minor felsic components. A residue of olivine and pyroxenes is left behind in the mantle and may be represented by the sheared harzburgites preserved in some ophiolites.

Depletion in **large ion lithophile (LIL) elements** (K, Rb, Ba, Th, U, etc.) in **NMORBs** (normal MORBs) indicates a mantle source that has been depleted in these elements by earlier magmatic events. Low $^{87}Sr/^{86}Sr$ and $^{206}Pb/^{204}Pb$ and high $^{143}Nd/^{144}Nd$ isotopic ratios also demand an NMORB source that is depleted relative to chondrites. Incompatible element contents and isotopic ratios vary in MORBs along ocean ridges and from ocean to ocean as illustrated by the distribution of Nb and Zr in modern MORBs from the North Atlantic Basin (Figure 3.1). Although some of this variation can reflect differences in

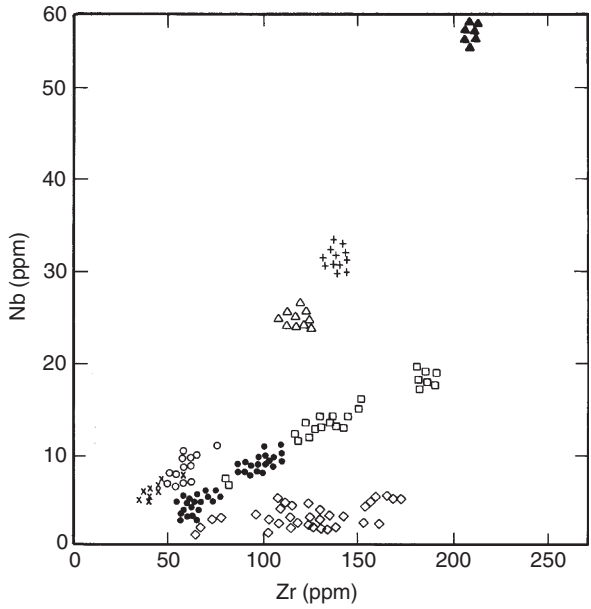

FIGURE 3.1 Zr and Nb distribution in ocean ridge basalts from the North Atlantic. Each symbol is for a different geographic location along the Mid-Atlantic Ridge. *Data from Wood et al. (1979).*

degree of melting of the source, fractional crystallization, or magma mixing, the large differences between some sites require variation in the composition of the mantle source. This subject is further discussed in Chapter 4.

Ophiolites

General Features

Ophiolites are tectonically emplaced successions of mafic and ultramafic rocks that are considered to represent fragments of oceanic or back-arc basin crust (Coleman, 1977; Moores, 1982; Dilek & Robinson, 2003). An ideal ophiolite includes from bottom to top the following units (Figure 3.2): (1) ultramafic tectonite (mostly comprising harzburgites), (2) layered cumulate gabbros and ultramafic rocks, (3) noncumulate gabbros, diorites and plagiogranites, (4) sheeted diabase dykes, and (5) pillowed basalts. Overlying this succession in many ophiolites are abyssal or/and pelagic sediments or arc-related volcaniclastic sediments. Due to faulting or other causes, the idealized ophiolite succession is rarely found in the geologic record. Instead, one or more of the ophiolite units are missing or they have been dismembered by faulting and occur as blocks in a tectonic melange.

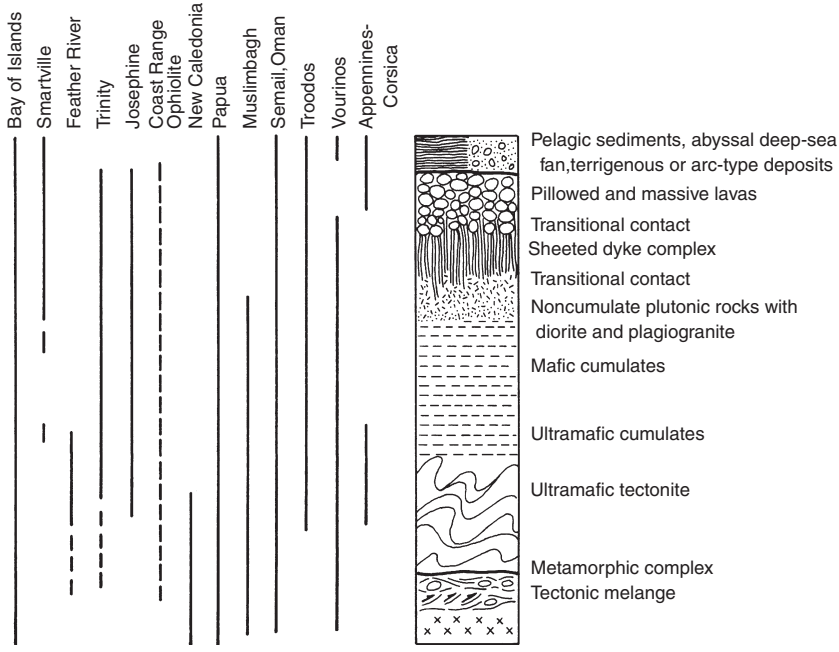

FIGURE 3.2 An idealized ophiolite succession compared with various exposed ophiolites. *Modified after Moores (1982).*

Some ophiolites are in fault contact with underlying shallow marine sediments, while others occur as tectonic slivers in accretionary prisms with graywackes and other arc-related rocks. These ophiolites appear to be emplaced along passive and active continental margins, respectively. The basal ophiolite melange (Figure 3.2) consists of a chaotic mixture of diverse rocks in a highly sheared matrix. Clast lithologies include ophiolite-derived rocks, pelagic and abyssal sediments, graywackes, and various metamorphic and volcanic rocks. Matrices are commonly sheared serpentinite. Ophiolite melanges are of tectonic origin formed during ophiolite emplacement.

Sheared and serpentinized ultramafic rock is an important component in many ophiolites. These tectonites are composed chiefly of harzburgite (ultramafic rock composed of orthopyroxene and olivine) with pronounced foliation and generally less deformed dunite (an extremely depleted ultramafic rock composed mostly of olivine) pods. Lenses of dunite and chromite also occur within the harzburgites. Overlying the tectonites are cumulate ultramafic and gabbroic rocks that formed by fractional crystallization. These rocks have cumulus textures and well-developed compositional banding. Plagiogranite, a minor component in some ophiolites, is tonalite composed of quartz and sodic plagioclase with minor mafic silicates. These rocks typically have granophyric intergrowths and may be intrusive into layered gabbros (Coleman, 1977).

Above the cumulate unit in an idealized ophiolite is a **sheeted dyke complex** (Baragar et al., 1990) (Figure 3.2). Dykes may crosscut or be gradational with cumulate rocks. Although dominantly diabase, dykes range from diorite to pyroxenite in composition, and dyke thickness is variable, commonly from 1 to 3 m. One-way chilled margins are common in sheeted dykes, a feature generally interpreted to reflect vertical intrusion in an oceanic axial rift zone, where one dyke is intruded in the center of another as the lithosphere spreads. The transition from sheeted dykes into pillow basalts generally occurs over an interval of 50–100 m, where screens of basalt between dykes become more abundant. The uppermost unit of ophiolites is ocean ridge basalt occurring as pillowed flows or hyaloclastic breccias. The thickness of this unit varies from a few meters to 2 km and pillows form a honeycomb network with individual pillows ranging up to 1 m across. A few dykes cut the pillowed basalt unit.

Many ophiolites are overlain by sediments reflecting pelagic, abyssal, or arc depositional environments. Pelagic sediments include radiolarian cherts, red fossiliferous limestones, metalliferous sediments, and abyssal sediments. Abyssal sediments are chiefly pelites and siltstones that were deposited on abyssal plains and often show evidence of both volcanic and continental provenance. Modern abyssal plains occur adjacent to passive continental margins, and hence have significant input of sediment from continental shelves. Graywackes and volcaniclastic sediments of arc provenance overlie some ophiolites.

Tectonic Setting and Emplacement of Ophiolites

Ophiolites are known from three tectonic settings: ocean ridges, back-arc and forearc basins, and in some instances, like the Metchosin Complex in British Columbia, immature island arcs (Coleman, 1977; Massey, 1986; Takashima et al., 2002). Incompatible element distributions in many ophiolitic basalts, for example the Semail ophiolite in Oman and the Troodos Complex in Cyprus, show a **subduction geochemical component** (relative depletion in Ta and Nb; Figure 3.3) suggesting they are fragments of arc-related oceanic crust (Moores et al., 2000). Relatively few ophiolites have basalts showing NMORB element distributions.

Ophiolites are emplaced in arcs or collisional orogens by three major mechanisms (Dewey & Kidd, 1977; Cawood & Suhr, 1992) (Figure 3.4): (1) **obduction** or thrusting of oceanic lithosphere onto a passive continental margin during a continental collision; (2) splitting of the upper part of a descending slab and obduction of a thrust sheet onto a former arc; and (3) transfer of a slab of oceanic crust to an accretionary prism in an arc system. Most ophiolites were emplaced by the last mechanism.

Compared to seismic sections of oceanic or arc crust, most ophiolites are considerably thinner (chiefly <5 km compared to 7–10 km for oceanic crust and 10–15 km for arcs) (Figure 3.5). In some highly deformed ophiolites, thickness is controlled by thinning during emplacement. Many ophiolites, however, are not severely deformed and may have been thickened during emplacement (Moores, 1982). So where in the oceanic crust do most ophiolites actually come from? Perhaps ophiolites are decoupled from the mantle at the

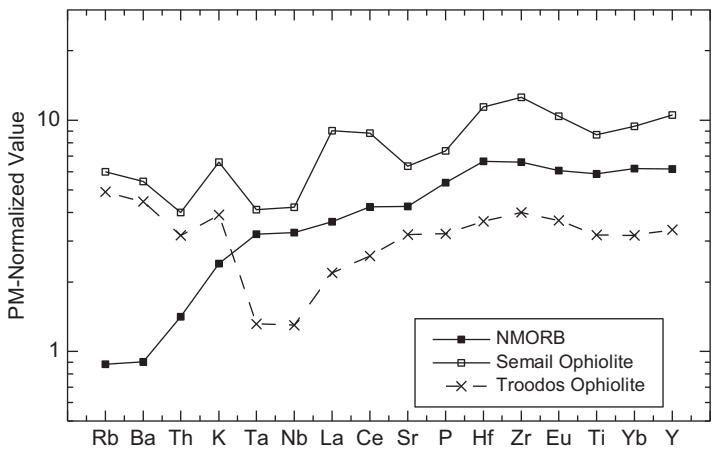

FIGURE 3.3 Primitive mantle normalized incompatible element distributions in ocean ridge basalts (NMORBs) and basalts from two ophiolites. *Primitive mantle values from Sun & McDonough (1989) and other data from Bednarz & Schmincke (1994) and Alabaster et al. (1982).*

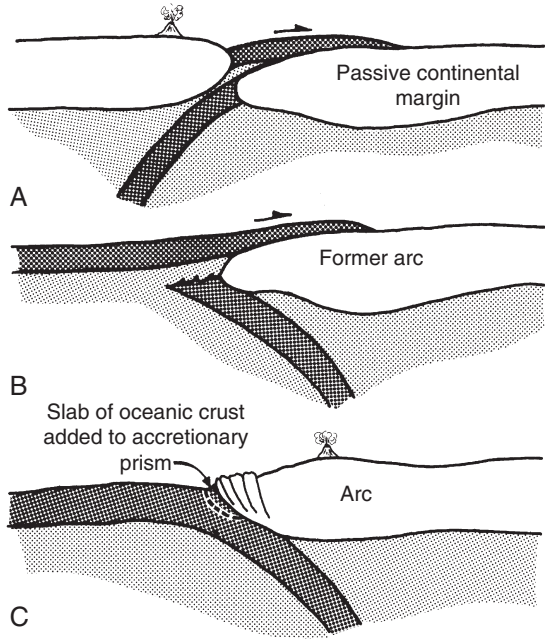

FIGURE 3.4 Three mechanisms of ophiolite emplacement: (A) obduction at a passive continental margin; (B) obduction of oceanic lithosphere; (C) transfer of a slab of oceanic lithosphere to an accretionary prism.

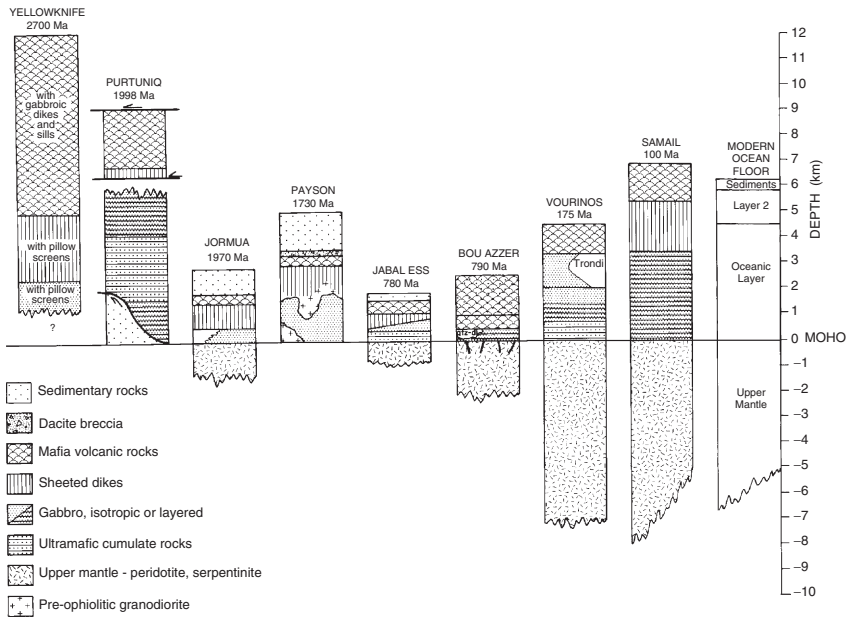

FIGURE 3.5 Simplified stratigraphic sections of ophiolites compared to average oceanic crust. *Modified after Helmstaedt & Scott (1992).*

asthenosphere–lithosphere boundary in the vicinity of spreading centers where oceanic lithosphere is thin (Karsten et al., 1996; Bortolotti et al., 2002). In a closing ocean basin, lithosphere decoupling may occur when an ocean ridge enters a subduction zone or during a continent–continent collision. If decoupling occurs only at the asthenosphere–lithosphere boundary, it may not be possible to obduct thicker segments of oceanic lithosphere (up to 150 km thick at the time of subduction), thus accounting for the absence of ophiolites much thicker than 5 km.

Formation of Ophiolites

Although details continue to be controversial, the overall mechanism by which a complete ophiolite succession forms is reasonably well understood. As pressure decreases in rising asthenosphere beneath ocean ridges, garnet lherzolite partially melts to produce basaltic magma (Figure 3.6). These magmas collect in shallow chambers (3–6 km deep) and undergo fractional crystallization. Layered ultramafic and gabbroic rocks accumulate in the magma chamber forming the cumulate section of ophiolites. The tectonized harzburgites represent residue left after melting, which is highly deformed and sheared due to lateral advective motion of the asthenosphere and/or to deformation during emplacement. Dykes are ejected from the magma chamber forming the sheeted dyke complex and many are erupted forming pillow lavas in the axial rift. Fractional crystallization in the magma chamber also gives rise locally to diorites and plagiogranites, which are intruded at the top of the layered cumulate series.

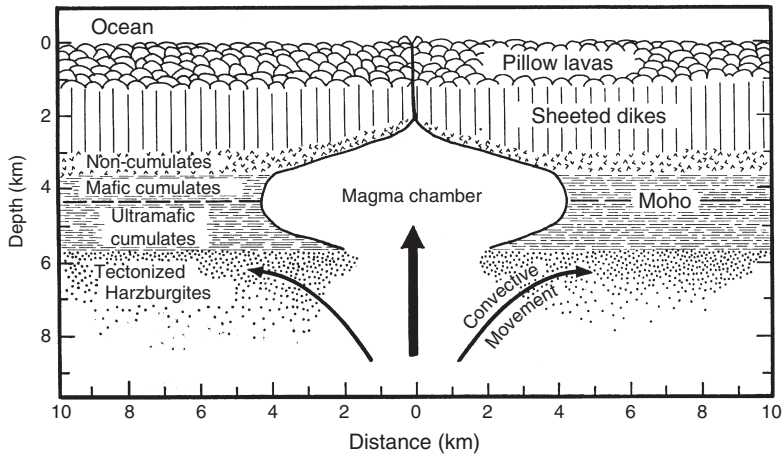

FIGURE 3.6 Schematic cross section of oceanic crust near an ocean ridge showing possible relationships to ophiolite successions.

Precambrian Ophiolites

Ophiolites and associated deep-sea sediments are first recognized in the geologic record about 2 Ga (Kusky, 2004). One of the oldest recognized ophiolites that has all of the essential components in the correct stratigraphic order is the 1.95-Ga Jormua Complex in northern Finland. Although older ophiolites have been reported (de Wit & Aswal, 1995; Helmstaedt & Scott, 1992; Kusky, 2004), most lack a convincing sheeted dyke complex and tectonized harzburgites. The thickest most laterally extensive Paleoproterozoic ophiolite is the Purtuniq ophiolite in the Cape Smith orogen in Canada with an age of about 2 Ga (Scott et al., 1992). Although few well-documented ophiolites have been reported that are older than about 1000 Ma, numerous occurrences in the age range of 1000 to 600 Ma are reported from the Pan-African provinces in Africa and South America and from areas around the North Atlantic. Estimated thicknesses of most Neoproterozoic ophiolites range up to 8 km, but most are less than 5 km. They are bounded by thrust faults and appear to have been emplaced by obduction. Although the range in metamorphic grade and degree of deformation is considerable, many Proterozoic ophiolites preserve primary textures and structures.

As with Phanerozoic ophiolites, many Proterozoic ophiolites carry a weak to strong subduction zone geochemical imprint. This suggests that they represent fragments of arc-related oceanic crust from either back-arc or forearc basins. Why there are few if any occurrences of ophiolites older than 2 Ga is an important question that we will return to in Chapter 7.

TECTONIC SETTINGS RELATED TO MANTLE PLUMES

Large Igneous Provinces

Large igneous provinces, commonly referred to as **LIPs,** comprise mostly volcanic or near-surface intrusions, with outcrop areas $\geq$100 000 km^2. Most LIPs have volumes of $>$100 000 km^3 and maximum life spans of about 50 Ma (Bryan & Ernst, 2008). Although the term is usually applied to mafic igneous rocks related to mantle plumes (Condie, 2001), a much broader usage is advocated by some investigators (Sheth, 2007). Some large rhyolite provinces, such as the Whitsunday Province in eastern Australia, clearly belong to this group, and large batholiths, such as the Andean batholith, are included as LIPs by some investigators. This discussion does not include subduction-related igneous provinces as LIPs. Only those provinces that appear to be directly (plume melts) or indirectly (lower crustal melts in which the heat source is probably a mantle plume) related to mantle plumes are considered to be LIPs (Bryan & Ernst, 2008) (Figure 3.7). Seamounts are not considered to be LIPs, whereas giant dyke swarms, large felsic igneous provinces, and basalt-komatiite greenstones (usually Archean in age) are classified as LIPs.

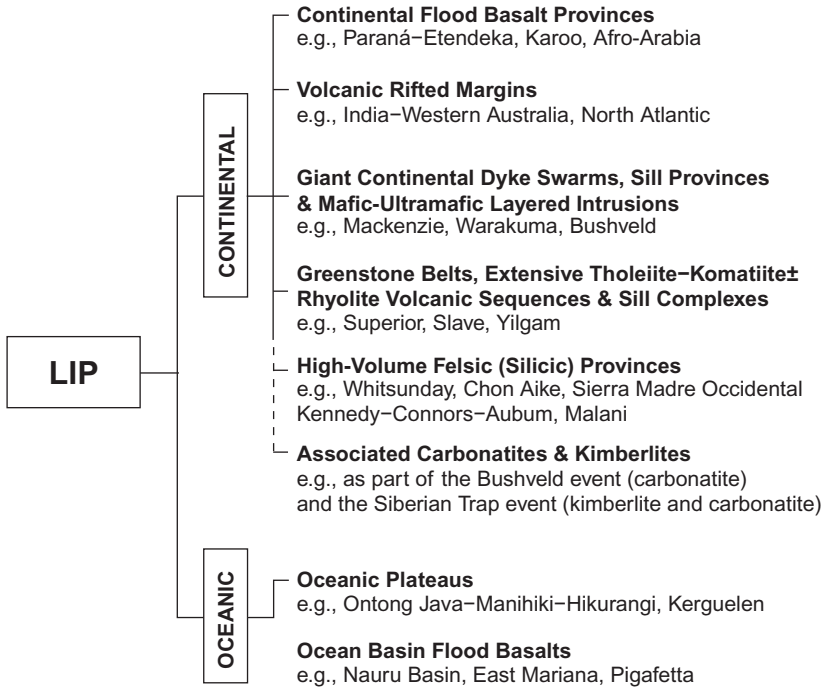

FIGURE 3.7 Classification of LIPs (large igneous provinces). Examples are given for each group. *Modified after Bryan & Ernst (2008).*

Oceanic Plateaus and Aseismic Ridges

Oceanic plateaus, which are composed chiefly of basalt flows erupted beneath the oceans, are the largest topographic features on the seafloor. **Aseismic ridges** are extinct volcanic ridges on the seafloor. About 10% of the ocean floors are covered by oceanic plateaus and aseismic ridges, and more than 100 are known (Figure 3.8), many of which are in the western Pacific (Coffin & Eldholm, 1994). These features rise thousands of meters above the seafloor and some, such as the Seychelles Bank in the Indian Ocean (SEYC, Figure 3.8), rise above sea level. Some have a granitic basement (e.g., Lord Howe Rise north of New Zealand, and the Agulhas Plateau south of Africa [AGUL]) suggesting they are rifted fragments of continental crust. Others such as the Cocos and Galapagos ridges west of South America are of volcanic origin, related to hotspot activity. Some aseismic ridges, such as the Palau-Kyushu ridge south of Japan (not shown in Figure 3.8), are extinct oceanic arcs. Others, such as the Walvis and Rio Grande ridges in the South Atlantic, are hotspot tracks.

Together with flood basalts on the continents, oceanic plateaus are thought to be the products of magmas erupted from mantle plumes (Coffin & Eldholm,

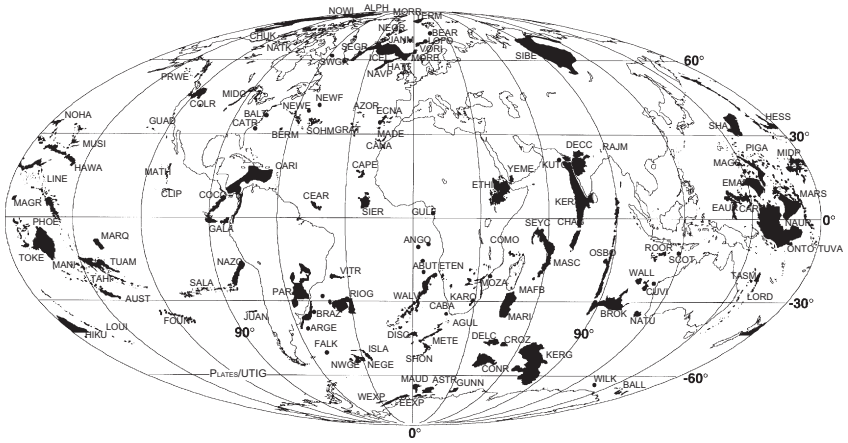

FIGURE 3.8 Distribution of Phanerozoic oceanic plateaus, aseismic ridges, and flood basalts. Some important examples referred to in this or later chapters: CARI, Caribbean Plateau; COCO, Cocos Ridge; COLR, Columbia River basalts; DECC, Deccan traps; GALA, Galapagos Ridge; ICEL, Iceland; KERG, Kerguelen oceanic plateau; LORD, Lord Howe Rise; NAVP, North Atlantic Volcanic Province; ONTO, Ontong Java oceanic plateau; PARA, Parana flood basalts; RIOG, Rio Grande Ridge; SIBE, Siberian flood basalts; WALV, Walvis Ridge. *After Coffin & Eldholm (1994).*

1994; Coffin et al., 2006). The largest oceanic plateau, which straddles the equator in the southern Pacific, is the Ontong Java plateau erupted from a mantle plume about 120 Ma in the South Pacific (Mann & Taira, 2004). This plateau is capped by seamounts and is covered by a veneer of pelagic sediments (limestone, chert, and radiolarite) in places over 1 km thick (Berger et al., 1993). Because only the tops of oceanic plateaus are available for sampling, to learn more about their rock assemblages, we must go to older plateaus that are preserved in the continents as terranes. Studies of the Wrangellia terrane, which is composed largely of an oceanic plateau accreted to western North America in the Cretaceous (Greene et al., 2008), show that pillow basalts and hyaloclastic breccias comprise most of the succession with only a thin capping of pelagic limestone, shale, and chert. Some oceanic plateaus (like Kerguelen in the southern Indian Ocean) emerge above sea level and are capped with subaerial basalt flows and associated pyroclastic volcanics. Oceanic plateau basalts are largely tholeiites with only minor amounts of alkali basalt, and most show incompatible elements only slightly enriched compared to NMORBs (Figure 3.9).

Rifted Continental Margins

During continental breakup, rifted continental margins may be underplated with significant volumes of mafic magma, such as along the coast of southeast Greenland and the coast of Norway during the breakup of Laurentia and Baltica

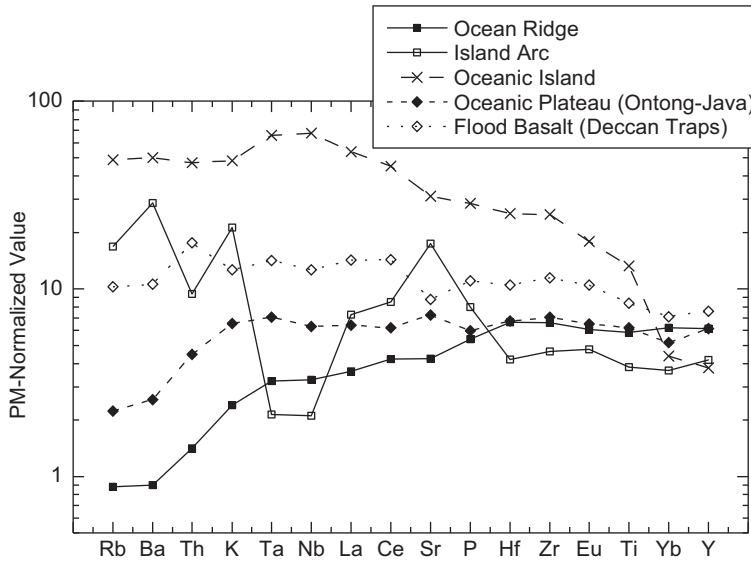

FIGURE 3.9 Primitive mantle normalized incompatible element distributions in various basalts. *Primitive mantle values and NMORBs from Sun & McDonough (1989).*

in the Late Cretaceous (SWGR, NEGR, and NAVP, Figure 3.8) (Holbrook & Kelemen, 1993). Rifted volcanic margins evolve by a combination of flood basaltic volcanism, intrusive magmatism, extension, uplift and erosion (Menzies et al., 2002; Reston, 2009). In the North Atlantic, at least 75% of the rifted continental margins are associated with contemporary volcanism during the last 200 Ma. The transition from continental flood basalt volcanism to ocean ridge volcanism is marked by prerift to synrift magmatism with development of submarine seaward-dipping seismic reflectors and up to 15 km of underplated mafic crust along and seaward of the rifting continental margin (Figure 3.10). There is a gradation from volcanic rifted margins to nonvolcanic rifted margins, for instance along the southern Red Sea.

Rifted margins are characterized by early flood basaltic volcanism reaching up to 7 km in thickness and including both mafic and felsic components (Menzies et al., 2002). In most dated examples, this volcanism is short lived, lasting less than 3 Ma. Magmatism and rifting are not always synchronous. In some rifted margins, a magmatic gap coincides with the peak in extension. The seaward-dipping seismic reflectors comprise a combination of volcanic flows and intrusive rocks, hyaloclastic deposits, and nonvolcanic sediments. The contribution of plume-derived and ocean ridge–derived magmas to rifted continental margins appears to vary in both space and time.

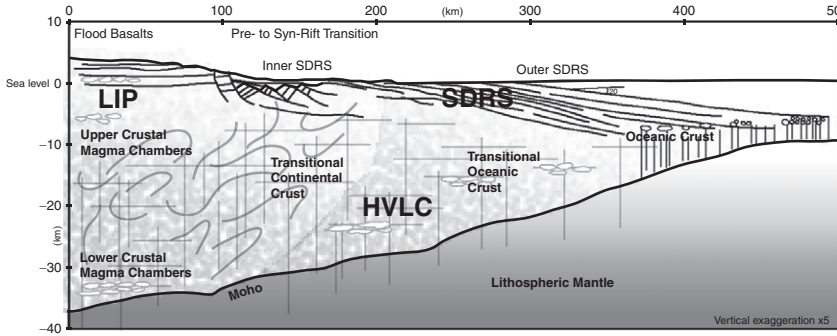

FIGURE 3.10 Schematic rifted continental margin. SDRS, seaward-dipping seismic reflectors; HVLC, high-velocity lower crust (mafic underplate). Extrusive episodes are prerift (flood basalts), synrift (inner subaerial SDRS), and synrift to postrift (outer submarine SDRS). *Courtesy of Martin Menzies and the Geological Society of America.*

Continental Flood Basalts

Flood basalts are thick successions of basalt erupted onto the continents over short periods of time, like the Columbia River basalts in the northwest United States and the Deccan traps in India (Figure 3.8). They are composed chiefly of the tholeiitic basalt flows, and like oceanic plateau basalts, they appear to be derived from mantle plumes, or in some cases, from melting of the subcontinental lithosphere triggered by mantle plumes (Condie, 2001). Thick successions of flood basalts comprise important plateaus on the continents. One of the characteristic features of both oceanic plateau basalts and flood basalts is the rapidity with which large volumes of basaltic magma are erupted. The Deccan traps, which were erupted at the Cretaceous/Tertiary boundary 65 Ma, include a preserved volume of basalt of about 1.5×10^6 km^3 erupted in ≤ 1 My, probably more than 80% of these flows $<500\,000$ y. The Columbia River basalts formed at 17.5 to 6 Ma, at which time 0.17×10^6 km^3 of magma were erupted. Eruption rates of flood basalts and oceanic plateau basalts range from about 0.5 to >1 km^3/y, considerably greater than rates typical of ocean ridges or volcanic islands like Hawaii (with rates of 0.02–0.05 km^3/y) (White & McKenzie, 1995).

Continental flood basalts tend to be lower in Mg and Fe and other compatible elements than MORBs or island basalts. They typically show Fe enrichment trends, but in some instances have lower Ti than other oceanic basalts. Incompatible element distributions vary widely in flood basalts, often within the same volcanic field. Those with relatively high contents of LIL elements, like the Deccan traps (Figure 3.9), are either contaminated by continental crust, or come from enriched sources in the subcontinental lithosphere. In both cases a

subduction geochemical component, as shown by the Deccan basalts, may be transferred to the magmas, either by magma contamination, or in the case of the lithosphere, directly from the source.

Hotspot Volcanic Islands

The hotspot model (Wilson, 1963), which suggests that linear volcanic chains and ridges on the seafloor form as oceanic crust moves over relatively stationary magma sources, has been widely accepted in the geologic community. Hotspots are generally thought to form in response to mantle plumes, which rise like salt domes in sediments, through the mantle to the base of the lithosphere (Duncan & Richards, 1991; Condie, 2001). Partial melting of plumes in the upper mantle leads to large volumes of magma, which are partly erupted (or intruded) at Earth's surface. Hotspots also may be important in the breakup of supercontinents.

Hotspots are characterized by the following features:

1. In ocean basins, hotspots form topographic highs of 500 to 1200 m with typical widths of 1000 to 1500 km. These highs are probably indirect manifestations of ascending mantle plumes.
2. Many hotspots are capped by active or recently active volcanoes. Examples are Hawaii and Yellowstone Park in the western United States.
3. Most oceanic hotspots are characterized by gravity highs reflecting the rise of more dense mantle material from the mantle.
4. One or two aseismic ridges of mostly of extinct volcanics lead away from many oceanic hotspots. Similarly, in continental areas, the age of magmatism and deformation may increase with distance from a hotspot. These features are known as **hotspot tracks** (Figure 3.11).
5. Most hotspots have high heat flow, probably reflecting a mantle plume at depth.

Chains of seamounts and volcanic islands are common in the Pacific Basin, and include such well-known island chains as the Hawaiian-Emperor, Line, Society, and Austral Islands, all of which are subparallel to either the Emperor or Hawaiian chains and approximately perpendicular to the axis of the East Pacific Rise (Figure 3.11). Closely spaced volcanoes form aseismic ridges such as the Ninetyeast Ridge in the Indian Ocean and the Walvis and Rio Grande Ridges in the South Atlantic (Figure 3.8). Isotopic ages demonstrate that the focus of volcanism in the Hawaiian chain has migrated to the southeast at a linear rate of about 10 cm/y for the last 30 Ma. Linear decreases in the age of volcanism that occurred in the Marquesas, Society, and Austral hotspot tracks in the South Pacific during the last 30 Ma (Figure 3.11) have inferred rates of plate migration the order of 11 cm/y, similar to the Hawaiian track. The Pratt-Welker seamount chain in the Gulf of Alaska, however, records a rate of plate motion of about 4 cm/y. Until recently, the bend in the Hawaiian-Emperor chain at about

FIGURE 3.11 Hotspot tracks on the Pacific plate. Tracks assume fixed hotspots and show 10-Ma tick marks. *Modified after Steinberger & O'Connell (1998) and courtesy of Bernhard Steinberger.*

43 Ma was assumed to reflect a change in spreading direction of the Pacific plate. However, paleomagnetic results show that prior to 43 Ma the hotspot track was caused by rapid movement of the hotspot, rather than by a change in plate motion (Tarduno et al., 2003). This rapid movement may be caused by a change in the locus of upwelling related to capture by an ocean ridge, followed by changes in sub-Pacific mantle flow regimes (Tarduno et al., 2009).

Hotspot tracks also occur in the continents, although they are less well defined than in ocean basins due the thicker lithosphere. For example, North America moved northwest over the Great Meteor hotspot in the Atlantic Basin between 125 and 80 Ma (Van Fossen & Kent, 1992). The trajectory of the hotspot is defined by the New England seamount chain in the North Atlantic (see Figure 1.3) and by Cretaceous kimberlites and alkalic complexes in New England and Quebec. Dated igneous rocks fall near the calculated position

of the hotspot track at the time they formed. The calculated trajectory of the Trindade hotspot east of Brazil matches the locations of three dated kimberlites from Brazil and also roughly coincides with the distribution of alluvial diamond deposits (which are derived from nearby kimberlites). High heat flow, low seismic wave velocities and densities at shallow depth, and high electrical conductivity at shallow depth beneath Yellowstone National Park in Wyoming reflect a mantle hotspot at this locality (Figure 3.11) (Smith & Braile, 1994). A 600-m-high topographic bulge is centered on the Yellowstone caldera and extends across an area 600 km in diameter. Direct evidence of a mantle plume at depth is manifest by anomalously low P-wave velocities that extend to depths of 200 km. The movement of the North American plate over this hotspot during the past 16 Ma has been accompanied by eruption of the Columbia River basalts in Oregon (Figures 3.8 and 3.11) and the development of the Snake River volcanic plain, with the oldest hotspot-related volcanics found in southeastern Oregon.

As exemplified by Hawaii, hotspot volcanic islands are some of the largest mountains on Earth, often rising many kilometers above the seafloor. During the subaerial stages of eruption, volcanoes typically evolve from a shield-building stage (like Mauna Loa and Kilauea), through a caldera-filling stage (like Mauna Kea), terminating in a highly eroded shield volcano with small, often alkaline magma eruptions (like most of the extinct volcanoes in Hawaii). Hotspot islands are composed chiefly of tholeiitic basalts, with only minor amounts of alkali basalts and their derivatives erupted during terminal volcanism. Dredging of seamounts and oceanic slopes of islands reveals a dominance of hyaloclastic volcanics, in contrast to the abundance of flows found along oceanic ridges (Bonatti, 1967). This difference indicates that island-seamount magmas are considerably more viscous than MORB magmas and readily fragment upon eruption into seawater (Kokelaar, 1986). In striking contrast to subduction-related basalts, many island basalts show a relative enrichment in Nb and Ta (Figure 3.9), reflecting a mantle plume source enriched in these elements.

Giant Mafic Dyke Swarms

Vast swarms of mafic dykes have been intruded into the continents, covering areas of tens to hundreds of thousands of square kilometers (Ernst et al., 1995; Ernst & Buchan, 2001). These swarms, which range up to 500 km in width and over 3000 km in length, occur on all Precambrian shields and include many thousands of dykes. Individual dykes range from 10 to 50 m in width, with some up to 200 m. Most dykes have rather consistent strikes and dips, and individual dykes have been traced for up to 1000 km. Dyke widths tend to be greater where depth of erosion is least, suggesting that dykes widen in the upper crust, and dyke spacing ranges generally from 0.5 to 3 km with dykes branching both vertically and along strike. Major swarms appear to have been

intruded episodically with important ages of intrusion at 2500, 2390–2370, 2150–2100, 1900–1850, 1270–1250, and 1150–1100 Ma. Structural studies indicate that most swarms are intruded at right angles to the minimum compression direction, and except near the source, most are intruded laterally, not vertically. Some swarms, such as the giant Mackenzie swarm in Canada (Figure 3.12), appear to radiate from a point, commonly interpreted as a plume head (Baragar et al., 1996). The Mackenzie swarm is also an example of a swarm associated with flood basalts (Coppermine River basalts, Cb in Figure 3.12) and a layered intrusion (Muskox intrusion, M). U-Pb dating of baddeleyite shows that most swarms are emplaced in very short periods of time,

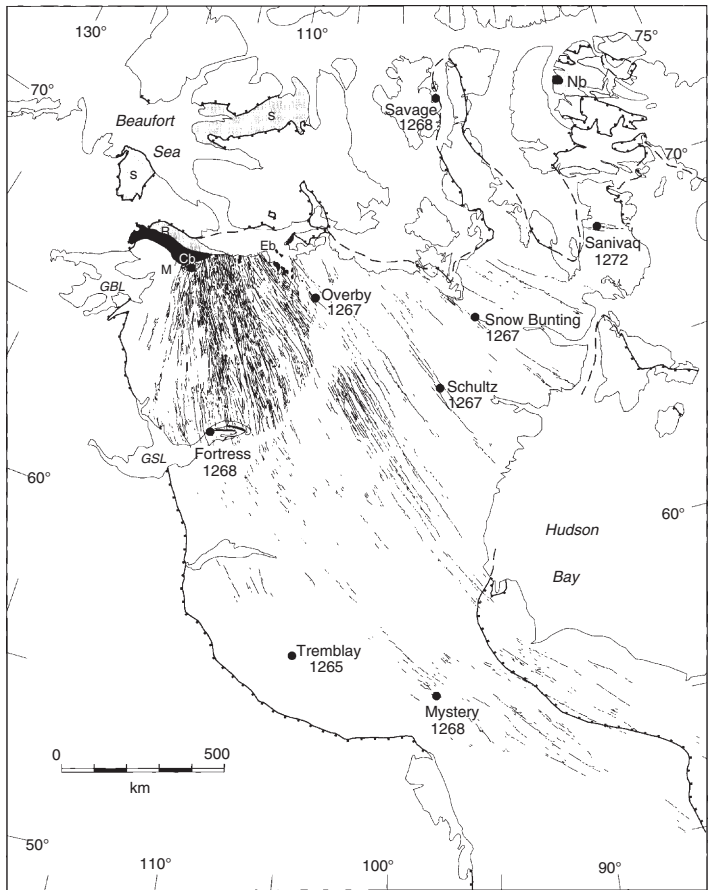

FIGURE 3.12 The giant Mackenzie dyke swarm in northern Canada. This dyke swarm was intruded at 1267 Ma, probably in response to a mantle plume located at that time south of Beaufort Sea. The Muskox intrusion (M) and the Coppermine River flood basalts (Cb) are part of the same event. GBL, Great Bear Lake; GSL, Great Slave Lake. *Courtesy of A. N. LeCheminant.*

often less than 2–3 Ma (Tarney, 1992). Giant dyke swarms are typically composed of tholeiites, although norite swarms are also important in the Proterozoic.

Like the Mackenzie swarm, many giant dyke swarms appear to be associated with mantle plumes, and their emplacement is accompanied by significant extension (over 30%) of the continental crust (Tarney, 1992; Baragar et al., 1996). During the early stages of plume activity and rifting, dykes may develop radial patterns from an underlying plume source (Figure 3.13, stage 1). As with the Red Sea and Gulf of Aden rifts associated with the Afar hotspot, an ocean basin may open between two of the radiating dyke swarms, leaving the third swarm as part of a failed arm or aulacogen (aborted rift) (stage 2). Later, during closure of the ocean basin and continental collision, dykes are consumed or highly deformed. The swarms intruded into aulacogens, however, are more likely to be preserved if they are on the descending plate (stage 3). Hence, major dyke swarms that radiate from a point, such as the Mackenzie swarm, may indicate the presence of a former ocean basin. Some giant dyke swarms may have been emplaced during supercontinent fragmentation and their ages and distributions can be helpful in reconstructing supercontinents (as discussed in Chapter 8).

CONTINENTAL RIFTS

General Features

Continental rifts are fault-bounded basins produced by extension of continental crust. They may be single, like the rifts in East Africa, or multiple, as in the case of the Basin and Range Province in the western United States (see Figure 1.3). Also included in this category are **aulacogens**, which are failed or less active arms of triple junctions, such as the Ethiopian and Benue Rifts in Africa. Spreading began in the Red Sea and Gulf of Aden 15–25 Ma and may be beginning today in the Ethiopian aulacogen. The Benue Rift became a failed arm in the Late Cretaceous as the other two rift segments opened as part of the Atlantic Basin. Rifts are of different origins and occur in different regional tectonic settings. Although the immediate stress environment of rifts is extensional, the regional stress environment may be compressional, extensional, or nearly neutral. Rifts that form in cratons, such as the East African rift system, are commonly associated with domal uplifts, although the timing of doming relative to rifting may vary (Mohr, 1982). Geophysical data indicate that both the crust and lithosphere are thinned beneath rifts and that most or all of the crustal thinning occurs in the ductile lower crust, over a much broader area than represented by the surface expression of the rift (Thompson & Gibson, 1994). Extension in rifts ranges from as little as 10 km in the Baikal Rift to >50 km in the Rio Grande Rift. Magma chambers have been described in rifts based on seismic data, of which the best documented cases are magma chambers in central New Mexico beneath the Rio Grande Rift and in Iceland

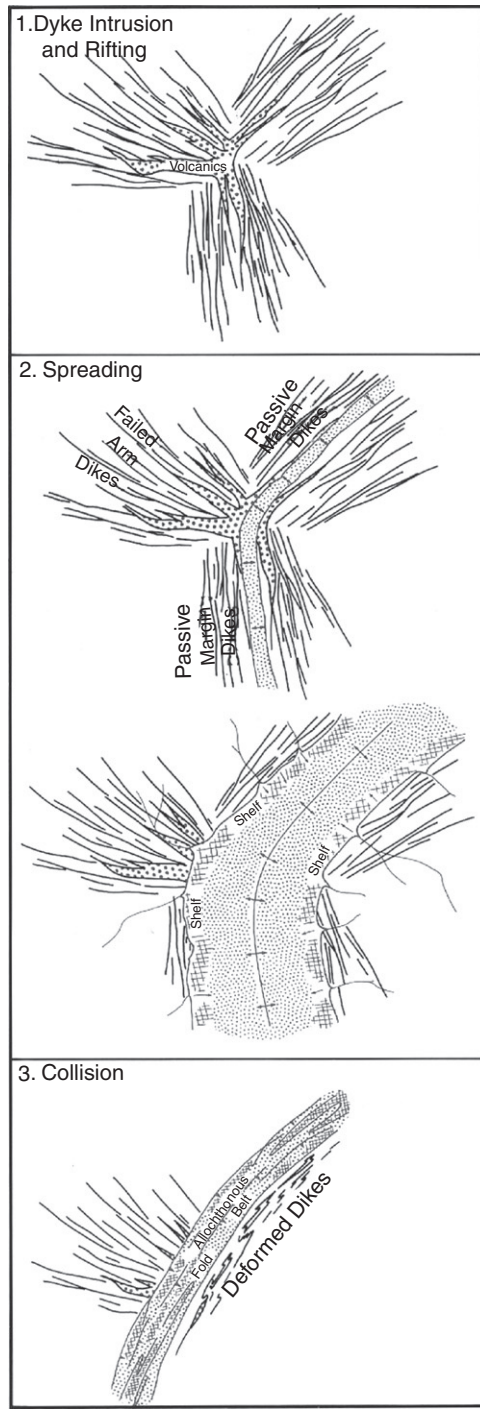

FIGURE 3.13 Three stages in the tectonic evolution of mafic dyke swarms. *From Fahrig (1987).*

(Sanford & Einarsson, 1982). Although in some instances tectonic and volcanic activity in rifts are related in space and time; in many cases they are not. Zones of major eruption seldom coincide with the main rift faults.

Rock Assemblages

Continental rifts (hereafter referred to as rifts) are characterized by immature terrigenous clastic sediments and bimodal volcanics (Wilson, 1993). **Bimodal volcanics** are basalts (tholeiites) and felsic volcanics, like those found, for instance, in the Rio Grande Rift, or alkali basalts and phonolites, like those in the East African Rift. Few, if any, igneous rocks of intermediate composition occur in rifts. Felsic volcanics are emplaced usually as ash flow tuffs or glass domes. In older rifts that are uplifted, the plutonic equivalents of these rocks are exposed, as in the Oslo Rift in Norway. Granitic rocks range from granite to monzodiorite in composition with granites and syenites usually dominating (Williams, 1982). The Kenya and Oslo Rifts show a decrease in magma alkalinity with time, a feature that probably reflects a secular decrease in depth of magma generation. Geochemical and isotopic studies of rift basalts show that they are derived either from mantle plumes or from the subcontinental lithosphere, or both (Bradshaw et al., 1993; Thompson & Gibson, 1994; Peate, 1997).

Layered igneous intrusions are common in exhumed rifts, although they also occur in other tectonic settings such as LIPs and convergent margins. These intrusions are large mafic to ultramafic bodies that exhibit internal layering formed by accumulation of crystals during fractional crystallization of basaltic parent magmas. Cyclic layering in large mafic intrusions is generally interpreted to reflect episodic injections of new magma into fractionating magma chambers. The largest well-studied intrusion is the vast Bushveld Complex in South Africa, which is over 8 km thick, covers a minimum area of 66 000 km^2, and was intruded 2 Ga (Figure 3.14). Although the origin of the Bushveld is still problematic, it may be the roots of a LIP associated with a mantle plume. Large layered intrusions are major sources of metals, such as Cr, Ni, Cu, and Fe and, in the case of the Bushveld Complex, also Pt.

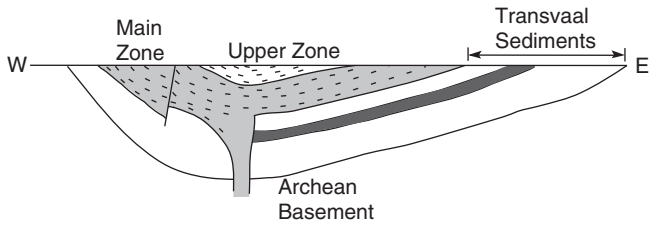

FIGURE 3.14 Idealized cross section of the 2-Ga Bushveld Complex in South Africa. Length of section about 150 km. *After Hunter (1975).*

Rift sediments are chiefly arkoses, feldspathic sandstones, and conglomerates derived from rapidly uplifted fault blocks, in which granitoids are important components. Evaporites also are deposited in many rifts. If a rift is inundated with seawater, as exemplified by the Rhine Graben in Germany, marine sandstones, shales, and carbonates may also be deposited.

Rift Development and Evolution

As a starting point for understanding rift development and evolution, rifts are classified into two categories, depending on the mechanisms of rifting (Sengor & Burke, 1978; Ruppel, 1995). **Active rifts** are produced by doming and cracking of the lithosphere, which results from upwelling asthenosphere or rising mantle plumes (Figure 3.15). **Passive rifts**, on the other hand, are produced by stresses in moving lithospheric plates or by drag at the base of the lithosphere. Active rifts are represented by ocean ridges, continental rifts, and back-arc basins. As continental rifts and back-arc rifts continue to open, they can evolve into ocean ridges. Active rifts contain relatively large volumes of volcanic rock, while in passive rifts, immature clastic sediments exceed volcanics in abundance. Active rifts are also characterized by early uplift and basement stripping resulting from crustal expansion due to a deep heat source. In general, uplift in passive rifts is confined to the stretched and faulted near-surface region and to the shoulders of the rift zone, whereas in active rifts, uplift commonly extends for hundreds of kilometers beyond the rift zone proper. Lithospheric thinning is laterally confined to the rift zone in passive rifts, while in active rifts the zone of thinning is several times wider than the rift width (Thompson & Gibson, 1994).

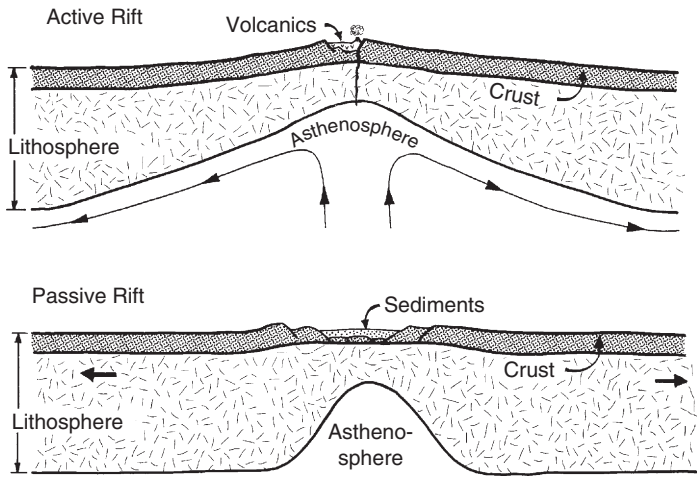

FIGURE 3.15 Diagrammatic cross sections of active and passive continental rifts.

Although active rifts may form in a number of tectonic settings, they commonly exhibit similar overall patterns of development. The major stages are as follows (after Mohr, 1982):

1. A broad, shallow depression develops prior to doming or volcanism.
2. Diapiric asthenosphere or a mantle plume is forcefully injected into the base of the lithosphere. During injection, diapirs undergo adiabatic decompression leading to partial melting and the onset of basaltic magmatism.
3. Buoyant isostatic uplift of heated lithosphere leads to doming.
4. Doming and extensional forces cause crustal attenuation and thinning of the lithosphere.
5. Episodic dyke injection and volcanism alternate with faulting, and the duration of episodes and volumes of magma erupted decrease with time.
6. Rift valleys develop and may be associated with voluminous felsic magmatism, both extrusive and intrusive.
7. An active rift may be aborted at an early stage of its development, such as the Mesoproterozoic Keweenawan rift in the north-central United States, or it may continue to open and evolve into an ocean basin, such as the Red Sea.

Passive rifts develop along faulted continental margins, in zones of continental collision, and in arc systems (Ingersoll, 1988). Examples of rifts associated with faulted continental margins are those found adjacent to the San Andreas and related faults in California and the rifts in western Turkey associated with the Anatolian transform fault. Rifts are generated along collisional boundaries by irregularities in continental margins and by transcurrent and normal faulting caused by nonperpendicular collision. The Rhine Graben in Germany is an example of a rift that developed at a steep angle to a collisional boundary, and the term *impactogen* has been applied to this type of rift. This graben appears to have been produced as Africa collided with an irregularity along the European continental margin. An aborted attempt to subduct the irregularity resulted in depression and rifting. Numerous studies confirm that stresses associated with the Tibet–India collision were transmitted great distances into the Eurasian plate as transcurrent and normal faults, forming such rifts as the Baikal Rift in Siberia and the Shanshi Graben system in China.

As rifts evolve, their rock assemblages change. Oceanic rifts are represented by ophiolites. Arc-related rifts contain arc volcanics and graywackes, and moderate to large back-arc basins are characterized by mixed assemblages including some combination of ophiolites and deep-sea sediments, arc-derived graywackes, and cratonic sediments. Continental rifts and aulacogens contain arkoses, feldspathic sandstones, conglomerates, and bimodal volcanics. Passive rifts contain a variety of immature sediments and, in some instances, minor volcanic rocks.

CRATONS AND PASSIVE MARGINS

As discussed in Chapter 2, cratons are large tectonically stable regions of the continents. **Passive margins** are continental margins that develop around the edges of opening ocean basins such as the Atlantic Ocean today. Rock assemblages deposited in cratonic basins and passive margins are mature clastic sediments, chiefly quartz arenites and shales, and shallow marine carbonates. In Late Archean/Paleoproterozoic successions, banded iron formation may also be important (Klein & Beukes, 1992; Eriksson & Fedo, 1994). Because passive continental margins began as continental rifts, rift assemblages generally underlie passive margin successions. When back-arc basins develop between passive margins and arcs, like the Sea of Japan, cratonic sediments may interfinger with arc sediments in the basins. Cratonic sandstones are relatively pure quartz sands that reflect intense weathering, low relief in source areas, and prolonged transport across subdued continental surfaces. Commonly associated marine carbonates are deposited as blankets and as reefs around the basin margins. Transgression and regression successions in large cratonic basins reflect the rise and fall of sea level, respectively.

Depositional systems in cratonic and passive margin basins vary depending on the relative roles of fluvial, eolian, deltaic, wave, storm, and tidal processes. Spatial and temporal distribution of sediments is controlled by regional uplift, the amount of continent covered by shallow seas, and climate (Klein, 1982). If tectonic uplift is important during deposition, continental shelves are narrow and sedimentation is dominated by wave and storm systems. However, if uplift is confined chiefly to craton margins, sediment yield increases into the craton and fluvial and deltaic systems may dominate. For transgressive marine clastic sequences, shallow seas are extensive and subtidal, and storm-dominated and wave-dominated environments are important. During regression, fluvial and eolian depositional systems become dominant.

The rates of subsidence and uplift in cratons are a function of the time interval over which they are measured. Current rates are of the order of a few centimeters per year, whereas data from older successions suggest rates 1–2 orders of magnitude slower. In general, Phanerozoic rates of uplift appear to have been 0.1–1 cm/y over periods of 10^4–10^5 years and over areas of 10^4–10^6 km^2. One of the most significant observations in cratonic basins is that they exhibit the same exponential subsidence as ocean basins (Sleep et al., 1980). After about 50 Ma, the depth of subsidence decreases exponentially to a constant value.

Several models have been suggested to explain cratonic subsidence (Bott, 1979; Sleep et al., 1980). Sediment loading, lithosphere stretching, and thermal doming followed by contraction are the most widely cited mechanisms. Although the accumulation of sediments in a depression loads the lithosphere and causes further subsidence, calculations indicate that the contribution of sediment loading to subsidence must be minor compared to other effects.

Subsidence at passive margins may result from thinning of continental crust by progressive creep of the ductile lower crust toward the suboceanic upper mantle. As the crust thins, sediments accumulate in overlying basins. Alternatively, the lithosphere may be domed by upwelling asthenosphere or by a mantle plume, and uplifted crust is eroded. Thermal contraction following doming results in platform basins or a series of marginal basins around an opening ocean basin. Most investigators now agree that subsidence along passive continental margins is due to the combined effects of thermal contraction of continental and adjacent oceanic lithosphere together with sediment loading.

Igneous rocks are rare in cratonic and passive margin basins, and when found, they are small intrusive bodies, dykes, sills, or volcanic pipes, generally of alkaline compositions. **Kimberlites** are ultramafic breccias found in cratonic areas, and they are significant in that they contain xenoliths of ultramafic rocks from the upper mantle as well as diamonds and other high-pressure minerals that indicate depths of origin for kimberlitic magmas of $\geq$300 km (Pasteris, 1984). They range in age from Archean to Tertiary and most occur as pipes or dykes <1 km^2 in cross-sectional area. Kimberlite magmas appear to have been produced by partial melting of enriched sources in the subcontinental lithosphere.

ARC SYSTEMS

Subduction-Related Rock Assemblages

Numerous geologic environments are associated with subduction. In an idealized arc system, three zones are recognized: the arc–trench gap, the arc, and the arc-rear area (Hamilton, 1988; Stern, 2002). From the ocean side landward, a continental-margin arc is characterized by the trench; an accretionary prism with overlying forearc basins; the volcanic arc with intra-arc basins; a fold-thrust belt; and a retroarc foreland basin (Figure 3.16a). An oceanic arc (Figure 3.16b) differs from a continental-margin arc primarily in the arc-rear area where it includes some combination of active and inactive back-arc basins and, in some instances, remnant arcs. Each of these arc environments is characterized by different rock assemblages as described below.

Trenches

Trenches form where oceanic lithospheric slabs begin to descend into the mantle. Trench sediments are dominantly fine-grained graywacke turbidites with minor pelagic components. Turbidity currents generally enter trenches at oceanic canyons and flow along trench axes. Sediments can be transported along trenches for up to 3000 km as seen, for example, in the Sunda trench south of Sumatra, where detritus from the Himalayas enters the trench on the north from the Bengal oceanic fan (Moore et al., 1982). Although most detrital sediment is clay or silt, sand and coarser sediments may be deposited in proximal facies. Down-axis changes in facies suggest that trenches are filled by a succession

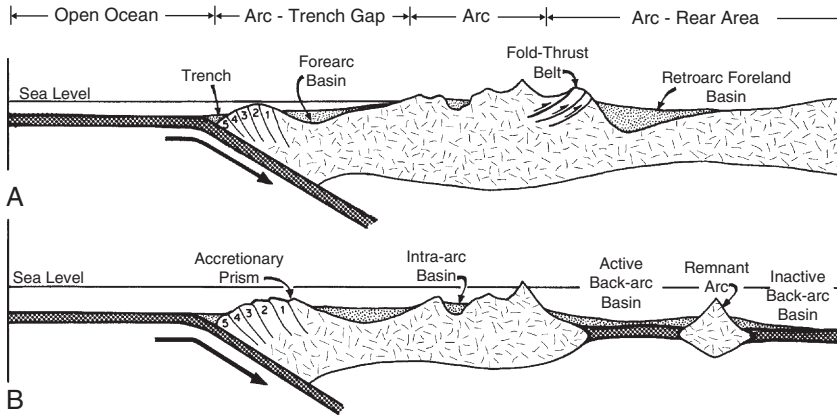

FIGURE 3.16 Diagrammatic cross sections of (A) a continental margin arc and (B) an oceanic arc showing major tectonic divisions. Numbers in accretionary prism indicate relative age of slabs, with 1 being the oldest.

of radiating oceanic fans and that most sediments are derived from local arc volcanic and plutonic sources.

Accretionary Prisms

The **accretionary prism** (or subduction zone complex) consists of a series of steeply inclined, fault-bounded wedges of sediment and volcanic rock above a descending slab. These wedges represent oceanic crust and trench sediments that have been accreted to the front of the arc. Individual wedges in the accretionary prism decrease in age as the trench is approached (Figure 3.16). Accretionary prisms are intensely deformed producing **melange**, which is a mappable body of rock characterized by the lack of continuous bedding and the inclusion of fragments of rocks of all sizes (up to more than a kilometer across) contained in a fine-grained, deformed matrix. Both sedimentary and tectonic processes can give rise to melange. **Olistostromes** are melanges produced by gravitational sliding and accumulate as semifluid bodies that do not have bedding, but include associated turbidites. Melange clasts may be exotic (derived from another environment) or native (reworked from the immediate environment) and are generally matrix supported (Figure 3.17). Clast lithologies include graywacke, mudstone, chert, basalt (greenstone) and other ophiolite lithologies, arc volcanics, and rare granitoids. Melanges are commonly folded and may contain more than one cleavage or foliation. Sheared matrices are usually composed of serpentine and fine-grained rock and mineral fragments.

Although melanges are typical of accretionary prisms, they are formed by several different processes and occur in different tectonic environments (Lash, 1987). Tectonic melanges are produced by compressive forces along the upper part of descending slabs at shallow depths. Fragmentation and mixing of largely

FIGURE 3.17 Franciscan melange near San Simeon, California. Fragments of greenstone metabasalt (large fragment one-third of the way down from top) and graywacke (large fragment near top) are enclosed in a sheared matrix of serpentine and chlorite. *Courtesy of Darrel Cowan.*

lithified rocks may occur along a migrating shear zone subparallel to a subducting slab. Fragments of oceanic crust and trench sediment are scraped off the descending plate and accreted to the overriding plate. Gravitational slumping may produce olistostromes or debris flows on oversteepened trench walls or along the margins of a forearc basin. Debris flows, in which clay minerals and water form a single fluid possessing cohesion, are probably the most important transport mechanism of olistostromes.

Forearc Basins

Forearc basins are marine depositional basins on the trench side of arcs (Figure 3.16), and they vary in size and abundance with the evolutionary stage of an arc. In continental-margin arcs, such as the Sunda arc in Indonesia, forearc

basins range to 700 km in strike length. They overlie the accretionary prism, which may be exposed as oceanic hills within and between forearc basins. Sediments in forearc basins, which are chiefly turbidites with sources in the adjacent arc system, range up to many kilometers in thickness. Hemipelagic sediments (mixed continental and oceanic sources) are also of importance in some basins, such as in the Mariana arc. Olistostromes can form in forearc basins by sliding and slumping from locally steepened slopes. Forearc basin clastic sediments may record progressive unroofing of adjoining arcs, as is seen, for instance, in the Great Valley Sequence (Jur-Cret) in California (Dickinson & Seely, 1986). Early sediments in this sequence are chiefly volcanic detritus from active volcanics and later sediments reflect progressive unroofing of the Sierra Nevada batholith. Volcanism is rare in modern forearc regions and neither volcanic nor intrusive rocks are common in older forearc successions.

Arcs

Volcanic arcs range from entirely subaerial, such as the Andean and Middle America arcs, to mostly or completely oceanic, such as many of the immature oceanic arcs in the Southwest Pacific. Other arcs, such as the Aleutians, change from subaerial to partly oceanic along the strike. Subaerial arcs include flows and associated pyroclastic rocks, which often occur in large stratovolcanoes. Oceanic arcs are built of pillowed basalt flows and large volumes of hyaloclastic tuff and breccia. Volcanism begins rather abruptly in arc systems at a volcanic front. Both tholeiitic and calc-alkaline magmas characterize arcs, with basalts and basaltic andesites dominating in oceanic arcs, and andesites and dacites often dominating in continental-margin arcs. Felsic magmas are generally emplaced as batholiths, although felsic volcanics are common in most continental-margin arcs.

Back-Arc Basins

Active **back-arc basins** occur over descending slabs behind arc systems (Figure 3.16) and commonly have high heat flow, relatively thin lithosphere, and in many instances, an active ocean ridge, which is enlarging the size of the basin (Jolivet et al., 1989; Fryer, 1996). Sediments are varied depending on basin size and nearness to an arc. Proximal to arcs and remnant arcs, volcaniclastic sediments generally dominate, whereas in more distal regions, pelagic, hemipelagic, and biogenic sediments are widespread (Klein, 1986). During the early stages of basin opening, thick epiclastic deposits, largely representing gravity flows, are important. With continued opening of a back-arc basin, these deposits pass laterally into turbidites, which are succeeded distally by pelagic and biogenic sediments (Leitch, 1984). Discrete layers of air-fall tuff may be widely distributed in back-arc basins. Early stages of basin opening are accompanied by diverse magmatic activity including felsic volcanism, whereas later evolutionary stages may be characterized by an active ocean

ridge. As previously mentioned, many ophiolites carry a subduction zone geochemical signature, and thus appear to have formed in either back-arc or forearc basins.

Subaqueous ash flows may erupt or flow into back-arc basins and form in three principal ways (Fisher, 1984). The occurrence of felsic welded ash flow tuffs in some ancient back-arc successions suggests that hot ash flows enter water without mixing and retain enough heat to weld. Alternatively, oceanic eruptions may eject large amounts of ash into the sea, which falls onto the seafloor, forming a dense, water-rich debris flow. In addition to direct eruption, slumping of unstable slopes composed of pyroclastic debris can produce ash turbidites.

Because of the highly varied nature of modern back-arc sediments and the lack of a direct link between sediment type and tectonic setting, one cannot assign a distinct sediment assemblage to these basins. It is only when a relatively complete stratigraphic succession is preserved and detailed sedimentologic and geochemical data are available that ancient back-arc successions can be identified. Inactive back-arc basins, such as the western part of the Philippine plate, have a thick pelagic sediment blanket and lack evidence for recent seafloor spreading.

Remnant Arcs

Remnant arcs are oceanic aseismic ridges that are extinct portions of arcs that have been rifted away by the opening of a back-arc basin (Figure 3.16b) (Fryer, 1996). They are composed chiefly of subaqueous mafic volcanic rocks similar to those formed in oceanic arcs. Once isolated by rifting, remnant arcs subside and are blanketed by progressively deep-water pelagic and biogenic deposits and distal ash showers.

Retroarc Foreland Basins

Retroarc foreland basins form behind continental-margin arc systems (Figure 3.16a), and they are filled largely with clastic terrigenous sediments derived from a fold-thrust belt behind the arc. A key element in foreland basin development is the syntectonic character of the sediments (Graham et al., 1986). The greatest thickness of foreland basin sediments borders the fold-thrust belt, reflecting enhanced subsidence caused by thrust-sheet loading and deposition of sediments. Another characteristic feature of retroarc foreland basins is that the proximal basin margin progressively becomes involved with the propagating fold-thrust belt (Figure 3.18). Sediments shed from the rising fold-thrust belt are eroded and redeposited in the foreland basin, only to be recycled again with basinward propagation of this belt. Coarse, arkosic alluvial-fan sediments characterize proximal regions of foreland basins, and distal facies by fine-grained sediments and variable amounts of marine carbonates. Progressive unroofing in the fold-thrust belt should lead to an "inverse" stratigraphic sampling of the source in foreland basin sediments as illustrated

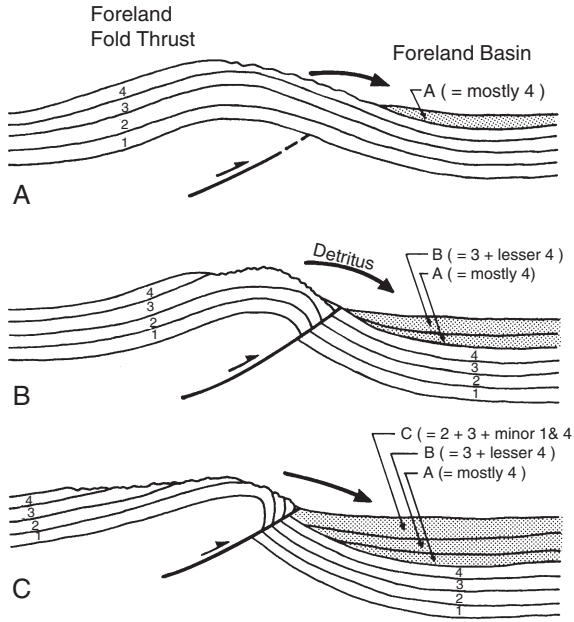

FIGURE 3.18 Progressive unroofing of an advancing foreland thrust sheet. *After Graham et al. (1986).*

in Figure 3.18. Such a pattern is well developed in the Cretaceous foreland basin deposits in eastern Utah (Lawton, 1986). In this basin, early stages of uplift and erosion resulted in deposition of Paleozoic carbonate-rich clastic sediments followed later by quartz-feldspar–rich detritus from the elevated Precambrian basement. Foreland basin successions also typically show upward coarsening and thickening of terrigenous sediments, a feature that reflects progressive propagation of the fold-thrust belt into the basin.

Arc Processes

Seismic reflection profiling and geologic studies of uplifted and eroded arc systems have led to a greater understanding of arc evolution and of the development of accretionary prisms and forearc basins (Stern, 2002). Widths of modern arc–trench gaps (75–250 km) are proportional to the ages of the oldest igneous rocks exposed in adjacent arcs (Dickinson, 1973). As examples, the arc–trench gap width in the Solomon Islands is about 50 km, with the oldest igneous rocks about 25 Ma, and the arc–trench gap width in northern Japan (Honshu) is about 225 km, with the oldest igneous rocks about 125 Ma. The correlation suggests progressive growth in width of arc–trench gaps with time. Such growth appears to reflect some combination of outward migration of the

subduction zone by accretionary processes and inward migration of the zone of maximum magmatic activity. **Subduction zone accretion** involves the addition of sediments and volcanics to the margin of an arc in the accretionary prism (Figure 3.19) (von Huene & Scholl, 1991). Seismic profiling suggests that accretionary prisms are composed of sediment wedges separated by high-angle thrust faults produced by offscraping of oceanic sediment (Figure 3.19b). During accretion, oceanic sediments and fragments of oceanic crust and mantle are scraped off and added to the accretionary prism (Hilde 1983; Scholl & von Huene, 2009). This offscraping results in outward growth of the prism, and also controls the location and evolutionary patterns of overlying forearc basins. Approximately half of modern arcs are growing by offscraping accretion. Reflection profiles suggest that deformational patterns are considerably more

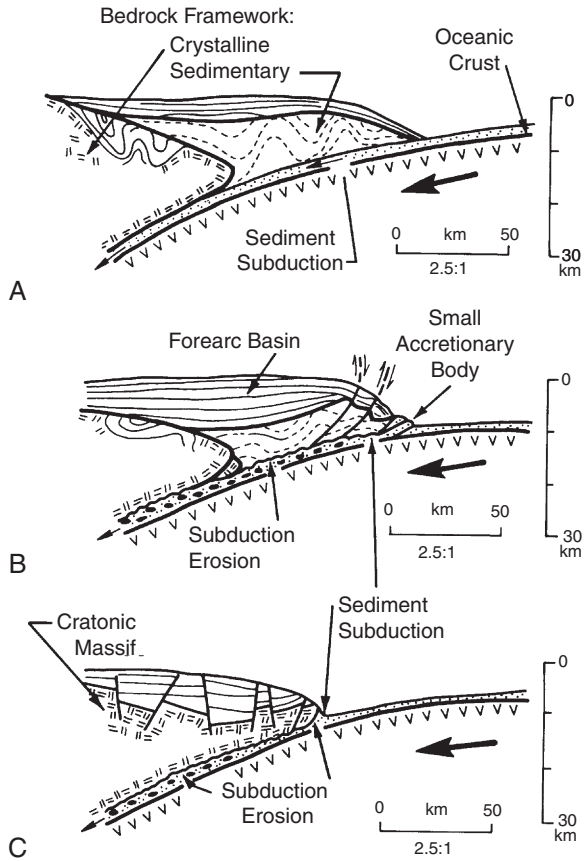

FIGURE 3.19 Sediment subduction and sediment erosion at a convergent plate boundary. *Modified after Scholl et al. (1980).*

complex than simple thrust wedges. Deformation may include large-scale structural mixing and infolding of forearc basin sediments (Figure 3.19a). Geologic evidence for such mixing comes from exposed accretionary prisms, exemplified by parts of the Franciscan Complex in California. Fluids also play an important role in facilitating mixing and metasomatism in accretionary prisms (Tarney et al., 1991).

In addition to accretion to the landward side of the trench, material can be underplated beneath the arc by a process known as duplex accretion. A duplex is an imbricate package of isolated thrust slices bounded on top by a thrust and below by a low-angle detachment fault (Sample & Fisher, 1986). During transfer of displacement from an upper to a lower detachment horizon, slices of footwall are accreted to the hanging wall (accretionary prism) and rotated by bending of the frontal ramp. Observations from seismic reflection profiles, as well as exposed accretionary prisms, indicate that duplex accretion occurs at greater depths than offscraping accretion. Although some arcs, such as the Middle America and Sunda arcs, appear to have grown by accretionary processes, others such as the New Hebrides arc, have little if any accretionary prism. In these latter arcs, either very little sediment is deposited in the trench or most sediment is subducted. One possible way to subduct sediments is in grabens in the descending slab, a mechanism supported by the distribution of seismic reflectors in descending plates. **Sediment subduction** is a major process by which continental crust is returned to the mantle. Interestingly, if sediments are subducted in large amounts beneath arcs, they cannot contribute substantially to arc magma production as constrained by isotopic and trace element distributions in modern arc volcanics.

Subduction erosion is another process that occurs in arcs with insignificant accretionary prisms (von Huene & Scholl, 1991). It involves mechanical plucking and abrasion along the top of a descending slab, which causes a trench's landward slope to retreat shoreward. Subduction erosion may occur either along the top of the descending slab (Figure 3.19b) or at the leading edge of the overriding plate (Figure 3.19c). Evidence commonly cited for subduction erosion includes (1) an inland shift of the volcanic front, as has occurred in the Andes in the last 100 Ma; (2) truncated seaward trends and seismic reflectors in accretionary prisms and forearc basins; (3) not enough sediment in trenches to account for the amount delivered by rivers; and (4) evidence for crustal thinning such as tilting of unconformities toward the trench, which is most easily accounted for by subsidence of the accretionary prism. All of these can be explained by erosion along the top of the descending slab. Subduction erosion rates have been estimated along parts of the Japan and Chile trenches at 25–50 km^3/Ma for each kilometer of shoreline.

Accretion, mixing, subduction erosion, and sediment subduction are all potentially important processes in subduction zones and any one of them may dominate at a given place and evolutionary stage. Studies of modern arcs indicate that about half of the ocean floor sediment arriving at trenches is

subducted and does not contribute to growth of accretionary prisms either by offscraping or duplex accretion (von Huene & Scholl, 1991). At arcs with significant accretionary prisms, 70–80% of incoming sediment is subducted, and at arcs without accretionary prisms, all of the sediment is subducted. The combined average rates of subduction erosion (1.4 km^3/y) and sediment subduction (1.1 km^3/y) suggest that on average, 2.5 km^3 of sediment are subducted each year.

High-Pressure Metamorphism

Blueschist-facies metamorphism is important in subduction zones, where high-pressure, relatively low-temperature mineral assemblages form. Glaucophane and lawsonite, both of which have a bluish color, are common minerals in this setting. In subduction zones, crustal fragments can be carried to great depths (>50 km), yet remaining at rather low temperatures, usually <400°C (see Figure 2.9). A major unsolved question is how these rocks return to the surface. One possibility is by continual underplating of the accretionary prism with low-density sediments, resulting in fast, buoyant uplift during which high-density pieces of the slab are dragged to the surface (Cloos, 1993). Another possibility is that blueschists are thrust upward during later collisional tectonics.

One of the most intriguing fields of research at present is seeing just how far crustal fragments are subducted before returning to the surface. Discoveries of coesite (high-pressure silica phase) and diamond inclusions in pyroxenes and garnet from eclogites from high-pressure metamorphic rocks in eastern China record astounding pressures of 4.3 GPa (about 150-km burial depth) at 740°C (Schreyer, 1995; Zheng, 2008). Several other localities have reported coesite-bearing assemblages recording pressures of 2.5–3 GPa. Also, several new high-pressure hydrous minerals have been identified in these assemblages, indicating that some water is recycled into the mantle and that not all water is lost by dehydration to the mantle wedge. Perhaps the most exciting aspect of these findings is that for the first time we have direct evidence that crustal rocks (both felsic and mafic) can be recycled into the mantle.

Igneous Rocks

The close relationship between active volcanism in arcs and descending plates implies a genetic connection between the two. Subduction zone–related volcanism starts abruptly at the **volcanic front**, which roughly parallels oceanic trenches and begins 200–300 km inland from trench axes adjacent to the arc–trench gap (Figure 3.20). It occurs where the subduction zone is 125–150 km deep, and the volume of magma erupted decreases in the direction of subduction zone dip. The onset of volcanism at the volcanic front reflects the onset of melting above the descending slab, and the decrease in volume of

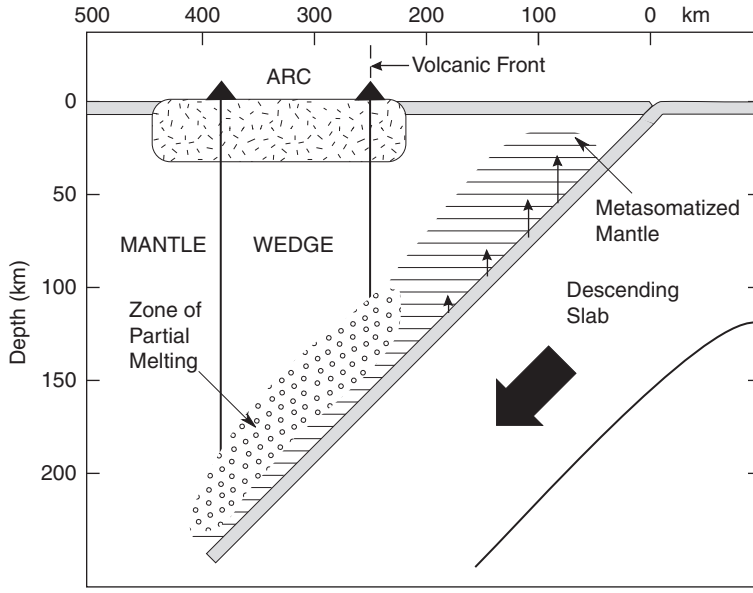

FIGURE 3.20 Cross section of a subduction zone showing shallow devolatilization of descending slab (short vertical arrows) and magma production in the mantle wedge.

erupted magma behind the volcanic front is caused by either a longer vertical distance for magmas to travel or a decrease in the amount of water liberated from the slab as a function of depth.

The common volcanic rocks in most island arcs are basalts and basaltic andesites, while andesites and more felsic volcanics also become important in continental-margin arcs. Whereas basalts and andesites are erupted chiefly as flows, felsic magmas are commonly erupted as plinian eruptions in which case most of the ejecta are ash and dust. These eruptions give rise to ash flows and associated pyroclastic (or hyaloclastic) deposits. Arc volcanic rocks are generally porphyritic, containing up to 50% phenocrysts in which plagioclase dominates.

Arc volcanoes are typically steep-sided stratovolcanoes composed of varying proportions of lavas and fragmental materials (Figure 3.21). Their eruptions range from mildly explosive to violently explosive, and contrast strikingly to the eruptions of oceanic island and continental rift volcanoes. Large amounts of water are given off during eruptions. Rapid removal of magmas may result in structural collapse of the walls of stratovolcanoes, producing calderas such as Crater Lake in Oregon. The final stages of eruption in some volcanic centers are characterized by the eruption of felsic pyroclastic flows that may travel great distances. Seismic shadow-zone studies indicate that modern magma reservoirs in subduction zone areas are commonly 50–100 km deep. The migration of

FIGURE 3.21 Eruption of Mayon volcano in the Philippines, September 2006. Notice the pyroclastic flows moving down the right flank of the volcano.

earthquake hypocenters from depths of up to 200 km over periods of a few months prior to eruption reflects the ascent of magmas at rates of 1–2 km/day.

The cores of arc systems comprise granitic batholiths as evidenced in deeply eroded arcs. Such batholiths, which are composed of numerous plutons, range in composition from diorite to granite, with granodiorite often dominating.

In contrast to oceanic basalts, arc basalts are commonly quartz normative, with high Al_2O_3 (16–20%) and low TiO_2 (<1%) contents. Igneous rocks of the tholeiite and calc-alkaline series are typical of island arcs and continental-margin arcs, respectively. Ratios of $^{87}Sr/^{86}Sr$ in volcanics from island arcs are low (0.702–0.705), whereas those from continental-margin arcs are variable, reflecting variable contributions of continental crust to the magmas. Arc basalts also exhibit a subduction zone component (depletion in Nb and Ta relative to neighboring incompatible elements on a primitive mantle normalized graph; Figure 3.9) (Hawkesworth et al., 1994; Pearce & Peate, 1995). Arc granitoids are chiefly I-types, typically meta-aluminous, with tonalite or granodiorite dominating.

Compositional Variation of Arc Magmas

Both experimental and geochemical data show that most arc basalts are produced by partial melting of the mantle wedge in response to the introduction of volatiles (principally water) from the breakdown of hydrous minerals in descending slabs (Pearce & Peate, 1995; Poli & Schmidt, 1995) (Figure 3.20). The degree and nature of melting is controlled by the temperature of the mantle wedge and the supply of water from the breakdown of hydrous phases (such as chlorite) in the descending plate. In contrast, the major control on location of melting is primarily slab dip, and to a lesser degree the rate of plate convergence (Grove et al., 2009). Other processes such as fractional crystallization, assimilation of

crust, and contamination by subducted sediment, however, also affect magma composition. Trace element and isotope distributions often cannot distinguish between a subducted sediment contribution to arc magmas and continental assimilation. The very high Sr and Pb isotope ratios and low Nd isotope ratios in some felsic volcanics and granitic batholiths from continental-margin arcs, such as in the Andes, suggest that these magmas were produced either by partial melting of older continental crust or by significant contamination with this crust.

One unsolved problem is that of how the subduction zone geochemical component is acquired by the mantle wedge. Whatever process is involved, it requires decoupling of Ta-Nb and Ti, from large-ion lithophile (LIL) elements and REE (McCulloch & Gamble, 1991). One of the most widely cited models to explain depletion of these three elements calls on rutile left in the mantle wedge after melt extraction. (In addition to Ti, rutile retains both Nb and Ta in the wedge, and thus the escaping magmas are depleted in these elements.) However, the absence of rutile in mantle lherzolites and the high solubility of rutile in basaltic magma present a problem for this mechanism. A more likely mechanism is that liberation of aqueous fluids from oceanic crust may carry LIL elements, which are soluble in such fluids, into the overlying mantle wedge, metasomatizing the wedge, and leaving behind Nb, Ta, and Ti whose solubilities are very low in these fluids (Saunders et al., 1980; Keppler, 1996; Baier et al., 2008). The net result is relative enrichment in Nb-Ta and Ti in the descending slab and corresponding depletion in the mantle wedge. Thus, magmas produced in the mantle wedge should inherit this **subduction zone signature**. A potential problem with this model is that hydrous secondary minerals in descending oceanic crust (e. g., chlorite, biotite, amphiboles, talc) break down and liberate water at or above 125 km (Figure 3.20). Only phlogopite may persist to greater depths. Yet the volcanic front appears at subduction zone depths of 125–150 km. Devolatilization of descending slabs by 125 km should add a subduction component only to the mantle wedge above this segment of the slab, which is shallower than the depth of partial melting. How then, do magmas acquire a subduction zone component in the mantle wedge? Two possibilities have been suggested, although neither have been fully evaluated: (1) asthenosphere convection extends into the "corner" of the mantle wedge and carries ultramafic rocks with a subduction component to greater depths (Figure 3.20), or (2) frictional drag of the descending plate drags mantle with a subduction component to greater depths.

OROGENS

Three Types of Orogens

Three types of orogens are recognized in continental crust (Figure 3.22): collisional, accretionary, and intracratonic (Cawood et al., 2009). **Collisional orogens** form during collision of two or more cratonic segments of the lithosphere. When the direction of colliding plates is orthogonal, the crust is greatly thickened, and thrusting, metamorphism, and partial melting may rework the

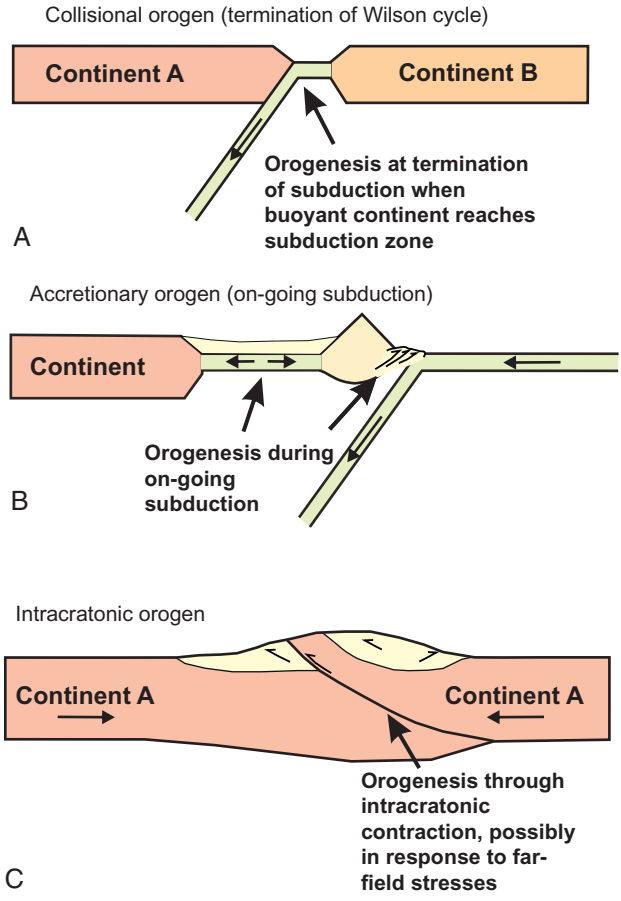

FIGURE 3.22 Schematic cross sections of collisional, accretionary, and intracratonic orogens. *Courtesy of Peter Cawood and the Geological Society of London.*

colliding cratons. A relatively small amount of juvenile crust is produced or tectonically "captured" during collisional orogeny. In contrast, **accretionary orogens** involve collision and suturing of largely juvenile crustal blocks (ophiolites, island arcs, oceanic plateaus, etc.) to continental crust at sites of continuing oceanic plate subduction. Most accretionary orogens contain relatively small volumes of reworked older crust. **Intracratonic orogens** form within continents, often far from active plate margins.

Collisional Orogens

During continental collisions, major thrusts and nappes are directed toward the converging plate as the crust thickens by ductile deformation, and perhaps by underplating with mafic magmas. In some instances, sheet-like slabs commonly

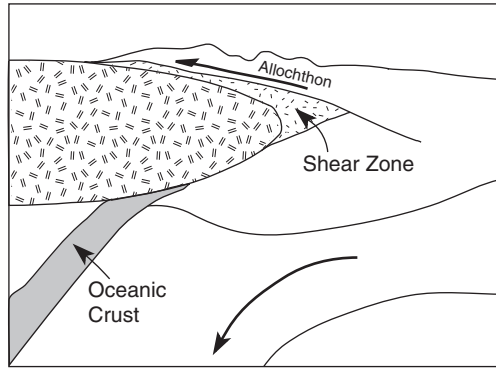

FIGURE 3.23 Schematic cross section showing the emplacement of an allochthon (flake) during a continent–continent collision.

referred to as flakes or **allochthons** may be sheared from the top of the converging plate and thrust over the overriding plate (Figure 3.23). In the Eastern Alps, for instance, Paleozoic metamorphic rocks have been thrust more than 100 km north over the Bohemian Massif and a zone of highly sheared Mesozoic metasediments lies within the thrust zone (Pfiffner, 1992). The allochthon is less than 12 km thick and appears to represent part of the Carnics plate that was detached during the Mid-Tertiary. Seismicity along continent–continent collision boundaries suggests partial subduction of continental crust. Thickening of crust in collisional zones results in partial melting of the lower crust, producing felsic magmas that are chiefly intruded as plutons, with some surface eruptions. Fractional crystallization of basalts may produce anorthosites in the lower crust, and losses of fluids from the thickened lower crust may leave behind granulite-facies mineral assemblages. Isostatic recovery of collisional orogens is marked by the development of continental rifting with fluvial sedimentation and bimodal volcanism, as evident in the Himalayas and Tibet (Dewey, 1988).

Each collisional belt has its own character. In some instances, plates lock together with relatively little horizontal transport, such as along the Caledonian suture in Scotland or the Kohistan suture in Pakistan. In other orogens, such as the Alps and Himalayas, allochthons are thrust for considerable distances and stacked one upon another. Many hundred kilometers of shortening may occur during such a collision. In a few collisional belts, such as the Neoproterozoic Damara belt in Namibia, a considerable amount of deformation and thickening may occur in the overthrust plate. In the Caledonides and parts of the Himalayan belt, ophiolite obduction precedes continent–continent collision and does not seem to be an integral part of the collisional process. In some cases, the collisional zone is oblique, with movement occurring along one or more transform faults. Still in other examples, one continent will indent another, thrusting thickened crust over the indented block. Thickened crust tends to spread

by gravitational forces, and spreading directions need not parallel the regional plate movement. Which block has the greatest effects of deformation and metamorphism depends on such factors as the age of the crust, its thermal regime, crustal anisotropy, and the nature of the subcrustal lithosphere. Old lithosphere generally has greater strength than younger lithosphere.

Accretionary Orogens

Accretionary orogens, such as the western Cordillera in Alaska and western Canada, develop as terranes collide with a continent along a convergent margin (Figure 3.22b). Components include, in addition to an accretionary prism, island arcs, back-arcs, ophiolites, oceanic plateaus, cratonic fragments, postaccretion granitoids, exhumed high-pressure metamorphic rocks, and clastic sedimentary basins (Cawood et al., 2009). Collisions may occur between oceanic terranes, producing a superterrane, before collision with a continent. In some instances, older continental blocks may also be involved in the collisions, such as those found in the 1.9-Ga Trans-Hudson orogen in eastern Canada and in the Ordovician Taconian orogen in the eastern United States. Seismic reflection profiles in western Canada show west-dipping seismic reflectors that are probably major thrusts, suggesting that accretionary orogens comprise stacks of thrusted terranes. Because some accretionary orogens contain large amounts of juvenile crust, they represent one of the major components of continental growth. As an example, during the Paleoproterozoic, an aggregate area of new crust up to 1500 km wide and over 5000 km long was added to the southern margin of the Baltica-Laurentia supercontinent (Figure 2.21) (Hoffman, 1988; Karlstrom et al., 2001).

Accretionary orogens are commonly grouped into two end members: retreating and advancing (Royden, 1993), based on contrasting geologic character and evolution. **Retreating orogens** undergo long-term extension in response to retreat of the lower plate (trench rollback), including opening of back-arc basins as exemplified by the Tertiary history of the western Pacific. In contrast, **advancing orogens** develop as the overriding plate advances toward the downgoing plate resulting in overall compression of the upper plate. A typical example is the eastern Pacific where the North and South American plates have overridden descending oceanic plates along their western margins. This has resulted in the accretion of arc and microcontinental ribbons previously rifted off the continental margins and extensive retroarc fold and thrust belts. Plate convergence may switch from one mode to the other, as it has done in Eastern Australia during the Mesozoic, although the mechanism of switching is poorly understood (Collins, 2002).

Intracratonic Orogens

The most recent addition to the orogen classification is the intracratonic orogen (Figure 3.22c) (Cawood et al., 2009). Many intracratonic orogens are related to subduction zones around continents. In Australia, for instance, a mid-Paleozoic

intracratonic orogen occurs up to 1300 km inboard from the inferred convergent margin that was responsible for the deformation. Similar inboard orogens are found at distances up to 1000 km from associated subduction zones in China during the Mesozoic and along the west coast of South America during the Tertiary. In all of these cases, the orogens paralleled associated convergent plate margins and formed in response to strain localization in the weak back-arc lithosphere, possibly related to flat-slab (buoyant) subduction. Other intracratonic orogens, such as the Altai and Tianshan in East Asia, occur inboard and are related continent–continent collisions (for these orogens, the India–Tibet collision). In this case, stress appears to be transmitted through weak quartz-rich continental rocks.

The preferential hinterland deformation in Asia associated with the India–Tibet collision probably reflects warm, thin Tibetan lithosphere produced by precollisional subduction and accretion. Extensional collapse zones, such as the Aegean basin, are generally of local occurrence in foreland areas and may develop in response to rollback of a partially subducted slab.

Orogenic Rock Assemblages

It is difficult to assign any particular rock assemblage to collisional and accretionary orogens, because rock assemblages change both with time and space as collision progresses. Also, one is faced with sorting out a myriad of older rock assemblages contained in the colliding blocks and representing every conceivable tectonic setting. Sediments accumulate in peripheral foreland and hinterland basins, which develop in response to uplift and erosion of collisional zones. These basins and the sediments therein evolve in a manner similar to retroarc foreland basins. Classic examples of peripheral foreland basins developed adjacent to the Alps and the Himalayas during the Alpine–Himalayan collisions in the Tertiary (Figure 3.24). During the Alpine

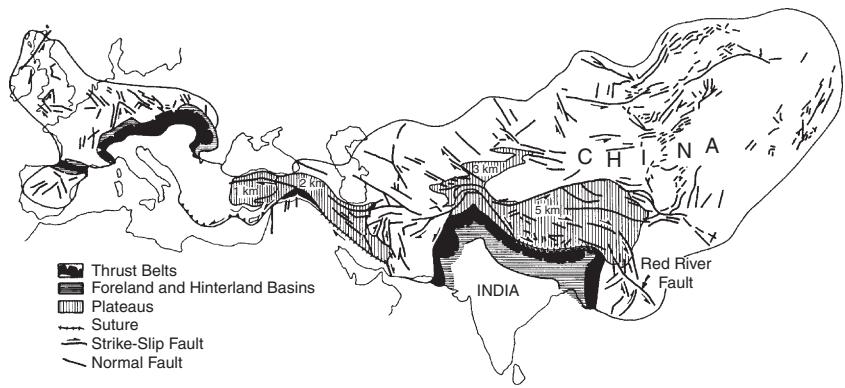

FIGURE 3.24 Simplified tectonic map of the Alpine–Himalayan orogen. Collisional plateau elevations given in kilometers. 1 km, Anatolia Plateau; 5 km, Tibet Plateau. *After Dewey et al. (1986).*

collision, up to 6 km of alluvial fan deposits were deposited in foreland basins (Homewood et al., 1986). Individual alluvial fans up to 1 km thick and 40 km wide have been recognized in the Alps. Coarsening upward cycles and intraformational unconformities characterize collisional deposits, both of which reflect uplift of an orogen and propagation of thrusts and nappes into foreland basins.

At deeper exposure levels (10–20 km), granitoids are common and appear to be produced by partial melting of the lower crust during collisions. Thickening of continental crust, both in descending and overriding plates, leads to the production of granulites at depths >20 km as fluids escape upward. Anorthosites may form as cumulates from fractional crystallization of basalt in the lower and middle crust. Basaltic magma also may underplate the crust and occur as gabbro or mafic granulites in uplifted crustal sections. Collisional granites include pre-collision, syncollisional, and postcollisional types (Pearce et al., 1984). Pre- and postcollisional granitoids are chiefly I-type granites, whereas syncollisional granites are commonly leucogranites (in collisional orogens) and many exhibit features of S-type granites (i.e., derived by partial melting of sediments). Silica contents of leucogranites exceed 70% and most show a subduction geochemical component inherited from their lower crustal source. Supporting a crustal source for many collisional granitoids are their high $^{87}Sr/^{86}Sr$ ratios (>0.725) and high $\delta^{18}O$ values (Vidal et al., 1984). Postcollisional granites, which generally postdate collision by 40 to 50 My, are sharply cross-cutting and are dominantly tonalite to granodiorite in composition.

Tectonic Elements of Collisional Orogens

Continental collision involves progressive compression of buoyant terranes within subduction zones. These terranes may vary in scale from seamounts or island arcs to large continents. The scale of colliding terranes dictates the style, duration, intensity, and sequence of strain systems (Dewey et al., 1986; von Raumer et al., 2003). If colliding continental margins are irregular, the strain sequences are variable along great strike lengths. Prior to terminal collision, one or both continental margins may have had a long complex history of terrane assembly. Continental collisional boundaries are wide complicated structural zones, where plate displacements are converted into complex and variable strains (Figure 3.25).

Collisional orogens can be considered in terms of five tectonic components (Figures 3.25 and 3.26): thrust belts, foreland flexures, plateaus, foreland/hinterland deformational zones, and zones of orogenic collapse. **Foreland** and **hinterland** refer to regions beyond major overthrust belts in the direction and away from the direction of principal orogenic vergence, respectively. Thrust belts develop where thinned continental crust is progressively restacked and thickened toward the foreland. If detachment occurs along a foreland thrust, rocks in the allochthon can shorten significantly independent of shortening in the basement. The innermost nappes and the suture zone are usually steepened

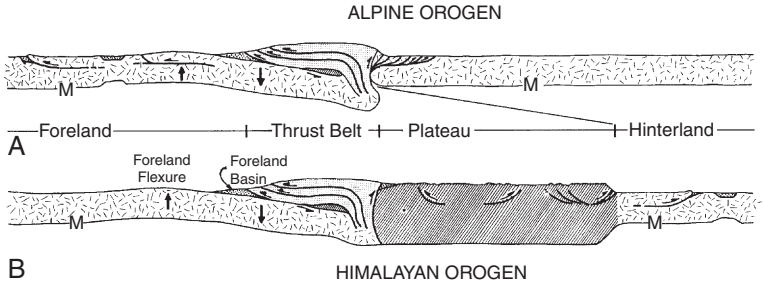

FIGURE 3.25 Schematic cross sections of (A) Alpine and (B) Himalayan collisional orogens. M, Moho. *After Dewey et al. (1986).*

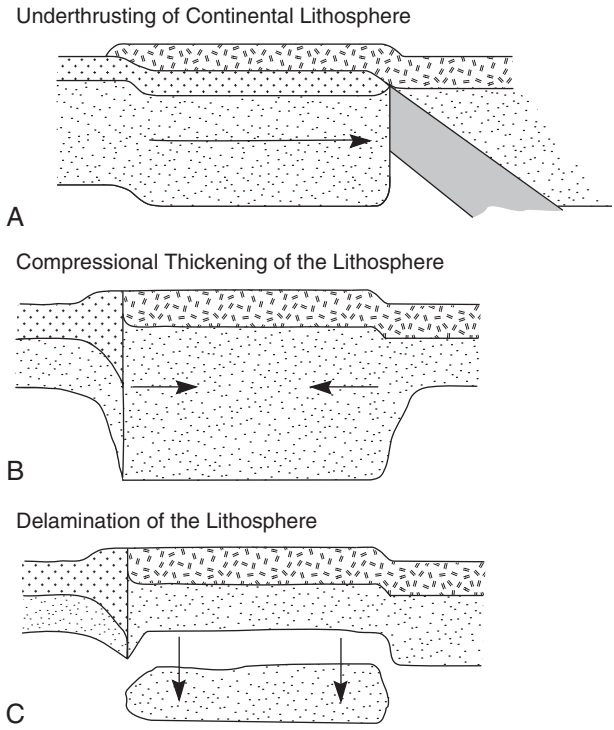

FIGURE 3.26 Schematic cross sections of Tibet showing three tectonic models for the uplift of the Tibet Plateau.

and overturned during advanced stages of collision. The upper crust in collisional orogens is a high-strength layer that may be thrust hundreds of kilometers as relatively thin, stacked sheets that merge along a décollement surface. For instance, in the southern Appalachians a décollement has moved westward over the foreland for at least 300 km. Foreland flexures are upwarps

in the foreland lithosphere caused by progressive downbending of the lithosphere by advancing thrust sheets.

Collisional plateaus, such as the Tibet and Anatolia plateaus (Figure 3.25), form in the near-hinterland area adjacent to the suture and may rise to 1–5 km above sea level. Three models have been suggested to explain collisional plateaus (Harrison et al., 1992) (Figure 3.26): (1) underthrusting of continental crust and lithosphere, which buoyantly elevates the plateau; (2) compressive shortening and thickening of both the crust and lithosphere, followed by isostatic rebound to form the plateau; and (3) either model 1 or 2 followed by delamination of the thickened lithosphere. Neither model 1 nor 2 adequately explains the delayed uplift of Tibet, which began 20 Ma, yet the India–Tibet collision began about 60 Ma. However, if mantle lithosphere was detached some 30 Ma after collision and sank into the mantle, it would be replaced with hotter asthenosphere, which would immediately cause isostatic uplift, elevating Tibet.

Sutures

Sutures are ductile shear zones produced by thrusting along converging plate boundaries, and they range from a few hundred meters to tens of kilometers wide (Coward et al., 1986). Rocks on the hinterland plate adjacent to sutures are chiefly arc-related volcanics and sediments from a former arc system on the overriding plate, whereas those on foreland plates are commonly passive-margin sediments. Fragments of rocks from both plates as well as ophiolites occur in suture melanges. These fragments are tens to thousands of meters in size and are randomly mixed in a sheared, often serpentine-rich, matrix.

One of the problems in recognizing Precambrian collisional orogens is the absence of well-defined suture zones. However, at the crustal depths exposed in most reactivated Precambrian terranes, suture zones are difficult to tell from other shear zones. The classic example of a Cenozoic suture is the Indus suture in the Himalayas. Yet, in the Nanga Parbat area where deep levels of this suture are exposed, it is difficult to identify the suture because it looks like any other shear zone (Coward et al., 1982). Rocks on both sides of the suture are complexly deformed amphibolites and gneisses indistinguishable from each other. If we compare equivalent crustal levels of the Indus suture with that of exhumed Precambrian orogens, there are striking similarities, and deep-seated shear zones in these orogens may or may not be sutures. Without precise geochronology and detailed geologic mapping on both sides of shear zones, it is not possible to correctly identify which shear zones are sutures and which are not.

Foreland and Hinterland Basins

Peripheral foreland and hinterland basins are like retroarc foreland basins in terms of sediment provenance and tectonic evolution. Major peripheral foreland and hinterland basins developed in the Tertiary in response to the

Alpine–Himalayan collisions (Figure 3.24) (Allen & Homewood, 1986). These basins exhibit similar stages of development that have been explained by thermal-mechanical models (Stockmal et al., 1986). In the case of foreland basins, during the first stage, a passive-margin sedimentary assemblage is deposited on a stretched and rifted continental margin. Collision begins as a terrane is thrust against and over continental crust on the descending slab. Continental convergence results in thickening of this terrane and partial melting of the root zones to form syntectonic granite magmas. Topographic relief develops at this stage as the thrust belt rises above sea level and sediments derived from erosion of the highland begin to fill a foreland basin. The first sediments come from distal low-relief terranes and are largely fine-grained, giving rise to deepwater marine shales and siltstones exposed in the lowest stratigraphic levels of foreland basin successions. In contrast, in hinterland basins the early sediments are commonly alluvial fan deposits, shed from the rising mountain range. Continued convergence causes thin-skinned thrust sheets to propagate into foreland basins and relief increases rapidly. Erosion rates increase as do grain size and feldspar content of derivative sediments in response to increased rates of tectonic uplift in the thrust belt. During this stage of development, thick alluvial fans also may be deposited in foreland basins.

The Himalayas

As an example of a young collisional mountain range, none can surpass the high Himalayas. The Himalayan story began some 80 Ma when India fragmented from Gondwana and started on its collision course with eastern Asia. Collision began about 65 Ma and is still going on today. Prior to collision, Tibet was a continental-margin arc system with voluminous andesites and felsic pyroclastic flow tuffs, and northern India was a passive continental margin with a marine shelf-facies on the south, passing into a deepwater Tethyan facies on the north. As the collision began, folds and thrusts moved southward onto the Indian plate (Searle et al., 1987). This resulted in thickening of the crust, high-pressure metamorphism, and partial melting of the root zones to produce migmatites and leucogranites. Thrusting continued on both sides of the Indus suture as India continued to converge on Tibet. By 40 Ma, deformation had progressed southward across both the Lower and Higher Himalayan zones (Figure 3.27). Collapse of the Lower and Sub-Himalayas during the Miocene juxtaposed lower Paleozoic shelf sediments north of the Main Boundary thrust against metamorphic rocks and leucogranites south of the thrust. Continued convergence of the two continental plates led to oversteepening of structures in the Indus suture, and finally to backthrusting on to the Tibet plate as well as continued southward-directed thrusting. The Siwaliks foreland basin continued to move to the south in the Sub-Himalayas as thrust sheets advanced from the north.

The amount of crustal shortening recorded across the Himalayan orogen is almost 2500 km for a time-averaged compression rate of ~5 cm/y

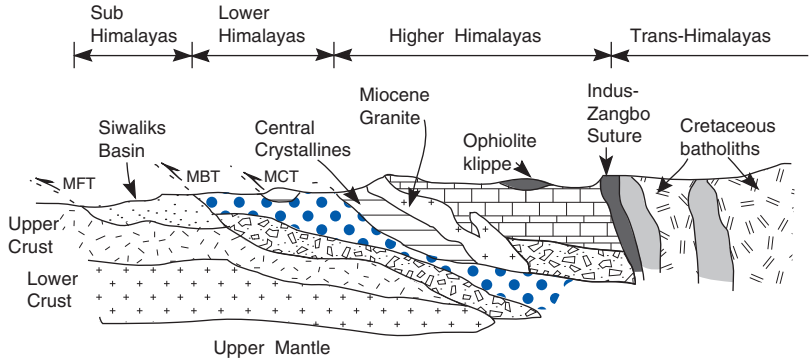

FIGURE 3.27 Schematic cross section of the Himalayas in Nepal and Tibet. MBT, Main Boundary thrust; MFT, Main Frontal thrust; MCT, Main Central thrust. *Modified after Windley (1993).*

(Searle et al., 1987). However, the crust of Tibet is only about 70 km thick, which can account for only about 1000 km of shortening. The remainder appears to have been taken up by transcurrent faulting north of the collision zone (Tapponnier et al., 1986; Windley, 1995). The Tertiary geologic record in SE Asia required 1000–1500 km of cumulative strike-slip offset in which India has successively pushed Southeast Asia followed by Tibet and China in an ESE direction. Most of the Mid-Tertiary displacement has occurred along the left-lateral Red River fault zone (Figure 3.24), accompanying opening of the South China Sea.

Most models for the India–Tibet collision involve buoyant subduction of continental crust. Earthquake data from the Himalayas suggest a shallow ($\sim$3°) northward-dipping detachment zone extending beneath the foreland basins on the Indian plate (Figure 3.27). This detachment surface is generally interpreted as the top of the descending Indian plate and may have a surface expression as the Main Frontal thrust. Convergence since the Early Miocene has been taken up chiefly along the Main Central thrust and its splays by counterclockwise rotation of India beneath Tibet.

UNCERTAIN TECTONIC SETTINGS

Anorogenic Granites

General Features

A wide belt of Proterozoic granites and associated anorthosites extends from southwestern North America to Labrador, across southern Greenland and into the Baltic shield in Scandinavia and Russia. The granites are massive and relatively undeformed, thus the name *anorogenic* granite (Anderson & Morrison, 1992; Windley, 1993). Many have rapakivi textures and other features of A-type granitoids. Two important field observations for anorogenic granites are that (1) they are emplaced chiefly in accretionary orogens and (2) often there

is a close spatial and temporal relation between granite magmatism and crustal extension. Proterozoic anorogenic granites in the Baltica-Laurentia belt range in age from about 1.8 Ga to 1.0 Ga. Most of those in North America are 1.5–1.3 Ga and tend to increase from 1.4 Ga in the southwestern United States to around 1.5 Ga in the midcontinent area (Figure 3.28). Two subprovinces of 1.4–1.34 Ga and 1.5–1.42 Ga granites are recognized in the midcontinent region. The largest and oldest anorogenic granites in this Proterozoic belt occur in Finland and Russia and date from 1.8 to 1.65 Ga (Haapala & Ramo, 1990). Large anorthosite bodies are associated with some anorogenic granites, and most occur in the Grenville Province and adjacent areas in eastern Canada (Figure 3.28). Although Mesoproterozoic anorogenic granites have received most attention, granites with similar field and geochemical characteristics are also known in the Archean and Phanerozoic, some of the youngest of which are in the American Cordillera.

Proterozoic anorogenic granites are A-type granites enriched in K and Fe and depleted in Ca, Mg, and Sr relative to I- and S-type granitoids. They are subalkalic to marginally peraluminous and plot near the minimum in the Q-Ab-Or system at 5–10 kb of pressure (Anderson, 1983). **A-type granites** are typically enriched in REE, Zr, and Hf and have striking depletions in Sr, P, and Ti compared to most other granites. In addition, they appear to have been emplaced under relatively dry conditions at temperatures of 650–800°C

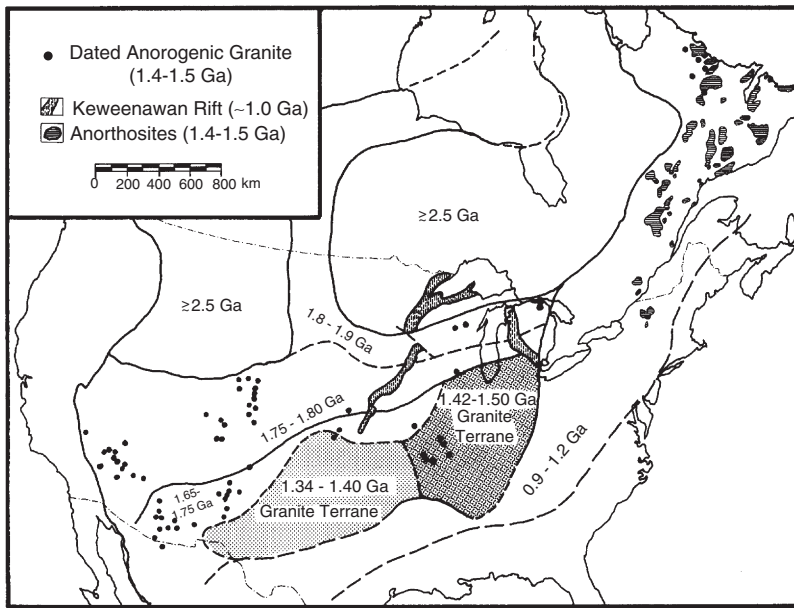

FIGURE 3.28 The Proterozoic anorogenic granite-anorthosite belt in North America. *After Anderson (1983).*

and depths of chiefly <15 km. Rapakivi textures may have developed by volatile losses at shallow depths during emplacement. Another characteristic feature of A-type granites is that they crystallized over three orders of magnitude of oxygen fugacity as reflected by their Fe-Ti oxide mineralogy. Their relatively high initial $^{87}Sr/^{86}Sr$ ratios (0.705 ± 0.003) and negative or near-zero ϵ_{Nd} values are consistent with a lower crustal source, as are incompatible-element and oxygen isotope distributions.

Associated Anorthosites

Associated anorthosites, which are composed of more than 90% plagioclase ($An_{45\text{-}55}$), are interlayered with gabbros and norites and exhibit cumulus textures and rhythmic layering. Most bodies range from 10^2 to 10^4 km^2 in surface area. Gravity studies indicate that anorthosites are from 2 to 4 km thick and are sheetlike in shape, suggesting they represent portions of layered igneous intrusions. The close association of granites and anorthosites suggests a genetic relationship. Geochemical and isotopic studies, however, indicate that the anorthosites and granites are not derived from the same parent magma by fractional crystallization or from the same source by partial melting. Data are compatible with an origin for the anorthosites as cumulates from fractional crystallization of high-Al_2O_3 tholeiitic magmas produced in the upper mantle (Emslie, 1978). The granitic magmas, on the other hand, appear to be the products of partial melting of lower crustal rocks of intermediate or mafic composition (Anderson & Morrison, 1992) or by fractional crystallization of basaltic magmas that did not give rise to anorthosites (Frost & Frost, 1997).

Tectonic Setting

The tectonic setting of anorogenic granites continues to baffle geologists. Unlike most other rock assemblages, young counterparts are recognized in different tectonic settings. The general lack of preservation of associated supracrustal rocks further hinders identifying the tectonic setting of these granites. The only well-documented outcrops of coeval supracrustal rocks and anorogenic granite are in the St. Francois Mountains of Missouri where felsic pyroclastic flow tuffs and calderas appear to represent surface expressions of granitic magmas. Both continental rift and convergent-margin models have been proposed for anorogenic granites, and both models have problems. The incompatible element distributions in most anorogenic granites are suggestive of a within-plate tectonic setting. If an extensive granite-rhyolite province of late Paleozoic to Jurassic age in Argentina represents an anorogenic granite province (Kay et al., 1989), this would favor a back-arc continental setting. The intrusion of anorogenic granites in the Mesoproterozoic belt in Baltica-Laurentia described above usually follows the main deformational events in this accretionary orogen by 60–100 Ma. This may reflect the time it takes to heat the lower crust to the point at which it begins to melt. Although our current database

seems to favor an extensional regime for anorogenic granites (± anorthosites), we cannot draw a strict parallel to modern continental rifts. The anorogenic granite event that transcended time from about 1.9 to 1.0 Ga in Baltica-Laurentia is closely tied to a large accretionary orogen of the same age. Although this event is clearly the most widespread anorogenic granitic event recognized, it is not the only one, and it now seems clear that other events have occurred in both the Archean and Phanerozoic.

Archean Greenstones

Although at one time it was thought that greenstones were an Archean phenomenon, it is now clear that they have formed throughout geologic time (Condie, 1994). It is equally clear that all greenstones do not represent the same tectonic setting, nor do the proportions of preserved greenstones of a given age and tectonic setting necessarily reflect the proportions of that tectonic setting at the same time. The term *greenstone* is used rather loosely in the literature. We will define **greenstone belt** as a submarine supracrustal succession in which the combined mafic volcanic and volcaniclastic component exceeds 50%. From a modern perspective, greenstones are volcanic-dominated successions that have formed in arcs, oceanic plateaus, volcanic islands, and oceanic ridges. It is now known that greenstones contain various packages of supracrustal rocks separated by unconformities or faults (Thurston & Chivers, 1990; Desrochers et al., 1993). Greenstone belts are linear to irregularly shaped volcanic-rich successions that average 20 to 100 km wide and extend for distances of several hundred kilometers. They contain several to many greenstone assemblages or tectonic domains, and in this sense, we might equate a greenstone belt to a terrane, or more specifically to an oceanic terrane. As an example, the largest preserved Archean greenstone belt, the Late Archean Abitibi belt in eastern Canada, contains several greenstone domains that formed and were amalgamated at about 2.7 Ga. Subprovinces in the Archean Superior Province, such as the Wawa-Abitibi and Wabigoon subprovinces (Figure 3.29), may be superterranes and represent amalgamations of greenstone terranes of various oceanic settings. High-precision U-Pb zircon isotopic dating of Archean greenstone terranes indicates that they formed in short periods of time, generally <50 Ma. In some areas, more than one volcanic-plutonic cycle may be recorded for a cumulative history of 200–300 Ma. Although Archean greenstones are dominantly submarine in origin, their tectonic settings continue to a subject of lively debate among Archean investigators. Let us review some of the principal features of Archean greenstones that are useful in constraining tectonic settings.

General Features

Although field evidence indicates that most greenstones are intruded by surrounding granitoids, there are some areas in which greenstone successions lie unconformably on older granitic basement (Condie, 1981; de Wit & Ashwal,

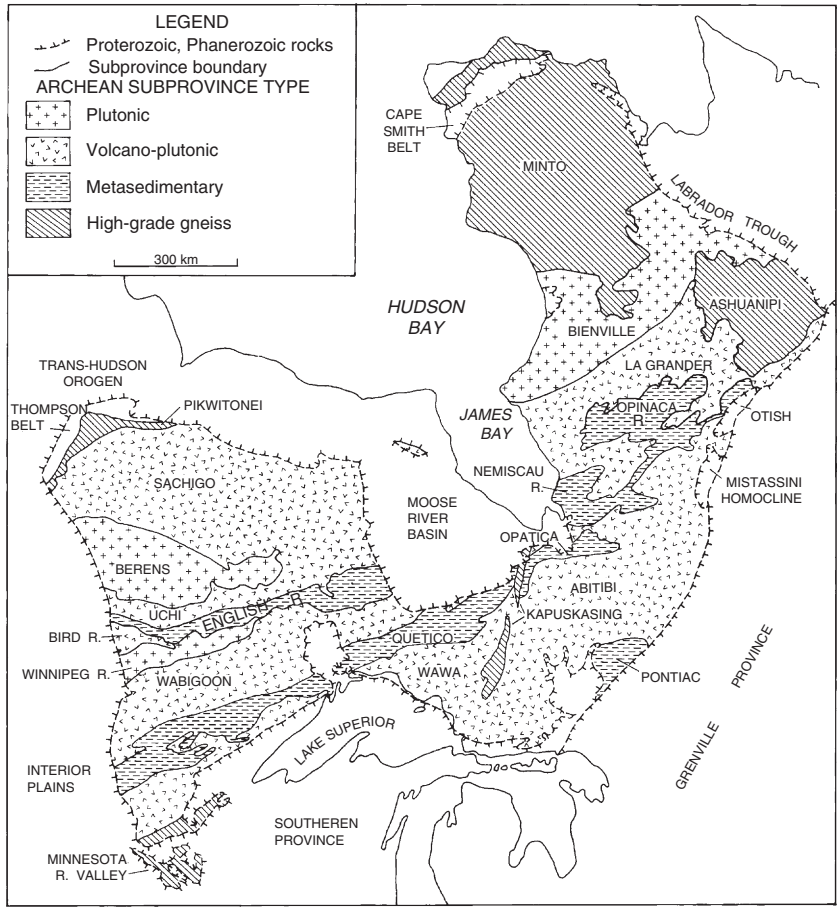

FIGURE 3.29 Generalized geologic map of the Archean Superior Province in eastern Canada. *Modified after Card and Ciesielski (1986).*

1995). In a few greenstone belts, such as Kambalda in southwest Australia, volcanic rocks contain zircon xenocrysts from gneissic basement that is at least 700 Ma older than the host rocks. Thus, although many Archean greenstones are clearly juvenile oceanic terranes, some were erupted on or close to continental crust, and may be contaminated by this crust.

In Canadian Archean greenstones, four lithologic associations are recognized (Thurston & Chivers, 1990; Thurston, 1994). Most widespread are the basalt-komatiite (mafic plain) and mafic to felsic volcanic cycle associations, comprising most of the major greenstone belts in Canada. These two associations are also the most common associations on other continents. The basalt-komatiite assemblages probably represent some combination of oceanic

plateaus and oceanic crust, whereas the mafic-felsic assemblages are likely arc related (Condie, 1994). Of more local importance are the calc-alkaline volcanic and fluvial sediment association (also probably arc related) and the carbonate-quartz arenite association, the latter of which is volumetrically insignificant. In the Archean Superior Province in eastern Canada, greenstone subprovinces alternate with metasedimentary subprovinces (Figure 3.29). Granitoids are more abundant than volcanic and sedimentary rocks in both subprovinces, with gneisses and migmatites most abundant in the metasedimentary belts. U-Pb zircon ages indicate younging in volcanism and plutonism from the northwest (Sachigo subprovince) to the southeast (Wawa-Abitibi subprovinces). The oldest magmatic events in the northwest occurred at 3.0, 2.9–2.8, and 2.75–2.7 Ga followed by major deformation, metamorphism, and plutonism at about 2.7 Ga. In the south, magmatism occurred chiefly between 2.75 and 2.7 Ga. The near contemporaneity of magmatic and deformational events along the lengths of the volcanic subprovinces, coupled with structural and geochemical evidence, supports a subduction-dominated tectonic regime in which oceanic terranes were successively accreted from northwest to southeast.

Greenstone Volcanics

Archean greenstones are structurally and stratigraphically complex. Although thicknesses up to 20 km have been reported, because of previously unrecognized tectonic duplication, it is unlikely that any sections exceed 5 km (Condie, 1994). Most Archean greenstones are composed chiefly of subaqueous basalts (Figure 3.30) and komatiites (ultramafic volcanics) with minor amounts of felsic tuff and layered chert. Many Archean volcanics are highly

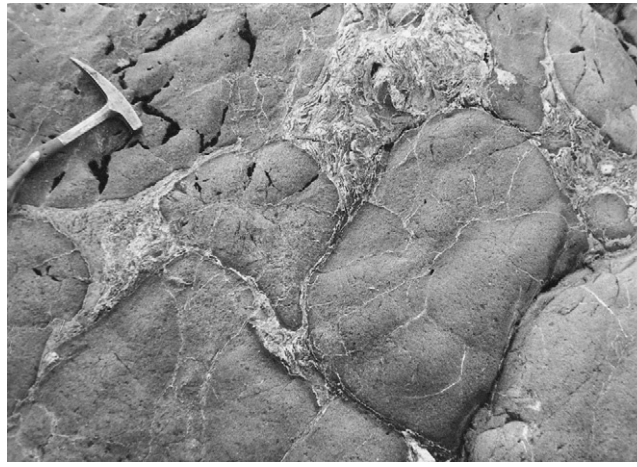

FIGURE 3.30 Pillows in Archean basalts from the Abitibi greenstone belt in southern Ontario.

altered and silicified, probably from oceanic hydrothermal fluids in a manner similar to that characteristic of modern oceanic arcs and ocean ridges. Three general trends observed with increasing stratigraphic height in some late Archean greenstone successions are (1) a decrease in the amount of komatiite, (2) an increase in the ratio of volcaniclastics to flows, and (3) an increase in the abundance of altered volcanics and in the abundance of felsic volcanics. These changes reflect an evolution from voluminous oceanic eruptions of basalt and komatiite, commonly referred to as a **mafic plain** (oceanic plateau?), to more localized calc-alkaline and tholeiitic stratovolcanoes (volcanic arc), which may become emergent with time, and intervening sedimentary basins.

Archean submarine stratovolcanoes were in some respects similar to modern oceanic volcanoes in arc systems (Ayers & Thurston, 1985). Similarities include (1) a general upward change from basalts to calc-alkaline and tholeiitic volcanics, (2) eventual emergence of subaqueous volcanoes to form islands, (3) a linear alignment of volcanoes, and (4) flanking sedimentary aprons leading into basins between volcanoes. Differences between modern arc volcanoes and Archean volcanoes include (1) the occurrence of komatiites in many Archean volcanoes, (2) the bimodal character of some Archean volcanics, especially in older greenstone successions, (3) the paucity of Archean shoshonitic volcanics, (4) extensive hydrothermal silicification in the upper parts of volcanic cycles, and (5) thick, laterally continuous oceanic flows, which collectively form large oceanic mafic plains upon which Archean volcanoes grew.

Perhaps the most distinctive volcanic rock of the Archean is komatiite (Arndt et al., 2008). **Komatiites** are ultramafic lava flows (or hypabyssal intrusives) that exhibit a quench texture known as spinifex texture and contain >18% MgO. Although komatiites are common in mafic plain Archean greenstone successions, they are uncommon in the Proterozoic and very rare in the Phanerozoic. Spinifex texture is commonly preserved in the upper parts of komatiite flows. This texture is characterized by randomly oriented skeletal crystals of olivine or pyroxene (Figure 3.31), and forms by rapid cooling in the near absence of crystal nuclei. Archean komatiite and basalt flows range from about 2 to >200 m thick, are commonly pillowed, and may be associated with sills or hyaloclastic rocks of similar composition. Intrusive mafic and ultramafic igneous rocks are also found in most greenstone successions and geochemical studies indicate they are closely related to enclosing volcanic rocks. Archean komatiitic and mafic volcanics are depleted in incompatible elements and show variable amounts of light-REE depletion. While Archean mafic plain basalts have incompatible element distributions similar to those of modern oceanic plateaus or less commonly, oceanic crust, Archean calc-alkaline basalts (associated with andesites and felsic volcanics) show a distinct subduction zone geochemical component (Condie, 1989, 1994).

Andesites and felsic volcanic rocks in greenstone successions occur chiefly as volcaniclastic rocks and minor flows. Tuffs, breccias, and agglomerates are common, and their distribution can be used to define volcanic centers. Archean

FIGURE 3.31 Spinifex texture in an Archean komatiite from the Barberton greenstone in South Africa (×6). Radiating crystals are serpentine pseudomorphs after olivine.

andesites are similar to modern andesites from volcanic arcs in incompatible element distributions. Alkaline volcanic rocks are rare in Archean greenstone successions and when found, occur chiefly as volcaniclastics and associated hypabyssal intrusives.

Greenstone Sediments

Four types of sediments are recognized in Archean greenstones (Mueller, 1991; Lowe, 1994b), which are, in order of decreasing importance, volcaniclastic, chemical, biochemical, and terrigenous sediments. Volcaniclastic sediments (including graywackes) range from mafic to felsic in composition and are commonly turbidites. Chemical and biochemical sediments, principally chert, banded iron formation, and carbonate, are of minor importance but of widespread distribution, and terrigenous sediments such as shale, quartzite, arkose, and conglomerate are of only local significance. Although plutonic sources are of importance in some graywackes, most greenstone detrital

sediments are clearly derived from nearby volcanic sources. Layered chert and banded iron formation are the most important nonclastic sediments in greenstones. Most cherts are very local in extent and are probably hydrothermal vent deposits. The earliest evidence of life on Earth occurs in the form of microstructures in Archean cherts. Few if any Archean cherts appear to represent pelagic sediments. Low $\delta^{18}O$ values for many Archean cherts support a volcanigenic origin. Carbonates and barite are very minor components in some greenstone belts. The barites appear to represent hydrothermal deposits and the carbonates, either hydrothermal or evaporite-related deposits.

Five different sedimentary environments are recognized in Archean greenstones (Lowe, 1994b). In some greenstones, such as the Northern Volcanic zone in the Abitibi belt, more than one sedimentary environment occurs in the same succession (Figure 3.32). The most widespread environment, especially in early Archean greenstones, is the mafic plain environment. In this setting, large volumes of basalt and komatiite were erupted to form a mafic plain, which may have risen to shallow depths beneath sea level or even became emergent. Sediments in this setting include hyaloclastic sediments, chert, banded iron formation, carbonate, and locally, shallow-water evaporites and barite. These rocks, which commonly preserve primary textures such as mudcracks, oolites,

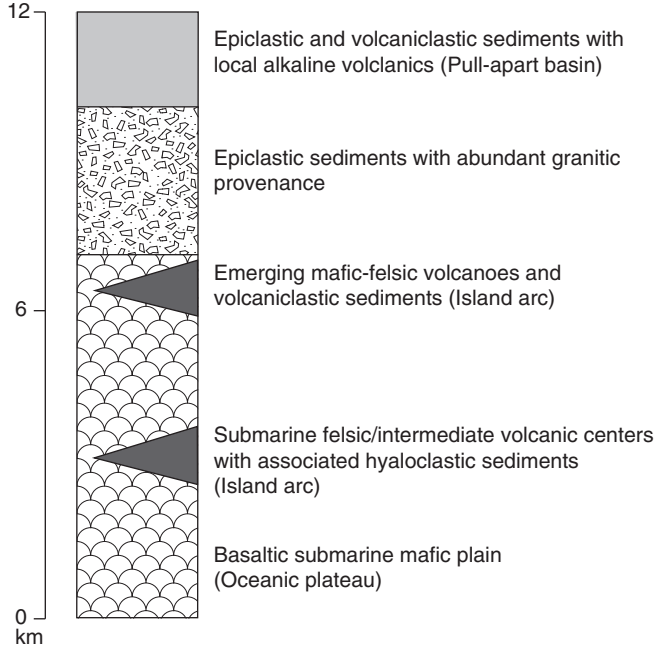

FIGURE 3.32 Generalized stratigraphic section of the Northern Volcanic Zone in the Abitibi greenstone belt, Quebec, showing the major lithologic assemblages. *Modified after Lowe (1994b).*

and gypsum casts, indicate shallow-water deposition. A second environment is a deepwater, nonvolcanic environment in which chemical and biochemical chert, banded iron formation, and carbonate are deposited. The third association, a graywacke-volcanic association very widespread in late Archean greenstones, and often stratigraphically on top of the mafic plain succession, is composed chiefly of graywackes and interbedded calc-alkaline volcanics and may have been deposited in or near island arcs. Fluvial and shallow-marine detrital sediments probably deposited in pull-apart basins, and mature sediments (quartz arenites, etc.) deposited in continental rifts, are the last two environments. These two environments are not volumetrically important in most Archean greenstones, although the pull-apart basin setting is widespread.

Granitoids

Granitoids associated with Archean greenstones fall into one of three categories: gneissic complexes and batholiths, diapiric syntectonic plutons of variable composition, and late discordant granite plutons (Martin, 1994; Sylvester, 1994). Gneissic complexes and batholiths, which are dominantly tonalite, trondhjemite, and granodiorite, the so-called **TTG suite**, comprise most of the preserved Archean crust. They contain large infolded remnants of supracrustal rocks as well as numerous inclusions of surrounding greenstone belts. Contacts between TTG complexes and greenstones are generally intrusive and usually strongly deformed. Granitic plutons range from foliated to massive, discordant to concordant, and some are porphyritic. Geophysical studies indicate that most Archean plutons extend to depths of less than 15 km. Diapiric plutons have well-developed concordant foliation around their margins and appear to have been deformed during forceful injection. Others, which are post-tectonic, are usually granite (*sensu strictu*) in composition and have discordant contacts and massive interiors. Most of these are post-tectonic (anorogenic?) plutons with A-type characteristics.

All but the post-tectonic granites are geochemically similar to felsic volcanics in greenstones. Together with their common syntectonic mode of emplacement, this fact suggests that most granitoids and felsic volcanics are genetically related. In areas where detailed U-Pb zircon chronology is available, such as in parts of the Superior Province in Eastern Canada, entire cycles of volcanism, sedimentation, deformation, and plutonism occur in <50 Ma, and late discordant granites are generally emplaced during the following 50 Ma. In some early Archean greenstones (Pilbara, Barberton), plutonism can continue for up to 500 Ma after major volcanism.

Geochemically, the TTG suite and most diapiric plutons are I-type granitoids, and they are extremely depleted in heavy REE (Martin, 1995). Most show a subduction geochemical component (Ta-Nb depletion) and no significant Eu anomalies. Geochemical and experimental data favor an origin for these rocks as partial melts of garnet amphibolites or eclogites in the deep crust. Archean

post-tectonic and anorogenic granites are calc-alkaline, strongly peraluminous, and commonly have A- or S-type affinities (Sylvester, 1994). They appear to be the products of partial melting of igneous and sedimentary rocks in the lower crust.

MINERAL AND ENERGY DEPOSITS

Plate tectonics provides a basis for understanding the distribution and origin of mineral and energy resources in space and time (Rona, 1977; Sawkins, 1990). The occurrence of energy and mineral deposits can be related to plate tectonics in three ways: (1) geologic processes driven by energy liberated at plate boundaries control the formation of energy and mineral deposits; (2) deposits form in specific tectonic settings, which are controlled by plate tectonics; and (3) reconstruction of fragmented supercontinents can be used in exploration for new mineral and energy deposits. In attempting to relate mineral and energy deposits to plate tectonics, it is important to know the relationship between the deposits and their host rocks. If deposits are syngenetic with host rocks, then they formed in the same tectonic setting. If, however, mineral and energy deposits are secondary in origin and entered the host rocks later (such as by hydrothermal fluids or migration of oil), they may have formed in a tectonic setting different from the host rocks. Major *in situ* mineral and energy deposits in various tectonic settings are summarized in Table 3.1.

Mineral Deposits

Ocean Ridges

Employing deep-sea photography and using small submersibles, numerous hydrothermal fields have been identified on ocean ridges (Rona et al., 1986; Von Damm, 1990). The submersibles allow direct observations and measurements on the seafloor. On the Galapagos and Juan De Fuca ridges, hydrothermal veins ranging in size from 500 to 1600 m^2 are spread along fissure systems for 500–2500 m. The TAG hydrothermal field on the Mid-Atlantic Ridge (26 °N) occurs along a fault zone on the east wall of the medial rift valley, and vent waters have temperatures up to 300°C. Animal communities living near the vents appear to be totally dependent on energy derived from seawater–rock reactions and sulfur-oxidizing bacteria. Seafloor observations also indicate that hydrothermal vents are locally developed in areas of the youngest seafloor and occur along both fast and slow-spreading ridge segments. Each hydrothermal field has multiple discharge sites, with sulfide chimneys rising up to 10 m above the seafloor. Minerals recovered from chimneys are chiefly Fe, Cu, and Au sulfides with minor amounts of anhydrite and amorphous silica (Humphris et al., 1995). Hydrothermal waters are acid, rich in H_2S, and are major sources of Mn, Li, Ca, Ba, Si, Fe, Cu, and Au. These metals are either deposited in the chimneys or with sediments near the vents.

TABLE 3.1 Summary of Major Mineral and Energy Deposits by Tectonic Setting

Tectonic setting	Mineral deposit	Energy deposit
Oceanic Settings		
a. Ophiolite	Cyprus-type Cu-Fe massive sulfides; podiform chromite	
b. Ocean ridge		Geothermal
c. Back-arc basin		Hydrocarbons
Subduction Zone		
a. Arc	Hydrothermal: Au, Ag, Cu, Mo, Pb, Sb, Hg, Sn, W Porphyries: Cu, Mo, Sn Massive sulfides: Cu, Pb, Zn	Geothermal Hydrocarbons
b. Foreland basin	Red bed U, V, Cu	Hydrocarbons Coal
c. Forearc basin		Hydrocarbons
Orogens		
a. Highlands	Sn-W granites Gemstones Deposits from older tectonic settings	
b. Foreland/ hinterland basin	Redbed U, V, Cu Stratiform Pb-Zn-Ag	Hydrocarbons Oil shale Coal
Continental rifts	Stratiform Pb-Zn REE, Nb, U, Th, P, Cl, F, Ba, Sr associated with alkaline intrusives Sn granites Stratiform Cu Evaporites	Geothermal
Cratons, passive margins	Diamonds (kimberlites) Bauxite Ni laterite Evaporites Clays	Hydrocarbons Coal
Archean greenstones	Cu-Zn massive sulfides Ni-Cu sulfides Au quartz veins	

The hydrothermal water erupted along ocean ridges is seawater that has circulated through hot oceanic crust with thermal gradients of >150°C/km. The seawater circulates by convection through the upper part of the permeable crust (1–2 km deep), and is heated at depth and discharges along active fissures in the medial rift. The discharging water leaches metals from the oceanic crust and alters the crust by additions of H_2O and elements such as Mg. Upon erupting on the seafloor, the hydrothermal waters are rapidly cooled and increase in pH resulting in deposition of sulfides and sulfates.

In considering ancient oceanic crust, two major mineral deposits are formed in ophiolites: Cyprus-type Cu-Fe massive sulfides and podiform chromite. Cyprus-type ores occur as stratiform deposits in pillowed basalt layers. These ores are exhalative deposits formed by hydrothermal vents along ancient ocean ridges as described above. Podiform chromite deposits are formed in ultramafic cumulates, and relict textures suggest they are the products of fractional crystallization.

Arc Systems

Metalliferous mineral deposits are important in both continental-margin arcs and island arcs. Base metals (Zn, Cu, Mo, Pb), precious metals (Ag, Au), and other metals (Sn, W, Sb, Hg) are found in hydrothermal veins and lodes formed in arc systems. Following erosion, placer deposits of these metals are important in some geographic areas. Veins and lodes are commonly associated with volcanics or granitic plutons, where they represent late-stage fluids derived from differentiated arc magmas. Cu, Mo, and Sn porphyry deposits are formed also in arc systems. These large-volume, low-grade disseminated deposits occur in altered porphyritic granites and are important sources of Cu and Mo in the Southwestern United States and in the Andes. Kuroko-type massive sulfides (Cu, Pb, Zn) are important in intra-arc and back-arc basin successions where they have formed as exhalatives on the seafloor. Redbed U, V, and Cu deposits occur in some retroarc foreland basins such as in the Mesozoic redbeds of the Colorado Plateau.

Zonation of metallic mineral deposits has been reported in Late Tertiary rocks from the Andes (Sillitoe, 1976). In the direction of the dipping lithospheric slab, the major metallic mineral zones encountered are contact metasomatic Fe deposits, Cu, Au and Ag veins, porphyry Cu-Mo deposits, Pb-Zn-Ag vein and contact metasomatic deposits, and Sn and Mo vein and porphyry deposits. Zonation is believed to result from progressive liberation of metals from the descending slab, with Sn coming from an extreme depth of about 300 km. Geochemical and isotopic data support the general concept that metal deposits associated with subduction are derived from some combination of the descending slab and the overlying mantle wedge. Metals move upward in magmas or in fluids and are concentrated in late hydrothermal or magmatic phases.

Orogens

Metalliferous deposits are abundant at collisional boundaries where a variety of tectonic settings exist, depending on location and stage of evolution. In addition, older mineral deposits associated with ophiolites, arc, craton, and continental rift assemblages occur in collisional zones. Sn and W deposits are associated with collisional leucogranites in the Himalayas and in the Variscan orogen, and at deeper crustal levels, Fe and Ti deposits occur associated with anorthosites. Many gemstones (ruby, sapphire) also are found in high-grade metamorphic rocks or in syntectonic nepheline syenites from collisional orogens. In peripheral foreland basins, stratiform Pb-Zn-Cu sulfides and redbed U-V-Cu deposits may be of economic importance.

Continental Rifts

Pb-Zn-Ag stratiform deposits occur in ancient continental rift sediments (Sawkins, 1990). These deposits, which are not associated with igneous rocks, occur in marine carbonates and are probably deposited from brines, which migrate to the edge of rift basins. REE, Nb, U, Th, Ba, P, Sr, and halogens are concentrated in carbonatites and other alkaline igneous rocks that occur in some continental rifts. Granites intruded during the late stages of rifting are often associated with Sr and fluorite. Stratiform Cu deposits occur in rift-related shales and sandstones as exemplified by deposits in the Zambian Copperbelt, where the Cu appears to be derived from associated basalts. Evaporites are important nonmetallic deposits found in some rifts.

Some of the major occurrences of Cr, Ni, Cu, and Pt are found in Proterozoic layered igneous intrusions. Chromite occurs as primary cumulates within the ultramafic parts of these intrusions and Cu and Ni generally occur as late-stage hydrothermal replacements. Pt occurs in a great variety of cumulus minerals, the most famous occurrence of which is the Merensky Reef in the Bushveld Complex in South Africa. In addition, some layered intrusions have magmatic ore deposits of Sn (in late granites) and Ti or V-rich magnetite.

Cratons and Passive Margins

Other than placer deposits, few if any metallic deposits are known to form on modern cratons or passive continental margins. Among the nonmetallic deposits formed in cratonic areas are diamonds from kimberlite pipes and associated placer deposits, bauxite, Ni-laterite deposits, and evaporites.

Important mineral deposits are the placer deposits of Au and U that occur in quartz arenites and conglomerates in cratonic successions. The largest deposits are in the Witwatersrand (3000 Ma) and Huronian (2400 Ma) Supergroups (Pretorius, 1976). Detrital Au and uraninite appear to have been concentrated by fluvial and deltaic processes in shallow-water, high-energy environments. Sources for the Au and U are older greenstone-granite terranes. Other important Proterozoic sedimentary mineral deposits include banded iron formation and

manganese-rich sediments. Banded iron formation, described more fully in Chapter 6, reached the peak of its development at about 2450 Ma. It occurs as alternating quartz-rich and magnetite (or hematite)-rich laminae and some was deposited in basins that are hundreds of kilometers across. Most banded iron formation is not associated with volcanic rocks and appears to have been deposited in shallow cratonic or passive margin basins. Manganese-rich sediments occur also in cratonic successions associated with carbonates.

Archean Greenstones

Some of the world's major reserves of Cu, Zn, and Au occur in Archean greenstone belts (Groves & Barley, 1995). Those greenstones $\geq$3.5 Ga contain only minor mineral deposits, including Cu-Mo porphyry and stockwork deposits and small occurrences of barite and banded iron formation. Late Archean greenstones contain major Cu-Zn massive sulfides associated with oceanic felsic volcanics and Ni-Cu sulfides associated with komatiites. The latter sulfides appear to have formed as cumulates by fractional crystallization of immiscible sulfide melts associated with komatiite magmas. Minor occurrences of banded iron formation occur in most late Archean greenstones. One of the most important deposits in greenstones is Au, which occurs in quartz veins and in late disseminated sulfides commonly associated with hydrothermal chert or carbonate deposits.

Energy Deposits

Several requirements must be met in any tectonic setting for the production and accumulation of hydrocarbons such as oil or natural gas. First of all, the preservation of organic matter requires restricted seawater circulation to inhibit oxidation and decomposition. High geothermal gradients are needed to convert organic matter into oil and gas and, finally, tectonic conditions must be such as to create traps for the hydrocarbons to accumulate. Several tectonic settings potentially meet these requirements (Table 3.1).

Both oil and gas are formed in forearc and back-arc basins, which can trap and preserve organic matter, and geothermal heat facilitates conversion of organic matter into hydrocarbons. Later deformation, generally accompanying continental collisions, creates a variety of structural and stratigraphic traps in which hydrocarbons can accumulate. An important site of hydrocarbon formation is in foreland basins. The immense accumulations in the Persian Gulf area formed in a peripheral foreland basin associated with the Arabia–Iran collision in the Tertiary.

The majority of the oil and gas reserves in the world have formed either in intracratonic or passive margin basins (Table 3.2). During the early stages of opening of a continental rift, seawater can move into the rift valley and if evaporation exceeds inflow, evaporites are deposited. This environment is also

TABLE 3.2 Oil Reserves in Devonian and Younger Reservoirs (in percent)

	Intracratonic basin	Passive margin	Foreland basin
Cenozoic	5	8	18[a]
Mesozoic	43	5	6
Paleozoic	13	1	1
Total	**61**	**14**	**25**

[a] *14% in the Persian Gulf and 4% elsewhere.*

characterized by restricted water circulation in which organic matter is preserved. As a rift continues to open, water circulation becomes unrestricted and accumulation of organic matter and evaporite deposition ceases. High geothermal gradients beneath an opening rift and increasing pressure due to burial of sediments facilitate the conversion of organic matter into oil and gas. At a later stage of opening, salt in the evaporite succession, because of its gravitational instability, may rise as salt domes and trap oil and gas. Oil and gas may also be trapped in structural or stratigraphic traps as they move upward in response to increasing pressures and temperatures at depth. Supporting this model are data from wells in the Red Sea, which represents an early stage of ocean-basin development. These wells encounter hydrocarbons associated with high geotherms and with rock salt up to 5 km thick. Also, around the Atlantic Basin there is a close geographic and stratigraphic relationship between hydrocarbons and evaporite accumulation.

Hydrocarbon production in intracratonic basins may also be related to plate tectonic processes (Rona, 1977). Increases in seafloor spreading rates and ocean-ridge lengths may cause marine transgression, which results in deposition in intracratonic basins. Decreasing spreading rates cause regression, which results in basins with limited circulation, and hence organic matter and evaporites accumulate. Unconformities also develop during this stage. Burial and heating of organic matter in intracratonic basins facilitates hydrocarbon production, and salt domes and unconformities may provide major traps for accumulation.

Coal is formed in two major tectonic settings: cratonic basins and foreland basins. For coal to form, plant remains must be rapidly buried before they decay, and such rapid burial occurs in swamps with high plant productivity. Widespread transgression in the Cretaceous was particularly suitable for coal swamps in cratonic areas. Swamps in foreland basins are generally part of large lake

basins, and the widespread late Paleozoic coals of central Europe appear to have formed in such environments. Oil shales can accumulate under similar conditions as exemplified by the oil shales in the early Tertiary foreland basins of eastern Utah.

Geothermal energy sources are associated with hotspots (such as Iceland and Yellowstone Park), arc systems (such as the Taupo area in New Zealand), and continental rifts (such as the Jemez site in New Mexico).

PLATE TECTONICS WITH TIME

As data continue to accumulate, it becomes more certain that plate tectonics in some form is the principal mechanism by which Earth has cooled for the last 4 Ga (Chapter 9). One way of tracking plate tectonics with time is with petrotectonic assemblages as summarized in this chapter. How far back in time do we see modern petrotectonic assemblages, and are their time/space relationships, tectonic histories, and chemical compositions similar to modern assemblages? Except for ophiolites, the greenstone and TTG assemblages are recognized throughout the geologic record from the oldest known rocks at 4.0–3.6 Ga to the present (Figure 3.33). The oldest well-preserved cratonic/passive margin sediments at 2.7–2.5 Ga are in the Kaapvaal craton in South Africa and the Pilbara Craton in Western Australia. Thus, it would appear that cratons,

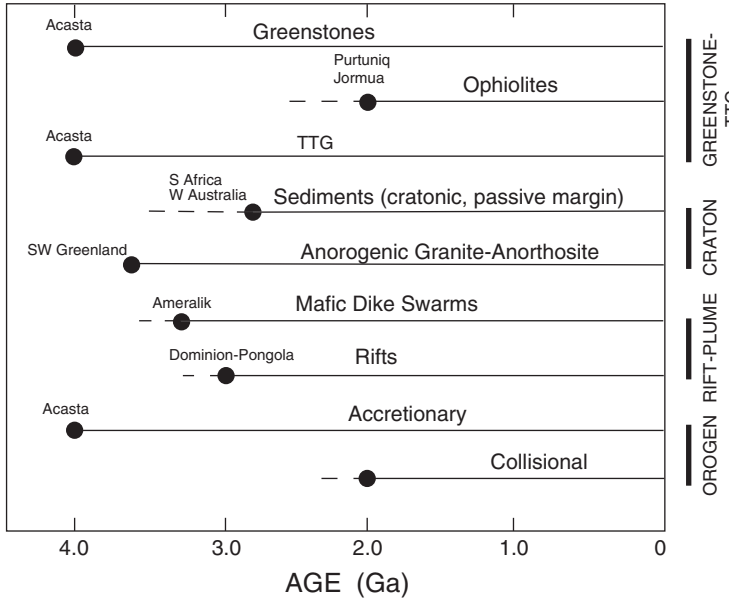

FIGURE 3.33 Distribution of petrotectonic assemblages with time.

although probably small, were in existence by the late Archean. Although the oldest isotopically dated mafic dyke swarm is the Ameralik swarm in Southwest Greenland intruded at about 3.25 Ga, deformed remnants of dykes in TTG complexes indicate that there were earlier swarms, perhaps as early as 4 Ga in the Acasta gneisses. The oldest dated anorogenic granite-anorthosite is in Southwest Greenland at about 3.7 Ga. Clasts of granite with anorogenic characters in conglomerates of the Moodies Group have igneous zircons with U-Pb isotopic ages of 3.6 Ga, indicating that highly fractionated granites also formed in other parts of the early Archean crust. The oldest known continental rift assemblages are in parts of the Dominion and Pongola Supergroups in South Africa, which were deposited on the Kaapvaal craton at about 3 Ga. The oldest accretionary orogens are the Acasta gneisses (4.0 Ga) and the Amitsoq gneisses (3.9 Ga) in Northwest Canada and Southwest Greenland, respectively. Although the oldest well-documented collisional orogens are Paleoproterozoic in age (such as the Wopmay orogen in Northwest Canada and the Capricorn orogen in Western Australia), it is likely that late Archean collisional orogens exist in the granulite terranes of East Antarctica and southern India.

Greenstones, TTG, anorogenic granites, mafic dyke swarms, and accretionary orogens all appear in the very earliest vestiges of our preserved geologic record at 4.0–3.5 Ga. Although some of these assemblages may have formed in non–plate tectonic settings, by 3.0–2.7 Ga, cratonic/passive margin sediments and continental rifts had appeared, recording the development of the earliest continental cratons and for the first time, a widespread distribution of plate tectonics seems unavoidable (see Chapter 9). Although plate tectonics appears to have been with us since at least 3 Ga, there are differences between some Archean and post-Archean rocks that indicate that Archean tectonic regimes must have differed in some respects from modern ones, and these are discussed in Chapter 9. These differences have led to the concept of having our cake and eating it too, or in other words, plate tectonics operated in the Archean, but differed in some ways from modern plate tectonics. We are now faced with the question of how and to what degree Archean plate tectonics differed from modern plate tectonics and what these differences mean in terms of the evolution of Earth.

FURTHER READING

Condie, K. C. (Ed.). (1994). *Archean Crustal Evolution* (528 pp). Amsterdam: Elsevier.

de Wit, M. J., & Ashwal, L. D. (1997). *Greenstone Belts* (840 pp). Oxford, UK: Oxford University Press.

Ernst, R. E., & Buchan, K. L. (Eds.). (2001). *Mantle Plumes: Their Identification Through Time* (593 pp). Special Paper 352. Geological Society of America.

Hatcher, R. D., Jr., Carlson, M. P., McBride, J. H., & Catalan, J. R. M. (2007). *4-D Framework of Continental Crust* (641 pp). Memoir 200. Geological Society of America.

Leitch, E. C., & Scheibner, E. (Eds.). (1987). *Terrane Accretion and Orogenic Belts.* (Vol. 19, 354 pp) Geodynamics Series. Geological Society of America-American Geophysical Union.

Moores, E. M., & Twiss, R. J. (1995). *Tectonics* (415 pp). New York: W. H. Freeman.

Olsen, K. H. (Ed.). (1995). *Continental Rifts: Evolution, Structure, Tectonics* (520 pp). Amsterdam: Elsevier.

Smellie, J. L. (1994). *Volcanism Associated with Extension at Consuming Plate Margins* (272 pp). Special Publication No. 81. Geological Society of London.

Stern, R. J. (2002). Subduction zones. *Reviews of Geophysics*, *40*(4), 3-1–3-38.

Treloar, P. J. (1993). *Himalayan Tectonics* (640 pp). Special Publication No. 74. Geological Society of London.

Windley, B. F. (1995). *The Evolving Continents* (3rd ed.). New York: John Wiley & Sons.

Chapter 4

The Mantle

INTRODUCTION

Earth's mantle plays an important role in the evolution of the crust and provides the thermal and mechanical driving forces for plate tectonics. Heat liberated by the core is transferred into the mantle where most of it (>90%) is convected through the mantle to the base of the lithosphere. The remainder may be transferred upward by mantle plumes generated in the core–mantle boundary layer. The mantle is also the graveyard for descending lithospheric slabs, and the fate of these slabs in the mantle is the subject of ongoing discussion and controversy. Do they partially collect at the 660-km discontinuity in the upper mantle or do they descend to the bottom of the mantle? Does what happens to these slabs control convection in the mantle? If they do not penetrate the 660-km discontinuity, the upper mantle may convect separately from the lower mantle, whereas if they sink to the base of the mantle, whole-mantle convection is probable. A related question is whether mantle plumes exist, and if they exist, how and where are they generated and what role do they play in mantle-crust evolution?

Another exciting mantle topic is that of the origin and growth of the lithosphere and if its role in plate tectonics has changed with time. The Archean continental lithosphere, for instance, is considerably thicker than post-Archean continental lithosphere, and geochemical data from xenoliths suggest it had quite a different origin. Still another hot topic is the origin of isotopic differences in basalts, which reflect different compositions and ages of mantle sources. How did these sources form and survive for billions of years in a convecting mantle? These are some of the questions we will address in this chapter.

SEISMIC STRUCTURE OF THE MANTLE

Upper Mantle

From studies of spectral amplitudes and travel times of body waves, we can refine details of the structure of the mantle. The P- and S-wave velocity structure beneath several crustal types is shown in Figure 4.1 (Helffrich & Wood, 2001).

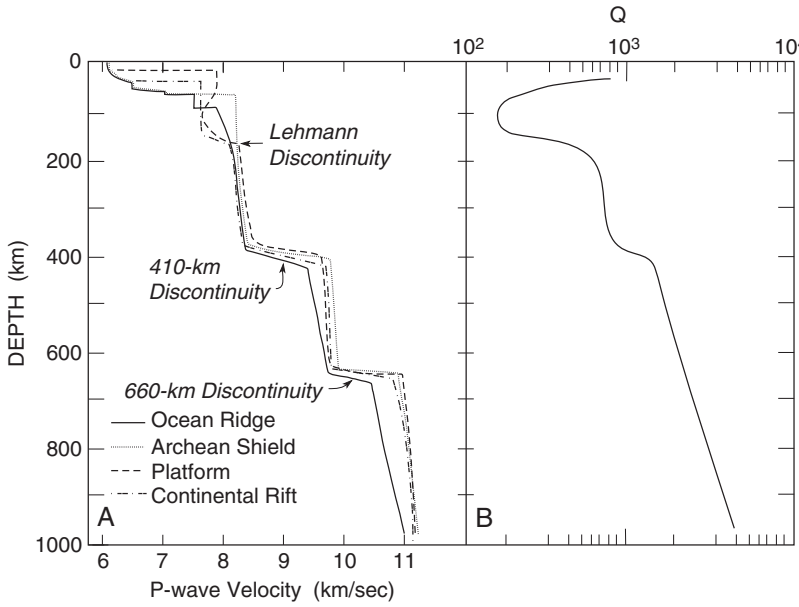

FIGURE 4.1 (A) P-wave velocity distribution in the mantle; (B) average distribution of Q, the specific attenuation factor, in the mantle (excluding regions beneath Precambrian shields). Q varies inversely with the amount of seismic wave attenuation, thus low values of Q show the greatest attenuation. The P-wave resolution is not sensitive enough to show the 520-km discontinuity in these sections. *Part (a), after Walck, 1985.*

Cratons are typically underlain by a high-velocity lid ($V_P > 7.9$ km/s) overlying, in turn, the low-velocity zone (LVZ) beginning at depths as shallow as 100 km and in some cases extending to depths of 300 km. A prominent minimum in Q, a measure of the attenuation of seismic wave energy, coincides with the LVZ (Figure 4.1). The top of the LVZ is generally assumed to mark the base of the lithosphere and averages 50–100 km deep beneath oceans. Beneath ocean ridges and most continental rifts, the LVZ may extend nearly to the Moho at depths as shallow as 10 km. The LVZ is minor or not detected beneath most Precambrian shields and may be nonexistent beneath Archean shields. The thickest lithosphere also occurs beneath shields ($\geq$200 km), and beneath Archean shields it may be >300 km thick.

At depths <200 km, seismic wave velocities vary with crustal type, whereas at greater depths the velocities are rather uniform regardless of crustal type. From the base of the LVZ to the 410-km discontinuity and from the 410-km discontinuity to the 660-km discontinuity, P-wave velocities increase only slightly (Figure 4.1). Unlike P waves, S-wave velocities show significant lateral variation in the upper mantle, indicating compositional heterogeneity and/or anisotropy. S-wave velocities beneath ocean ridges are strongly correlated with

spreading rates at shallow depths (<100 km), and very slow velocities are limited to depths of <50 km (Zhang & Tanimoto, 1993). Also, some hotspots are associated with very slow S-wave velocities.

Lower Mantle

In the lower mantle, seismic wave velocities continue to increase with depth and no further discontinuities are recognized until the D″ zone at the base of the mantle (Figure 1.2). However, seismic tomographic studies have shown that various "velocity domains" exist in both the upper and lower mantle. **Seismic tomography**, like its medical analogue, combines information from a large number of criss-crossing waves to construct three-dimensional images of the interior of Earth. Relatively hot and cool regions of Earth's interior can be mapped because seismic velocities vary inversely with temperature. Orientation of minerals in convecting mantle can also increase seismic velocities parallel to "fast" crystallographic axes of minerals. The accumulation of digital data from global seismic networks makes it possible to construct reliable three-dimensional models of mantle structure, and such information provides important constraints on the style of convection in Earth (Hager & Clayton, 1989; Boschi & Dziewonski, 1999).

Combining data from surface and body waves, we can compare the seismic structure of the upper and lower mantle. Models of seismic wave velocity distribution in the deep mantle clearly show that large inhomogeneities exist in the mantle on the scale of thousands of kilometers and that they extend to great depths (Li et al., 2008) (Figure 4.2). Low-velocity zones (in red, Figure 4.2) underlie ocean ridges to depths up to 450 km, especially evident beneath the northern Mid-Atlantic Ridge. At greater depths, large low-velocity regions underlie the South Pacific and southern Africa. High-velocity zones (in blue) underlie regions around the Pacific Basin and reflect recently subducted slabs. The high-velocity zone at 750 km extending from eastern North America into the northern part of South America probably represents the descending Farallon plate, an oceanic plate that is almost completely subducted. Although the origin and significance of all of the anomalies shown on these sections are not yet understood, the fact that many anomalies cross the 660-km discontinuity favors whole-mantle rather than layered-mantle convection.

MANTLE UPWELLINGS AND GEOID ANOMALIES

To balance subducted slabs that sink into the mantle, there must be an upward return flow. Because subducted plates are relatively cool, they decrease the temperature of nearby mantle, thus leaving relatively warm mantle in the regions between subduction zones. These broad, warm regions of mantle, known as **mantle upwellings** or **superplumes**, are relatively buoyant, and may provide the return flow in the mantle. A comparison of seismic images of these

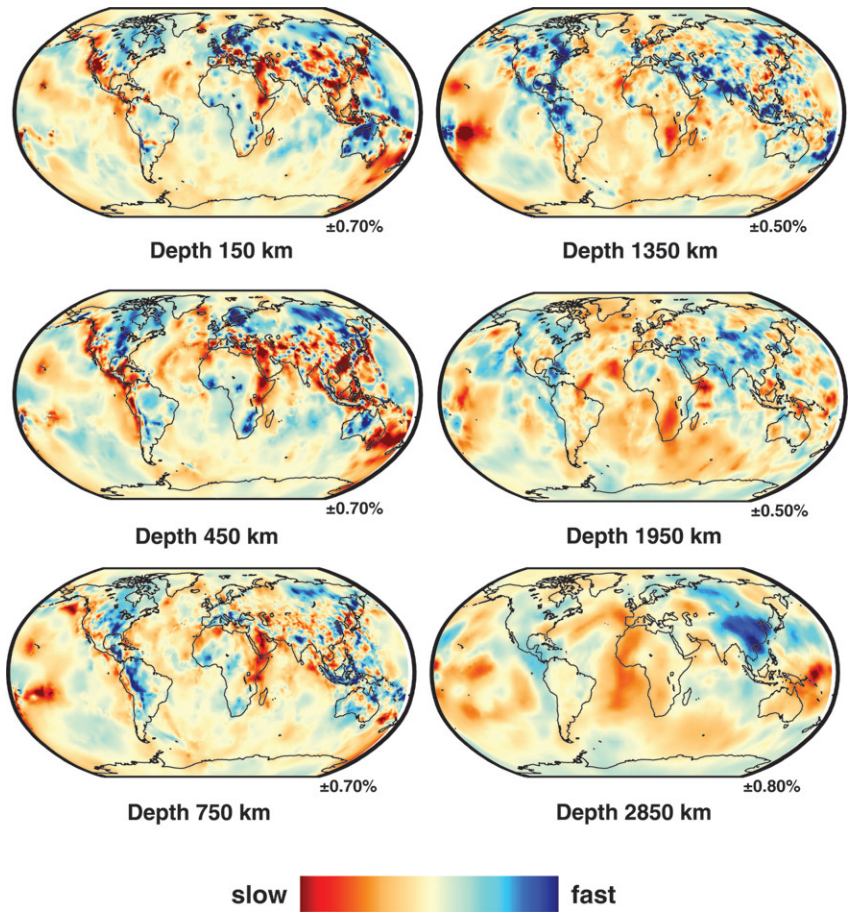

FIGURE 4.2 Global P-wave tomographic sections of Earth at various depths using the Robinson projection centered on Africa. Red refers to slow velocities and blue to fast velocities. *From Li et al. (2008). Reproduced with permission of American Geophysical Union, courtesy of Chang Li.*

upwellings with convection studies based on laboratory and numerical experiments suggests that the upwellings are relatively hot and perhaps chemically distinct from surrounding mantle. Today, two large upwellings are recognized in the mantle, one beneath the African plate and one beneath the Pacific plate (Maruyama, 1994; Ni & Helmberger, 2003). Anomalously low P- and S-wave velocity distributions in the mantle are consistent with the existence of these two upwellings, especially prominent at depths >500 km (red colors in Figure 4.2). Seismic images of the upwellings indicate that large-scale low-velocity anomalies (in excess of 1000 km) extend from the bottom of the mantle to a depth of about 1000 km (Suetsugu et al., 2009). In addition, small-scale anomalies occur along the tops and margins of the large upwellings, and these

may represent mantle plumes rising from the upwellings. As discussed more fully in Chapter 8, the mantle upwellings appear to form under large plates and especially beneath supercontinents, and their production may lead to the breakup of supercontinents.

An important characteristic of upwellings is that they contain most of the modern hotspots, and hence most of the modern mantle plumes. A possible explanation for this is that deep flow in a mantle upwelling, just above the core–mantle boundary, sweeps material upward, thus thickening the D″ layer. This promotes instability in D″, which gives rise to new plumes that rise within the upwelling. Consistent with this idea is the fact that plumes with the highest buoyancy flux are concentrated in the Pacific upwelling (Ribe & de Valpine, 1994). Also supporting this interpretation is the correlation of hotspots and seismic velocity anomalies with the geoid highs described below (Richards et al., 1989). Davaille (1999) has shown experimentally that upwellings and associated plumes (hotspots) can form with only a small amount of density layering ($\sim$1%) in the mantle.

The **geoid** is the gravitational equipotential surface of Earth and coincides with sea level in oceanic areas. Because gravitational potential decreases inversely with distance to source mass, whereas gravitational acceleration decreases inversely with the square of the distance, the geoid provides a long-range probe into Earth. Deviations of the geoid from an idealized hydrostatic ellipsoid are known as **geoid anomalies.** Because upwellings are hotter than surrounding mantle, they are less dense and produce a negative mass anomaly in the mantle. The upward flow elevates the surface of Earth and produces a positive geoid anomaly since air or water is being replaced with rock (Lassak et al., 2007). Because both of the terrestrial upwellings are characterized by large positive geoid anomalies, they can be contoured much like a topographic map (Figure 4.3). The core–mantle boundary is also raised beneath the upwellings (Figure 4.3b); that is, the upper and lower surfaces of the mantle (+ crust) are deformed in the same direction and in the same geographic locations. Of the order of 3 km of relief occurs on the core–mantle anomalies. Probability density models of the deep mantle indicate that the upwellings cannot be accounted for entirely by heating of the deep mantle. Results clearly show that compositional differences are at least partially responsible for the seismic wave anomalies and such differences are the dominant cause in the lower 1000 km of the mantle (Trampert et al., 2004). The fact that both the Pacific and African upwellings correspond to high rather than low density material supports this conclusion (Figure 4.4).

The bipolar nature of mantle upwellings is thought to be a fundamental characteristic of planets with plate tectonics. During the growth of the Pacific plate in the last 175 Ma, the center of the plate remained more or less symmetrical with respect to the equator centered over the Pacific upwelling (Pavoni, 1997). At 180°, Africa was centered over the other upwelling, with plates fragmenting from its margins and dispersing as Pangea broke up. Thus, the upwellings are bipolar with nearly fixed plates above them, and rifted plates

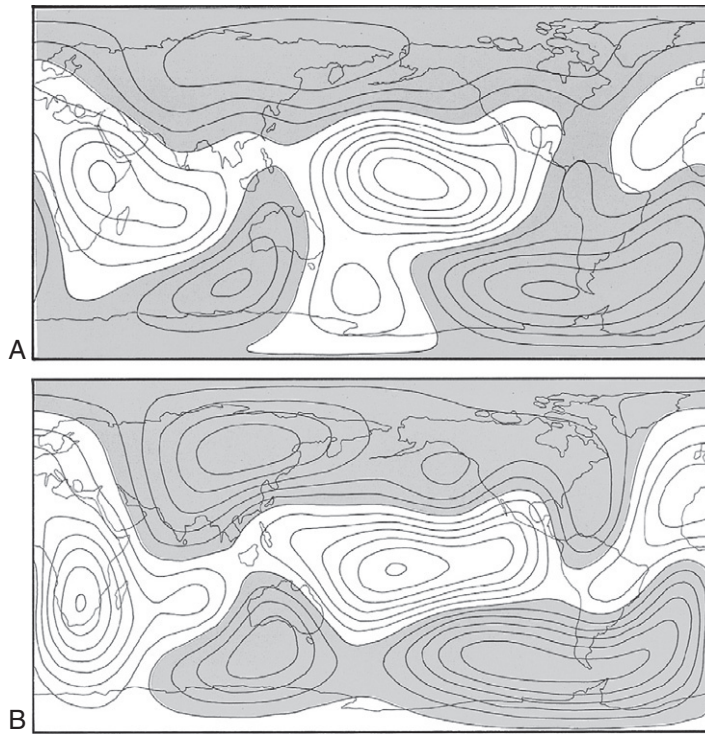

FIGURE 4.3 (A) The calculated geoid for a convecting Earth. Density contrast assumed equal to 2.3 g/cm^3, contour interval 200 m, and degrees 1–6. Geoid lows shaded. (B) Calculated topography at the core–mantle boundary. Density contrast across the boundary assumed to be 4.5 g/cm^3, contour interval 400 m, and degrees 1–6. Geoid lows shaded. *After Hager & Clayton (1987).*

spreading away from these two centers. This probably reflects bipolar convection in the mantle, which may be a fundamental feature of planets with plate tectonics and the supercontinent cycle.

TEMPERATURE DISTRIBUTION IN THE MANTLE

The most accessible energy measure for a planet is the total amount of heat released at the surface. Estimates of this range from about 43 to 49 terawatts (TW) averaging 46 $\pm$ 3 TW (Lay et al., 2008). Of the total radiogenic heat production for a chondritic Earth (20 TW), 6–8 TW comes from the crust (almost all from the continental crust) leaving 12–14 TW coming from radioactivity in the mantle (Figure 4.5). Cooling of the mantle supplies 8–28 TW (mostly from the lower mantle) and cooling of the core, 5–15 TW. In round numbers, about 40% of Earth's heat comes from radioactivity, another 40% from mantle cooling, and only 20% from cooling of the core.

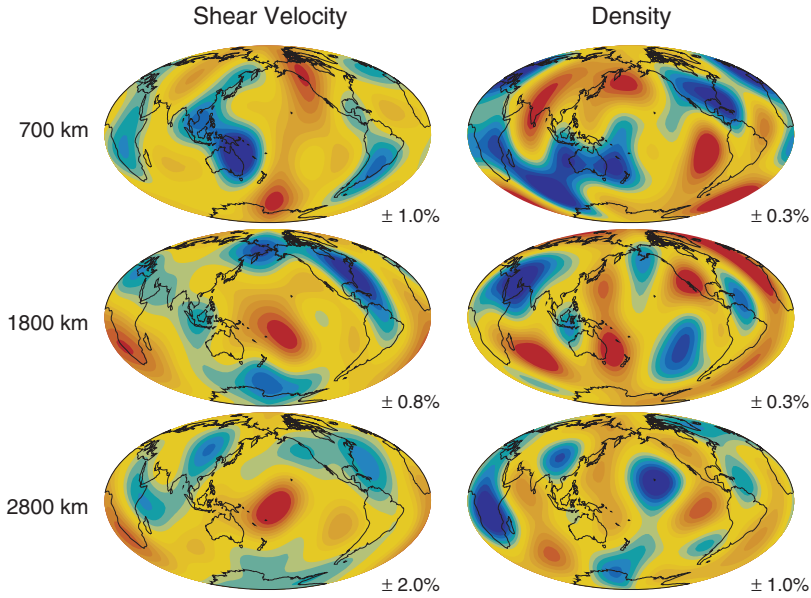

FIGURE 4.4 S-wave velocity distribution and calculated densities for three depths in the mantle. Colors as in Figure 4.2. *Courtesy of Maki Ishii.*

Estimates of temperatures in the lower crust and mantle can be made from surface heat flow measurements, models of heat production, and thermal conductivity distributions with depth (Artemieva & Mooney, 2001). **Convection** is the dominant mode of heat transfer in the asthenosphere and mesosphere where an adiabatic gradient is maintained, and thus temperature increases at a very slow rate with depth. This gradient, known as the **mantle adiabat**, is an idealized curve in P-T space describing a state in which heat is neither lost nor gained. In detail, the lithosphere comprises both a mechanical and a thermal boundary as shown in Figure 4.6. The mechanical boundary layer is separated from the asthenosphere by the thermal boundary layer in which small-scale convection occurs. The **mantle potential temperature** (T_p) is defined as the extrapolation of the mantle adiabat to Earth's surface. In contrast to the convecting mantle, heat is lost from the lithosphere by **conduction** where temperatures change rapidly with depth and with tectonic setting. C**onductive geotherms** show this heat loss in P-T space in Figure 4.7.

Although major differences in temperature distribution exist in the upper mantle, it is necessary for all geotherms to converge at depths of $\leq$400 km, or large unobserved gravity anomalies would exist between continental and oceanic areas. Heat flow distribution, heat production calculations, and seafloor spreading rates suggest that most geotherms to about 50 km deep range from 10 to 30°C/km. With the exception of beneath-ocean ridge axes, geotherms must

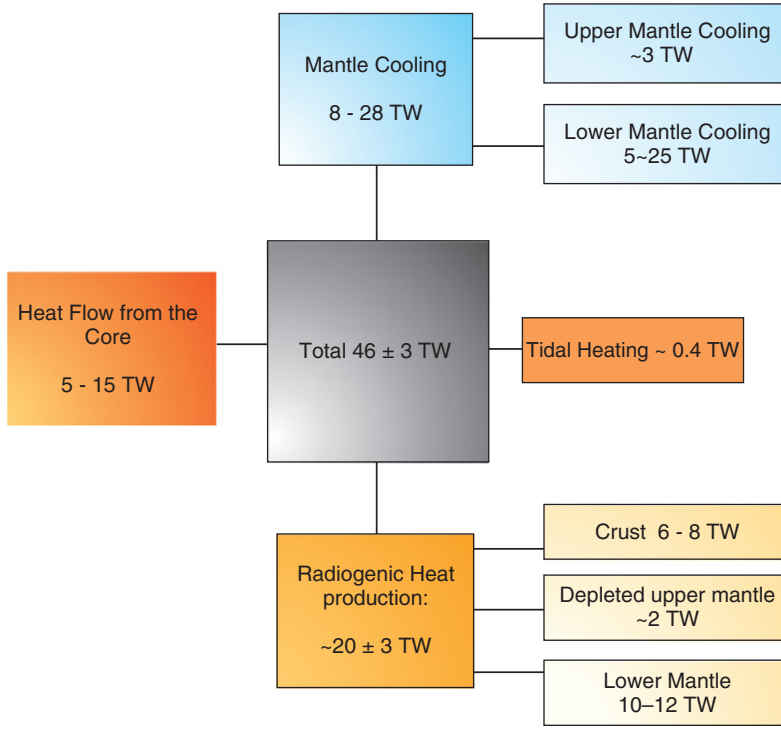

FIGURE 4.5 Global heat flow balance for Earth (TW, terawatts). *Modified after Lay et al. (2008). Courtesy of Thorne Lay. Used with permission of Nature Publishing Group, permission conveyed through Copyright Clearance Center, Inc.*

decrease rapidly between 50 and 200 km to avoid a large amount of melting in the upper mantle, which is not allowed by seismic or gravity data. Oceanic geotherms intersect the mantle adiabat at depths of <200 km, whereas continental geotherms intersect the adiabat at greater depths. Beneath ocean ridges (A, Figure 4.7) geotherms are very steep and intersect the **mantle solidus** (i.e., the temperature at which the mantle begins to melt) at depths of <50 km. Thus, ocean ridge basaltic magma is produced at shallow depths beneath ridges. With increasing distance from a ridge axis as the lithosphere cools, geotherms decrease at a rate inversely proportional to lithosphere spreading rates (Bottinga & Allegre, 1973). The decrease results in progressively greater depths of intersection of the geotherm with the mantle solidus, and hence to a deepening of the lower thermal boundary of the oceanic lithosphere as it ages. After about 100 Ma, the thermal lithosphere is about 100 km thick, in good agreement with thicknesses estimated from seismic surface wave studies. On average, neutral buoyancy of the oceanic lithosphere is reached at about 20 Ma, and further cooling leads to negative buoyancy and to subduction, where the mean age is about 120 Ma. Rarely are plates >100 km thick when they subduct.

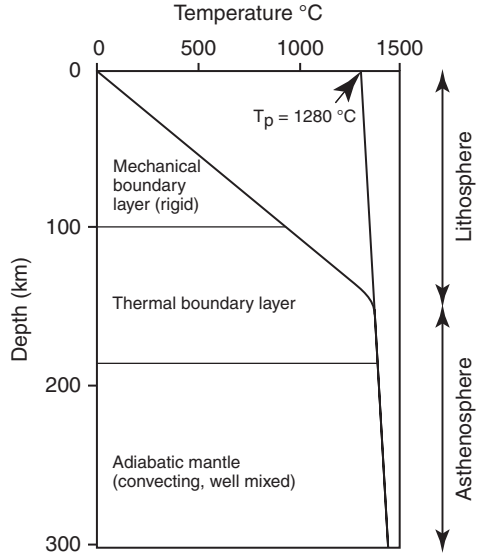

FIGURE 4.6 Thermal structure of the oceanic upper mantle showing the lithosphere-asthenosphere relationship and the mantle potential temperature T_p (extrapolation of adiabat to the surface).

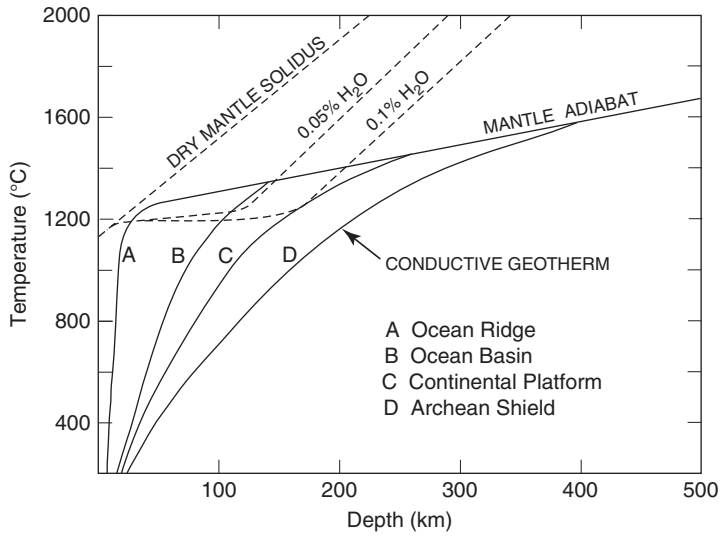

FIGURE 4.7 Typical lithosphere conductive geotherms. Note that geotherms intersect the mantle adiabat at variable depths. Also shown is the dry mantle solidus and mantle solidus with 0.1% and 0.05% H_2O.

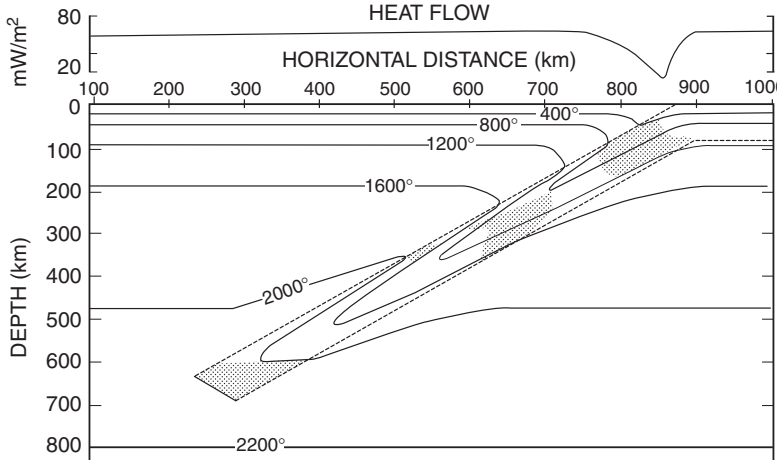

FIGURE 4.8 Temperature distribution in a descending slab 10 Ma after initiation of subduction for a spreading rate of 8 cm/y. Shaded areas are the gabbro-eclogite, olivine-wadsleyite, and the 660-km discontinuity phase changes, in order of increasing depth. *Modified after Toksoz et al. (1971).*

Geotherms beneath Archean shields are not steep enough to intersect the mantle solidus, whereas most other continental geotherms intersect a slightly hydrous mantle solidus at depths of 150–200 km (Figure 4.7). Subduction geotherms vary with the age of the onset of subduction. In most cases, however, they are not steep enough for the descending slab to melt. The temperature distribution beneath a descending slab 10 Ma after the onset of subduction is shown in Figure 4.8. Note that isotherms are bent downward as the cool slab descends, and the phase changes at 150 km (gabbro-eclogite) and 410 km (olivine-wadsleyite) occur at shallower depths in the slab than in surrounding mantle, in response to cooler temperatures in the slab. As slabs descend into the mantle, they warm up by heat transfer from surrounding mantle, adiabatic compression, frictional heating along the upper surface of the slab, and exothermic phase changes in the slab (Toksoz et al., 1971).

THE LITHOSPHERE

Understanding the structure and evolution of the lithosphere is critical to understanding the origin and evolution of both the oceanic and continental crust. Although the lithosphere can be loosely thought of as the outer rigid layer of Earth, more precise definitions in terms of thermal and mechanical characteristics are useful. For oceanic lithosphere, where cooling controls thickness, it is defined as the outer shell of Earth with a conductive temperature gradient overlying the convecting adiabatic interior (White, 1988; Jaupart & Mareschal, 1999; Jackson et al., 2008). Asthenosphere can be converted to oceanic lithosphere simply by cooling. The thickness of the rigid part of the outer layer of

Earth that readily bends under a load, known as the **elastic lithosphere**, is less than that of the thermal lithosphere. The base of the oceanic elastic lithosphere varies with composition and temperature increasing from about 2 km at ocean ridges to 50 km just before subduction. It corresponds roughly to the 500–600°C isotherm. In continental lithosphere, the elastic thickness is less than the crustal thickness, often by 10–15 km. Unlike the oceanic lithosphere, the continental lithosphere is thick, old, and relatively strong. Archean subcontinental lithosphere represents a thick, cold underplate that is probably responsible for the preservation of Archean cratons. In addition, it has higher P- and S-wave velocities than its post-Archean counterparts. Subcontinental lithosphere is a mantle domain that is isolated from the rest of the mantle and provides a source of information on early Earth processes and evolution.

The mineralogical and chemical composition of the mantle lithosphere can be approximated from the combined results of seismic velocity distributions, high-pressure and -temperature experimental studies, and geochemical and isotopic studies of mantle xenoliths. Several lines of evidence indicate that ultramafic rock composes most of the upper mantle. Geochemical, isotopic, and seismic studies all agree that the mantle is heterogeneous. The distribution of radiogenic isotopes in basalts clearly indicates the existence of distinct mantle reservoirs that have been in existence for more than 10^9 years. The sizes, shapes, and locations of these reservoirs, however, are not well constrained by the isotopic data and it is only through increased resolution of seismic velocity distributions that these reservoirs can be more accurately characterized.

Oceanic Lithosphere

Oceanic lithosphere is produced at ocean ridges and cools, thickens, and increases in age as it moves away from ridges. The standard model involves cooling by conduction and increasing in thickness until about 70 Ma, reaching a maximum thickness of about 120 km. In contrast, the underlying asthenosphere is mixed by shallow convection and is thought to convert to lithosphere by cooling with little or no change in composition. Between the oceanic lithosphere and asthenosphere is a thermal boundary layer about 80 km thick in which small-scale convection occurs (Figure 4.6). As expected, hotspots (plumes), such as Hawaii and Iceland, are associated with slow velocities between 50 and 200 km deep. Thermal and geochemical modeling has shown that oceanic lithosphere can be thinned by as much as 50 km by extension over mantle plumes (White & McKenzie, 1995).

Both P- and S-wave splitting is observed in the depth range of 80–220 km in the oceanic lithosphere. This anisotropy develops in response to the alignment of olivine and pyroxene that accompanies seafloor spreading with the [100] axes of olivine and [001] axes of orthopyroxene oriented normal to ridge axes (the higher velocity direction) (Estey & Douglas, 1986). Supporting evidence for alignment of these minerals comes from studies of ophiolites and upper

mantle xenoliths, and flow patterns in the oceanic upper mantle can be studied by structural mapping of olivine orientations (Nicholas, 1986). The mechanism of mineral alignment requires upper mantle shear flow, which aligns minerals by dislocation glide. The crystallographic glide systems have a threshold temperature necessary for recrystallization of about 900°C, which yields a thermally defined lithosphere depth similar to that deduced from seismic data (~100 km). Creep actively maintains mineral alignment below this boundary in the LVZ, and it is preserved in a fossil state in the overlying lithosphere. Together with a relatively constant seismic lid thickness beneath the Pacific, results suggest that the oceanic lithosphere is a dry, chemically depleted layer overlying hydrated, fertile, and possibly partially molten asthenosphere. Because this layer lies in the same depth range in the Pacific, regardless of plate age, it suggests a rather uniform lithosphere thickness, whereas cooling models predict thickening of the lithosphere with age (Fischer et al., 2010). Although still not understood, it is possible that the constant depth range of the anisotropic layer reflects gradual cooling of the mantle beneath the aging oceanic lithosphere. Changes in hydration, fertility, and amount of melting beneath this lithosphere may also contribute to deviation from the standard cooling model.

Continental Lithosphere

Composition

Seismic Velocity Constraints

Studies of density and S-wave velocity distribution provide strong evidence of compositional variations in the subcontinental lithosphere (van Gerven et al., 2004). Laboratory measurements of seismic velocities at pressures up to 5 GPa provide valuable constraints on mineral assemblages in this part of the upper mantle (Christensen, 1966; Christensen & Mooney, 1995). Dunite, pyroxenite, harzburgite, various lherzolites, and eclogite or some mixture of these rock types are consistent with observed P-wave velocities in the upper mantle. Higher than normal temperatures and/or some combination of garnet granulite or serpentinite may account for regions with anomalously low velocities ($V_P <$ 8.0 km/s). Measured velocities of highly serpentinized ultramafic rocks (5.1–6.5 km/s), however, are too low for most upper mantle. The high temperatures characteristic of the upper mantle also exceed the stability of serpentine, thus greatly limiting the extent of even slightly serpentinized lherzolite in the mantle.

The subcontinental lithosphere exhibits seismic anisotropy of S waves parallel to the surface of Earth. This is evidenced by **S-wave splitting**, in which the incident wave is polarized into two orthogonal directions traveling at different velocities (Silver & Chan, 1991). As with the oceanic lithosphere, this seismic anisotropy also appears to be caused by a strain-induced preferred orientation of anisotropic crystals such as olivine. Seismic and thermal modeling indicates

that the continental anisotropy occurs within the lithosphere at depths of 150–400 km. The major problem in the subcontinental lithosphere has been to determine how and when such alignment occurred in tectonically stable cratons. Was it produced during assembly of the craton or supercontinent or is it a recent feature caused by deformation of the base of the lithosphere as it moves about?

Complicating the definition of the base of lithosphere are results that show a rather sharp boundary beneath Precambrian cratons at an 80- to 95-km depth (Rychert & Shearer, 2009; Fischer et al., 2010). Recent studies using seismic wave receiver functions show the distinct presence of two lithospheric layers in North America with strikingly different seismic anisotropies (Yuan & Romanowicz, 2010). The top layer is about 150 km thick and tapers outward to Phanerozoic continental margins, whereas the second layer (180–240 km thick) is relatively flat, consistent with the existence of a thermal conductive root that wraps around the depleted top layer (Figure 4.9). The second layer may have been accreted during assembly of the Laurentian craton in the Paleoproterozoic, as supported by the correlation of the fast axis direction with northeast to east-trending sutures that weld some of the Archean blocks together. In contrast to the two upper layers, at the lithosphere–asthenosphere boundary (LAB), the azimuth of the fast S wave is closely aligned with the direction of absolute plate motion for the last 100 Ma (Figure 4.10) (Silver & Chan, 1991; Vinnik et al., 1995; Marone & Romanowicz, 2007). This coincidence indicates that the anisotropy is not a Precambrian feature, but results from resistive drag along the base of the lithosphere related to present-day plate motions.

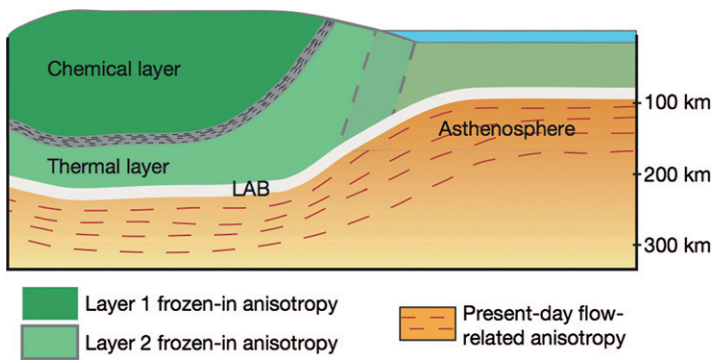

FIGURE 4.9 Diagrammatic cross section of lithospheric structure of an Archean craton based on seismic anisotropy (based on the Superior Province in North America). LAB, lithosphere-asthenosphere boundary. Layer 1 is depleted thick Archean keel and layer 2 is a thermal layer probably accreted during assembly of the craton during the Paleoproterozoic. *From Yuan & Romanowicz (2010), courtesy of Barbara Romanowicz. Used with permission of Nature Publishing Group, permission conveyed through Copyright Clearance Center, Inc.*

FIGURE 4.10 Fast S-wave velocity directions in the subcontinental lithosphere compared to motion directions of modern plates (bold arrows). *After Silver & Chan (1991).*

Mantle Xenoliths

Mantle xenoliths are fragments of the mantle brought to Earth's surface during volcanic eruptions. They are common in alkali basalts and in kimberlite pipes and provide an important constraint on mineral assemblages in the upper mantle. Experimental studies of coexisting minerals at elevated temperature and pressure, known as **thermobarometry studies**, provide a means to constrain the temperature and pressure at which xenoliths last crystallized in the mantle (Ryan et al., 1996; O'Reilly et al., 1997). Results sometimes define a P-T curve, which may be a "**paleogeotherm**" through the lithosphere (O'Reilly & Griffin, 1985; Boyd, 1989). Supporting such an interpretation is the fact that these P-T paths are similar in shape to calculated modern geotherms.

From measured seismic velocities, mantle xenolith compositions, and high-pressure experimental data, possible upper mantle mineral assemblages are shown in Figure 4.11. Also shown are the mantle solidus and ocean ridge, ocean basin, and Archean shield geotherms. Xenoliths from kimberlites indicate sources with depths >100 km, and those from alkali basalts record depths of 50–100 km. The data are consistent with an upper mantle lithosphere beneath both the oceans and post-Archean continents composed chiefly of spinel lherzolite (olivine-cpx-opx-spinel) and lherzolite (olivine-cpx-opx), whereas in the thick Archean lithosphere and in the asthenosphere, garnet lherzolite (olivine-cpx-opx-garnet) is the dominant rock type. Although measured seismic wave velocities also allow dunite (all olivine), pyroxenite (all pyroxenes),

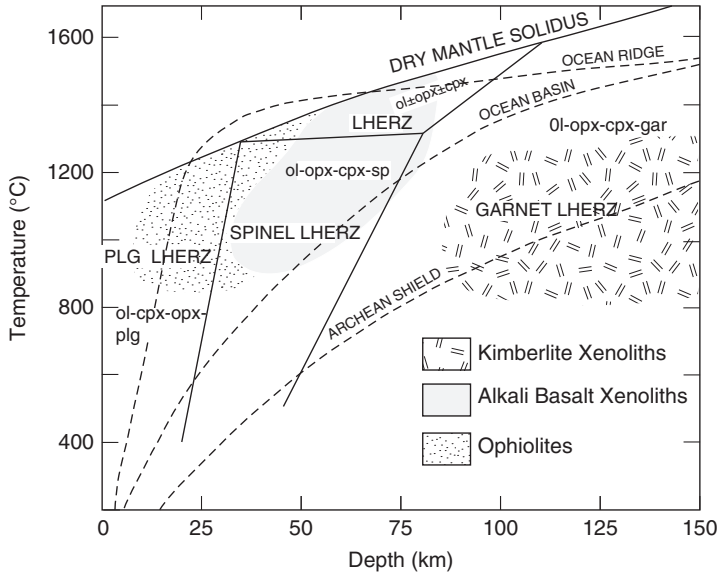

FIGURE 4.11 Stability fields of mantle mineral assemblages in pressure-temperature space. Also shown are lithosphere geotherms and the dry mantle solidus. sp, spinel; plg, plagioclase; gar, garnet; ol, olivine; cpx, clinopyroxene; opx, orthopyroxene; LHERZ, lherzolite.

eclogite (garnet-cpx), and harzburgite (olivine-opx) in the upper mantle, the fact that the first three of these rocks are not abundant in xenolith populations or ophiolites suggests that they are not important constituents in the upper mantle. Harzburgites, however, are widespread in most ophiolites and may be the most important rock type in the shallow oceanic upper mantle. As suggested by the steep ocean ridge geotherm in Figure 4.11, some ophiolite ultramafics are dominantly plagioclase lherzolite (olivine-cpx-opx-plag). Ultramafic rocks from ophiolites record source depths of 10–75 km, and verify the interpretation that they are slices of the oceanic upper mantle. Ophiolites interpreted as fast-spreading ocean ridges (>1 cm/y) commonly contain harzburgites from which >20% basaltic melt has been extracted. Ophiolites from slow-spreading ridges (<1 cm/y) record less melt extraction (<20%) and a residual mineral assemblage in which plagioclase lherzolite dominates.

One of the exciting applications of thermobarometry is to "map" the distribution of mantle mineral assemblages in the lithosphere with increasing depth. With multiple sample locations, mantle lithosphere stratigraphy can be mapped and followed laterally producing three-dimensional images of the lithosphere that can be correlated with geophysical data and surface geology (Figure 4.12) (Griffin et al., 1999; Poudjom Djomani et al., 2001). The fact that lithosphere domains often correlate with crustal age provinces implies that crustal province boundaries are really lithospheric boundaries and that each

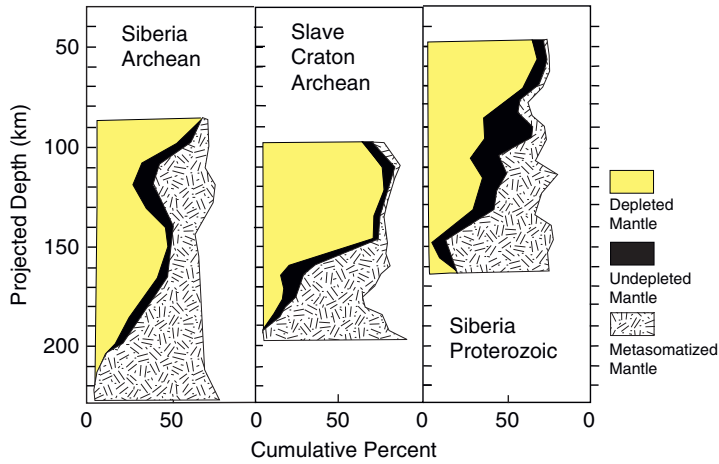

FIGURE 4.12 Compositional cross sections of the subcontinental lithosphere based on geochemical data from mantle xenolith and xenocryst populations. *Modified after Griffin et al. (1999).*

province carried its own lithospheric root during assembly of cratons and supercontinents. In the Slave Province in northwestern Canada, lithosphere mapping suggests two layers, with the upper layer (100–150 km) consisting of depleted harzburgite and the lower layer (150–220 km) of less depleted and metasomatized lherzolite (Figure 4.12). Although the lithosphere is thinner, a similar pattern is shown by Proterozoic lithosphere in Siberia. In the Archean Siberian lithosphere, however, the metasomatized layer extends to shallower depths.

Chemical Composition

Using the compositions of mantle xenoliths together with the results of model calculations, estimates of the average composition of primitive mantle, mantle lithosphere, and depleted mantle are given in Table 4.1. All four estimates have a combined total of more than 90% of MgO, SiO_2, and FeO, and no other oxide exceeds 4%. In a plot of modal olivine versus the Mg number of olivine, ophiolite ultramafics and spinel lherzolite xenoliths from post-Archean lithosphere define a distinct trend, whereas those from the Archean lithosphere define a population with a relatively high Mg number but no apparent trend (Figure 4.13). The trends for oceanic and post-Archean xenolith suites are readily interpreted as restite trends, where **restite** is the material remaining in the mantle after extraction of variable amounts of basaltic magma (Boyd, 1989). In the case of ophiolites, ultramafic rocks represent the restite remaining after extraction of ocean ridge basalts, and the xenoliths from post-Archean lithosphere may be restites from extraction of plume-related basalts (flood basalts). The high Mg numbers of olivines from some Archean xenoliths suggest that they are restites from the extraction of komatiite (ultramafic) magmas. Because

TABLE 4.1 Average Chemical Composition of the Mantle

	Primitive mantle	Post-Archean lithosphere	Archean lithosphere	Depleted mantle
SiO_2	46.0	44.1	46.6	43.6
TiO_2	0.18	0.09	0.04	0.134
Al_2O_3	4.06	2.20	1.46	1.18
FeOT	7.54	8.19	6.24	8.22
MgO	37.8	41.2	44.1	45.2
CaO	3.21	2.20	0.79	1.13
Na_2O	0.33	0.21	0.09	0.02
K_2O	0.03	0.028	0.08	0.008
P_2O_5	0.02	0.03	0.04	0.015
Mg/Mg+Fe	90	90	93	91
Rb	0.64	0.38	1.5	0.12
Sr	21	20	27	13.8
Ba	7.0	17	25	1.4
Th	0.085	0.22	0.27	0.018
U	0.02	0.04	0.05	0.003
Zr	11.2	8.0	7.3	9.4
Hf	0.31	0.17	0.17	0.26
Nb	0.71	2.7	1.9	0.33
Ta	0.04	0.23	0.10	0.014
Y	4.6	3.1	0.63	2.7
La	0.69	0.77	3.0	0.33
Ce	1.78	2.08	6.3	0.83
Eu	0.17	0.10	0.11	0.11
Yb	0.49	0.27	0.062	0.30
Co	104	111	115	87
Ni	2080	2140	2120	1730

Major elements in weight percent of the oxide and trace elements in ppm.
Mg number = Mg/Mg+Fe mole ratio × 100. Depleted mantle calculated from NMORB; Archean lithosphere from garnet lherzolite xenoliths and post-Archean lithosphere from spinel lherzolite xenoliths.
Source: Data from Hofmann (1988), Sun & McDonough (1989), McDonough (1990), Boyd (1989), and miscellaneous sources.

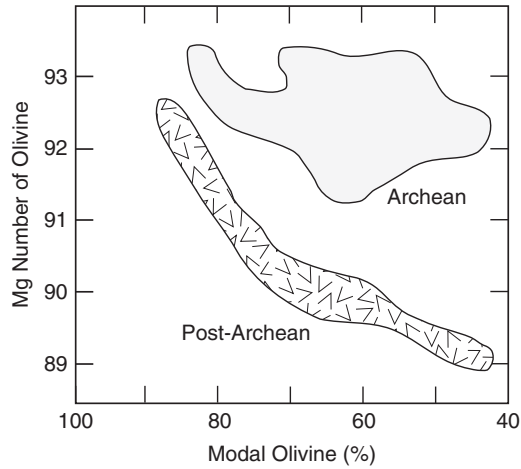

FIGURE 4.13 Mg number versus modal olivine in post-Archean mantle xenoliths and ophiolite ultramafics and in Archean lithosphere xenoliths from South Africa. Mg number (Mg/Mg+Fe molecular ratio) is a measure of the amount of melt that has been removed from a mantle source (higher values reflect more lost melt). *After Boyd (1989).*

garnet, the densest mineral in the upper mantle, is preferentially removed compared to olivine and orthopyroxene during melting, the restites in all cases are less dense than a primitive mantle of garnet lherzolite, and thus they tend to rise and remain part of the lithosphere.

Isotopic and geochemical data from mantle xenoliths indicate that the mantle lithosphere beneath Archean shields formed during the Archean and that it is chemically distinct and strongly depleted in incompatible elements compared to post-Archean lithosphere. One line of evidence for the depletion comes from surface heat flow. It has long been known that heat flow from Archean cratons is less than that from Proterozoic cratons. Two explanations for this relationship have been proposed (Nyblade & Pollack, 1993; Jaupart &Mareschal, 1999): (1) There is greater heat production in Proterozoic crust than in Archean crust, and (2) it is due to a thick lithospheric root beneath the Archean lithosphere that is depleted in radiogenic elements. Although Proterozoic upper continental crust is enriched in K, U, and Th, whose isotopes produce most of the heat in Earth (Condie, 1993), only part of the difference between the heat flow from Proterozoic and Archean lithosphere can be explained. Thus, it would appear that the thick root beneath the Archean cratons must also be depleted in radiogenic elements and contribute to the difference in heat flows.

Earth's **primitive mantle** composition is calculated from geochemical modeling and represents the average composition of the silicate part of Earth just after planetary accretion (Sun & McDonough, 1989). Compared to primitive mantle, incompatible element distributions in the mantle lithosphere and depleted mantle are quite distinct (Table 4.1). The striking depletion in the most

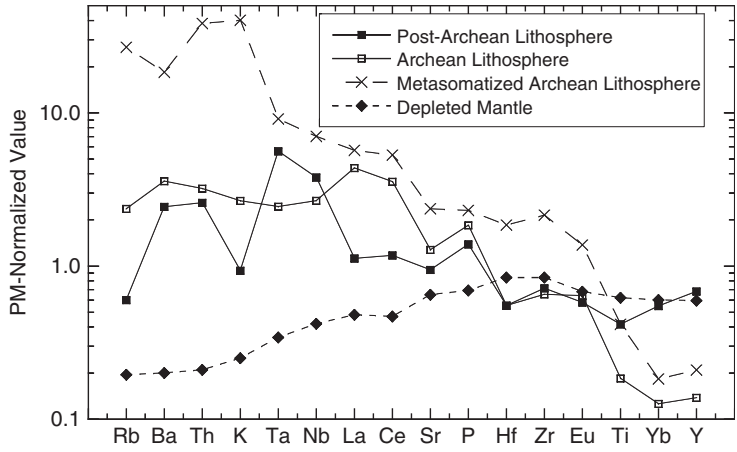

FIGURE 4.14 Primitive mantle normalized incompatible element distributions in subcontinental lithosphere and depleted mantle. *Primitive mantle values from Sun & McDonough (1989) and data from Nixon et al. (1981), Hawkesworth et al. (1990), Wood (1979), and miscellaneous sources.*

incompatible elements (Rb, Ba, Th, etc.) in depleted mantle (Figure 4.14), as represented by ophiolite ultramafics and mantle compositions calculated from ocean ridge basalts, reflects removal of basaltic liquids enriched in these elements (Hofmann, 1988). In striking contrast to depleted mantle, lithosphere mantle shows prominent enrichment in the most incompatible elements. Spinel lherzolites from post-Archean lithosphere shows a positive Nb-Ta anomaly, suggestive that they represent plume material plastered on the bottom of the lithosphere (Figure 4.14) (McDonough, 1990). Archean garnet lherzolites commonly show textural and mineralogical evidence for metasomatism (i.e., modal metasomatism), such as veinlets of amphibole, micas, and other secondary minerals (Waters & Erlank, 1988). The very high content of the most incompatible elements in modally metasomatized xenoliths probably records metasomatic additions of these elements to the lithosphere, and in some cases, as in the xenoliths from Kimberley in South Africa (Hawkesworth et al., 1990), these additions occurred after the Archean.

Thickness

The continental lithosphere varies in thickness depending on its age and mechanism of formation. Shear wave tomographic studies of the upper mantle have been most definitive in estimating the thickness of continental lithosphere (Grand, 1987; Polet & Anderson, 1995; Jackson et al., 2008). Seismic velocity variations of a nonthermal origin show a strong correlation with age and with regional variations in subcontinental lithosphere thickness (Artemieva, 2009). Most post-Archean lithosphere is 100–200 km thick, whereas lithosphere beneath Archean shields is commonly >200 km thick.

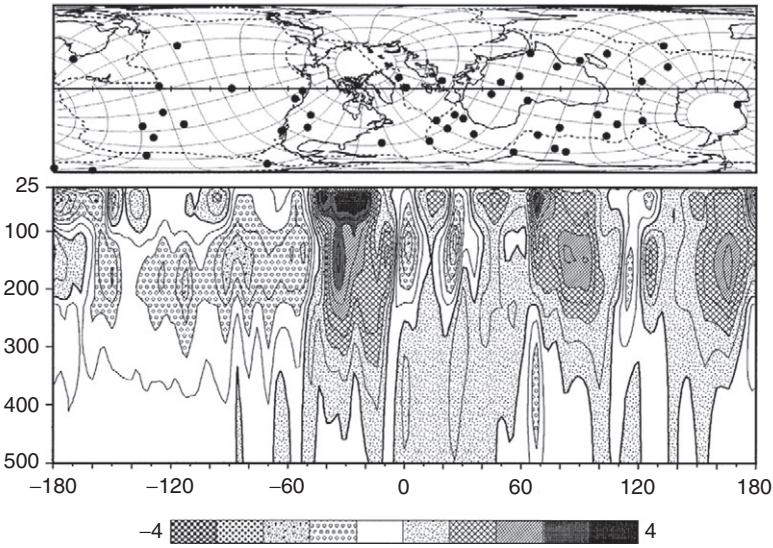

FIGURE 4.15 S-wave velocity distribution in the upper mantle along a great circle passing through Hawaii and Iceland. Darker shades indicate faster velocities. Map shows location of great circle and major hotspots (black dots). *From Zhang & Tanimoto (1993).*

Rheological models also suggest thicknesses of 100–300 km for continental lithosphere (Ranalli, 1991). In a shear wave tomographic cross section around the globe, high-velocity roots underlie Archean crust, as for example in northern Canada, central and southern Africa, and Antarctica (Figure 4.15). The base of the lithosphere in these and other areas overlain by Archean crust may nearly reach the 410-km discontinuity. In the Kaapvaal Craton in southern Africa, the mantle keel extends to 225–300 km deep and is consistent with compositional variations of mantle xenoliths brought up in kimberlite pipes (Fouch et al., 2004). Under Proterozoic shields, however, lithospheric thicknesses rarely exceed 200 km. Consideration of elongation directions of Archean cratons relative to directions of modern plate motions suggests that the thick Archean lithosphere does not aid or hinder plate motions (Stoddard & Abbott, 1996).

Because of the buoyant nature of depleted Archean lithosphere, it tends to ride high compared to adjacent Proterozoic lithosphere, as evidenced by the extensive platform sediment cover on Proterozoic cratons compared to Archean cratons (Hoffman, 1990). The thick roots of Archean lithosphere often survive later tectonic and thermal events, such as continental collisions and supercontinent rifting. However, mantle plumes or extensive later reactivation can remove the thick lithosphere keels, as is the case, for instance, with the Archean Wyoming Province in North America and the North China Craton.

Subductability

It is generally assumed that continental lithosphere, because of its increased buoyancy, is essentially unsubductable. However, the occurrence of ultra-high-pressure metamorphic minerals within rocks from continental collision zones indicates that continental rocks may descend into subduction zones up to 300 km or more. Because of its relative overall buoyancy, continental crust should resist subduction, and thus end up in either collisional or accretionary orogens. To quantitatively test this conclusion, Wu et al. (2009) have conducted experimental studies up to 24 GPa and 1800°C on gneiss samples that have returned to the surface from great depths. They found that the upper continental crust is no longer buoyant with respect to the surrounding mantle when it has been transported to a depth of 250 km ($\sim$ 8–9 GPa), which they suggest defines a "depth of no return" for the subducted upper continental crust. This depth is consistent with the depth limit for most exposed ultra-high-pressure rocks. The experimental results suggest that subducted upper continental crust with a jadeite-stishovitite mineralogy has the potential to sink into the mantle transition zone. However, unless continental crust is carried into the deep mantle by associated mafic and ultramafic rocks, the density relationship is reversed at the base of the transition zone, and the felsic crust could be trapped at the 660-km discontinuity.

Age of Subcontinental Lithosphere

In terms of crust/mantle evolution, it is important to know if the thick lithospheric roots beneath Archean cratons formed in the Archean in association with the overlying crust, or if they were added later by underplating. Although in theory we can use mantle xenoliths to isotopically date the lithosphere, because later deformation and metasomatism may reset isotopic clocks, ages obtained from xenoliths are generally too young. What we really need to determine the original age of the subcontinental lithosphere are minerals that did not recrystallize during later events, or an isotopic system that was not affected by later events. At this point diamonds and Os isotopes enter the picture. Diamonds, which form at depths $>$150 km, are very resistant to recrystallization at lithosphere temperatures, and sometimes they trap silicate phases as they grow, shielding these minerals from later recrystallization (Richardson, 1990). Pyroxene and garnet inclusions in diamonds, which range from about 50 to 300 μm in size, have been successfully dated by the Sm/Nd isotopic method, and appear to record the age of the original ultramafic rock that housed the diamonds. Often more than one age is recorded by diamond inclusions from the same kimberlite pipe, as is seen, for instance, in the Premier pipe, in South Africa. Diamonds in this pipe with garnet-orthopyroxene inclusions have Nd and Sr mineral isochron ages $>$3.0 Ga, suggesting that the mantle lithosphere formed in the early Archean at the same time the overlying crust formed (Richardson et al., 1993). Those diamonds with garnet-clinopyroxene-orthopyroxene inclusions record an age of 1.93 Ga and

those with garnet-clinopyroxene (eclogitic), an age of 1.15 Ga, an age that is only slightly older than the age of kimberlite emplacement. The younger ages clearly indicate multiple events in the South African lithosphere. Diamond inclusion ages from lithosphere xenoliths from Archean cratons in South Africa, Siberia, and western Australia all indicate that the lithosphere in these regions is also Archean in age.

The Re/Os isotopic system differs from the Sm/Nd and Rb/Sr systems in that Re is very incompatible in the mantle, whereas Os is compatible. In contrast, in most other isotopic systems used in dating rocks, both parent and daughter elements are incompatible. Hence, during the early magmatic event that left the Archean mantle lithosphere as a restite, Re was completely or largely extracted from the rock while Os was unaffected (Carlson et al., 1994; Pearson et al., 2002; Brueckner et al., 2010). When Re was extracted from the rock, the Os isotopic composition was "frozen" into the system, and hence by analyzing a mantle xenolith later brought to the surface, we can date the Re depletion event. Calculated Os isotopic ages of xenoliths from two kimberlite pipes in South Africa are shown in Figure 4.16, plotted at depths of origin inferred from thermobarometry. In the Premier and North Lesotho pipes, ages range from

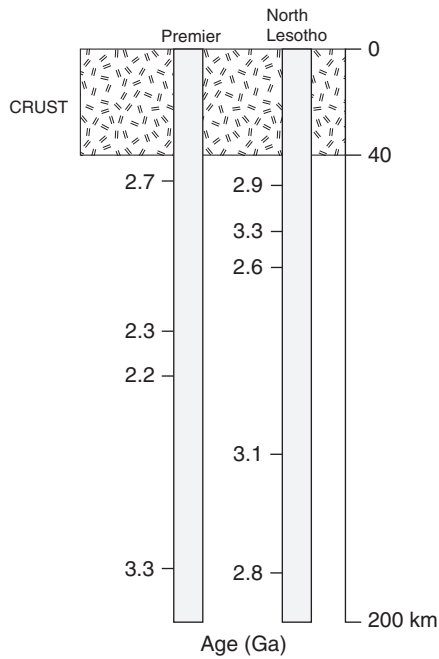

FIGURE 4.16 Idealized cross section of the Archean lithosphere in South Africa constructed from mantle xenoliths from two kimberlite pipes. *Ages are redepletion model ages (in Ga) from Carlson et al. (1994).*

3.3 to 2.2 Ga, similar to the ranges found in xenoliths from pipes in other Archean cratons. It is not yet clear if the range in ages from a given pipe really records the range in formation ages of the lithosphere or a series of metasomatic events of lithosphere that occurred after 3 Ga.

The maximum isotopic ages obtained for mantle keels in the Siberia and Kaapvaal Cratons are similar to the oldest isotopic ages obtained from the overlying crust (Figure 4.16) (Carlson et al., 1994; Pearson et al., 1995; 2002; Griffin et al., 2003; Simon et al., 2007). This suggests that substantial portions of the mantle keels beneath the continents formed at the same time as the overlying crust and that they have remained firmly attached to the crust ever since.

Because S-wave velocities correlate with the thermal regime in the continental lithosphere, the age of the last major thermal event in the lithosphere can be mapped with S-wave velocities (Artemieva & Mooney, 2001; Artemieva, 2006, 2009). Poupinet and Shapiro (2009) have used global S-wave velocity in the crust and upper mantle to compute vertical S-wave travel times in the continental lithosphere. Their map is a "thermal history" map of the continental lithosphere (Figure 4.17), and the ages shown represent the last major thermal/orogenic event to affect the lithosphere. It is not a map showing

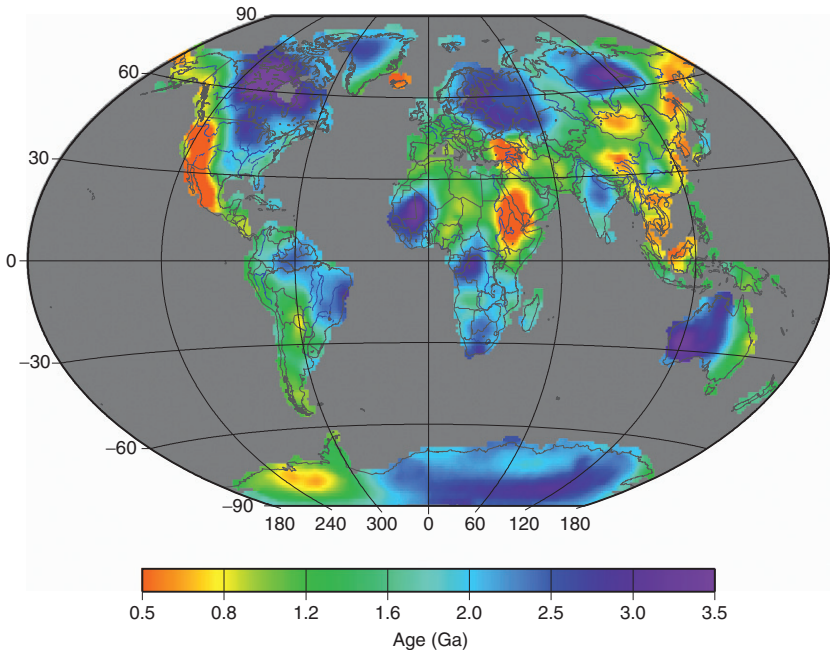

FIGURE 4.17 Map of the thermal age distribution of continental lithosphere constructed from a correlation of thermal lithospheric age to S-wave vertical traveltime delay. Ages represent the last major thermal event. *From Poupinet and Shapiro (2009), courtesy of N. M. Shapiro.*

juvenile continental crust, and some areas shown in green, for instance, may be reworked Archean crust. It is noteworthy, however, that large portions of the continents formed in the Archean (especially in Antarctica and North America, deep blue color) and have not been overprinted by later thermal events.

THE LOW-VELOCITY ZONE

The low-velocity zone (LVZ) in the upper mantle is characterized by low seismic wave velocities, high seismic energy attenuation, and high electrical conductivity. The bottom of the LVZ, sometimes referred to as the **Lehmann discontinuity,** has been identified from the study of surface wave and S-wave data in some continental areas (Figure 4.1) (Gaherty & Jordan, 1995). This discontinuity, which occurs at depths of 180–220 km, appears to be thermally controlled and at least in part reflects a change from an anisotropic lithosphere to a more isotropic asthenosphere. A zone of high electrical conductivity in the LVZ has been explained by the presence of small amounts of water, perhaps inducing partial melting (Eaton et al., 2009). The LVZ plays a major role in plate tectonics, providing a relatively low-viscosity region on which lithospheric plates can slide with very little friction.

Because of the dramatic drop in S-wave velocity and increase in attenuation of seismic energy, it would appear that partial melting must contribute to producing the LVZ (Kawakatsu et al., 2009). This drop in velocity can be explained by horizontal melt-rich layers embedded in the mantle, and it can account for the large viscosity contrast at the base of the lithosphere that facilitates horizontal plate motions. The probable importance of incipient melting is attested to by the high surface heat flow observed when the LVZ reaches shallow depths, such as beneath ocean ridges and in continental rifts. Experimental results show that incipient melting in the LVZ requires a minor amount of water to depress silicate melting points (Wyllie, 1971). With only 0.05–0.1% water in the mantle, partial melting of garnet lherzolite occurs in the appropriate depth range for the LVZ as shown by the geotherm–mantle solidus intersections in Figure 4.7. The source of water in the upper mantle may be from the breakdown of minor hydrous phases such as amphibole, mica, titanoclinohumite, or other hydrated silicates. The theory of elastic wave velocities in two-phase materials indicates that only $\leq$1% melt is required to produce the lowest S-wave velocities measured in the LVZ (Anderson et al., 1971). If, however, melt fractions are interconnected by a network of tubes along grain boundaries, the amount of melting may exceed 5% (Marko, 1980). The downward termination of the LVZ appears to reflect the depth at which geotherms pass below the mantle solidus. Also possibly contributing to the base of the LVZ is a rapid decrease in the amount of water available (perhaps free water enters high-pressure silicate phases at this depth). The width or even the existence of the LVZ depends on the steepness of the geotherms. With steep geotherms like those characteristic of ocean ridges and continental rifts, the range of penetration of the mantle solidus is large,

and hence the LVZ should be relatively wide (A and B, Figure 4.7). The gentle geotherms in continental platforms, which show a narrow range of intersection with the hydrated mantle solidus, produce a thin or poorly defined LVZ (C). Beneath Archean shields, geotherms do not intersect the mantle solidus, and hence there is no LVZ (D).

THE TRANSITION ZONE

The 410-km Discontinuity

The transition zone is that part of the upper mantle where two major seismic discontinuities occur: one at 410 km and the other at 660 km (Figure 4.1). High-pressure experimental studies document the breakdown of Mg-rich olivine to a high-pressure phase known as **wadsleyite** (B phase) at about 14 GPa, which is equivalent to 410 km of depth in the Earth (Figure 4.18). There is no change in chemical composition accompanying this phase change or other phase changes described below. Mantle olivine (Fo_{90}) completely transforms to wadsleyite over a <300-MPa pressure range at appropriate temperatures for the 410-km discontinuity (~1000°C) (Ita & Stixrude, 1992; Helffrich & Wood, 2001). This pressure range is in good agreement with the <10-km width of the 410-km discontinuity deduced from seismic data (Vidale et al., 1995). In some places the discontinuity is broader than normal (20–25 km), a feature that

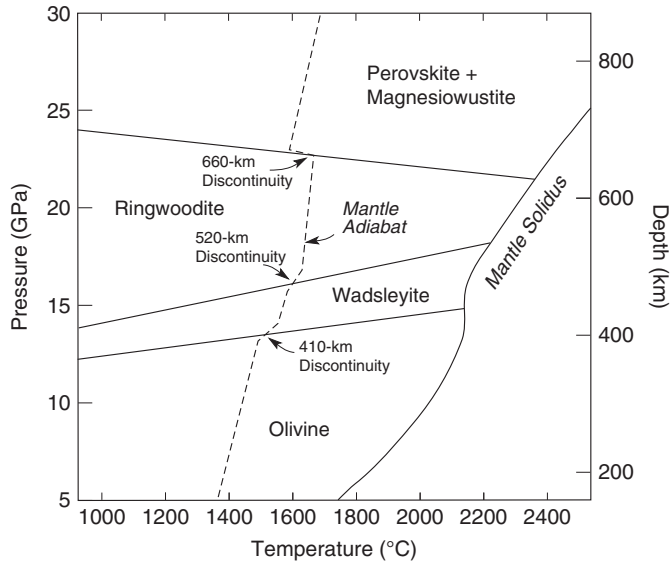

FIGURE 4.18 Summary of phase relations for Mg_2SiO_4 in the mantle from experimental studies at high pressure and temperature. The dashed line is the mantle adiabat. *Modified after Christensen (1995).*

may reflect water incorporated into the wadsleyite crystal structure (van der Meijde et al., 2003). If olivine composes 40–60% of the rock, as it does in garnet lherzolite, the olivine-wadsleyite phase change may account for the approximately 6% increase in density observed at this discontinuity (Table 4.2).

TABLE 4.2 Summary of Mantle Mineral Assemblages for Average Garnet Lherzolite from High-Pressure Studies

	Depth (km)	Mineral assemblage (minerals in vol%)	Density contrast (%)	Slope of reaction (MPa/°C)
	<410	Olivine 58 Opx 11 Cpx 18 Garnet 13		
	350–450	Opx-Cpx → Majorite	6	+1.5
410-km discontinuity	410	Olivine (α phase) → Wadsleyite (B phase)	6	+5.5
	410–550	Wadsleyite 58 Majorite 30 Cpx 9 Opx 3		
520-km discontinuity	520	Wadsleyite → Ringwoodite (γ phase) Ca-garnet → Ca-perovskite	1	+3.0
	550–660	Ringwoodite 58 Majorite 37 Ca-Perovskite 5		
660-km Discontinuity	660	Ringwoodite → Perovskite + Magnesiowustite	5	–0.5 to –1.3 (dry); –2 (wet)
	650–680 680–2600	Majorite → Perovskite Ilmenite → Perovskite Perovskite 77 Magnesiowustite 15 Ca-Perovskite 8 Silica (?)		+1.5 to +2.5
D″ discontinuity	2600–2750	Perovskite → post-Perovskite	1	7–10

Opx, orthopyroxene; Cpx, clinopyroxene.
Source: Data from Ita & Stixrude (1992), Christensen (1995), Mambole & Fleitout (2002), Hirose (2002), Katsura et al. (2003), Fei et al. (2004), Litasov et al. (2005).

Measurements of the elastic moduli of olivine at high pressures suggest that 40% olivine explains the velocity contrast better than 60% olivine (Duffy et al., 1995). Because garnet lherzolites typically have 50–60% olivine, modal olivine may decrease with depth in the upper mantle to meet this constraint.

Studies using receiver functions provide additional high-resolution data on the nature of the 410-km discontinuity. The **receiver function method** is a seismic technique that uses the interconversion (P-to-S and S-to-P) of near-planar teleseismic body waves propagating toward the surface of Earth to resolve geometry and contrast details at seismic discontinuities, such as those in the mantle transition zone. Results from subduction zones often show a double discontinuity at 410 km of depth near descending slabs. This may result from water collected near the slab and fed into the 410-km discontinuity, giving rise to a localized melt layer on top of the discontinuity (Schmerr & Garnero, 2007). Geophysical models suggest that such a melt layer at about 350 km deep could attain thicknesses of 10–20 km, consistent with seismic velocity distributions (Leahy & Bercovici, 2010; Benoit et al., 2010). Alternatively or in addition, a second discontinuity may reflect other reactions at the 410-km discontinuity (see below). In any case, the detection of multiple discontinuities supports the existence of lateral heterogeneity and possibly the existence of a melt layer above the 410-km discontinuity.

High-pressure experimental data indicate that at depths of 350–450 km, both clino- and orthopyroxene are transformed into a garnet-structured mineral known as **majorite**, involving a density increase of about 6% (Christensen, 1995). This transition has been petrographically observed as pyroxene exsolution laminae in garnet in mantle xenoliths and as inclusions in diamonds, both found in kimberlites derived from the Archean lithosphere at depths of 300–400 km (Haggerty & Sautter, 1990; Nishi et al., 2010). It is probable that an increase in velocity gradient sometimes observed beginning at 350 km and leading up to the 410-km discontinuity is caused by these pyroxene transformations. Both of the phase changes that occur at or near the 410-km discontinuity have positive slopes in P-T space, and thus the reactions are exothermic.

The 520-km Discontinuity

Experimental data indicate that wadsleyite should transform to a more densely packed spinel structured phase (γ phase) at equivalent burial depths of 520 km. This mineral, known as **ringwoodite**, has the same composition as Mg-rich olivine, but the crystallographic structure of spinel. Because of the very small density contrast associated with this transition ($\sim$1%), the 520-km discontinuity is not resolvable in all seismic sections. Recent improvements in the resolution of seismic structure, however, show that in some regions the discontinuity splits into two discontinuities, one at 500 km and another at 560 km (Saikia et al., 2008). Because the depth of these two discontinuities varies, they are probably caused by two phase transitions responding to changes in composition or temperature. The shallower discontinuity is probably due to the wadsleyite transformation, whereas the deeper discontinuity may be caused by the formation

of Ca-perovskite from Ca-garnet (Table 4.2) (Saikia et al., 2008). Variations in the splitting depth of the discontinuity may arise from variability in Ca concentration in the mantle and its areal distribution and can yield information on both the fertility of mantle (low Ca) and the proportion of recycled oceanic crust (high Ca).

The 660-km Discontinuity

One of the most important questions related to the style of mantle convection in Earth is the nature of the 660-km discontinuity (Figure 4.1). If descending slabs cannot readily penetrate this boundary or if the boundary represents a compositional change, two-layer mantle convection is favored with the 660-km discontinuity representing the base of the upper layer. Large increases in both seismic-wave velocity (5–7%) and density (5%) occur at this boundary. High-frequency seismic waves reflected at the boundary suggest that it has a width of only about 5 km, but has up to 20 km of relief over distances of hundreds to thousands of kilometers (Wood, 1995).

As with the 410-km discontinuity, it appears that a phase change in Mg_2SiO_4 is responsible for the 660-km discontinuity (Christensen, 1995; Helffrich & Wood, 2001). High-pressure experimental results indicate that ringwoodite transforms to a mixture of perovskite and magnesiowustite at a pressure of about 23 GPa (Figure 4.18), and can account for both the seismic velocity and density increases at this boundary if the rock contains 50–60% ringwoodite:

$$\begin{gathered} Mg_2SiO_4 \rightarrow MgSiO_3 + MgO \\ \text{ringwoodite} \rightarrow \text{perovskite} + \text{magnesiowustite} \end{gathered} \tag{4.1}$$

Mg **perovskite** and **magnesiowustite** are extremely high-density minerals and appear to comprise most of the lower mantle.

Unlike the shallower phase transitions, the ringwoodite-perovskite transformation is endothermic and has a negative Clapeyron slope in P-T space (Figure 4.18 and Table 4.2). However, because recent measurements by Katsura et al. (2003) and Fei et al. (2004) show that the slope is only slightly negative (–0.5 to –1.3 MPa/°C instead of strongly negative as earlier measurements suggested), it will have little or no ability to impede slabs from sinking into the deep mantle or prevent plumes from rising into the upper mantle (Fukao et al., 2009). The latent heat associated with phase transitions in descending slabs and rising plumes can deflect phase transitions to shallower depths for exothermic (positive P-T slope) reactions and to greater depths for endothermic (negative P-T slope) reactions (Liu, 1994). For a descending slab in the exothermic case, like the olivine-wadsleyite transition, the elevated region of the denser phase exerts a strong downward pull on the slab or upward pull on a plume, thus helping drive convection. In contrast, for an endothermic reaction the low-density phase is depressed, enhancing a slab's buoyancy and resisting further sinking of the slab. This effect may be significant for

the ringwoodite-perovskite transformation only if water is available in the mantle at this depth (Litasov et al., 2005), which makes the Clapeyron slope more negative (about –2 MPa/°C; Table 4.2). As with the 410-km discontinuity, a double discontinuity is observed around some descending slabs. This may be caused by a somewhat deeper and weaker discontinuity due to the ilmenite-perovskite transformation, which high-pressure experiments show should occur in cooler regions of the mantle (Schmerr & Garnero, 2007).

Also in the depth range of 650–680 km, majorite transforms to perovskite (Table 4.2), but unlike the ringwoodite transition, the majorite transition is gradual and does not produce a seismic discontinuity. This transition is very sensitive to the temperature and aluminum content of the system. Unlike the ringwoodite-perovskite reaction, the garnet-perovskite reaction has a positive slope (1.5 to 2.5 MPa/°C) (Hirose, 2002; Mambole & Fleitout, 2002).

Computer models by Davies (1995) suggest that stiff slabs can penetrate the 660-km discontinuity more readily than plume heads, and plume tails are the least able to penetrate it. Some investigators have suggested that slabs may locally accumulate at the discontinuity, culminating in occasional "avalanches" of slabs into the lower mantle. The fate of the oceanic crust in descending plates may be different from suboceanic lithosphere due to their different compositions. Irifune and Ringwood (1993) suggested that the 660-km discontinuity may be a density "filter," which causes the crust to separate from the mantle lithosphere in descending slabs. At depths less than 660–700 km, basaltic crust has a greater density than surrounding mantle, which could cause separation of the two components when they intersect the discontinuity. At about 700 km of depth, however, the crust becomes less dense than surrounding mantle due to the majorite-perovskite transition (Hirose et al., 1999). Hence, if the mafic parts of slabs accumulate to sufficient thickness (>60 km) just beneath the 660-km discontinuity, the density of the basaltic component will increase and may drive the slabs into the deep mantle.

THE LOWER MANTLE

General Features

High-pressure experimental studies clearly suggest that Mg perovskite is the dominant phase in the lower mantle (Table 4.2). However, it is still not clear if the seismic properties of the lower mantle necessitate a change in major element composition (Wang et al., 1994). Results allow, but do not require, the Fe/Mg ratio of the lower mantle to be greater than that of the upper mantle. If this were the case, it would greatly limit the mass flux across the 660-km discontinuity to maintain such a chemical difference, and thus favor layered convection. It is also possible that free silica could exist in the lower mantle. Stishovite (a high-P phase of silica) inverts to an even more dense silica polymorph with a $CaCl_2$ structure at about 50 GPa (Kingma et al., 1995), and it is possible that this silica phase exists at depths >1200 km.

New interpretations of the isostatic rebound of continents following Pleistocene glaciation, together with gravity data, indicate that the viscosity of the mantle increases with depth by two orders of magnitude, with the largest jump at the 660-km discontinuity. This conclusion is in agreement with other geophysical and geochemical observations. For instance, although mantle plumes move upward relatively fast, it would be impossible for them to survive convective currents in the upper mantle unless they were anchored in a "stiff" lower mantle. Also, only a mantle of relatively high viscosity at depth can account for the small number (two today) of mantle upwellings. Geochemical domains that appear to have remained isolated from each other for billions of years in the lower mantle (as discussed later) can also be accounted for in a stiff lower mantle that resists mixing.

Descending Slabs

Although variation is seen in seismic wave tomography sections and the density distribution of the mantle among different investigators, some of the general features of the deep mantle are becoming well established (Figures 4.2 and 4.4). S-wave anomalies continue over distances of many thousands of kilometers with apparent widths as small as several hundred kilometers (van der Hilst et al., 1997; Grand et al., 1997). Fast anomalies can be tracked thousands of kilometers into the mantle and may represent descending oceanic plates. One very prominent anomaly extending from about 30 °S to 50 °N in North and South America can be traced into the deep mantle and is interpreted as remnants of the subducted Farallon plate. High-velocity anomalies also extend beneath Asia, probably all the way to the base of the mantle (Figures 4.2 and 4.19). The low-velocity anomalies beneath Africa and the South Pacific reflect the two large mantle upwellings previously discussed.

Data suggest that the degree of slab penetration below the 660-km discontinuity is related to slab dip, slab roll back, viscosity jump, and the metastable persistence of ringwoodite in cold slabs (Zhong & Gurnis, 1995; Li & Yuan, 2003; Ganguly et al., 2009). Slabs with steep dip angles and relatively stationary trenches, like the Mariana and Tonga slabs (van der Hilst, 1995), are more likely to descend into the lower mantle (Figure 4.19a). In contrast, those with shallow dip angles, like the Izu-Bonin and Japan slabs, are commonly associated with rapid retrograde trench migration and these have greater difficulty in penetrating the 660-km discontinuity. Estimates of viscosity in the transition zone lie in the range of 10^{20}–10^{21} Pa-s; higher viscosities could result in piling up or flattening of slabs at the 660-km discontinuity (Quinteros et al., 2010).

Stagnant slabs at the 660-km discontinuity are observed at many locations around the circum-Pacific (Figure 4.19a) (Fukao et al., 2009). The Clapeyron slope of the ringwoodite reaction appears to be more negative at these locations than that of the dry reaction, suggesting that water is available in some descending slabs at depths as great as 660 km. There is growing evidence of both

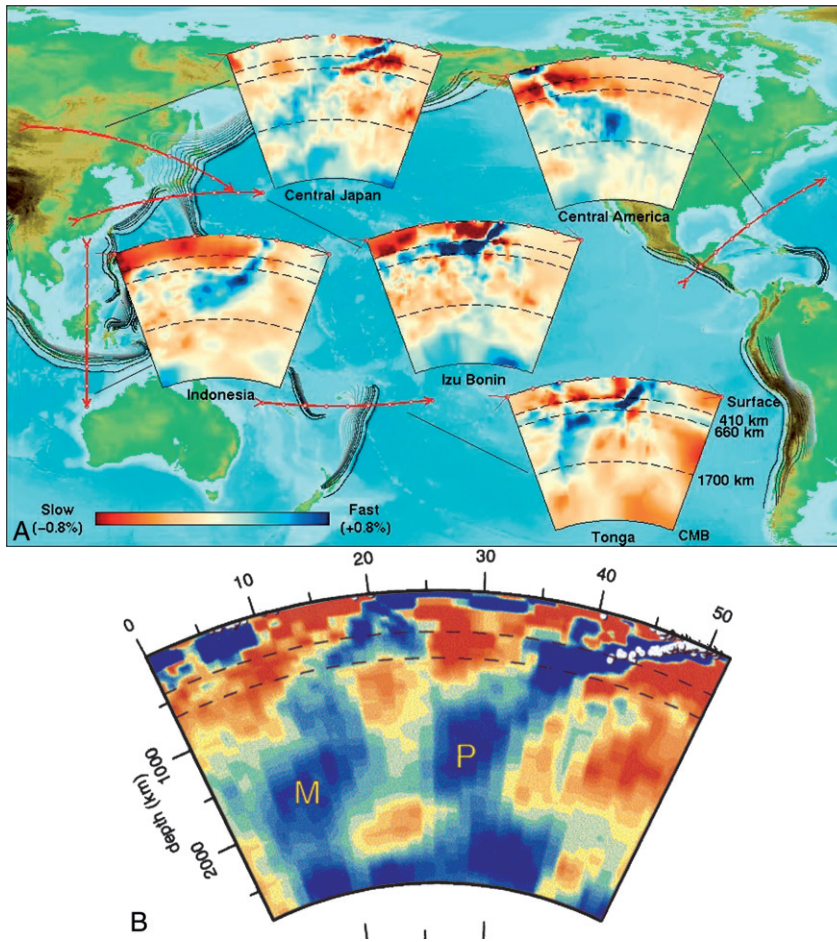

FIGURE 4.19 **(A)** Seismic tomographic cross sections of subduction zones around the Pacific basin. Colors as in Figure 4.2. Although most plates descend into the deep mantle, some are temporarily stalled at the 660-km discontinuity. Courtesy of Rob van der Hilst. Reprinted from Karason et al. (2000) with permission of the American Geophysical Union. **(B)** Seismic tomographic section of northeastern Asia. Colors as in Figure 4.2. Note that the Pacific (P) and Mongol-Okhotsk (M) slabs (in blue) extend all the way to the core-mantle boundary. White dots are earthquakes in descending Pacific plate beneath Japan. Courtesy of Rob Van der Voo. Reprinted with permission of Nature, Copyright 1999 Macmillan Magazines Ltd.

stagnant slabs at the 660-km discontinuity and of falling slabs in the lower mantle, and data suggest that the seismic signals are primarily of thermal rather than compositional origin (Fukao et al., 2009). Although some slabs may be delayed at the 660-km discontinuity, tomographic images suggest that all or most modern slabs eventually sink into the lower mantle. Thus, there is little evidence for layered convection in Earth in terms of slab distributions in the mantle.

The high-velocity anomaly beneath Asia that extends all the way to the lower mantle appears to represent ancient oceanic slabs (Mongol-Okhotsk plate) subducted into the mantle during closure of several ocean basins as microcontinents collided to form Asia in the Mesozoic (M in Figure 4.19b) (Van der Voo et al., 1999). Subduction ended about 135 Ma at which time the subducted slabs became detached from the lithosphere and continued to sink into the mantle. These slabs have sunk into the mantle at about 1 cm/y. The Pacific plate (P in Figure 4.19b), which subducts beneath Japan, is also apparent in the tomographic section, and it appears to merge with the Mongol-Okhotsk plate in the very deep mantle.

One interesting yet controversial feature of some tomographic sections is the fact that many, if not most, descending plates seem to break up below the 660-km discontinuity (Figure 4.19a). The pattern of high-velocity anomalies beneath this depth is much less regular and dispersed. This suggests to some investigators that the deep mantle may be convectively isolated from the upper part of the mantle (van der Hilst & Karason, 1999; Kaneshima & Helffrich, 1999).

The D″ Layer

The D″ layer is a region of the mantle just above the core where seismic velocity gradients are anomalously low (Figure 4.20) (Young & Lay, 1987; Loper & Lay, 1995; Helffrich & Wood, 2001). Estimates of the thickness of the D″ layer suggest that it ranges from 100 to about 400 km. Calculations indicate that only a relatively small temperature gradient (1–3°C/km) is necessary to conduct heat from the core into the D″ layer. Because of diffraction of seismic waves by the

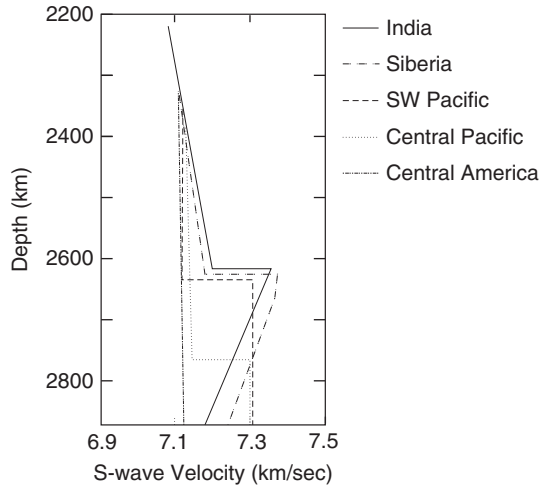

FIGURE 4.20 S-wave velocity distribution for various geographic regions in the lower mantle. Although most regions show a discontinuity near 2600 km, the velocity profiles show a great deal of lateral heterogeneity in this region. *Data after Knittle & Jeanloz (1991).*

core, the resolution in this layer is not as good as at shallower mantle depths, and thus details of its structure are not well known. However, results clearly indicate that D″ is a complex region that is both vertically and laterally heterogeneous, and that it is layered on a kilometer scale in the lower 50 km (Kendall & Silver, 1996; Sidorin et al., 1999; Thybo et al., 2003). Data also indicate the presence of a major solid–solid phase transition about 200 km above the core–mantle interface (Figure 4.20) (Sidorin et al., 1999). Recent seismic results furthermore confirm the existence of a 5- to 50-km-thick ultra-low-velocity layer just above the core–mantle boundary where S-wave velocity decreases by 10–50%, consistent with more than 15% melt in this layer (Thybo et al., 2003). As an example of lateral heterogeneity in D″, regions beneath circum-Pacific subduction zones have anomalously fast P and S waves, interpreted by many to represent lithospheric slabs that have sunk to the base of the mantle.

There are three possible contributions to the complex seismic structures seen in D″: temperature variations, compositional changes, and mineralogical phase changes. Temperature variations are caused chiefly by slabs sinking into D″ (a cooling effect that produces relatively fast velocities) and heat released from the core (causing slow velocities). Subduction of oceanic crust also may give rise to widespread heterogeneity in the mantle possibly extending into the D″ layer. Because of the mineralogical differences between basalt and ultramafic rocks at such high pressures, negative and positive jumps in seismic wave velocities are expected and this could explain some of the velocity variation in D″ (Ohta et al., 2008). Mixing of molten iron from the core with high-pressure silicates can also lead to compositional changes with corresponding velocity changes. Experiments have shown, for instance, that when liquid iron comes in contact with silicate perovskite at high pressures, these substances vigorously react to produce a mixture of Mg perovskite, a high-pressure silica polymorph, wustite (FeO), and Fe silicide (FeSi) (Knittle & Jeanloz, 1991; Dubrovinsky et al., 2003). These experiments also suggest that liquid iron in the outer core will seep into D″ by capillary action to hundreds of meters above the core–mantle boundary and that the reactions will occur on timescales of less than 10^6 years.

The S-wave velocity discontinuity at about 2600 km (Figure 4.20) may be caused by a phase change, and this phase change should have a positive Clapeyron slope of about >6 MPa/°C (Sidorin et al., 1999). The verification of this transformation by ultra-high-pressure experiments in which Mg-perovskite inverts to a **post-perovskite phase** with a Clapeyron slope in the range of 7–10 MPa/°C is remarkably consistent with the theoretical prediction (Oganov & Ono, 2004):

$$\begin{array}{c} MgSiO_3 \rightarrow MgSiO_3 \\ \text{perovskite} \rightarrow \text{post-perovskite} \end{array} \qquad (4.2)$$

The post-perovskite phase is composed of densely packed SiO_6 octahedra sharing edges and corners to form sheets with layers of Mg and Fe cations (Duffy, 2008).

As mentioned in Chapter 1, the D″ layer is a thermal boundary layer in which heat is transferred from the core to the mantle. Hence, like the lithosphere upstairs, the D″ has a steep thermal gradient (i. e., a geotherm) between the core and the convecting mantle. The large Clapeyron slope of the post-perovskite reaction, unlike other reactions in the mantle, allows the phase boundary to be crossed by the geotherm at two depths (Hernlund et al., 2005) (Figure 4.21). In fact, seismic migration techniques have revealed a pair of oppositely polarized discontinuities beneath Eurasia and the Caribbean regions, in good agreement with the predictions of the double-crossing thermal model. The depth and complexity of the boundary is dependent on lateral changes in temperature in D″ (Kawai & Tsuchiya, 2009). Three scenarios are shown in Figure 4.21: (1) Relatively cold mantle temperatures where descending plates accumulate give rise to a thick stability field for the post-perovskite phase, whereas in warmer regions, (2) the stability field is thinner. For a hot scenario, which may be beneath a mantle plume or superplume, (3) the geotherm may not intersect the phase boundary, and thus Mg-perovskite would be stable all the way to the core–mantle interface. This may explain why the seismic discontinuity is absence in some regions (Figure 4.20).

Because the low seismic wave velocities in D″ reflect high temperatures, thus a lowering of mantle viscosity, this layer is commonly thought to be the source of mantle plumes. The lower viscosity will also enhance the flow of material into the base of newly forming plumes, and the lateral flow into plumes will be balanced by slow subsidence of the overlying mantle. The results of Davies and Richards (1992) suggest that a plume could be fed for 100 Ma from a volume of D″ only a few tens of kilometers thick and 500–1000 km in

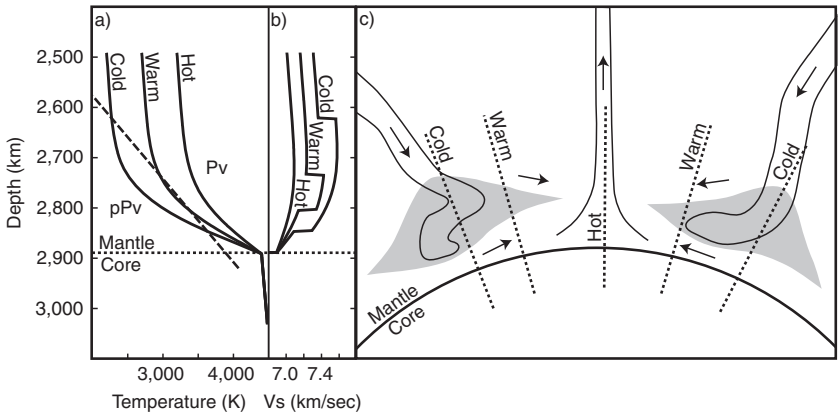

FIGURE 4.21 Schematic diagram of possible structure in the lowermost mantle. (A) Geotherms (pPv, post-perovskite; Pv, perovskite); (B) Vs profiles; and (C) possible structure of the D″ layer. Gray area is the stability field of post-perovskite and dashed lines are geotherms from part (a). *After Hernlund et al. (2005). Courtesy of John Hernlund. Used with permission of Nature Publishing Group, permission conveyed through Copyright Clearance Center, Inc.*

diameter. These results are important for mantle dynamics because they suggest that plumes are fed from the lowermost mantle, whereas ocean ridges are fed from the uppermost mantle.

Spin Transitions

It is predicted that at very high pressures in the deep mantle the electron orbitals of iron should collapse from a high spin to a low spin state. This would represent a major change in chemical bonding of iron that should lead to significant changes in the physical and chemical properties of the lower mantle, and these changes may be discernible in seismic wave velocities. Recent high-P experiments have confirmed the existence of spin transitions in iron in magnesiowustite and perovskite (Ohtani & Sakai, 2008). Although the depth of spin transitions in these phases is too broad to produce an abrupt seismic discontinuity in the lower mantle, the transitions may explain a correlated anomaly for both P and S waves that extends throughout most or all of the lower mantle (Crowhurst et al., 2008). Also, observed changes in sound velocity and bulk modulus in the lower mantle may be due to an iron spin transition in lower mantle minerals (Lin et al., 2005).

WATER IN THE MANTLE

Large quantities of water are returned to the mantle in subduction zones (Peacock, 1990; Mookherjee et al., 2008). Estimates indicate that around 10^{12} kg/y of water as sediments and altered oceanic crust enter subduction zones, and at this rate our current hydrosphere would be cycled into the mantle every 1.5 Ga. The rate at which Earth degasses water at ocean ridges is about an order of magnitude less than that lost to subduction, and the rate of degassing of water at hotspot volcanism is an order of magnitude less than ridge degassing. The bottom line is that Earth's oceans are decreasing in volume with time and the mantle is becoming more hydrated. If this observation is correct, the role of water in the mantle has been greatly underestimated, especially in terms of possible melting and convection regimes in the deep mantle.

Just how all this water is stored in the mantle has been the subject of many studies. Water (or hydrogen) can be stored in a broad suite of minerals, as defects in anhydrous minerals and as dissolved hydrogen atoms in iron-rich minerals and melts (Litasov et al, 2003). In the shallow mantle (50–300 km deep), water is stored in metamorphic minerals such as serpentine, amphibole, mica, and lawsonite (contains 11% water), and by defect hydration of olivine and pyroxenes. Numerical simulations to constrain the distribution of water in and around subducting slabs suggest that hydrous minerals are stable above the slab and that they carry water into the mantle transition zone (Tonegawa et al., 2008). At greater depths a group of hydrated Mg-silicates have been synthesized, the so-called "alphabet" phases, which have not as yet been given mineral names. Below 300 km, water may be retained in defects and in hydrous phases A, B, D, and E (D may be stable to 1250 km). In addition, Mg- and Ca-perovskite,

magnesiowustite, and post-perovskite may retain significant amounts of water in the deep mantle as defect substitutions (10–1000 ppm in each phase). Both wadsleyite and ringwoodite are each likely to contain about 0.5% water under normal mantle conditions. The solubility of water in these phases decreases with increasing temperature, and hence subduction of these phases can introduce significant amounts of free water into the deep mantle.

Because of changing solubilities of water with temperature and pressure, there is considerable interest in describing what occurs when water-enriched phases in the transition zone are convected upward or downward (Bercovici & Karato, 2003). If enhanced water contents accompany the high water solubility within transition zone phases, then hot upwellings would release water as they rise and correspondingly cool downwellings would release water as they sink. This water release has been proposed to generate global melting just above the 410-km discontinuity, which could explain a widespread low S-wave velocity anomaly at this depth (Hirschmann, 2006; Sakamaki et al., 2006). However, modeling of the advective transfer of water in the mantle by convection and diffusion indicates that water is not readily concentrated in the transition zone, but rather it is homogenized over broad depth ranges (Richard et al., 2002). The key point here is that the hydration of the deep mantle is still relatively uncertain (Hirschmann, 2006). If significant amounts of water are stored here, the lower mantle could contain one or two oceans of water!

PLATE DRIVING FORCES

Although the question of what drives Earth's plates has promoted a lot of controversy in the past, we now seem to be converging on an answer. Most investigators agree that plate motions must be related to thermal convection in the mantle, although a generally accepted model relating the two processes remains elusive. The shapes and sizes of plates and their velocities exhibit large variations and do not show simple geometric relationships to convective flow patterns. Most computer models, however, indicate that plates move in response chiefly to slab-pull forces as plates descend into the mantle at subduction zones, and that ocean-ridge push or stresses transmitted from the asthenosphere to the lithosphere are very small (Vigny et al., 1991; Lithgow-Bertelloni & Richards, 1995; Conrad & Lithgow-Bertelloni, 2002). Ridge-push forces are caused by two factors: (1) horizontal density contrasts resulting from cooling and thickening of the oceanic lithosphere as it moves away from ridges, and (2) the elevation of the ocean ridge above the surrounding seafloor (Spence, 1987). The slab-pull forces in subduction zones reflect the cooling and negative buoyancy of the oceanic lithosphere as it ages. The gabbro-eclogite and the other high-pressure phase transitions that occur in descending slabs also contribute to slab-pull by increasing the density of slabs.

Stress distributions are consistent with the idea that at least oceanic plates are decoupled from underlying asthenosphere (Wiens & Stein, 1985). Using an

analytical torque balance method, which accounts for interactions between plates by viscous coupling to a convecting mantle, Lithgow-Bertelloni and Richards (1995) show that the slab-pull forces amount to about 95% of the net driving forces of plates. Ridge-push and drag forces at the base of the plates are no more than 5% of the total. Computer models using other approaches and assumptions also seem to agree that slab-pull forces dominate (Vigny et al., 1991; Carlson, 1995). Although slab-pull cannot initiate subduction, once a slab begins to sink, the slab-pull force rapidly becomes the dominant force for continued subduction.

MANTLE PLUMES

A **mantle plume** is a buoyant mass of material in the mantle, which because of its buoyancy, rises. The existence of mantle plumes in Earth was first suggested by J. Tuzo Wilson (1963) as an explanation of oceanic island chains, such as the Hawaiian-Emperor chain, which change progressively in age along the chain. Wilson proposed that as a lithospheric plate moves across a fixed hotspot (the mantle plume), volcanism is recorded as a linear array of volcanic seamounts and islands parallel to the direction the plate is moving. However, we know today that plumes can also move, so this simplified model will not hold for all hotspot tracks. In fact, a few investigators question whether mantle plumes really exist at all.

Laboratory experiments show that plume viscosity has an important effect on the shape of a plume. If a plume has a viscosity greater than its surroundings, it rises as a finger, whereas if it has a lower viscosity, it rises with a mushroom shape and has a distinct head and tail (Figure 4.22). The tail contains a hot fluid that "feeds" the head as it buoyantly rises. The characteristic head-tail structure likely results from strong cooling of the mantle by large-scale stirring driven by plate tectonics (Jellinek & Manga, 2004). Griffiths and Campbell (1990) were the first to confirm by experiment and theory the existence of thermal plume heads and tails and to distinguish between thermal and compositional plumes. In thermal plume heads, the boundary layer around the plume is heated by conduction, becomes buoyant, and rises. This results in a plume head that reaches a diameter of 1000 km or more. This size is consistent with many large igneous provinces, which may reach diameters of 500 to 3000 km. Because of the thermal buoyancy of the head, it entrains material from its surroundings as it grows, and depending on the rate of ascent, it may entrain up to 90% of its starting mass. Streamlines in computer models show that most of the entrained fraction should come from the lower mantle (Hauri et al., 1994).

Although most Earth scientists accept the plume hypothesis, there is a minor, but vocal group who do not (Anderson, 2003; Anderson & Natland, 2005). They point out that it has not yet been possible with seismic tomography to image narrow vertical structures that may represent plume tails over the entire mantle (although, as pointed out below, this is rapidly changing). Another problem with some plumes is the lack of high heat flow. The critics also

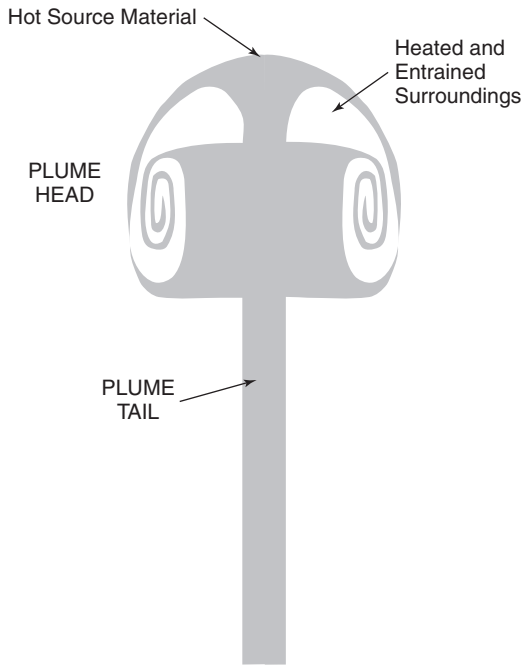

FIGURE 4.22 Photograph of a starting plume in a laboratory experiment showing the large head and narrow tail. The plume was produced by continuously injecting hotter, lower viscosity dyed fluid into the base of a cool, higher viscosity layer of the same fluid. Light regions in the head are entrained from surrounding undyed fluid. *Courtesy of Ian Campbell.*

show that geochemical arguments used to support the plume hypothesis are ambiguous and can be explained without calling on plumes (Foulger & Natland, 2003). However, the plume critics have failed to come up with another model to explain the widely distributed evidence suggestive of mantle plumes. Although many details of plumes and their effects are still controversial and debated, the basic theory of mantle plumes is well established and there is considerable observational evidence to support the plume concept. In addition, recently the resolution of seismic tomography has improved sufficiently such that at least some plumes in the upper mantle can be detected seismically (Li et al., 2000; Rhodes & Davies, 2001; Ritsema & Allen, 2003) (Figure 4.23).

Hotspots

As discussed in Chapter 3, hotspots are generally thought to form in response to mantle plumes that reach the base of the lithosphere (Duncan & Richards, 1991). Partial melting of plumes in the upper mantle leads to large volumes of magma, which are partly erupted (or intruded) at Earth's surface as large igneous provinces (LIPs) or oceanic islands.

Somewhere between 40 and 150 active hotspots have been described on Earth. The best documented hotspots have a rather irregular distribution occurring in both oceanic and continental areas (Figure 4.24). Some occur on or near ocean ridges, such as Iceland, St. Helena, and Tristan in the Atlantic Basin, while others occur near the centers of plates (such as Hawaii). How long do hotspots last? One of the oldest hotspots is the Kerguelen hotspot in the southern Indian Ocean, which began to produce basalts about 117 Ma. Most modern hotspots, however, are <100 Ma. The life spans of hotspots depend on such parameters as plume size and the tectonic environment into which a plume is emplaced. On the Pacific plate, three volcanic chains were generated by hotspots between 70 and 25 Ma, whereas 12 chains have been generated in the last 25 Ma. The large number of hotspots in and around Africa and in the Pacific Basin correspond to the two major geoid highs (Figure 4.3) (Stefanick & Jurdy, 1984). The fact that the geoid highs appear to reflect mantle upwellings supports the idea that hotspots are caused by mantle plumes rising from the deep mantle.

A major problem that has stimulated a great deal of controversy is whether hotspots remain fixed relative to plates (Duncan & Richards, 1991). If they have remained fixed, they provide a means of determining absolute plate velocities. The magnitude of interplume motion can be assessed by comparing the geometry and age distribution of volcanism along hotspot tracks with reconstructions of past plate movements based on paleomagnetic data. If hotspots are stationary

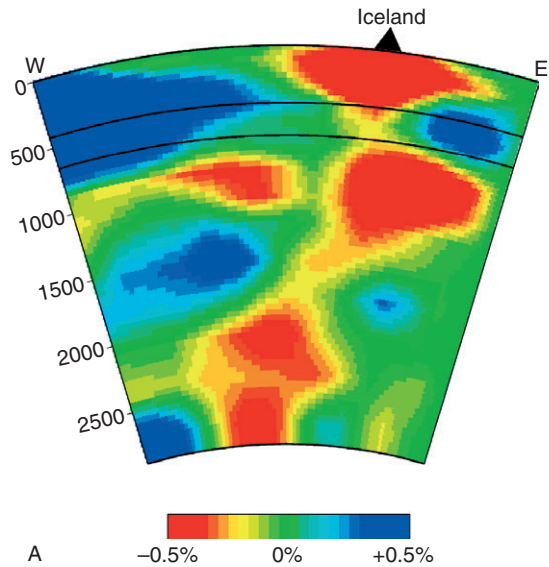

FIGURE 4.23 **(A)** P-wave seismic tomographic image of the Iceland plume. Colors as in Figure 4.2. *Courtesy of Dapeng Zhao.*

Continued

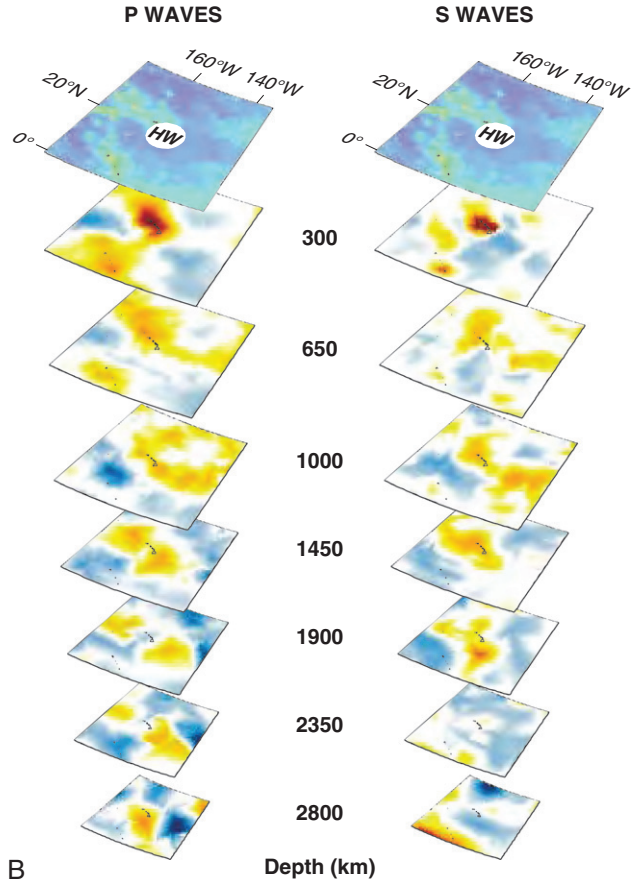

FIGURE 4.23—cont'd **(B)** Three dimensional view of the mantle plume beneath Hawaii for both P and S waves. Colors as in Figure 4.2. From Montelli et al. (2006). *Courtesy of R. Montelli. Reproduced with permission of American Geophysical Union.*

beneath two plates, then the calculated motions of both plates should follow hotspot tracks observed on them. The close correspondence between observed and modeled tracks on the Australian and African plates (Figure 4.25) supports the idea that these hotspots are fixed relative to each other and are maintained by deeply rooted mantle plumes. Also, the almost perfect fit of volcanic chains in the Pacific plate with a pole of rotation at 70 °N, 101 °W and a rate of rotation about this pole of about 1 deg/Ma for the last 10 Ma suggests that Pacific hotspots have remained fixed relative to each other over this short period of time (Steinberger & O'Connell, 1998).

If all hotspots have remained fixed with respect to each other, it should be possible to superimpose the same hotspots in their present positions on their

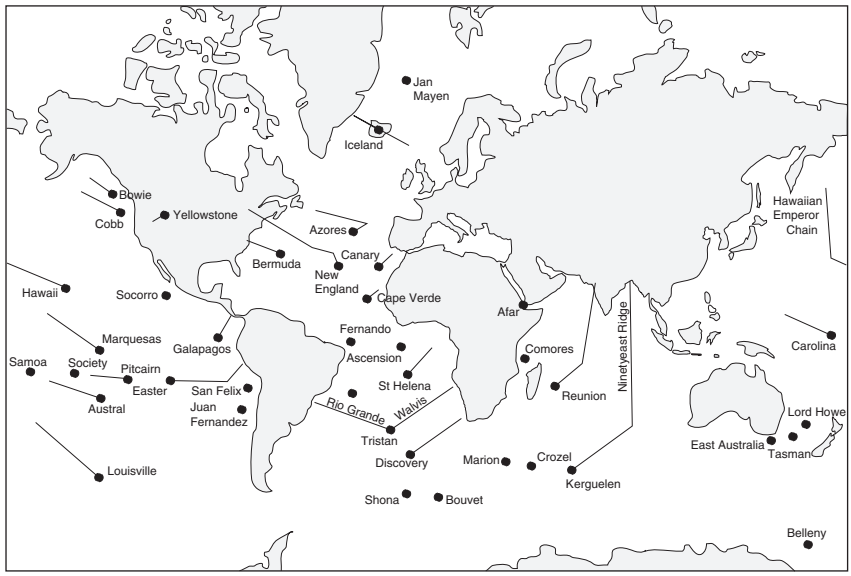

FIGURE 4.24 Geographic distribution of major terrestrial hotspots (dots) and tracks (lines).

predicted positions at other times in the last 150–200 Ma. Except for hotspots in proximity to each other, however, it is not possible to do this, suggesting that hotspots move in the upper mantle (Duncan & Richards, 1991; Van Fossen & Kent, 1992). As mentioned in Chapter 3, there is now strong paleomagnetic evidence for movement of the Hawaiian hotspot prior to 43 Ma (Tarduno et al., 2003). Also, in comparing Atlantic with Pacific hotspots, significant differences are seen between calculated and observed hotspot tracks (Molnar & Stock, 1987). Using paleolatitudes deduced from seamounts, Tarduno and Gee (1995) show that Pacific hotspots have moved relative to Atlantic hotspots at a rate of about 30 mm/y.

Plume Characteristics

Theoretical, geochemical, and laboratory models have clarified the dynamics of plumes and have suggested numerous ways that plumes may interact with the mantle (White, 2010). The numerical models of Davies (1999) and others of temperature-dependent viscosity plumes confirm and expand on laboratory experiments. A sequence of snapshots of a mantle plume as it ascends and spreads over a 176-Ma period is shown in Figure 4.26. The plume ascends rapidly in the first 100 Ma and then more slowly afterward as it begins to flatten against the lithosphere. As the hot fluid in the plume tail reaches the top of the head, it flattens against the lithosphere and the head becomes very thin and increases significantly in radius (176 Ma). Heat liberated from the plume partly escapes

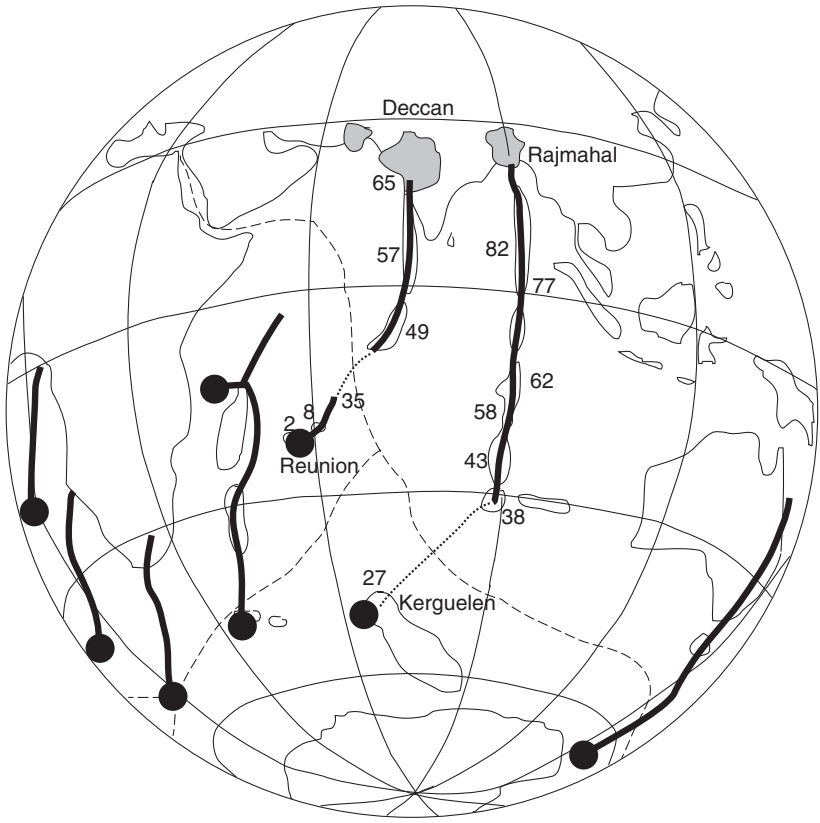

FIGURE 4.25 Computer-generated hotspot tracks for the Indian and South Atlantic Oceans, showing calculated (heavy lines) and observed hotspot trajectories. Current hotspots at black dots and past ages of hotspot basalts given in millions of years ago. *After Duncan (1991).*

and partly heats material entrained in the plume head so the head has a temperature intermediate between the tail and the surrounding mantle. Such features were also recognized in the experimental models of Griffiths and Campbell (1990). As the head continues to grow and cool, it rises more slowly than the tail, which continues to feed the head. More recent experimental results indicate that plumes may reach a level of neutral buoyancy before arriving at the base of the lithosphere at which point they stagnate and denser parts of the plume actually begin to sink (Kumagai et al., 2008). This can produce fat and patchy plumes such as the Iceland plume (Figure 4.23a).

Davies (1995) has shown by computer models that for the temperature- and depth-dependent viscosity in Earth, most plumes should pass through the ringwoodite-perovskite phase boundary unimpeded. As a plume head approaches the lithosphere, it begins to flatten and eventually intersects the mantle

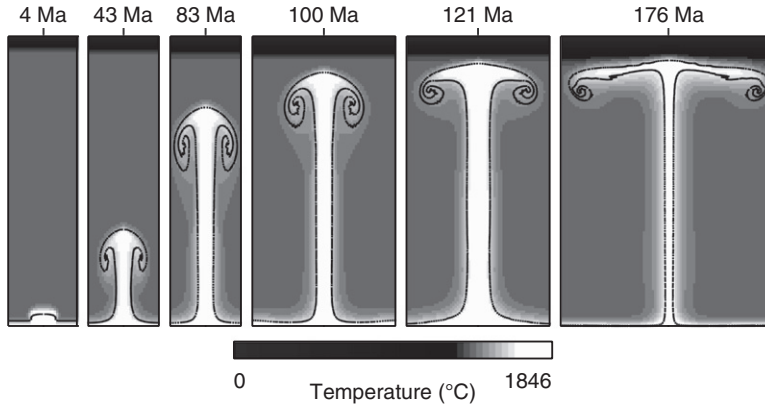

FIGURE 4.26 Numerical model showing rise and growth of a mantle plume from the D″ thermal boundary layer for 176 Ma. Viscosity is a strong function of temperature and ambient viscosity is 10^{22} Pa sec. The bottom boundary temperature is 430°C above the interior plume temperature and plume viscosity here is about 1% of the plume interior. *Courtesy of Geoff Davies.*

solidus, resulting in the production of large volumes of basaltic magma in relatively short times (White & McKenzie, 1995). Plumes with flattened heads $\geq$1000 km diameter are plausible sources for flood basalts and large oceanic plateaus as discussed in Chapter 3.

The geochemistry of basalts derived from hotspot volcanoes provides yet another characteristic of mantle plumes (White, 2010). First of all, oceanic island basalts are usually, although not always, geochemically distinct from ocean ridge basalts as discussed below. Also, geothermometry studies of olivine from oceanic island basalts indicates they are derived from mantle sources that are several hundred degrees hotter than mantle beneath ocean ridges.

Tracking Plume Tails

Tomographic images of S-wave velocity distribution in the mantle seem to confirm the existence of plumes with long tails beneath many of Earth's hotspots (Montelli et al., 2006; Zhao, 2007). For instance, deep mantle plumes probably exist beneath Hawaii, Azores, Afar, Canary, Samoa, and Tahiti, and in some cases tails can be tracked to the core–mantle boundary (for instance, Hawaii, Cape Verde, Cook Island, and Kerguelen). This is illustrated in Figure 4.23b for Hawaii, which shows a composite seismic tomographic cross section of the Hawaiian plume. Plumes that reach only midmantle depths are recognized at Bowie, Eastern Australia, and Juan Fernandez, but these plumes may have weak tails that cannot be resolved in the deep mantle. Probable plumes starting in the D″ layer occur south of Java in Indonesia, east of the Solomon Islands in the South Pacific, and beneath the Coral Sea. All of the currently imaged plumes are wide and do not show well-developed plume heads, suggesting a very weak

temperature dependence of viscosity in the lower mantle or/and compositional variations in the plumes. Most plumes that can be traced to the lower mantle, such as the Hawaiian plume (Figure 4.23b), are associated with well-defined slow/hot regions in or just above the core–mantle interface.

Plume Sources

Although the base of both the upper and the lower mantle have been suggested as sites of mantle plume generation, four lines of evidence suggest that many plumes are produced just above the core–mantle boundary in the D″ layer (Campbell & Griffiths, 1992a; Davies & Richards, 1992):

1. Computer modeling indicates that plume heads can only achieve a size (~1000 km diameter) required to form large volumes of flood basalt and large submarine plateaus, like the Ontong Java plateau, if they come from the deep mantle.
2. The approximate fixed position of hotspots relative to each other in the same geographic region is difficult to explain if plumes originate in the convecting upper mantle, but is consistent with a high-viscosity, lower mantle source.
3. The amount of heat transferred to the base of the lithosphere by plumes, which is $\leq$12% of Earth's total heat flux, is comparable to the amount of heat estimated to be emerging from the core as it cools.
4. Periods of increased plume activity in the past seem to correlate with normal polarity epochs and decreased pole reversal activity in plume-related basalts (Larson, 1991a, b). Correlation of plume activity with magnetic reversals implies that heat transfer across the core–mantle boundary starts a mantle upwelling in D″, and at the same time changes the pattern of convective flow in the outer core, which in turn affects Earth's magnetic field.

An excess of radiogenic Os in some oceanic island basalts may also support a deep source for mantle plumes, but the argument is less robust. By analogy with iron meteorites, Earth's core should be enriched in Os with a high $^{187}Os/^{188}Os$ ratio compared to the mantle (Walker et al., 1995). Thus, plumes produced in the D″ layer could be contaminated with radiogenic Os from the core. Some plume-derived basalts have $^{187}Os/^{188}Os$ ratios up to 20% higher than primitive or depleted mantle. However, because these basalts do not show evidence of tungsten (W) contamination (W is also concentrated in the core as it is a siderophile element), the high radiogenic Os values may be due to a recycled crustal component in the deep mantle (Schersten et al., 2004).

Not all data, however, are interpreted to reflect deep plume sources. Another interpretation of seismic tomographic data by Boschi et al. (2007) suggests that only a small fraction of plumes associated with known hotspots may have sources in the D″ layer. Many LIPs erupted in the last 300 Ma lie vertically above the margins of the large African and South Pacific upwellings (Burke et al., 2008). The sites of 24 active hotspots project downward to these same

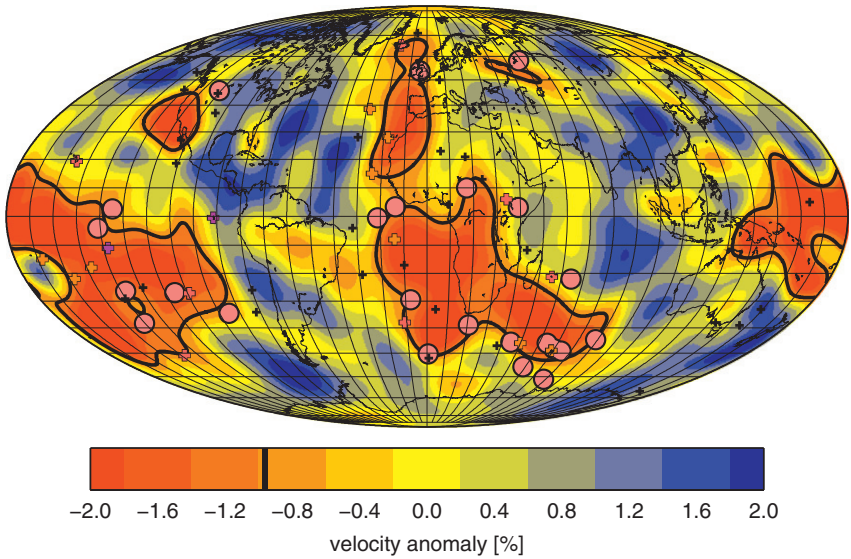

FIGURE 4.27 Large igneous province (LIP) eruption sites (pink circles) and young hotspots (crosses) plotted on an S-wave tomographic model of the D″ layer. Average separation of LIPs from the 0.96% contour of velocity anomaly on the map (bold black line) is only 3.7 degrees. *From Burke et al. (2008), courtesy of Kevin Burke and Trond Torsvik.*

narrowly defined upwelling margins (Figure 4.27). This correlation suggests that the plume generation zones of these hotspots are around the margins of the two giant upwellings. Furthermore, because all LIP eruption sites younger than 300 Ma lie above the margins of these upwellings today, plume generation zones are inferred to have remained in the same places for the last 300 Ma. Steep horizontal temperature gradients at the upwelling intersections with normal mantle are important controls for the generation of these plumes.

MANTLE GEOCHEMICAL COMPONENTS

Radiogenic isotopes can be used as geochemical "tracers" to track the geographic and age distribution of crustal or mantle reservoirs from which the elements that house the parent (P) and daughter (D) isotopes have been fractionated from each other. For instance, any process that fractionates U from Pb or Sm from Nd will result in a changing rate of growth of the daughter isotopes ^{207}Pb and ^{206}Pb (from ^{235}U and ^{238}U, respectively) and ^{143}Nd (from ^{147}Sm). If the element fractionation occurred geologically long ago, the change in P/D ratio will result in a measurable difference in the isotopic composition of the melt and its source. This is the basis for the isotopic dating of rocks. On the other hand, if the chemical change occurs during a recent event, such as partial melting in the mantle just prior to magma eruption, there is not enough

time for the erupted lava to evolve a new isotopic signature distinct from the source material reflecting its new P/D ratio. Hence, young basalts derived from the mantle carry with them the isotopic composition of their mantle sources, and this is the basis of the **geochemical tracer** method (Hart, 1988; Hofmann, 1997; 2003; White, 2010). Tracer studies clearly show that the mantle is heterogeneous on scales of a few hundred meters or less to thousands of kilometers (Paulick et al., 2010).

When isotopic ratios from young oceanic basalts are plotted against the P/D ratio, they often scatter along a line known as a **mantle isochron** (Brooks et al., 1976; Rudge, 2006). The interpretation of mantle isochrons, however, is ambiguous. They could represent ages of major fractionation events in the mantle, or alternatively, they may be mixing lines between end member components in the mantle. However, the fact that most ages calculated from U/Pb and Rb/Sr isotopic data from young oceanic basalts fall between 1.8 and 1.6 Ga, and most Sm/Nd results yield ages of 2.0–1.8 Ga seem to favor their interpretation as ages of mantle events. Even if the linear arrays on isochron diagrams are mixing lines, at least one of the end members has to be $\geq$2.0 Ga.

Identifying Mantle Components

Summary

Isotopic ratios from basalts show that at least four, and perhaps as many as six, isotopic components exist in the mantle (Hart, 1988; Hart et al., 1992; Helffrich & Wood, 2001) (Figures 4.28 and 4.29). These are **depleted mantle** (**DM**), the source of **ocean ridge basalts** (**MORBs**); **HIMU**, distinguished by its high $^{206}Pb/^{204}Pb$ ratio, which reflects a high U/Pb ratio ($\mu = {}^{238}U/^{204}Pb$) in the source; and at least two enriched sources (**EM1** and **EM2**), which reflect long-term enrichment in light REE in the source. A fifth component, **primitive mantle** (**PM**), may be preserved in parts of the mantle.

The existence of at least four mantle geochemical components is now well documented. What remains to be verified is the origin and location of each of these and their mixing relations. As summarized below, much progress has been made on these questions by also using rare gas isotopic data and trace element ratios. Also, the hierarchy of mixing of components in basalts from single islands or island chains can provide useful information on the location of the components in the mantle.

Depleted Mantle

Depleted mantle (DM) is mantle that has undergone one or more periods of fractionation involving extraction of basaltic magmas (Hofmann, 2003). It is known to underlie ocean ridges and probably extends beneath ocean basins, although it is not the source of oceanic island magmas. The depleted isotopic character (low $^{87}Sr/^{86}Sr$, $^{206}Pb/^{204}Pb$ and high $^{143}Nd/^{144}Nd$) (Figures 4.28 and 4.29) and low large ion lithophile element contents of MORB require the existence of a

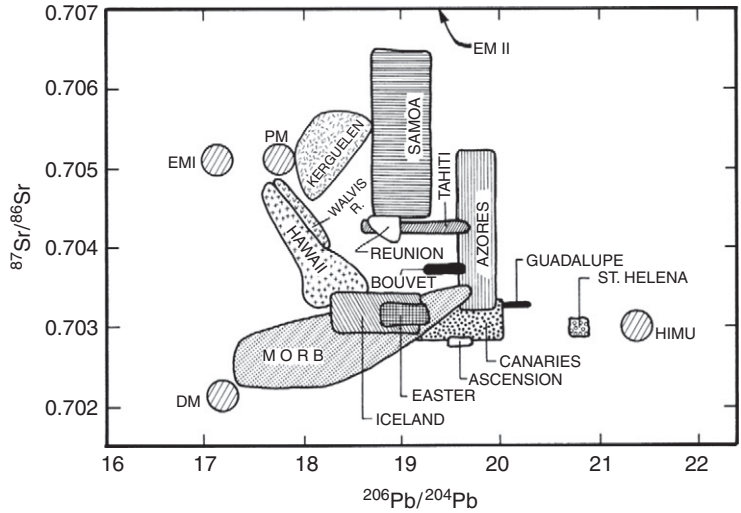

FIGURE 4.28 Sr and Pb isotope distributions in MORB and ocean island basalts. DM, depleted mantle; PM, primitive mantle; HIMU, high U/Pb component; EMI and EM2, enriched mantle components. *Modified after Zindler & Hart (1986).*

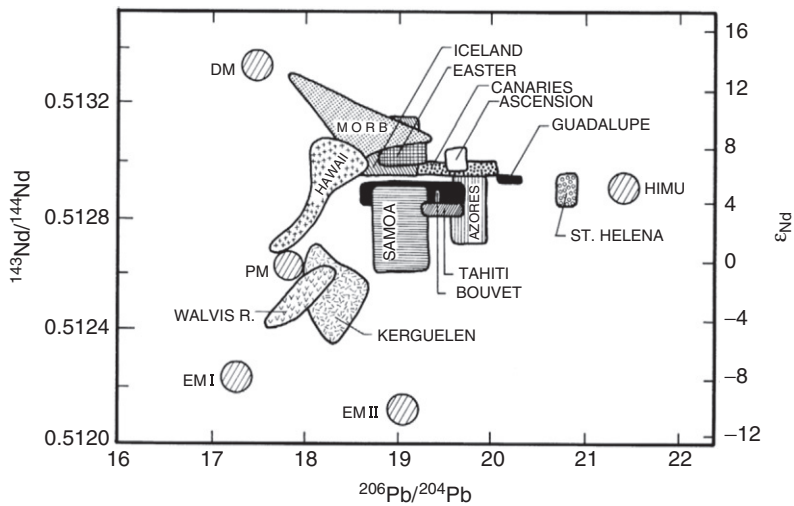

FIGURE 4.29 Nd and Pb isotope distributions in MORB and ocean island basalts. DM, depleted mantle; PM, primitive mantle; HIMU, high U/Pb component; EM1 and EM2, enriched mantle components. *Modified after Zindler & Hart (1986).*

widespread depleted mantle reservoir. Rare gas isotopic compositions also require that this reservoir be highly depleted in rare gases compared to other mantle components. Although most of the geochemical variation within MORB can be explained by processes such as variable degrees of melting, variations in isotopic ratios demand that the depleted mantle reservoir is heterogeneous, at least on scales of 10^2–10^3 km and probably less. This heterogeneity may be caused by small amounts of mixing with enriched mantle components. The most important of these enriched components appears to be recycled continental crust: oxygen isotopic data suggest that the upper mantle globally contains an average of 5–10% of recycled continental crust (Cooper et al., 2009).

Although depleted mantle beneath ocean ridges is widely thought to be well mixed, abyssal peridotites from some slow-spreading ocean ridges have Nd and Os model ages of $\geq$2 Ga, implying a long-term preservation of old mantle components, which have not been eliminated by later convective mixing (Liu et al., 2008). This suggests that mixing in the upper mantle is not effective in eliminating ancient domains.

HIMU

The extreme enrichment in ^{206}Pb and ^{208}Pb in some oceanic island basalts (such as those from St. Helena; Figures 4.28 and 4.29) requires the existence of a mantle source enriched in U+Th relative to Pb, and mantle isochrons suggest an age for this HIMU source on the order of 2.0–1.5 Ga. This reservoir is also enriched in radiogenic ^{187}Os (Hauri & Hart, 1993). Because HIMU has ^{87}Sr/^{86}Sr ratios similar to MORB, however, it has been suggested that it represents subducted oceanic crust in which the U+Th/Pb ratio was increased by preferential loss of Pb in volatiles escaping upward from descending slabs during subduction. Supporting a recycled oceanic crust origin for HIMU are relative enrichments in Ta and Nb in many oceanic island basalts. As discussed in Chapter 3, devolatilized descending slabs should be relatively enriched in these elements since neighboring incompatible elements like Th, U, K, and Ba have been lost to the mantle wedge. Thus, the residual mafic part of the slab that sinks into the mantle and may later become incorporated in mantle plumes should be relatively enriched in Ta and Nb. Although an origin for HIMU as recycled oceanic crust is widely accepted, Kamber and Collerson (1999) have proposed that in terms of helium and Pb isotopes, it can best be explained as recycled oceanic lithosphere that has been metasomatized.

An equally difficult question is that of where HIMU resides in the mantle. There are two main contenders: (1) mantle plumes and (2) dispersed blobs or steaks in the depleted upper mantle. The common assumption that hotspots are synonymous with mantle plumes is clearly not the case. For example, it is not easy to reconcile with mantle plumes the large number of isolated islands and seamounts (>70 000 with heights >1 km in the Pacific alone) that are not aligned in chains. Most of these have volcanics that carry a HIMU or an

enriched source geochemical signature (EM, see below), yet they probably do not come from plumes. In this case the HIMU-EM component may be acquired by small degrees of melting, which tends to preferentially sample the more highly fusible parts of the mantle where the HIMU-EM component resides, whereas higher degrees of melting at ocean ridges will homogenize the mixture, sampling a large proportion of depleted mantle, and thus produce more depleted melts (MORB).

Enriched Mantle

Enriched mantle components are enriched in incompatible elements such as Rb, Nd, U, and Th. At least two enriched components are required to explain the isotopic and trace element distributions in the sources of oceanic basalts (Figure 4.30) (Zindler & Hart, 1986; Willbold & Stracke, 2006): EM1 with moderate $^{87}Sr/^{86}Sr$ ratios and low $^{206}Pb/^{204}Pb$ ratios and EM2 with high $^{87}Sr/^{86}Sr$ ratios and moderate $^{206}Pb/^{204}Pb$ ratios. Both have low $^{143}Nd/^{144}Nd$ ratios. Among the numerous candidates proposed for EM1 are old oceanic mantle lithosphere (± sediments) that has been recycled back into the mantle (Hart et al., 1992; Hauri et al., 1994) and metasomatized lower mantle (Kamber & Collerson, 1999). Also Hf isotope distributions in Hawaiian basalts have been interpreted to indicate the presence of old pelagic sediments in their plume

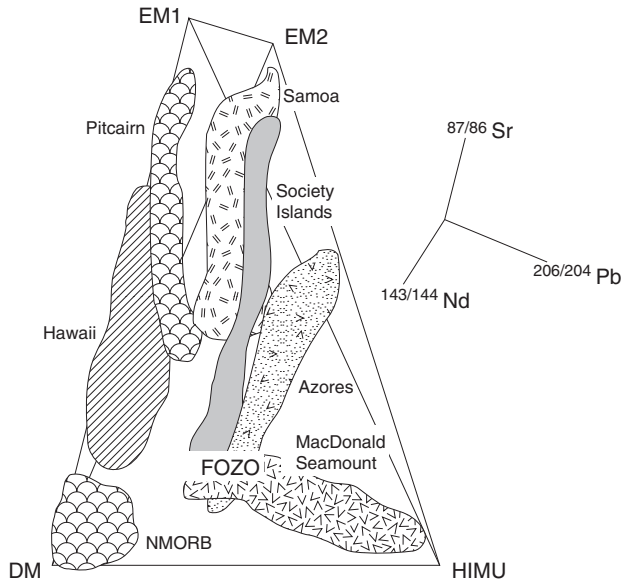

FIGURE 4.30 Three-dimensional plot of Sr, Nd, and Pb isotopic ratios from intraplate ocean basalts. The tetrahedron is defined by the mantle end members EM1, EM2, DM, and HIMU. *Modified after Hauri et al. (1994).*

sources (Blichert-Toft et al., 1999). At some localities (Walvis ridge, SW Indian ridge, Marion hotspot), low but variable $^{206}Pb/^{204}Pb$ ratios occur in the volcanics, and also a large range of $^{207}Pb/^{204}Pb$ and $^{208}Pb/^{204}Pb$ ratios are found relative to the $^{206}Pb/^{204}Pb$ ratio (e.g., Mahoney et al., 1995; Douglass et al., 1999). These variations clearly indicate that EM1 cannot be considered as one mantle component, but it must represent several components. All of these components must be depleted in the more highly incompatible element U relative to Pb on a time-integrated basis compared to average depleted mantle from which MORB comes, and they must have a time-integrated Rb/Sr ratio similar to that of primitive mantle.

EM2, if there is a single EM2 component, has isotopic ratios closer to average upper continental crust or to modern subducted continental sediments (i.e., $^{87}Sr/^{86}Sr > 0.71$ and $^{143}Nd/^{144}Nd \sim 0.5121$). Subducted continental sediments are favored by some investigators for this end member because EM2 commonly contributes to island-arc volcanics in which continental sediments have been subducted, such as the Lesser Antilles and the Sunda arc (Hauri et al., 1994; Willbold & Stracke, 2010). Samoan lavas typically carry an EM2 signature and oxygen isotopes, and $^{87}Sr/^{86}Sr$ ratios clearly define continental crust or its sedimentary derivative in the mantle sources (Workman et al., 2008). However, based on helium and Pb isotope distributions in Hawaiian lavas, Kamber and Collerson (1999) propose that EM2 is recycled subcontinental lithosphere and that it has a variable composition, and Workman et al. (2003) suggest that it may be recycled oceanic lithosphere with trapped melt fractions. It would appear that EM2 represents more than one component or a complex mixture of components in the mantle.

Helium Isotopes

One of the most important observations in oceanic basalts is that their helium isotope ratios differ according to tectonic setting. There are two isotopes of helium: ^{3}He, which is a primordial isotope that was incorporated in Earth as it accreted, and ^{4}He, an isotope produced by radioactive decay of U and Th isotopes. Plume-related basalts in oceanic areas have relatively high $^{3}He/^{4}He$ ratios often more than 20 times that of air ($R/R_A \geq 20$), whereas MORB generally has R/R_A values of 7–9 (Hanan & Graham, 1996). In some Pacific MORB, R/R_A values increase with increasing $^{206}Pb/^{204}Pb$ ratios, whereas in the Atlantic the opposite trend is observed. Also, in the Atlantic and Indian Oceans, helium isotope ratios tend to be higher in basalts with EM1 characteristics. These high ratios, which apply to both MORB and oceanic island basalts, may be sampling two different EM1 reservoirs, both with low U/Pb and high Th/Pb ratios.

Two classes of models have been suggested to explain the origin of the high $^{3}He/^{4}He$ reservoir in the mantle. Some investigators interpret the high ratios to reflect recycled oceanic lithosphere in the deep mantle (Albarede, 1998). Such lithosphere should have a high $^{3}He/^{4}He$ ratio because partial melting at ocean ridges extracts almost all of the U and Th from the mantle source. Because these

elements are responsible for accumulation of ^{4}He over time, causing the $^{3}He/^{4}He$ ratio to decrease in the source, without U and Th, the depleted oceanic lithosphere would acquire a high $^{3}He/^{4}He$ ratio. Alternative models call upon primitive, unfractionated sources deep in the mantle that still retain their original high $^{3}He/^{4}He$ ratios (Helffrich & Wood, 2001; Porcelli & Elliott, 2008). However, new experiments on the behavior of helium in the mantle do not require a deep primordial source (White, 2010). The most convincing case for truly primitive helium isotope ratios comes from young plume-related basalts from Baffin Island in Canada. The basalts have very high $^{3}He/^{4}He$ ratios and exhibit primitive Pb and Nd isotope ratios, the combination of which suggests preservation, at least locally, of a very primitive source ($\geq$4.5 Ga) deep in the mantle (Jackson et al., 2010).

Archean Geochemical Components

Although geochemical mantle components are defined from isotopic ratios in young basalts, because many of the isotopes (such as Sr, Pb and U) are subject to remobilization during secondary processes, it has proved difficult to extend these characterizations to Archean basalts. One way around this problem is to use relatively immobile incompatible elements, or better yet, immobile incompatible element ratios (Weaver et al., 1987; Condie, 2003a). Incompatible element ratios also have the advantage that they do not change with time as isotopic ratios do. Condie (2003a, 2004) suggests that it is possible to characterize at least some mantle domains with four incompatible element ratios in tholeiites: Nb/Th, Zr/Nb, Zr/Y, and Nb/Y. Although these ratios cannot identify mantle geochemical reservoirs with the resolution of radiogenic isotopes, in some cases they can be used to distinguish plume from nonplume mantle sources. However, they cannot, without additional data, distinguish subduction-derived basalts from plume-derived basalts that are contaminated with continental crust or subcontinental lithosphere. If age relationships are well known in a given greenstone succession, the Zr/Y-Nb/Y and Nb/Th-Zr/Nb relationships may be useful in tracking plume histories, supercontinent breakup, and the mixing of deep and shallow depleted mantle sources. They should be used, however, only when stratigraphic and lithologic assemblages are well characterized, and then only to supplement and complement other data. Trace element ratios in Archean greenstones suggest that modern mantle geochemical components were in place by the late Archean.

Mixing Regimes in the Mantle

When viewed in Nd-Sr-Pb isotopic space, arrays defined by various oceanic basalts tend to cluster along two and three component mixing lines with DM, HIMU, EM1, and EM2 at the corners of a tetrahedron (Figure 4.30). There is, however, a notable lack of mixing arrays joining EM1, EM2 and HIMU, which seems to rule out random mixing in the mantle (Hart et al., 1992; Hauri et al., 1994). The mixing arrays are systematically oriented originating from points along the EM1-HIMU and EM2-HIMU joins and converging in a region

within the lower part of the tetrahedron, but not at DM. This convergence suggests the existence of another mantle component that appears in oceanic mantle plumes. This component, which is called **FOZO** (or C) after the focal zone from the converging arrays, is a depleted mantle component (Hart et al., 1992) (Figure 4.30). Helium isotope ratios also progressively increase toward FOZO, and because ^{3}He may have been incorporated in Earth during planetary accretion, the high ^{3}He/^{4}He ratios are commonly interpreted to mean that the FOZO component is relatively primitive, and probably resides deep in the mantle. Alternatively, as mentioned above, the high ^{3}He/^{4}He ratios in FOZO may represent a recycled oceanic lithosphere in this source.

The fact that mixing arrays do not emanate from the EM1-EM2 join nor from the EM1-EM2-HIMU face of the tetrahedron indicates that there was some process that caused juxtaposition of EM components and HIMU that predates the mixing with FOZO. The probability that most or all hotspot sources do not mix with the shallow depleted mantle DM is consistent with most plume entrainment occurring in the lower mantle.

The isotopic mixing arrays do not tell us which components occur in the plume sources and which have been entrained in the mantle. A high ^{3}He/^{4}He ratio in FOZO in contrast to a low ^{3}He/^{4}He ratio in DM may indicate that FOZO is in the lower mantle and does not mix with DM in the upper mantle. It is not possible from isotopic data alone to determine if the EM-HIMU components are plume sources in the D″ layer, and FOZO is entrained in the lower mantle as the plumes rise, or the other way around (FOZO is the plume and EM-HIMU are entrained). When coupled with geophysical data previously discussed, however, the former model seems most acceptable.

Although isotopic, rare gas, and trace element distributions in oceanic basalts demand a heterogeneous mantle, the nature, scale, preservation, and history of mantle heterogeneities remain problematic. Experimental studies on diffusion rates of cations in mantle minerals provide a basis to constrain the minimum scale of mantle heterogeneities. Results suggest that even in the presence of a melt where diffusion rates are high, heterogeneities larger than 1 km in size can persist for several billion years (Zindler & Hart, 1986; Kellogg, 1992). Geochemical heterogeneities in ultramafic portions of ophiolites occur on scales of centimeters to kilometers indicating that small-scale heterogeneities survive in the upper mantle. Geochemical and isotopic variations in basalts from a single volcano require heterogeneity on the scale of several kilometers and variations in MORB along ocean ridges or of arc basalts along single volcanic arcs demand heterogeneities on scales of 10^2–10^3 km. Numerical stirring models show that if the viscosity of the lower mantle is 1–2 orders of magnitude greater than the upper mantle, mantle heterogeneities on a variety of scales should survive for billions of years as isotopic data from oceanic island basalts suggest (Davies & Richards, 1992; Ogawa, 2003).

Because the mantle was hotter in the Archean, and hence probably convected more rapidly and chaotically, it is of interest to see if mantle

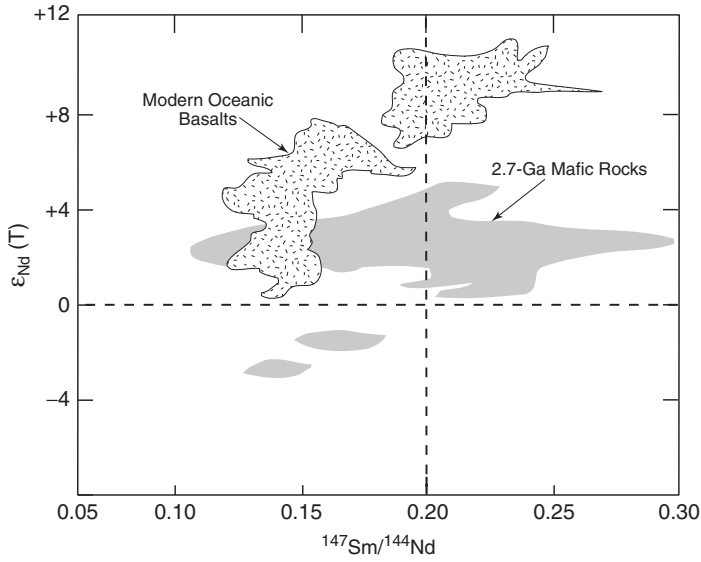

FIGURE 4.31 Distribution of late Archean and modern basalts on an ϵ_{Nd} (T) versus $^{147}Sm/^{144}Nd$ graph. T (age) = 0 Ma for modern basalts and 2.7 Ga for Archean rocks. *After Blichert-Toft & Albarede (1994).*

heterogeneities were preserved in the Archean mantle. Nd isotopic ratios and Sm/Nd ratios provide a means to compare the Archean mantle with the modern mantle, by analyzing for these quantities in greenstone basalts. The Archean mantle array on an ϵ_{Nd}-$^{147}Sm/^{144}Nd$ plot varies significantly from the modern arrays (Figure 4.31). For a similar overall range in Sm/Nd ratio, the Archean array varies by only 1 epsilon unit compared to at least 8 epsilon units in modern arrays (Blichert-Toft & Albarede, 1994). These results demonstrate that both long-term depletion and enriched mantle domains had developed in the mantle by the late Archean. The absence of a larger range in ϵ_{Nd} values in the Archean mantle must mean that heterogeneities with variable Sm/Nd ratios did not survive long enough to be recorded in the $^{143}Nd/^{144}Nd$ isotopic ratio. This, in turn, suggests faster mixing in the Archean mantle.

Overview

By way of summary, perhaps the most significant chemical signatures recorded by the mantle are the complementary relationships between incompatible element enrichment in the continental crust (Figure 2.20) and the probable siderophile element (Fe, Ni, Co, Cr, etc.) enrichment of the core, and the corresponding depletion of these elements in the DM reservoir (Carlson, 1994). It would seem that the key events controlling compositional variations in Earth are early core formation, followed by gradual or episodic extraction of

continental crust to leave at least part of the mantle depleted in incompatible and siderophile elements. The DM and FOZO components may represent depleted mantle remaining from these events. The other mantle components would appear to reflect subducted inhomogeneities that were not sufficiently remixed into the convecting mantle so as to lose their geochemical and isotopic signatures. Many of these components, together with DM, may have been "fossilized" in the subcontinental lithosphere by accretion of spent plume material to the base of the lithosphere throughout geologic time (Menzies, 1990; White, 2010). Both the HIMU and FOZO components are carried in mantle plumes, but their compositions still do not give a clear picture of where plumes come from in the mantle. Plumes are chemically heterogeneous and often carry both incompatible-element enriched and depleted components. However, the depleted component in plumes appears to be distinct from the depleted component in the MORB source, and may represent an early restite later recycled into the deep mantle. Geochemical evidence for layering in the mantle is equivocal and controversial. Although the data do not exclude chemical layering, the nonrandom occurrence of geochemical components in plume sources would seem to require exchange between the upper and lower mantle.

CONVECTION IN THE MANTLE

The Nature of Convection

It is generally agreed that convection in the mantle is responsible for driving plate tectonics (Schubert et al., 2001). Convection occurs because of buoyancy differences with lighter material rising and denser material sinking. In terms of quantitative laboratory models, **Rayleigh-Bernard convection** is best understood. This type of convection arises because of heating at the base and cooling at the surface of fluid. Lord Rayleigh was the first to show that the convective behavior of a substance is dependent on a dimensionless number, now known as the **Rayleigh number**. For a simple homogeneous liquid to convect as it is heated at the base, the Rayleigh number must exceed 2000, and for the convection to be vigorous it must be of the order of 10^5. Irregular turbulent convection begins when the Rayleigh number reaches about 10^6 and such convection probably exists in Earth where the Rayleigh number is greater than 10^6. Calculations indicate that the mass flux in the upper mantle caused by lateral slab motions also may be an important contribution to large-scale mantle convection (Garfunkel et al., 1986).

A voluminous literature exists on models for convection in the mantle. In general, they fall into two categories: (1) layered convection and (2) whole-mantle convection. In **layered convection** models, convection occurs separately below and above the 660-km discontinuity, whereas **whole-mantle convection** involves the entire mantle, although parts of the deep mantle may be isolated from convection because of their high viscosity. It is important to remember that

these types of convection are two end-member scenarios, and that convection in Earth may be somewhere in between (i. e., partially layered convection). Seismic images of the mantle previously discussed suggest that most subducted slabs eventually sink all the way to the bottom of the mantle, and this rules out complete layering at the 660-km discontinuity, favoring some style of whole-mantle convection. However, both depletion in incompatible elements in the upper mantle and the existence of isotopically distinct components or domains in the mantle must be accommodated in any whole-mantle convection model.

In addition to the layered and whole-mantle convection end-member scenarios, several other models of mantle structure and convection have appeared in recent years. The lava-lamp model of Kellogg et al. (1999) proposes that the mantle is divided into an upper layer about 2000 km thick (in contrast to the 660-km boundary) and a compositionally distinct lower layer enriched in iron and heat-producing elements. The model incorporates seismic tomographic observations of deep subduction while keeping the geochemical distinctiveness of various reservoirs in the mantle. A variant of this model proposed by Tolstikhin and Hofmann (2005) shifts the lower boundary of the upper layer to the base of the mantle but preserves the geochemical characteristics of the D″ layer. An alternative to the lava-lamp model is the **"plume pudding"** model in which chemically distinct blobs are scattered throughout the mantle like plums in a pudding. Often the plum pudding model is combined with models of whole-mantle convection to accommodate the preservation of geochemical reservoirs as described above.

Passive Ocean Ridges

Classical pictures of convection in Earth show convective upcurrents coming from the deep mantle beneath ocean ridges, and downcurrents returning at subduction zones. However, it is now clear that ocean ridges are shallow passive features, not related to deep convection in the mantle. S-wave velocity distributions beneath ocean ridges are useful in distinguishing between shallow and deep sources for upwelling mantle. As shown in Figure 4.32, ocean ridges are typically underlain by broad low-velocity regions in the upper 200 km of the mantle. In most cases, the lowest velocities occur at depths of around 100 km (Zhang & Tanimoto, 1992). The widths of the low-velocity regions correlate positively with spreading rates, a feature that may be due to dragging of the shallow asthenosphere away from ridges by the separating plates. Also supporting shallow upwelling beneath ocean ridges is the fact that ocean ridges migrate in response to stress distributions in the plates rather than to buoyancy forces in the deep mantle, as they should if they had deep roots.

The low-velocity anomalies under ocean ridges indicate they have shallow roots probably caused by passive upwelling produced by deformation in plates in response to sinking slabs. Because plumes, on the other hand, are driven by density anomalies in the deep mantle, they should have low-velocity anomalies that

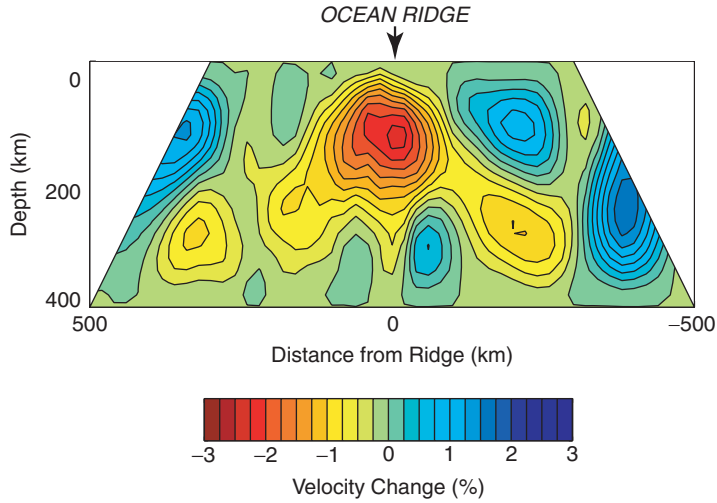

FIGURE 4.32 S-wave velocity distribution across the East Pacific Rise. Note that very slow velocities are confined to depths <200 km. *From Hammond & Toomey (2003), courtesy of Bill Hammond. Reproduced with permission of American Geophysical Union.*

extend much deeper into the mantle, as observed for Hawaii and the Azores. Both situations occur along the Mid-Atlantic Ridge, but only the hotspots on or near ocean ridges have deep low-velocity roots. Thus, it would appear that some degree of decoupling occurs between active and passive asthenosphere at depths of 100–200 km. Just how this occurs and evolves with time is not well understood.

Layered Convection Model

The layered convection model involves separately convecting upper and lower mantle reservoirs. The upper mantle, above the 660-km discontinuity, is generally equated with the geochemically depleted mantle (DM) reservoir and the lower mantle with the other mantle geochemical domains (Allegre, 1982; O'Nions, 1987). If DM is assumed to have formed chiefly by the extraction of continental crust from primitive mantle, calculations based on Nd and Pb isotopes indicate that it must comprise between 35% and 50% of the entire mantle.

One of the major lines of evidence used to support layered mantle convection comes from the isotopic composition of rare gases in basalts (O'Nions, 1987; Allegre et al., 1995a). Nonradiogenic ^{3}He is enriched in many ocean island basalts, and since these appear to be derived from mantle plumes, they may come from an undegassed source in the deep mantle, as discussed above. Similar arguments can be made from Ar, Ne, and Xe isotopes. The simplest model to satisfy these constraints is a two-layer convective mantle with the upper layer (DM) strongly depleted in rare gases and incompatible elements and the lower layer enriched in HIMU and EM components and in ^{3}He.

Despite the rare gas data, however, layered convection has numerous difficulties, among the most prominent are the following:

1. The aspect ratio (width/depth) of convection cells should be close to unity. This is not consistent with layered convection in which convection cells bottom out at 660 km, when horizontal measurements exceed 10^4 km as reflected by plate sizes.
2. Nd, Sr, and Pb isotopic data from oceanic basalts require not just two or three, but several ancient mantle geochemical components as discussed above.
3. As we have seen, seismic velocity studies indicate that descending lithosphere eventually sinks into the lower mantle, a feature that would promote whole-mantle convection.
4. Mantle plumes appear to be derived from the lowermost mantle, another feature consistent with whole-mantle convection.

As we pointed out above, however, layering in the mantle is not an all-or-none situation, and numerous factors influence the degree of layering (Christensen, 1995; Davies, 1995, 2002; Tackley, 2000). Among the more important contributing factors to the nature of convection are the following:

1. *Temperature*. As temperature increases so does the Rayleigh number, and higher Rayleigh numbers tend to favor layered convection (Christensen & Yuen, 1985). This is caused by the fact that the sensitivity of an endothermic phase change, like that at the 660-km discontinuity, to retard descending slabs increases with increasing Rayleigh number.
2. *Internal heating*. Model calculations indicate that internal heating of a substance, as compared to bottom heating, increases the propensity for layered convection. Thus, the amount and distribution of radiogenic heat sources in the mantle can affect the type of convection.
3. *Exothermic phase changes*. As previously discussed, all of the phase changes recognized in the upper mantle, except the 660-km perovskite phase change (which is only slightly endothermic), are exothermic, and hence enhance rather than retard the movement of descending slabs and rising plumes across the phase-change boundary.
4. *Plate lengths*. Models of Zhong and Gurnis (1994) show that the mass flux between the upper and lower mantle increases strongly with total plate length. For a ratio of plate length to mantle thickness of 1, for instance, perfectly layered convection is predicted, whereas for a ratio of 5, perfect whole-mantle convection should exist.
5. *Slab dip angle*. In seismic tomographic profiles of subduction zones, shallow dip angles of descending slabs decrease the chances of penetrating the 660-km discontinuity without some holding time.
6. *Reaction rates*. Slow reaction rates of phase changes can temporarily retard descending slabs. This is due to the time it takes to heat up the coldest parts of the slab to the temperatures necessary for the reaction to proceed.

7. *Change in chemical composition*. If, as some investigators suggest, there is an increase in the amount of Fe and perhaps Si at the 660-km discontinuity, some degree of layered convection seems necessary to preserve such a compositional boundary.

From the above considerations it appears there is a real possibility that convection in Earth involves partial layering, at least at certain times in the past. In fact, computer modeling by Tackley et al. (1994) suggests that descending slabs may be temporarily delayed at the 660-km discontinuity, where they accumulate and spread laterally. After some critical mass is reached, however, the plates sink into the lower mantle. At Raleigh numbers $<10^6$, a kind of "leaky" two-layer convection is predicted, which is really time-delayed whole-mantle convection, and this may be the best approximation of what is going on in the mantle today.

Toward a Convection Model for Earth

Perhaps the greatest challenge in understanding mantle convection is to compile, evaluate, and reconcile the wide range of observations and constraints from many disciplines, and especially from geochemistry and geophysics (Korenaga, 2008b). The isotopic and geochemical data discussed above, as well as heat production considerations, suggest the existence of distinct mantle reservoirs that have retained their identity for at least 2 Ga. The noble gas record in plume-derived basalts, which may require storage of primordial gases in the deep mantle, suggests that the deep mantle has not been extensively degassed, a feature that is difficult to reconcile with whole-mantle convection. Heat flow arguments also do not favor whole-mantle convection. The sum of the heat produced by continental crust and depleted mantle extending all the way to the core–mantle boundary accounts for only a small fraction of the present-day heat flow at Earth's surface (Albarede, 1998; Turcotte & White, 2001). This seems to require a high heat-producing reservoir in the lower mantle, which again is difficult to account for if the entire mantle is convecting.

On the other hand, seismic tomography indicates that most or all descending plates penetrate the 660-km discontinuity and sink to, or close to, the core–mantle boundary (van der Hilst et al., 1997). Numerical computer models furthermore suggest that it is difficult to maintain an impermeable boundary at the 660-km discontinuity or any place else in the mantle (McNamara & van Keken, 2000; Tackley, 2000; Davies, 2002). Some models indicate geochemical differences between the upper and lower mantle should disappear in a few hundred million years as long as plates continue to penetrate the boundary (Albarede & van der Hilst, 1999). Also, high-pressure mineral physics experiments together with seismic observations indicate that the Clapeyron slope of the 660-km phase transition is too small (or nonexistent) to cause long-term stratification of the mantle. In addition, no convincing evidence exists for a thermal or compositional boundary at the 660-km discontinuity, of which one or both would develop if the upper and lower mantle convected separately.

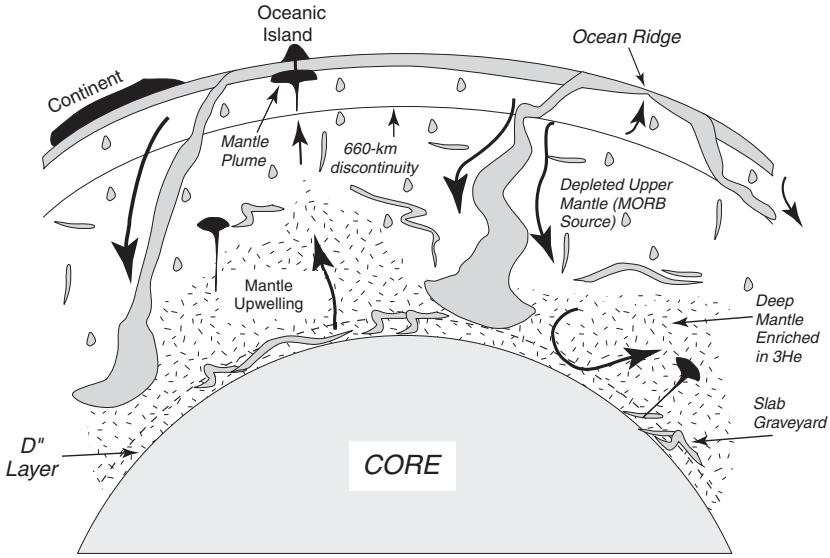

FIGURE 4.33 Convection model for Earth involving a thick zone deep in the mantle that is convectively isolated from the middle and upper mantle (random line pattern). Mantle plumes may be produced both in the D″ layer at the core–mantle interface and along the margins of mantle upwellings. *Modified after Kellogg et al. (1999).*

Can any model accommodate all of these apparently conflicting observations? The model of Kellogg et al. (1999) as modified by Albarede and van der Hilst (1999) seems to hold promise. In this model, the mantle to a depth of approximately 1700 km is relatively uniform in major element composition and largely represents a depleted and outgassed reservoir (Figure 4.33). A transition zone at 400–1000 km deep divides the mantle into two regimes with different timescales of mixing: (1) the upper mantle (DM), which mixes rapidly and is the source of MORB, and (2) the lower mantle, which mixes at a much slower rate. Remnants of subducted slabs occur throughout the mantle as plums in the pudding, and the entire mantle is heterogeneous on all length scales. Numerical modeling based on seismic tomographic data supports the existence of an isolated lower mantle (van der Hilst & Karason, 1999; Tackley, 2000). This deep mantle, which ranges from about 1700 km to near the core–mantle interface has a very high density and contains undegassed material enriched in radiogenic heat-producing elements and piles of subducted slabs (the slab graveyard). If there is a depleted component in the deep mantle as suggested by Kempton et al. (2000), it also resides in this dense lower mantle. Descending slabs, which are highly depleted in incompatible elements such as K, Rb, Ba, Th, and U, accumulate both in D″ and around the margins of the mantle upwellings. Numerical models of Kellogg et al. (1999) show that if portions of D″ are only 4% more dense than the overlying mantle, it will develop substantial

topographic relief as shown in Figure 4.33. Some of this topography also reflects lateral changes in the distribution of post-perovskite due to temperature variation. The D″ layer is thin or absent beneath descending plates and thicker far from these plates. Although some mantle plumes arise from D″, most are generated along the deep margins of the two mantle upwellings. The upwellings, which contain fragments of older crust and lithosphere mixed with lower mantle, impart the distinctive EM and HIMU geochemical signatures to rising plumes and their derivative basalts.

Whether this model will survive the test of rapidly accumulating new data remains to be seen. However, it would appear that any model for mantle convection must be consistent with the existence of a compositionally distinct and gravitationally stabilized lower mantle.

FURTHER READING

Condie, K. C. (2001). *Mantle Plumes and Their Record in Earth History* (306 pp). Cambridge, UK: Cambridge University Press.

Davies, G. F. (2010). *Mantle Convection for Geologists* (280 pp). Cambridge, UK: Cambridge University Press.

Fei, Y., Bertka, C. M., & Mysen, B. O. (Eds.), (1999). *Mantle Petrology: Field Observations and High Pressure Experimentation* (322 pp). Geochemical Society Special Publication No. 6. University of Houston.

Fowler, C. M. R. (2005). *The Solid Earth: An Introduction to Global Geophysics* (2nd ed., 685 pp). Cambridge, UK: Cambridge University Press.

Gurnis, M., Wysession, M. E., Knittle, E., & Buffett, B. A. (Eds.), (1998). *The Core–Mantle Boundary Region* (Vol. 28., 338 pp). *Geodynamic Series*, American Geophysical Union.

Helffrich, G. R., & Wood, B. J. (2001). The Earth's mantle. *Nature*, *412*, 501–507.

Hirose, K., Brodholt, J., Lay, T., & Yuen, D. (Eds.), (2007). *Post-Perovskite: The Last Mantle Phase Transition* (Vol. 174., 287 pp). *Monograph Series*, American Geophysical Union.

Schubert, G., Turcotte, D. L., & Olson, P. (2001). *Mantle Convection in the Earth and Planets* (940 pp). Cambridge, UK: Cambridge University Press.

Stacey, F. D., & Davis, P. M. (2008). *Physics of the Earth* (4th ed., 552 pp). Cambridge, UK: Cambridge University Press.

Chapter 5

The Core

INTRODUCTION

Earth's core is important for three main reasons: (1) it is responsible for the generation of Earth's magnetic field, (2) it contains information regarding the earliest history of accretion of the planet, and (3) thermal and compositional features established when the core formed have largely controlled the subsequent evolution of the core and also influence the evolution of the mantle, crust, and atmosphere (Nimmo, 2007). Seismic velocity data indicate that the radius of the core is 3485 $\pm$ 3 km and that the outer core does not transmit S waves (Jeanloz, 1990; Jacobs, 1992; Tkalcic & Kennett, 2008) (see Figure 1.2 in Chapter 1). This latter observation is interpreted to mean that the outer core is in a liquid state. Supporting this interpretation are radio astronomical measurements of Earth's normal modes of free oscillations. The inner core, with a radius of 1220 km, transmits S waves at very low velocities, suggesting that it is a solid near the melting point or partly molten. There is a sharp velocity discontinuity in P-wave velocity (0.8 km/s; see Figure 1.2) at the inner core boundary, and a low velocity gradient at the base of the outer core. Results suggest that the top of the inner core attenuates seismic energy more than the deeper part of the inner core. Detailed analysis of the travel times of seismic waves reflected from and transmitted through the core indicates that the outer liquid core is relatively homogeneous and well mixed, probably due to convection currents. Seismic data also suggest that relief on the core–mantle interface is limited to about 5 km. The viscosity of the outer core is poorly known with an estimated value of about 10^{-3} Pa s and in any case $<10^{4}$ Pa s.

Three lines of evidence indicate that the core is composed chiefly of iron. First, the internal geomagnetic field must be produced by a dynamo mechanism, which is only possible in a liquid-metal outer core. Because the fluidity and electrical conductivity of the mantle are too low to produce Earth's magnetic field, the outer core must be liquid metal for the geodynamo to operate (Jeanloz, 1990; Glatzmaier, 2002). Second, the calculated density and measured body wave velocities in the core are close to those of iron measured at appropriate pressures and temperatures. Third, iron is by far the most abundant element in the solar system that has seismic properties resembling those of the core.

CORE TEMPERATURE

An accurate knowledge of the temperature of the core is important for constraining both Earth's radioactivity budget and the generation of the magnetic field. Limits on the temperature profile in the core are determined by considering the solid–liquid interface at the inner core boundary from extrapolated phase equilibria and from high-pressure experimental studies of the melting of iron and iron alloys (Monnereau & Yuen, 2010). Depending on the approach used, significant differences exist in the estimates of core temperature. For instance, estimates of the minimum temperature at the core–mantle boundary range from 2500 to 5000°C. The core–mantle boundary and D″ layer probably reflect large gradients in both temperature and composition. Thermal gradients are inferred from radial and lateral seismic wave velocity gradients and from experimental data on the melting point of iron at high pressures (Boehler, 1996; Ahrens et al., 2002). Melting relationships of iron and Fe-O-S compounds measured at pressures up to 2 Mbar imply a temperature discontinuity at the core–mantle boundary in excess of 1300°C.

To generate Earth's magnetic field, the higher temperatures seem necessary, and using the high-pressure melting point data of iron, a value of 3700 ± 500°C is a reasonable estimate for the temperature at the core–mantle boundary (Duba, 1992; Ahrens et al., 2002). Corresponding temperatures at the inner-core/outer-core boundary and at Earth's center are about 5000 and 5500°C, respectively, each with at least a 400°C uncertainty (see Figure 1.2).

THE INNER CORE

Anisotropy of the Inner Core

Although seismic data indicate the inner core is solid, on geologic timescales it may behave like a fluid, undergoing solid-state convection like the mantle. Support for this idea comes from seismic anisotropy in which the P-wave velocity is higher in the inner core along Earth's rotational axis than in equatorial directions (Figure 5.1) (Jeanloz, 1990; Tromp, 2001). It is generally agreed that the uppermost layer of the inner core is a mushy zone with an estimated grain size of 1–2 km composed chiefly of an axial-oriented body-centered cubic iron or iron alloy phase (Tkalcic & Kennett, 2008; Mattesini et al., 2010). Solidification of the inner core along this boundary occurs under shear compression at the liquid–solid interface, a process that favors the development of oriented iron crystals. It has been known for many years that body waves traveling parallel to Earth's rotation axis arrive faster than waves traveling in the equatorial plane. Cylindrical anisotropy of the order of a few percent with the fast axis parallel to the rotation axis and the slow axis in the equatorial plane is the preferred explanation of these observations. Studies by Ishii and Dziewonski (2003) suggest that the symmetry axis in the inner core may be significantly tilted away from the rotational axis. Their results also imply that there is a seismically distinct

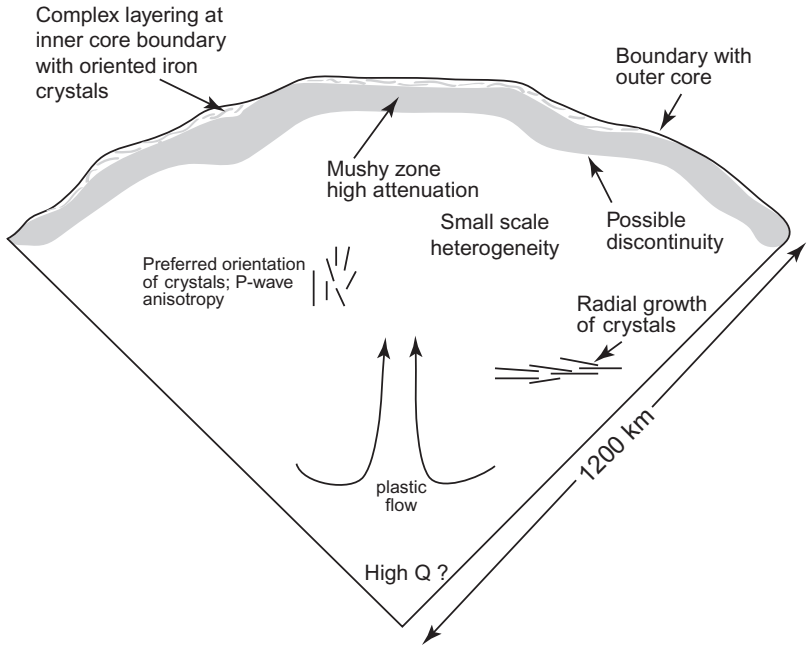

FIGURE 5.1 Schematic cross section of the inner core showing structure inferred from seismic wave studies. *Modified after Tkalcic & Kennett, 2008.*

region in the center of the core with a radius of about 300 km. Four mechanisms have been proposed for the inner-core anisotropy: solid-state convection, solidification texturing, anisotropic growth of the inner core, and the magnetic field (Tromp, 2001). We will briefly review each of these mechanisms.

Inner-core convection requires solid-state convection driven by radioactive sources in the inner core. Although still favored by some investigators, the high heat production and the high thermal conductivity are obstacles for inner-core convection (Yukutake, 1998). The existence of significant amounts of radioactive elements in the inner core also seems unlikely from geochemical arguments.

Solidification texturing involves radial dendritic growth of iron crystals in the inner core (Figure 5.1), in which dendrites grow along an axis that is aligned with the direction of dominant heat flow, which is generally assumed to be perpendicular to Earth's rotation axis (Bergman, 1997). The radial growth of dendritic iron crystals may be responsible for radial anisotropy in the inner core, an interpretation that is consistent with the observed depth dependence of the strength of anisotropy.

A similar model predicts that the inner core should grow faster in its equatorial regions than in its polar regions because heat transport is less effective near the poles (Yoshida et al., 1996). In this model, the viscous flow from

the equator to the poles produces stresses that are large enough to cause alignment of iron crystals. The main uncertainty of this explanation is the viscosity of the inner core: if it is too small, the flow-induced stresses may not be large enough to align the crystals in a reasonable amount of time.

Karato (1999) has shown that Earth's magnetic field induces a stress called the **Maxwell stress** that causes a seismically anisotropic fabric in the inner core. In this model, the Maxwell stresses squeeze iron crystals in the inner core toward the rotational axis, moving material from regions of high stress (the outer part of the inner core) to regions of low stress (near the rotational axis) (Figure 5.2). Material that reaches the low-stress region will melt and flow outward replacing material lost from the high-stress regions. Numerical modeling by Deguen and Cardin (2009) suggests that the inner core evolves gradually from a regime in which deformation penetrates into the deepest parts of the core to a regime confined to the uppermost region. In this case, the deep anisotropy is probably a fossil anisotropy inherited from horizontal Maxwell stresses or to

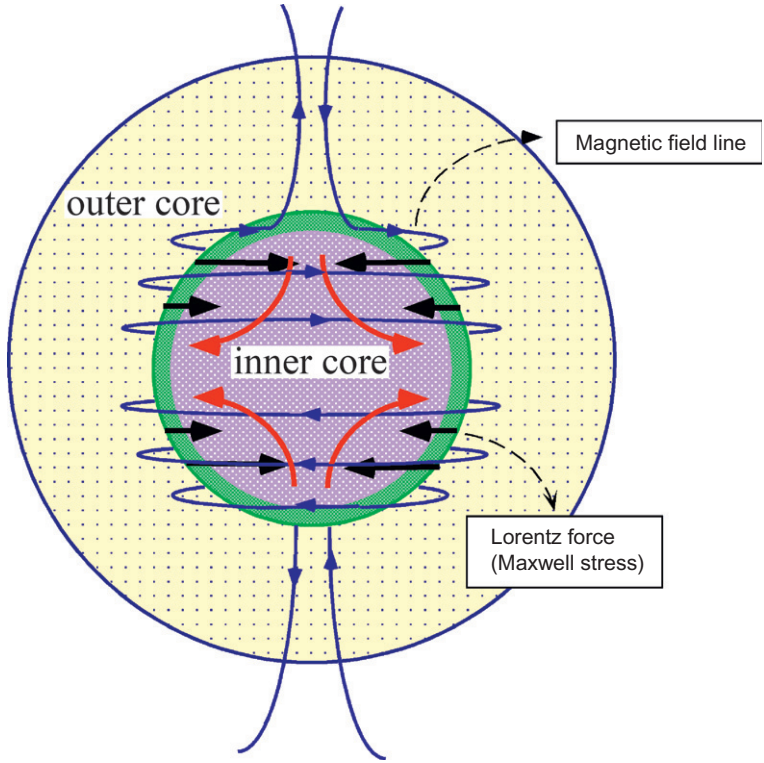

FIGURE 5.2 Diagram of the inner core showing the structure and dynamics caused by Earth's magnetic field. Shown are the magnetic field lines (blue), the induced Maxwell stresses (thick black arrows), and the flow lines (red arrows). *Courtesy of Shun-Ichiro Karato.*

texture deformation during solidification. The structure of the upper layers of the inner core, on the other hand, probably results from heterogeneous growth. Using normal mode splitting function measurements of large earthquakes, Deuss et al. (2010) have recognized differences in anisotropy between the western and eastern hemispheres of the inner core. The similarity of this pattern to that of the magnetic field suggests freezing-in of crystal alignment during solidification or texturing by the Maxwell stresses.

The Maxwell stress model has two major consequences: (1) the flow of core material results in large strains that could be responsible for the radial fabric in the inner core (Figure 5.1), and (2) the flow also causes nonuniform release of energy at the inner-core/outer-core boundary due to the melting and crystallization of iron. The energy released by these reactions is likely to have an important effect on the convection pattern in the outer core, and hence the inner core could influence the geodynamo (discussed below) through thermal effects.

Finally, there is at least permissive evidence for a seismic discontinuity within the inner core. Seismic waves passing along north-south paths in the inner core produce unusually broad pulse shapes at long periods and provide compelling evidence for a seismic discontinuity about 200 km below the inner-core boundary (Figure 5.1) (Song & Helmberger, 1998). This boundary seems to separate an isotropic upper layer from an anisotropic inner layer, and may be caused by a phase change between high-pressure phases of metallic iron.

Inner Core Rotation

A perplexing problem that has not yet been solved is the question of whether the inner core rotates slightly faster than the mantle and crust. Small but systematic temporal variations in the travel times of seismic waves passing near the center of Earth have been interpreted by some investigators as evidence that the solid inner core is rotating faster than the overlying mantle and crust by 0.2–3 deg/y. However, recent measurements based on Earth's large-scale free oscillations, rather than on travel times of seismic waves, seem to rule out differential rotational rates as high as 1 deg/y, but are marginally consistent with rates of $\leq$0.2 deg/y (Laske & Masters, 1999). The main problem with using seismic travel times to probe the inner core is the sensitivity of the measured times to local irregularities in the core. The free oscillation method sidesteps the need to resolve these irregularities because the long-wavelength oscillations are completely insensitive to small-scale structures in the core. Laske and Masters (1999) conclude from their study that the inner-core mean rotation rate is 0.0 ± 0.2 deg/y, which implies that the inner core is gravitationally "locked" to the mantle and that it does not rotate at a different rate. Supporting this conclusion are the hemispherical differences in the inner core reported by Deuss et al. (2010).

Using an improved seismic method involving scattering of seismic waves by the inner core, Vidale et al. (2000) have been able to greatly improve the resolution of seismic wave data. If the inner core rotates with respect to the mantle,

waves that are scattered by irregularities will arrive earlier from the side of the core getting closer, whereas waves coming from the retreating side will arrive later. This is exactly what is reported by Vidale et al. (2000). Their results suggest that the inner core rotates faster than the mantle, but at a considerably slower rate than predicted by earlier seismic wave results: only 0.15 deg/y, which is within the error of the free oscillation results discussed earlier.

COMPOSITION OF THE CORE

Constraints on the composition of Earth's core come from the study of iron meteorites (which may represent samples of asteroid cores), thermodynamic model studies, and high-pressure experimental studies. Only the diamond-anvil and shock-wave experiments, however, can reach inner-core pressures (up to 300 GPa) and temperatures (Stixrude & Brown, 1998). Three phases of iron are known at pressures that exist in the core: body-centered cubic (bcc), face-centered cubic (fcc), and hexagonal-close packed (hcp) iron. Most experimental data indicate that hcp iron is the dominant phase in the core (Tromp, 2001). Although theoretical studies agree that the hcp phase is stable at core pressures and the bcc phase is unstable, quantum mechanic studies indicate that bcc may also be stable in the core (Vocadlo et al., 2003). Belonoshko et al. (2003) take this one step further based on density function theory and suggest that the hcp–bcc transition is misinterpreted as a melting transition in experimental studies and that the bcc iron phase is really the stable phase in the inner core. We clearly need better resolution of the experimental data to resolve this problem.

The presence of 5–10% nickel in the core is supported by the composition of iron meteorites, which may represent fragments of core material from asteroids. Seismically, however, there is no reason for nickel to be in the core, since seismic velocities are essentially the same for iron and nickel. Although it is clear the core must be composed chiefly of iron, P-wave velocities and the density of the outer core are about 10% lower than that of liquid iron (Jacobs, 1992). Thus, at least the outer core requires 5–15% of one or more low atomic number elements to reduce its density. This also means there is not a single melting temperature at a given pressure, but that the core must melt over an interval given by its solidus and liquidus. Just which alloying element or elements occur in the core is intimately linked with various models that are proposed for the origin and evolution of the core. In addition to Sulfur, silicon and oxygen are the two elements that have received the most support from geochemical modeling as core contaminants.

Another approach to estimating the composition of the core is by using the composition of the bulk Earth and the primitive mantle as estimated from meteorite compositions, and then determining the core composition by difference. Results suggest that the total core contains about 7% silicon and traces of both sulfur (2%) and oxygen (4%) (Allegre et al., 1995b).

Although most investigators now believe that sulfur or/and silicon are the low mass elements in the outer core, considerable disagreement exists as to which of these two elements dominates. Although density calculations indicate that both silicon and sulfur may be present (Sherman, 1997), metal-silicate partitioning experiments at high pressure show that both elements are mutually exclusive under the same low oxygen fugacity in the core (Kilburn & Wood, 1997). The common presence of iron sulfides in meteorites is consistent with the presence of sulfur in the core, as is density modeling of Fe-S alloys at core pressures (Sherman, 1995). Experimental studies support the idea that the mantle is depleted in sulfur due to iron-silicate equilibria during core formation, and thus support sulfur as the dominant light element in the core (Li & Agee, 2001). If a significant amount of sulfur is in the core, it must have entered at low pressures as shown by the experimental data, and hence supports core formation during the late stages of planetary accretion some 4.6 Ga (Newsom & Sims, 1991).

The possibility that oxygen is the dominant alloying agent in the core is based on ultra-high-pressure experimental studies and thermodynamic calculations (Kato & Ringwood, 1989; Alfe et al., 2002), since the relevant oxide phases are not stable at low pressures nor are they found in meteorites. Experimental results document that oxygen can alloy with molten iron at pressures in excess of 10 GPa. Hence, in contrast to sulfur, alloying of oxygen would be expected well after the core began to form, and perhaps after planetary accretion was complete (Ito et al., 1995). The high-pressure experiments of Takafuji et al. (2005) show that a combination of oxygen and silicon in liquid iron can account for a 7% density deficit in the outer core. Badro et al. (2007) propose a model-based high-pressure experimental study in which both the outer and inner core contain 2.5–3.0% silicon, with traces of oxygen in the inner core and about 5% oxygen in the outer core.

It seems probable from comparing the seismically deduced density of the inner core to measured densities of iron and iron alloys at high pressures that the inner core also cannot be composed of a pure Fe-Ni alloy (Jephcoat & Olson, 1987). Like the outer core, it must contain a low-atomic-number element, presumably sulfur or silicon, but in small amounts of only 3–7%. Experiments by Antonangeli et al. (2010) find that inner-core density and both P- and S-wave velocities can be explained by 4–5% nickel and 1–2 % silicon. This also would be consistent with convection in the inner core, as mentioned above, since these elements would lower the effective viscosity enhancing the ability to convect. Thermodynamic calculations indicate that the bcc iron phase should be stabilized compared to the hcp phase by sulfur or silicon impurities in the inner core (Vocadlo et al., 2003). Possibly the bcc phase is responsible for the seismic complexity in the inner core. For instance, a phase change from the hcp to the bcc phase may be responsible for a possible seismic boundary in the inner core mentioned above (Song & Helmberger, 1998).

AGE OF THE CORE

It is obviously not possible to date the core since we do not have samples that have been brought to Earth's surface. However, indirect isotopic and geochemical arguments can be used to constrain the timing of core formation. Lead isotopes provide an estimate for the age of Earth of 4.57–4.45 Ga, and it appears that at this time U and Pb were fractionated from each other. A significant proportion of Earth's Pb (although still at trace concentrations) may have been incorporated in the core at this time, since it geochemically follows iron. If so, the Pb isotope age of Earth suggests that separation of the core from the mantle occurred very early in Earth's history, perhaps beginning during the late stages of planetary accretion. Another complicating factor is the effect of the Moon-forming collision early in the history of Earth. Computer simulations show that the core of the planet-size impactor (see Chapter 9) remains mostly intact during the collision and appears to merge with Earth's core (Canup, 2004).

More precise ages for core formation can be made using short-lived radiogenic isotopes in which parent and daughter isotopes are fractionated during accretion of Earth. One of the most productive isotopic systems is the ^{182}Hf-^{182}W system. Whereas W follows iron into the core, Hf remains in the silicate fraction in the mantle. The parent isotope ^{182}Hf has a half-life of about 9 Ma, and thus if the core forms rapidly soon after planetary accretion, the daughter isotope ^{182}W will remain in the mantle and will show up today as tungsten anomalies in mantle xenoliths. On the other hand, if the core forms slowly through geologic time, tungsten will enter the core and there will be no anomalies in mantle xenoliths. Tungsten isotopes can also be measured in iron meteorites, which constrain the timing of core formation in the asteroid parent bodies of these meteorites. The ^{182}Hf-^{182}W isotope data from iron meteorites support early segregation of parent body cores, in the first 30–50 Ma of planetary accretion (Harper & Jacobsen, 1996; Kleine et al., 2005). The correct interpretation of Hf-W ages, however, depends on the initial abundance of ^{182}Hf in the solar system, the tungsten isotopic composition of chondritic meteorites, and the material from which Earth was accreted. Using Hf and W data from chondrites as a starting material for Earth, Earth's core must have formed within about 30 Ma of the beginning of accretion of bodies in the solar system (see Chapter 10) (Kleine et al., 2002). Corresponding ages for the lunar core are between 26 and 33 Ma. Hf-W data from meteorites indicate the cores in their asteroid parent bodies formed in less than 10 Ma after the beginning of asteroid accretion. These ages indicate that the cores of the terrestrial planets and asteroids formed very rapidly, probably during the late stages of planetary accretion.

Also supporting early core formation is the lack of change in ratios of siderophile to lithophile elements in the mantle with time (Sims et al., 1990). If the core were to have grown gradually by blobs of liquid iron sinking through the mantle to Earth's center, the mantle should show progressive depletion of siderophile elements (like W, Mo, and Pb) relative to lithophile elements

(like Ce, Rb, and Ba) with time. However, it does not show such a trend. Even the oldest known basalts (~4 Ga), which carry a geochemical signature of their mantle sources, have element ratios comparable to ratios in modern basalts.

Although it is not possible to date the inner core with radiogenic isotopes, it is possible to constrain its age by considering the energy relationships associated with crystallization of the inner core. The age of the inner core is dependent on the heat flux from the core–mantle boundary and the concentrations of radiogenic elements in the core. Regrettably, neither of these parameters is well known. Calculations indicate that if radiogenic elements are absent in the core, the inner core cannot be older than about 2.5 Ga and it is most likely about 1 Ga (Labrosse et al., 2001). If this model is correct, it would appear that Earth's inner core did not begin to crystallize until 2–3 Ga after planetary accretion terminated.

GENERATION OF EARTH'S MAGNETIC FIELD

The Geodynamo

It is well known that Earth's magnetic field is similar to that of a giant bar magnet aligned with the rotational axis of the planet (Figure 5.3). The magnetic lines of force trace curved paths, exiting near the South Pole and entering near the North Pole. Maps of the magnetic field at the surface show a secular variation that occurs over periods of decades to tens of thousands of years. Among the most striking changes in the last few thousand years are a decrease in the dipole component of the field and a westward drift of part of the field. Earth's field can also reverse its polarity, and has done so many times in the geologic past. Most evidence strongly suggests Earth's magnetic field is generated in the fluid outer core by a dynamo-like action, although the details of how this occurs are poorly understood (Jacobs, 1992; Glatzmaier, 2002). How long has Earth had a magnetic field? Using a laser heating approach to obtain both paleodirections and intensities of the magnetic field of single crystals, Tarduno et al. (2007) report magnetic field strengths within 50% of present-day values in rocks that are 3.2 Ga. Early Archean rocks from the Barberton greenstone in South Africa retain magnetic signatures that suggest Earth's geodynamo was operational even earlier—by 3.45 Ga (Usui et al., 2009).

Fluid Motions in the Outer Core

It is possible to map fluid motions in the outer core using the flow lines of the magnetic field (Bloxham, 1992). The maps show current movements at the core surface (as vectors) and regions of upwelling and downwelling known as core spots (Figure 5.4). Four spots contribute most strongly to the dipole component, which have been interpreted by Bloxham (1992) as the tops and bottoms

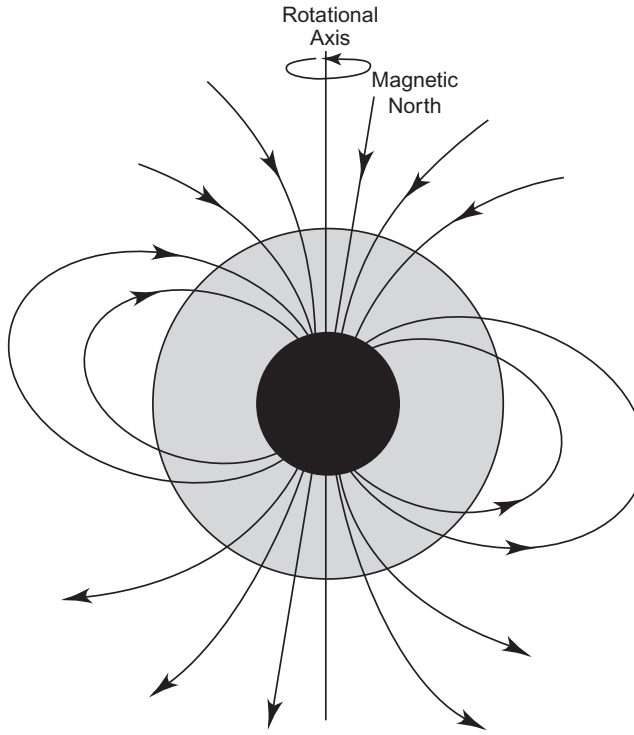

FIGURE 5.3 Earth's magnetic field showing lines of equal intensity and orientation.

of two columns of liquid that appear to touch the inner core and run parallel to Earth's rotational axis. Liquid iron may spiral down through the two columns creating a dynamo that concentrates magnetic flux within the columns. Magnetic field lines are "frozen" in the iron liquid, and as it moves they are carried with the liquid, thus mapping current patterns. Results show two prominent cells of circulating fluid beneath the Atlantic Basin, one south and one north of the equator (Figure 5.4). Also, there is a region of intense upwelling near the equator elongated in a N-S direction at 90 °E longitude beneath the Indian Ocean, with a strong equatorial jet extending westward between the two circulating cells. This westward current may in fact explain the slow westward drift of the magnetic field in this area. The core spots appear to be produced by intense upward and downward flow of liquid. Evidence is mounting that the fall in dipole component of the magnetic field during the last few hundred years is caused by the growth and propagation of the downward flux core spots beneath Africa and the Atlantic Basin. This is supported by a correlation between the intensity of the dipole component and the amount of lateral motion of these two spots in the last 300 years.

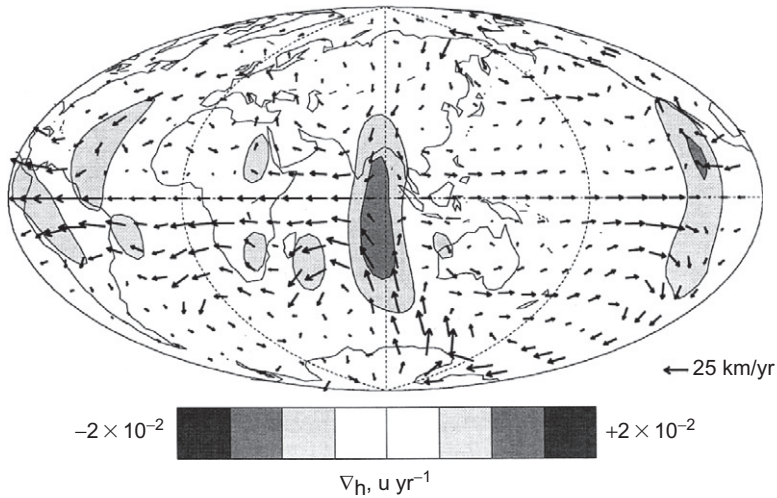

FIGURE 5.4 Current patterns in the outer core as shown by vectors. The gray scale shows the intensity of upcurrents and downcurrents. Upcurrents are beneath the Indian Ocean, South Africa, and beneath the Atlantic Ocean. Downcurrents are beneath the East Pacific Ocean, NW Australia, southeast of Madagascar, North Africa, and northern South America. *After Bloxham (1992).*

Fueling the Geodynamo

The energy for the geodynamo could be gravitational, chemical, or thermal, which in all cases is ultimately converted to heat that flows outward into the mantle (Jacobs, 1992; Glatzmaier, 2002; Stevenson, 2003). Remanent magnetism in rocks more than 3.45 Ga indicate that Earth's geodynamo was in action by that time. Also, paleomagnetic studies show the field intensity has never varied by more than a factor of 2 since the Archean, so the energy needed to drive the dynamo must have been available at about the same rate for at least 4 Ga.

The two serious candidates for the **geodynamo energy source** (Kutzner & Christensen, 2000; Stevenson, 2003; Labrosse, 2003) are (1) thermal convection of the outer core, and (2) compositional convection caused by growth of the inner core. Not favoring the first case is the fact that most of the heat should be carried away either by convection or conduction and not contribute to production of the magnetic field. In contrast, growth of the inner core can supply gravitational energy in two ways: (1) latent heat of crystallization as iron crystallizes on the surface of the inner core, and (2) as metal accretes to the inner core, a lighter fraction is concentrated in the outer core and, because of its buoyancy, leads to compositionally driven convection.

The near exclusion of light elements from the inner core as it grows provides an important source of buoyancy for convection (Buffett, 2000; Stevenson, 2003). The light elements rise into the fluid outer core, while the denser elements (Fe, Ni, and other metals) crystallize into the inner core. Although

thermal convection may also be important, it is difficult to evaluate the role of the overlying mantle on heat loss. Estimating the rate of cooling of the outer core is important because of the high thermal conductivity of liquid iron. The heat conducted through the core may be comparable to the total heat flow into the base of the mantle. Uncertainties in this heat loss make it difficult to estimate the role of thermal convection in generating the magnetic field. Convection in the core operates like a heat engine: heat is drawn from the core by the mantle and work is done to generate the magnetic field. As the inner core grows and light elements are concentrated more into the outer core, gravitational energy is released to power the geodynamo. Estimates suggest that compositional convection contributes about 80% to the power of the geodynamo and thermal convection about 20%. At earlier times in the history of the core, compositional convection should have been weaker because the inner core was smaller or nonexistent. Before formation of the inner core, the magnetic field would have been generated entirely by thermal convection.

How the Geodynamo Works

Many of the planets in the solar system, including Earth, have magnetic fields that originate from self-sustaining dynamos (Stevenson, 2003). Some planets like Mars and Venus do not have dynamos at present, but may have had dynamos in the distant past. Three basic ingredients are needed for an active dynamo: (1) a large volume of convecting fluid (Fe in the case of the terrestrial planets) in or near the center of the planet, (2) an energy source such as excess heat resulting in convection of the fluid, and (3) planetary rotation to control fluid motions. It is possible with high-speed computers to construct and test numerical models that may simulate Earth's geodynamo. Two general models have been widely discussed: polar vortex and differential rotation models (Kuang & Bloxham, 1997; Olson & Aurnou, 1999; Glatzmaier, 2002; Dumberry & Bloxham, 2003). Both models involve a hypothetical tangential cylinder inside the geodynamo (Figure 5.5). The two models call on similar convective energy, rotation rate, and fluid properties, and they produce comparable magnetic fields. Both models delegate a special role for the solid inner core: first as an energy source as described earlier, and second as a mechanical barrier to flow in the outer core.

The chief difference between the models is the assumed boundary conditions between the inner and outer cores, which have an important effect on the tangential cylinder (Figure 5.5). In the polar vortex model, the inner core is spun into a fast prograde rotation relative to the mantle, generating the magnetic field within the tangential cylinder. In the differential rotation model, the effect of viscosity is greatly reduced, and the polar vortices are largely suppressed, causing the magnetic field to be generated outside the cylinder. This situation gives rise to a westward drift of the magnetic field, as observed in Earth.

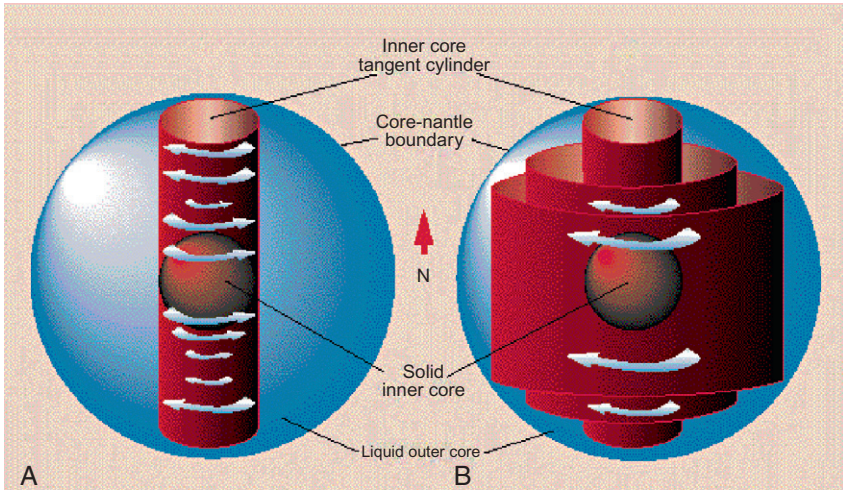

FIGURE 5.5 Two models for Earth's geodynamo: (A) Polar vortex model. In this model flow occurs inside the inner-core tangent cylinder. (B) Differential rotation model. Flow occurs outside the tangent cylinder. *After Olson (1997), reprinted with permission of* Nature, *copyright Macmillan Magazines Ltd., 1997.*

Perhaps the most remarkable outcome of these two models is in showing that computer simulations can be powerful and accurate tools for relating magnetic fields to the dynamics of planetary cores.

What Causes Magnetic Reversals?

First of all, why does Earth's field reverse polarity? It appears to be a random process: because the magnetic field varies all the time, it is a matter of chance whether a drop in intensity of the field ends up with the same or opposite polarity. How long does a reversal take? Reversals in Earth's magnetic field occur on different timescales and there are many aborted attempts to reverse when the field either immediately switched back or did not even reach the opposite polarity. Records show that the magnetic field becomes progressively weaker beginning several thousand years before a reversal, with the actual reversal occurring in less than 2000 years (Gubbins, 2008). The reversed field then grows in strength for another few thousand years. Reversals occur on average about every 300 000 years and the last reversal is recorded at 780 000 years ago. Since then, the polarity has started to change, but flipped back before a reversal was complete. The field has done this several times since the last reversal. An incomplete reversal (or immediate switchback), known as an excursion, likely results from some local instability at the core–mantle interface, and may not be global. Stable reversals, on the other hand, are always global in extent. The oldest well-documented reversed polarity interval is recorded in 2.7-Ga flood

basalts from Western Australia and clearly indicates that the reversal mechanism was operational by this time (Strik et al., 2003).

At the other end of the timescale are **superchrons**, which record intervals when the field maintained the same polarity for periods of 20–50 Ma. It is very unlikely that these changes of polarity on very different timescales are the result of the same processes in the core (Jacobs, 1995). The origin of superchrons is not well understood. Since the geodynamo is at least in part driven by cooling from the top of the outer core, and this cooling is controlled by plate tectonics and mantle convection, it would appear that changes in the deep mantle may have interrupted the pattern of fluid flow in the core for extended periods of time, greatly decreasing the frequency of reversals.

Reversals may be initiated either by changes at the core–mantle boundary or at the inner core boundary, and in both cases it appears that some physical or chemical process arising from an energy source independent of the source that powers the geodynamo actually initiates the reversal (Gubbins, 1994, 2008). For instance, instabilities may be generated at the core–mantle boundary by heat loss, which produces cooler, more dense blobs of molten iron that sink and destabilize the main convection in the outer core. Alternatively, hot plumes rising from the inner-core boundary may have the same effect. Hollerbach and Jones (1993) suggest that reversals may be caused by oscillations of the magnetic field in the outer core. Their modeling concludes that although the field oscillates strongly in the outer core, only weak oscillations should occur near the core surface, and reversals may be caused when these weak oscillations exceed some threshold value. This would occur only when the size ratio of the inner to outer core is greater than 0.25, and thus before the inner core crystallized there should have been no reversals. Changes in the frequency of reversals can arise either from changes in the total heat flux from the core to the mantle or from instabilities associated with lateral variations at the core–mantle boundary (Gubbins, 1994).

ORIGIN OF THE CORE

Segregation of Iron in the Mantle

Many models have been proposed to explain how molten iron sinks to Earth's center as the melting point of metallic iron or iron alloys is reached in the mantle (Rubie et al., 2007). Although molten iron could collect into layers and sink as small diapirs, the high surface tension of metallic liquids relative to solid silicates should cause melt droplets to collect at grain boundaries, rather than drain into layers (Stevenson, 1990; Newsom & Sims, 1991). During the late stages of planetary accretion, large amounts of molten iron should have been retained in the silicate mantle. At that time it appears that a giant impact between Earth and a Mars-size body led to rapid melting. Most or all of the silicate mantle melted, producing a magma ocean as described in Chapter 10. In this deep magma

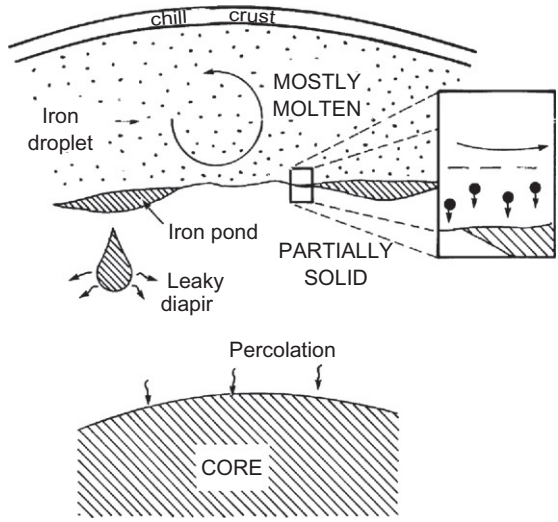

FIGURE 5.6 Possible core segregation processes. Molten metal droplets rapidly sink in a silicate magma ocean, large blobs of molten iron sink as diapirs, and alloying of oxygen with iron in the lower mantle triggers downward percolation of liquid alloy into the core. *Modified after Stevenson (1990) and Newsom & Sims (1991).*

ocean, droplets of liquid iron should separate from the silicate liquid and sink rapidly to the core (Stevenson, 1990; Bruhn et al., 2000). If the magma ocean were relatively shallow, metal droplets could accumulate at the bottom, eventually coalescing into larger blobs that would either sink as diapirs or percolate downward (Figure 5.6). One question that is still hotly debated is the role that the Moon-forming collision (see Chapter 9) had on the formation of the core. The key issue is whether Earth accretion was accompanied by (1) direct merging of the cores of Earth and the colliding planet or (2) if the core grew by continuous segregation and sinking of metal from a hot magma ocean (with some of the iron coming from the colliding planet).

Siderophile Element Distribution in the Mantle

Until recently, it was generally assumed that the concentrations of siderophile elements in the mantle are higher than predicted for models of core segregation (Newsom & Sims, 1991). Because of their very strong tendency to follow iron, most of these elements should have been scavenged by liquid iron as it sank to Earth's center during core formation. Yet the concentrations of many siderophile elements are similar to that of primitive mantle. Murthy (1991), however, has shown that this apparent depletion may not be real. In a molten planet the size of Earth, increasing pressure increases the melting point of metal and silicates significantly, so a large part of the mantle would be at very high

temperatures (2000–4000°C). Thus, the distribution of trace elements between liquid and solid would be governed by high-temperature distribution coefficients, and not the low-temperature distribution coefficients that have been used in most previous modeling. The siderophile element distributions in the mantle calculated with high-temperature distribution coefficients is similar to the element distributions in mantle xenoliths. Thus, the problem of excess siderophile elements in the mantle goes away when appropriate high-temperature modeling is done.

Growth and Evolution of the Core

Although high-pressure phase equilibria in the Fe-O and Fe-S systems are still not precisely known, it is informative using the available data to track the growth of the core during the first 50 Ma of Earth's history. During the late stages of planetary accretion, steepening geotherms in Earth should intersect the melting curve of iron and silicates at relatively shallow depths in the mantle. Continued heating raises the geotherms well above the melting point of both iron and silicates, producing a widespread magma ocean containing droplets of molten iron, which because of their gravitational instability, begin to sink to the center of the planet and form the core (Figure 5.6). During a collision with a Mars-size body at about 4530 Ma (Chapter 10), most of the mantle of the impactor should have accreted to Earth and its core probably penetrated Earth's core (Benz & Cameron, 1990), transferring iron to Earth's core. Thermal convection in the core started the geodynamo very early in Earth's history. Just when the core cooled enough for the inner core to begin to crystallize is unknown, but as previously mentioned, it was probably sometime between 1 and 2 Ga.

As the core cools in the future, the inner core should continue to grow at the expense of the outer core. Because the low-atomic-numbered diluting element or elements (S, Si, or O) are preferentially partitioned into the liquid phase, the outer core will become progressively enriched in these elements with time, and thus the melting point of the outer core should drop until the eutectic in the system is reached. The final liquid that crystallizes as the outermost layer of the core, some time in the distant geologic future, should be a eutectic mixture.

WHAT THE FUTURE HOLDS

Although the past 10 years have been extremely productive in learning more about Earth's core, we still have a long way to go. For instance, we know very little about the cause of the coincidence of geoid anomalies at the surface of Earth and at the core–mantle boundary (Chapter 4). Is this controlled by the transfer of heat to the mantle? How much interaction is there between the core and mantle at the core–mantle boundary and can we better resolve this interaction with seismic wave studies? Although it is clear that the inner core is

anisotropic, the causes of variations in anisotropy remain problematic. Another question about which we know very little is the rate at which the inner core is crystallizing and how it crystallizes. Is crystallization episodic, resulting in sudden bursts of heat loss, or is it very uniform and gradual? This could be important in understanding mantle plume events, which may be triggered by sudden losses of core heat. Although we are beginning to understand the geodynamo in more detail, to make significant progress on this question, we need 3D simulations, which will require significant time on high-speed computers at great expense.

So unlike our understanding of the crust and mantle, which has been significantly enhanced in the last decade, the information highway for the core is just beginning to open.

FURTHER READING

Buffett, B. A. (2000). Earth's core and the geodynamo. *Science*, *288*, 2007–2012.

Dehant, V., Creager, K. C., Karato, S., & Zatman, S. (2003). *Earth's Core: Dynamics, Structure, Rotation* (Vol. 31). *Geodynamic Series,* American Geophysical Union.

Merrill, R. T. (2010). *Our Magnetic Earth, the Science of Geomagnetism* (272 pp). Chicago, IL: University of Chicago Press.

Newsome, H. E., & Jones, J. H. (Eds.), (1990). *Origin of the Earth* (378 pp). Oxford, UK: Oxford University Press.

Rubie, D. C., Nimmo, F., & Melosh, H. J. (2008). Formation of the Earth's Core. In *Treatise on Geophysics* (pp. 51–90). Amsterdam: Elsevier, Chapter 9.03.

Tromp, J. (2001). Inner-core anisotropy and rotation. *Annual Review of Earth and Planetary Sciences*, *29*, 47–69.

Chapter 6

Earth's Atmosphere, Hydrosphere, and Biosphere

THE MODERN ATMOSPHERE

Earth is a unique planet in the solar system not just because of its plate tectonics, but because it is also the only planet with oceans and with an oxygen-bearing atmosphere capable of sustaining higher forms of life. How did such an atmosphere–ocean system arise and why only on Earth? Related questions include these: Once formed, how did the atmosphere and oceans evolve with time, and in particular, when and how did free oxygen enter the system? How have climates changed with time and what are the controlling factors, and when and how did life form? What is the role of plate tectonics, mantle plumes, and extraterrestrial impact in the evolution of atmosphere and oceans? It is these and related questions that we will address in this and subsequent chapters.

Atmospheres are the gaseous carapaces that surround some planets and satellites and because of gravitational forces, they increase in density toward planetary surfaces. Earth's atmosphere is divided into six regions as a function of height (Figure 6.1). The magnetosphere, the outermost region, is composed of high-energy nuclear particles trapped in Earth's magnetic field. This is underlain by the exosphere in which lightweight molecules (such as H_2) occur in extremely low concentrations and escape from Earth's gravitational field. Temperature decreases rapidly in the ionosphere (to about –90°C) and then increases again to near 0°C at the base of the mesosphere. It drops again in the stratosphere and then rises gradually in the troposphere toward the surface. Because warm air overlies cool air in the stratosphere, this layer is relatively stable and undergoes very little vertical mixing. The temperature maximum at the top of the stratosphere is caused by absorption of ultraviolet (UV) radiation in the ozone layer. The troposphere is a turbulent region that contains about 80% of the mass of the atmosphere and most of its water vapor. Tropospheric temperature decreases toward the poles, which together with vertical temperature change causes continual convective overturn in the troposphere.

Earth's atmosphere is composed chiefly of nitrogen (78%) and oxygen (21%) with very small amounts of other gases such as argon and carbon dioxide.

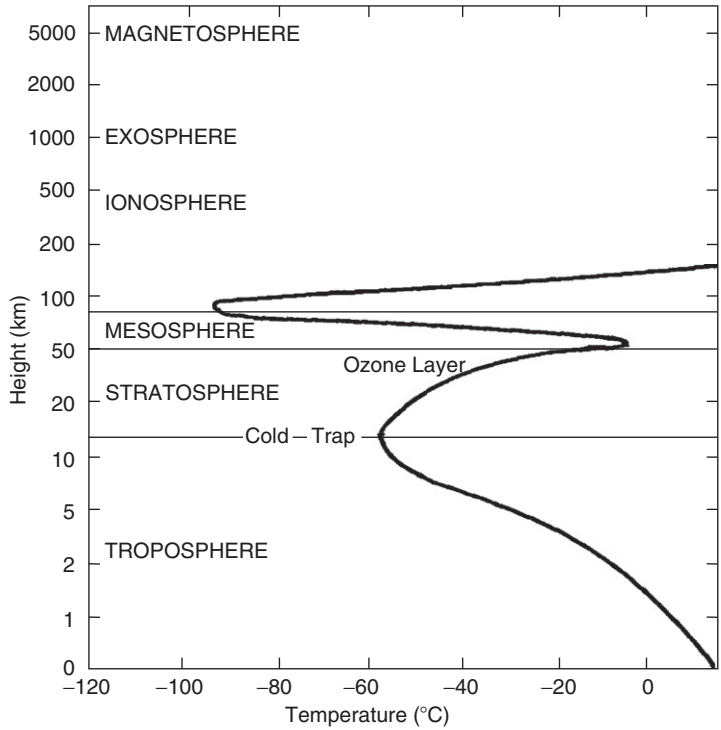

FIGURE 6.1 Major divisions of the Earth's atmosphere showing average temperature distribution.

In this respect, the atmosphere is unique among planetary atmospheres (Table 6.1). Venus and Mars have atmospheres composed largely of CO_2, and the surface pressure on Venus ranges up to 90 times that on Earth, whereas the surface pressure of Mars is $<10^{-2}$ of that of Earth. The surface temperatures of Earth, Venus, and Mars are also very different (Table 6.1). The outer planets are composed largely of hydrogen and helium and their atmospheres consist chiefly of hydrogen and, in some cases, helium and methane.

The concentrations of minor gases such as CO_2, H_2, and **ozone** (O_3) in Earth's atmosphere are controlled primarily by reactions in the stratosphere caused by UV solar radiation. Solar photons fragment gaseous molecules (such as O_2, H_2, CO_2) in the upper atmosphere producing free radicals (C, H, O), a process called **photolysis**. One important reaction produces free oxygen atoms that are unstable, and recombine to form ozone:

$$\begin{aligned} &\overset{\text{UV}}{O_2 \rightarrow O + O} \\ &O + O + O \rightarrow O_3 \text{ or} \\ &O + O_2 \rightarrow O_3 \end{aligned} \qquad (6.1)$$

TABLE 6.1 Composition of Planetary Atmospheres

	Surface temperature (°C)	Surface pressure (bars)	Principal gases
Earth (early Archean)	55 to 85	~11	CH_4, N_2 (CO_2, OCS, SO_2)
Earth	–20 to 40	1	N_2, O_2
Venus	400 to 550	92	CO_2 (N_2)
Mars	–140 to 25	0.008	CO_2 (N_2)
Jupiter	–160 to –90	>1000	H_2, He
Saturn	–190 to –140	>1000	H_2, He
Uranus	–220 to –200	>1000	H_2, He, CH_4
Neptune	–220 to –200	>1000	H_2, He, CH_4
Pluto	–235 to –210	≤0.005	CH_4, N_2

This reaction occurs at heights of 30–60 km with most ozone collecting in a relatively narrow band at about 25–40 km (Figure 6.1). Ozone, however, is unstable and continually breaks down to form molecular oxygen. The production rate of ozone is approximately equal to the rate of loss, and thus the ozone layer maintains a relatively constant thickness in the stratosphere. Ozone is an important constituent in the atmosphere because it absorbs UV radiation from the Sun, which is lethal to most forms of life. Hence, the ozone layer provides an effective shield that permits a large diversity of living organisms to survive on Earth. It is for this reason we must be concerned about the release of synthetic chemicals into the atmosphere that destroy the ozone layer. The distributions of N_2, O_2, and CO_2 in the atmosphere are controlled by volcanic eruptions and by interactions between these gases and the solid Earth, the oceans, and living organisms.

THE PRIMITIVE ATMOSPHERE

Although most investigators agree that the present atmosphere, except for oxygen, is chiefly the product of degassing, whether a primitive atmosphere existed and was lost before extensive degassing began is a subject of controversy. Three possible sources have been considered for an early atmosphere on Earth (Halliday, 2003; Williams, 2007): (1) residual gases remaining after planetary accretion, (2) extraterrestrial sources such as the Sun, and (3) early degassing of Earth by volcanism. Models suggest that all three may have played roles, although the relative importance of each remains problematic

(Shaw, 2008). One line of evidence supporting the existence of an early atmosphere is the fact that volatile elements should collect around planets during their late stages of accretion. This follows from the very low temperatures at which volatile elements condense from the solar nebula (Chapter 10). The distribution of volatile elements in Earth is very different from that in the Sun (Figure 6.2). Although the relative abundances of volatiles are similar to those found in carbonaceous chondrites (a low-temperature group of meteorites), the absolute abundances are smaller. The depletion in rare gases in Earth compared to carbonaceous chondrites and the Sun indicates that if a primitive atmosphere collected during accretion, it must have been lost (Pepin, 1997; Halliday, 2003). The reason for this is that gases with low atomic weights (e.g., CO_2, CH_4, He, H_2) that probably composed this early atmosphere should be lost even more readily than rare gases with high atomic weights (Cl, Br, I, Kr, Xe) and greater gravitational attraction. Xenon is peculiar in that it is depleted relative to other noble gases in Earth, but not in meteorites, a feature often referred to as "Earth's missing xenon" (Figure 6.2).

Just how a primitive atmosphere may have been lost is not clear, but xenon isotopic data suggest that >99% of this early atmosphere was lost in the first 100 Ma of Earth's history. One possibility is by a **T-Tauri solar wind**

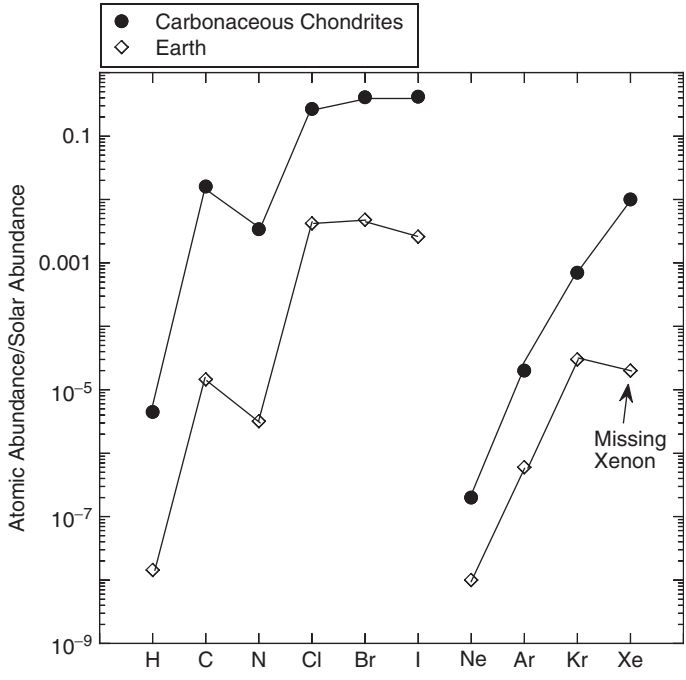

FIGURE 6.2 Volatile element abundances in carbonaceous chondrites and Earth relative to solar abundances. *Modified after Kramers (2003).*

(Ozima & Podosek, 1999) (see Chapter 10). If the Sun evolved through a T-Tauri stage during or soon after (<50 Ma) planetary accretion, this wind of high-energy particles could readily blow volatile elements out of the inner solar system. Another way an early atmosphere could have been lost is during impact with a Mars-size body in the late stages of planetary accretion, which resulted in formation of the Moon (Chapter 9). Calculations indicate, however, that less than 30% of a primordial atmosphere would be lost during the collision of the two planets (Genda & Abe, 2003).

In summary, the noble gas data provide strong evidence that Earth had an early atmosphere that was far more massive than the present atmosphere. If so, this has two important consequences for the early history of the planet: (1) the blanketing effect of the atmosphere would have caused very high surface temperatures, thus contributing to the existence of magma oceans; and (2) with such a thermal blanket, it would have been easy to dissolve small amounts of the atmosphere into the magma oceans, providing a mechanism to transport primitive gases (such as ^{3}He) into the deep mantle by convection.

THE POST-COLLISION ATMOSPHERE

Earth's present atmosphere appears to have formed largely by degassing of the mantle and crust and is commonly referred to as the **post-collision** or **secondary atmosphere** (Kershaw, 1990; Kasting & Howard, 2006). This is the atmosphere that began to accumulate after the planetary collision that formed the Moon and the "new" Earth about 4520 Ma (Chapter 9). **Degassing** is the liberation of gases from within a planet, and it may occur directly during volcanism, or indirectly by weathering of igneous rocks on a planetary surface. For Earth, volcanism appears to be most important both in terms of current degassing rates and calculated past rates. After the Moon-forming collision, a thick rock vapor with a temperature in excess of 2600°C may have collected around the new Earth (Sleep et al., 2001). Although the lifetime of this atmosphere would have been very short (of the order of 1000 years), the mass of the steam portion of the atmosphere would be dictated by the solubility of water in the magma ocean. As the magma ocean solidified, gases collected in the atmosphere and rapidly condensed within the first 50–100 Ma to form the proto-oceans.

Composition of the Early Atmosphere

Two models have been proposed for the composition of the early post-collision atmosphere depending on whether metallic iron existed in the mantle. If metallic iron was present, equilibrium chemical reactions would liberate large amounts of H_2, CO, and CH_4 and small amounts of CO_2, H_2O, H_2S, and N_2 (Holland, 1984; Kasting et al., 1993a). If iron was not present, reactions would liberate mostly CO_2, H_2O, and N_2 with minor amounts of H_2, HCl, and SO_2. If degassing began during or immediately after re-accretion of Earth, metallic

iron would have been present in the mantle and the first atmosphere would have been a hot steamy one composed chiefly of H_2, CO_2, H_2O, CO, and CH_4. However, because core formation and most degassing were probably complete in <50 Ma after re-accretion, the composition of the early atmosphere may have changed rapidly during this time interval in response to decreasing amounts of metallic iron in the mantle. It is likely that H_2 rapidly escaped from the top of the atmosphere and water vapor rained out, forming oceans. This leaves an early atmosphere rich in CO_2, CO, N_2, and CH_4 (Holland et al., 1986; Kasting, 1993). As much as 15% of the carbon now found in the continental crust may have resided in this early atmosphere, which is equivalent to a partial pressure of CO_2, CH_4, and N_2 of about 11 bars (Table 6.1). The mean surface temperature of such an atmosphere would have been about 85°C.

Even after the main accretionary phase of the new Earth had ended, major asteroid and cometary impacts continued to about 3.9 Ga, as inferred from the lunar impact record. Cometary impactors could have added more carbon as CO to the atmosphere, and produced NO by shock heating of atmospheric CO_2 and N_2. A major contribution of cometary gases to the early atmosphere also solves the "missing xenon" problem. Being heavier, xenon should be less depleted and less fractionated than krypton in Earth's atmosphere, whereas the opposite is observed (Figure 6.2) (Dauphas, 2003). Any fractionation event on the early Earth would have resulted in high Xe/Kr ratios, not low ratios as observed. Noble gases such as Xe and Kr trapped in comets, however, show a depletion in Xe relative to Kr. Hence, a significant contribution of cometary gases to the early atmosphere could account for the missing xenon in Earth's atmosphere. Some investigators have suggested that Earth received much of its water supply from the accretion of comets. However, the D/H (deuterium/hydrogen) ratio of Earth (1.49×10^{-4}) is similar to that of the carbonaceous chondrites and very different from that of comets (3.1×10^{-4}), suggesting that our water came from accretion of asteroid-like materials (Robert, 2001). This conclusion, however, is questioned by Genda and Ikoma (2007) who present a case for the terrestrial D/H changing during the last 4.5 Ga.

Growth Rate of the Atmosphere

Two extreme scenarios are considered for growth rate of the post-collision atmosphere: the **big burp model**, in which the atmosphere grows by rapid degassing during or soon after planetary re-accretion (Fanale, 1971), and the **steady-state model**, in which the atmosphere grows slowly over geologic time (Rubey, 1951). One way of distinguishing between these models is to monitor the buildup of ^{40}Ar and ^{4}He in sedimentary rocks that have equilibrated with the atmosphere–ocean system through time. Argon-40 is produced by the radioactive decay of ^{40}K in Earth, and as it escapes from the mantle it collects in the atmosphere. Because ^{36}Ar is nonradiogenic, the $^{40}Ar/^{36}Ar$ ratio should record distinct evolutionary paths for Earth degassing. The steady-state model is characterized by a gradual increase in the $^{40}Ar/^{36}Ar$ ratio with time, while the

big burp model should show initial small changes in this ratio followed by rapid increases as ^{40}K decays.

Some argon degassing models suggest that the atmosphere grew very rapidly in the first 100 Ma after the Moon-forming event followed by more continuous growth to the present (Sarda et al., 1985). These models indicate a mean age for the atmosphere of 4.5 Ga, suggesting rapid early degassing of Earth. The fraction of the atmosphere released during early degassing is unknown, but may have been substantial (Marty & Dauphas, 2002). On the other hand, relatively young K/Ar ages of MORB mantle sources (<1 Ga) show that the depleted upper mantle was not completely degassed, and that it decoupled from the atmosphere early in Earth's history (Fisher, 1985). These data, together with the relatively young U/He and U/Xe ages of depleted mantle suggest that some degassing has continued to the present.

The Faint Young Sun Paradox

Models for the evolution of the Sun indicate that it was less luminous when it entered the main sequence about 5 Ga. This is because with time the Sun's core becomes denser and therefore hotter as hydrogen is converted to helium. Calculations indicate that the early Sun was 25–30% less luminous than it is today and that its luminosity has increased with time in an approximately linear manner (Kasting, 1987). The paradox associated with this luminosity change is that Earth's average surface temperature would have remained below freezing until 2–1 Ga for an atmosphere composed mostly of nitrogen (Figure 6.3).

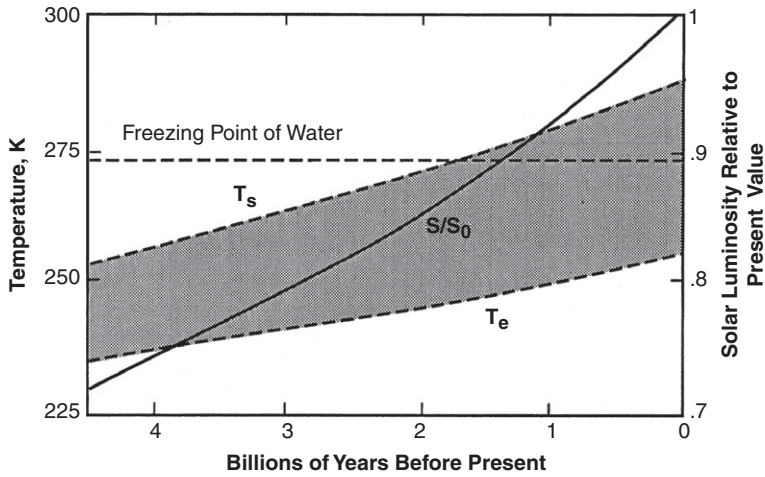

FIGURE 6.3 Estimated increase in solar luminosity with time and its effect on Earth's surface temperature. S, solar luminosity; S_o, present solar luminosity; T_s, surface temperature with nitrogen atmosphere; T_e, surface temperature with no atmosphere. *Modified after Kasting & Ono (2006), courtesy of Jim Kasting.*

Yet the presence of sedimentary rocks as old as 3.8 Ga indicates the existence of oceans and running water. A probable solution to the faint young Sun paradox is that the early atmosphere contained a much larger quantity of greenhouse gases than it does today. For instance, CO_2 or CH_4 levels of even a few tenths of a bar could prevent freezing temperatures at Earth's surface due to an enhanced greenhouse effect. The **greenhouse effect** is caused by gases that allow sunlight to reach a planetary surface, but absorb infrared radiation reflected from the surface, which heats both the atmosphere and the planetary surface. An upper bound on the amount of CO_2 in the early Archean atmosphere is provided by the carbon cycle and appears to be about 1 bar. Although CO_2 was undoubtedly an important greenhouse gas during the Archean, studies of a 3.5-Ga paleosol (ancient soil horizon) suggest that atmospheric CO_2 levels in the Archean were at least five times lower than required by the faint young Sun paradox (Rye et al., 1995; Sheldon, 2006). This constrains the Archean CO_2 levels to about 0.2 bar. The mineralogy of banded iron formation also suggests that CO_2 levels were <0.15 bar at 3.5 Ga. Hence, another greenhouse gas, probably CH_4 with contributions from nitrogen (N_2) (Goldblatt et al., 2009), may have been the most important greenhouse gas in the Archean atmosphere (Table 6.1) (Catling et al., 2001; Kasting & Howard, 2006). As pointed out by Kasting (2010), however, the methane greenhouse effect is limited because organic haze begins to form when the CH_4/CO_2 ratio is >0.1, creating an "anti-greenhouse" effect that cools the surface if the haze becomes too thick. Ueno et al. (2009) have shown from SO_2 photolysis calculations that carbonyl sulfide (OCS), which is a strong greenhouse gas, may have been abundant enough in the Archean atmosphere to resolve the faint young Sun paradox.

Another factor that may have aided in warming the surface of the early Earth is decreased **albedo**, that is, a decrease in the amount of solar energy reflected by cloud cover. To conserve angular momentum in the Earth–Moon system, Earth must have rotated faster in the Archean (about 14 h/day), which decreases the fraction of global cloud cover by 20% with a corresponding decrease in albedo (Jenkins et al., 1993). Also contributing to lower albedo in the early Archean is a probable smaller total surface area of continents (Rosing et al., 2010).

So the bottom line of the faint young Sun paradox is that some combination of CH_4, N_2 and OCS in the atmosphere, together with a contribution of decreased albedo kept planet Earth from freezing over before 2 Ga.

The Precambrian Atmosphere

By 3.8 Ga, it would appear that Earth's atmosphere was composed chiefly of CH_4, N_2, and CO_2, with small amounts of CO, H_2, H_2O, and reduced sulfur gases (Kasting, 1993; Des Marais, 1994; Pavlov et al., 2000). Based on the paleosol data described earlier, an average CO_2 level of about 10^3 PAL (PAL = fraction of present atmospheric level) seems reasonable at 3 Ga. Photochemical models, however, indicate that methane levels approximately

1000 times the present level in the atmosphere can also explain the paleosol data (Pavlov et al., 2000; Catling et al., 2001). Such levels could readily be maintained in the Archean by **methanogenic bacteria** (i.e., methane-producing bacteria; also called **methanogens**), which appear to have been an important part of the biota at that time (Chapter 9). With little if any land area in the early Archean, removal of CO_2 by seafloor alteration and carbonate deposition should have been more important than today. Beginning in the late Archean, however, when continental cratons emerged above sea level, the volcanic inputs of CO_2 were ultimately balanced by weathering and perhaps to a lesser degree by carbonate deposition.

During the Proterozoic, the increasing biomass of algae may have contributed to a CO_2 drawdown caused by photosynthesis, and rapid chemical weathering was promoted by increased greenhouse warming. However, small amounts of methane in the atmosphere (100–300 ppm) also may have contributed to maintaining a warm climate during the Proterozoic (Pavlov et al., 2003). An overall decrease in atmospheric CO_2 level with time may be related to changes in the carbon cycle, in which CO_2 is removed from the atmosphere by carbonate deposition and photosynthesis, followed by burial of organic matter faster than it is resupplied by volcanism and subduction (Figure 6.4). Methane levels in the atmosphere may also drop during this time by continued photolysis in the upper atmosphere, followed by hydrogen escape (Catling et al., 2001). Shallow marine carbonates deposited in cratonic basins are effectively removed from the carbon cycle and are a major sink for CO_2 from the

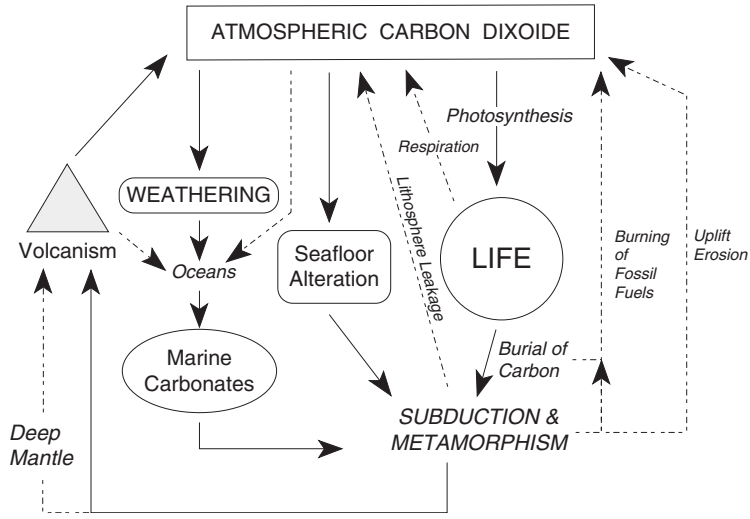

FIGURE 6.4 Simplified version of the carbon cycle. Solid arrows are major controls and dashed arrows minor controls on atmospheric CO_2 levels.

Mesoproterozoic onward. Decreasing solar luminosity and the growth of ozone in the upper atmosphere beginning in the Paleoproterozoic also reduced the need for CH_4 and CO_2 as greenhouse gases. Rapid extraction of CO_2 by deposition of marine carbonates and decreases of CH_4 caused by photolysis and hydrogen escape may have resulted in sufficient atmospheric cooling to cause the widespread glaciation recognized in the geologic record at 2.4–2.3 Ga.

THE CARBON CYCLE

The most important chemical system controlling the CO_2 content of the terrestrial atmosphere is the **carbon cycle**. CO_2 enters Earth's atmosphere by volcanic eruptions, the burning of fossil fuels, uplift and erosion, and the respiration of living organisms (Figure 6.4). Of these, only volcanism appears to have been important in the geologic past, but the burning of fossil fuels is becoming more important today. For instance, records indicate that during the last 100 years, the rate of release of CO_2 from the burning of fossil fuels has risen 2.5% per year and could rise to three times its present rate in the next 100 years. CO_2 returns to the oceans by chemical weathering of silicates, alteration on the seafloor, and dissolution of atmospheric CO_2 in the oceans, of which only the first two are significant at present (Figure 6.4). The ultimate sink for CO_2 in the oceans is deposition of marine carbonates. Although CO_2 is also removed from the atmosphere by photosynthesis, it is not as important as carbonate deposition. Weathering and deposition reactions can be summarized as follows (Walker, 1990; Brady, 1991):

Weathering:

$$CaSiO_3 + 2CO_2 + 3H_2O \rightarrow Ca^{2+} + 2HCO_3^{-1} + H_4SiO_4 \qquad (6.2)$$

Deposition:

$$Ca^{2+} + 2HCO_3^{-1} \rightarrow CaCO_3 + CO_2 + H_2O \qquad (6.3)$$

The cycle is completed when pelagic carbonates are subducted and metamorphosed and CO_2 is released and again enters the atmosphere either by volcanism or by leaking through the lithosphere. The metamorphic reactions that liberate CO_2 can be summarized by the carbonate-silica reaction:

$$CaCO_3 + SiO_2 \rightarrow CaSiO_3 + CO_2 \qquad (6.4)$$

For equilibrium to be maintained in the carbon cycle, increased input of CO_2 into the atmosphere causes a negative feedback resulting in more weathering and carbonate deposition, thus avoiding buildup of CO_2 in the atmosphere. Various negative feedback mechanisms in the carbon cycle may have stabilized Earth's surface temperature in the geologic past (Walker, 1990; Berner & Canfield, 1989). As an example, if the solar luminosity were to suddenly drop, the surface temperature would fall, causing a decrease in the rate of silicate

weathering due to a decrease in evaporation from the oceans (and hence a decrease in precipitation). This results in CO_2 accumulation in the atmosphere, which increases the greenhouse effect and restores higher surface temperatures. The converse of this feedback would occur if the surface temperature were to suddenly increase. Although increased CO_2 in the Archean atmosphere would result in greenhouse warming of Earth's surface, it should also cause increased weathering rates resulting in a decrease in CO_2. However, this would only occur in the late Archean after a large volume of continental crust had stabilized above sea level to be weathered.

THE CARBON ISOTOPE RECORD

General Features

Carbon isotopes in carbonates and organic matter offer the most effective way to trace the growth of the crustal reservoir of reduced carbon (Des Marais et al., 1992). The fractionation of ^{13}C and ^{12}C is measured by the $^{13}C/^{12}C$ ratio in samples relative to a standard such that

$$\delta^{13}C\ (‰) = \{[(^{13}C/^{12}C)_{sample}/(^{13}C/^{12}C)_{std}] - 1\} \times 1000 \qquad (6.5)$$

This expression is used to express both carbonate (δ_{carb}) and organic (δ_{org}) isotopic ratios. The relative abundance of carbon isotopes is controlled chiefly by equilibrium isotopic effects among inorganic carbon species, fractionation associated with the biochemistry of organic matter, and the relative rates of burial of carbonate and organic carbon in sediments. Most of the carbon in Earth's near-surface systems is stored in sedimentary rocks with only about 0.1% in living organisms and the atmosphere–hydrosphere. Oxidized carbon occurs primarily as marine carbonates and reduced carbon as organic matter in sediments. In the carbon cycle, CO_2 from the oceans and atmosphere is transferred into sediments as carbonate carbon (C_{carb}) or organic carbon (C_{org}), with the former monitoring the composition of the oceans (Figure 6.4). The cycle is completed by uplift and weathering of sedimentary rocks and by volcanism, both of which return CO_2 to the atmosphere.

Because organic matter preferentially incorporates ^{12}C over ^{13}C, there should be an increase in the $^{13}C/^{12}C$ ratio (as measured by $\delta^{13}C$) in buried carbon with time, and indeed this is what is observed (Worsley & Nance, 1989; Des Marais et al., 1992). The amount of $\delta^{13}C_{org}$ increases from values of $< -40‰$ in the Archean to modern values of –20 to –30‰. On the other hand, seawater carbon as tracked with $\delta^{13}C_{carb}$ remains roughly constant with time, with $\delta^{13}C_{carb}$ averaging about 0‰. The carbon cycle can be monitored by an isotopic mass balance (Des Marais et al., 1992) as follows:

$$\delta_{in} = f_{carb}\,\delta^{13}C_{carb} + f_{org}\,\delta^{13}C_{org} \qquad (6.6)$$

where δ_{in} represents the isotopic composition of carbon entering the global surface environment comprised of the atmosphere, hydrosphere, and biosphere. The right side of the equation represents the weighted-average isotopic composition of carbonate ($\delta^{13}C_{carb}$) and organic ($\delta^{13}C_{org}$) carbon buried in sediments, and f_{carb} and f_{org} are the fractions of carbon buried in each form ($f_{carb} = 1 - f_{org}$). For timescales longer than 100 Ma, $\delta_{in} = -5$ ‰, the average value for crustal and mantle carbon (Holser et al., 1988). Thus, where values of sedimentary $\delta^{13}C_{carb}$ and $\delta^{13}C_{org}$ can be measured, it may be possible to determine f_{org} for ancient carbon cycles. For example, higher values of $\delta^{13}C_{carb}$ indicate either a higher value of f_{org} or a greater negativity of average $\delta^{13}C_{org}$.

During the Phanerozoic, there are several peaks in $\delta^{13}C_{carb}$, the largest at about 110, 280, 300, 400, and 530 Ma (Figure 6.5). These peaks appear to reflect an increase in burial rate of organic carbon (Des Marais et al., 1992; Frakes et al., 1992). This is because organic matter selectively enriched in ^{12}C depletes seawater in this isotope, raising the $\delta^{13}C$ values of seawater. In the late Paleozoic (300–250 Ma), the maxima in $\delta^{13}C_{carb}$ correspond to the rise and spread of vascular land plants, which provided a new source of organic debris for burial (Berner, 1987, 2001). Also conducive to preservation of organic remains at this time were the vast lowlands on Pangea, which appear

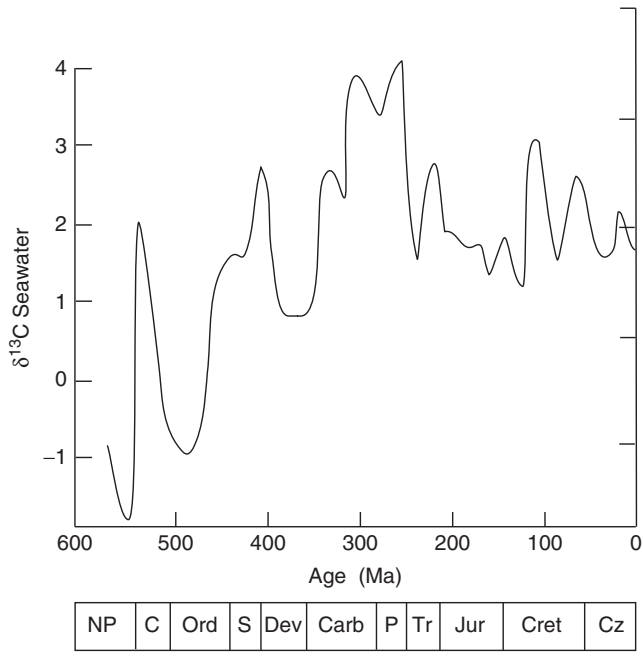

FIGURE 6.5 Secular changes in $\delta^{13}C$ in seawater in the last 600 Ma based on data from marine carbonates.

to have been sites of widespread swamps where bacterial decay of organic matter is minimized. A drop in $\delta^{13}C_{carb}$ at the end of the Permian is not understood. Perhaps large amounts of photosynthetic O_2 generated by Carboniferous forests led to extensive forest fires that destroyed large numbers of land plants in the Late Permian.

The 2200-Ma Carbon Isotope Excursion

It is now well established that a global positive excursion in $\delta^{13}C$ occurs in marine carbonates at about 2200 Ma, the largest known excursion in the geologic record (Figure 6.6) (Karhu & Holland, 1996; Holland, 2002). Zircon ages constrain the timing of this event from 2200 Ma to between 2100 and 2060 Ma, for a duration of 100–140 Ma (Melezhik et al., 2007). Other Paleoproterozoic carbon isotope excursions are reported in the Transvaal Group in South Africa, but it is not clear if these are of global extent or reflect local sedimentary conditions. During the 2200-Ma event, the fraction of carbon gases reduced to organic carbon was much larger than before or after the event (Holland, 2002, 2006). At the peak, $\delta^{13}C$ in marine carbonates reached values as high as +12 and corresponding organic carbon values, although variable, averaged about –24.

Using Eq. (6.6), there are two ways to explain a positive excursion of carbonate $\delta^{13}C$: (1) increase the fraction of carbon buried in the organic carbon reservoir or (2) increase the negativity of $\delta^{13}C_{org}$ in the organic reservoir. If the average $\delta^{13}C$ input into the atmosphere was about –5‰ as it is today, about 50% of the carbon at this time would have to be buried as organic carbon to produce the carbonate $\delta^{13}C$ excursion. However, there is no evidence for extensive carbon burial in shallow marine basins nor for the oxygen growth in the

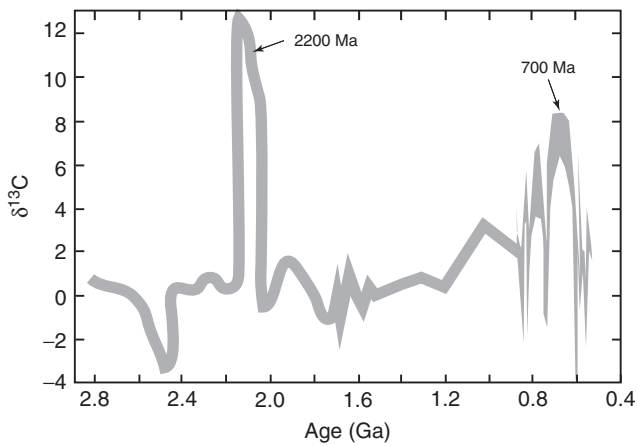

FIGURE 6.6 The isotopic composition of carbon in marine carbonates, between 2.8 and 0.4 Ga.

atmosphere that would accompany the burial at this time. It is possible, however, that organic matter may have been deposited in deepwater settings that were later subducted. Another possibility is that an increasing importance of methanogenic diagenesis at this time may have played a significant role (Hayes & Waldbauer, 2006). If methanogens became more widespread, the negativity of $\delta^{13}C_{org}$ would increase. The unanswered question is what would cause methanogens to increase and then decrease again in relative importance? The age of the excursion also corresponds to the breakup of a late Archean supercontinent (see Chapter 8). Could such an event possibly affect methanogens by increasing the geographic area of reducing environments in which they live? Alternatively, could photosynthesis increase at this time, increasing the food supply of the methanogens? In either case, we need a shutoff valve to end the excursion.

THE SULFUR ISOTOPE RECORD

The geochemical cycle of sulfur resembles that of carbon (Figure 6.7). During this cycle ^{34}S is fractionated from ^{32}S with the largest fractionation occurring during bacterial reduction of marine sulfate to sulfide. Isotopic fractionation is expressed as $\delta^{34}S$ in a manner similar to that used for carbon isotopes. Sedimentary sulfates appear to record the isotopic composition of sulfur in seawater. Mantle ^{34}S is near zero per mil and bacteria reduction of sulfate strongly prefers ^{32}S, thus reducing $\delta^{34}S$ in organic sulfides to negative values (–180‰) and leaving oxidized sulfur species with approximately equivalent positive values (+17‰). Hence, the sulfur cycle is largely controlled by the biosphere, and in particular by sulfate-reducing bacteria that inhabit shallow marine waters. Due to the mobility of dissolved sulfate ions and rapid mixing of marine reservoirs, $\delta^{34}S$ values of residual sulfate show limited variability ($+17 \pm 2$‰) compared to the spread of values in marine sulfides (–5 to –35‰).

The sulfur isotopic record may also help constrain the growth of oxygen in the atmosphere as discussed more fully in Chapter 9. The time distribution of

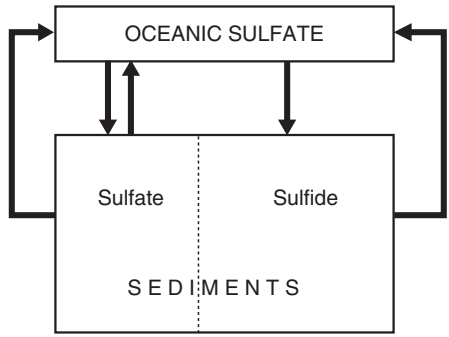

FIGURE 6.7 Schematic diagram of the sulfur cycle.

sulfates and sulfate-reducing bacteria should track the growth of oxygen (Ohmoto et al., 1993; Canfield et al., 2000). The overall sulfur isotope trends in marine sulfates and sulfides from 3.8 Ga to the present suggest a gradual increase in sulfate $\delta^{34}S$ and corresponding decrease in sulfide $\delta^{34}S$ (Figure 6.8). Changes in $\delta^{34}S$ with time reflect (1) changes in the isotopic composition of sulfur entering the oceans from weathering and erosion, (2) changes in the relative proportions of sedimentary sulfide and sulfate receiving sulfur from the atmosphere–ocean system, and (3) the temperature of seawater (Schidlowski et al., 1983; Ohmoto & Felder, 1987; Canfield et al., 2000).

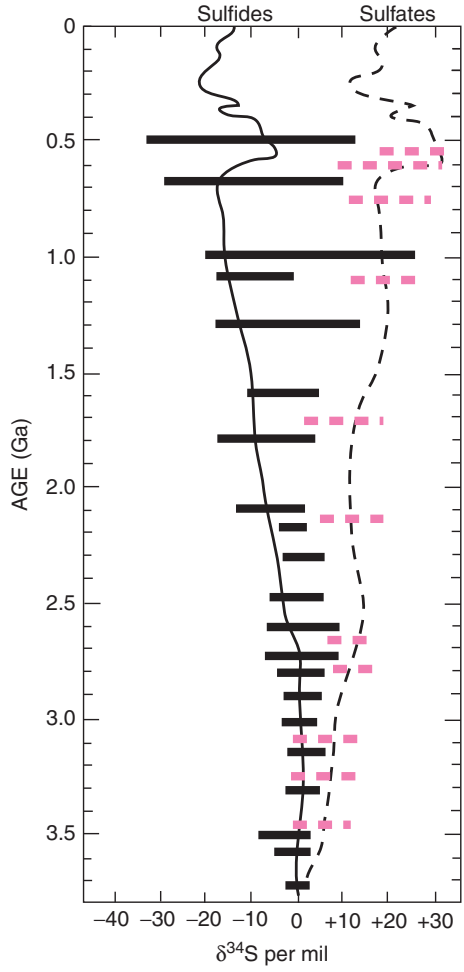

FIGURE 6.8 The isotopic composition of sulfur in marine sulfates and sulfides with geologic time. *Modified after Schidlowski et al. (1983) and Canfield (1998).*

Because weathering tends to average out sulfide and sulfate input, one or both of the latter two effects probably accounts for oscillations in the sulfate $\delta^{34}S$ with time. Three causes have been suggested for the tight grouping of $\delta^{34}S$ in marine sulfates and sulfides in the Archean (Figure 6.8) (Canfield et al., 2000): (1) low fractionation of sulfur isotopes due to high sulfate reduction rates and moderate concentrations of sulfate in the oceans, (2) low fractionation of isotopes in sulfides that form a closed system of poorly mixed sediments, or (3) sulfide formation in sulfate-poor oceans. In all three scenarios, sulfate-reducing bacteria are able to reduce sulfates to sulfur very efficiently, resulting in limited isotopic fractionation between sulfides and sulfates. Although with our current database a distinction between the above three causes is not possible, the increase in spread of $\delta^{34}S$ values beginning at about 2.3–2.2 Ga is consistent with the carbon isotope data in suggesting rapid growth in oxygen in the atmosphere at this time (see Chapter 9).

PHANEROZOIC ATMOSPHERIC HISTORY

It is possible to track the levels of CO_2 and O_2 in Earth's atmosphere during the Phanerozoic using the burial and weathering rates of organic carbon, Ca and Mg silicates, and carbonates as deduced from the preserved stratigraphic record. Other factors such as the effect of changing solar radiation on surface temperature and weathering rates and the use of the $^{87}Sr/^{86}Sr$ seawater curve to estimate the effect of tectonics on weathering and erosion rates can be used to fine-tune the results (Berner & Canfield, 1989; Berner, 1994, 2001). Although CO_2 shows a gradual drop throughout the Phanerozoic, it is very high in the early to middle Paleozoic and shows a pronounced minimum around 300 Ma (Figure 6.9). Variations in atmospheric CO_2 are controlled by a combination of tectonic and biologic processes, often with one or the other dominating, and by the increasing luminosity of the Sun. An increase in solar luminosity since the beginning of the Paleozoic is probably responsible for the gradual drop in atmospheric CO_2. This drawdown is caused by enhanced weathering rates due to the greenhouse warming of the atmosphere. The dramatic minimum in CO_2 about 300 Ma appears to be related to (1) enhanced silicate weathering and (2) the appearance and rapid development of land plants, which, through photosynthesis followed by burial, rapidly removed carbon from the atmosphere–ocean system. Rapid weathering rates in the early and middle Paleozoic probably reflect a combination of increasing solar luminosity and the fragmentation of Gondwana (early Paleozoic only), during which enhanced ocean ridge and mantle plume activity pumped large amounts of CO_2 into the atmosphere, resulting in increased weathering rates.

The small increase in CO_2 in the early Mesozoic (225 Ma), which resulted in worldwide warm climates, may have been caused by enhanced ocean ridge and mantle plume activity associated with the onset of fragmentation of Pangea. The gradual drop in CO_2 in the Late Cretaceous and Tertiary may reflect increased

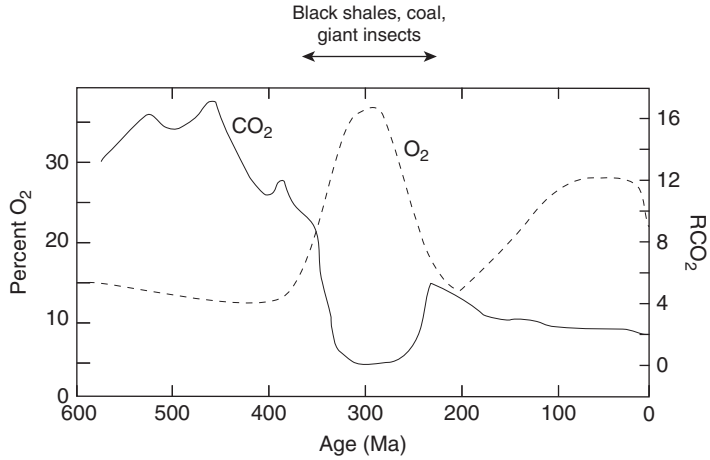

FIGURE 6.9 Oxygen and CO_2 atmospheric concentrations during the Phanerozoic. RCO_2 = mass ratio of CO_2 at a given time divided by the modern value. *After Berner & Canfield (1989) and Berner (1994, 2001).*

weathering and erosion rates in response to terrane collisions around the Pacific (exposing more land area for weathering).

Unlike CO_2, the variation in O_2 during the Phanerozoic appears to be controlled chiefly by the burial rate of carbon and sulfur, which in turn is controlled by sedimentation rates (Berner, 2001). Oxygen levels were relatively low and constant during the early and middle Paleozoic, followed by a high peak about 300 Ma (Figure 6.9). This peak correlates with the minimum in CO_2 and appears to have the same origin: enhanced burial rate of organic carbon accompanying the rise of vascular land plants (Berner et al., 2007). Because land plants are high in lignin, a degradation-resistant organic substance, widespread burial in swamps led to major coal deposits and wildfires (as evidenced by abundant fossil charcoal) during the late Paleozoic (360–260 Ma). This increase in oxygen may have enhanced diffusion-dependent processes such as respiration, and hence some organisms could attain large body sizes (Graham et al., 1995; Berner, 2001). The most spectacular examples are the insects, where some forms attained gigantic sizes probably in response to increased diffusive permeation of oxygen into the organisms. Also, the increased oxygen levels would result in a denser atmosphere (21% greater than at present), which may have led to the evolution of insect flight by offering greater lift. Increased aquatic oxygen levels during the Carboniferous-Permian would permit greater biomass densities and increased metabolic rates, both of which could lead to increases in radiation of taxa and in organism sizes. Impressive examples of both of these changes occur in brachiopods, foraminifera, and corals.

The decrease in O_2 around 200 Ma at the beginning of the Triassic appears to be mainly related to decreases in the lateral extent of lowland forests and

swamps. This resulted in a drop in burial rate of carbon, and hence to a decrease in O_2 production. As Pangea began to fragment, depositional basins changed from coal swamps to oxidized terrestrial basins, largely eolian and fluvial, thus no longer burying large quantities of carbon. Also, a dramatic drop in sea level at the end of the Permian resulted in oxidation and erosion of previously buried organic material, thus reducing atmospheric O_2 levels. During the Mesozoic O_2 gradually increased, probably in response to burial of land plants in coal swamps. A drop in sea level during the Late Tertiary exposed these organics to oxidation and erosion, probably leading to the fall in atmospheric O_2 beginning in the Late Tertiary.

THE HYDROSPHERE

The oceans cover 71% of Earth's surface and comprise most of the hydrosphere. The composition of seawater varies geographically and with depth and is related principally to the composition of rivers and hydrothermal water entering along ocean ridges. Chemical precipitation, melting of ice, and evaporation rate also affect the salinity of seawater. Dissolved nutrients such as bicarbonate, nitrate, phosphate, and silica vary considerably in concentration as a result of removal by planktonic microorganisms such as foraminifera, diatoms, and algae. Seawater temperature is rather constant in the upper 300 m ($\sim$18°C), then drops dramatically to a depth of about 1 km where it remains relatively constant (3–5°C) to the ocean bottom. The cold bottom water in the oceans forms in polar regions, where it sinks because of its high density, and travels toward the equator displacing warm surface waters that travel poleward. The geologic history of seawater is closely tied to the history of the atmosphere, and oceanic growth and the concentration of volatile elements in seawater are controlled, in part, by atmospheric growth (Holland et al., 1986). Most paleoclimatologists agree that the oceans formed early in Earth history by condensation of atmospheric water. Some water, however, may have been added to Earth by early cometary impacts. For instance, with the current rate of water accretion from small comets, it is possible to increase mean global sea level by 2–10 mm in about 3600 years (Deming, 1999). However, as discussed previously, because the deuterium/hydrogen ratio in cometary water (3.1×10^{-4}) is considerably higher than in terrestrial water (1.49×10^{-4}), the contribution of cometary water to the oceans in the past probably has been very small (<10%) (Robert, 2001).

Because of a higher CO_2 content of the early atmosphere, the first seawater to condense must have had a low pH (<7) due to dissolved CO_2 and other acidic components (H_2S, HCl, etc.). However, this situation was probably short lived in that submarine volcanic eruptions and seawater recycling through ocean ridges would introduce large amounts of Na, Ca, and Fe. Thus, a pH between 8 and 9 and a neutral or negative Eh were probably reached rapidly in the early oceans and maintained thereafter by silicate-seawater buffering reactions and recycling at ocean ridges.

Sea Level

Global sea level is controlled by changes in the volume of seawater or in the volume of ocean basins. Water volume changes are controlled chiefly by the growth and loss of continental ice sheets, resulting in high-amplitude, rapid eustatic changes (up to 200 m with rates up to 20 m/1000 years) (Miller et al., 2005). Other processes affecting sea level at high rates (10 m/1000 years) and low amplitudes (5–10 m) include thermal expansion and contraction of seawater and variations in groundwater and lake storage (Figure 6.10). In contrast, changes in ocean basin volumes are controlled chiefly by changes in seafloor spreading rates and ocean ridge lengths (100–300 m at rates of 10 m/Ma). In addition, growth of oceanic plateaus can produce moderate changes (60 m/Ma). Three scales of sea level change are apparent (Figure 6.10): long term (10^7–10^8 years), related to changing ocean ridge systems and the supercontinent cycle; (2) intermediate term (10^6–10^7 years); and (3) short-term changes (10^4–10^5 years) due chiefly to changes in ice volume.

Changes in sea level leave an imprint in the geologic record by the distribution of sediments and biofacies, by the aerial extent of shallow seas as manifest by preserved cratonic sediments, and by calculated rates of sedimentation (Eriksson, 1999). A widely used approach to monitor sea level is to map successions of transgressive and regressive facies in marine sediments. During **transgression**, shallow seas advance on the continents, and during **regression** they retreat. Transgressions and regressions, however, are not always accompanied by rises or drops in sea level and in order to estimate sea level changes,

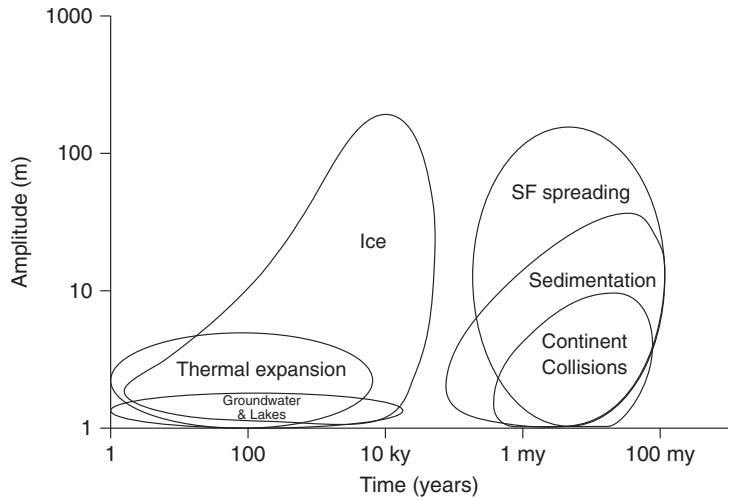

FIGURE 6.10 Timing and amplitudes of factors controlling eustatic changes in sea level. SF, seafloor. *From Miller et al. (2005), courtesy of Ken Miller and the American Association for the Advancement of Science.*

it is necessary to correlate facies and unconformities over large geographic regions on different continents and different tectonic settings using sequence stratigraphy (Steckler, 1984; Vail & Mitchum, 1979). Using this technique, onlap and offlap patterns are identified in seismic reflection profiles and used to construct maps of the landward extent of coastal onlap, from which changes in sea level are estimated. Major transgressions are recorded in the early Paleozoic and in the Late Cretaceous (Figure 6.11). Estimates of the amplitude of these sea level rises range from 100 to more than 350 m above present sea level (Algeo & Seslavinsky, 1995; Miller et al., 2005). Cyclicity in sea level change has been proposed by many investigators with periods in the range of 10 to 80 Ma.

Short-term changes in sea level are controlled dominantly by changes in ice volume, which, in turn, reflect astronomical variations in Earth's orbital properties, the Milankovitch cycles as described later in the chapter (Eriksson, 1999; Miller et al., 2005). Also waves and tides, storm winds and hurricanes, tsunamis, melting of methane hydrates (clathrates), and catastrophic sediment slumps can affect tidal range. Tectonic controls seem to produce sea level changes at rates <1 cm/10^3 years, whereas glacial controls can produce changes up to 10 m/10^3 years. With the present ice cover on Earth, the potential amplitude for sea level rise if all the ice were to melt is 200 m.

Long-term changes in sea level are related largely to rates of seafloor spreading, with secondary contributions from changes in subduction zones, the motion of continents with respect to geoid highs and lows, and supercontinent

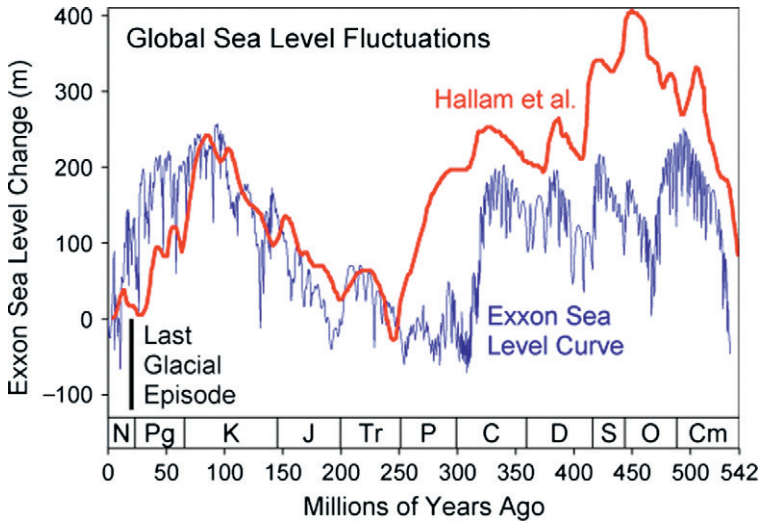

FIGURE 6.11 Global changes in sea level during the Phanerozoic. *Courtesy of Global Warming Art and Robert A. Rohde.*

insulation of the mantle (Gurnis, 1993; Eriksson, 1999; Miller et al., 2005). The most important cause of long-term sea level change is the volume of the ocean ridge systems, which increase and decrease as supercontinents assemble and disperse. The cross-sectional area of an ocean ridge is dependent on the spreading rate, since its depth is a function of its age. For instance, a ridge that spreads 6 cm/y for 70 Ma has three times the cross-sectional area of a ridge that spreads at 2 cm/y for the same amount of time. The total ridge volume at any time is dependent on the spreading rate (which determines cross-sectional area) and total ridge length. A long-term rise in sea level that may be controlled by increasing total ocean ridge volume is the breakup of Pangea beginning about 185 Ma and reaching a peak at about 90 Ma (Figure 6.11). Likewise, the rapid decrease in sea level in the late Paleozoic reflects the loss of ocean ridges as Pangea is forming. The sea level rise in the Cambrian may reflect new ocean ridges accompanying the breakup of the short-lived supercontinent Pannotia.

It is the intermediate scale sea level changes that are most perplexing and controversial (i.e., those that occur in cycles of 10^6–10^7 years). However, they often correlate with changes in global surface temperature, suggesting an ice volume control. The drops in sea level at 475, 420, and 375 Ma (Figure 6.11) probably reflect glaciations at these times. However, many intermediate-scale sea level changes occurred when Earth is thought to have been ice free, such as during the Late Cretaceous. One recently developed model that calls on pulsating convection in the shallow asthenosphere seems to have promise to explain these changes. Variations in the intensity of the upwelling beneath ocean ridges, together with blobs of hot mantle that are brought up on occasion, may control the ups and downs of sea level on a timescale of a few million years to tens of millions of years (Lovell, 2010).

The Early Oceans

Thermal modeling of the cooling rate of magma oceans after the Moon-forming event indicate that surface temperatures probably fell to less than 100°C between 4.54 and 4.51 Ga (Sleep et al., 2001). A steam atmosphere would begin to condense at temperatures of 300–400°C, thus giving rise to an early liquid ocean. The earliest history of the oceans comes from an unusual source: oxygen isotopes in ancient igneous zircons preserved in detrital sediments (Mojzsis et al., 2001). Most or all of these zircons appear to come from granitic sources. The $\delta\ ^{18}O$ values of detrital zircons ranging in age from about 4.4 to 2.7 Ga are slightly higher than the primitive value of Earth's mantle ($5.3 \pm 0.3‰$) (Figure 6.12) (Valley et al., 2002). To explain these high values, the granitic magmas must have interacted with water or involved sources that interacted with water that had high $\delta\ ^{18}O$ (such as shales). The relatively high $\delta\ ^{18}O$ in all of the early Archean zircons suggests, but does not prove, that oceans existed by at least 4.4 Ga. Liquid-water oceans are also required by 3.8 Ga to explain the precipitation of the chemical sediments found in Southwest Greenland and by 3.5 Ga to explain pillow basalts and stromatolites.

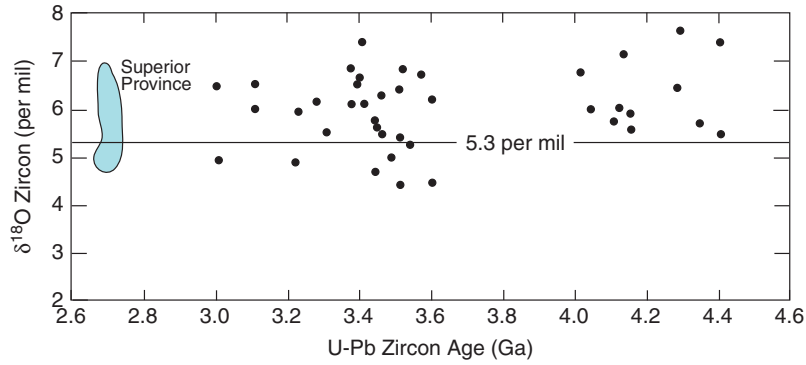

FIGURE 6.12 Oxygen isotopic composition of Archean detrital zircons. The value of 5.3‰ for average mantle is also shown. *Modified after Valley et al. (2002).*

It is likely that the growth rate of the early oceans paralleled that of the atmosphere, perhaps with a slight delay reflecting the time it took for a steam atmosphere to cool and condense. Although continental freeboard has been used to monitor the volume of seawater with time (Wise, 1973), as discussed in Chapter 7, uncertainties in the magnitude of the various factors that control freeboard render any conclusions suspect. In any case, a large fraction of the oceans probably formed soon after re-accretion of Earth after the Moon-forming event, such that by 4 Ga most of the current volume of seawater (>90%) was in place on Earth's surface. The presence of positive Eu anomalies in marine carbonates and the occurrence of ankerite in the Warrawoona Group in Western Australia by 3.45 Ga strongly suggest that seawater was anoxic at this time (Van Kranendonk et al., 2003). Also, the presence of siderite in banded iron formation in the Warrawoona Group suggests that hydrothermal input into the oceans at this time was more significant than afterward.

Changes in the Composition of Seawater with Time

Marine Carbonates

The two primary sources for dissolved ions in seawater are (1) runoff from the continents and (2) hydrothermal input from ocean ridges and arc-related submarine volcanism. The balance of inputs from these two sources is often preserved in marine sedimentary rocks such as carbonates, evaporites, banded iron formations, and chert. Although it is commonly assumed that the composition of seawater has not changed with time, observational and theoretical data challenge this assumption. For instance, some Archean marine carbonates contain giant botryoids of aragonite and Mg-calcite beds up to several meters thick that extend for hundreds of kilometers (Grotzinger & Kasting, 1993) (Figure 6.13). By comparison, Paleoproterozoic carbonates have much less

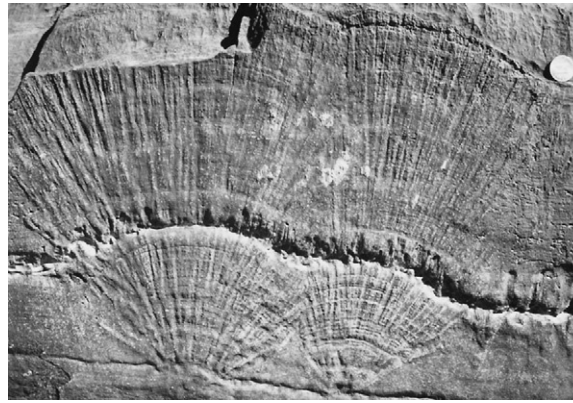

FIGURE 6.13 Aragonite botryoid pseudomorphs from the late Archean (2.52 Ga) Transvaal Supergroup in South Africa. Two aragonite fans nucleated on the sediment surface and grew upward. Width of photo about 30 cm. *Courtesy of John Grotzinger.*

spectacular occurrences of these minerals, although cement crusts in tidal flat deposits are common. In contrast, all younger marine carbonates lack these features, or in the case of the cements, show a progressive decline in abundance with age. Despite the fact that the modern ocean is oversaturated in carbonate, cement crusts are not deposited today. These secular changes strongly suggest that Precambrian seawater was greatly oversaturated in carbonate and that saturation decreased with time (Grotzinger & Kasting, 1993; Hardie, 2003). In addition, major ion concentrations and small-scale secular variations in Precambrian seawater composition are similar to those in Phanerozoic seawater.

Secular changes in the mineralogy of marine limestones and evaporites during the Phanerozoic may also be related to the supercontinent cycle. Periods of marine aragonite deposition are also times when $MgSO_4$ evaporites are widespread, whereas periods of dominantly calcite deposition correspond to an abundance of KCl evaporite deposition (Hardie, 1996; Horita et al., 2002). This distribution may be controlled by chemical reactions associated with hydrothermal alteration at ocean ridges in which there is a net transfer of $Na + Mg + SO_4$ from seawater to rock and of $Ca + K$ from rock to seawater. The intensity of these reactions is a function of the volume of seawater circulated through the ocean ridge system, which in turn is a function of the heat flux associated with ocean crust production. Thus, during times of high production of oceanic crust, the oceans should be depleted in Na-Mg sulfates and enriched in Ca and K ions, as for instance during the early Paleozoic. The Mg/Ca mole ratio in seawater can be used to track these reactions, in that at mole ratios of less than 2, only calcite is deposited, whereas at higher ratios both high-Mg calcite and aragonite are deposited. Also, during episodes of high Mg/Ca in seawater when aragonite is deposited, seawater has low Sr/Ca ratios due to the preferential incorporation

of Sr into aragonite (Steuber & Veizer, 2002). Because the production rate of oceanic crust is tied closely to the supercontinent cycle, the mineralogy of marine carbonates and evaporites should also reflect this cycle. The Mg/Ca mole ratio of seawater calculated from oceanic crust production rate during the Paleozoic agrees well with the observed secular changes in composition of carbonates and evaporites, supporting the model (Hardie, 1996, 2003).

Another attribute of carbonate deposition not well understood is the scarcity of Archean carbonates. Among the causes proposed for this observation are the following: (1) the pH of Archean seawater was too low for carbonate deposition, (2) carbonates were deposited on stable cratonic shelves during the Archean and later eroded away, and (3) carbonates were deposited in deep ocean basins during the Archean and later destroyed by subduction. A possible high-CO_2 content for the Archean atmosphere has been appealed to by some to explain the scarcity of Archean marine carbonates (Cloud, 1968a). The reasoning is that a high-CO_2 content in the atmosphere results in more CO_2 dissolved in seawater, thus lowering seawater pH and allowing Ca^{2+} to remain in solution because of its increased solubility. However, the CO_2 content of seawater is not the only factor controlling pH. Mineral stability considerations suggest that although the $CO_2 - CO_3^{2-}$ equilibria may have short-term control of pH, silicate equilibria have long-term control. In seawater held at a constant pH by silicate buffering reactions, the solubility of Ca^{2+} decreases with increasing CO_2 levels. Hence, the CO_2 mechanism does not seem capable of explaining the scarcity of Archean carbonates.

As for the second explanation, carbonate rocks in Archean shallow marine successions are very rare, and thus removal of such successions by erosion will not solve the missing Archean carbonate problem. The third possibility tentatively holds the most promise. Because of the small number of stable cratons in the Archean, carbonate sedimentation was likely confined to deep ocean basins. If so, these carbonates would be largely destroyed by subduction accounting for their near absence in the geologic record.

The Dolomite-Limestone Problem

It has long been recognized that the ratio of dolomite to calcite in sedimentary carbonates has decreased with decreasing age for the last 3 Ga (Holland & Zimmermann, 2000). This is also reflected by the MgO/CaO ratio of marine carbonates. Most investigators agree that these trends are primary and are not acquired during later diagenesis, metasomatism, or alteration. The molar MgO/MgO+CaO ratio in igneous rocks ($\sim$0.2) is close that observed in pre-Mesozoic marine carbonates (0.2–0.3), which suggests that Mg and Ca were released during weathering in the same proportions that they occur in source rocks prior to 100 Ma (Holland, 1984). The residence times of CO_2, Mg^{2+}, and Ca^{2+} in seawater are short and delicately controlled by the input and removal rates of diagenetic silicates and carbonates.

The short-term variations in the dolomite/calcite ratio have been explained by changes in the distribution of sedimentary environments with time. For instance, dolomite is widespread during times in which large evaporite basins and lagoons were relatively abundant, such as in the Permian (Sun, 1994). Although the origin of the long-term secular change in the dolomite/calcite ratio is not fully understood, one of two explanations has been most widely advocated (Holland, 1984; Holland & Zimmermann, 2000):

1. *Change in Mg and/or Ca depository*. Removal of Mg^{2+} from seawater may have changed from a dominantly carbonate depository in the Proterozoic to a dominantly silicate depository in the late Phanerozoic. There is a tendency for the MgO/Al_2O_3 in shales to increase over the same time period, providing some support for this mechanism, in that Mg appears to be transferred from carbonate to silicate reservoirs with time. Alternatively, the decrease in dolomite deposition with time may be caused by the gradual transfer of $CaCO_3$ deposition from shallow-water to deepwater environments with time due to the growing importance of planktonic calcareous organisms.
2. *Decrease in atmospheric CO_2*. Silicate-carbonate equilibria are dependent on the availability of CO_2 in the atmosphere–ocean system. When only small amounts of CO_2 are available in the ocean, silicate-carbonate reactions shift such that Ca^{2+} is precipitated chiefly as calcite rather than in silicates. If the rate of CO_2 input into the ocean exceeds the release rate of Ca^{2+} during weathering, both Mg^{2+} and Ca^{2+} are precipitated as dolomite. Hence, a greater amount of dolomite in the Precambrian may reflect an atmosphere–ocean system with greater amounts of CO_2.

Evaporites

Another difference between Precambrian and Phanerozoic sediments is the sequence of evaporite deposition. In Paleoproterozoic sediments, halite (NaCl) is often deposited immediately on top of carbonate without intervening sulfates. Although minor occurrences of evaporitic gypsum are reported in the Archean (Buick & Dunlop, 1990), they appear to reflect the local composition of seawater controlled by local source rocks. The first really extensive sulfate deposits appear in the MacArthur Basin in Australia at 1.7–1.6 Ga, which coincides with the last examples of deposition of seafloor carbonate cements. The paucity of gypsum evaporites before 1.7 Ga may have been due to (1) low concentrations of sulfate in seawater before this time or (2) a sufficiently high bicarbonate/Ca ratio such that during progressive seawater evaporation, Ca was exhausted by carbonate precipitation before the gypsum stability field was reached (Grotzinger & Kasting, 1993).

Evaporite deposition also may have influenced the composition of the oceans during the Phanerozoic. The large mass of evaporites deposited during some time intervals may have been important in lowering the NaCl and $CaSO_4$ contents of world oceans (Holser, 1984). For instance, the vast volumes of salt

(chiefly NaCl) deposited in the Late Permian may have caused average ocean salinity to drop significantly during the Triassic and Jurassic. Evaporite deposition has been sharply episodic and erosion of older evaporites has been relatively slow in returning salts to the oceans. The distribution of evaporites of all ages coupled with a slow recycling rate into the oceans suggests that the mean salinity of seawater may have decreased since the Mesoproterozoic due to evaporite deposition.

Banded Iron Formation

Banded iron formation or **BIF** is a chemical sediment, typically thin-bedded or laminated with >15% iron of sedimentary origin. BIF has a very distinct distribution with time (see Figure 9.32 in Chapter 9). It is found in minor amounts in the early Archean and in large amounts in the late Archean, appears again around 1.9 Ga, and then disappears from the geologic record for 1 Ga, appearing again briefly in the Neoproterozoic, before it disappears entirely. As discussed in Chapter 9, the deposition of BIF is controlled by the availability of ferrous iron and oxygen in seawater. Rare earth element distributions in BIF and marine cherts in particular have proven to be useful in distinguishing continental from hydrothermal inputs to the oceans. BIF has variable amounts of Eu, which is a signature element for hydrothermal input. Positive Eu anomalies, indicative of hydrothermal sources, are common in BIF older than 2.7 Ga (Kato et al., 2006), whereas they are much smaller in younger BIF. This suggests that after the end of the Archean runoff from continental sources was considerably increased, probably due to the extensive growth of continental cratons in the late Archean. The enhanced continental input carried the typical negative Eu anomaly, which overwhelmed the hydrothermal Eu signature of the early oceans.

The Biochemical Record of Sulfur

Sulfate-reducing bacteria appear to have been in place by at least 3.5 Ga as suggested by the sulfur isotope fractionation between coexisting sulfates and sulfides of this age (see Figure 6.8). The biochemical record of sulfur is consistent with sulfate-poor Archean oceans changing to modest sulfate concentrations, but not until about 2.3 Ga do we see a significant separation between $\delta^{34}S$ in sulfides and sulfates. As discussed in Chapter 9, this probably reflects rapid growth of oxygen in the atmosphere at this time. These results suggest that the oceans were oxygenated only to shallow depths during the Paleoproterozoic and that more extensive oxygenation did not occur until the Neoproterozoic (see later discussion about euxinia) (Anbar & Knoll, 2002; Anbar, 2008). If sulfide conditions were common through much of the Proterozoic, geochemical redox indicators should provide evidence of widespread anoxia, and seawater sulfate concentrations should have been lower than at present. Both predictions are observed in black shales deposited between 1730 and 1640 Ma in Australia

and Laurentia. In addition, the relatively large isotopic variability in Mesoproterozoic sulfate evaporites, not seen in Phanerozoic evaporites, suggests a smaller Mesoproterozoic global reservoir of oceanic sulfate ion.

In summary, available data point to globally extensive sulfate-reducing bacteria in low-sulfate oceans, oxygenation in the ocean insufficient to support widespread deposition of sulfate evaporites, and sulfide-rich bottom waters in at least some marine basins during most of the Proterozoic (Anbar & Knoll, 2002; Knoll, 2003). Sulfur isotope studies further indicate that the sulfur content of the oceans increased by as much as an order of magnitude during the Great Oxidation Event (Chapter 9) around 2350 Ma, and then again in the Neoproterozoic at about 700 Ma.

Sedimentary Phosphates

Phosphorus is a major building block of all forms of life, and hence a knowledge of the spatial and temporal distribution of phosphates in marine sediments should provide insight into patterns of organic productivity (Follmi, 1996; Papineau, 2010). It is well known that sedimentary phosphates in the Phanerozoic have an episodic distribution, with well-defined periods of major phosphate deposition in the Neoproterozoic/Early Cambrian, Late Cretaceous/Early Tertiary, Miocene, Late Permian, and Late Jurassic (Cook & McElhinny, 1979). Most sedimentary phosphates occur at low paleolatitudes ($<40°$), and appear to have been deposited in arid or semiarid climates either in narrow east–west seaways in response to dynamic upwelling of seawater, or in broad north-south seaways in response to upwelling along the east side of the seaway. In both cases, shallow seas are necessary for the upwelling.

The secular distribution of phosphate deposition may be related in part to the supercontinent cycle. For instance, major peaks of phosphate deposition at 0.8–0.6 and <0.25 Ga correlate with the breakup of supercontinents during which the area of shallow seas increased as continental fragments dispersed. This resulted in a rise in sea level providing extensive shallow-shelf environments into which there was a transfer of deep phosphorous-rich ocean water to the shallow photic zone. During diagenesis, phosphorus can be released from both organic matter and iron oxides, thus becoming available for living organisms. Post-glacial oceanic overturn can also drive a rise in sea level and upwelling around continental margins (Papineau, 2010). Also, rifting during supercontinent breakup can form new basins around and within supercontinents into which phosphates may accumulate. Increased erosion rates resulting from rapidly rising collisional mountain belts during supercontinent assembly can bring more phosphate into the oceans, promoting both phosphate deposition and an increase in biomass.

A rapid increase in abundance of sedimentary phosphates at the base of the Cambrian is particularly intriguing, and appears to be the largest of several phosphate "events" near the Cambrian/Precambrian boundary (Cook, 1992).

The extensive phosphate deposition at this time may have triggered changes in biota, including both an increase in biomass and the appearance of metazoans with hard parts. Late Cretaceous and Eocene peaks in phosphate deposition may be related to the formation of narrow east-west seaways accompanying the continuing fragmentation of Pangea. The most dramatic example of this is the Tethyan Ocean, an east-west seaway that closed during the last 200 Ma, providing numerous rifted continental fragments with shallow shelves that are potential sites for phosphate deposition.

The Temperature of Seawater

Oxygen-18 is fractionated from oxygen-16 in the atmosphere–ocean system during evaporation, with the vapor preferentially enriched in ^{16}O. Fractionation of these isotopes also decreases with increasing temperature and salinity. The fractionation of the two isotopes is measured by the deviation of $^{18}O/^{16}O$ from standard mean ocean water (SMOW) in terms of $\delta^{18}O$ where

$$\delta^{18}O\ (‰) = [\{(^{18}O/^{16}O)_{sample}/(^{18}O/^{16}O)_{SMOW}\} - 1] \times 1000 \quad (6.7)$$

Because marine chert and banded iron formation (BIF) are resistant to secondary changes in $\delta^{18}O$, they are useful in monitoring the composition of seawater with geologic time (Knauth & Lowe, 1978; Gregory, 1991). The $\delta^{18}O$ of marine chert is a function of temperature of deposition, the isotopic composition of seawater, and secondary changes in the chert. A summary of published $\delta^{18}O$ from Precambrian cherts and BIF clearly shows that Archean cherts have low $\delta^{18}O$, but they overlap with Proterozoic cherts (Figure 6.14). Although relatively few samples are available from Proterozoic cherts, there is a clear increase in Proterozoic $\delta^{18}O$ values towards the Phanerozoic values of 25–35‰ (Knauth & Lowe, 1978, 2003). Recent measurements of $\delta^{18}O$ in single quartz grains in Proterozoic chert at the micron scale show two populations: one apparently records seawater temperature and the other diagenetic fluid temperatures (Marin et al., 2010). Hence, the range of values shown in Figure 6.14 probably represents varying proportions of these two types of quartz in reported whole-rock analyses, and the lower end of the range may be the best estimate of seawater temperature.

Two models have been proposed to explain increasing $\delta^{18}O$ in chert and BIF, and hence in seawater, with geologic time:

1. *The mantle–crust interaction model* (Perry et al., 1978). If Archean oceans were about the same temperature as modern oceans, they would have a $\delta^{18}O$ of 34‰ less than chert precipitated from them or about 14‰. For seawater to evolve to a $\delta^{18}O$ of 0‰ with time, it is necessary for it to react with substances with $\delta^{18}O$ values greater than 0‰. Recycling seawater at ocean ridges and interactions of continent-derived sediments and river waters are processes that can raise seawater $\delta^{18}O$ values. Large volumes of seawater

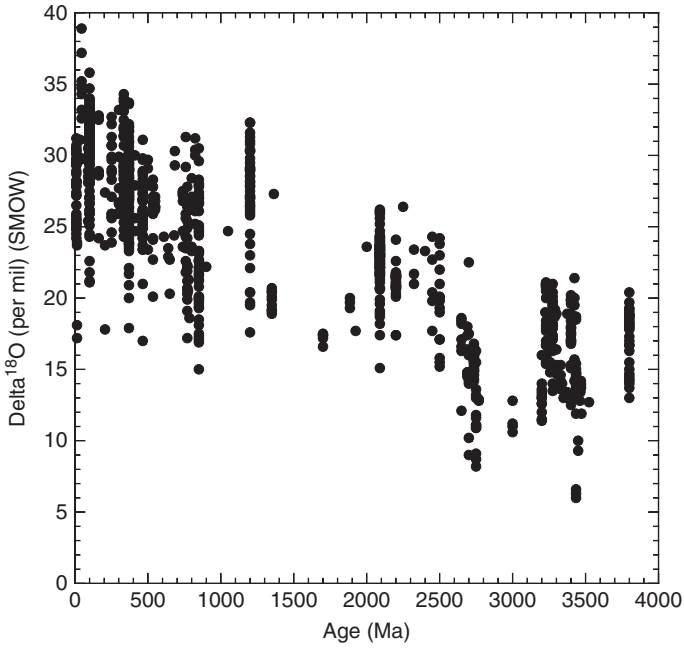

FIGURE 6.14 Distribution of oxygen isotopes in marine cherts with time relative to standard mean seawater (SMOW). *Data from Knauth (2005) and Robert & Chaussidon (2006).*

are recycled through the crust at ocean ridges and react with basalt that has a $\delta^{18}O$ of 5.5–6‰, and continental sediments have $\delta^{18}O$ values even higher (7–20‰). This model is consistent with increasing volumes of continental crust preserved with time.

2. *The seawater-cooling model* (Knauth and Lowe, 1978, 2003). In this model, the oxygen isotope trend is explained by a gradual cooling of Earth's surface temperature from 60 to 85°C at 3.5 Ga to present temperatures. The $\delta^{18}O$ of seawater may or may not be constant over this time; however, if not constant it must have changed in such a way so as not to have affected the temperature control. Chert with $\delta^{18}O < 15‰$ reflects formation during deepest burial or in local areas of enhanced geothermal activity. Chert with higher $\delta^{18}O$ values formed during early diagenesis and indicates an extremely hot Archean ocean. Some investigators suggest that the evidence for gypsum deposition in the Archean is an obstacle for this model, since gypsum cannot be deposited at temperatures >58°C. However, the only well-documented examples of Archean gypsum deposition are seen in sediments from the Pilbara in Western Australia, and it appears to reflect local and not worldwide ocean compositions.

Muehlenbachs and Clayton (1976) argued persuasively that recycling of seawater at ocean ridges has caused the oxygen isotopic composition of

seawater to remain constant with time. However, not until studies of ophiolite alteration (Holmden & Muehlenbachs, 1993; Lecuyer et al., 1996) were reported did it became clear that the $\delta^{18}O$ of seawater has probably not changed in the last 2 Ga, since the distribution of $\delta^{18}O$ in low- and high-temperature alteration zones in 2-Ga ophiolites is the same as that found in young ophiolites. Hoffman et al. (1986) furthermore suggest that the stratigraphic distribution of $\delta^{18}O$ in alteration zones of the 3.5-Ga Barberton greenstone belt may also indicate that the oxygen isotopic composition of seawater has not changed appreciably since the early Archean. Thus, if the secular change in $\delta^{18}O$ in chert and BIF is real, it would appear that the temperature of Archean seawater must have been greater than at later times, as originally suggested by Knauth and Lowe (1978).

However, the long-term cooling of the oceans based on oxygen isotope data in cherts has been questioned, because the isotopic signature could have been changed by exchange with hydrothermal fluids after sediment deposition. Silicon isotopes, which are much more resistant to secondary remobilization in cherts, however, seem to corroborate the oxygen isotope story (Robert & Chaussidon, 2006). The silicon isotope data imply a change in seawater temperature from about 70°C at 3.5 Ga to 20°C at 800 Ma (Figure 6.15).

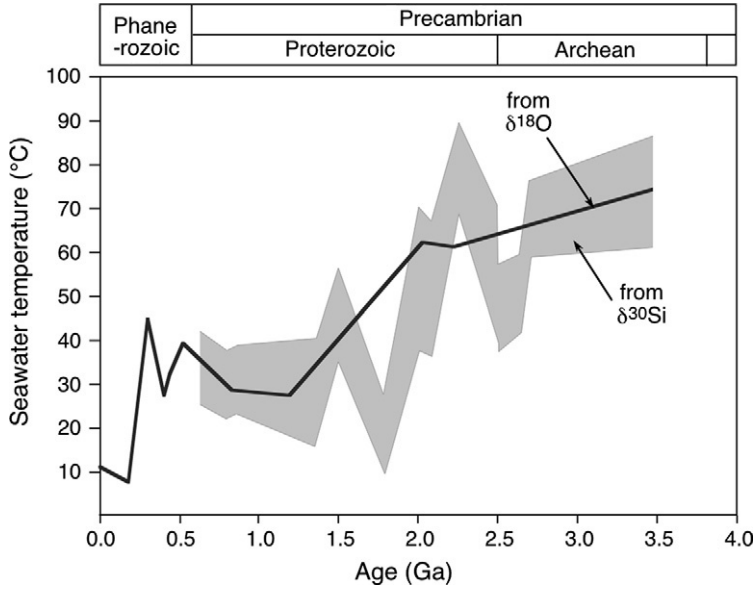

FIGURE 6.15 Variation in seawater temperature modeled with $\delta^{30}Si$ in marine cherts (gray pattern) compared with temperatures calculated from $\delta^{18}O$ from Figure 6.14. *From Robert & Chaussidon (2006), courtesy of Francois Robert. Used with permission of Nature Publishing Group, permission conveyed through Copyright Clearance Center, Inc.*

Not all results, however, support hot Archean oceans. For instance, such an interpretation does not easily accommodate the evidence for widespread glaciation at 2.4–2.3 Ga, which necessitates cool oceans. Also, combined oxygen and hydrogen isotopic results from 3.4-Ga cherts do not allow for seawater temperatures much greater than 40°C at this time (Hren et al., 2009). These results suggest that Archean seawater was isotopically depleted in both oxygen and hydrogen isotopes and far cooler than the Knauth model predicts. Jaffres et al. (2007) suggest that long-term trends in chemical weathering and hydrothermal circulation affect the oxygen isotope composition of chemical sediments. These authors suggest that the low $\delta^{18}O$ level in Archean cherts reflects higher weathering rates in a greenhouse gas atmosphere and a greater abundance of easily weathered mafic and komatiitic volcanic rocks. It would appear that the jury is still out with regard to the temperature of the Archean oceans, and they are probably not going to make a decision any time soon.

Ocean Volume through Time

Whether the oceans have grown, shrunk, or remained the same through time is still an outstanding question. The answer to this question is simply the difference between the degassing rate of water from the mantle and the recycling rate at subduction zones, neither of which is precisely known. Although the constancy of the freeboard of continents (mean elevation above sea level) through time has been known for some time, its interpretation still remains uncertain. For instance, freeboard is dependent on water volume, continental volume, depth of the ocean basins (and hence the mean age and heat flow), and oceanic crustal thickness (Galer & Mezger, 1998). As discussed earlier, most degassing models suggest that a volume equivalent to the present oceans was degassed very rapidly from the mantle, probably within 100 Ma after the Moon-forming event (Williams, 2007).

Some scenarios predict greater degassing volumes followed by recycling of water back into the mantle as described in Chapter 4. Korenaga (2008b) presents a model of secular cooling of Earth in which the early Archean mantle convects more slowly than today because it generates a thicker, more buoyant and dehydrated lithosphere, which resists subduction (see Chapter 7). This model predicts that Archean ocean basins should be deeper and have about twice as much water as today. Thus, Earth's global water cycle is dominated by regassing, not degassing, of the mantle with time, and the corresponding loss of ocean volume by a factor of 2.

Euxinia in the Proterozoic Oceans

The standard model for the growth of oxygen in Earth's atmosphere suggests that the disappearance of banded iron formation (BIF) at about 1900 Ma records the beginning of an oxygenated ocean (Holland, 2006). However, as pointed out

by Canfield (1998) this sudden disappearance of BIF may indicate that the deep oceans became **euxinic** (containing dissolved H_2S) and reducing rather than oxic and that iron was now deposited as insoluble Fe-sulfides, leading to what is now called the "Canfield Ocean" (Figure 6.16). Canfield and associates developed a model based on sulfur isotopes in biogenetic sedimentary sulfides that reflect sulfate availability and redox conditions at the time of formation (Lyons et al., 2009). Changes is sulfur isotope systematics in the Precambrian sedimentary record support the Canfield model. Sulfide-reducing bacteria appear to have been in action by 3.5 Ga as suggested by S-isotope fractionation between evaporitic barite and sulfide inclusions (see discussion above). In comparison to younger isotopic fractionation, this result is consistent with sulfate-poor Archean oceans increasing to modest values in the Proterozoic (Anbar & Knoll, 2002). Presumably this reflects the rise of a moderately oxidizing atmosphere facilitating, for the first time, delivery of large amounts of sulfate to the oceans. It is pyrite burial on the deep sea floor and its eventual subduction that maintains low sulfate levels in the ocean. After a billion years of shuttling sulfate from the continents to the oceans, the oceans returned for a brief period at about 700 Ma to iron control with BIF deposition again (see Figures 6.16 and 9.32). This may have been the result of a Snowball Earth (see Chapter 9), where a nearly complete frozen surface shuts off the supply of sulfate from river input.

Another important aspect of the euxinic model is the ecology and evolution of eukaryotes, which were tied to the ocean redox state during the Proterozoic (Lyons et al., 2009). The persistence of sulfides in the deep ocean may have stripped the ocean of essential nutrients, such as Mo and Fe, as we see today

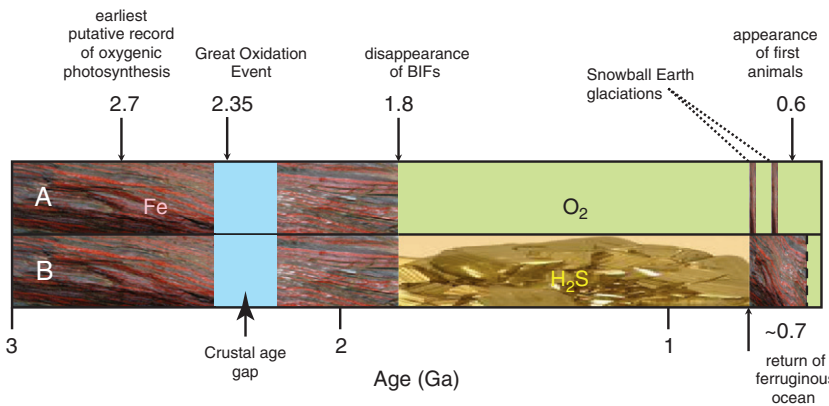

FIGURE 6.16 Comparison of (A) the standard oxidation model and (B) the Canfield euxinic model for the oceans from 1800 and 700 Ma. Fe, ferruginous conditions; H_2S, euxinia; O_2, oxic to suboxic. *Modified after Lyons et al. (2009), courtesy of Tim Lyons. Reprinted with permission from the* Annual Review of Earth and Planetary Sciences.

in the Black Sea. Supporting this idea is the fact that mid-Proterozoic fossil diversity is low and eukaryotic biomarker molecules are limited in both abundance and diversity. Also placing severe constraints on eukaryotic evolution may have been incursions of sulfide from the deep ocean into the oxygenated surface waters (Poulton et al., 2010). Only in the very late Neoproterozoic, when the deep oceans became oxidizing, did morphologically complex eukaryotic phytoplankton and branching macroalgal benthos diversify. Thus, the fossil record of algal diversification parallels the history of ocean oxidation inferred from sulfur isotopes (see Figure 9.32).

PALEOCLIMATES

To better understand the history of the atmosphere and oceans, it is necessary to turn to Earth's paleoclimatic record (Barnes, 1999). Major worldwide changes in climate are related to plate tectonics, volcanism, or astronomical phenomena. Plate tectonic processes govern the size, shape, and distribution of continents, which, in turn, influence ocean current patterns. The distribution of mountain ranges, volcanic activity, and changes in sea level are also controlled by plate tectonics and each of these factors may affect climate. Volcanism influences climate in two ways: (1) volcanic peaks may produce a rain shadow effect similar to other mountain ranges and (2) volcanism can introduce large amounts of volcanic dust and CO_2 into the atmosphere, the former of which reduces solar radiation and the latter increases the greenhouse effect. Clearly, the distribution of continents and ocean basins is an important aspect of paleoclimatology, and reconstructions of past continental positions are critical to understanding ancient climatic regimes. Astronomical factors, such as changes in the Sun's luminosity, changes in the shape of Earth's orbit about the Sun, and changes in the angle between Earth's equator and the ecliptic also influence climate.

Changes in the surface temperature of Earth with time are related chiefly to three factors: (1) an increase of solar luminosity, (2) variation in albedo, and (3) variation in the greenhouse effect. Albedo and the greenhouse effect are partly controlled by other factors such as plate tectonics and global volcanism. All three factors play an important role in long-term (10^8–10^9 years) secular climate changes, while plate tectonics and volcanism appear to be important in climate changes occurring on time scales of 10^6–10^8 years (Crowley, 1983).

Paleoclimatic Indicators

The distribution of ancient climates can be constrained with **paleoclimatic indicators**, which are sediments, fossils, or other information from ancient rocks that is sensitive to paleoclimate. A summary of major paleoclimatic indicators and their interpretation is given in Table 6.2. Some sediments reflect primarily precipitation regimes rather than temperature regimes. Coal, for instance, requires abundant vegetation and an adequate water supply but can form at various

TABLE 6.2 Examples of Paleoclimatic Indicators

Indicator	Interpretation
Widespread glacial deposits	Continental glaciation; widespread cold climates
Coal	Abundant vegetation, moist climate, generally midlatitudes
Eolian sandstones	Arid or semiarid; generally but not always hot or warm temperatures
Evaporites	Arid or semiarid; generally but not always hot or warm temperatures
Redbeds	Arid to subtropical; commonly semiarid or arid
Laterites and bauxites	Tropical, hot and humid climates
Corals and related invertebrate fauna	Subtropical to tropical, near-shore marine

temperature regimes, excepting arid hot or arid cold extremes (Robinson, 1973). Sand dunes may form in cold or hot arid (or semiarid) environments (as exemplified by modern dunes in Mongolia and the Sahara, respectively). Evaporites form in both hot and cold arid environments, although they are far more extensive in the former. Laterites and bauxites seem to unambiguously reflect hot, humid climates. The distribution of various floral and faunal groups may also be useful in reconstructing ancient climatic belts. Modern hermatypic hexacorals, for instance, are limited to warm surface waters (18–25°C) between latitude 38 °N and 30 °S. It is also possible to estimate paleoclimatic temperatures with oxygen isotopes in marine carbonates and cherts, provided the rocks have not undergone isotopic exchange since their deposition.

Glacial **diamictites** (poorly sorted sediments containing coarse- to fine-grained clasts) and related glacial-fluvial and glacial-marine deposits are important in identifying cold climates. Extreme care must be used in identifying glacial sediments in that sediments formed in other environments can possess many of the features characteristic of glaciation. For instance, subaqueous slump, mud flow, and landslide deposits can be mistaken for tillites, and indeed some ancient glaciations have been proposed based on inadequate or ambiguous data (Rampino, 1994). It also has been proposed that fallout from ejecta from large asteroid or comet impacts can produce large debris flows with characteristics similar to glacial tillites including striated clasts and striated pavements (Oberbeck et al., 1993). The bottom line is that no single criterion should be accepted in the identification of continental glacial deposits. Only a convergence of evidence from *widespread* locations such as tillites, glacial pavement,

faceted and striated boulders, and glacial dropstones should be considered satisfactory.

Long-Term Paleoclimatic Driving Forces

Paleoclimatic data are often interpreted to mean that long-term variations in climate are driven by natural variations in the CO_2 content of the atmosphere (Crowley & Berner, 2001). Veizer et al. (2000), however, point out some serious discrepancies when CO_2 levels calculated for the Phanerozoic are compared to the paleoclimatic record. They suggest that for at least part, if not all, of the Phanerozoic an alternative driving force for climate is necessary. These investigators furthermore proposed a cyclic component of paleoclimate with a period of about 135 Ma. There are no terrestrial phenomena known that recur at this frequency. Shaviv and Veizer (2003) propose that at least 66% of the variance in the paleotemperature of Earth's surface during the Phanerozoic may be caused by variations in the galactic cosmic ray flux as the solar system passes through the spiral arms of the Milky Way with a period of about 143 My.

Reevaluation of the paleoclimatic CO_2 data by Crowley and Berner (2001), however, show first-order agreement between the CO_2 record and continental glaciation, which supports the conventional CO_2 driving force theory for long-term climate change. To solve this problem will require more sophisticated climatic models that consider more climatic variables and interactions of these variables.

Glaciation

Direct evidence for major terrestrial glaciation exists for perhaps 5–10% of Earth's history. At least eight major periods of continental glaciation are recognized in the geologic record (Table 6.3) (Young, 1991). The earliest glaciation at about 3 Ga is represented only in South Africa in the Pongola Supergroup (von Brunn & Gold, 1993) and is probably of only local geographic extent. The first evidence of widespread glaciation is the Huronian glaciation at 2.4–2.3 Ga, evidence for which has been found in Laurentia, Baltica, Siberia, and South Africa. At least two major ice caps existed in Laurentia at this time, as recorded by marine glacial deposits around their perimeters (Figure 6.17). Although the evidence for Neoproterozoic glaciation (720–580 Ma) is overwhelming, the number, geographic distribution, and specific ages of individual glaciations are not well known (Eyles, 1993). Major Neoproterozoic ice sheets were located in central Australia, west-central Africa, the Baltic shield, Greenland and Spitsbergen, western North America, and possibly in eastern Asia and South America. At least three glaciations are recognized as given in Table 6.3. Puzzling features of the Neoproterozoic glacial deposits include their association with shallow marine carbonates, which is suggestive of warm climatic regimes giving rise to the Snowball Earth hypothesis described in Chapter 9.

TABLE 6.3 Summary of Major Terrestrial Glaciations

Age (Ma)	Geographic areas
3000–2900	Pongola Supergroup, southern Africa
2400–2300	Huronian: Laurentia, Baltica, Siberia, South Africa
717–712	Sturtian: Australia, Laurentia, South Africa
635	Marinoan: Eurasia, South Africa, China, Australia, Antarctica, Laurentia, South America
584	Gaskiers: Laurentia, Australia, China, Baltica, Avalonia
450–400	Gondwana
350–250	Gondwana
15–0	Antarctica, North America, Eurasia

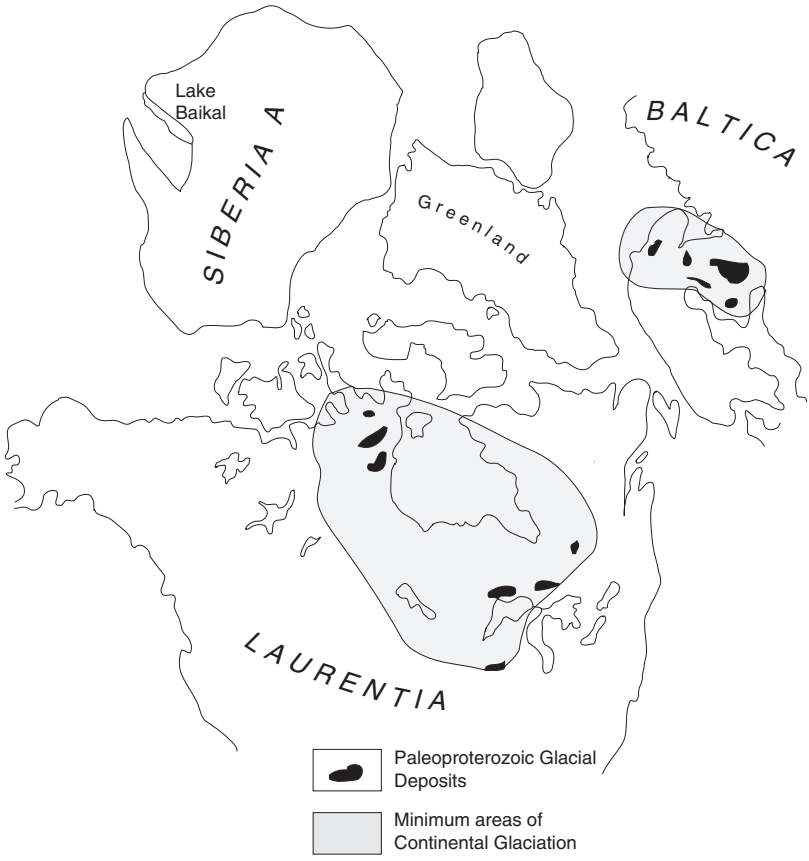

FIGURE 6.17 Minimum distribution of Paleoproterozoic (2.4–2.3 Ga) glaciation in Laurentia-Baltica.

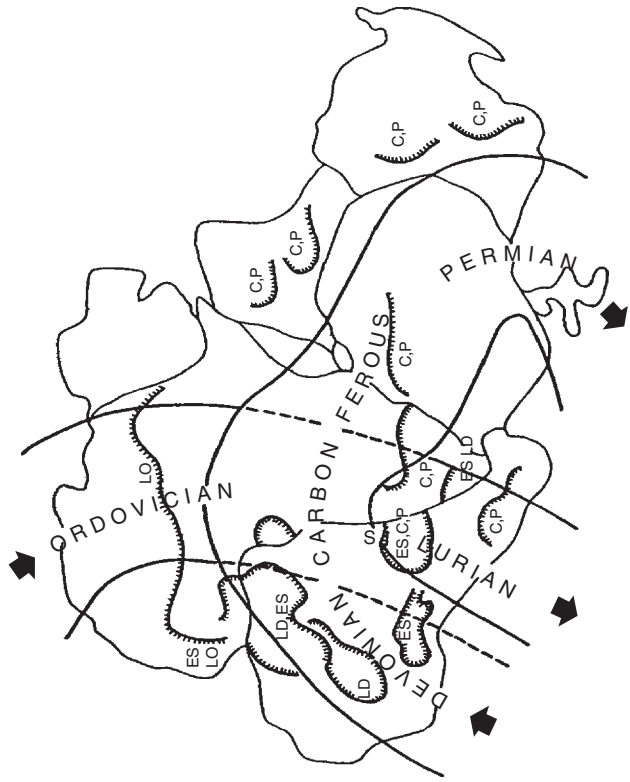

FIGURE 6.18 Apparent polar wander paths and major glacial centers across western Gondwana during the Paleozoic. E, Early; L, Late; O, Ordovician; S, Silurian; D, Devonian; C, Carboniferous; P, Permian. Major glacial centers shown with hachured lines. *Modified after Caputo and Crowell (1985).*

During the Paleozoic, Gondwana migrated over large latitudinal distances, crossing the South Pole several times. Major glaciations in Gondwana occurred in the Late Ordovician, Late Carboniferous, and Early Permian (Figure 6.18) and are probably responsible for drops in sea level at these times. Minor Gondwana glaciations are also recorded in the Cambrian and Devonian. Although minor glaciations may have occurred in the Mesozoic, the next large glaciations were in the late-Cenozoic culminating with the multiple glaciations in the Quaternary.

Precambrian Climatic Regimes

Using paleoclimatic indicators together with models of atmospheric evolution, it is possible to characterize average surface temperatures and precipitation regimes with time. The abundance of CH_4 and CO_2 in the Archean atmosphere

resulted in greenhouse warming to average surface temperatures greater than at present (Figure 6.19) (Sleep & Zahnle, 2001; Kasting & Ono, 2006). Few climatic indicators are preserved in Archean supracrustal successions. Archean BIF is commonly thought to have been deposited in shallow marine waters, and hence implies low wind velocities to preserve the remarkable planar stratification. This is consistent with a CH_4-CO_2–rich atmosphere in which differences in temperature gradient with latitude are small, as are corresponding wind velocities (Frakes et al., 1992). The earliest evaporites and stromatolitic carbonates appear at about 3.5 Ga and also favor generally warm climates. The relative abundance of shallow marine carbonates and the preservation of lateritic

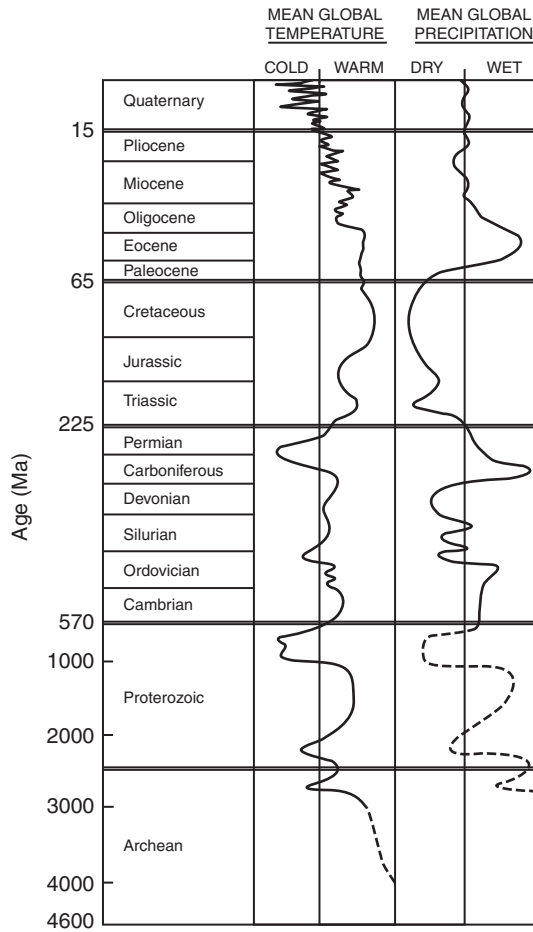

FIGURE 6.19 Generalized average surface temperature and precipitation history of Earth. *Modified after Frakes (1979).*

paleosols in the Proterozoic suggest a continuation of warm, moist climates after the end of the Archean. The increasing proportion of evaporites and redbeds after 2 Ga appears to record the increasing importance of semiarid to arid climatic regimes. Colder climates as recorded by widespread glaciations alternated with warm, moist climates as reflected by marine carbonates in the Neoproterozoic.

Also supporting an unusually warm Archean climate are geochemical data related to weathering rates. Studies of modern weathering show that Ca, Na, and Sr are rapidly lost during chemical weathering and that the amount of these elements lost is proportional to the degree of weathering (Condie, 1993). The **Chemical Index of Alteration (CIA)**, commonly referred to as the paleoweathering index (Nesbitt & Young, 1982), has been used to estimate the degree of chemical weathering in the source areas of shales. The CIA is calculated from the molecular proportions of oxides, where CaO is the amount in only the silicate fraction:

$$\mathrm{CIA} = [\mathrm{Al_2O_3}/(\mathrm{Al_2O_3} + \mathrm{CaO} + \mathrm{Na_2O} + \mathrm{K_2O})] \times 100 \qquad (6.8)$$

The higher the CIA, the greater the degree of chemical weathering in sediment sources. For example, CIA values of more than 85 are characteristic of residual clays in tropical climates. Most post-Archean shales show moderate losses of Ca, Na, and Sr from source weathering with CIA indices of 80–95 and Sr contents of 75–200 ppm. These values reflect the "average" intensity of chemical weathering of the shale sources. Most Archean shales, however, show greater losses of all three elements with typical CIA indices of 90–98 and Sr contents $<$100 ppm. This suggests that the average intensity of chemical weathering may have been greater during the Archean than afterward, a conclusion that is consistent with a CH_4-CO_2–rich atmosphere in the Archean.

Although data clearly indicate that Archean and Paleoproterozoic climates were warmer than at present, at least two glaciations must somehow be accommodated (Kasting & Ono, 2006). Calculations indicate that a drop of only 2°C is enough to precipitate an ice age (Kasting, 1987). Causes of glaciations at 3.0–2.9 and 2.4–2.3 Ga remain illusive. The absence of significant amounts of volcanic rock beneath tillites of both ages does not favor volcanic dust injected into the atmosphere (reducing sunlight) as a cause of either glaciation. The 3.0- to 2.9-Ga glaciation is recorded only in the eastern part of the Kaapvaal craton in South Africa, and may have been caused by local conditions. However, for the Paleoproterozoic glaciation, it would appear we need a widespread drawdown mechanism for atmospheric greenhouse gases. One possibility is that increasing numbers of photosynthetic microorganisms may have extracted large amounts of CO_2 from the atmosphere faster than it could be returned by chemical weathering, thus reducing the greenhouse effect. However, such a model does not explain how glaciation should end nor why large amounts of marine carbonate produced during the CO_2 withdrawal do not occur beneath 2.4- to 2.3-Ga tillites. Another possibility that has not been fully explored is the

possible effect of rapid continental growth in the late Archean on the CO_2 content of the atmosphere. Perhaps rapid chemical weathering of newly formed supercratons reduced CO_2 levels in the atmosphere and led to cooling and glaciation. Still another mechanism continually growing in popularity is that oxygen entering the atmosphere during the Great Oxidation Event at 2350 Ma destroyed CH_4, which led to rapid cooling of the planetary surface.

Phanerozoic Climatic Regimes

Most of the early and middle Paleozoic is characterized by climates that were warmer than at present, while late Paleozoic climates show wide variation (Figure 6.19) (Frakes et al., 1992). Europe and North America underwent relatively small changes in climate during the Paleozoic, while Gondwana underwent several major changes. This is due to the fact that the continental fragments comprising Laurasia remained at low latitudes during the Paleozoic, while Gondwana migrated over large latitudinal distances. Major glaciations occurred in Gondwana in Late Ordovician, Late Carboniferous, and Early Permian.

The Mesozoic is characterized by warm, dry climates that extend far north and south of equatorial regions (Barron et al., 1995). Paleontologic and paleomagnetic data also support this interpretation. Initial Triassic climates were cool and humid like the late Paleozoic, and they were followed by a warm, drying trend until Late Jurassic. The largest volumes of preserved evaporites are in the Late Triassic and Early Jurassic and reflect widespread arid climates on Pangea. Most of the Cretaceous is characterized by warm, commonly humid climates regardless of latitude, with tropical climates extending from 45°N to perhaps 75°S. Glacial climates are of local extent and only in polar regions. Mean annual surface temperatures during the Mid-Cretaceous, as determined from oxygen isotope data, are 10–15°C higher than today. The Late Cretaceous is a time of maximum transgression of the continents, and the warm Cretaceous climates appear to reflect a combination of increased atmospheric CO_2 levels and low albedo of the oceans (Wilson & Norris, 2001). The Early Tertiary was a time of declining temperatures, significant increased precipitation, and falling sea levels. The Middle and Late Tertiary are characterized by lower and more variable temperature and precipitation regimes. These variations continued and became more pronounced in the Quaternary, leading to the alternating glacial and interglacial epochs.

Glaciation

Both early and late Paleozoic glaciations appear to be related to plate tectonics. During both of these times, Gondwana was glaciated as it moved over the South Pole (Figure 6.18) (Caputo & Crowell, 1985; Frakes et al., 1992). Major glaciations occurred in central and northern Africa in the Late Ordovician when

Africa was centered over the South Pole. As Gondwana continued to move over the pole, major ice centers shifted into southern Africa and adjacent parts of South America in the Early Silurian. Gondwana again drifted over the South Pole beginning with widespread glaciation in the Late Devonian and Early Carboniferous in South America and central Africa, shifting to India, Antarctica, and Australia in the Late Carboniferous and Permian. Paleozoic glaciations also may be related to prevailing wind and ocean currents associated with the movement of Gondwana over the pole.

The next major glaciations began in the Mid-Tertiary and were episodic with interglacial periods. Between 40 and 30 Ma, the Drake Passage between Antarctica and South America opened and the Antarctic circumpolar current was established, thus thermally isolating Antarctica (Crowley, 1983). The final separation of Australia and Antarctica at about this time may also have contributed to cooling of Antarctica by inhibiting poleward transport of warm ocean currents. Glaciation appears to have begun in Antarctica 15–12 Ma and by 3 Ma in the Northern Hemisphere. Initiation of Northern Hemisphere glaciation may have been in response to formation of Panama, which resulted in relocation of the Gulf Stream, which had previously flowed westward about the equator, to flow north along the coasts of North America and Greenland. This shift in current brought warm, moist air into the Arctic, which precipitated and began to form glaciers. Four major Quaternary glaciations are recorded, with the intensity of each glaciation decreasing with time: the Nebraskan (1.46–1.3 Ma), Kansan (0.9–0.7 Ma), Illinoian (550–400 ka), and Wisconsin (80–10 ka). All but the Wisconsin glaciation lasted 100–200 ka, with interglacial periods of 200–400 ka.

Two factors may have been important in controlling the multiple glaciations in the Pleistocene (Eyles, 1993): cooling and warming of the oceans and cyclic changes in Earth's rotation and orbit. Cyclical changes in the temperature of the oceans caused by changes in the balance between evaporation and precipitation may be in part responsible for multiple glaciations. Cyclical changes in the shape of Earth's orbit about the Sun and in the inclination and wobble of the rotational axis can bring about cyclical cooling and warming of Earth. Today, Earth's equatorial plane is tilted at 23.4 degrees to the ecliptic, but this angle varies from 21.5 to 24.5 degrees with a period of about 41 ka. Decreasing the inclination results in cooler summers in the Northern Hemisphere and favors ice accumulation. Earth's orbit also changes in shape from a perfect circle to a slightly ellipsoidal shape with a period of 92 ka and the ellipsoidal orbit results in warmer than average winters in the Northern Hemisphere. Earth also wobbles as it rotates with a period of about 26 ka and the intensity of seasons varies with the wobble. When variations in oxygen isotopes or fauna are examined in deep-sea cores, all three of these periods, known as the **Milankovitch periods**, can be detected, with a 92-ka period being prominent. These results suggest that on timescales of 10–400 ka, variations in the Earth's orbit are the fundamental cause of Quaternary glaciations (Imbrie, 1985). Spectral analyses of $\delta^{18}O$ and orbital time series strongly support the model.

THE BIOSPHERE

Perhaps no other system is as unique to planet Earth as the biosphere, which includes all forms of life. Life occurs nearly everywhere on and even under the surface of the planet. In terms of actual biomass, it is likely that microbes that live beneath the surface exceed that of all the surface life, plants and animals. Some microbes survive in the upper atmosphere as high as 25 km and as deep in the crust as several kilometers. The temperature range of life continues to increase as we learn more about microbes, which today is from about 120°C around thermal springs to as low as –20°C in some glacial environments. The origin of life is the subject of ongoing research and is considered one of the great events in Earth's history, and thus is covered in Chapter 9. In this section, we pick up the story with the evolution of life-forms that need an oxygenated atmosphere to survive, which includes chiefly the Eukarya (see Figure 9.13 in Chapter 9), those life-forms comprised of advanced or eukaryotic cells.

Appearance of Eukaryotes

It was not until about 2 Ga that microbes entirely dependent on the use of molecular O_2 appeared in the geologic record (Runnegar, 1995). This correlates with the rapid growth of oxygen in the atmosphere at this time. These are **eukaryotes**, which are advanced cells with a cell nucleus enclosing DNA and with specialized organs in the cell. Eukaryotes also are able to sexually reproduce. RNA studies of living unicellular eukaryotes suggest they are derived from archaebacterial prokaryotes sometime about 2.7 Ga (Brocks et al., 1999). Although the earliest fossil eukaryotes appear about 1.9 Ga, they did not become widespread in the geologic record until 1.7–1.5 Ga. The oldest fossil thought to represent a eukaryote is *Grypania* from 1.9-Ga sediments in Michigan. *Grypania* is a coiled, cylindrical organism that grew to about 50 cm in length and 2 mm in diameter (Figure 6.20). Although it has no certain living relatives, it is regarded as a probable eukaryotic alga because of its complexity, structural rigidity, and large size.

RNA studies of modern eukaryotes suggest that the earliest forms to evolve were microsporidians, amoebae, and slime molds. Between 1.3 and 1.0 Ga, eukaryotes began to accelerate, leading to the appearance of red algae. A minimum date for this radiation is given by well-preserved, multicellular red algae fossils from 1.2- to 1.0-Ga sediments in Arctic Canada. According to RNA data, this was followed by major radiation leading to ciliates, brown and green algae, plants, fungi, and animals.

RNA studies suggest that modern algal and plant chloroplasts have a single origin from a free-living cyanobacterium. Margulis (1970) was the first to point out that a number of parts of the eukaryotic cell probably formed by the fusion of separate species of prokaryotes. She drew attention to the fact that many traits

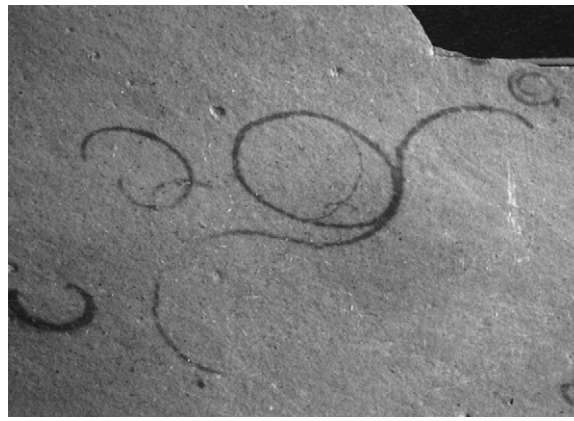

FIGURE 6.20 Grypania, the oldest known fossil of eukaryotic algae from the 1.9-Ga Negaunee Iron Formation, Marquette, Michigan. Scale ×2. *Courtesy of Bruce Runnegar.*

of the mitochondria in eukaryote cells are similar to those of bacteria. Later studies support this idea in that genes in mitochondria closely resemble genes in bacteria (Zimmer, 2009). The **symbiotic theory** of cell evolution suggests that the remarkable complexity of eukaryotes requires a long period of time and probably developed from symbioses between prokaryotes and amitochondriate protists (Cavalier-Smith, 1987). Purple bacteria were probably acquired first to provide mitochondria, whereas photosynthetic prokaryotes were acquired later to form chloroplasts. It is likely that host–photosymbiont relationships take long periods of time to develop, perhaps hundreds of millions of years. Such evolution may have occurred during a period of remarkable stability in the carbon cycle from about 1.9 to 0.8 Ga (Brasier & Lindsay, 1998).

Whatever the exact series of steps leading to eukaryotes, their appearance triggered a biological revolution. Prokaryotes can generate energy only by moving charged atoms across their membranes, which contributes to limiting their size. In contrast, eukaryotes pack hundreds of energy-generating mitochondria into single cells. This allows them to grow to sizes considerably larger than prokaryotes and adapt to new ecological niches.

Studies of the size of organisms with time indicate that the maximum size increased by 16 orders of magnitude since life first appeared in the fossil record (Payne et al., 2009). The majority of this increase occurred in two distinct steps of approximately equal magnitude. The first around 1.9 Ga and the second at 0.6–0.45 Ga. Each step required a major innovation in organismal complexity: first the appearance of the eukaryotic cell and second the appearance of metazoans. It is noteworthy that each of these steps comes just after the two major oxidation events of the atmosphere (at 2.35 Ga and 0.7–0.6 Ga), suggesting a cause-and-effect relationship between oxygen and body size.

Origin of Metazoans

Metazoans (multicellular animals) appear to have evolved from single-celled ancestors that developed a colonial habit. The adaptive value of a multicellular way of life relates chiefly to increases in size and the specialization of cells for different functions. For instance, more suspended food settles on a large organism than on a smaller one. Because all cells do not receive the same input of food, food must be shared among cells and a "division of labor" develops among cells. Some concentrate on food gathering, others on reproduction, while still others specialize in protection. At some point in time when intercellular communication was well-developed, cells no longer functioned as a colony of individuals but as an integrated organism.

The trace fossil record suggests that metazoans were well established by 1000 Ma (Figure 6.21), and the great diversity of metazoans of this age suggests that more than one evolutionary line led to multicellular development. Leaf-shaped fossils in North China suggest that some form of multicellular life had evolved by 1.7 Ga (Shixing & Huineng, 1995). On the basis of their size (5–30 mm long), probable development of organs, and possible multicellular structures, these forms are likely benthic multicellular algae (Figure 6.22). Recently discovered centimeter-sized structures from 2.1-Ga black shales from West Africa are interpreted as colonial organisms, also probably metazoans (El Albani et al., 2010). Although metazoans appeared by about 2 Ga, because of an inadequate fossil record we cannot yet trace these organisms back to their unicellular ancestors.

Stromatolites

Stromatolites are finely laminated sediments composed chiefly of carbonate minerals that have formed by the accretion of both detrital and biochemical precipitates on successive layers of microorganisms (commonly cyanobacteria)

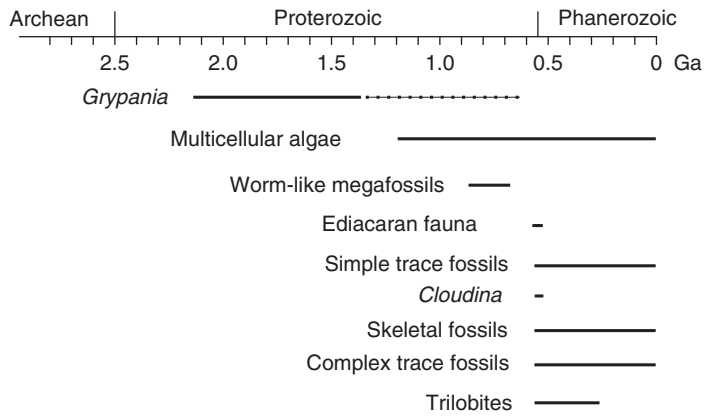

FIGURE 6.21 Time distribution of various Proterozoic fossil groups.

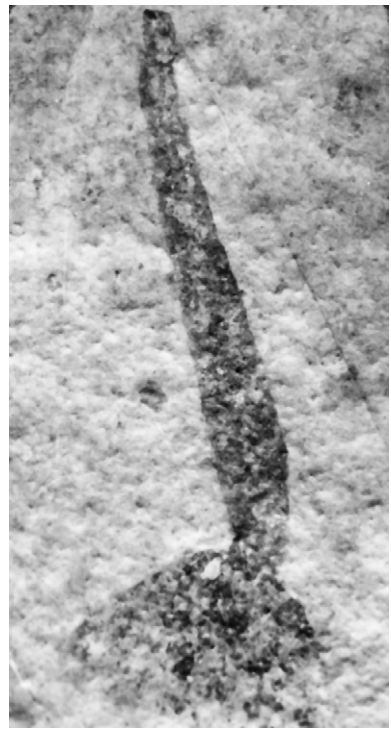

FIGURE 6.22 A carbonaceous multicellular fossil (*Antiqufolium clavatum*) from the 1.7-Ga Tuanshanzi Formation, North China. Fossil is about 25 mm long. *Courtesy of Zhu Shixing.*

(see Figure 9.15). They exhibit a variety of domical forms and range in age from about 3.5 Ga to modern (Grotzinger & Knoll, 1999). Two parameters are especially important in stromatolite growth: water currents and sunlight. There are serious limitations to interpreting ancient stromatolites in terms of modern ones, however. First of all, modern stromatolites are not well understood and occur in a great variety of aqueous environments (Walter, 1994; Grotzinger & Knoll, 1999). The distribution in the past is also controlled by the availability of shallow stable shelves, the types of organisms producing the stromatolites, the composition of the atmosphere, and perhaps the importance of burrowing animals. It is possible to use stromatolite reefs to distinguish deepwater from shallow-water deposition, because reef morphologies are different in these environments.

Paleoproterozoic stromatolites formed in peritidal and relatively deep subtidal environments, and for the most part appear to be built by cyanobacteria. Stromatolites increased in numbers and complexity from 2.2 Ga to about 1.2 Ga, after which they decreased rapidly (Grotzinger, 1990; Walter, 1994). Whatever the cause or causes of the decline, it is most apparent initially in quiet

subtidal environments and spreads later to the peritidal realm. Perhaps the major cause is the decreasing saturation of carbonate in the oceans, resulting in decreasing stabilization of algal mats by precipitated carbonate. The extent to which stromatolites can be used to establish a worldwide Proterozoic biostratigraphy is a subject of controversy, which revolves around the role of environment and diagenesis in determining stromatolite shape and the development of an acceptable taxonomy. Because the growth of stromatolites is at least partly controlled by organisms, it should in theory be possible to construct a worldwide biostratigraphic column.

Neoproterozoic Multicellular Organisms

The Ediacaran fauna is a group of fossil remains of uncertain ancestry that survived for a short time interval just before the Cambrian (Figure 6.21). Although most paleontologists regard Ediacaran fossils as metazoans, some have suggested that some or all of these fossils may represent an extinct line of primitive plant-like organisms similar to algae or fungi (Seilacher, 1994; Narbonne, 1998). However, there are more similarities of the Ediacarans to primitive invertebrates than to algae or fungi (Runnegar, 1994; Weiguo, 1994). From the widespread fossil record, some 31 Ediacaran species have been described including forms that may be ancestral to flatworms, coelenterates, annelids, soft-bodied arthropods, and soft-bodied echinoderms. The most convincing evidence for Neoproterozoic animals comes from trace fossils associated with the Ediacaran fauna. Looping and spiraling trails up to several millimeters in width and strings of fecal pellets point to the presence of soft-bodied animals with a well-developed nervous system, asymmetry, and a one-way gut.

U-Pb zircon ages from ash beds associated with Ediacaran fossils in Namibia in Southwest Africa indicate that this fauna is no older than about 575 Ma, and that some forms are as young as 543 Ma (Grotzinger et al., 1995). This places their age just before the Cambrian/Precambrian boundary at 542 Ma (Figure 6.23). Although not part of the Ediacaran assemblage, recently discovered sponge-like fossils from Australia are somewhat older, at least 650 Ma. Prior to these isotopic ages, a large gap was thought to have existed between the Ediacaran fossils and the diverse invertebrate forms that suddenly appear in the Cambrian. It now appears that some of the shelly Cambrian forms overlap with the Ediacaran forms (Kimura & Watanabe, 2001). These new findings support the idea, but do yet prove, that some Ediacaran forms were ancestral to some Cambrian invertebrates.

The Cambrian Explosion

All of the major invertebrate phyla (except the Protozoa) made their appearances in the Cambrian, a feature sometimes referred to as the **Cambrian explosion** (Figure 6.23) (Weiguo, 1994; Bengtson, 1994; Marshall, 2006;

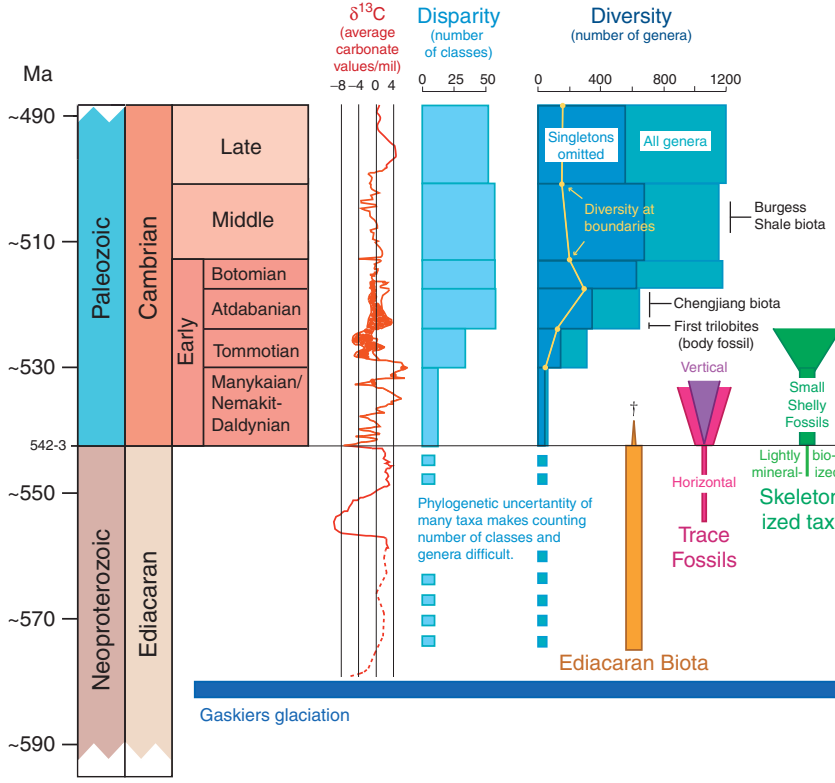

FIGURE 6.23 Summary of the Cambrian explosion of life. *From Marshall (2006), courtesy of Charles Marshall. Reprinted with permission from the* Annual Review of Earth and Planetary Sciences.

Meert & Lieberman, 2008). Four major questions are related to the Cambrian explosion that need to be explained: the spectacular increase in disparity (origin of specific groups), the rise in animal and plant diversity, what initiated the explosion at about 540 Ma, and why the duration was rather short, a few tens of millions of years. Molecular clocks indicate that metazoans are rooted to about the time of the Marinoan glaciation at 635 Ma, with the bilaterians emerging just prior to the Gaskiers glaciation at 584 Ma. The trilobite stem groups emerged sometime between 600 and 550 Ma although they do not appear in the fossil record until about 525 Ma (Figure 6.23). Even more striking is the fact that the two major groups of trilobites, the redlichiids and olenellids, developed in two different geographic regions, indicating a much earlier split of their ancestors. These lines of evidence suggest that the roots of the Cambrian explosion extend 50–70 Ma before its expression in the fossil record.

The increase in numbers and diversity of organisms is matched by a sharp increase in the diversity of trace fossils and the intensity of bioturbation

(the churning of subaqueous sediments by burrowing organisms). One of the immediate results of bioturbation is the return of buried organic matter to the carbon cycle and, hence, a decrease in the net release of oxygen due to decay. The Cambrian explosion may have been triggered by environmental change near the Proterozoic–Cambrian boundary and later amplified by interactions within reorganized ecosystems (Knoll & Carroll, 1999). Two biological inventions permitted organisms to invade sediments (Fischer, 1984). First, the development of exoskeletons allowed organisms (such as trilobites) to dig by using appendages and, second, the appearance of coelomes permitted worm-like organisms to penetrate sediments. Although calcareous and siliceous skeletons did not become widespread until the Cambrian, the oldest known metazoan with a mineralized exoskeleton is *Cloudina*, a tubular fossil of worldwide distribution predating the base of the Cambrian by at least 10 Ma (appearing about 550 Ma) (Figure 6.21).

The reasons that hard parts were developed in so many different groups at about the same time is a puzzling problem. Possibly it was for armor that would give protection against predators. However, one of the earliest groups to develop a hard exoskeleton is the trilobites, which were the major predators of the Cambrian seas. Although armor has a role in the development of hard parts in some forms, it is probably not the only or original reason for hard parts. The hard parts in different phyla developed independently, and are made of different materials. More plausible ideas are that hard parts are related to an improvement in feeding behavior, locomotion, or support. As an example of improved feeding behavior, in brachiopods the development of a shell enclosed the filter-feeding "arms" and permitted the filtration of larger volumes of water, similar in principle to how a vacuum cleaner works. Possibly the appearance of a hard exoskeleton in trilobites permitted a more rapid rate of locomotion by extending the effective length of limbs. Additional structural support may have been the reason that an internal skeleton developed in some echinoderms and in corals.

Still another factor that may have contributed to the Cambrian explosion is the growth of oxygen in the atmosphere. A continuing increase in the amount of fractionation of sulfur isotopes between sulfides and sulfates beginning in the Early Cambrian may record increased levels of oxygen in the atmosphere caused by repeated cycles of oxidation of H_2S (Canfield & Teske, 1996). The increase in oxygen levels at this time may have contributed to the rapid growth and diversification of organisms in the Cambrian.

Recent very precise U/Pb zircon ages that constrain the base of the Cambrian to about 542 Ma have profound implications for the rate of the Cambrian explosion (Bowring et al., 1993). These results show that the onset of rapid diversification of phyla probably began within 10 Ma of the extinction of the Ediacaran fauna. All of the major groups of marine invertebrate organisms reached or approached their Cambrian peaks by 530–525 Ma, and some taxonomic groupings suggest that the number of Cambrian phyla actually exceeded

the number known today. Assuming the Cambrian ended at about 490 Ma, the evolutionary turnover among the trilobites is among the fastest observed in the Phanerozoic record. Using 542 Ma for the base of the Cambrian, the average longevity for Cambrian trilobite genera is only about 1 Ma, much shorter than was previously thought.

The increase in disparity and diversity of organisms in this short time interval probably results from an interplay of the development of bilateral symmetry and an increase in the number of needs these organisms had to meet as complex ecological systems developed (Marshall, 2006). The time of onset of the explosion seems to be related chiefly to evolution of environments and perhaps the extinction of the Ediacaran fauna, which opened up many new ecological niches. The duration of the explosion, in contrast, is controlled by the rates at which innovations evolved.

Evolution of Phanerozoic Life-Forms

In recent years, progress in both systematic and developmental genetics has revolutionized our perspective on animal relationships and provided new ideas about early animal evolution. With most of the 35 modern metazoan phyla represented or inferred by the end of the Cambrian from the fossil record, the age, rate of divergence, and number of branches in the phylogenetic tree are beginning to emerge (Knoll & Carroll, 1999). New molecular phylogenies based on 18S ribosomal RNA sequences suggest that most animals fall into three major groups: the deuterostomes, lophotrochozoans, and ecdysozoans. One implication of this new phylogeny is that early-diverging groups within each group may display ancestral and derived characters in combination. At present, however, the three-branched tree provides no evidence for the kind of animal that could represent the last common ancestor.

From the fossil record, it is possible to track the major evolutionary development of life (Figure 6.24). Cambrian faunas are dominated by trilobites (~60%) and brachiopods (~30%), and by the Late Ordovician, most of the common invertebrate classes that occur in modern oceans were well established. Trilobites reached the peak of their development during the Ordovician, with a great variety of shapes, sizes, and shell ornamentation. Bryozoans, which represent the first attached communal organisms, appeared in the Ordovician. Graptolites, cephalopods, crinoids, echinoderms, molluscs, and corals also began to increase in numbers at this time. Vertebrates first appeared during the Ordovician as primitive fish-like forms without jaws. Marine algae and bacteria continued to be the important plant forms during the early Paleozoic.

The late Paleozoic is a time of increasing diversification of plants and vertebrates and of decline in many invertebrate groups. Brachiopods, coelenterates, and crinoids all increase in abundance in the late Paleozoic, followed by a rapid decrease in numbers at the end of the Permian. The end of the Paleozoic was also a time of widespread extinction, with trilobites, eurypterids, fusulines,

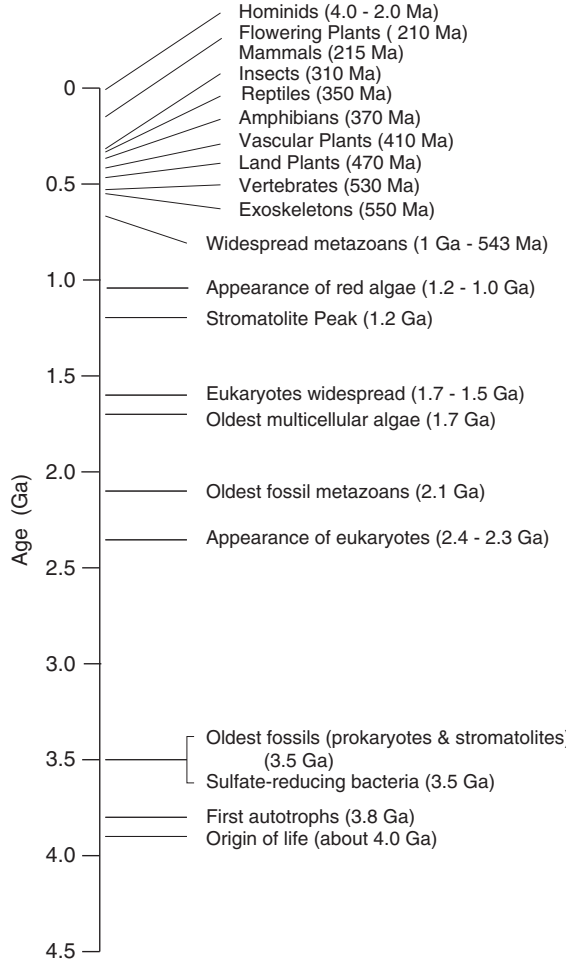

FIGURE 6.24 Biological benchmarks in the geologic past.

and many corals and bryozoa becoming extinct. Insects appeared in the Late Devonian. Fish greatly increased in abundance during the Devonian and Mississippian, amphibians appeared in the Mississippian, and reptiles in the Pennsylvanian. Plants increased in numbers during the late Paleozoic as they moved into terrestrial environments. Among the plants, psilopsids are most important during the Devonian, with lycopsids, ferns, and conifers becoming important thereafter. Perhaps the most important evolutionary event in the Paleozoic was the development of vascular tissue in plants, which made it possible for land plants to survive under extreme climatic conditions. Seed plants also began to be more important relative to spore-bearing plants in the late Paleozoic and early Mesozoic. The appearance and rapid evolution of amphibians in the late

Paleozoic was closely related to the development of forests, which provided protection for these animals. The appearance for the first time of shell-covered eggs and of scales (in the reptiles) allowed vertebrates to adapt to a greater variety of climatic regimes.

During the Mesozoic, gymnosperms rapidly increased in numbers with cycads, ginkgoes, and conifers being most important. During the Early Cretaceous, angiosperms (flowering plants) made their appearance and rapidly grew in numbers thereafter. The evolutionary success of flowering plants is due to the development of a flower and enclosed seeds. Flowers attract birds and insects that provide pollination, and seeds may develop fleshy fruits, which, when eaten by animals, can serve to disperse the seeds. Marine invertebrates, which decreased in numbers at the end of the Permian, made a comeback in the Mesozoic (such as bryozoans, molluscs, echinoderms, and cephalopods). Gastropods, pelecypods, foraminifera, and coiled cephalopods are particularly important Mesozoic invertebrate groups. Arthropods in the form of insects, shrimp, crayfish, and crabs also rapidly expanded in number during the Mesozoic. Mesozoic reptiles are represented by a great variety of groups, including dinosaurs. Dinosaurs are of herbivorous and carnivorous types, as well as marine and flying forms. Birds and mammals evolve from reptilian ancestors in the Early Jurassic. The development of mammals is a major evolutionary breakthrough, in that their warm-blooded nature allowed them to adapt to a great variety of natural environments (including marine), and their increased brain size allowed them to learn more rapidly than other vertebrates. During the Cenozoic, mammals evolved into large numbers of groups filling numerous ecological niches. Hominids appeared about 4 Ma. In the Cenozoic, the vertebrate groups characteristic of the Mesozoic continued to increase in numbers and angiosperms expanded exponentially.

Biological Benchmarks

Many benchmarks have been recognized in the appearance and evolution of new life-forms on Earth as summarized in Figure 6.24. The first is that life on Earth originated probably between 4.4 and 4.0 Ga at least 100 Ma after the Moon-forming impact (Chapter 9). The first autotrophs may have appeared by 3.8 Ga, and by 3.5 Ga anaerobic prokaryotes were widespread and stromatolites, probably constructed by cyanobacteria, had appeared. Sulfate-reducing bacteria were also present by 3.5 Ga, although probably not widespread. After the Great Oxidation Event at 2350 Ma, oxygen levels in the atmosphere increased enough for eukaryotes to appear, although the oldest eukaryotic fossils are 1.9 Ga. The oldest metazoan fossils at 2.1 Ga suggest that metazoans may have evolved soon after the appearance of eukaryotic cells. Unicellular eukaryotes became the dominant life-forms by 1.7–1.5 Ga and stromatolites, probably constructed chiefly by cyanobacteria, peaked in abundance and diversity about 1.2 Ga. Soft-bodied metazoans increased rapidly in numbers between

1 Ga and 550 Ma, culminating with the Ediacaran fauna at 575–543 Ma. *Cloudina*, the first metazoan with an exoskeleton, appeared about 550 Ma.

Important Phanerozoic benchmarks include the explosion of marine invertebrates between 540 and 530 Ma, the appearance of vertebrates (hemichordates) at about 530 Ma, land plants at 470 Ma, vascular plants at 410 Ma, amphibians at 370 Ma, reptiles and the amniote egg at about 350 Ma, insects at 310 Ma, mammals at 215 Ma, flowering plants at 210 Ma, and hominids at about 4 Ma (*Australopithecus* at 4 Ma, *Homo* at 2 Ma).

MASS EXTINCTIONS

Another important and controversial topic dealing with living systems is that of **mass extinctions**, when many diverse groups of organisms become extinct over short periods of time (Bambach, 2006). Mass extinctions affect a great variety of organisms, marine and terrestrial, stationary and swimming forms, carnivores and herbivores, protozoans and metazoans. Hence the causal processes do not appear to be related to specific ecological, morphological, or taxonomic groups. Important mass extinctions occurred at eight different times during the Phanerozoic (McLaren & Goodfellow, 1990).

Causes of mass extinction fall into three groups: extraterrestrial, physical, and biological. Extraterrestrial causes that have been suggested include increased production of cosmic and X-radiation from nearby stars, increased radiation during reversals in Earth's magnetic field, and climatic changes caused by supernova events or by impact on Earth's surface. Among the physical environmental changes that have been proposed to explain extinctions are rapid climatic changes, reduction in oceanic salinity caused by widespread evaporite deposition, fluctuations in atmospheric oxygen level, and changes in sea level. Collision of continents may also lead to extinction of specialized groups of organisms over longer periods of time as discussed in Chapter 8. Rapid changes in environmental factors lead to widespread extinctions, while gradual changes permit organisms to adapt and may lead to diversification. Correlation analysis between times of microfossil extinctions in deep-sea sediments and polarity reversals of the magnetic field does not support a relationship between the two (Plotnick, 1980). As discussed in Chapter 9, a great deal of evidence seems to support impact on Earth's surface as a cause for the mass extinction at the Cretaceous-Tertiary (K/T) boundary. One of the most significant problems in constraining the causes of mass extinction is precise isotopic dating of time boundaries. Precise isotopic ages using the U/Pb system require zircon-bearing ash beds that bound mass extinction events, a situation that is not commonly found in key stratigraphic sections. Even when these conditions exist, mass extinction events cannot as yet be dated to better than about 500 ka.

It has been suggested by Courtillot and Olson (2007) that a strong correlation exists between major Phanerozoic mass extinctions and LIP (large

igneous province) volcanism. This suggestion is quantitatively evaluated in Figure 6.25a, which shows the difference in age between LIP volcanic events and mass extinction events (Kelley, 2007). The major observation in the graph is that of the 15 major LIP eruptions in the last 300 Ma, only 6 fall within error of mass extinction events. Although there must have been changes in the environment during LIP eruptions, the peak eruption ages of many LIPs do not coincide with mass extinctions. There are only three striking correlations with extinctions: the North Atlantic II, Deccan, and Karoo-Ferrar. Some LIP eruptions postdate major extinctions, such as the Parana-Etendeka event (134.7 Ma), which is 10 Ma after a mass extinction (Figure 6.25a). Other LIPs, like the Rajmahal-Kerguelen event predates the early Aptian extinction by as much as 5 Ma. For comparison, a similar graph for major impact structures and mass extinctions is shown in Figure 6.25b. The data show that the ages of confirmed craters >40 km in diameter overlap with mass extinction events for only four sites: Chicxulub, within error of the K/T extinction at 65.5 Ma; Morokweng and Mjolnir within error of the end-Jurassic extinction (145.5 Ma); and the Siljan within error of the Late Devonian extinction at 374.5 Ma. Of these only Chicxulub shows a striking correlation with an extinction event.

Although it is clear that no single cause is responsible for all major extinctions, many mass extinctions share common characteristics suggestive of a catastrophic event. Perhaps no other subject in geology has received more attention or has been more controversial than the question of what catastrophic process or processes are responsible for major mass extinctions.

Episodic Distributions

Eight mass extinctions are recognized in the Phanerozoic, and the same peaks are found for terrestrial and marine organisms, indicating that the major extinctions affected organisms on land and in the sea at the same time (Sepkoski, 1989; Benton, 1995; Foote, 2003) (Figure 6.26). The Late Carboniferous, Late Jurassic, and Early Cretaceous extinctions are more prominent for terrestrial than marine organisms. Five major mass extinctions are recognized: Late Ordovician, Late Devonian, Late Permian, Late Triassic, and Late Cretaceous (Figure 6.27). Of these, the Permian extinction rate is highest, with a mean family extinction rate of 61% for all life, 63% for terrestrial organisms, and 49% for marine organisms (Benton, 1995). Peaks in origination of species generally follow extinction peaks by <30 Ma, which appears to reflect the time necessary to fill abandoned ecological niches with new species (Figure 6.26). Extinction events tend to occur during times of high preservation potential, whereas origination events following these extinctions are more likely to occur at times that are more poorly represented by the fossil record (Foote, 2003).

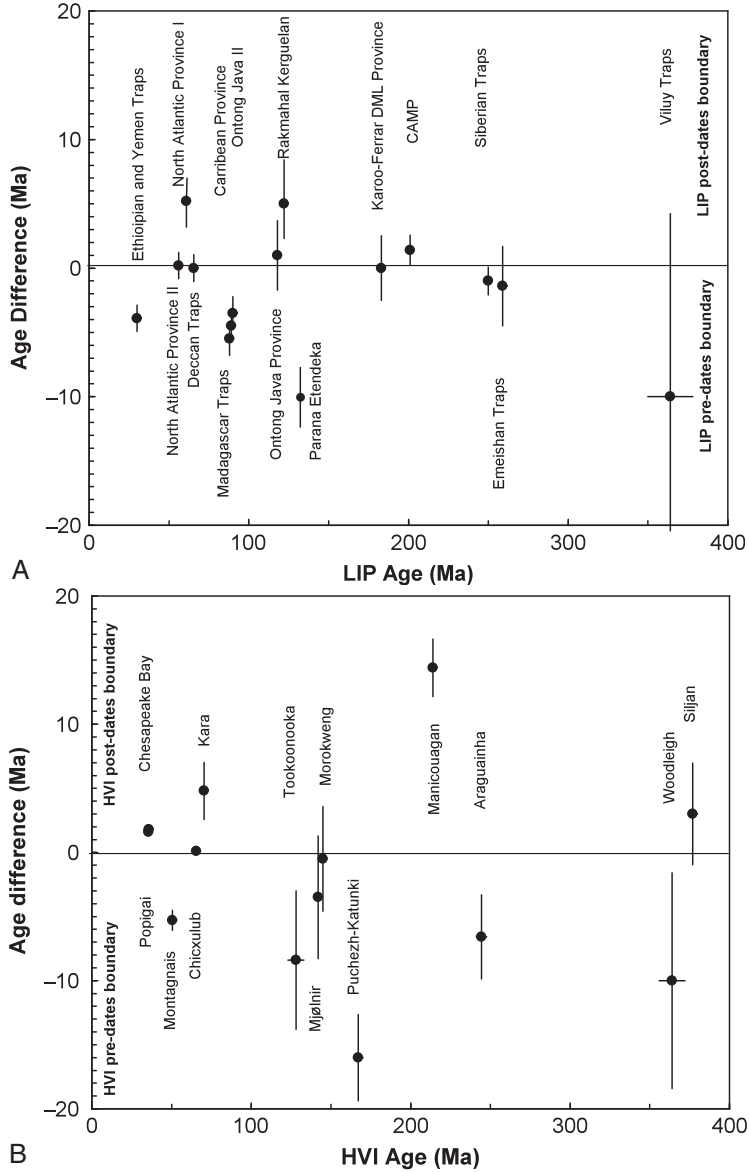

FIGURE 6.25 Age differences between (A) large igneous province (LIP) and mass extinction events and (B) high-velocity impact craters (HVI) (>40 km diameter) and mass extinction events. CAMP, Central Atlantic Magmatic Province. Events predate extinctions for positive differences and postdate extinctions for negative differences. Vertical lines are estimated age uncertainties. *From Kelley (2007), courtesy of Simon Kelley and the Geological Society of London.*

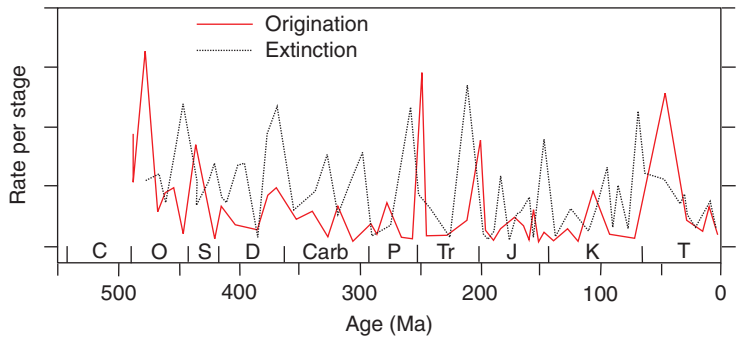

FIGURE 6.26 Rates of origination and extinction of marine animals during the Phanerozoic. *Modified after Foote (2003).*

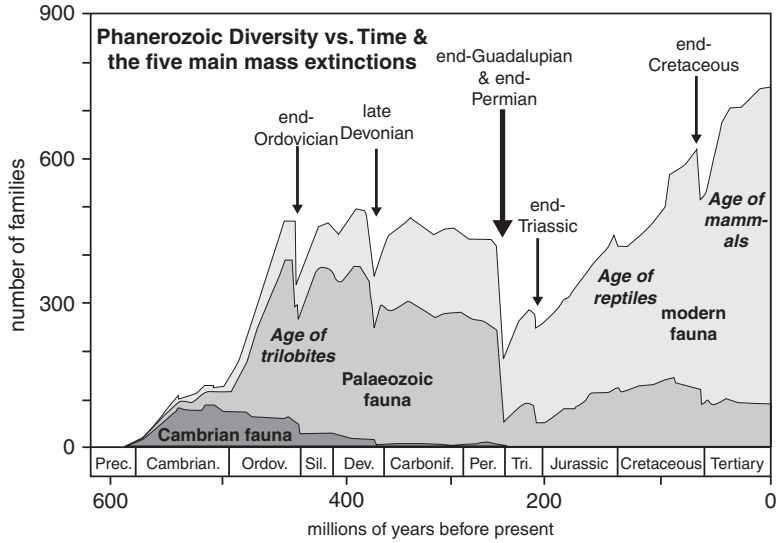

FIGURE 6.27 Major mass extinctions during the Phanerozoic showing number of families as a measure of biologic diversity. *From Metcalf & Isozaki (2009), courtesy of Ian Metcalf.*

Glaciation and Mass Extinction

Perhaps the best example of a mass extinction that may be related to glaciation is that at the end of the Ordovician (Sheehan, 2001). At this time about 26% of families and 49% of genera became extinct (Figure 6.27) (Sepkoski, 1996). Two environmental changes associated with the Ordovician glaciation may be responsible for the Late Ordovician extinction (Sheehan, 2001): (1) cooling global climates and (2) sea level decline, which drained the large shallow seas

and eliminated the habitats of shallow marine life. In some regions, like Scandinavia, sea level drawdown was more than 100 m. The Ordovician extinction was severe in terms of number of taxa lost, but less severe in terms of ecological consequences. Unlike many mass extinctions, there was relatively little evolutionary innovation during the recovery that followed the Ordovician extinction. Newly developing communities were drawn largely from surviving taxa that had previously lived in similar ecological settings.

During the Ordovician extinction, strong thermal gradients appear to have been established between the poles and equator resulting in movement of cold polar seawater into deep tropical seawater. At the end of the glaciation, sea level rebounded rapidly and temperature gradients returned to normal, with the entire glaciation lasting perhaps only 500 ka. At the onset of glaciation, initial extinctions occurred chiefly in the receding shallow seas. Cool temperatures in the open ocean led to the development of the cool-water *Hirnantia* fauna. At the end of the glaciation, sea level rise and atmosphere warming resulted in a second pulse of extinction leading to the rapid demise of open marine faunas including the *Hirnantia* fauna.

Impact-Related Extinctions

Environmental Changes

It is important to distinguish between the ultimate cause of mass extinctions, such as impact, and the immediate cause(s) such as rapid changes in environment that kill plants and animals in large numbers worldwide. The impact of an asteroid or comet on Earth's surface clearly will cause changes in the environment, some of which could result in extinction of various groups of organisms (Toon et al., 1997). The timescale of associated environmental changes ranges from minutes or hours to many decades as summarized in Table 6.4.

As an example, the major consequences of the collision of a 10-km-diameter asteroid with Earth's surface that may contribute to a mass extinction can be summarized as follows:

1. *Darkness.* Fine dust and soot particles will spread worldwide in the upper atmosphere, completely cutting out sunlight for a few months after the impact. This will suppress photosynthesis and initiate a collapse of food chains causing death to many groups of organisms by starvation. For instance, major groups that became extinct at the end of the Cretaceous, such as most or all dinosaurs, marine planktonic and nektonic organisms, and benthic filter feeders were in food chains tied directly with living plants (Chapter 9). Organisms less affected by extinction, including marine benthic scavengers, deposit feeders, and small insectivorous mammals, are in food chains that depend on dead plant material.
2. *Cold.* The dust will produce darkness and be accompanied by extreme cold, especially in continental interiors that are far from the moderating

TABLE 6.4 Summary of Environmental Changes Resulting from Impact of a Large Comet or Asteroid (10–15 km in diameter)

Environmental agent	Timescale
Fireball radiation	Minutes
Burial beneath ejecta	Minutes to hours
Impact-related wildfires	Hours
Winds and tsunamis	Hours
Dust veil darkness (no photosynthesis)	Months
Fires (burning, soot, pyrotoxins)	Months
Dust veil cooling	Months to years
Acid rain (nitric and sulfuric)	Years
Ozone depletion (UV exposure)	Years
Heavy metal poisons and mutagens	Many years
CO_2 greenhouse effect	Many years
Stratospheric aerosols (cold)	Decades
H_2O greenhouse effect	Decades to centuries

influence of oceans. Within 2 or 3 months, continental surface temperatures will fall to –20°C (Figure 6.28).

3. *Increased greenhouse effect*. If an asteroid collided in the ocean, both dust and water vapor will be spread into the atmosphere. Fallout calculations indicate that after the dust settles, water vapor will remain in the upper atmosphere for many decades producing an enhanced greenhouse effect that could raise surface temperatures well in excess of the tolerance limits of many terrestrial organisms. A carbon dioxide greenhouse effect could last for many hundreds of years.
4. *Acid rain*. Energy liberated during an impact may cause atmospheric gases to react, producing nitric and sulfuric acids and various nitrogen oxides. Hence, another side effect of an impact bearing on extinctions is the possibility of acid rain. These rains could last as long as a few years and would lower the pH of surface water in the upper 100 m sufficiently to kill a large number of planktonic organisms.
5. *Wildfires*. The soot particles reported in clays at the K/T boundary may be the result of widespread wildfires ignited by infrared radiation from the

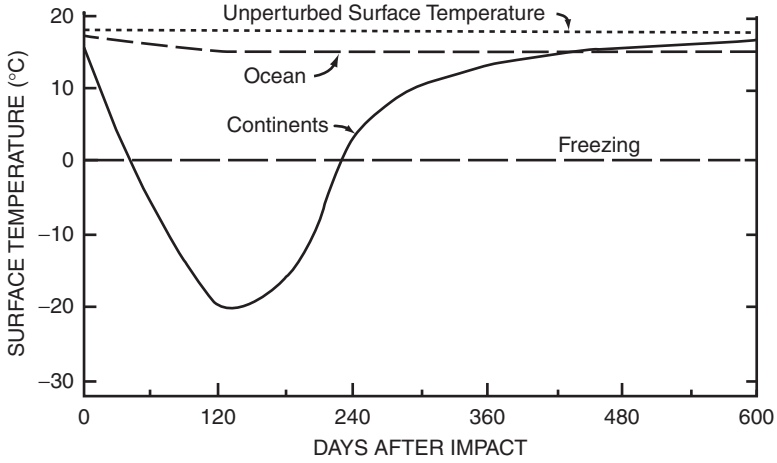

FIGURE 6.28 Change in terrestrial surface temperature of the oceans and continents following impact with asteroid about 10 km in diameter. Atmospheric dust density following impact is 1 g/cm^3. *Modified from Toon (1984).*

initial impact and lasting for many hours. Studies of the soot particles indicate they come chiefly from the burning of coniferous forests. Charcoal is even more definitive and can be used to locate the region in which impact-ignited fires occurred (Belcher et al., 2003).

6. *Toxic seawater*. Asteroid collision should also result in the introduction of a wide variety of trace elements, many of which are toxic, into the oceans (such as Hg, Se, Pb, and Cd). Organisms living in surface marine waters will be exposed to these toxic elements for many years, contributing perhaps to their extinction.

Earth-Crossing Asteroids

Is it possible from our understanding of asteroid orbits and how they change by collisions in the asteroid belt that asteroids have collided with Earth? The answer is yes. Today there are approximately 50 Earth-crossing asteroids with diameters greater than 1 km, and a total population of more than 1000. **Earth-crossing asteroids** are asteroids that are capable of colliding with Earth with only small perturbations of their orbits. To be effective in mass extinctions, the "killer-asteroid" would have to be at least 10 km in diameter. Today there are about eight Earth-crossing asteroids with diameters $\geq$10 km, and probability calculations suggest that about 10 asteroids of this size have collided with Earth since the end of the Precambrian (McLaren & Goodfellow, 1990).

Comets

About three long-period and 10 short-period (<20 per year) comets pass inside Earth's orbit each year. Because long-period comets have velocities greater than asteroids, collisions with Earth should liberate approximately an order of magnitude more energy. Statistical calculations indicate that Earth-crossing comets make about 9 returns to the inner solar system before being ejected into different orbits, and this corresponds to a mean lifetime of about 500 ka. Estimates based on frequency of cometary showers suggest that about 50% of the preserved craters on Earth are the products of cometary rather than asteroid or meteorite impact. A major shower involving $\sim 10^9$ comets >3 km in diameter will result in about 20 impacts on Earth's surface and should occur every 300–500 Ma, and smaller showers ($\sim 10^8$ comets) involving about two impacts should occur every 30–50 Ma. The probable ages of known impact structures (and impact glasses) on Earth's surface suggest episodes of cometary impact with major peaks at 99, 65, and 35 Ma. Recognized mass extinctions that annihilate 50–95% of ecologically diverse lower taxa are recognized at 93, 65, and 36 Ma. The similarity in timing is consistent with the possibility that cometary showers may be responsible for these extinctions. A major problem with the periodic extinction model, however, is that periodicity has not been recognized in the Paleozoic and early Mesozoic. It would appear that any explanation of extinctions involving periodic cometary collisions must also explain why these extinctions only started in the last 100 Ma.

The Triassic Extinction

The end-Triassic mass extinction is recognized as one of the "big five" mass extinctions in the Phanerozoic with more than 50% loss in both marine and terrestrial realms (Figure 6.27) (Tanner et al., 2004; Deenen et al., 2010). A drop in global sea level near the end of the Triassic may explain these declines in many organisms in the marine realm, although it is not yet clear if these changes are eustatic. In the terrestrial realm, extinctions may be related to widespread drying in response to strengthening of the monsoonal climate and breakdown of zonal climatic belts. Volcanism in the Central Atlantic Magmatic Province (CAMP) precisely dated at 201.4 Ma is close to the age of the Late Triassic extinction (Figure 6.25a). If the extinction is related to the LIP eruption, sulfur gases may have led to abrupt climate changes, thus stressing many organisms. In particular, palynological evidence for severe cooling at the Triassic-Jurassic boundary is consistent with large-scale emission of sulfur gases. Also, the strong drop in global sea level at this time (Figure 6.11) suggests that short-term cooling may have resulted in glaciation. In addition, a pronounced decrease in $\delta^{13}C$ is found in both marine and terrestrial environments around 200 Ma and it appears to be tied

directly to a longer term CO_2 supergreenhouse and a marine biocalcification crisis (Whiteside et al., 2010). The approximate coincidence in timing of CAMP volcanism, widespread extinctions, and carbon isotope excursions is supportive of LIP volcanism being the major cause of the Late Triassic mass extinction.

Impact and a 580-Ma Extinction

Biostratigraphic and chemostratigraphic results from Neoproterozoic successions in Australia that contain Ediacaran fossils and acritarchs (unicellular microfossils of unknown or variable biologic affinity) show a striking correlation between acritarch changes, a short-lived excursion in the carbon isotopic record of kerogens, and an ejecta layer from the 580-Ma Acraman impact in southern Australia (Grey et al., 2003). Acritarchs changed from assemblages dominated by long-range simple spheroids to a diverse assemblage characterized by short-range, large complex shapes. Also, at this time, 57 species of acritarchs make their first appearance in the geologic record. In addition, a negative carbon isotopic excursion occurs just before the acritarch radiation. It is possible, if not likely, that the global extinction and recovery of acritarchs at about 580 Ma were associated with the Acraman impact in southern Australia at 580 Ma. Stratigraphic relationships in Neoproterozoic sediments in southern Australia imply that the Acraman impact occurred during a glaciation (Gostin et al., 2010).

EPILOGUE

Although we understand the overall processes in Earth's atmosphere, hydrosphere, and biosphere and how they operate on short timescales, we are just beginning to learn about long-term changes and how the three spheres interact with the solid Earth. To better understand this long-term history, we must better understand how the modern systems react during global changes related to mantle processes. It also means that we need more precise ages of events in the past: a million year uncertainty on ages in the Precambrian is not going help distinguish volcanic eruptions from long-term climate change. We also need increasingly more sophisticated numerical modeling of complex system interactions with high-speed computers. One thing, however, is very clear: the atmosphere, hydrosphere, and biosphere cannot be considered in isolation from the solid Earth. The supercontinent cycle as well as mantle plume events, as discussed in Chapter 8, may have profound effects not only on long-term variations in the atmosphere–ocean system, but also on life on this planet.

FURTHER READING

Bambach, R. K. (2006). Phanerozoic biodiversity mass extinctions. *Annual Review of Earth and Planetary Sciences*, *34*, 127–155.

Holland, H. D. (2003). The Geologic History of Seawater. In *Treatise on Geochemistry* (pp. 583–625). Amsterdam: Elsevier, Chap. 6.21.

Huber, B. T., Wing, S. L., & MacLeod, K. G. (Eds.). (1999). *Warm Climates in Earth History* (480 pp). Cambridge, UK: Cambridge University Press.

Marshall, C. R. (2006). Explaining the Cambrian "explosion" of animals. *Annual Review of Earth and Planetary Sciences*, *34*, 355–384.

Pepin, R. O. (2006). Atmospheres of the terrestrial planets: Clues for origin and evolution. *Earth and Planetary Science Letters*, *252*, 1–14.

Sreenivas, B., & Murakami, T. (2005). Emerging views on the evolution of atmospheric oxygen during the Precambrian. *Journal of Mineralogical and Petrological Sciences*, *100*, 184–201.

Wigley, T. M. L., & Schimel, D. S. (2000). *The Carbon Cycle* (310 pp). Cambridge, UK: Cambridge University Press.

Williams, Q. (2007). *Water, the Solid Earth, and the Atmosphere: The Genesis and Effects of a Wet Surface on A Mostly Dry Planet*, Treatise on Geophysics (pp. 121–142). Amsterdam: Elsevier, Chap. 9.05.

Chapter 7

Crustal and Mantle Evolution

INTRODUCTION

One of the unique features of Earth is its crust. None of the other terrestrial planets has a crust similar that of Earth, and the reason for this is related to plate tectonics, which in turn is related to the way the mantle cools and how it has evolved. Most investigators now agree that the history of Earth's crust and mantle are closely related, and that many of the features we find in the crust are controlled by processes in the mantle. In this chapter we will show just how closely the evolution of the crust is tied to that of the mantle, and review how this dynamic system has evolved as planet Earth has cooled during the last 4.6 Ga.

THE HADEAN

There is confusion in the literature as to the definition of the Hadean as a period of time. Some investigators define it as the era older than the oldest rocks (4 Ga), and others as the era older than the first evidence of life (3.5 Ga) (both of which are subject to change as we acquire more data). Another approach is to place the end of the Hadean at the end of Late Heavy Bombardment (3.9 Ga) in the inner solar system, which has the advantage of being able to compare events with other planets. We will refer to the **Hadean** herein as the period time prior to 4 Ga extending back to the accretion of Earth around 4560 Ma (see Chapter 10).

Extinct Radioactivity

Radiogenic isotopes with short half-lives that were present when the solar system formed decayed rapidly leaving a record of their presence in daughter isotopes. This is known as **extinct radioactivity**. These isotopes, with half-lives of the order of a few million to a few tens of millions of years, can be useful in constraining the timing of accretionary events in the very earliest stages in the history of the solar system. Their usefulness is dependent not only on their half-lives, but also on how effectively accretion fractionates parent from daughter isotope. If this fractionation is strong, anomalous amounts of the daughter isotope will occur in planetary bodies today, and will also show up in Earth's

mantle and in basalts derived from the mantle. From the amount of daughter isotope present (over background level), ages of early fractionation events can be estimated. The most useful isotopic pairs are $^{92}Nb/^{92}Zr$ ($t_{1/2} = 36$ Ma), $^{182}W/^{182}Hf$ ($t_{1/2} = 9$ Ma), $^{146}Sm/^{142}Nd$ ($t_{1/2} = 103$ Ma), $^{129}I/^{129}Xe$ ($t_{1/2} = 16$ Ma), and $^{244}Pu/^{136}Xe$ ($t_{1/2} = 82$ Ma). An example of using the $^{182}W/^{182}Hf$ method to constrain the age of Earth's core was given in Chapter 5.

Differences in the $^{142}Nd/^{144}Nd$ ratio in terrestrial samples and meteorites indicate different evolutionary histories (Figure 7.1) (Kramers, 2007). Fractionation of the Sm/Nd ratio by magmatic processes leads to differences in the $^{142}Nd/^{144}Nd$ isotopic ratio only during the lifetime of ^{146}Sm (about the first 400 Ma of Earth history), and hence the $^{142}Nd/^{144}Nd$ ratio of terrestrial rocks is a sensitive indicator of differentiation events that occurred early in Earth's history. Although later mixing in the mantle tends to eliminate isotopic inhomogeneities, the 3.7-Ga Isua metasediments in Southwest Greenland have $^{142}Nd/^{144}Nd$ anomalies ($\varepsilon^{142}Nd = 0.1$–$0.2$) showing that some domains in the mantle escaped stirring and provide a "memory" of the earliest history of the planet (Figure 7.1). These anomalies may record production of an early crust

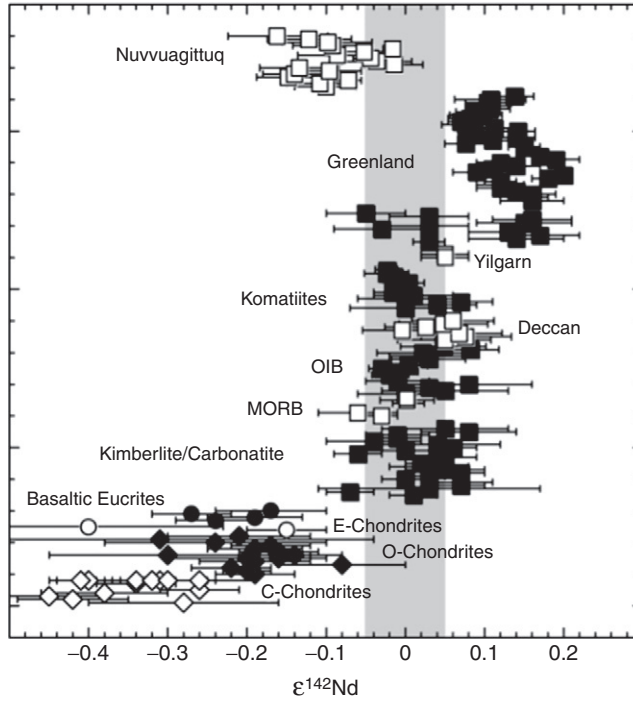

FIGURE 7.1 Distribution of $^{142}Nd/^{144}Nd$ in meteorites and terrestrial rocks. The gray vertical band is the range of most terrestrial samples. $\varepsilon^{142}Nd = \{[(^{142}Nd/^{144}Nd)sample/(^{142}Nd/^{144}Nd)\ standard] - 1\} \times 10^6$.

in the first 30–50 my of Earth's history (Bennett et al., 2007). Note that ages measured forward from the age of the solar system will be expressed as "my" rather than "Ma," the latter of which refers to time measured backwards from the present. The Hf-W system provides a powerful complement to the Sm/Nd results for early Earth, because both core formation and silicate differentiation fractionate Hf from W. Calculations of Moynier et al. (2010), which describe the isotopic evolution of a chondritic reservoir and core segregation as well as silicate differentiation, show that the W isotopic composition of terrestrial samples provides the most stringent time constraint for early core formation of 28–38 my after time zero followed by early crustal formation at 38–75 my, which is consistent with the ^{142}Nd results.

However, as pointed by Caro and Bourdon (2010), the Nd isotopic results can be interpreted in more than one way. If for instance, Earth accreted from material with a higher Sm/Nd ratio than chondritic meteorites, the need for an early crustal formation event disappears.

Hadean Zircons

No crust is known to have survived that is older than the 4.0-Ga Acasta gneisses in Canada (Figure 7.2). However, evidence of even older crust is provided by detrital zircons in metasediments from the Mt. Narryer and Jack Hills areas in Western Australia (Amelin et al., 1999; Wilde et al., 2001; Nutman, 2001; Mojzsis et al., 2001; Harrison et al., 2008). Detrital zircons with ages between 4.3 and 3.5 Ga have been reported from these sediments. One deep purple zircon measuring 220 by 160 μm, with internal complexities or inclusions, has a domain with a concordant ^{207}Pb/^{206}Pb age of 4404 ± 8 Ma, which is

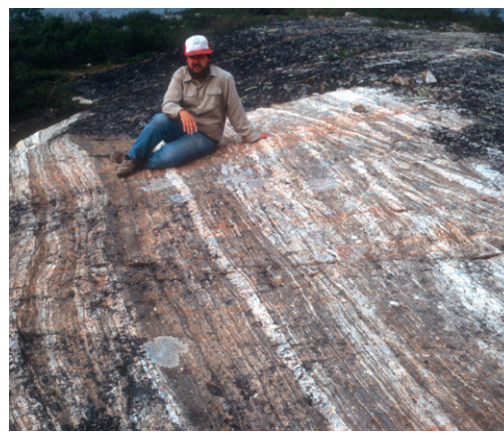

FIGURE 7.2 The 4.0-Ga Acasta gneisses from the Archean Slave province, northwest of Yellowknife, NWT, Canada. This outcrop, with the founder Sam Bowring, shows interlayered TTG and granite (light bands).

interpreted as the age of crystallization of this domain (Figure 7.3a) (Wilde et al., 2001). This is the oldest reported mineral age from planet Earth. Although this represents only one SHRIMP analysis, it is not affected by cracks and has a relatively small error. The other U/Pb ages from this zircon ≥4.3 Ga may represent actual geologic events (Figure 7.3b), whereas the more discordant ages

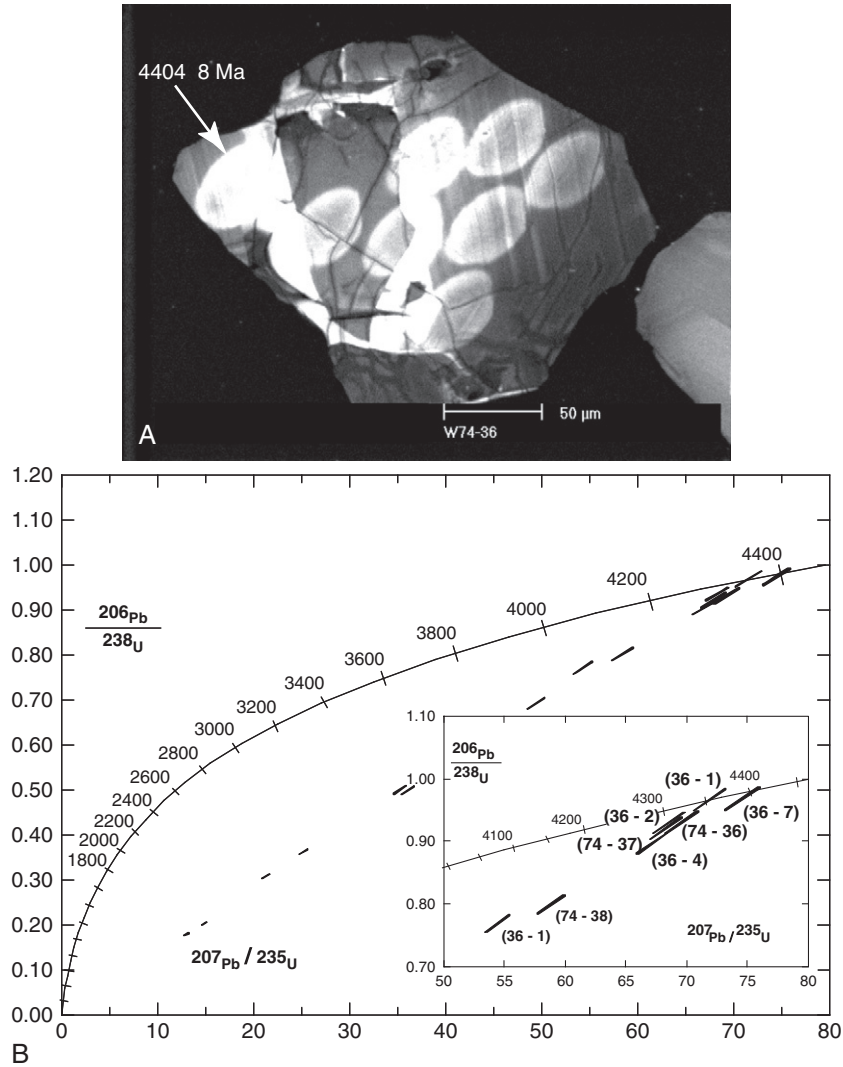

FIGURE 7.3 (A) Cathodoluminescence image of early Archean zircon W74/2-36, from Western Australia. White ovoids are locations of individual SHRIMP analyses, with the oldest domain at 4404 Ma labeled. (B) Combined Concordia plot for grain W74/2-36. *Courtesy of Simon Wilde.*

may represent Pb loss during impact events. These old detrital zircons are important in that they indicate the presence of felsic sources, some of which contained components that were up to 4.4 Ga. These components may have been remnants of continental crust, although the lateral extent of any given domain could have been much smaller than microcontinents the size of Madagascar.

Rare earth element (REE) distributions in the Jack Hills zircons typically show enrichment in heavy REE, a positive Ce anomaly and a negative Eu anomaly, indicating that they crystallized from granitic melts (Harrison et al., 2008; Harrison, 2009). This observation is important because it means that granitoids were produced on Earth by 4.4–4.3 Ga. Hafnium isotopic results from the Jack Hills detrital zircons suggest continuous derivation of crust from the mantle from 4.5 to 4.2 Ga, with concurrent recycling into the mantle.

Oxygen isotope ratios are fractionated by low-temperature processes in the crust, but are not significantly affected by high-temperature processes. Hence, the oxygen isotope signatures preserved in detrital zircons are thought to reflect the nature of the source rock from which the granitoid that hosted the zircon was derived (Valley et al., 2005). The $\delta^{18}O$ values from the Jack Hills zircons extend to 7.5‰, a range significantly above the mantle value of 5.3‰ (see Figure 6.12 from Chapter 6). This implies that the source of the granitic magma originally contained clays that formed at Earth's surface by hydrous weathering or hydrothermal alteration. It also means that liquid water was present on the surface of Earth before 4 Ga (Harrison, 2009). Supporting this conclusion is the occurrence of hydrous mineral inclusions in the zircons and the relatively low crystallization temperatures ($\leq 700^{\circ}C$) and water contents calculated for the zircon protoliths.

Another important source of information housed in Hadean zircons comes the Lu-Hf isotopic system (Kramers, 2007). During melting in the mantle, the Lu/Hf ratio is fractionated, and the residue left behind has a higher Lu/Hf ratio than the starting material. The most robust feature of the Hf isotope results from a selected group of the Jack Hills zircons is the fact that they fall along a Hf isotopic growth line ($^{176}Lu/^{177}Hf = 0.02$) characteristic of mafic crust (Kemp et al., 2010). The U/Pb ages and Hf isotopic compositions were measured concurrently in these zircons using laser ablation microprobe ICP-MS and they are considered to be the most precise data set from Jack Hills zircons. How do you get zircons from mafic crust? One possibility is that partial melting of mafic crust under hydrous conditions produced TTG (tonalite-trondhjemite-granodiorite) melts, which hosted the zircons. When extrapolated back to a depleted mantle growth curve, the tight cluster of data suggests that crustal extraction from the mantle occurred at or before 4.4 Ga. Complementing the $^{142}Nd/^{144}Nd$ system, the Hf isotopic systematics support formation of a primitive mafic crust soon after the Moon-forming event around 4520 Ma. Where is this early crust today? One possibility is that it was rapidly recycled into the mantle during the Hadean and now resides in the deep mantle.

Origin of the First Crust

Although a short-lived crust may have formed on a magma ocean prior to the Moon-forming event, the only crust that we have a record of with both short- and long-lived radiogenic isotopes is the crust that formed on Earth after the planetary collision that formed the Moon at 4520 Ma. With our ever-increasing database, we can address several outstanding questions related to the origin of this early crust:

1. Was the first crust of local or global extent?
2. When and by what process did the first crust form?
3. What was the composition of the early crust?
4. When and how did oceanic and continental crustal types develop?

As we will see below, the oldest preserved fragments of continental crust at 4.0–3.8 Ga are chiefly of TTG gneisses containing fragments of komatiite and basalt (amphibolite), some of which may be remnants of early oceanic crust. Although the original extent of Early Archean continental fragments is not known, they comprise less than 10% of preserved Archean crust (Figure 7.4). The sparsity of rocks older than 3 Ga may be related to losses resulting from recycling of early crust into the mantle as discussed later in the chapter. We may be able to learn more about the first terrestrial crust by comparison with the lunar crust and crusts of other terrestrial planets. The lunar highlands, for instance, are remnants of an early crust (~4.4 Ga), which covered most or

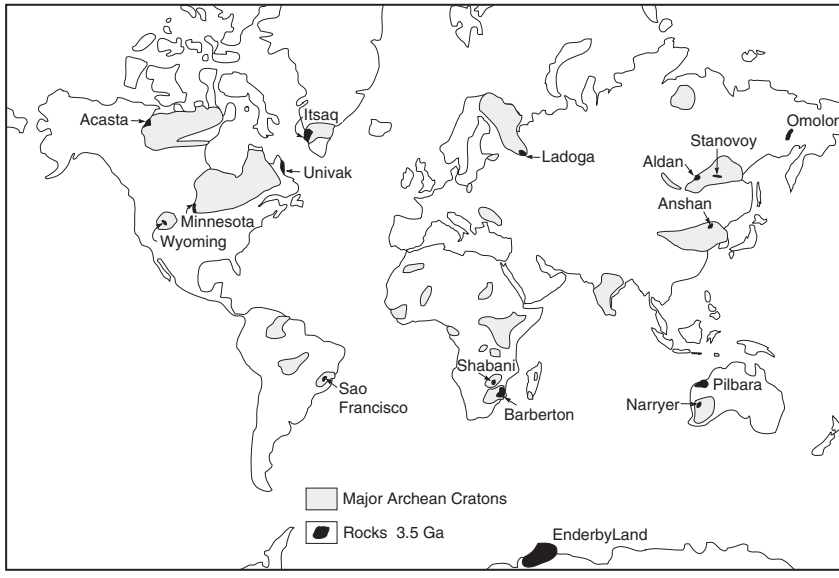

FIGURE 7.4 Map showing the distribution of Earth's oldest rocks.

all of the Moon's surface (Taylor, 1982). Studies of topographic features and the cratering histories of Mercury and Mars also suggest the preservation of widespread primitive crusts. If the early history of Earth was similar to the histories of these planets, it also may have had an early crust that covered most of its surface. Because remnants of this crust are not preserved in the continents (or at least not yet recognized), if such a crust existed it must have been destroyed by continuing impacts on the surface or/and by recycling into a magma ocean.

Theories for the origin of Earth's primitive crust fall into two broad categories: impact models and terrestrial models. Several models have been proposed for crustal origin either directly or indirectly involving impact of accreting objects. All call on surface impacting that leads to melting in the mantle producing either mafic or felsic magmas that rise to form a crust. Large impacts may have produced mare-like craters on the terrestrial surface that were filled with impact-produced magmas (Grieve, 1980). If the magmas or their differentiation products were felsic, continental nuclei may have formed and continued to grow by magmatic additions from within the planet. Alternatively, if the impact craters were flooded with basalt, they may have become the first oceanic crust. Although initially attractive, impact models are faced with many difficulties in explaining crustal origin. For instance, most or all of the basalts that flood lunar mares formed later than the impacts and are not related directly to impacting. Also, only relatively small amounts of magma were erupted into lunar mare craters. Perhaps the most significant problem with the lunar mare analogy is that mare basins formed in still older anorthositic crust.

Models that call on processes operating within Earth have been most popular in explaining the origin of the early crust. The fact that textures and geochemical relationships indicate that the early anorthositic crust on the Moon is a product of magmatic processes favors a similar origin for Earth's earliest crust. It is likely that enough heat was retained in Earth, after or during the late stages of planetary accretion, that the upper mantle was partially or entirely melted, as discussed later in the chapter. Complete melting of the upper mantle would result in a magma ocean, which on cooling should give rise to a widespread crust. Whether or not plate tectonics was operative at this time is not known. However, some mechanism of plate creation and recycling must have been operative to accommodate the large amounts of heat loss and vigorous convection in the early mantle.

Composition of the Primitive Crust

Numerous compositions have been suggested for the earliest terrestrial crust. In part responsible for diverging opinions are the different approaches to estimating composition. The most direct approach is to find and describe a relict of the primitive crust ($\geq$4.4 Ga). Although some investigators have not given up on this approach, the chances that a remnant of this crust is preserved seem very

small. Another approach is to deduce the composition from studies of the preserved Archean crust. However, compositions and field relations of rock types in the oldest preserved Archean terranes may not be representative of the earliest terrestrial crust. Another approach has been to assume that Earth and the Moon have undergone similar early histories and hence to go to the Moon, where the early record is well preserved, to determine the composition of Earth's primitive crust. Geochemical models based on crystal-melt equilibria and a falling geothermal gradient with time have also been used to constrain the composition of the early terrestrial crust.

Felsic Models

Some models for the production of a primitive felsic or andesitic crust rely on the assumption that low degrees of partial melting in the mantle will be reached before high degrees, and hence felsic magmas should be produced before mafic ones. Other models call on fractional crystallization of basalt to form andesitic or felsic crust. Shaw (1976) proposed that the mantle cooled and crystallized from the center outward, concentrating incompatible elements into a near-surface basaltic magma layer. This layer underwent fractional crystallization, resulting in the accumulation of an anorthositic scum in irregular patches and in residual felsic magmas that crystallized to form the first stable crust by about 4 Ga.

Two main obstacles face felsic crustal models. First, the high heat generation in the early Archean probably produced large degrees of melting of the upper mantle, and hence it is unlikely that felsic melts could form directly. Although felsic or andesitic crust could be produced by fractional crystallization of basaltic magmas, this requires a large volume of basalt, which itself probably would have formed the first crust. Despite these problems, the fact that the Jack Hills zircons clearly demand granitic sources means that felsic crust existed, at least locally by $\geq$4350 Ma. Rollinson (2008) has argued that this early felsic crust may have been similar to the Na-rich granitoids associated with ophiolites (e.g., plagiogranites, Chapter 3). The ophiolitic granitoids are produced by partial melting or fractional crystallization of associated mafic rocks. Support for this idea comes from an overlap in the trace element and oxygen isotopic compositions of young zircons from ophiolites and the 4-Ga Jack Hills zircons in Western Australia. The scarcity of detrital zircons older than 3 Ga, however, would seem to imply that any early felsic crust was of local rather than global extent.

Anorthosite Models

Studies of lunar samples indicate that the oldest rocks on the lunar surface are gabbroic anorthosites and anorthosites of the lunar highlands, which are remnants of a widespread crust formed about 4.4 Ga (Taylor, 1982; Taylor & McLennan, 2009). This primitive crust appears to have formed in response to

catastrophic heating that led to widespread melting of the lunar interior and production of a voluminous magma ocean. As the magma ocean rapidly cooled and underwent fractional crystallization, pyroxenes and olivine sank and plagioclase (and some pyroxenes) floated, forming a crust of anorthosite and gabbroic anorthosite. Impacts disrupted this crust and produced mare craters, and these craters were later filled with basaltic magmas (3.9–2.5 Ga).

If Earth had an early melting history similar to that of the Moon, the first crust may have been composed dominantly of anorthosites and gabbroic anorthosites. However, the increased pressure gradient in Earth limits the stability range of plagioclase to depths considerably shallower than on the Moon. Experimental data suggest that plagioclase is not a stable phase at depths >35 km in Earth. Hence, if such a model is applicable to Earth, the anorthosite fraction, either as floating crystals or as magmas, must find its way to very shallow depths to be preserved. The most serious problem with the anorthosite model, however, is related to the hydrous nature of Earth. Plagioclase will readily float in an anhydrous lunar magmatic ocean, but even small amounts of water in the system causes it to sink (Taylor, 1987, 1992). Hence in the terrestrial system, where water was probably abundant in the early mantle, an anorthosite scum on a magma ocean would not form.

Basalt and Komatiite Models

In terms of our understanding of Earth's early thermal history and from the geochemical and experimental database related to magma production, it seems likely that Earth's primitive crust was mafic to ultramafic in composition. If a magma ocean existed, cooling would produce a widespread basaltic crust, probably with komatiite components. Without a magma ocean or after its solidification, basalts also may have composed an important part of the early crust. The importance of basalt and komatiite in early Archean greenstone successions attests to their probable importance on the surface of Earth prior to 4 Ga.

EARTH'S OLDEST ROCKS

The oldest preserved rocks occur as small, highly deformed terranes tectonically incorporated within Archean crustal provinces (Figure 7.4). These terranes are generally <500 km across, and are separated from surrounding crust by shear zones. Although the oldest known rocks on Earth are about 4.0 Ga, the oldest minerals are detrital zircons from the 3-Ga sedimentary rocks in Western Australia as described earlier.

The oldest isotopically dated rocks on Earth are the Acasta gneisses in northwestern Canada (Figure 7.2). These gneisses are a heterogeneous assemblage of highly deformed TTG, tectonically interleaved on a centimeter scale with amphibolites, ultramafic rocks, granites, and at a few locations, metasediments (Bowring, 1990; Bowring et al., 1989; Iizuka et al., 2007). Acasta amphibolites

appear to represent basalts and gabbros, many of which are deformed dykes and sills. The metasediments include calc-silicates, quartzites, and biotite-sillimanite schists. The rare occurrence of the assemblage tremolite-serpentine-talc-forsterite in ultramafic rocks indicates that the metamorphic temperature was in the range of 400–650°C. The ages of zircon from the tonalitic and amphibolite fractions of the gneiss range from 4 to 3.6 Ga with TTG emplacement events recorded at 4.03–3.94, 3.74–3.72, and 3.6 Ga (Iizuka et al., 2007). Thus, it would appear that this early crustal segment evolved over about 400 Ma, and developed a full range in composition of igneous rocks from mafic to K-rich felsic types. Because of the severe deformation of the Acasta gneisses, the original field relations between the various lithologies are not well known. However, the chemical compositions of the Acasta rocks are very much like less deformed Archean greenstone-tonalite-trondhjemite-granodiorite assemblages, suggesting a similar origin and tectonic setting.

The largest and best preserved fragment of early Archean continental crust is the Itsaq Gneiss Complex in Southwest Greenland (Nutman et al., 1996, 2002; Manning et al., 2006). In this area, three terranes have been identified, each with its own tectonic and magmatic history, until their collision at about 2.7 Ga (Figure 7.5) (Friend et al., 1988). The Akulleq terrane is dominated by the Amitsoq TTG complex most of which formed at 3.9–3.8 Ga and underwent high-grade metamorphism at 3.6 Ga. The Akia terrane in the north comprises 3.2- to 3.0-Ga tonalitic gneisses that were deformed and metamorphosed at 3.0 Ga, and the Tasiusarsuaq terrane, dominated by 2.9- to 2.8-Ga rocks, was deformed and metamorphosed when the terranes collided in the late Archean. Although any single terrane records <500 Ma of precollisional history, collectively the terranes record over 1 Ga of history before their amalgamation in the late Archean. Each of the terranes also contains remnants of highly deformed supracrustal rocks. The most extensively studied is the Isua sequence in the Isukasia area in the northern part of the Akulleq terrane (Figure 7.5). Although highly altered by submarine metasomatism, this succession comprises from bottom to top: basalts and komatiites with intrusive ultramafics interbedded with banded iron formation; intrusive sheets of tonalite and granite; basalts and ultramafic rocks; mafic volcanigenic turbidites; and basalts with interbedded banded iron formation (Rosing et al., 1996). Recent remapping of the Isua succession suggests that at least some of the schists are highly deformed tonalitic gneisses or pillow basalts (Fedo et al., 2001). Carbonates in the Isua succession are now considered to be mostly, or entirely, metasomatic in origin; some may represent the products of seafloor alteration. The Isua succession is similar to island-arc greenstone successions, thus supporting the existence of plate tectonics in the early Archean.

The Pilbara craton in Western Australia also comprises a group of accreted terranes, the most widespread of which is the Warrawoona terrane, which formed between 3.7 and 3.2 Ga. Although extensively altered by submarine processes, the Warrawoona sequence is the best preserved early Archean

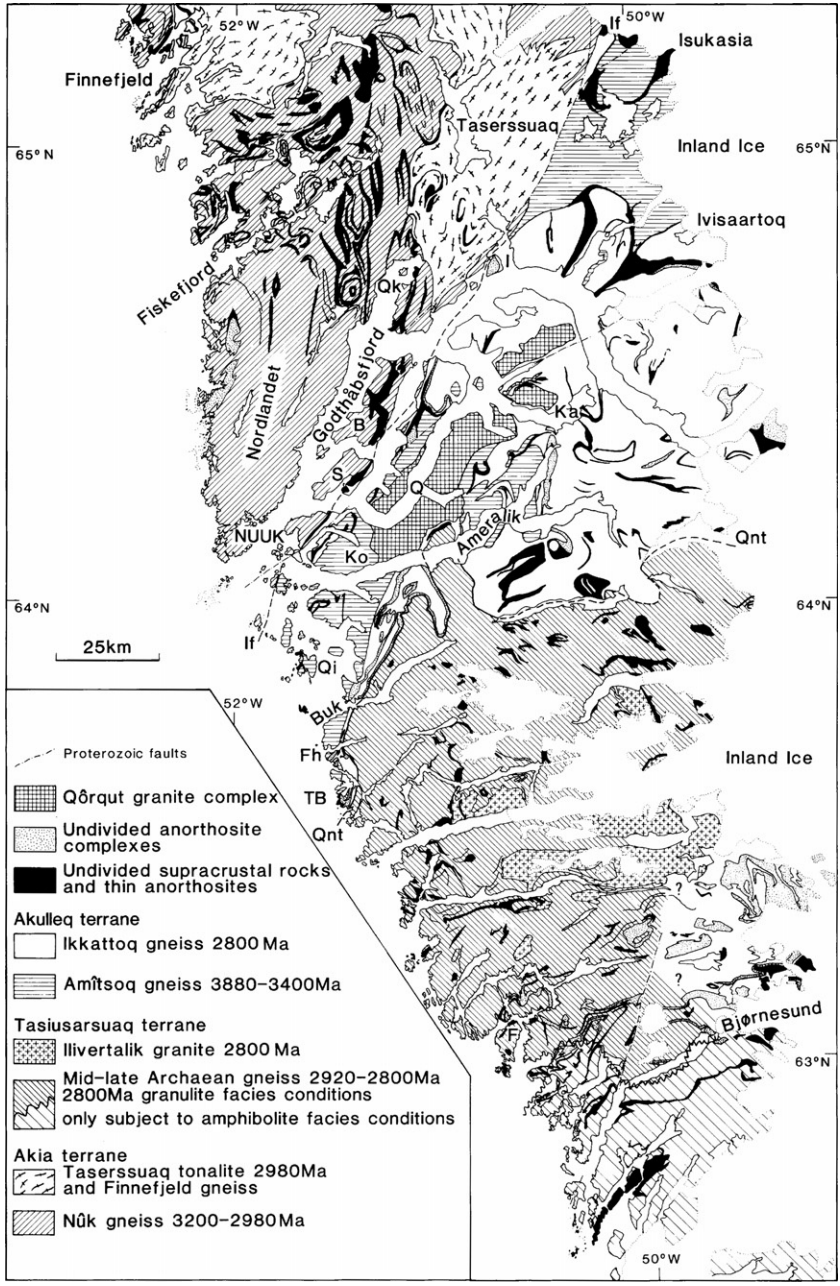

FIGURE 7.5 Generalized geologic map of the Nuuk region in Southwest Greenland showing three early Archean terranes. *Courtesy of Clark Friend.*

greenstone (Barley, 1993; Krapez, 1993). It rests unconformably on an older greenstone-TTG complex with a U/Pb zircon age of about 3.5 Ga (Buick et al., 1995b). This is important because it indicates that not only was the Warrawoona deposited on still older continental crust, but that land emerged above sea level by 3.5 Ga in this region.

Detailed investigations in the Pilbara indicate the existence of three separate terranes, each with unique stratigraphy and deformational histories (Van Kranendonk et al., 2002): an eastern terrane (3.72–2.85 Ga), a western terrane (3.27–2.92 Ga), and the Kuranna terrane ($\leq$3.29 Ga). The oldest supracrustal rocks in the eastern Pilbara terrane (the Coonterunah and Warrawoona Groups, 3.5–3.3 Ga) were deposited unconformably on older felsic crust dated at 3.72 Ga. The Warrawoona Group is divided into three volcanic cycles including, from base to top, the Talga Talga (3.49–3.46 Ga), Salgash (3.46–3.43 Ga), and Kelly (3.43–3.31 Ga) Subgroups (Figure 7.6). These dominantly mafic rocks include chert beds, containing Earth's oldest stromatolites, and are interbedded with felsic volcanics erupted intermittently between 3.49 and 3.43 Ga. The Pilbara successions appear to be remnants of one or more oceanic plateaus that were erupted on to thin, submerged continental crust.

The Barberton greenstone in southern Africa is one of the most studied early Archean greenstones. Together with coeval TTG plutons, the Barberton succession formed at 3.55 to 3.2 Ga (Kamo & Davis, 1994; Kroner et al., 1996). It includes four tectonically juxtaposed terranes, with similar stratigraphic

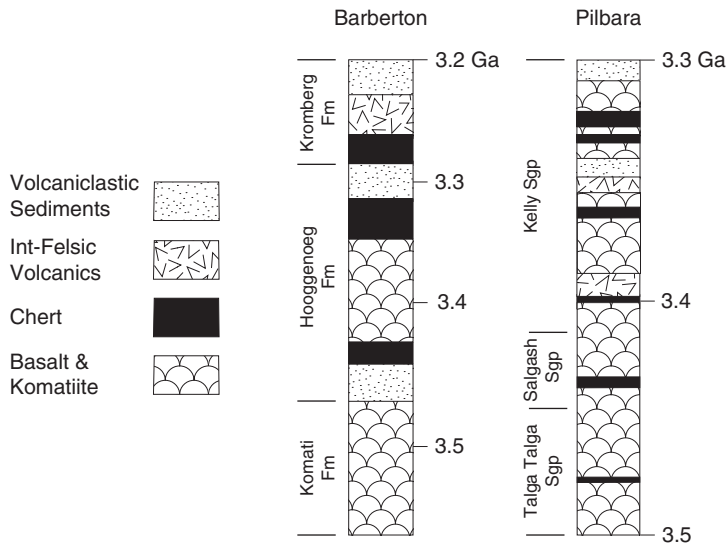

FIGURE 7.6 Generalized stratigraphic sections of early Archean greenstones from the Barberton greenstone in South Africa and the Pilbara succession in Western Australia. Fm, formation; Sgp, supergroup.

successions in each terrane (Lowe, 1994a). Each succession (known as the Onverwacht Group) begins with submarine basalts and komatiites of the Komati Formation (Figure 7.6), an Archean mafic plain succession that could represent remnants of oceanic crust. Overlying the mafic plain succession are the Hooggenoeg and Kromberg Formations, a suite of felsic to basaltic submarine volcanics, fine-grained volcaniclastic sediments, and cherts, possibly representing an oceanic arc. The terminal Moodies Group (not shown in Figure 7.6), which includes orogenic sediments, may have been deposited during amalgamation of the four terranes just after 3.2 Ga.

Unlike most late Archean greenstones, many of which evolved in less than 50 Ma, early Archean greenstones had long histories of >500 Ma before colliding and stabilizing as part of a continent (Condie, 1994). In the Barberton greenstone, individual cycles lasted 50–80 Ma and included rifting and eruption of thick successions of mafic flows, magmatic quiescence with deposition of chemical sediments, and finally crustal thickening caused by intrusion of TTG plutons. Unlike most late Archean terranes, which accreted into cratons almost as they formed, early Archean terranes appear to have bounced around like bumper cars for hundreds of millions of years. Why they did not accrete into continents is an important question that still remains unresolved. Perhaps there were too few of these terranes and collisions were infrequent. Alternatively, most of these terranes may have been recycled into the mantle before having a chance to collide and make a continent.

CRUSTAL ORIGIN

The probable characteristics of Earth's early oceanic and continental crust are summarized in Table 7.1. Oceanic crust is generated today at ocean ridges by partial melting of the upper mantle, and there is no reason to believe that early

TABLE 7.1 Characteristics of Earth's Early Crust

	Oceanic crust	Continental crust
First appearance	~4.5 Ga	≥4.35 Ga
Where formed	Ocean ridges	Oceanic plateaus
Composition	Mafic	Felsic (TTG)
Lateral extent	Widespread, rapidly recycled	Local, rapidly recycled
How generated	Partial melting of ultramafic rocks in upper mantle	Partial melting of wet mafic rocks with garnet left in residue

TTG = tonalite-trondhjemite-granodiorite.

oceanic crust did not form the same way. Just when the first oceanic crust began to be produced is unknown because it was undoubtedly recycled into the mantle, but it is likely it became widespread in the late Archean. Because of the greater amount of heat in the Archean upper mantle, oceanic crust may have been produced four to six times faster than at present; if that was the case, it would have been considerably thicker than modern oceanic crust. Like modern oceanic crust, however, it was probably widely distributed on Earth's surface.

As far as we know, Earth is the only terrestrial planet with continental crust. If so, what is unique about Earth that gives rise to continents? Two factors immediately stand out: (1) the Earth is the only planet with significant amounts of water and (2) it appears to be the only planet with plate tectonics. An important constraint on the origin of Archean continents is the composition of Archean TTG. Experimental data favor an origin for TTG by partial melting of amphibolite or eclogite in the presence of significant amounts of water (Rapp & Watson, 1995). Without water, TTG magmas cannot form. The production of large amounts of Archean continental crust require subduction of large quantities of hydrated basalt and large quantities of water. Hence, with the possible but unlikely exception of Venus, the absence of continental crust on other terrestrial planets may reflect the small amount or absence of water and the absence of plate tectonics on these planets.

It is possible that the earliest TTG crust developed from mafic oceanic plateaus, either by partial melting of the thickened mafic roots of the plateaus or by melting of slabs subducted around their margins as discussed later in the chapter. In either case, the resulting TTG magmas rise and underplate mafic and komatiitic rocks, some of which are preserved today in greenstone belts. Large granite plutons do not appear in the geologic record until about 3.2 Ga and do not become important until after 2.6 Ga (here granite is used *sensu stricto*). Geochemical and experimental data suggest that these granites are produced by partial melting or fractional crystallization of TTG (Condie, 1986). It is not until TTG is relatively widespread that granites appear in the geologic record. Thus, the story of early continental crust is the story of three rock types: basalt, TTG, and granite listed in the general order of appearance in the Archean geologic record. Field relations in most Archean granite-greenstone terranes also indicate this order of relative ages. It would appear that early Archean basalts were hydrated by seafloor alteration and later they partially melted, either in descending slabs or in thickened root zones of oceanic plateaus, giving rise to TTG magmas. TTG, in turn, was partially melted or fractionally crystallized to produce granites.

Thus, unlike the first oceanic crust, which probably covered much or all of Earth's surface, the first continental crust was probably of more local extent associated with subduction zones and oceanic plateaus. Now that we have a beginning for continental crust, the next question is that of how and at what rate did continents grow?

HOW CONTINENTS GROW

General Features

Although most investigators agree that production of post-Archean continental crust is related to subduction, just how continents are produced in arc systems is not well understood. Oceanic terranes such as island arcs and oceanic plateaus may be important building blocks for continents as they collide and accrete to continental margins. However, the fact that these terranes are largely mafic (Kay & Kay, 1985; DeBari & Sleep, 1991), yet upper continental crust is felsic, indicates oceanic terranes must have undergone dramatic changes in composition to become continental crust. Although details of the mechanisms by which mafic crust evolves into continental crust are poorly known, fractionation of mafic rock to make felsic rock, by either partial melting or fractional crystallization, involves production of a thick depleted restite (>100 km thick). Perhaps colliding terranes partially melt and felsic magmas rise to the upper continental crust, leaving a depleted restite in the lower crust. Because we do not see seismic evidence for thick depleted continental roots beneath recently accreted crust, if this mechanism is important, the depleted root must delaminate and sink into the mantle, perhaps during the plate collisions.

Various mechanisms have been suggested for the growth of continents, the most important of which are magma additions by crustal underplating and by terrane collisions with continental margins (Figure 7.7) (Rudnick, 1995). Magma from the mantle may be added to the crust by **underplating**, involving

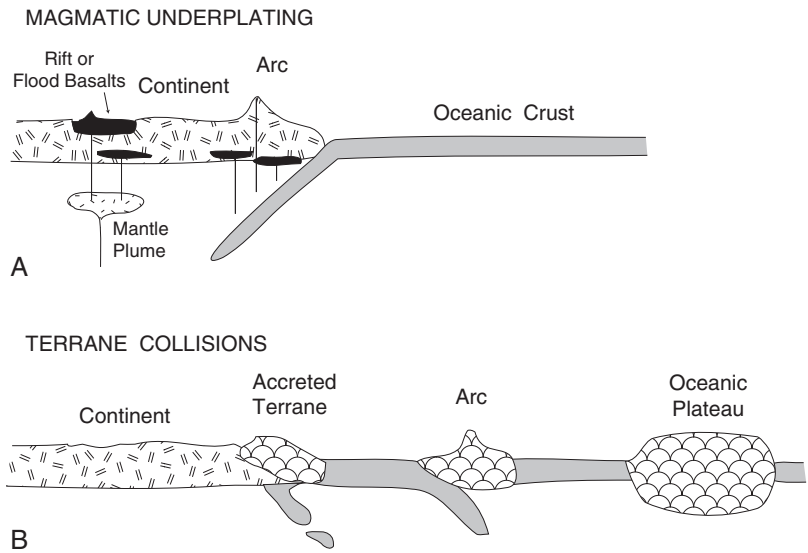

FIGURE 7.7 Mechanisms of continental growth.

the intrusion of sills and plutons. Magma additions can occur in a variety of tectonic environments, the most important of which are arcs, continental rifts, and over mantle plumes. Up to 20% of the crust in the Basin and Range Province in western North America was added during the Tertiary by juvenile volcanism and plutonism (Johnson, 1993). Large volumes of juvenile magma from the mantle are added to both oceanic and continental margin arcs. Major continental growth by this mechanism can occur during seaward migration of subduction zones, when arc magmatism must keep up with slab migration. However, two important observations indicate that island arcs are not important components in the lower continental crust: (1) they are generally $<$25 km thick and as such should be subducted (Cloos, 1993), and (2) lower crustal xenoliths contain too much Ni, Cr, and Co for an arc source (Condie, 1994; Abbott, 1996). Also, current studies indicate that Phanerozoic accretionary orogens contain relatively few remnants of island arcs.

At the onset a clear distinction needs to be made between juvenile and reworked additions to the crust. **Juvenile crust** is produced in the mantle by partial melting and rapid extraction, whereas **reworked crust** is produced by partial melting and/or intense metamorphism of older crust. The growth of continents involves both types of crust, but only juvenile crust represents net additions to continental crust.

Growth by Mafic Underplating

Field relationships in exposed lower crustal sections, such as the Ivrea zone in Italy, suggest that many mafic granulites are intrusive gabbros and that additions of mafic magmas to the lower continental crust may be important. Also, a high-velocity layer at the base of Proterozoic shields has been interpreted as a mafic underplate (Durrheim & Mooney, 1991). This accounts for a difference in average thickness of Archean shields ($\sim$35 km) and Proterozoic shields ($\sim$45 km). Just why Archean continents also were not underplated with mafic magma is not understood, but may be related to the thick depleted lithospheric roots beneath Archean cratons that somehow protect the crust from underplating.

One line of evidence that the lower continental crust has grown, at least in part, by underplating of basaltic magma comes from seismology (Nelson, 1991). Strong reflectors, which are widespread in the lower continental crust (see Figure 2.17 in Chapter 2), have generally been interpreted as flows, sills, and layered mafic intrusions. Supporting this conclusion is the fact that some shallow reflectors have been traced to the surface and identified (Percival et al., 1992). Crustal xenolith studies and studies of uplifted segments of the lower crust clearly show mafic intrusions in the lower crust, some of which are considerably younger than their host rocks (Rudnick, 1995; Rudnick & Fountain, 1995).

Another potentially important source of juvenile crust is crustal underplating associated with the eruption of continental flood basalts. Our largest data source for mafic underplating of continental crust comes from the

North Atlantic Igneous Province, where both seismic studies and deep-sea drilling help constrain the volumes of underplated igneous rock (Fitton et al., 1998). Results of these studies show that large volumes of mafic magma (both as basalt flows and intrusives) were emplaced along the transition between continental and oceanic crust during rifting of Laurentia from Baltica. Along more than 2600 km of the propagating coastlines in the North Atlantic (coasts of Greenland and North Europe) during the Early Tertiary, both submarine and subaerial volcanism occurred mainly concentrated in a 1- to 2-Ma period about 57 Ma. Similar widespread volcanism, but more prolonged, occurred along the eastern Coast of North America during the opening of this part of the Atlantic in the Mesozoic (White et al., 1987).

Oceanic Plateaus and Continental Growth

Some or most oceanic plateaus have arc systems erupted along their margins, such as the Solomon Arc along the southern margin of the Ontong-Java Plateau and the Lesser Antilles Arc along the eastern edge of the Caribbean Plateau. During collision and obduction, it is these arcs that are obducted at shallow levels onto continental crust. Although in some instances thick slices of oceanic plateau can also be obducted (20 km for the Caribbean Plateau) or underplated (10 km for the Siletz terrane in Oregon), arcs should greatly dominate in obducted fragments. Perhaps this is the reason for the relative abundance of arc-related greenstones in the geologic record. The high-velocity layer in the lower crust beneath many oceanic plateaus (see Figure 2.3) may represent a mafic underplate composed largely of mafic and ultramafic layered intrusions (Ridley & Richards, 2010).

So what is the fate of oceanic plateaus that collide with continents and lose their surficial arcs by obduction? Three scenarios have been suggested: (1) the oceanic plateaus are completely subducted and thus have no effect on continental growth, (2) the uppermost part of the plateau and its overlying sediments are obducted on to continent, and (3) at least part of the oceanic plateau is underplated beneath the continental margin, thus adding a significant volume of new crust to the continent (Mann & Taira, 2004). In the third case, the plateaus may evolve into lower continental crust with time. Although crustal thickening during collision could result in the production of eclogites in the root zones of accreted plateaus, leading to minor recycling of plateaus into the mantle as suggested by Saunders et al. (1996), a significant volume of these plateaus may be accreted to the continents. This idea has important implications for continental development in that the lower continental crust would comprise a significant contribution of accreted and underplated oceanic plateaus, whereas the upper continental crust would form by subduction-related processes, perhaps beginning before accretion of oceanic plateaus to continental margins. Most of the upper continental crust, however, must develop after collision by subduction-related magmatism as discussed below.

If oceanic plateaus are important in the lower crust, mafic xenoliths derived from the lower crust should carry the geochemical signatures of oceanic plateau basalts. Unfortunately, results are complicated by arc basalts and MORB contained in oceanic plateaus, upper crustal contamination of basaltic magmas, remobilization of elements during high-grade metamorphism and metasomatism, and possibly by later plume-derived and asthenosphere-derived magmas injected into the lower crust (Rudnick, 1992; Downes, 1993; Rudnick & Fountain, 1995). Also at given xenolith localities, the range of compositions can be large, reflecting a mixture of plume and arc-derived components in the lower crust. Clearly, it is going to be a challenging problem using Nd, Sr, and Pb isotopes to sort out accreted plateau sources from later underplated magmas in lower crustal xenolith suites.

The most convincing test for oceanic plateau accretion as a process of continental growth is to identify young accreted oceanic plateaus that are in the process of evolving into continental crust. It is well established that the Mesozoic Cordilleran crust in northwestern North America is relatively immature, and on the whole, more mafic in composition than Precambrian cratonic crust (Condie & Chomiak, 1996; Patchett & Gehrels, 1998). Wrangellia, a dismembered oceanic plateau accreted to northwestern North America in the Late Cretaceous, provides a test for this continental evolution model (Condie, 1997). Using results from several seismic reflection sections from the LITHOPROBE project in Canada (Varsek et al., 1993), Wrangellia can be traced laterally at depth into central British Columbia (Figure 7.8). The eastern margin of Wrangellia is a major transcurrent fault (the Fraser fault) separating the accreted oceanic plateau from the Precambrian craton. Although greenstone basalts with both arc and plume geochemical characters occur in Wrangellia, the average composition of these basalts clearly is plume-like in character. Since accretion to the North American craton, the upper crust in Wrangellia has been intruded by the Coast Range batholith, a complex of felsic plutons carrying a subduction-zone geochemical signature (Nb and Ta depletion) and having juvenile isotopic characters (Samson & Patchett, 1991). Also, the Cascade-Garabaldi arc system and its predecessors have been erupted on the surface of Wrangellia. With the emplacement of the Coast Range batholith and the eruption of arc volcanics, the upper crust of Wrangellia has become more felsic and appears to be evolving into more typical upper continental crust. Perhaps Wrangellia provides us with a young and still evolving example of how continental crust is formed from two sources: the lower crust from an accreted oceanic plateau and the upper crust from subduction-related processes.

Growth by Plate Collisions

Most of the Cordilleran and Appalachian orogens in North and South America represent collages of oceanic terranes added by collision, either at convergent plate boundaries or along transform faults. Lithologic associations, chemical

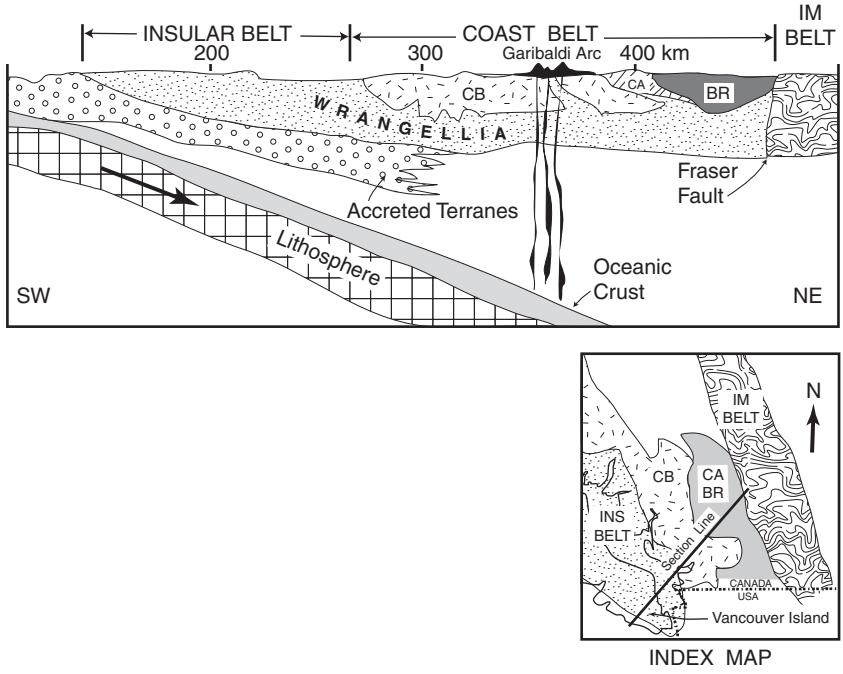

FIGURE 7.8 Interpretive geologic cross section of southeastern British Columbia, Canada, showing possible extent of Wrangellia. INS, Insular belt (Alexander + Wrangellia); CB, Coast Range batholith; CA, Cadwallader terrane; BR, Bridge River terrane; IM, Intermontane belt. *Modified after Clowes et al. (1992) and Condie (1997).*

compositions, terrane life spans, and tectonic histories of Cordilleran terranes in northwestern North America are consistent with collisional growth of the continent in these areas (Condie & Chomiak, 1996; Bahlburg et al., 2009). In addition to the Wrangellia collision described above, remnants of other oceanic plateaus and oceanic crust are found in the American Cordillera. Although some of these terranes began to evolve into continental crust before accretion to North America, most terranes probably began this evolution at or not long before the time they accreted to the continent. This was accomplished largely by incompatible element enrichment resulting from subduction-related processes associated with collisionally thickened crust. In both the North and South American Cordillera, accretionary growth can be tracked from the present day back to the Paleoproterozoic.

One of the highest rates of continental growth by terrane accretion is in the Altaids in eastern Asia. Most of the action in this orogen was between the late Paleozoic and early Mesozoic when numerous juvenile terranes were added to the continental margin of Siberia (Xiao et al., 2009; Wang et al., 2009). Similar accretionary mechanisms have been proposed for Archean orogens based on detailed

mapping, attesting to the operation of plate tectonics at this time (Percival & Williams, 1989; Windley & Garde, 2009). As evidenced by the Andes (Terra Australis orogen) during the Mesozoic-Cenozoic, however, a considerable amount of reworking and recycling of older crust also can occur in accretionary orogens (Bahlburg et al., 2009). Although rates of addition of juvenile continental crust are probably greater in accretionary than in collisional orogens, geochemical and Nd isotopic studies of young collisional orogens such as the Himalayas, show that collisional orogens are also sites of net crustal growth (Mo et al., 2008).

Rates of terrane accretion are also useful in constraining the rates of continental growth. The total lifetimes of accretionary orogens range from as small as 50 Ma in the Archean to more typically 100–300 Ma afterwards (Condie, 2007). The average terrane life span, defined as the difference between the age of the oldest rocks in a terrane (excluding basement) and the age of accretion, is 100–200 Ma in post–1-Ga orogens, 50–100 Ma in Proterozoic orogens, and 70–700 Ma in Archean orogens. The terrane life span is controlled chiefly by (1) terrane tectonic setting, (2) the complexity of precollisional terrane history, and (3) the plate history of ocean basins adjacent to accretionary orogens. Rates of terrane accretion are faster in the Precambrian (100–200 km^3/km/Ma) than afterwards (70–150 km^3/km/Ma), possibly related to more rapid convection in the Precambrian mantle.

CONTINENTAL GROWTH RATES

Continental growth is the net gain in mass of continental crust per unit time. Because continental crust is both extracted from and returned to the mantle, the continental growth rate can be positive, zero, or even negative. Many different models of continental growth rate have been proposed (Figure 7.9). These are

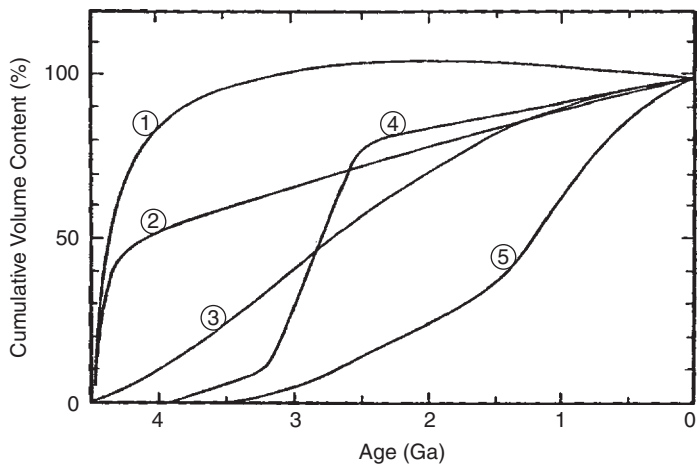

FIGURE 7.9 Examples of published continental growth rate models. See text for explanation.

based on one or a combination of (1) Pb, Sr, and Nd isotopic data from igneous rocks; (2) Sr isotope ratios of marine carbonates; (3) the constancy of continental freeboard through time; (4) Phanerozoic crustal addition and subtraction rates; (5) the aerial distribution of isotopic ages; and (6) estimates of crustal recycling rates into the mantle. Most investigators have proposed growth models in which the cumulative volume of continental crust has increased with time at the expense of primitive mantle, leaving a complementary depleted mantle behind. Some models tacitly assume that the aerial extent of continental crust of different ages preserved today directly reflects the amount of crustal growth through time, an assumption we now know is unrealistic. The earliest models for continental growth were based chiefly on the geographic distribution of isotopic ages in the continents (Hurley & Rand, 1969). These models suggested that continents grew slowly in the Archean and rapidly after 2 Ga (curve 5, Figure 7.9). We now realize that this is not a valid approach to estimating crustal growth rates because many of the Rb-Sr and K-Ar dates used in such studies have been reset during later orogenic events, and the true crustal formation age is older than the reset dates. On the opposite extreme are models that suggest very rapid growth early in Earth's history, followed by extensive recycling of continental sediment back into the mantle (curves 1 and 2) (Reymer & Schubert, 1984). In the model proposed by Fyfe (1978) (curve 1), the volume of continental crust in the Proterozoic actually exceeds that present today. Recycling into the mantle is necessary in the latter two models because we do not see large volumes of old continental crust on Earth today. Other growth models fall between these extremes and include approximately linear growth with time (curve 3) and episodic growth, where continents grow rapidly during certain periods of time, such as in the late Archean (curve 4) (Taylor & McLennan, 1985).

The Role of Recycling

The distribution of juvenile continental crust is a function of two factors: (1) continental extraction rate from the mantle and (2) the rate of recycling of continent back into the mantle. The difference in these two rates is the **net continental growth rate**, which can also be considered as the preservation rate of continental crust. The degree and rate at which continental crust is returned to the mantle is a subject of considerable disagreement and radiogenic isotopic data do not clearly resolve the problem (Armstrong, 1991). One of the major lines of evidence used to argue against a large volume of early Archean continental crust is the small volume of preserved crust $\geq$3.5 Ga, either as crustal blocks or as sediments. Although small in volume, continental crust $\geq$3.5 Ga is very widespread, with one or more examples known on all continents (Figure 7.4), a feature that could indicate that early Archean continental crust was much more extensive than at present. Recycling of this early crust into the mantle is not surprising, as proposed long ago by Armstrong (1981), in that a

hotter mantle in the early Archean should lead to faster and more vigorous convection, which could result in faster crustal recycling than we see today.

The Nd isotopic composition of both detrital and chemical sediments also supports extensive sediment recycling. For instance, on a plot of stratigraphic age versus Nd model age, progressively younger sediments deviate farther from the equal age line (Figure 7.10). This reflects recycling of older continental crust and a progressively greater proportion of older crust entering the sediment record with time. Another process that may have contributed to early crustal recycling is bombardment of Earth's surface with asteroid-size bodies (McLennan, 1988). It is well established that planets in the inner solar system underwent intense bombardment with large impactors until about 3.9 Ga and that such impact on the terrestrial surface could have aided in the destruction and recycling of early continental crust.

Veizer and Jansen (1985) have shown that various tectonic settings on Earth have finite lifetimes in terms of recycling. Contributing to their life spans are rates of uplift and erosion, as well as subduction and delamination. Active plate settings, such as oceanic crust, arcs, and back-arc basins, are recycled much faster than continental cratons. Most active plate settings have recycling half-lives of <50 Ma, whereas collisional orogens and cratons have half-lives of >250 Ma, with finite lifetimes (or oblivion ages) of <100 Ma and >1000 Ma, respectively (Figure 7.11). Because we see small remnants of rocks formed at active plate settings in the geologic record, small amounts of even these tectonic settings may be tectonically trapped in the continents and sheltered from recycling.

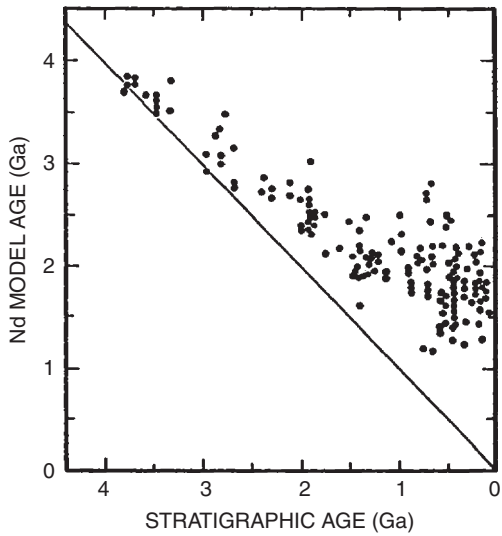

FIGURE 7.10 Comparison of stratigraphic and Nd model ages of fine-grained terrigenous sediments. The diagonal line shows where Nd model age equals the stratigraphic age. Data compiled from many sources.

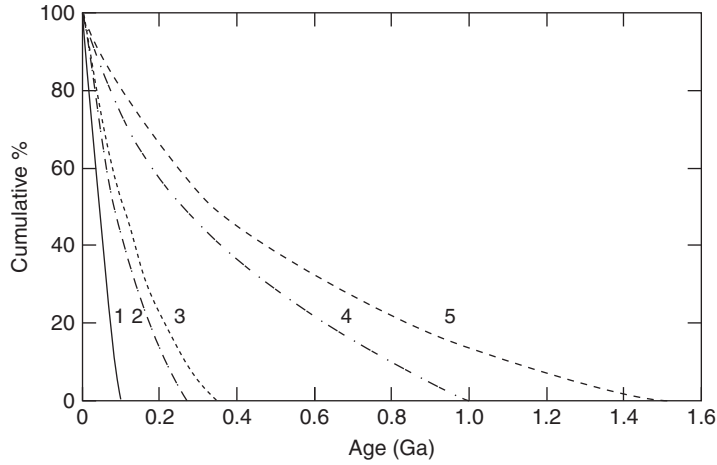

FIGURE 7.11 Mass-age distributions of tectonic settings. Key to tectonic settings with corresponding half-lives: 1, oceanic crust (50 Ma); 2, arc (80 Ma); 3, passive margin (100 Ma); 4, collisional orogen (250 Ma); 5, craton (350 Ma). *Data from Veizer & Jansen (1985).*

There are three processes by which modern continental crust may be destroyed and returned to the mantle (von Huene & Scholl, 1991; Armstrong, 1991; Scholl & von Huene, 2009). These are (1) sediment subduction, (2) subduction erosion, and (3) delamination and sinking of the lower crust into the mantle during collisional orogeny. Sediment subduction refers to sediments that are transported into subduction zones and the sediment is either underplated beneath the arc or carried into the deep mantle (Chapter 3). Subduction erosion is the mechanical plucking and abrasion along the top of a descending slab, which causes a trench's landward slope to retreat shoreward. Subduction erosion and sediment subduction are both potentially important processes in subduction zones. Long-term (10–20 Ma) addition rates and losses can be estimated from data gathered along modern subduction zones. Studies of modern arcs indicate that about half of the ocean floor sediment arriving at trenches is subducted and does not contribute to growth of accretionary prisms (von Huene & Scholl, 1991; Scholl & von Huene, 2009). At arcs with significant accretionary prisms, 70–80% of incoming sediment is subducted, and at arcs without accretionary prisms, all of the sediment is subducted. The combined average rates of subduction erosion (1.4 km^3/y) and sediment subduction (1.1 km^3/y) suggest that, on average, 2.5 km^3 of sediment are subducted each year.

Delamination

Delamination, or **detachment** as it is sometimes referred to**,** is the decoupling and sinking into the asthenosphere of lower crust and lithosphere from the overlying crust. The most important driving force for delamination is negative

buoyancy of the lower continental lithosphere, due primarily to the eclogite phase transition (Meissner & Mooney, 1998; Schott & Schmeling, 1998). Delamination leads to crustal uplift as the dense lithosphere is replaced by lower density asthenosphere. Where negative buoyancy exists in continental lithosphere, whether delamination occurs or not depends on the existence of a suitable zone of decoupling between the less dense portions of the lithosphere and the mantle lithosphere. Viscosity-depth calculations show low-viscosity zones at three depths (Meissner & Mooney, 1998): (1) the base of the felsic upper crust, (2) just above the Moho in the lower crust, and (3) tens of kilometers below the Moho. These low-viscosity zones, in addition to being zones of potential decoupling, are avenues for lateral flow during both compressive and extensional deformation.

Supporting the possibility of modern collisional delamination is a major vertical seismic gap in the Western Mediterranean basin. Tomographic images in this region indicate the presence of a high-velocity slab beneath low-velocity mantle, interpreted to be a piece of delaminated continental mantle lithosphere (Seber et al., 1996). Another example of delamination in an accretionary orogen is the North American Cordillera in California (Lee et al., 2007). Dense restitic material in the lower crust left over from batholith generation may have foundered into the mantle, leaving behind a more felsic crust. Large-scale decoupling between crust and upper mantle in this area is consistent with the distribution of strain in the lithosphere as inferred from such proxies as low P-wave velocities and mafic magmatism (Wernicke et al., 2008).

Delamination is not limited to convergent margins. It would appear that large portions of the root zones of cratons can be removed by later thermal and tectonic activity, as for instance recorded in the North China craton and also probably in the Wyoming craton. Hafnium isotope data from zircons from igneous rocks in the eastern North China craton indicate that widespread late Mesozoic granitoids formed by partial melting of ancient crust with significant input of a mantle component (Yang et al., 2008). The Hf isotopic signatures are interpreted to record the addition of juvenile crust beneath the eastern part of the craton, and the magmatism may have resulted from removal and modification of lithospheric mantle, accompanied by asthenospheric upwelling. Whatever the mechanism, it is apparent that since 200 Ma, ancient lithosphere beneath the eastern North China craton has been progressively reactivated and replaced, resulting in "decratonization."

Juvenile Crust

In this section we describe some of the most important methods used to identify juvenile additions to continental crust, that is, additions that come directly from the mantle with little or no contribution from older continental materials. The primary signals of mantle-derived continental crust are recorded in isotopic systems, of which we describe three: oxygen, neodymium, and hafnium.

Oxygen Isotopes

Oxygen isotopes as discussed in Chapter 6 are fractionated at relatively low temperatures by processes at and near Earth's surface. Thus, if rocks with crustal/atmospheric oxygen isotopic signatures are buried in the crust, for instance during a continental collision, and later they are involved as source materials in magma production, the derivative magmas carry a crustal $\delta^{18}O$ isotopic signature.

The oxygen isotope ratio of zircon has also been shown to effectively trace the contribution of young surface rocks to later magmas (Valley et al., 2005). The asthenospheric mantle is a remarkably homogenous oxygen isotope reservoir and igneous zircons in equilibrium with mantle-derived magma will have average $\delta^{18}O = 5.3 \pm 0.6‰$ (see Figure 6.12 in Chapter 6). Although whole-rock $\delta^{18}O$ values will increase during fractional crystallization, the corresponding $\delta^{18}O$ of zircon does not change significantly (Be'eri-Shlevin et al., 2009). Thus, $\delta^{18}O$ in zircon can be used to track sources of magmas and contamination of magmas by continental crust. For instance, granitoids that have $\delta^{18}O$ values significantly higher than the mantle value have clearly been contaminated with or derived from rocks that once resided at Earth's surface and interacted with the atmosphere–ocean system.

Neodymium Isotopes

One way to recognize juvenile continental crust is with Nd isotopes. Positive εNd(T) values are interpreted to reflect derivation from juvenile sources, whereas negative εNd(T) values reflect derivation from enriched sources (Arndt & Goldstein, 1987). Ages of crust must be determined by some other isotopic system, the most accurate of which is the U/Pb system in zircons. It is now widely recognized that both positive and negative εNd(T) values are recorded in Precambrian crustal rocks, even in the earliest Archean rocks (Figure 7.12a). The vertical arrays of εNd(T) values on an εNd(T)–time plot may be explained by mixing of crustal [negative εNd(T)] and juvenile mantle components [positive εNd(T)] (Figure 7.12b). If this is the case, most of the individual data points cannot be used to estimate the rates and amounts of continental growth and corresponding mantle depletion (Bowring & Housh, 1995). Calculated εNd(T) values as high as +3.5 in 4.0- to 3.8-Ga rocks indicate the presence of a strongly depleted mantle reservoir at that time. The isotopic composition of this reservoir changed very little during the Precambrian, and some of it may be the source of modern ocean ridge basalts. This implies that the isotopic composition of the depleted mantle reservoir was buffered by the addition of either an enriched mantle component or continental crust. Otherwise, the Nd isotopic composition would have evolved along a Nd growth line steeper than that of depleted mantle (DM) (Figure 7.12a). We now recognize that continental crust was available for recycling by 4 Ga as evidenced by the detrital zircon ages from Western Australia.

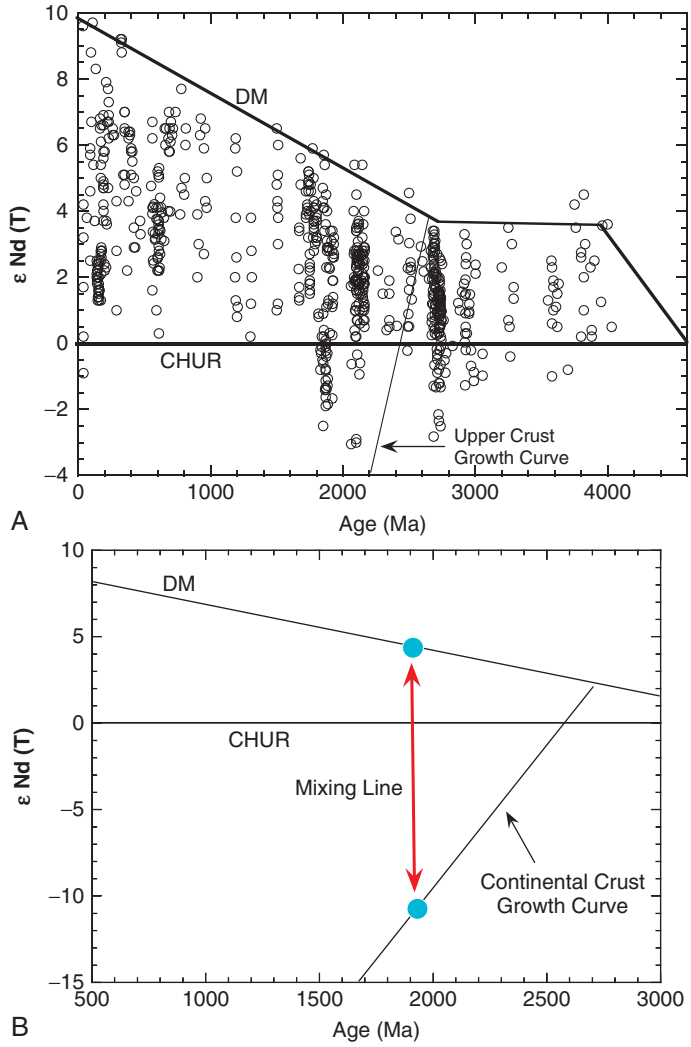

FIGURE 7.12 (A) εNd(T) versus age plot of igneous rocks from convergent margin and greenstone environments. DM, depleted mantle; CHUR, chondritic uniform reservoir. Positive epsilon values reflect depleted mantle sources and negative values reflect enriched mantle sources. $\varepsilon^{143}\text{Nd(T)} = \{[(^{143}\text{Nd}/^{144}\text{Nd})\text{sample}/(^{143}\text{Nd}/^{144}\text{Nd})\text{ standard}] - 1\} \times 10^4$. (B) εNd(T) versus age plot showing how vertical arrays of data can be explained by mixing of juvenile crust from a depleted source (DM) and older continental crust.

A wide range of εNd(T) in the Acasta gneisses and other early Archean rocks requires extreme early fractionation accompanied by efficient recycling to generate these differences in the early Archean (Bowring & Housh, 1995). Because of the relative enrichment of Nd in the continents, it is easier to buffer mantle evolution with subducted continental sediments than with an enriched

mantle reservoir, because of the much smaller volumes of crust required. Armstrong (1981, 1991) proposed a model for continental growth, whereby the amount of recycling decreased with age in parallel with the cooling of Earth. It is interesting that the calculated growth curve for εNd(T) in his model falls near the DM growth curve in Figure 7.12a. Thus, the paucity of early Archean rocks in Precambrian shields may reflect the efficiency of recycling rather than a lack of production of early continental crust. The gradual increase in εNd(T) values in the last 2.5 Ga is consistent with rapid growth of continental crust in the late Archean, causing a decrease in the Sm/Nd ratio in the mantle source, such that later juvenile crust increases more rapidly in εNd(T).

The volume of juvenile continental crust preserved can be estimated from whole-rock Nd isotopes in conjunction with U/Pb zircon ages and geologic maps of varying scales. A new estimate from Condie and Aster (2010) is shown as a histogram in Figure 7.13. Collectively, about 60% of the preserved continental crust falls into one of the four peak clusters. Only 24% of this continental crust formed during the late Archean (2800–2600 Ma), much less than some previous estimates (Taylor & McLennan, 1985; Campbell, 2002). About 20% formed during the Paleoproterozoic (1900–1650 Ma); thereafter, continental preservation rates were relatively small: only 6–10% during each of the Grenvillian (1200–1000 Ma) and Pan-African events (700–500 Ma). Approximately 45% of the existing continental crust appears to have formed in the Archean, and only 15% in the last 700 Ma.

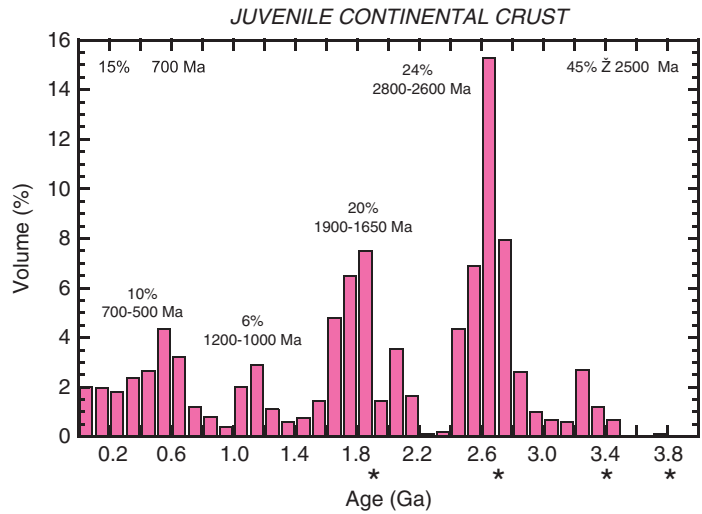

FIGURE 7.13 Volume distribution of juvenile continental crust in 50-Ma bins based on a total volume of continental crust of 7.177×10^9 km^3. Ages are U/Pb zircon ages used in conjunction with Nd isotope data and lithologic associations and percents are the amounts of juvenile continental crust preserved. Asterisks denote episodes of mafic crust formation. *After Kemp et al., 2006; Pietranik et al., 2008. Modified after Condie (1998, 2000).*

Hafnium Isotopes and Detrital Zircons

No other method has had such an impact on dating and tracing the sources of ancient igneous rocks than the combined Hf isotope and U/Pb age analysis of single zircons. The development of laser probe ICP-MS (inductively coupled plasma mass spectrometry) has made it relatively easy to obtain precise U/Pb ages and Hf isotopic compositions from the same zircon, and many such studies have appeared in the last few years (Pietranik et al., 2008; Harrison et al., 2008; Condie et al., 2009a). Although the method is applicable to both igneous and detrital zircons, an advantage of using detrital zircons from modern river systems is that a variety of biases related to sampling of bedrock can be avoided, and river drainages, which sample both bedrock zircons and recycled zircons, may approach a more random sample of the continents. Because single-river drainages clearly show geographic biases in zircon sampling (Condie et al., 2009a; Iizuka et al., 2010), when a global database is used, results show that major age clusters of juvenile crust coincide with reworked crust, and both correlate with supercontinent assembly as discussed in Chapter 8 (Condie et al., 2011). It is noteworthy that there is a scarcity of zircons greater than 3 Ga, indicating that modern river systems do a poor job of sampling very old crust.

The most striking feature of the epsilon distributions in Figure 7.14 is the vertical arrays of data, which define eight peak clusters centered at 2700, 2500, 2010, 1840, 1600, 1150, 600, and 300 Ma. The clusters extend vertically into both positive and negative εHf(T) space, suggesting that whatever their origin, they involve both juvenile [positive εHf(T)] and reworked [negative εHf (T)] continental crust. The greatest contribution of juvenile continental crust is associated with the 1600- and 1150-Ma clusters where more than 40% of the zircons have εHf(T) values greater than +2. The spread of εHf(T) values to less than –10 is more frequent in zircons less than 1000 Ma, indicating a greater degree of reworking and recycling of older continental crust after this time.

Hafnium model ages may be useful in estimating crustal extraction times from the mantle. They are calculated by extrapolating the isotopic growth curve for a sample back to a source, which is often assumed to be depleted mantle (DM). The age intersection may represent the time at which the sample was extracted from the mantle. Hafnium model ages of the detrital zircons calculated with reference to depleted mantle (HfT_{DM}) show an age distribution very different from the U/Pb zircon age distribution (Figure 7.15) (Kemp et al., 2006; Condie et al., 2009a). The model ages do not show distinct pulses like the U/Pb ages, but rather show two broad highs around 3300–2700 and 2200–1800 Ma and suggest that at least 50% of the existing continental crust was extracted from the mantle by 2.5 Ga and 80% by 1.6 Ga (compare this to Figure 7.16). This also implies that the U/Pb zircon ages do not represent crustal production pulses, but "preservation" pulses as discussed in Chapter 8. If significant juvenile continental crust was produced before 3300 Ma, most of it was rapidly recycled into the mantle, since very little continental crust is preserved with older ages.

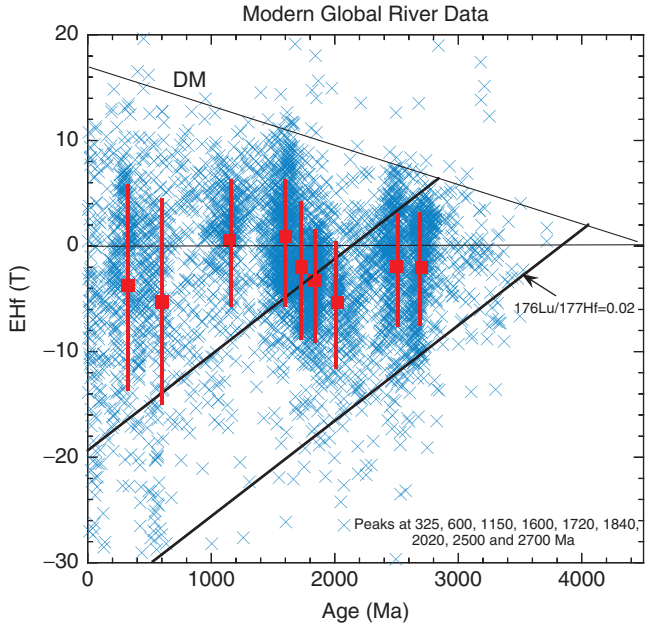

FIGURE 7.14 Distribution of U/Pb ages of detrital zircons from modern river sediments on an εHf(T) versus age plot. DM, depleted mantle growth line. Two growth lines for average continental crust ($^{176}Lu/^{177}Hf = 0.02$) are also shown. Mean values with 1σ uncertainty given for major age clusters. Total number of data points = 3961. $\varepsilon_{Hf}(T) = \{[(^{176}Hf/^{177}Hf)sample/(^{176}Hf/^{177}Hf)\ standard] - 1\} \times 10^4$. *From Condie & Aster (2010).*

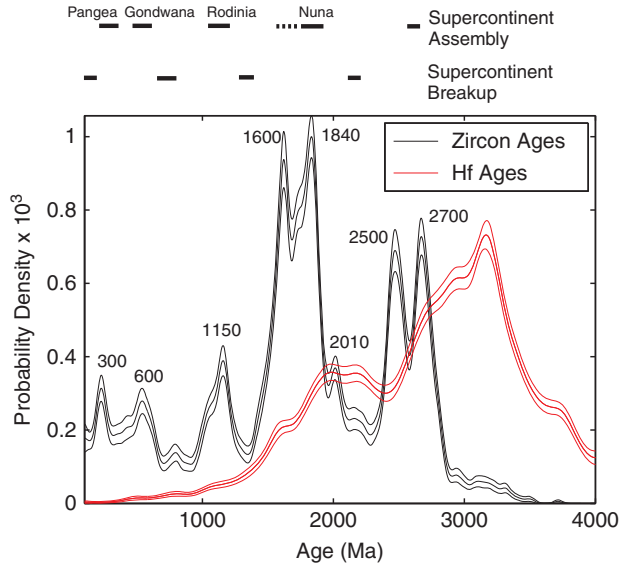

FIGURE 7.15 Probability density distribution of U/Pb detrital zircon ages and Hf model ages of data shown in Figure 7.14. Multiple lines for each spectrum show error bounds of 1σ. Periods of supercontinent assembly and breakup are shown at the top.

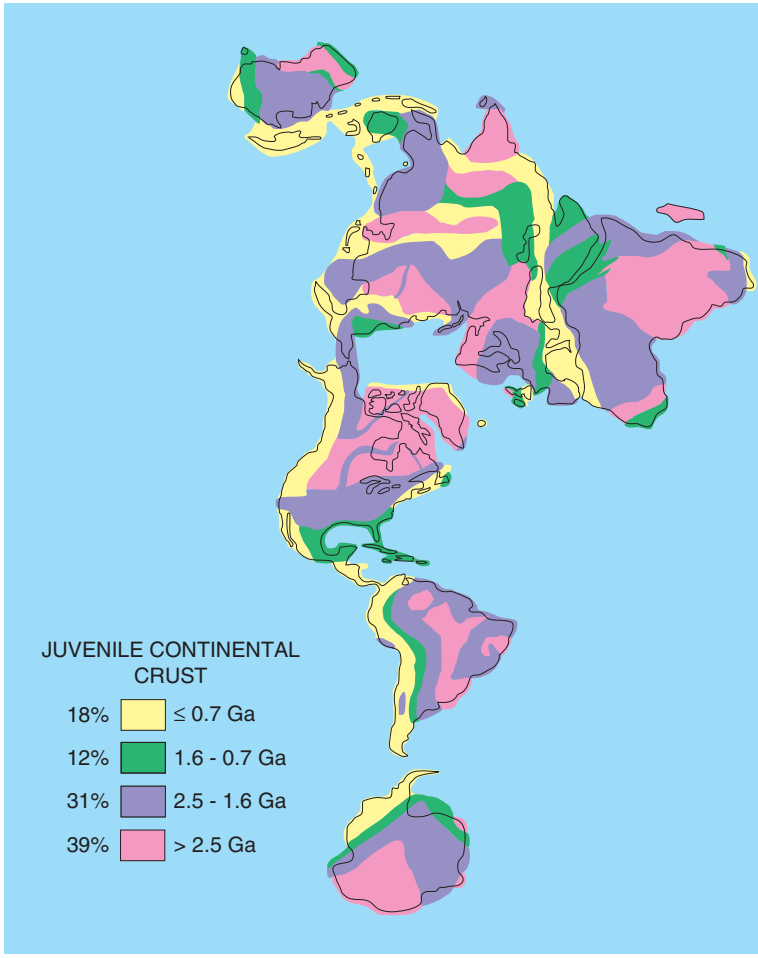

FIGURE 7.16 Distribution of juvenile continental crust shown on an equal-area projection of the continents. Percent by volume. See Figure 7.13 for other information.

The HfT_{DM} model ages also suggest that production of juvenile continental crust after about 1500 Ma was relatively minor. Results from combined Hf and oxygen isotopic data from detrital zircons suggest episodes in production of juvenile mafic crust at about 2700 and 1900 Ma (Kemp et al., 2006; Pietranik et al., 2008) (asterisks in Figure 7.13). This mafic crust may have served, at least in part, as a source for the felsic crust produced at these times. Although very little crust survives that is older than 3 Ga, the detrital Hf isotope data also indicate that 3400 and 3800 Ma were important in terms of mafic crust production (Pietranik et al., 2008). Combined U/Pb and Hf isotope results from global pre–3.2-Ga zircons (both igneous and detrital) suggest three major pulses of

crustal growth: 4.3, 3.9, and 3.3 Ga (Nebel-Jacobsen et al., 2010). The first period around 4.3 Ga was probably mafic crust and the two younger periods largely felsic crust. Significant reworking of 3.9-Ga felsic crust also occurred during the 3.3-Ga event.

Juvenile Crust in Extensional Settings

Although juvenile continental crust is also produced during rifting of supercontinents, the amount of such crust contributing to continents is probably very small. For instance, Stern and Scholl (2010) estimate that at most only 15% of juvenile additions to continents comes from the combined input of continental rift, hotspot (including flood basalts), and rifted continental margin settings. Seismic studies of young passive margins, such as the North Atlantic, reinforce how minor the underplated mafic component is during the opening of ocean basins (Larsen & Saunders, 1999; Reston, 2009). The fact that some unknown amount of the mafic underplate comes from the remelting of the lower continental lithosphere means that even less has juvenile characteristics. Hence, it would appear that at least 80% of juvenile input into the continental crust is associated with subduction zones. In any case, the mafic component added during the breakup of supercontinents would contribute few if any zircons to the detrital zircon database.

Freeboard

If continental area changes by as little as 5%, either significant erosion or flooding of the continental margins should occur (Whitehead & Clift, 2009). The **freeboard** of continents, the mean elevation above sea level, is commonly assumed to be constant with time (Reymer & Schubert, 1984; Armstrong, 1991). If freeboard has remained roughly constant, the ratio of continental to oceanic crust could still change depending on the relative volumes of continental crust and seawater. Together with the volume of ocean ridges, continental crustal thickness exerts a first-order control on global sea level over hundreds of millions of years. Supporting the constant freeboard assumption for the Phanerozoic is the fact that collisional stages of supercontinent growth coincide with global low sea levels and periods of active ocean ridge activity correlate with high sea levels and transgressions (Eriksson, 1999). If freeboard has been constant with time and ocean ridges have diminished in volume due to cooling of the mantle, then the continents must have grown at a steady rate to accommodate the decreasing volume of seawater (curve 2, Figure 7.9).

Although the constant freeboard model is supported by observations from the Phanerozoic, we now realize that this assumption may be inaccurate for the Precambrian (Galer, 1991). One problem is the thick Archean lithosphere, since a thicker lithosphere tends to offset the effects of shrinking ocean ridge volume.

Another is thicker Archean oceanic crust, which would make the Archean oceanic lithosphere more buoyant, and thus add to the volume discrepancy required by a larger volume of Archean ocean ridges. Also, freeboard is especially sensitive to asthenosphere temperature, which was greater in the Archean. For instance, if the upper mantle temperature in the early Archean were 1600°C (about 200°C hotter than at present), much of the continental crust would have been below sea level (Galer, 1991). In terms of the geologic record, evidence for subaerial weathering and erosion first appears in rocks about 3.8 Ga, thus prior to this time continents may very well have been deeply submerged.

The freeboard concept and a constant or variable freeboard over post-Archean time are closely linked to the growth of continents. However, because of the uncertainties in the freeboard of continents with time, and especially because we do yet fully understand the magnitudes of all of the controlling factors, extreme caution should be used when using freeboard to constrain continental growth models.

Continental Growth in the Last 200 Ma

Reymer and Schubert (1984) were the first to estimate the growth rates of young continental crust by estimating the various crustal addition and subtraction rates. Table 7.2 is an updated and revised spreadsheet for continental crust produced in the last 200 Ma based principally on the work Scholl and von Huene (2009) and Stern and Scholl (2010). The results for arc and oceanic plateau crustal addition rates include both arcs and plateaus in ocean basins today and an estimate of the volume of arcs and plateaus accreted to continental margins in the last 200 Ma. Hence, the arc accretion rate (2.5 km^3/y) is considerably greater than the 1.1 km^3/y value of Reymer and Schubert based on "nonaccreted" arcs only. The estimate of 0.5 km^3/y for a combination of plume-related additions (oceanic plateaus, hotspot volcanism, continental underplating) is probably a minimum value. The volume of subducted sediments and material recycled into the mantle by subduction erosion are from Stern and Scholl (2010). The amount of crust returned to the mantle by delamination is poorly known, with estimates ranging from none to perhaps 0.2 km^3/y (I have assumed a value of 0.1 km^3/y). It is striking that the balance sheet comes out approximately to zero (3.2 km^3/y out and 3.3 km^3/y in). This suggests that for at least the last 200 Ma continental crust has been in a state of equilibrium, neither growing nor shrinking in volume.

It is of interest to see if this rate of crustal growth can account for the volume of juvenile continental crust formed in the last 200 Ma as estimated from precise geochronology and Nd isotope studies. Neodymium isotopic data suggest that about 80% of subducted continental crust (by any mechanism) is not recycled at shallow levels in subduction zones, but is instead carried into the deep mantle (Clift et al., 2009). An exception is beneath the Andes, where most of the subducted sediment is underplated beneath the forearc region (Clift & Hartley,

TABLE 7.2 Growth Rate of Continents in the Last 200 Ma

	Rate (km^3/y)
Gains	
Island arcs (1.5), continental arcs (1.0)	2.5
Additions at crust-suturing subduction zones	0.2
Hotspot volcanism, oceanic plateau accretion, continental underplating	0.5
Total Additions	3.2
Losses	
Sediment subduction	–1.1
Subduction erosion	–1.4
Losses at crust-suturing subduction zones	–0.7
Delamination	–0.1
Total	–3.3
Net Growth Rate (3.2 km^3/y – 3.3 km^3/y)	–0.1

Arcs, oceanic plateaus, and hotspot volcanics include also an estimate of those accreted to the continents in the last 200 Ma.
Source: After Scholl & von Huene (2009) and Stern & Scholl (2010).

2007). Regional sedimentation rates suggest that most orogens have their topography removed by erosion in 100–200 Ma. Accretion of sediment to active continental margins is a small contribution to crustal construction (ca. 0.2–0.3 km^3/y). Similarly, LIP flood basalts add only around 0.12 km^3/y, including their intrusive roots. If oceanic plateaus are accreted to continental margins, average construction rates may be as high as 1.1 km^3/y, meaning that to keep constant crustal volumes, recycling rates into the mantle would have to be around 3.8 km^3/y, which is considerably higher than the estimated rates (Table 7.2). This result clearly suggests that oceanic plateaus are at best only partly accreted to continental margins.

Toward a Continental Growth Model

The Approach

Net continental growth rate in the geologic past, which can also be considered as the preservation rate of continental crust, is critically dependent on two factors (Condie, 1990b): (1) the proportion of reworked crust within a given crustal

province and (2) the growth length intervals assumed. The volume of juvenile crust g extracted from the mantle during a specified time interval $\triangle t$ is given by:

$$g = a - r + m \tag{7.1}$$

where a is the volume of crust formed during $\triangle t$; r is the volume of reworked crust that must be subtracted; and m is the volume of crust formed in $\triangle t$, but now tectonically trapped as blocks in younger crust. The value of a is determined from the scaled area of crustal provinces/terranes of a given age times the average crustal thickness. The final crustal thickness includes a 10-km-thick restoration of crust lost by erosion for a total average thickness of 45 km. Values for r and m are estimated from published Nd isotopic data, Hf isotope data and U/Pb zircon ages, and detailed geologic maps. Growth is considered in 100-Ma increments. The amount of reworked crust in a given crustal province is estimated from Nd and Hf isotopic data, assuming mixing of juvenile and evolved end members (Arndt & Goldstein, 1987) and from the distribution of detrital and xenocrystic zircon ages. Volumes of reworked crust are redistributed into appropriate earlier growth intervals.

The Model

Because of extensive reworking of older crust in some areas, only the most intense and widespread orogenic events are used in delineating the distribution of juvenile crust. Most crustal provinces <2.5 Ga contain variable amounts of reworked older crust. Early Archean (>3.5 Ga) crustal provinces, although widely distributed, are very small (chiefly <500 km across; Figure 7.4) and may represent remnants of Earth's early continents.

Isotopic age data have been compiled and major juvenile crustal provinces are shown on an equal area map projection of the continents in Figure 7.16. Aerial distributions indicate that at least 45% of the presently exposed continental crust formed in the Archean, 28% at 2.5–1.6 Ga, 12% at 1.6–0.7 Ga, and 15% in the last 0.7 Ga. Clearly portrayed on the map is the strikingly irregular distribution of juvenile crust with time. Whereas most of Africa, Antarctica, Australia, and the Americas formed in the Archean and Paleoproterozoic, much of Eurasia formed in the Meso-Neoproterozoic and Phanerozoic. Late Archean provinces (3.0–2.5 Ga) are widespread on all continents and probably underlie much of the platform sediment (or ice) in Canada, Africa, Antarctica, and Siberia. Paleoproterozoic provinces (2.0–1.7 Ga) are widespread in North America and in the Baltic shield in Europe, and form less extensive but important orogens in South America, Africa, and Australia. Mesoproterozoic provinces (chiefly 1.3–1.0 Ga) occur on almost all continents where they form narrow belts along which the Mesoproterozoic supercontinent Rodinia was sutured together. Unlike older crustal provinces, little juvenile crust is known of this age. Neoproterozoic provinces (0.8–0.55 Ga) are of importance only in South America, Africa, southern Asia, and perhaps in Antarctica.

THE 2.4- TO 2.2-GA CRUSTAL AGE GAP

The distribution of U/Pb zircon ages from both granitoids and detrital sediments shows an exceptionally strong minimum between about 2400 and 2200 Ma (Figure 7.17) (Condie et al., 2009b). The fact that the minimum is well defined in both granitoid and in detrital zircon populations is remarkable, since the sampling control and bias are very different in the two populations. While the granitoid zircon ages largely reflect areas where geologists have worked, the detrital zircon ages sample parts of the continental crust where river systems

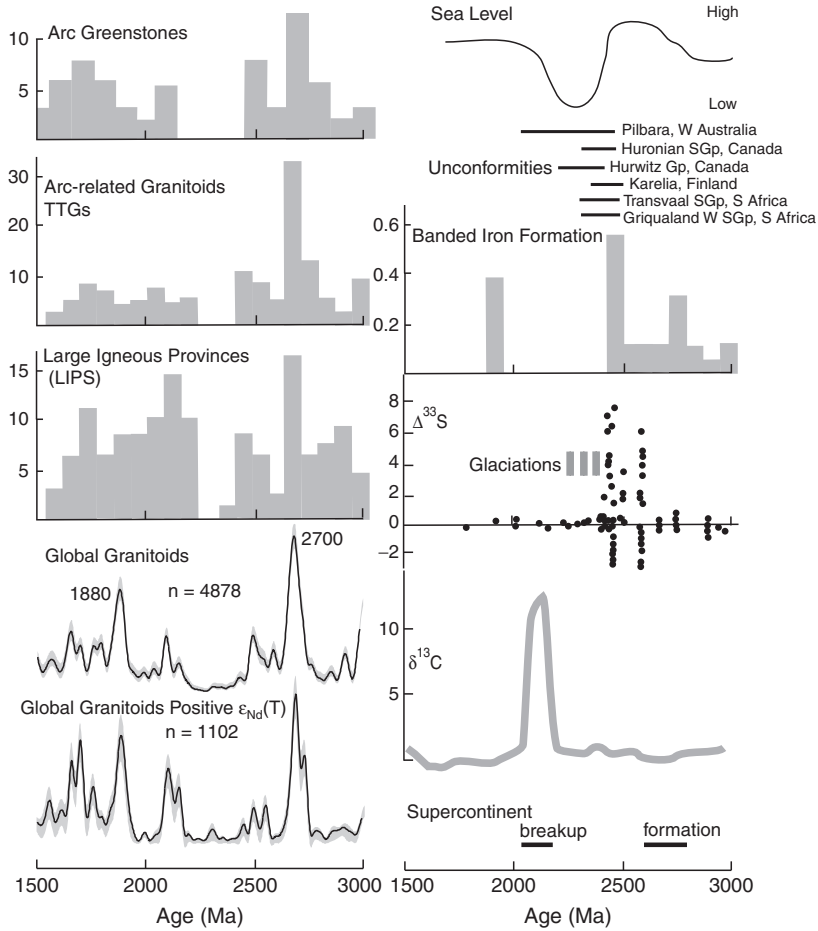

FIGURE 7.17 Secular distribution of U/Pb zircon ages, rock types, and other features between 3000 and 1500 Ma. Vertical axis for greenstones, granitoids, and LIPs is number of occurrences; vertical axis for banded iron formation is fraction of known iron ore reserves. *Modified after Condie et al. (2009).*

have propagated and sediments have been preserved. As the database of zircon ages has grown, the 2400- to 2200-Ma minimum has persisted, suggesting that it is robust and not due to inadequate sampling of rocks of these ages. In addition there is little Nd or Hf isotopic evidence to support significant additions to the continental crust at convergent plate margins between 2.4 and 2.2 Ga (Figures 7.12a, 7.13, and 7.14). Condie et al. (2009b) have suggested that this unusual period of time be referred to as a **crustal age gap**. During the crustal age gap, arc-type greenstones show a dramatic decrease in abundance, and the TTG suite, which is widespread in Archean continental crust, is also rare. Granitoids produced during the 2.4- to 2.2-Ga crustal age gap are chiefly granites with continental rift or continental back-arc affinities (Hartlaub et al., 2007) derived from older crustal sources. Remnants of large igneous provinces (LIPs), which probably formed from mantle plume sources, show a similar age distribution to arc-type greenstones (Figure 7.17).

Constraints from the geologic record suggest that a global reduction in magmatic activity and crust production between 2.4 and 2.2 Ga could be caused by a period of extended tectonic quiescence due to widespread lithospheric stagnation characteristic of an episodic mantle overturn regime (O'Neill et al., 2007b). Also, ocean ridge volume should have dropped as oceanic lithosphere cooled, leading to deeper ocean basins and lower sea level (Moucha et al., 2008), and a drop in sea level should lead to extensive erosion on the continents and, therefore, to widespread unconformities in the stratigraphic record. As shown in Figure 7.17, this is precisely what is observed: major unconformities representing 100 to over 300 Ma of time occur on most cratons during the crustal age gap.

The largest volume of banded iron formation (BIF) was deposited at about 2.45 Ga (Hamersley basin, Western Australia) followed by a BIF depositional gap until about 1.9 Ga. This is consistent with a widespread shutdown of submarine magmatism, which would decrease Fe^{2+} input into the oceans, and thus the rate of BIF deposition. The resumption of submarine volcanic activity and LIP activity at 2.2 Ga may have led to renewed deep-sea hydrothermal activity with Fe^{2+} input, as well as redevelopment of marginal basins, and thus contribute to renewed deposition of BIF at 1.9 Ga.

What changes in the carbon cycle might result from a lull in global magmatism? A widespread slowdown of global volcanism and the increased area of the continents exposed to weathering due to a sea level drop would decrease the rate of CO_2 input into the atmosphere–ocean system. This, in turn, could lead to global cooling and hence to the global glaciation observed at 2.4–2.3 Ga. The end of mass-independent sulfur isotope fractionation (S-MIF) and associated oxygenation of the atmosphere at 2.35 Ga (the Great Oxidation Event, Chapter 9) approximately coincides with the onset of the hypothesized magmatic slowdown (Figure 7.17). Contributing to oxidation is a global drop in submarine volcanism, which decreases the input of H_2 and H_2S into the oceans, which normally act as reductants for oxygen. In addition, an increase in phosphorus delivered to the oceans from extensive erosion of the

continents could enhance biomass production, leading to more O_2 production (Aharon, 2005). All three of these effects may have provided positive feedback for oxygen entering the atmosphere at 2.35 Ga. As discussed in Chapter 6, the positive $\delta^{13}C$ excursion in inorganic carbon at about 2.2 Ga, which coincides with the proposed resumption of widespread magmatism, may reflect increased burial of organic carbon at this time or/and enhanced methanogen activity. At about 2.2–2.1 Ga, late Archean supercratons began to fragment and disperse (see Chapter 8), and thus create anoxic basins where methanogen activity may have increased.

Although it is clear that a large number of geologic events occurred during the 2.4- to 2.2-Ga time window, it is not yet understood how and if these events are related. If they are related, some global change must have occurred in planet Earth that had far-reaching effects into many if not all terrestrial subsystems, including not only deep-seated reservoirs but also shallow and surficial reservoirs. One global change that might tie all of these seemingly unrelated events together is a partial shutdown of global magmatism. Because most of Earth's magmatism is closely tied to plate tectonics, could this mean that plate tectonics shut down, or at least slowed down, for 200 Ma? We will return to this exciting possibility in Chapter 9.

SECULAR CHANGES IN THE CONTINENTAL CRUST

As a constraint on the evolution of the crust–mantle system, it is important to know if the composition of continental crust has changed with time. Some investigators have used fine-grained terrigenous sediments to monitor changes in upper crustal composition (Rudnick & Gao, 2004). Justification of this approach relies on mixing of sediments during erosion and sedimentation, such that shale, for instance, reflects the composition of large continental areas. Only those elements that are relatively insoluble in natural waters, and thus transferred in bulk to sediments, can be used to estimate crustal composition (such elements as Th, Sc, and the rare earth elements [REE]). Some studies have compared sediments of different ages from different tectonic settings, thus erroneously identifying secular changes in crustal composition, which in fact, reflect different tectonic settings (Gibbs et al., 1986). The prime example of this is comparison of Archean greenstone sediments (dominantly volcanigenic graywackes) with post-Archean cratonic sediments (dominantly cratonic shales) and interpreting differences in terms of changes at the Archean–Proterozoic boundary (Veizer, 1979; Taylor & McLennan, 1985). Another limitation of sediments in monitoring crustal evolution results from recycling of older sediments, which leads to a buffering effect through which changes in juvenile crustal composition may not be recognizable (Veizer & Jansen, 1985; McLennan, 1988). For sediment geochemical results to be meaningful, sediments should be grouped by average grain size and by lithologic association, which in turn reflects tectonic setting.

Major Elements

There have been numerous studies of secular changes in major element distributions, most of which have concentrated on detrital sediments. Some investigators have suggested that the proportions of sedimentary rocks have changed with time and are responsible for possible secular changes in major element concentrations (Engel et al., 1974; Schwab, 1978; Ronov et al., 1992). However, all of these studies suffer from the same problem: indiscriminately lumping sediments together from different tectonic settings. Thus, although significant changes in lithologic proportions and element distributions have been proposed, their existence is questionable.

Only three major element trends are well documented from sampling of bedrock in Precambrian shields as described in Chapter 2. Results suggest that Ti increases and Mg decreases, and that there is an increase in the K/Na ratio near the end of the Archean (Figure 7.18) (Condie, 1993, 2008). The changes in Ti and Mg appear to reflect a decrease in the amount of komatiite and high-Mg basalt in continental sources after the Archean. The increase in K/Na ratio at the end of the Archean reflects a decrease in the proportion of TTG (Na-rich) to calc-alkaline granitoids (K-rich) (Condie, 2008).

Rare Earth and Related Elements

Based on bedrock sampling of Precambrian shields, at the end of the Archean, average upper continental crust increases in P, Nb, Ta, and to some degree in Zr and Hf (Condie, 1993). Also, Rb/Sr and Ba/Sr ratios increase at this time. The Th/Sc

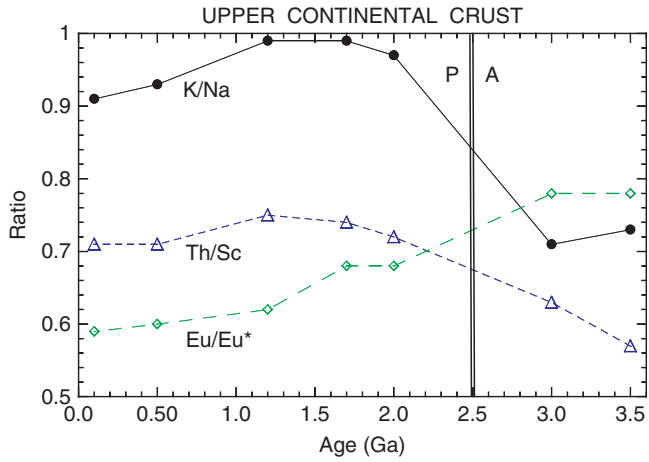

FIGURE 7.18 Distribution of K/Na, Th/Sc, and Eu/Eu* in upper continental crust with time. Eu/Eu* is a measure of the Eu anomaly with positive Eu anomalies having values >1 and negative anomalies with values <1. $Eu/Eu^* = Eu_n/(Sm_n \times Gd_n)^{0.5}$, where n stands for chondrite-normalized values. (Eu* is the interpolated Eu value on a chondrite-normalized REE plot). Estimated errors for ratios range from 1 to 2 times the size of the plotting symbol. A, Archean; P, Proterozoic. *Data from Condie (1993).*

ratio shows only a moderate increase at the A/P (Archean–Proterozoic) boundary (Figure 7.18). Although the sediment data suggest that the Th/U ratio increases with time, there is no evidence for secular variation of this ratio in the shield data (Figure 7.19).

At the end of the Archean, there is also a notable decrease in fractionation of REE, as shown by a decrease in the (La/Yb)n ratio and a small increase in the Sm/Nd ratio in the upper crust (Figure 7.19). The Sm/Nd ratio of continental shales has remained about constant with time at 0.18, and agrees well with the average ratio of upper crust today.

Taylor and McLennan (1985) have long maintained that post-Archean sediments differ from Archean sediments by the presence of a negative Eu anomaly (represented by Eu/Eu* <1; Figure 7.18). However, it is difficult to test their conclusion because it is based on comparing largely greenstone sediments from the Archean with cratonic sediments in the post-Archean. Precambrian shield results indicate that both Archean shales and Archean upper continental crust have sizable negative Eu anomalies (Eu/Eu* <1), and that there is only a modest change at the end of the Archean (Condie, 1993; Gao & Wedepohl, 1995) (Figure 7.18). The major contributing factor appears to be a decrease in the proportion of TTG (high Eu/Eu*) to calc-alkaline granitoids (low Eu/Eu*) after the Archean (Condie, 2008). Negative Eu anomalies, however, are not limited to post-Archean rocks, and both Archean shales and granites typically show sizable anomalies.

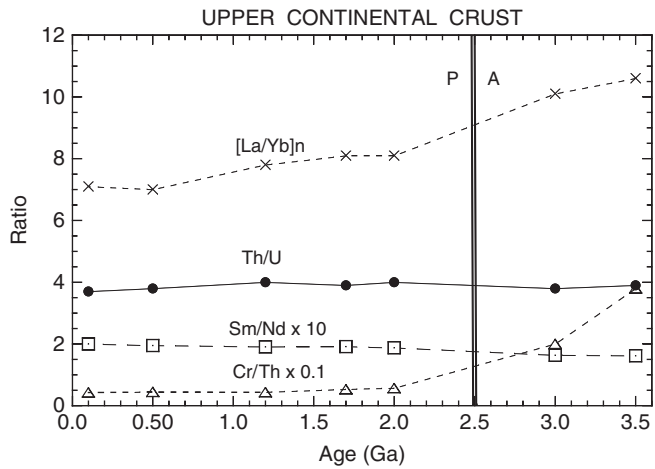

FIGURE 7.19 Distribution of Cr/Th, Th/U, Sm/Nd, and (La/Yb)n in upper continental crust with time, where n refers to chondrite-normalized ratio. See Figure 7.18 for other information.

Nickel, Cobalt, and Chromium

Decreases in Ni, Co, and Cr as well as in Cr/Th, Co/Th, and Ni/Co ratios are observed at the A/P boundary in both upper continental crust and in fine-grained cratonic sediments (Taylor & McLennan, 1985; Condie, 1993) (Figures 7.19 and 7.20). These changes reflect a decrease in the amount of both high-Mg basalt and komatiite in continental sources after the end of the Archean. A striking example of this decrease occurs in Precambrian cratonic sediments of the Kaapvaal craton in southern Africa (Condie & Wronkiewicz, 1990). A decrease in Cr/Th ratio in Kaapvaal sediments near the A/P boundary probably reflects a decrease of komatiite and high-Mg basalt sources.

Oceanic Plateaus as Starters for Archean Continents

If plate tectonics did not become really widespread on Earth before the late Archean (Chapter 9) yet we have evidence of at least small patches of continental crust produced before this time, how did this crust form? Perhaps the first continental nuclei were oceanic plateaus produced from mafic and komatiitic melts extracted from mantle plumes. The plume model provides a means of obtaining komatiites and basalts from the same source: komatiites from the high-temperature plume tail and basalts from the cooler head (Campbell et al., 1989). The residual material would be depleted from melt extraction, and thus be relatively low in garnet, which would make it buoyant. This spent plume material may underplate the oceanic plateaus, thus contributing to the thickening of the lithosphere beneath Archean cratons (Wyman & Kerrich, 2002).

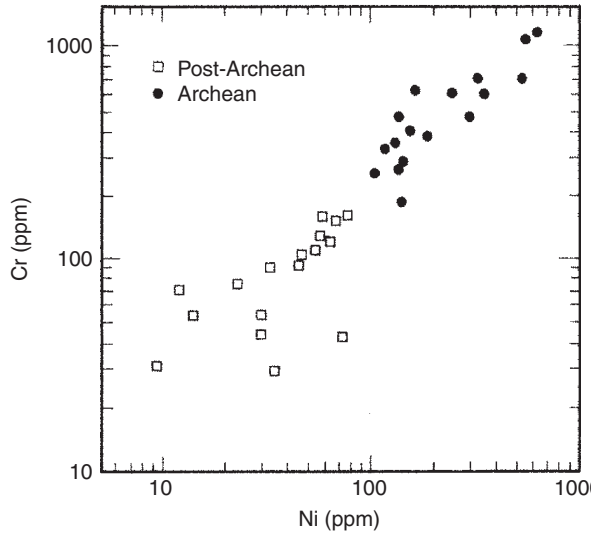

FIGURE 7.20 Cr-Ni distribution in cratonic fine-grained detrital sediments.

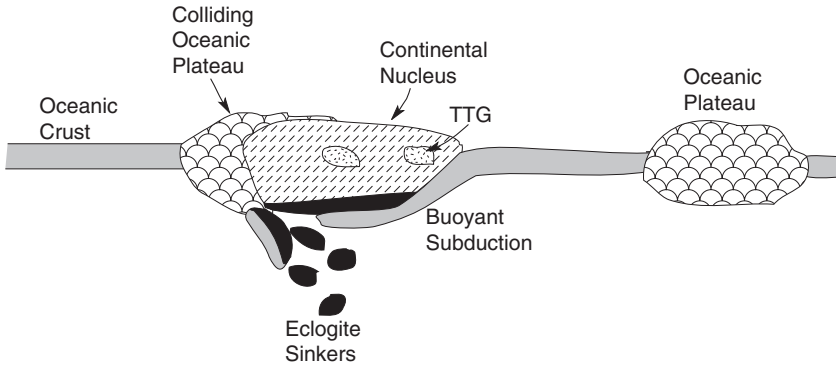

FIGURE 7.21 An oceanic plateau model for the formation of early Archean continents. TTG, tonalite-trondhjemite-granodiorite.

Whether subduction processes or partial melting of thick oceanic plateaus formed the first Archean felsic crust is a hotly debated subject. Young dacites have been found in Iceland that have many of the geochemical features of Archean TTGs, and model calculations indicate that they were produced by deep partial melting of mafic lower crust followed by fractional crystallization of amphibole, plagioclase, and ilmenite (Willbold et al., 2009). Similar results are reported for a partially subducted oceanic plateau in Jamaica (Hastie et al., 2010). Hence, it is possible that the mafic roots of oceanic plateaus can give rise Archean TTG magmas (Figure 7.21). Buoyant subduction around the perimeters of the plateaus should result in both lateral continental growth and thickening of the lithosphere (Abbott & Mooney, 1995). Thin slabs of oceanic crust may be obducted, remnants of which may be preserved in some Archean greenstones. Because these slabs are thin, they would not include complete ophiolites. Collision of other oceanic plateaus (and island arcs if plate tectonics was operative) would also contribute to the growing continental nuclei. Descending slabs would sink, either because of their negative buoyancy or/and because of eclogite production in buoyantly subducted oceanic crust (Figure 7.21). TTG could be produced in the mafic descending slabs, in the thickened mafic continental roots, or in the sinking eclogite blocks (Bedard, 2006). The major requirement is that garnet must be left in the restite to explain heavy REE depletion in Archean TTG.

SECULAR CHANGES IN THE MANTLE

To track secular changes in the mantle, we use a combination of direct and indirect approaches. Incompatible element distributions in basalts carry the signature of their mantle sources, provided they have not been disturbed by later events or contaminated with continental crust. Hence, we can learn a great deal

about the Precambrian mantle by using the compositions of basalts from oceanic greenstones if we can avoid or filter out the effects of secondary processes. Another approach to tracking mantle composition is the use of mantle xenoliths derived directly from the mantle lithosphere. Here we have to worry about the effects of mantle metasomatism on changing the distributions of incompatible elements. Finally, we can use thermal modeling of the mantle to track the history of convection and plate tectonics.

Tracking Mantle Geochemical Components into the Archean

Because most isotopic ratios can be changed during metamorphism and alteration of greenstones, ratios of high-field-strength elements (Zr, Nb, Th, REE), which are more resistant to change, are used to characterize Archean greenstone mantle sources, rather than the Sr, Pb, and Nd isotopes used today (Chapter 4). Using Zr/Nb and Nb/Th ratios to track mantle source compositions, there are two general populations of late Archean oceanic, non–arc-related basalts (Figure 7.22). Most of the data plot in a broad array between continental lithosphere (EN) and primitive mantle (PM). Those basalts that fall near the EN component are suggestive of mixing between deep mantle sources and continental lithosphere. The scattering of many Archean oceanic basalts around

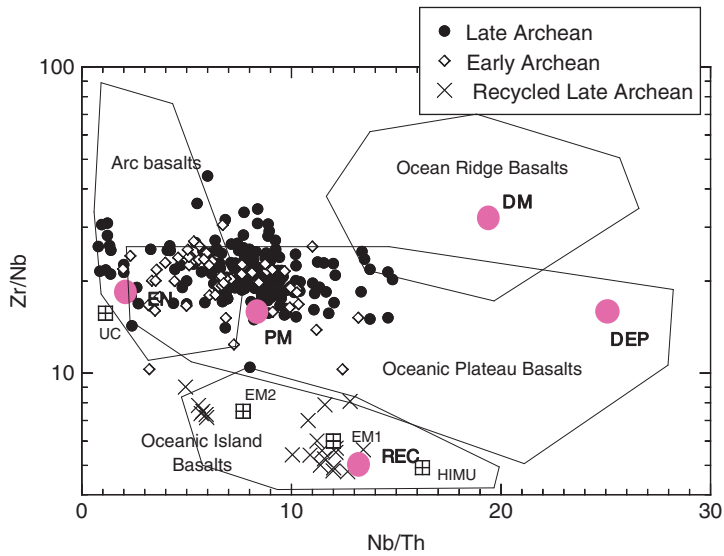

FIGURE 7.22 Nb/Th–Nb/Zr graph showing distribution of non–arc-related Archean greenstone basalts. UC, upper continental crust; PM, primitive mantle; DM, depleted mantle; DEP, deep depleted mantle; EN, enriched mantle (subcontinental lithosphere); REC, recycled mantle components; EM1, EM2, enriched components in the mantle; HIMU, high μ component. Each data point is average value from specific greenstones.

PM may reflect derivation from relatively undepleted, pristine mantle sources. Perhaps the most striking observation is that there is no clear indication for a shallow depleted mantle source (DM) in the Archean. However, if Archean ocean ridge basalts came from an undepleted PM-like source, it may not be possible to distinguish ocean ridge from oceanic plateau basalts in the Archean (Figure 7.22). A second population, represented only by late Archean data, falls near the recycled mantle component (REC), suggestive of affinities to modern oceanic island basalts. This indicates that significant recycling of oceanic crust into the deep mantle did not begin until the late Archean, an observation consistent with plate tectonics not becoming widespread until this time (Chapter 9). Thus, it would appear that geochemistry by itself cannot distinguish between oceanic and oceanic plateau basalts in the Archean.

Mantle Lithosphere Evolution

Continental Lithosphere

The continental lithosphere has had a complicated history, perhaps involving more than one growth mechanism and changes in growth mechanisms at the end of the Archean. The post-Archean subcontinental lithosphere may contain remnants of "spent" mantle plumes. That is, mantle plumes that rose to the base of the lithosphere partially melted, producing flood basalts, and the restite remained behind as a lithospheric underplate. Seismic reflection results, however, suggest that at least some of the continental lithosphere represents remnants of partially subducted oceanic lithosphere (see Figure 2.2). In northern Scotland, for instance, dipping reflectors in the lower lithosphere are thought to represent fragments of now eclogitic oceanic crust, a relic of pre-Caledonian oceanic subduction (Warner et al., 1996). Isotopic data from xenoliths also indicate that some asthenosphere is added directly to the subcontinental lithosphere.

The relationship of mantle lithosphere to its overlying crust is important in understanding the origin of continents and whether plate tectonics and crustal growth have changed with time. As discussed in Chapter 4, average subcontinental lithospheric mantle composition is broadly correlated with the age of overlying crust, suggesting that mantle lithosphere and overlying crust formed at approximately the same time (Griffin et al., 1999). In terms of Al and Ca, lithospheric mantle has become progressively less depleted from the Archean to the Phanerozoic (Figure 7.23). High Ca and Al contents reflect primitive, unfractionated mantle and low values indicate depleted mantle in which significant amounts of basaltic melt have been removed. Garnet lherzolite xenoliths from young extensional regimes are chemically similar to primitive mantle, indicating very small amounts of melt extraction. In contrast, Archean xenoliths have very low Ca and Al, indicating significant melt loss. Although the details of this secular evolution in composition are not well understood, in a general way it probably reflects the cooling of the mantle with time

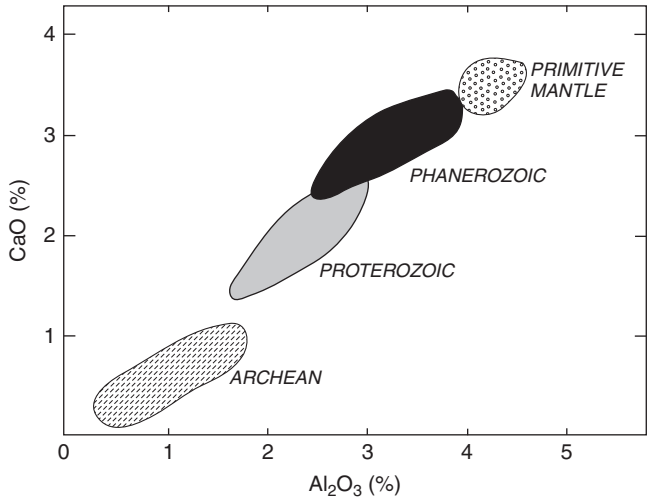

FIGURE 7.23 $CaO–Al_2O_3$ plot showing the range of mantle lithosphere compositions calculated from garnet xenocrysts. *Modified after O'Reilly et al. (2001).*

(Griffin et al., 2003). Higher degrees of melting in the Archean led to greater melt production and as the mantle cooled, melt production gradually decreased.

As discussed in Chapter 4, the lithospheric roots of Archean cratons are anomalously thick, some extending to 350 km deep. These cool, buoyant roots may be the reason that Archean cratons have survived to the present. Why and how did these roots get so thick? Three tectonic scenarios have been proposed (Lee, 2006; Arndt et al., 2009). The first is melting in a mantle plume head, with the restite material plastered beneath the new crust forming a thick root (Figure 7.24a). This mechanism results in progressive change of the residue with time from fertile lherzolite at first through residues of varying degrees of melting to the last stage of very refractory dunite. The process leaves very Mg-rich olivine in the restite, which is similar to that found in mantle xenoliths from beneath Archean cratons. Because melt extraction removes volatiles, the residue is anhydrous, has a low density, and is gravitationally stable; thus, it contributes to the long-term stability of the craton.

A second model (Figure 7.24b) calls upon underthrusting of oceanic slabs along marginal subduction zones, accreting the slabs to the base of the lithosphere. This model is attractive in that it explains the dipping seismic reflectors in the Archean crust (see Figure 2.2). One of the main problems with the model is that eclogite xenoliths, which would represent fragments of the underthrust oceanic crust, are rare in most Archean cratons. Also, with such a high proportion of garnet-rich lherzolites (undepleted), the accreted slabs would probably have not been buoyant enough to survive for billions of years.

The last model calls on reprocessing of material in the mantle wedge above subduction zones (Figure 7.24c). Here, relatively fertile lherzolite is transformed into a more refractory residue by melting, which is triggered by fluids escaping from

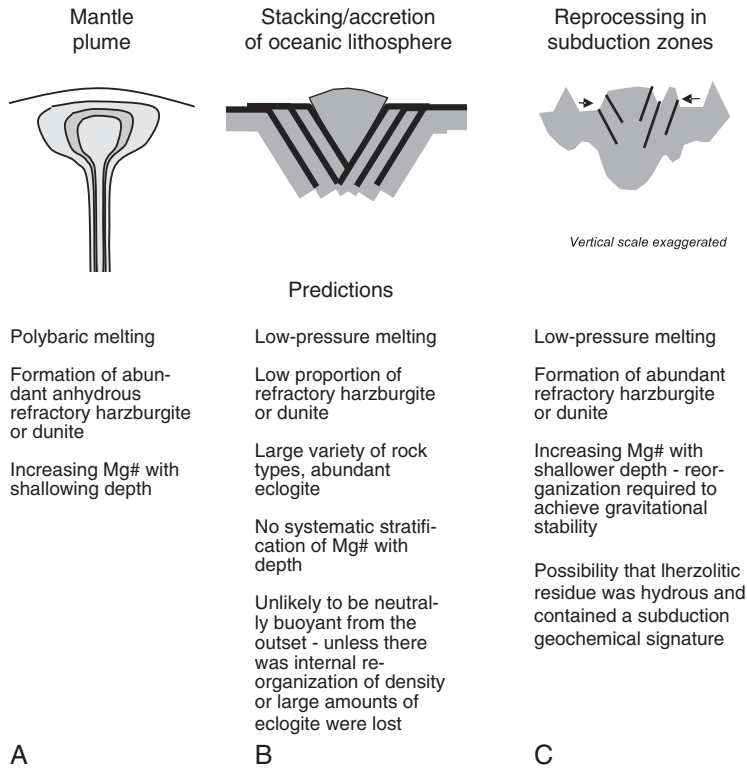

FIGURE 7.24 Models for development of thick lithospheric roots. *Modified after Lee (2006). Reproduced with permission of American Geophysical Union.*

dehydrating descending slabs. One problem with the model is the question of whether or not hydrous melting can leave a residue, which is anhydrous, a feature necessary for long-term survival. Also, the xenoliths from this underplate do not typically show a subduction geochemical signature (Nb-Ta depletion; Chapter 3).

Although the mechanism of thickening the lithosphere beneath Archean cratons continues to be a subject of hot debate, the mantle plume residue model (Figure 7.24a) seems to have the fewest number of obstacles (Arndt et al., 2009). The highly refractory, Fe-poor composition of mantle xenoliths can be explained only by melting in a high-temperature source, for which mantle plumes seem to be the only way to provide such high temperatures.

Oceanic Lithosphere

Ophiolites

As discussed in Chapter 3, a complete ophiolite includes, from bottom to top, ultramafic tectonite, layered and nonlayered gabbros and ultramafic rocks, sheeted diabase dykes, and pillow basalts. If we adhere strictly to this

definition, the oldest known ophiolites are about 2 Ga. Although older Archean ophiolites have been described, they lack one or more of the ophiolite components and, hence, may not be fragments of oceanic crust (Bickle et al., 1994). They cannot be rejected as oceanic crust on this basis only, however, because like most younger ophiolites, they may be "dismembered" ophiolites. The oldest sequence claimed to be an ophiolite is part of the 3.8-Ga Isua supracrustal sequence in Southwest Greenland (Furnes et al., 2007). However, other investigators have shown that, although largely mafic and ultramafic, the Isua rocks are highly sheared and altered and the protolith is problematic. Other Archean "ophiolites" are equally controversial (Kusky & Polat, 1999; Kusky, 2004; de Wit, 2004). A summary of ophiolite characteristics is given in Table 7.3 comparing young ophiolites with rocks that have been described as Archean ophiolites. Very few characters are diagnostic and most of these are relatively rare even in Cenozoic ophiolites. Although it is likely that remnants of Archean oceanic crust survive in Archean greenstones, it would appear that a convergence of characteristics is necessary to identify these remnants—and that is the case *only* if Archean oceanic crust were similar to young oceanic crust.

Why are complete ophiolites extremely rare or missing in the Archean? There are at least two possible explanations assuming that plate tectonics was operating in the Archean: (1) Archean ophiolites have been overlooked

TABLE 7.3 Characteristics of Ophiolites

Character	Importance	Cenozoic ophiolites	Archean "ophiolites"
Full sequence (Figure 3.2)	Diagnostic	Rare, ≤15%	None
Podiform chromite	Diagnostic	Uncommon 10–15%	None
Sheeted dykes	Diagnostic	20–30%	Rare to absent
Mantle tectonites	Distinctive	20–30%	Rare
Cumulates	Inconclusive	~70%	Present
Layered gabbro	Typical	~70%	Present
Pillow lavas	Ubiquitous	≥90%	Common
Chert	Typical	≥90%	Common
Seafloor alteration	Distinctive	All	Present
Hydrothermal vents	Distinctive	Rare, ≤15%	Common

Source: After Kusky (2004).

or not recognized as such or (2) remnants of Archean oceanic crust do not look like post-Archean ophiolites. Considering the detailed geologic mapping in Archean greenstones, it is becoming less and less likely that ophiolites have been overlooked. If higher heat production in the Archean mantle resulted in production of thicker oceanic crust, because of the greater amount of melting beneath ocean ridges, complete ophiolites may not have been preserved by obduction or underplating mechanisms (Moores, 2002). Because ophiolites are generally <7 km thick, a tectonic slice off the top of Archean oceanic crust that was 20 km thick may only include the pillow basalt unit, and pillow basalts are prolific in Archean greenstones. If indeed this were the case, we are immediately faced with the question of how to distinguish slices of oceanic crust from slices of oceanic plateaus or arcs in Archean greenstone belts. One has to be very careful when using basalt geochemistry as discussed earlier.

One possible way to distinguish between oceanic crust and oceanic plateaus may be by the presence of komatiites. If komatiites require plume sources, as seems likely, only those greenstone successions without komatiites could be candidates for Archean oceanic crust. Certainly renewed effort seems warranted in our hunt for remnants of Archean oceanic crust.

Blueschists and Ultra-High-Pressure Metamorphic Rocks

Blueschists are formed in association with subduction and continental collision and reflect burial to high pressures at relatively low temperatures (see Figure 2.10). It has long been recognized that blueschists older than about 1000 Ma are apparently absent in the geologic record (Ernst, 1972). Those with aragonite and jadeitic clinopyroxene, which reflect the highest pressures, are confined to arc terranes <200 Ma. Lawsonite-bearing blueschists and eclogites, and ultra-high-pressure (UHP) metamorphic rocks characterized by coesite or diamond are a predominantly Phanerozoic phenomena related to deep subduction (Brown, 2006, 2007). UHP metamorphism is the first evidence of deep subduction of continental crust in the geologic record.

Three general ideas have been proposed for the absence of pre–1000-Ma blueschists and UHP metamorphic rocks: (1) steeper geotherms beneath pre–1000-Ma arcs prevented rocks from entering the blueschist and UHP stability fields, (2) uplift of blueschists and UHP rocks led to recrystallization to lower pressure mineral assemblages, and (3) erosion has removed old blueschists and UHP rocks. It may be that all three of these factors contribute to the absence of pre–1000-Ma blueschists and UHP rocks. Prior to 2 Ga, steeper subduction geotherms may have prevented formation of high-pressure low-temperature rocks. After this time, however, when geotherms were not much steeper than at present, the second two factors may control preservation of these rocks. Calculated P-T-t trajectories for blueschists suggest that they may increase in temperature prior to uplift (see Figure 2.10), resulting in recrystallization of blueschist-facies assemblages to greenschist- or amphibolite-facies assemblages. After 500 Ma of uplift

and erosion, only the latter two assemblages would be expected to survive at the surface. Uplift and erosion after continental collisions may also remove blueschists and UHP rocks. Even in young collisional mountain chains such as the Himalayas, only a few minor occurrences of blueschist have not been removed by erosion.

Higher radioactive heat production in the Archean predicts that metamorphic rocks in Archean collisional orogens should have experienced maximum temperatures several hundreds of degrees centigrade higher than those recorded by metamorphic rocks in modern collisional orogens. However, there is no evidence for this and the Archean record is dominated by ordinary P-T conditions and crustal melting at relatively low temperatures (Brown, 2007). The Neoproterozoic transition to a "modern plate tectonic thermal regime" registers a change to subduction of continental crust deeper into the mantle and its (partial) return from depths up to 300 km, a change perhaps related to the thickening of oceanic lithosphere with decreased thermal gradients.

EARTH'S THERMAL HISTORY

Two lines of evidence indicate that the mantle was hotter during the Archean. The most compelling evidence is that the present-day heat loss from Earth is approximately twice the amount of heat generated by radioactive decay, which requires that the excess heat come from cooling. Isotopes of U, Th, and K provide most of Earth's radiogenic heat (Chapter 4), and from the decay rates of these isotopes, it would appear that heat production in the Archean was three to four times higher than today (Richter, 1988). A second argument for higher Archean mantle temperatures is the presence of high-Mg komatiites in Archean greenstones, which require higher mantle temperatures for their generation. Estimates of the average Archean mantle temperature at 3 Ga vary from about 100 to 300°C higher than modern temperatures (Figure 7.25).

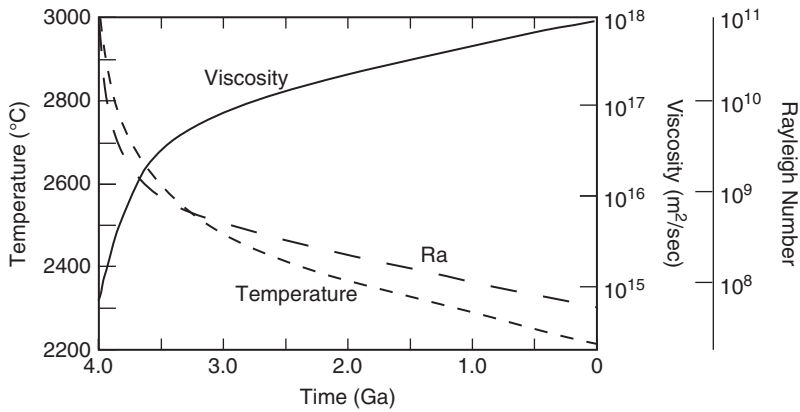

FIGURE 7.25 Average temperature, viscosity, and Rayleigh number of the mantle with time. *Modified after McGovern & Schubert (1989).*

One approach to calculating Earth's thermal history is by using parameterized convection models in which expressions are solved that relate convective heat transport to the temperature difference between the surface and interior of a convecting cell in the mantle and to the viscosity distribution in that cell. Results for whole-mantle convection show that mantle temperature, heat production, and Rayleigh number (see Chapter 4) decrease with time, whereas mantle viscosity increases with time, all in accordance with a cooling Earth (McGovern & Schubert, 1989) (Figure 7.25). Early in Earth's history when the mantle was very hot, viscosity was low and convection rapid, perhaps chaotic, as dictated by the high Rayleigh numbers. During this period of about 500-Ma duration, Earth cooled rapidly, followed by gradual cooling of about 100°C/Ga to the present time.

Magma Oceans

During the first 50–100 Ma after the Moon-forming event, it is likely that Earth retained enough heat to melt a large portion if not all of the mantle, giving rise to what is generally termed a **magma ocean**. A variety of physical and chemical processes guided the crystallization of the magma ocean, long before solid-state convection took over (Solomatov, 2007). This involves vigorous convection of the liquid, crystal settling, and extraction of residual melts during the late stages of crystallization. After the Moon-forming collision, re-accretion of Earth and first-time accretion of the Moon retained enough heat to largely melt both bodies. Any solids, including much of the newly formed cores, sink to the bottom of the magma ocean (Figure 7.26). The viscosity of the magma ocean is very low, convection is vigorous, and the temperature profile is adiabatic. Because the melting curve is unlikely to be steeper than the adiabat, crystallization of the magma ocean proceeds from the bottom upward. Thermal models indicate that more than 50% crystallization, mostly in the deep mantle, should occur in 10^3–10^4 years, leading to higher viscosity (Figure 7.26). Dissolution of smaller crystals and growth of larger ones decreases the number of crystals per unit volume and thus increases the average crystal size. Crystallization beyond 60% is accomplished by solid-state creep convection, the rate of which remains high. During the last stages of crystallization, the purely molten region disappears and cumulus crystals continue to grow. At this time, the early dusty atmosphere changes to a steam atmosphere, whose blanketing effect can reduce the heat flux from the magma ocean by several orders of magnitude. Convection continues to weaken the mantle and the crystals grow larger. Crystal settling (or/and floating) forms stratification, which tends to suppress the convection except near the surface, and when the packing of crystals reaches about 60% all the way to the surface, the heat flux drops dramatically. Formation of a crust would further reduce the surface heat flux.

Final crystallization of the magma ocean takes 10^7–10^8 years depending on the nature of mantle convection, and thereafter radioactivity and convection

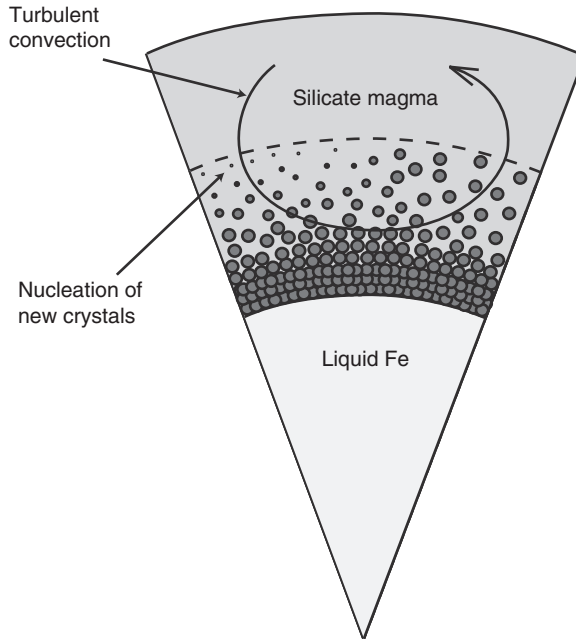

FIGURE 7.26 Schematic cross section of a magma ocean during the early stages of crystallization. *From Solomatov (2007).*

largely control the subsequent thermal history. Any liquid iron left in the mantle would continue to settle into the core.

How Hot Was the Archean Mantle?

Most petrologists agree that the dramatic decrease in abundance of komatiites at the end of the Archean reflects a decrease in mantle temperature. However, no agreement has been reached on just where and how komatiites are produced in the mantle. Although generally assumed to form by partial melting of the mantle under dry conditions, some experimental studies show that if water is present, the liquidus temperature of komatiitic magma is reduced substantially (Asahara et al., 1998; Grove & Parman, 2004). However, experimental data also show that it is difficult to erupt wet komatiitic lavas, because they should erupt explosively and show widespread textural evidence of degassing, or they should solidify before eruption (Stone et al., 1997; Arndt et al., 1998). Although pyroclastic komatiites may reflect wet magmatic eruptions, they are rare in the geologic record. Also, the effect of water on liquidus temperature is reduced at the high degrees of melting (30–50%) necessary to produce komatiitic magmas. In addition, trace element distributions and isotopic characteristics of komatiites indicate that their source was depleted in incompatible elements,

including water, prior to magma formation, leaving a dry source to melt. Chromium content of olivine in equilibrium with chromite is also sensitive to melting temperature. Olivines with Cr contents of >1550 ppm crystallize at temperatures above 1500°C, whereas those with Cr contents of <1000 ppm crystallize at temperatures below 1250°C (Li et al., 1995). Komatiites typically have Cr contents of >2000 ppm, confirming that they are high- rather than low-temperature melts. This is in contrast to low-temperature, high-Mg island-arc magmas that have olivine with Cr contents of <800 ppm. Also supporting hot, dry komatiitic magmas are measurements of Fe^{3+}/Fe^{2+} ratios in melt inclusions in Archean komatiites from Zimbabwe, which are consistent with near anhydrous melting of the source rock (Berry et al., 2008).

Arndt et al. (2008) conclude that most komatiites are derived from dry mantle sources and, thus, that komatiite liquidus temperatures, as deduced from MgO content, can be used to constrain source temperatures in the Archean mantle and to track the temperature of komatiite sources with time (McKenzie & Bickle, 1988; Abbott et al., 1994). Because of alteration, however, it is difficult to estimate the original MgO content of komatiite magmas. Maximum values of MgO range from 29% to 32%, with the lower value from the least altered komatiites (Nisbet et al., 1993). The eruptive temperature of a komatiite with 30% MgO is about 1600°C (Figure 7.27). In comparison, the hottest modern magmas are basaltic komatiites (MgO = 20%) from Gorgona Island that erupted at temperatures of 1400°C, and typical basalts are not erupted at temperatures over 1300°C. If 1600°C is taken as the maximum eruption

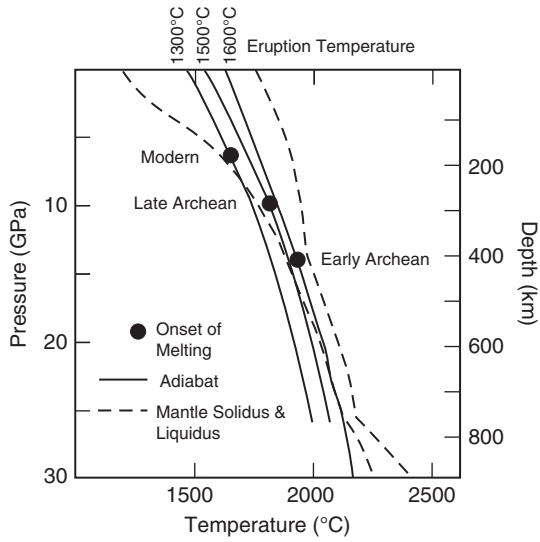

FIGURE 7.27 Pressure-temperature diagram showing mantle liquidus and solidus and various adiabats for basalt and komatiite.

temperature of komatiites in the Archean, following a mantle adiabat suggests their mantle source would have a temperature near 2000°C (Figure 7.27). Because this temperature is greater than that predicted by the secular cooling curve of the mantle, it would appear that komatiites come from hot, rising plumes with temperatures that are 200–300°C hotter than surrounding mantle, similar to the temperature difference calculated between modern plumes and surrounding mantle. Campbell and Griffiths (1992b) have argued from the fact that komatiites are a very minor component in Archean greenstones, that it is Archean tholeiites that more closely reflect the temperature of the upper mantle. Because most Archean tholeiites have MgO contents of <10% MgO, similar to modern oceanic basalts, it would seem that most of the late Archean upper mantle was <50°C hotter than modern upper mantle of about 1300–1400°C.

Because garnet is stabile in the mantle relative to pyroxenes, the solubility of garnet in silicate liquids is reduced, resulting in magmas that have very low concentrations of Al_2O_3, similar to many Al-depleted komatiites (Herzberg, 1995). Because CaO varies much less with residual mineralogy, the CaO/Al_2O_3 ratio is strongly pressure dependent, and an Al_2O_3–CaO/Al_2O_3 plot can be used to estimate the depth of melting of primary picrite and komatiite magma. As shown on Figure 7.28, high-Mg picrites and komatiites <100 Ma have large Al_2O_3 values and CaO/Al_2O_3 ratios near one. In contrast, late Archean komatiites have intermediate values of these indices and early Archean

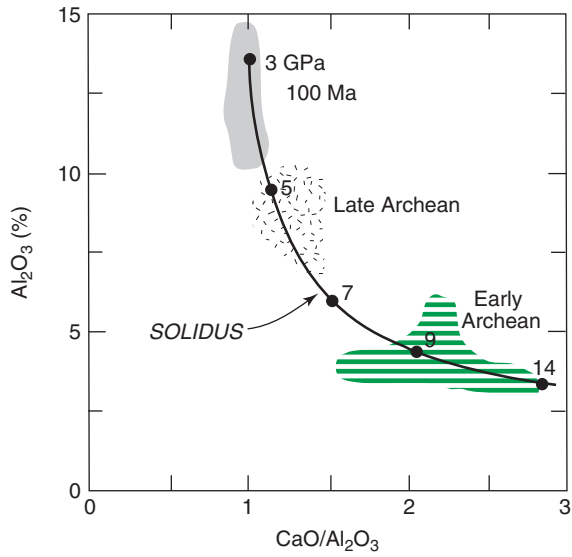

FIGURE 7.28 Al_2O_3 versus CaO/Al_2O_3 graph showing the mantle solidus as a function of increasing pressure. Pressure given in GPa. Also shown is the distribution of komatiite and picrite as a function of age (patterned areas). *Modified after Herzberg (1995).*

komatiites have low Al_2O_3 and high CaO/Al_2O_3. This suggests that young komatiites come from depths of up to 100 km, late Archean komatiites from depths of 150–200 km, and early Archean komatiites from depths of 300–450 km (Herzberg, 1995).

Many petrologists agree that komatiites are produced in the hot central tail region of mantle plumes, and associated basalts probably come from the cooler plume head (Campbell & Griffiths, 1992a). Each follows a different adiabat, suggesting that both temperature and depth of magma segregation in plumes have decreased with time (Figure 7.29), presumably in response to the cooling of the mantle. If this is true, the secular compositional changes in komatiites may be the result of a hotter bulk Earth rather than just hotter plume sources in the Archean.

Finally, calculations of melting temperatures of non–arc-type greenstone basalts clearly indicate high ambient mantle temperatures in the Archean (Herzberg et al., 2010). The temperatures are calculated from the MgO and FeO contents of relatively unfractionated non-arc basalts using the method of Herzberg and Asimow (2008). Figure 7.29 shows that mantle potential temperatures inferred from the petrologic modeling converge to the present-day ambient value, suggesting that the modeled lavas formed from hot ambient mantle. Shown for comparison is the range of temperatures calculated from komatiites. If some of the non-arc Archean basalts came from mantle plumes,

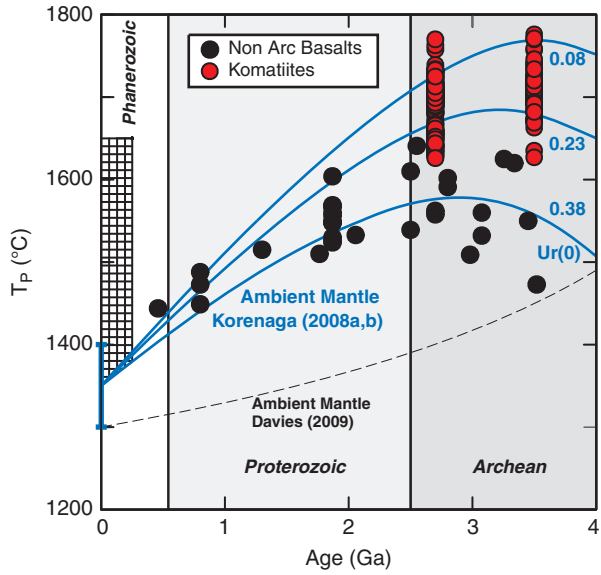

FIGURE 7.29 Secular cooling Earth models for ambient mantle (Korenaga, 2006) compared with calculated mantle potential temperatures from non-arc greenstone basalts. *After Herzberg et al. (2010).*

they must have come from distal plume margins that approached ambient mantle temperatures. These petrologic estimates on the thermal evolution of ambient mantle are in substantial agreement with the cooling curves of Korenaga (2006). Even with the large degree of scatter, the models capture the form of the curves, which are concave toward the time axis. The agreement is well within the uncertainties in both the petrologic estimates and the parameterized convection models (i.e., 60 and ~50°C, respectively). These results clearly suggest that non-arc basalts of Precambrian age provide a viable petrologic record of the heating and cooling history of Earth.

Thermal Models

Numerous models have been published to describe the cooling of Earth and they all share one thing in common: there is considerable uncertainty in many of the parameters used in the models, and none of them perfectly describes all of the data we have available. All depend on a balance between heat production in the mantle by radioactivity and heat loss by convection. The standard models conclude that a hotter mantle in the Archean would have produced more melt at ocean ridges and hence thicker oceanic crust. Calculations suggest that the Archean oceanic crust should have been about 20 km thick (maybe even thicker in the early Archean) compared to the present thickness of about 7 km (Sleep & Windley, 1982). Because oceanic crust is less dense than the mantle, the Archean oceanic lithosphere would have been more buoyant, and thus more difficult to subduct. A hotter mantle would also convect faster, probably causing plates to move faster, and thus oceanic lithosphere would have less time to thicken and become gravitationally unstable. In support of these models are paleomagnetic results from 2.7-Ga rocks in the Pilbara craton of Western Australia which suggest that late Archean plate motions were faster than today (Strik et al., 2003).

Many thermal models do not take into account plate tectonics nor variations in the **Urey ratio** (γ_0), which is the ratio of heat production in the mantle to heat loss from the top of the mantle. Rather than discussing the pros and cons of various models, we will discuss briefly a model that does take into account both plate tectonics and the Urey ratio. This model, presented by Korenaga (2006), is based on plate tectonic convection and a relatively small Urey ratio of 0.15 to 0.3 (Figures 7.30a and d). Three main features that set the model apart from other models are (1) decompression melting beneath ocean ridges, (2) the role of water in lithosphere rheology, and (3) plate bending at subduction zones. The Archean oceanic lithosphere is strong because it is chemically depleted and dehydrated during melting in the upper mantle. Also, plate bending is a source of resistance to subduction. The net result is that plates actually move slower in a hotter mantle and with time they speed up (Figure 7.30b). One difficulty with the model, as mentioned above, is that paleomagnetic data do not support slower plate motions in the Archean. Although the model extends to 4 Ga, it should not be interpreted to mean that plate tectonics was operational at this time.

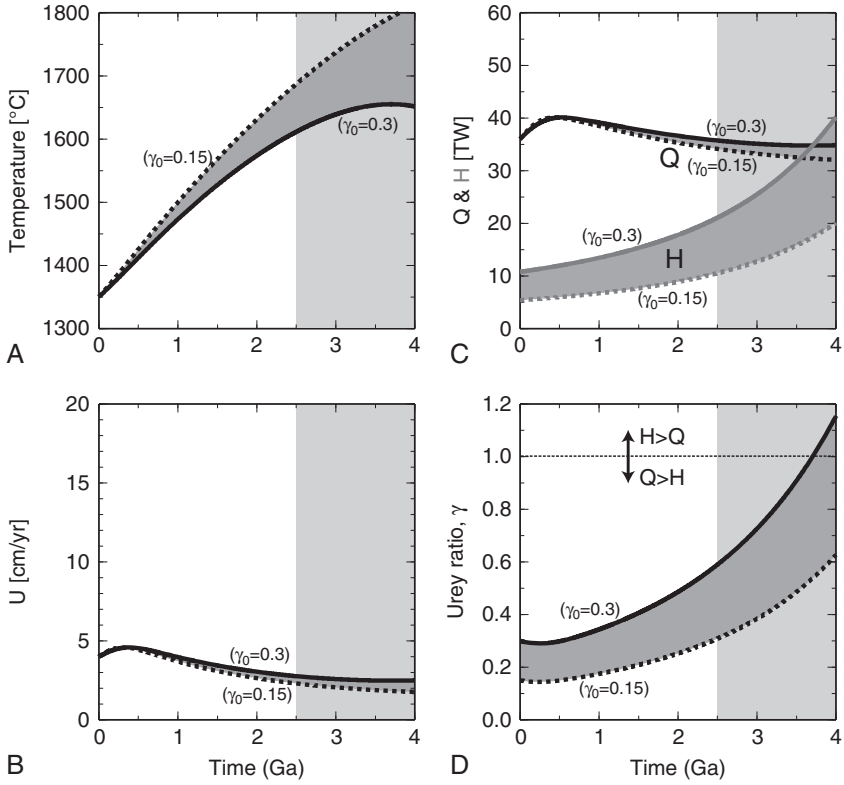

FIGURE 7.30 Thermal model for cooling of the mantle assuming plate tectonics. U, average plate velocity (cm/y); Q, heat flow from mantle; H, mantle heat generation in terawatts (TW); γ_o, Urey ratio (H/Q). *After Korenaga (2006), courtesy of Jun Korenaga. Reproduced with permission of American Geophysical Union.*

As with other thermal models, the Korenaga model shows heat production in the mantle decreasing with age, primarily due to decreasing radioactivity. However, the secular cooling curve is very different from that of Papuc and Davies (2008) (Figure 7.29) and Labrosse and Jaupart (2007), which are based on the more conventional heat-flow scaling with more rapid plate tectonics in the past and a higher Urey ratio. The low-Urey-ratio model with sluggish convection in the past predicts a cooling curve concave toward the time axis, because in the past mantle heat flux was lower and internal heating was higher. In particular, the apex of the concave cooling curve (for $\gamma_0 = 0.3$) corresponds to the time when the Urey ratio was unity. Prior to this time, internal heating exceeded surface heat loss, resulting in mantle warming. In contrast, the high-Urey-ratio models with rapid convection in the past predict a convex cooling curve with mantle heat flux always exceeding internal heat production.

As mentioned earlier, the ambient mantle temperatures calculated from basalts seem to support the Korenaga model (Figure 7.29). It would appear that a better understanding of physical and chemical properties of the early mantle are necessary to decide between these two types of thermal models for Earth.

FURTHER READING

Brown, M., & Rushmer, T. (2006). *Evolution and Differentiation of the Continental Crust*. Cambridge, UK: Cambridge University Press.

Condie, K. C. (2001). *Mantle Plumes and Their Record in Earth History*. Cambridge, UK: Cambridge University Press.

Davies, G. F. (2008). *Thermal Evolution of the Mantle*. Treatise on Geophysics (pp. 197–216). Amsterdam: Elsevier, Chap. 9.08.

Halliday, A. N. (2003). *The Origin and Earliest History of the Earth,* Treatise on Geochemistry (pp. 509–557). Amsterdam: Elsevier, Chap. 1.20.

Harrison, T. M. (2009). The Hadean crust: Evidence from >4 Ga zircons. *Annual Review of Earth and Planetary Sciences*, *37*, 479–505.

Korenaga, J. (2006). *Archean Geodynamics and the Thermal Evolution of Earth,* Monograph Series 164 (pp. 7–32). American Geophysical Union.

Kusky, T. M. (2004). Precambrian ophiolites and related rocks. In *Developments in Precambrian Geology* (Vol. 13, 748 pp), Amsterdam: Elsevier.

Rollinson, H. (2008). *Early Earth Systems: A Geochemical Approach*. Oxford, UK: Blackwell Publishers.

Schubert, G., Turcotte, D. L., & Olson, P. (2001). *Mantle Convection in the Earth and Planets*. Cambridge, UK: Cambridge University Press.

Chapter 8

The Supercontinent Cycle

INTRODUCTION

Supercontinents are large continents that include most or all of the existing continents. Matching of continental borders, stratigraphic sections, and fossil assemblages are some of the earliest methods used to reconstruct supercontinents. Wegener (1912) pointed out the close match of opposite coastlines of continents and the regional extent of the Permo-Carboniferous glaciation in the Southern Hemisphere, and DuToit (1937) was first to propose an accurate fit for continents based on geologic evidence. Today, in addition to these methods, we have apparent polar wander paths, seafloor spreading directions, hotspot tracks, and correlation of crustal provinces using piercing points. The use of computers in matching continental borders has resulted in more accurate and objective fits.

The youngest supercontinent is **Pangea**, which formed between 450 and 320 Ma and includes most of the existing continents (Figure 8.1). Pangea began to fragment about 185 Ma and is still dispersing today. **Gondwana** is a Southern Hemisphere supercontinent comprised principally of South America, Africa, Arabia, Madagascar, India, Antarctica, and Australia (Figure 8.2). It formed in the latest Neoproterozoic and was largely completed by the Early Cambrian (~550 Ma) (Unrug, 1993). Later it became incorporated in Pangea as the largest piece. **Laurentia**, which is also part of Pangea, includes most of North America, Scotland and Ireland north of the Caledonian suture, Greenland, Spitzbergen, and the Chukotsk Peninsula of eastern Siberia. The oldest supercontinent for which we know at least a partial configuration is **Rodinia**, which formed between about 1200 and 900 Ma, fragmented at 750–600 Ma, and appears to have included many cratons in a configuration quite different from that of Pangea (Pisarevsky et al., 2003). Although the existence of older supercontinents is likely, their configurations are not well known. Geologic data strongly suggest the existence of supercontinents in the Paleoproterozoic and in the late Archean (Aspler & Chiarenzelli, 1998; Pesonen et al., 2003; Bleeker, 2003). Current thinking is that supercontinents have been episodic, giving rise to the idea of a supercontinent cycle (Nance et al., 1986; Hoffman, 1991). A **supercontinent cycle** consists of rifting and breakup of one supercontinent, followed by a stage

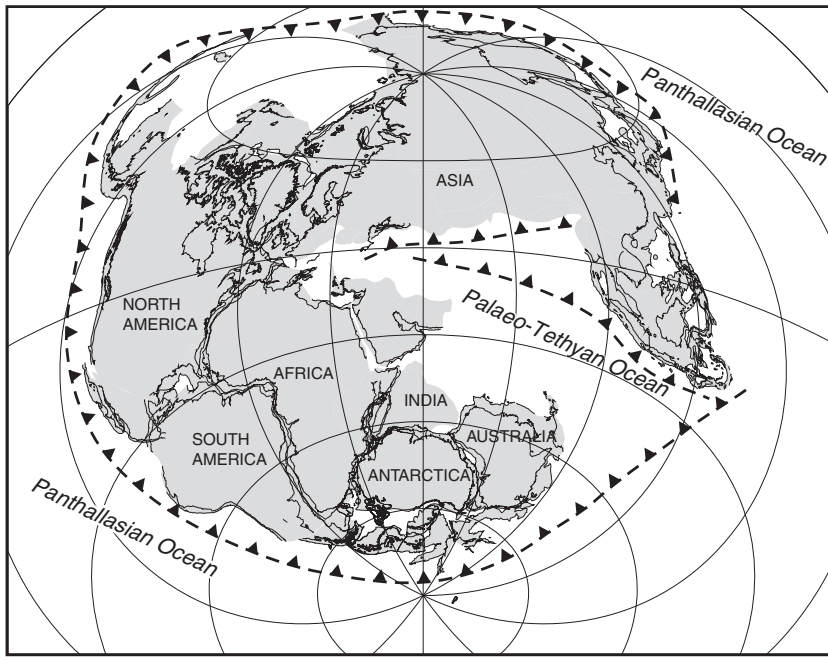

FIGURE 8.1 Pangea, the last supercontinent, formed between 450 and 320 Ma and began to fragment about 185 Ma. Barbed lines are inferred locations of subduction zones. *Modified after Vaughan & Storey (2007), courtesy of Alan Vaughan and the Geological Society of London.*

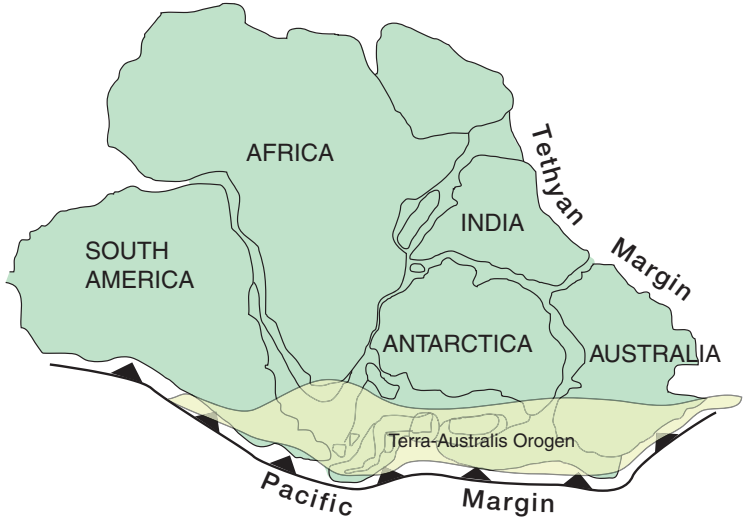

FIGURE 8.2 The supercontinent Gondwana formed between 750 and 550 Ma and became part of Pangea in the late Paleozoic. Barbed line, inferred subduction zone.

of reassembly in which dispersed cratons collide to form a new supercontinent, with most or all fragments in different configurations from the older supercontinent (Hartnady, 1991).

Supercontinents have aggregated and dispersed several times during Earth history, although our geologic record of supercontinent cycles is only well documented for the last two cycles: Gondwana-Pangea and Rodinia (Hoffman, 1989; Rogers, 1996). It is generally agreed that the supercontinent cycle is closely tied to mantle processes, including both convection, mantle upwellings (superplumes), and mantle plumes.

SUPERCONTINENT RECONSTRUCTION

We can precisely reconstruct the last supercontinent Pangea by simply reversing the direction of seafloor spreading until the continental margins meet (e.g., the margins of Africa and South America). However, because there is no intact seafloor older than about 200 Ma, we must use other approaches to reconstruct older supercontinents. Of these only the paleomagnetic approach is quantitative. We make use of rocks magnetized in Earth's magnetic field at times in the past, which carry the position of the magnetic poles, known as **paleopoles**. When a rock forms, it may acquire a magnetization parallel to the ambient magnetic field referred to as **primary remanent magnetization**. Information about both the direction and intensity of the magnetic field in which a rock formed can be obtained by studying its primary magnetization. The most important minerals controlling rock magnetization are magnetite and hematite. However, it is not always easy to identify primary magnetization in that rocks often acquire later magnetization known as **secondary remanent magnetization**, which must be removed by demagnetization techniques prior to measuring primary magnetization. Some rocks possess magnetization in a direction opposite to that of the present Earth's magnetic field, known as **reverse magnetization,** in contrast to **normal magnetization**, which parallels the present field. Detailed studies of magnetic stratigraphy show that Earth's field has reversed many times in the last 200 Ma.

Paleomagnetism is the study of ancient pole positions and makes use of remanent magnetization to reconstruct the direction and strength of the geomagnetic field in the past. To accomplish this, oriented samples are collected, the remanent magnetization is measured in the laboratory with a magnetometer, and calculated paleopole positions are plotted on equal-area maps as apparent polar wander paths. For a paleopole to have significance in terms of ancient plate motions, however, numerous problems must be addressed as follows:

1. *Dipole field*. The present Earth's field can be approximated as a geocentric dipole inclined at 11.5 degrees to the rotational axis. The nondipole field, which remains after subtraction of the dipole field from the measured field, is about 5% of the total field. In reconstructing ancient pole positions,

a dipole field is assumed to have existed in the past. The consistency of pole positions from different parts of a continent at the same geologic time and the worldwide agreement of paleoclimatic regimes with inferred paleolatitude calculated from paleomagnetic studies support this assumption. Because of the axial symmetry of the dipole field, however, paleolongitudes cannot be determined from paleomagnetic data. Thus, plate motions parallel to lines of latitude cannot be detected.

2. *True polar wander*. Ancient pole positions are generally plotted as **apparent polar wander paths** for a continent (or segment thereof) relative to its present position (Figure 8.3). Apparent polar wander paths (or APW paths) may result from either plate motions or true polar wander, or both. True polar wander results from changes in the magnetic pole position caused by global slip at the core–mantle boundary, at least in part in response to changes in mass redistribution at the surface caused by the formation and breakup of supercontinents. Movement of the entire lithosphere with respect to the mantle or of the mantle relative to the core can produce the same effect. Comparison of plate motions assuming a fixed hotspot framework indicates that true polar wander has amounted to about 12 degrees since the Early Tertiary. Because true polar wander affects equally all calculated poles of a given age in the same way, however, it does not usually influence relative plate motions deduced from APW paths.
3. *Normal or reversed pole*. For an isolated paleopole, it is not possible to tell if the pole is reversed or normal. This decision must be based on other information such as paleoclimatic data or an APW path constructed from other geographic localities, but including the age of the measured sample.
4. *Deformation*. The most reliable pole positions come from nearly flat-lying rock units. In rocks that acquired magnetization prior to deformation, it may be possible to estimate pole positions by "unfolding" the rocks. Strain associated with folding also must be removed. It is only in strata that have undergone rather simple folding that these structural corrections can be made. However, in complexly deformed metamorphic terranes, $^{40}Ar/^{39}Ar$ dating indicates that the major remanent magnetization is usually acquired after deformation, possibly during regional uplift. Thus, in many instances it is possible to obtain meaningful post-deformational paleopoles from strongly deformed and metamorphosed rocks in cratons.
5. *Dating of remanent magnetization*. The Curie temperature (the temperature at which thermal remanent magnetization is acquired) in magnetic minerals (Fe-Ti oxides) lies between 500 and 600°C, and it is possible date the magnetization using an isotopic system with a blocking temperature similar to Curie temperatures. The $^{40}Ar/^{39}Ar$ method has proved useful in this respect, generally using hornblende, which has an argon blocking temperature of about 500°C. It is very difficult, however, to assign meaningful $^{40}Ar/^{39}Ar$ ages to rocks that have multiple magnetizations. In this light, a new field of research in rock magnetization is the measurement of magnetic domains

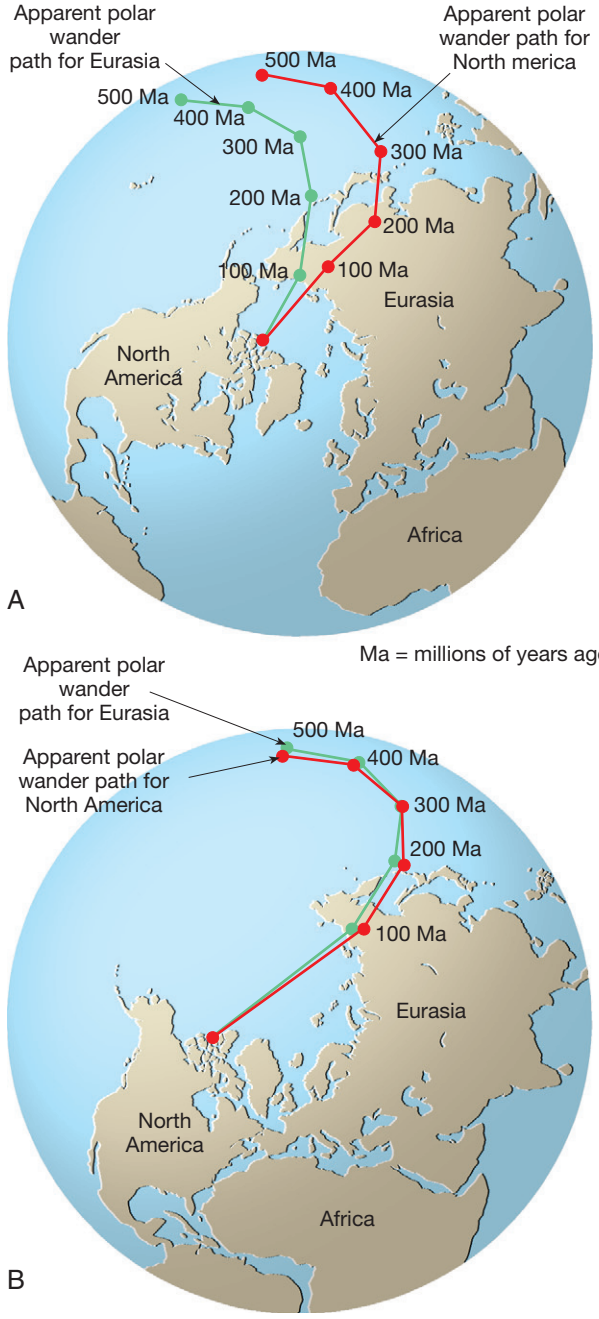

FIGURE 8.3 Apparent polar wander paths for Eurasia and North America for the last 500 Ma: (A) current positions and (B) reconstructed positions of continents after closing the Atlantic Basin. *Courtesy of Dennis Tasa.*

on a microscopic scale for individual minerals. From such studies, minerals that carry different fractions of the magnetization can be identified and multiple magnetizations can potentially be resolved. Further, using laser $^{40}Ar/^{39}Ar$ dating, it may be possible to date individual magnetic components in a rock, and thus to track magnetic poles for individual crystals.

6. *Separation of remanence components*. One of the most difficult problems in paleomagnetic studies is that of separating, identifying, and establishing the sequence of acquisition of multiple magnetizations. This is particularly a problem in metamorphic rocks where a primary magnetization is overprinted with one or more metamorphic magnetizations. Standard techniques for separating magnetic components include stepwise treatment of samples either by alternating magnetic fields or by heating. Depending on the history of a rock, it may be difficult or impossible to separate and date the various magnetic components, although the laser $^{40}Ar/^{39}Ar$ technique offers promise for overcoming this problem.

In using the paleomagnetic method, the APW paths of continents (or segments thereof) are plotted on equal-area projections of Earth, generally relative to the present positions of continents. If continents show the same APW paths, it is clear they did not move relative to each other. The fact that North American and Eurasian APW paths diverge from each other going back in time, however, indicates that these plates have moved separately for the last 100 Ma (Figure 8.3a). If we close the Atlantic Ocean using the magnetic stripes on the seafloor, this brings the two APW paths together (Figure 8.3b), showing that both continents were part of the same plate until about 100 Ma when the North Atlantic began to open. To illustrate the use of APW paths in reconstructing plate motions, four tectonic scenarios with corresponding APW paths are shown in Figure 8.4. The simplest case is for a single continent in which paleopole positions from various cratons lie on the same APW path (case A). Here, cratons have been part of the same continent over the period of time represented by the APW path. Such paths characterize most Precambrian cratons within a given continent for the last 600 Ma, central and eastern Asia being the major exception. Case B illustrates the assembly of a supercontinent by successive collisions of continents. Two continents collide at time 4 and are joined by two more continents at times 8 and 10 to form a supercontinent. A **Wilson Cycle** (the opening and closing of an ocean basin) is illustrated in case C. At time 4, a continent is rifted apart and an ocean basin opens, reaching a maximum width at time 8, when the two continental fragments begin to close again. The original continent is reformed at time 12 by collision of these fragments. The offset in APW paths from times 1 to 4 reflects the fact that the fragments did not return to their original positions. The opening and closing of the Iapetus Ocean during the Paleozoic is an example of a Wilson Cycle that can be tracked with APW paths. Case D illustrates offset along a major continental transform fault where motion begins at time 8.

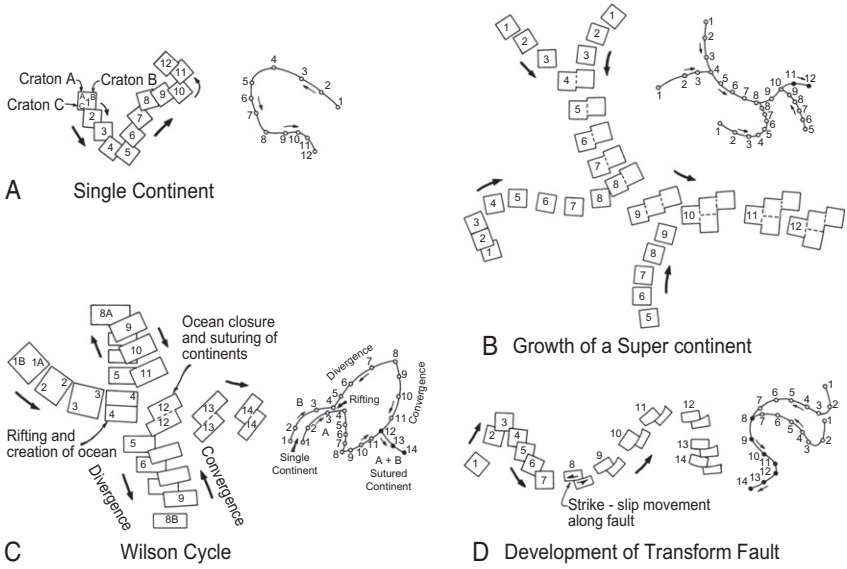

FIGURE 8.4 Apparent polar wander paths for various tectonic scenarios. Numbers are relative time with 1 being the oldest.

It is clear from paleomagnetic studies that continents grow by terrane collisions and that supercontinents, such as Pangea, have formed and dispersed several times in the geologic past. The paleomagnetic method has the unique property of being able to see through the breakup of Pangea 185 Ma. In principle, it is possible to reconstruct continental positions prior to 185 Ma provided the problems listed above can be overcome. Applications to the Precambrian, however, have not met with much success, due principally to the complex thermal histories of most Precambrian terranes and problems with separating and dating the various magnetizations. Despite inherent errors in interpretation, paleomagnetic data constrain the amount of independent motion between adjacent Precambrian crustal provinces. For instance, results from North America and Baltica (Scandinavia) suggest that these continents were part of the same supercontinent during the Paleoproterozoic and again, with somewhat different configurations, during the Neoproterozoic.

For Precambrian supercontinent reconstructions, piercing points and barcodes are at least equally reliable as paleomagnetism in supercontinent reconstructions (Bleeker & Ernst, 2006). A **piercing point** is a distinct geologic feature such as a fault or terrane that strikes at a steep angle to a rifted continental margin, the continuation of which should be found on the continental fragment that rifted away (Figure 8.5). Each well-defined high-angle piercing

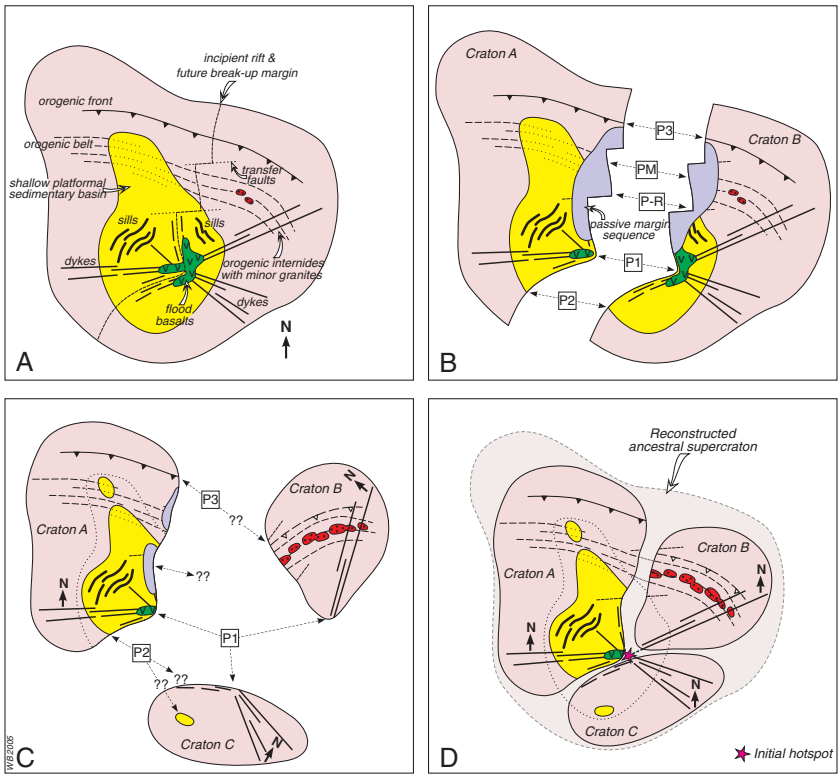

FIGURE 8.5 Use of piercing points in craton reconstruction. (A) A supercraton with various geologic elements prior to breakup. A LIP with flood basalts (green) and associated dykes (radiating black lines) is emplaced along the incipient rift. (B) Breakup of the supercraton has spawned to cratons (A and B). They may be matched up using a variety of piercing points, for example, P-R, the fitting of promontories and reentries along the rifted margins; PM, general correlation and fitting of the conjugate passive margins; P1, piercing points and reconstruction of the LIP; P2, piercing points provided by older sedimentary basins; and P3, piercing points provided by an ancient orogenic front or fold-thrust belt. (C) Further breakup, abrasion, and uplift of derivative cratons. Craton B is strongly uplifted and its sedimentary cover eroded. Piercing point P3 has shifted and an exhumed granitoid belt (red blobs) is unmatched in craton A. Craton C is also uplifted, erasing piercing point P2. Dykes related to the LIP, however, remain on all three cratons and precise isotopic dating suggests that they might be part of a single event. Primary paleomagnetic data may yield additional geometrical clues (North arrows). (D) Reconstruction of the original craton, based only on the precise piercing points and other information derived from the dyke swarms. *After Bleeker & Ernst (2006), courtesy of Wouter Bleeker.*

point must have a conjugate along the margin of another craton. Unfortunately, breakup margins sometimes follow older sutures or crustal boundaries, thus minimizing the number of well-defined high-angle piercing points. Figure 8.5a presents an idealized example of the use of piercing points to reconstruct a supercontinent. During the last two decades, short-lived magmatic

events, and the information inherent therein, have emerged as the key to unraveling pre-Pangea paleocontinental reconstructions. Multiple precisely dated events define "barcodes" for individual cratons or crustal fragments and provide a history of the short-lived magmatic events experienced by that piece of crust (Bleeker & Ernst, 2006; Ernst & Bleeker, 2010). Originally adjacent pieces of crust are likely to share at least part of their magmatic history, perhaps in the form of distant dyke swarms, and thus will show a partial match between their barcodes. Multiple matches among the barcodes of now distant cratons imply that the cratons were adjacent parts of an ancestral craton, which later fragmented.

CONTINENTAL COLLISIONS AND THE ASSEMBLY OF SUPERCONTINENTS

Supercontinents are made by collisions of plates carrying continental crust, which forms collisional orogens as described in Chapter 3. They continue to grow by collisions of terranes around their margins, such as island arcs, oceanic plateaus, and rifted pieces of continental crust. During collisions, buoyant continental material resists subduction, resulting in significant thickening of the lithosphere in both upper and lower plates (as for instance in the Himalayas today). As an example, the assembly of Gondwana, largely between 600 and 520 Ma, involved the accretion of continental blocks in a variety of orogenic belts (Cawood & Buchan, 2007). There are eight major blocks with at least six internal collisional orogens, followed by a long-lived accretionary orogen on the Pacific side, the Terra Australis orogen (Figure 8.2). Pangea is the last supercontinent that existed on the planet prior to the opening of the Atlantic, which led to the plate configuration we have today (Figure 8.1). Pangea formed by the suturing of Gondwana, Laurentia-Baltica, and several plates in northeastern Asia. Major amalgamation of these plates occurred along three primary orogens: (1) the Appalachian orogen in eastern North America and northwestern Africa, which sutured Laurentia to Africa; (2) the Variscan orogens in central Europe where Europe was sutured to northern Africa; and (3) the Ural orogen in west-central Asia where Europe was sutured to Siberia. Later rifting of small plates from Africa and Antarctica and collision of these plates with southern Europe or southern Asia to form the gigantic Alpine-Himalayan orogen in the Tertiary complicate the history of Pangea.

The collisions that were responsible for the assembly of Gondwana and Pangea were synchronous with the development of subduction and contractional orogenesis along the margins of the supercontinents. In the case of Gondwana, final assembly occurred between 570 and 510 Ma with final cooling and uplift complete by 490 Ma (Cawood & Buchan, 2007). This was coeval with the switch from passive margin to convergent margin activity along the Pacific margin of the supercontinent. Likewise, the final stage of amalgamation of Pangea occurred between 320 and 250 Ma, with major boundary reorganization

along the ongoing Terra Australis accretionary orogen along both the East and West Pacific margins, especially evident in Australia. It is likely that the approximate synchronicity of collisional and accretionary orogens during supercontinent assembly is related to global plate kinematic adjustments (Cawood & Buchan, 2007).

THE FIRST SUPERCONTINENT

One of the intriguing yet puzzling questions of the supercontinent cycle is that of just how and why the first supercontinent formed. No robust data are available to support the existence of a supercontinent prior to the late Archean, and even then evidence points to several supercratons (unusually large cratons) rather than one large supercontinent (Bleeker, 2003). There are about 35 Archean cratons today and most or all appear to be rifted fragments of larger landmasses. Bleeker (2003) suggests these cratons can be grouped into clans based on their degrees of similarity. There are at least three clans, each of which seems to come from a different supercraton. The Slave, Dharwar, Zimbabwe, and Wyoming cratons may be fragments of one supercraton that stabilized at about 2.6 Ga, and broke up between 2.2 and 2.0 Ga (Ernst & Bleeker, 2010). Superior, Rae, Kola, Hearne, and Volga may have been part of a second supercraton, and Kaapvaal and Pilbara part of a third.

Figure 8.6 shows an example of reconstruction of a late Archean supercontinent or more precisely, a supercraton often referred to as Kenorland (Aspler & Chiarenzelli, 1998; Bleeker & Ernst, 2006). Three events (ca. 2500 Ma, ca. 2446 Ma, and ca. 2110 Ma) are matched between the southern Superior and the Hearne cratons. Between the Superior and Karelia cratons no less than four key events can now be matched, allowing a tightly constrained fit. Breakup of these cratons must have occurred sometime after 2100 Ma but before 1980 Ma, the date of an important magmatic event in Karelia that has no match in the southern Superior craton. This implies that the cover sequences dated at 2400–2300 Ma in the Superior and Karelia cratons formed in intracratonic rifts and extensional basins and do not represent true passive margin successions along rifted craton margins. A second Archean supercraton, Vaalbara, is proposed for two cratons now in the Southern Hemisphere: Kaapvaal in southern Africa and Pilbara in Western Australia. Although no well-dated piercing points warrant such a supercraton, paleomagnetic poles from both cratons dated at 2.8–2.7 Ga at least permit its existence (de Kock et al., 2009).

For supercratons or supercontinents to form, a significant volume of continental crustal fragments that survive recycling into the mantle is required. Prior to the late Archean, the high mantle temperatures and inferred large mantle convection rates probably resulted in rapid recycling of continental crust, presumably before continental pieces had time to collide to make supercratons or a supercontinent (Armstrong, 1991; Bowring & Housh, 1995). So what happened in the late Archean that led to formation of the first supercratons?

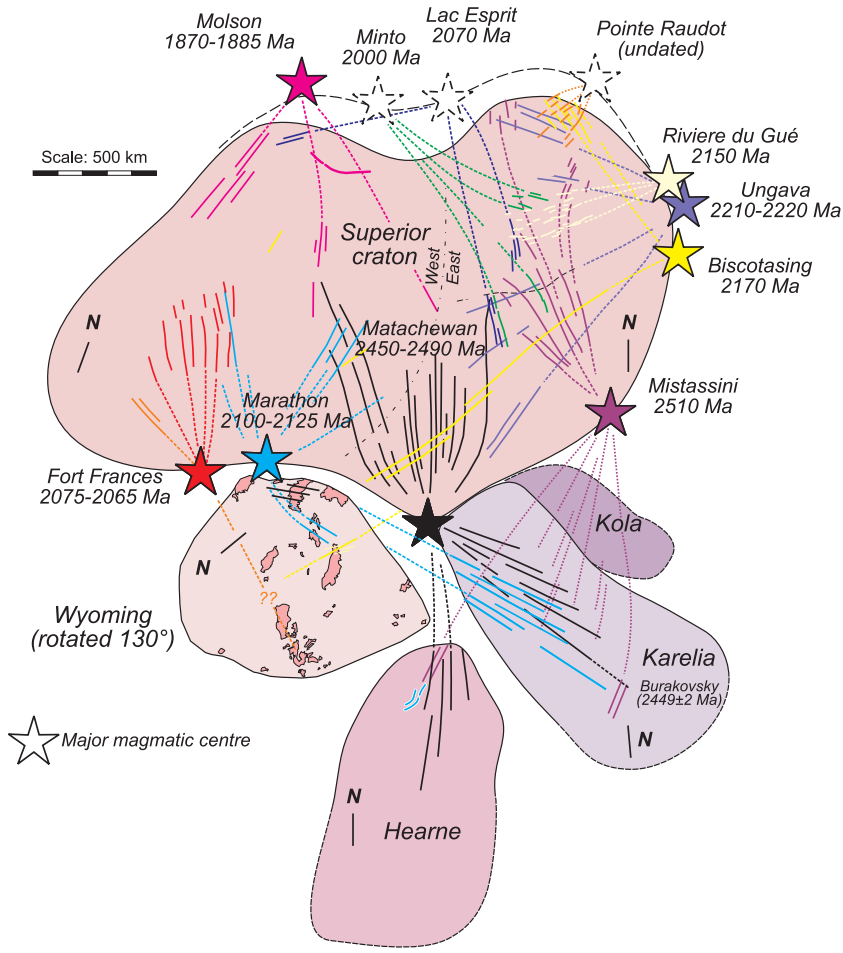

FIGURE 8.6 Possible configuration of a late Archean supercontinent or supercraton. Reconstruction based on correlation of short-lived LIP events and correlation of cover sequences. *Modified after Bleeker & Ernst (2006) and Ernst & Bleeker (2010), courtesy of Wouter Bleeker.*

One possibility, as described in Chapter 9, is that the widespread onset of plate tectonics led to the production of large volumes of continental crust in a relatively short period of time ($\leq$100 Ma). If this were the case, the first supercratons would form in response to the first widespread subduction. Also contributing to growth of late Archean supercratons is the thick Archean subcontinental mantle lithosphere that is relatively buoyant (Griffin et al., 1998), thus resisting subduction during plate collisions.

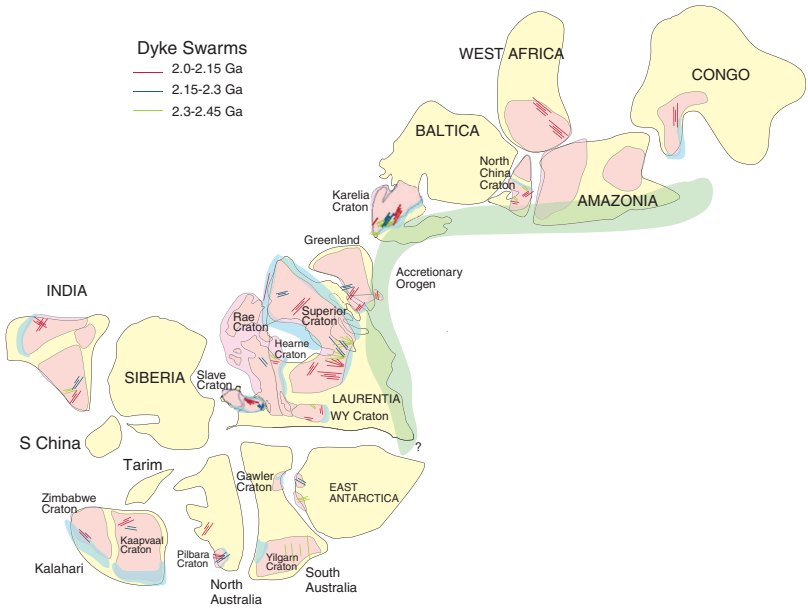

FIGURE 8.7 Schematic reconstruction of the supercontinent Nuna at 1500 Ma. Blue identifies passive margins and green, a long-lived accretionary orogen. *After Zhao et al. (2002), Hou et al. (2008), and Johansson (2009).*

LATER SUPERCONTINENTS

After the breakup of one or more late Archean supercratons at 2.2–2.1 Ga, the first true supercontinent, referred to as Nuna or Columbia, formed between 1900 and 1800 Ma and continued to grow until about 1650 Ma. It is not yet clear if Nuna fragmented or survived intact to become the largest piece of the next supercontinent. In the last 1000 Ma, three different supercontinents have come and gone. The Meso-Neoproterozoic supercontinent Rodinia formed as continental blocks collided primarily along what today is the Grenvillian orogen, which extends from Siberia along the coasts of Baltica, Laurentia, and Amazonia into Australia and Antarctica (Hoffman, 1991; Condie, 2002a). Gondwana formed chiefly between 600 and 520 Ma and Pangea between 450 and 320 Ma.

Nuna (Columbia)

Figure 8.7 is a speculative reconstruction of Nuna at about 1500 Ma based on both piercing points and paleomagnetic data (Zhao et al., 2002; Meert, 2002). Also shown on the reconstruction are passive margin sequences in the age range of 1400 to about 1900 Ma, which are useful in identifying the rifted margins of the late Archean supercraton(s) (Bradley, 2008). Notice that most

of the Superior craton in Laurentia is surrounded by passive margins, which became collisional margins during the assembly of Nuna. High-precision paleomagnetic poles from Laurentia, Baltica, Amazonia, and North China suggest that these four continents were laterally contiguous by 1.8 Ga. Also shown on the Nuna configuration are large dyke swarms that record the initial rifting (2.45–2.3 Ga), initial breakup (2.15–2.3 Ga), and final dispersal (2.0–2.15 Ga) of the late Archean supercraton(s). The radiating pattern of dyke swarms along the southern coast (present day) of the Superior craton suggests that mantle plumes may have been important in the formation of this boundary. Cratonic blocks in West Africa and Amazonia were welded together during the Transamazonian orogeny at 2.1–2.0 Ga; the Kaapvaal and Zimbabwe blocks during the Limpopo collision at 2 Ga; the North American, European, and Siberian fragments at 1.9–1.8 Ga; and the Archean blocks within India and within the North China craton at 1.85 Ga (Zhao et al., 2002). The position of Australia relative to Laurentia is still hotly debated. Some investigators place it adjacent to northwestern Laurentia (as shown in Figure 8.7) and others adjacent to southwestern Laurentia (Karlstrom et al., 2001). After assembly of Nuna, a long-lived accretionary orogen developed along the southern and eastern coast of Laurentia and extended into Baltica and probably into Amazonia (Figure 8.7, green belt).

The breakup timing of Nuna is not well known. It may have occurred between 1350 and 1250 Ma as suggested by large igneous province (LIP) dyke swarms, and especially the giant 1267-Ma Mackenzie swarm in northern Canada (see Figure 3.12 in Chapter 3) (Hou et al., 2008). Alternatively, Nuna may not have fragmented, or at least not fragmented completely. Reliably dated paleomagnetic poles from Laurentia, Baltica, and Siberia indicate that these three continents did not break up, but remained intact until the fragmentation of Rodinia in the Neoproterozoic (Wingate et al., 2009).

Rodinia

The last Precambrian supercontinent was Rodinia (Figure 8.8). Although Rodinia appears to have assembled largely between 1200 and 900 Ma (Z. X. Li et al., 2008), some collisions, such as those in the Grenville orogen in eastern Canada and collisions between the South and West Australian plates (Rivers, 1997; Condie, 2003b; Meert & Torsvik, 2003; Pesonen et al., 2003), began as early as 1300 Ma. The assembly process began with the accretion or collision of continental blocks around the margin of Laurentia and most of it was completed in about 150 Ma (Z. X. Li et al., 2008). Relatively minor collisions between 1000 and 900 Ma, such as Rockall-Amazonia and Yangtze-Cathaysia (in South China), added the finishing touches. Recent paleomagnetic data suggest that with the exception of Amazonia, most or all of the cratons in Africa and South America were never part of Rodinia

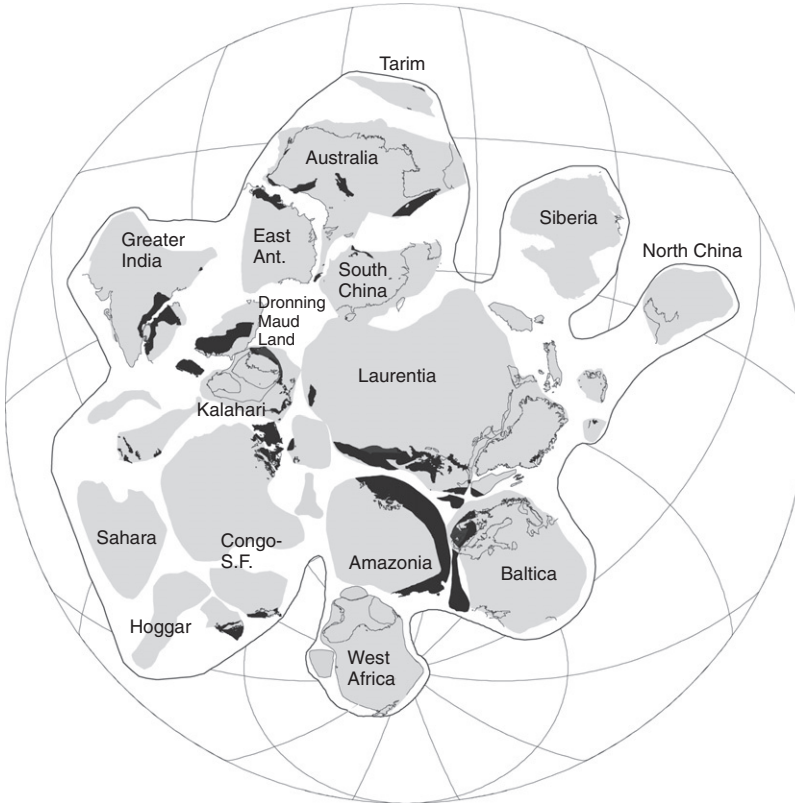

FIGURE 8.8 Rodinia, a supercontinent, formed between 1.2 and 0.9 Ga and fragmented 750–600 Ma. Black regions are major 1.1- to 1.0-Ga collisional orogens. *Reconstruction from Z. X. Li et al. (2008), courtesy of Zheng-Xiang Li.*

(Kroner & Cordani, 2003). These latter cratons, however, remained relatively close to each other from the Mesoproterozoic onward. Rodinia began to fragment at 780 Ma with the separation of India from Australia and East Antarctica, followed by the separation of South China from Laurentia-Australia by 750 Ma. Although rifting between Amazonia and Laurentia began about the same time, fragmentation along this boundary was not complete until about 600 Ma. At this same time, cratons in western Gondwana were amalgamating, and thus fragmentation of one supercontinent coincided with assembly of another supercontinent. Although most fragmentation occurred between 750 and 650 Ma, the opening of the Iapetus Ocean began about 600 Ma with the separation of Baltica-Laurentia-Amazonia. In addition, small continental blocks, such as Avalonia-Cadomia and several blocks from western Laurentia, were rifted away as recently as 600–550 Ma.

Gondwana and Pangea

The formation of Gondwana immediately followed the breakup of Rodinia with some overlap in timing between 650 and 600 Ma (Figure 8.9). The short-lived supercontinent Pannotia, which formed as Baltica, Laurentia, and Siberia, briefly collided with Gondwana between 580 and 540 Ma (Dalziel, 1997) assembled and fragmented during the final stages of Gondwana construction. As Rodinia fragmented, cratons scattered from Laurentia and at about 650 Ma began colliding on the opposite side of Earth to form Gondwana. Gondwana was largely intact by 600 Ma. By 550 Ma, India moved closer to Australia and Kalahari started to collide with Congo and Rio de la Plata. The final amalgamation of Gondwana occurred 540–530 Ma with the docking of India to Australia-East Antarctica, forming the Mozambique orogen in East Africa.

Pangea began to form about 450 Ma (Figure 8.9) with the Precordillera-Rio de la Plata, Amazonia-Laurentia, and Laurentia-Baltica collisions (Li & Powell, 2001). It continued to grow by collisions in Asia, of which the last major collision produced the Ural orogen between Baltica and Siberia about 280 Ma. It was not until about 185 Ma that Pangea began to fragment with rifting of the Lhasa and West Burma plates from Gondwana. Major fragmentation occurred between 150 and 100 Ma, with the youngest fragmentation, i.e., the rifting of Australia from Antarctica, beginning about 100 Ma. Small plates, such as Arabia (rifted at 25 Ma) and Baja California (rifted at 4 Ma),

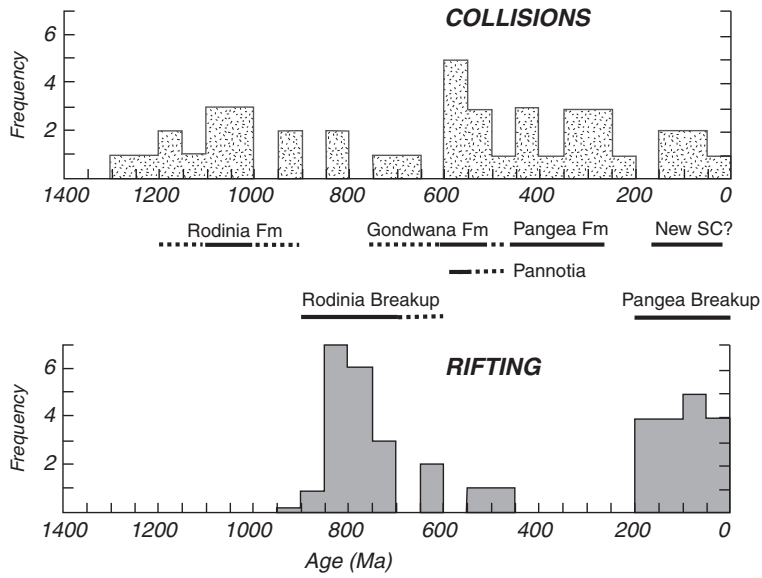

FIGURE 8.9 Distribution of rifting and collisional ages used in the construction of supercontinent cycles in the last 1400 Ma. SC, supercontinent.

continued to be rifted from Pangea up to the present. Although often overlooked, there are numerous examples of continental plate collisions that paralleled the breakup of Pangea. Among the more important are the China/Mongolia-Asia (150 Ma), West Burma-Southeast Asia (130 Ma), Lhasa-Asia (75 Ma), India-Asia (55 Ma), and Australia-Indonesia (25 Ma) collisions. In addition, numerous small plates collided with the Pacific margins of Asia and North and South America between 150 and 80 Ma (Schermer et al., 1984). These collisions in the last 150 Ma may very well represent the beginnings of a new supercontinent (Condie, 1998), and if so, the breakup phase of Pangea and growth phase of this new supercontinent significantly overlap in time (Figure 8.9).

THE SUPERCONTINENT CYCLE

Our most detailed and extensive coverage of the supercontinent cycle comes from the recent supercontinent Pangea. Pangea 200 Ma was centered approximately over the African mantle upwelling and geoid high (see Figures 4.3a and 4.27 in Chapter 4), and the other continents moved away from this high during the breakup of Pangea. Because the upwelling contains many of Earth's hotspots and is characterized by low seismic wave velocities in the deep mantle, it is probably hotter than average as discussed in Chapter 4. Except for Africa, which still sits over the geoid high, continents seem to be moving toward geoid lows that are also regions with relatively few hotspots and high lower mantle velocities, all of which point to cooler mantle (Anderson, 1982). These relationships suggest that supercontinents may affect the thermal state of the mantle, with the mantle beneath supercontinents becoming hotter than normal, expanding and producing mantle upwellings (Anderson, 1982; Gurnis, 1988). This is followed by increased mantle plume activity, which may fragment supercontinents or at least contribute to dispersal of cratons.

Episodic Ages

It is widely accepted that the isotopic ages of continental crust, including juvenile components, record episodic events (McCulloch & Bennett, 1994; Condie, 1998; Pietranik et al., 2008). What is not known, however, is whether the episodicity is caused by changes in crustal production rate, crustal preservation rate, or both. One way to address this question is with combined U/Pb ages and Hf isotope data from detrital zircons as discussed in Chapter 7. The development of laser probe ICP-MS (inductively coupled plasma mass spectrometry) has made it relatively easy to obtain precise U/Pb ages and Hf isotopic compositions from the same zircon, and many such studies have appeared in the last few years (Belousova et al., 2010; Condie et al., 2009a; Wang et al., 2009).

Results from detrital zircons with both U/Pb and Hf isotope data are shown on an εHf(T) versus age plot in Figure 7.14 and the composite age spectra are

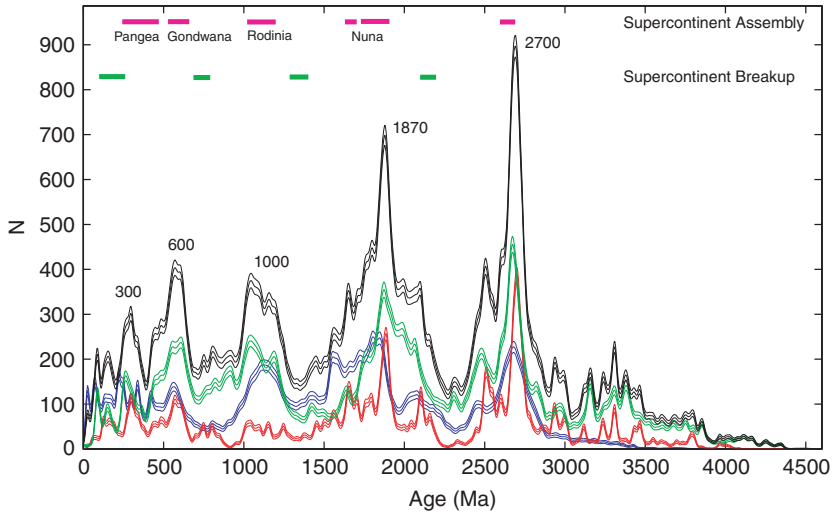

FIGURE 8.10 Distribution of U/Pb zircon ages in orogenic granitoids and detrital zircons for the last 4 Ga with 1σ error envelope, where N is representative of the number of samples as a function of age that would be observed in a histogram with bins of width 30 Ma. The detrital ancient sediment database is multiplied by two for comparative purposes. Number of zircon ages: orogenic granitoids, 8928; detrital modern sediments, 6978; detrital ancient sediments, 21 282; total ages, 37 188. Major peak clusters labeled in Ma and supercontinent cycle shown at the top. *Modified after Condie & Aster (2010).*

shown in Figure 8.10 as Monte Carlo simulations of density probability. All continents are represented in the database, and the εHf(T) diagram was discussed in Chapter 7. The major peak clusters in the detrital age distribution are similar to those found in orogenic granitoids and correlate well with supercontinent formation (Campbell & Allen, 2008; Condie & Aster, 2010) (Figure 8.10). The remarkable correlation with the supercontinent cycle suggests that these clusters are principally preservation peaks that reflect juvenile and reworked crust selectively sequestered from mantle recycling during continent–continent collisions. It is noteworthy and expected that the U/Pb age distribution of zircons from granitoids with a juvenile Nd isotopic signature shows the same distribution of peak clusters (Figure 7.13).

As discussed in Chapter 7, during the Cenozoic, the production and recycling rates of continental crust are approximately the same (Clift & Vannucchi, 2004; Scholl & von Huene, 2009). Although a significant amount of juvenile and reworked continental crust can be recycled into the mantle during continent–continent collisions by uplift/erosion or subduction (Stern & Scholl, 2010), some is preserved in cratons in the roots of collisional orogens, now elevated to the surface. Examples are found in the uplifted roots of the Trans-Hudson orogen in Canada (1.9 Ga; Schneider et al., 2007), the Limpopo belt in southern Africa (2.0 Ga; Zeh et al., 2007) and in the East African orogen

(Neoproterozoic; Stern, 2002). Thus, enhanced preservation of both juvenile and reworked continental crust during supercontinent assembly is caused by an increase in the "capture" rate of this crust from obduction and uplift during collision and tectonic isolation or sequestering from crust recycling in subduction zones (Scholl & von Huene, 2007). Both juvenile and reworked sources contribute to the production of syncollisional to post-collisional igneous rocks.

As recognized in earlier studies, the age clusters are few and broad in the Precambrian, but narrow and numerous in the Phanerozoic. Although part of this trend may reflect underestimation of uncertainties of Precambrian U/Pb zircon ages, it is possible also that it may reflect speeding up of the supercontinent cycle in the Phanerozoic (Chapter 7; Korenaga, 2006). Another factor that may be important in controlling widths of peak clusters is continuing accretion of terranes around the margins of supercontinents. For instance, it appears that the supercontinent Nuna largely assembled between 1900 and 1800 Ma, but a laterally extensive accretionary orogen continued to be active until about 1500 Ma (Karlstrom et al., 2001). Both the 1600- and 1840-Ma clusters comprise several embedded age peaks that are only resolvable in age spectra of detrital zircons from single-river systems. Single peaks within these clusters may record terrane collisions in specific geographic regions, such as in the Yavapai-Penokean accretionary orogen along the southern margin of Laurentia.

Another interesting feature of the U/Pb zircon age patterns (Figure 8.10) is the times during which very few ages are recorded, such as at 2400–2200, 1400–1300, 900–650, and 185–120 Ma. These age "gaps," which correlate in part with supercontinent breakup, may represent times when crustal production and recycling rates were about the same. Hence, they would reflect windows into the normal rate of continental growth, which is falling with time. As discussed in Chapter 7, the especially prominent 2400- to 2200-Ma gap may be an exception, if it represents a global slowdown of magmatism and plate tectonics. The late Archean supercratons appear to have broken up near the end of this time interval at 2200–2100 Ma (Bleeker, 2003), and the 1400- to 1300-Ma gap may correlate with the partial breakup of Nuna. The long gap at 900–650 Ma overlaps the assembly and breakup phases of Rodinia and perhaps the beginning of the assembly of Gondwana (Figure 8.10). Some studies have suggested that the Neoproterozoic was a time of significant continental growth (Rino et al., 2008; Stern, 2008). Indeed, there are two peaks (at about 750 and 800 Ma) in the detrital zircon age spectrum that could be enhanced if African, South American, and European river sediments were more heavily sampled for detrital zircons. These two peaks may correlate with the breakup of Rodinia and, thus, be an exception to the supercontinent assembly correlation. The 185- to 120-Ma gap, however, seems to correlate with major phases in the breakup of Pangea.

If the proposed correlations of zircon age peaks with the supercontinent cycle is correct, then during the breakup phase of supercontinents, the recycling rate of continental crust catches up with the production rate and hence explains a sparsity of detrital zircons formed during the age gaps. An example of this idea

may be the modern Andean subduction system in South America. Opening of the South Atlantic in the last 200 Ma did not develop new subduction zones, which would have rapidly formed new arc crust, but took advantage of a subduction system that had been in existence along the Pacific margin of South America for the last 500 Ma (Glodny et al., 2006). The result since the beginning of the breakup of southern Pangea has been a net loss (by a factor of ~2 over arc additions) of western South American continental crust (Scholl & von Huene, 2009). This could result in a gap in the zircon age distributions, which is testable as more detrital zircon age data become available from modern river sediments in South America. If the South American scenario is typical of supercontinent breakup, it could certainly lead to age gaps in detrital zircon populations from later river sediments.

If this interpretation of U/Pb ages and Hf isotopic compositions of detrital zircons is correct, it implies that any planet with plate tectonics and a supercontinent cycle should exhibit episodic ages in continental crust.

Patterns of Cyclicity

The timing of breakup and dispersal of supercontinents in the last 1000 Ma does not support a simple supercontinent cycle in which a breakup phase is always followed by a growth phase, the growth phase by a stasis phase, and the stasis phase by another breakup phase (Condie, 2002a). Rather, the data suggest that two types of supercontinent cycles may be operating: (1) a sequential breakup and assembly cycle and (2) a supercontinent assembly cycle only. In the sequential cycle, a supercontinent breaks up over a geoid high (mantle upwelling) (Anderson, 1982; Lowman & Jarvis, 1999) and the pieces move to geoid lows, where they collide and form a new supercontinent, in part during, but chiefly after, supercontinent breakup. The formation of Rodinia followed by its breakup and then by the assembly of Gondwana is an example of the sequential cycle (Figure 8.9). Up to 100-Ma overlap may occur between each stage of the cycle. The breakup of Pangea, which is still going on in East Africa, and the possible formation of a new supercontinent with collisions in Southeast Asia seem to completely overlap in time, but nevertheless, probably belong to the sequential cycle. The Rodinia–Gondwana cycle from the first breakup of Rodinia to the final aggregation of Gondwana lasted about 250 Ma (750–500 Ma) and the Pangea–new supercontinent cycle has been in operation for about 200 Ma.

The second type of supercontinent cycle, that which characterizes the growth of Rodinia (1200–900 Ma) and Pangea (450–320 Ma), appears to involve only the formation of a supercontinent without fragmentation of another supercontinent. But how can we explain such a cycle? Perhaps the answer is that an earlier supercontinent did not fully fragment, and thus the later supercontinent involved relatively few collisions of large, residual continental blocks. In the case of Pangea, Gondwana did not fragment before becoming part of

Pangea. In fact, Pangea is really the product of continued growth of Gondwana. Thus, Pangea formed from an already existing supercontinent that collided with three large residual fragments left over from the breakup of Rodinia (Laurentia, Baltica, and Siberia). In a similar manner, Rodinia may have formed from relatively few residual continental blocks that survived the incomplete breakup of the Paleoproterozoic supercontinent Nuna. Condie (2002b) has shown from the distribution of sutures in Rodinia that the predecessor supercontinent did not fully fragment. At least two large fragments, Atlantica (Amazonia, Congo, Rio de la Plata, West and North Africa) and Arctica (Laurentia, Siberia, Baltica, North China), survived the partial breakup of Nuna.

This immediately presents the problem of why some supercontinents do not fully fragment. Based on the models of Lowman and Jarvis (1999) and Lowman and Gable (1999) (discussed below), supercontinent fragmentation depends on supercontinent size. Small supercontinents do not produce sufficient mantle shielding to be fragmented. Only when supercontinents reach large sizes like Rodinia and Pangea can they completely fragment. Why should some supercontinents grow to large sizes while others remain relatively small? One possibility is that supercontinent size is related to the geographic distribution of subduction zones over which supercontinent growth is centered. If subduction zones are strung out in a linear, disconnected array rather than grouped in a few closely connected regions on Earth's surface, a large supercontinent would not form over the subduction zones at any one point. Rather, two or three relatively linear supercontinents of smaller size may form, and because these supercontinents do not provide adequate thermal shielding to the underlying mantle, they do not fragment. Nuna may have been an example of this type of supercontinent (Figure 8.7). It is these survivors that later collide to form a new supercontinent; thus, complete breakup of a supercontinent is not required for supercontinent formation in the second type of supercontinent cycle.

Relationship to Earth History

Mineral Deposit Age Patterns

It is now well established that the distribution of mineral deposits in both space and time is related to the supercontinent cycle (Groves et al., 2005; Goldfarb et al., 2010). Many of the patterns of mineral deposit distribution are controlled by cooling of the mantle, the widespread onset of plate tectonics (Chapter 9), and the depth of formation of ore-bearing fluids. Orogenic Au, volcanigenic massive sulfides (VMS), epithermal Au-Ag, and porphyry Cu and Mo deposits are associated with subduction zones during the assembly of supercontinents at 2700–2600, 1900–1800, 1200–900, 650–550, and 450–300 Ma (Figure 8.11). The present-day distribution of porphyry Cu and Mo and epithermal Au deposits are strongly skewed toward the late Cenozoic. Most of these deposits older than 20–30 Ma have been uplifted and removed by erosion and thus lost

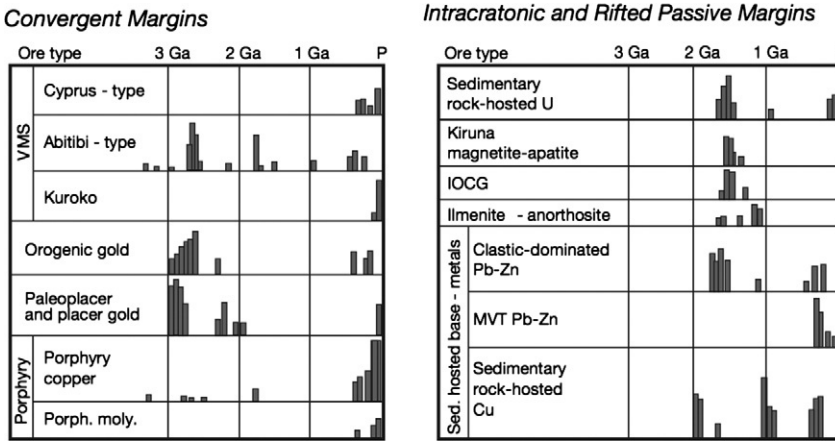

FIGURE 8.11 Distribution in time of important mineral deposits. VMS, volcanigenic massive sulfides; IOCG, iron-oxide Cu-Au deposits. Bin heights are relative estimated reserves. *Modified after Groves et al. (2005) and Goldfarb et al. (2010).*

from the geologic record, although a few examples are still preserved in rocks as old Archean. Mississippi Valley Type (MVT) Pb-Zn deposits and sediment-hosted Cu and U deposits also appear to form during supercontinent assembly, although at some distance from collisional zones. Associated with supercontinent breakup or attempted breakup (aborted rifting) are kimberlitic diamonds, Bushveld-type Ni-Cu and platinum group metals, IOCG (Fe oxide Cu-Au) deposits, and clastic-dominated Pb-Zn and Cu deposits in intracontinental rifts. All of these deposits form in extensional environments associated with the onset of supercontinent fragmentation.

Strontium Isotopes in Marine Carbonates

The isotopic composition of Sr in seawater is controlled chiefly by the composition of rivers entering the oceans and the hydrothermal input at ocean ridges (Veizer, 1989; Veizer & Mackenzie, 2003). Today the river influx greatly dominates in controlling the seawater $^{87}Sr/^{86}Sr$ ratio. Because of the long residence time of Sr in the oceans (~4 Ma) compared to ocean mixing times (~1000 years), the isotopic composition of modern seawater is very uniform (about 0.7099), even in partially landlocked seas like the Black Sea. Because marine carbonates record the seawater Sr isotopic composition, they have been used to monitor the composition of seawater in the geologic past. The evolution curve for seawater is generally chosen by connecting the lowest values (bold dashed line in Figure 8.12), since most secondary processes tend to increase Rb/Sr and the Sr isotopic ratios (Veizer & Mackenzie, 2003). When land areas are extensive and elevations relatively high, weathering and erosion transport large amounts of continental Sr into the oceans, which has relatively high

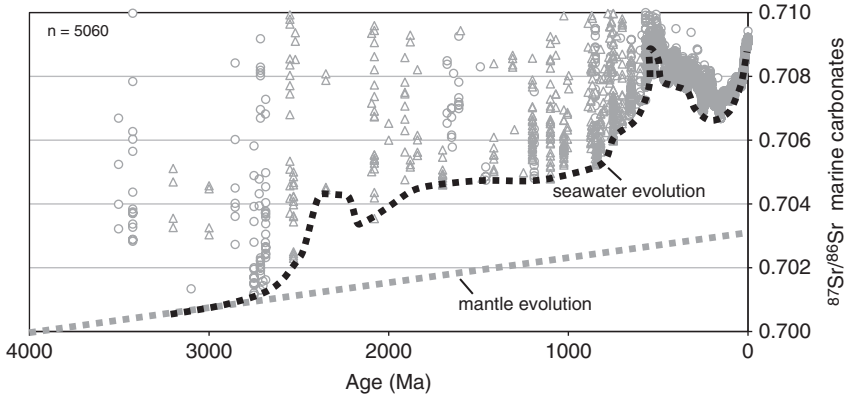

FIGURE 8.12 The record of $^{87}Sr/^{86}Sr$ ratio in seawater since the late Archean using marine carbonates as a proxy. Also shown is the mantle growth curve, where n is the number of samples. *Carbonate Sr isotope data from Mirota & Veizer (1994), courtesy of Jan Veizer.*

$^{87}Sr/^{86}Sr$ ratios. In contrast, when sea level is high and ocean ridges or/and mantle plumes are widespread and active, the input of mantle Sr into seawater is enhanced. Many of the long-term changes in the Sr isotopic composition of seawater may be related to the supercontinent cycle. In principle, we should be able to track the formation and destruction of supercontinents with the Sr isotopic record in seawater: during supercontinent formation, when land area is increasing the $^{87}Sr/^{86}Sr$ ratio of seawater should increase, and during fragmentation when ocean ridge activity increases, the ratio should decrease.

Although the Sr isotope record of seawater for the Phanerozoic is relatively well known (Veizer et al., 1999), except for the Neoproterozoic, the record for Precambrian seawater is still incomplete. Although several orders of variation in the Sr isotopic composition of ancient carbonates is recognized, only the first-order changes that occur over times of 500 Ma or more can be resolved in the Precambrian record. Veizer and Compston (1976) were the first to suggest that the growth rate of continental crust can be tracked with Sr isotopes using the $^{87}Sr/^{86}Sr$ ratio in marine carbonates. Prior to 2.5 Ga, $^{87}Sr/^{86}Sr$ ratios fall near the mantle growth curve (~0.702), suggesting that the oceans were largely buffered by mantle input, and that little continental crust existed, at least above sea level (Figure 8.12). After a probable major period of continental growth at 2.7 Ga and the formation of one or more supercratons, $^{87}Sr/^{86}Sr$ ratios in seawater began to rise, remaining high during the 2.4- to 2.2-Ga crustal age gap. The ratio drops at about 2.2 Ga, perhaps reflecting the reestablishment of global magmatism after a magmatic slowdown between 2.4 and 2.2 Ga. Between 2 Ga and about 700 Ma, $^{87}Sr/^{86}Sr$ remains rather constant, suggesting little change in the input ratio of continental to mantle Sr. The rapid increase in $^{87}Sr/^{86}Sr$ between 650 and 500 Ma probably reflects input of continental Sr from collisional orogens associated with the growth of Gondwana. The ratio remains rather

constant during the growth of Pangea in the mid- to late Paleozoic, and then falls as Pangea begins to fragment in the early Mesozoic. The rise in $^{87}Sr/^{86}Sr$ during the Cenozoic may reflect the beginning of formation of a new supercontinent, and the steep rise in the latest Cenozoic reflects erosion accompanying the rapid uplift of the Himalayas.

Sea Level Variations

Worsley et al. (1984, 1986) have proposed an intriguing model in which long-term change in sea level is directly tied to the supercontinent cycle, with a repeat time of about 400 Ma. The rapid increases in sea level observed at 600–500 Ma and 200–100 Ma correspond to the onset of the breakup of Laurasia (Laurentia-Baltica) and Pangea, respectively, and the Paleozoic long-term maximum coincides with the assembly of Pangea (Figure 8.13). The low sea level at about 600 Ma correlates with the assembly of Gondwana and the low at 300–200 Ma correlates with the final assembly of Pangea. The really low sea levels correlate with the growth of supercontinents, presumably times of decreasing ocean ridge activity. The models of Heller and Angevine (1985) show that both the magnitude and relative timing of highstands in sea level during supercontinent breakup may be related to increasing volume of ocean ridges and the formation of extensional passive margins. Supporting this idea is the fact that the number of continents with time also correlates with sea level (Figure 8.13). Also, as expected, the percent flooding of the continents increases during supercontinent dispersal and decreases during supercontinent assembly and stasis.

Comparisons of the ages of oceanic crust and sea level suggest that the breakup of Pangea controls a significant part of sea level variations (~50%)

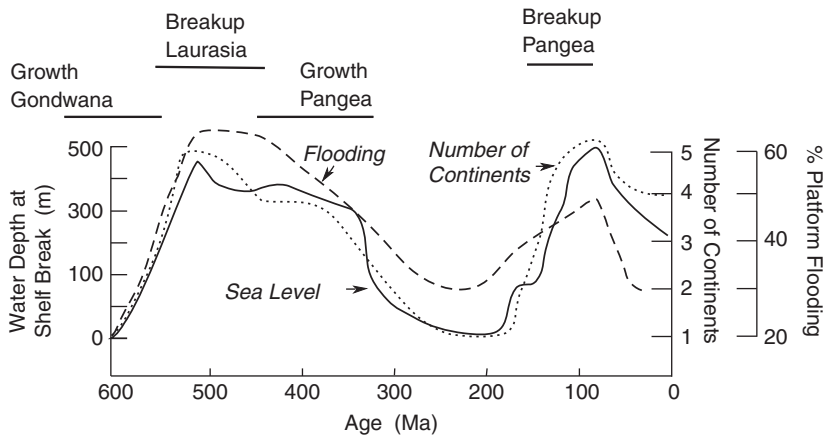

FIGURE 8.13 Comparison of variation in sea level, number of continents, and amount of flooding of shallow shelves by seawater for the last 600 Ma. Also indicated are the breakup and growth stages of supercontinents. *Modified after Worsley et al. (1984), Gaffin (1987), and Hardie (1996).*

in the last 180 Ma (Cogne et al., 2006). However, first-order sea level change is also controlled by oceanic plateau production and ice cap development, contributing respectively +60 m in the 120- to 70-Ma period, and − 60 to + 80 m in the last 40 Ma. First-order sea level change is a good proxy of mean oceanic lithospheric age, which is related to Wilson cycles of supercontinent fragmentation and amalgamation.

Supercontinents and Evolution

The supercontinent cycle has played a major role in the origination and extinction of some groups of organisms. Modern ocean basins are effective barriers not only to terrestrial organisms, but also to most marine organisms. Larval forms of marine invertebrates, for instance, can only survive several weeks, which means they can travel only 2000–3000 km with modern ocean current velocities. Hence, the geographic distribution of fossil organisms provides an important constraint on the sizes of oceans between continents in the geologic past. As illustrated in Figure 8.14, when a supercontinent fragments, organisms that cannot cross the growing ocean basin become isolated and this can lead to

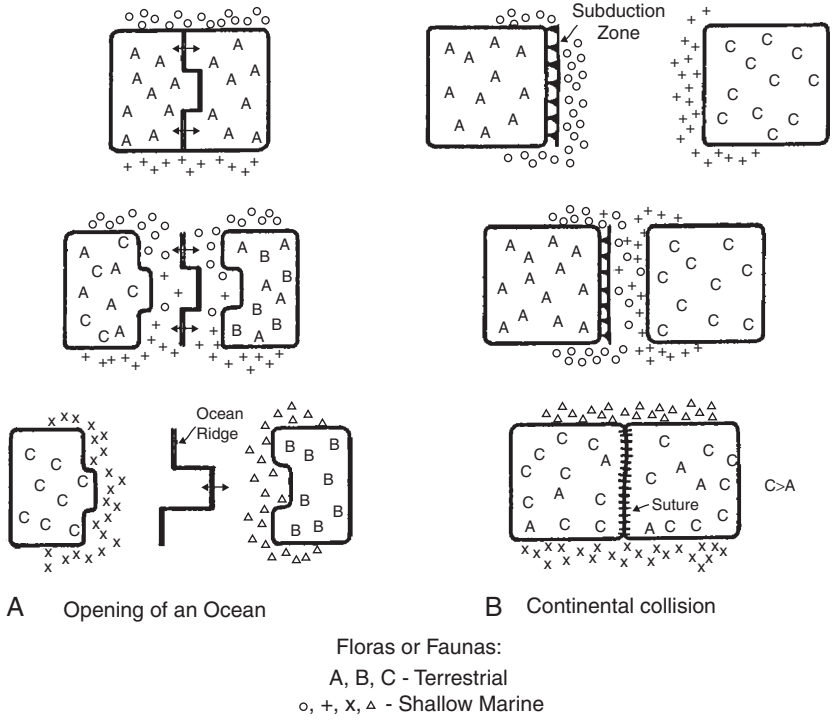

FIGURE 8.14 Possible effects of (A) breakup and (B) formation of a supercontinent on the origination and extinction of marine and terrestrial organisms.

the evolution of diverse groups on each of the separating continents (Hallam, 1974). This affects both marine and terrestrial organisms. Examples are the diversification and specialization of mammals in South America and in Africa following the opening of the South Atlantic in the Late Cretaceous. Similar changes occurred in bivalves of East Africa and India after the separation of these continents in the last 100 Ma. Continental collision (Figure 8.14b), on the other hand, removes an ocean barrier and formerly separate faunal and floral groups mix and compete for the same ecological niches. This leads to extinction of groups that do not successfully compete. Collision also creates a new land barrier between coastal marine populations. If these marine organisms cannot migrate around the continent (due perhaps to climatic barriers), diversification occurs and new populations evolve along opposite coastlines. As an example, during the Ordovician collisions in the North Atlantic many groups of trilobites, graptolites, corals, and brachiopods became extinct. The formation of new arc systems linking continents has the same effect as a collision. For instance, when the Panama arc was completed in the Late Tertiary, mammals migrated between North and South America, which led to the extinction of large endemic mammals in South America. Panama also separated marine populations, which led to divergence of Pacific and Caribbean marine organisms.

Although a correlation between the rate of taxonomic change of organisms and supercontinents seems to be well established, researchers have not agreed on the actual causes of such changes. At least three different factors have been suggested to explain rapid increases in the diversity of organisms during the Phanerozoic (Hallam, 1973; Hedges et al., 1996):

1. An increase in the aerial distribution of particular environments results in an increase in the number of ecological niches in which organisms can become established. For instance, an increasing diversification of marine invertebrates in the Late Cretaceous may reflect increasing transgression of continents (Figure 8.13), resulting in an aerial increase of the shallow-sea environment in which most marine invertebrates live.
2. Continental fragmentation leads to morphological divergence because of genetic isolation.
3. Some environments are more stable than others in terms of such factors as temperature, rainfall, and salinity. Studies of modern organisms indicate that stable environments lead to intensive partitioning of organisms into well-established niches and to corresponding high degrees of diversity. Environmental instability, decreases in environmental area, and competition of various groups of organisms for the same ecological niche can result in extinctions.

The biogeographic distribution of Cambrian trilobites indicates the existence of several continents separated by major ocean basins during the early Paleozoic as Gondwana was being assembled. Major faunal province boundaries commonly correlate with suture zones between continental blocks brought

together by later collisions. Wide oceans are implied in the Cambrian between Laurentia and Baltica, Siberia and Baltica, and China and Siberia, and paleomagnetic data support this interpretation. Minor faunal provincialism within individual blocks probably reflects climatic differences. Early Ordovician brachiopods belonged to at least five distinct geographic provinces, which were reduced to three provinces during the Baltica-Laurentia collision in the Late Ordovician. The opening of the North Atlantic in the Cretaceous resulted in the development of American and Eurasian invertebrate groups from an originally homogeneous Tethyan group. In addition, similar ammonite populations from East Africa, Madagascar, and India indicate that only shallow seas existed between these areas during the Jurassic.

The similarity of mammals and reptiles in the Northern and Southern Hemispheres prior to 200 Ma demands land connections between the two hemispheres (Hallam, 1973). The breakup of Pangea during the early to middle Mesozoic led to diversification of birds and mammals and the evolution of unique groups of mammals (e.g., the marsupials) in the Southern Hemisphere (Hedges et al., 1996). On the other hand, the fact that North America and Eurasia were not completely separated until the Early Tertiary accounts for the overall similarity of Northern Hemisphere mammals today. When Africa, India, and Australia collided with Eurasia in the mid-Tertiary, mammalian and reptilian orders spread both ways, and competition for the same ecological niches was keen. This competition led to the extinction of 13 orders of mammals.

Plant distributions are also sensitive to the comings and goings of supercontinents. The most famous are the *Glossopteris* and *Gangamopteris* flora in the Southern Hemisphere. These groups range in age from Carboniferous to Triassic and occur on all continents in the Southern Hemisphere as well as in northeastern China, confirming that these continents were connected from 350–200 Ma. The complex speciation of these groups could not have evolved independently on separate landmasses. The general coincidence of Late Carboniferous and Early Permian ice sheets and the *Glossopteris* flora appears to reflect adaptation of *Glossopteris* to relatively temperate climates and its rapid spread over high latitudes during the Permian. The breakup of Africa and South America is reflected by the present distributions of the rain forest tree *Symphonia globulifera* and a semiarid leguminous herb *Teramnus uncinatus,* both of which occur at approximately the same latitudes on both sides of the South Atlantic (Melville, 1973). Conifer distribution in the Southern Hemisphere reflects continental breakup, as evidenced by the evolution of specialized groups on dispersing continents after supercontinent breakup in the early Mesozoic.

MANTLE SUPERPLUME EVENTS

Condie (1998), Isley and Abbott (1999), and Maruyama et al. (2007) have presented arguments that mantle superplume events (sometimes called mantle plume events) have been important throughout Earth's history and are tied

closely with the supercontinent cycle and plate tectonics. Although the meaning of a "**mantle superplume event**" varies in the scientific literature, we shall constrain the term to refer to a short-lived mantle event ($\leq$100 Ma) during which one or more large mantle upwellings develop and mantle plumes related to these upwellings bombard the base of the lithosphere. During a mantle superplume event, plume activity may be concentrated in one or more mantle upwellings, as occurred during the mid-Cretaceous mantle plume event some 100 Ma, when activity was focused mainly in the Pacific mantle upwelling. Maruyama et al. (2007) propose that whole-Earth dynamics is directly tied to superplumes, which transport heat from the core to Earth's surface.

The duration of supercontinent formation and the total life span of supercontinents decreases with age. It took about 250–300 Ma each for Nuna and Rodinia to form, decreasing to 120–170 Ma each for Gondwana and Pangea. Paralleling this decrease is a decrease in the volume of juvenile continental crust preserved during each supercontinent cycle. Approximately 24% of the present continental crust was produced during formation of supercratons or a supercontinent in the late Archean, 20% during formation of the Paleoproterozoic supercontinent Nuna, and only about 6% during the formation of Rodinia (see Figures 7.13 and 7.16). The total amount of juvenile continental crust produced during the Phanerozoic appears to have been less than 15% of the total volume today. Only the first two supercontinent events at 2.7 and 1.9 Ga are associated with preservation of significant volumes of juvenile crust. What may have been responsible for decreases in the length of supercontinent cycles with time? One possibility, as discussed in Chapter 7, is that plate velocities are increasing with time, thus driving the supercontinent cycle at a faster rate.

Superplume Events

The insulating properties of large plates, continental or oceanic, result from the lithosphere inhibiting mantle convection currents from reaching the surface of the Earth (Gurnis, 1988). An equally, if not more, important effect is the fact that large plates prevent the mantle beneath them from being cooled by subduction. Numerical models show that large plates become increasingly effective as insulators when their width is much greater than the depth of the convecting layer (Lowman & Jarvis, 1996; Lenardic & Kaula, 1996). The net result of this effect is that large mantle upwellings develop beneath large plates. If a large plate happens to carry a supercontinent, the upwelling may promote weakening and eventual breakup of the supercontinent.

The models of Lowman and Jarvis (1999) have been useful in quantifying the relationships between mantle upwellings, supercontinent fragmentation, and whole-mantle versus layered mantle convection. Their results indicate that supercontinent rifting varies with the mode of mantle heating (basal heating versus internal radioactive heat sources) and supercontinent aggregation history. Whether tensile stresses in the interior of supercontinents exceed the yield stress

of the lithosphere of about 80 MPa depends on continental aggregation history, supercontinent size, the Raleigh number of the convecting mantle, the amount of radioactive heating in the mantle, and the viscosity distribution with depth. In the Lowman-Jarvis models, subduction-related forces are at least as important as mantle upwelling in supercontinent breakup. As observed in the breakup of Gondwana, whole-mantle model results predict that plate velocities should be rapid after supercontinent breakup, reducing in speed thereafter. For layered mantle convection, the Lowman-Jarvis models require unreasonably long periods of time to generate stresses necessary to rift supercontinents ($>$600 Ma). Model supercontinents survive for $>$500 Ma when internal heating in the mantle is 40% or less, but $<$250 Ma for models with 80% internal heating of the mantle.

Several superplume events have been suggested in the geologic past. The first and best documented, as discussed in Chapter 9, is the Cretaceous superplume event originally proposed by Larson (1991a, b). Based on weaker evidence, three events were suggested in the Paleozoic and a major global event at 1.9 Ga (Condie et al., 2000). Yet the 1.9-Ga event, which occupied nine pages in the first edition of this book, does not make an appearance in this edition. What happened to it? It turns out that several of the critical evidences are either not dated precisely (high sea level, CIA in shales, phosphate deposition, stromatolite diversity), represent preservational biases (black shales, evaporites), or, like banded iron formation, can now be explained in other ways.

Mantle Plumes and Supercontinent Breakup

One question not fully understood is the role of mantle plumes in the supercontinent cycle. Are they responsible for fragmenting supercontinents, or do they play a more passive role? Many investigators doubt that mantle convection provides sufficient forces to fragment continental lithosphere and that mantle plumes play an active role (Storey, 1995). Not all models require mantle plumes, however. Coltice et al. (2007) show by convection modeling that an internally heated mantle produces an upwelling that results in widespread melting without requiring the help of single mantle plumes. However, because plumes have the capacity to generate large quantities of magma, it should be possible to track the role of plumes in continental breakup by the magmas they leave behind as flood basalts and giant dyke swarms. Models involving mobile-lid convection in the mantle are characterized by alternating spherical harmonic degrees 1 and 2 planform (Zhong et al., 2007). When continents are not present, one hemisphere has a major upwelling and the other a downwelling. In contrast, when a supercontinent is present, the mantle has two antipodal major upwellings. Zhong et al. (2007) propose that due to modulation of continents, these two modes of mantle convection alternate, causing the cyclic processes of assembly and breakup of supercontinents including Rodinia and Pangea in the last 1 Ga. The models of Phillips et al. (2009) that couple mantle convection with mobile

continents involve two types of true polar wander (TPW). The first is driven by a hot upwelling axis that creates a stable maximum moment of inertia, and the second leads to homogenization of mantle thermal structure following dispersal of a supercontinent. Thus it is possible that the supercontinent cycle drives true polar wander.

As discussed in Chapter 4, young LIPs preferentially occur in the two large mantle upwellings beneath the South Pacific and Africa (see Figure 4.2). Unlike earlier views, this suggests a close association between mantle plumes and plate tectonics. McNamara and Zhong (2005) have shown that these large upwellings are better explained as thermochemical piles of "dead" slabs accumulated in the last 120 Ma, rather than purely as thermal superplumes. A time lag of 20–120 Ma occurs between the assembly of Pangea and the starting time of the African superplume, which approximately coincides with the later breakup of Pangea (Li & Zhong, 2009). This is consistent with the idea that mantle upwellings are the ultimate cause of supercontinent breakup.

Gurnis (1988) published a numerical model based on feedback between continental plates and mantle convection, whereby supercontinents insulate the mantle causing the temperature to rise beneath a supercontinent. This results in a mantle upwelling that fragments and disperses the supercontinent. Beginning with a supercontinent with cold downwellings along each side, a hot upwelling generated beneath the supercontinent by its insulation effect fragments the supercontinent (Figures 8.15a and b). After breakup, two smaller continental cratons begin to separate rapidly as the hot upwelling extends to the surface between the two plates, producing a thermal boundary layer (b). Both plates rapidly move toward the cool downwellings marked with a vertical arrow in (c). Approximately 150 Ma after breakup, the two continental fragments collide over a downwelling (d). Nearly 450 Ma after breakup, a new thermal upwelling develops beneath the new supercontinent, and the cycle starts over (e).

If the formation of mantle upwellings is related to the formation of supercontinents, then plate subduction rather than spontaneous boundary instabilities at the core–mantle interface appears to be the ultimate cause of mantle upwellings. Furthermore, the position of the upwelling is linked to the position of the supercontinent, which means that upwellings are not fixed in the mantle. As discussed earlier for Pangea, upwellings or/and clusters of plumes related to upwellings may lead to the breakup of supercontinents.

A possible relationship of mantle plume events to the supercontinent cycle is summarized in Figure 8.16. The timing of the various segments of this cycle is constrained chiefly by data from isotopic ages of continental crust and from computer simulations of mantle processes (Tackley et al., 1994; Condie, 1998, 2000). Results suggest that it takes on average 200–400 Ma for shielding of a large supercontinent to result in a mantle upwelling beneath it (Lowman & Jarvis, 1996). The upwelling and associated plumes break up the supercontinent over a 100- to 200-Ma period and the fragments disperse, heading for major

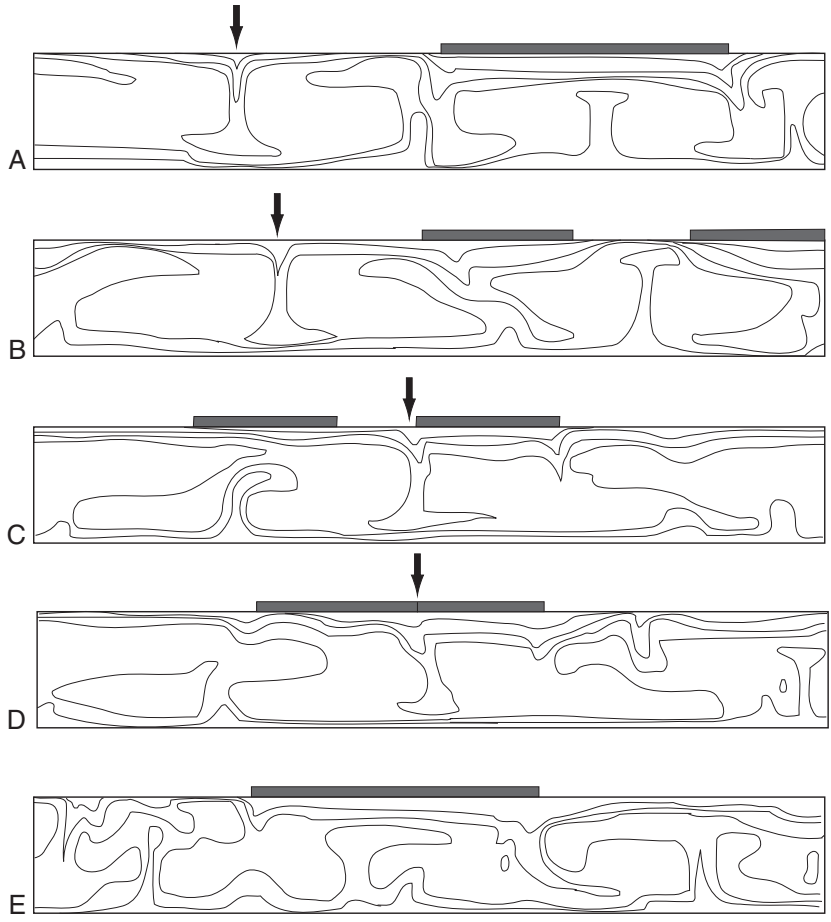

FIGURE 8.15 Computer-generated model of supercontinent breakup and formation of a new supercontinent. The frame of reference is fixed with respect to the left corner of the diagram, and the right continent moves with respect to the left continent, which is stationary. *Modified after Gurnis (1988).*

downwellings (subduction zones). Collisions over the downwellings lead to the assembly of a new supercontinent, which can last another 100–300 Ma, in part overlapping with the breakup phase of the previous supercontinent.

The breakup of Gondwana provides a means of testing the timing of plume magmatism and supercontinent fragmentation (Storey, 1995; Dalziel et al., 2000). The initial rifting stage beginning 180 Ma produced a seaway between West (South America and Africa) and East Gondwana (Antarctica, India, Australia) (Figure 8.17). Seafloor spreading began in the Somali, Mozambique, and Weddell Sea basins by 156 Ma (B). Approximately 130 Ma, South America

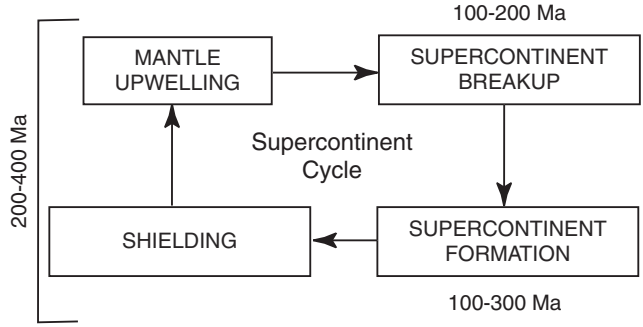

FIGURE 8.16 Box diagram showing possible relationship of the supercontinent cycle to mantle upwelling. *Modified after Condie (1998, 2000).*

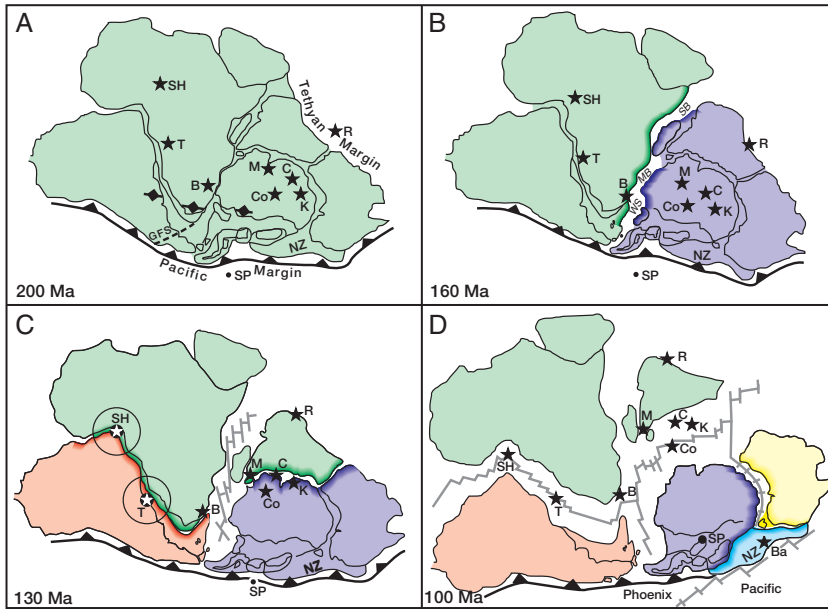

FIGURE 8.17 Gondwana reconstructions during the last 200 Ma. Also shown are subduction zones (barbed lines), major hotspots (stars), and inferred sizes of plume heads (circles). Ocean ridges are diagrammatic. Ba, Balleny; B, Bouvet; C, Crozet; Co, Conrad; K, Kerguelen; M, Marion; R, Reunion; SH, St. Helena; T, Tristan, GFS, Gastre fault system; MB, Mozambique Basin; NZ, New Zealand; SB, Somali Basin; SP, South Pole; WS, proto-Weddell Sea. *Modified after Storey (1995).*

separated from Africa-India and Africa-India separated from Antarctica-Australia (C). The breakup was complete by 100 Ma when Australia separated from Antarctica and Madagascar and the Seychelles separated from India as it migrated northward on a collision course with Asia (D). Precise isotopic dating suggests that continental separation is closely associated with plume volcanism (Figure 8.18).

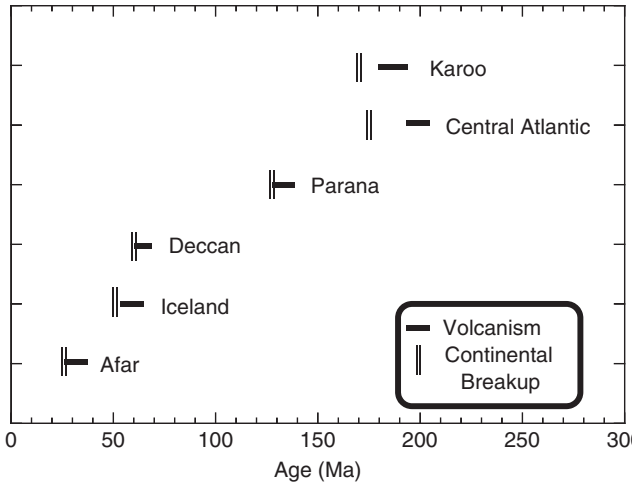

FIGURE 8.18 Timing of supercontinent breakup and plume volcanism associated with several LIPs. *Modified after Courtillot et al. (1999).*

As exemplified by the Deccan and Parana LIPs, volcanism typically begins 3 to 15 Ma before breakup, and the most intense volcanism accompanies initial fragmentation of the supercontinent. The onset of major volcanism in the Deccan traps is coeval with continental breakup and intense volcanism continues for more than 20 Ma. In the case of Iceland, melt production began 60 Ma followed by extensive rifting at 55 Ma and the first oceanic crust formed about 53 Ma as Greenland and Norway separated (Larsen & Saunders, 1998). In Afar (Ethiopia), oceanic volcanism has not yet begun in the Afar depression. The time duration between the onset of flood basalt eruption and the production of oceanic crust ranges from <5 Ma in the Parana and Deccan to 13 Ma for the Karoo and 25 Ma for the Central Atlantic Province (Figure 8.18).

The opening of other basins, such as the Red Sea, Gulf of Aden, Arabian Sea, and the Indian Ocean, also appears to be related to plume volcanism. In fact, with the exception of the Siberian and Emeishan traps in eastern Asia, all major flood basalt provinces in the last 200 Ma are associated with the opening of a new ocean basin (Coffin & Eldholm, 1994; Courtillot et al., 1999). The location of plume impacts on the lithosphere may not have been random or uniform in the mantle. In some instances, as illustrated by the breakup of Gondwana, plume impacts were centrally located under supercontinents (Figure 8.17). In all of the cases cited above, rifting either did not exist prior to flood basalt eruption or it jumped to a new location at or before major eruption began. If the plume head model for flood basalt magma generation is accepted, basalt eruption, uplift (if any), and rifting are all related to rising plume heads, yet they occur in slightly different time sequences in different

areas. Most ocean basins not lined with subduction zones may have been shaped by the episodic impact of large plume heads in the interior or at the edges of continents (Courtillot et al., 1999).

The earliest record of a superplume is that associated with the breakup of Rodinia, as evidenced by large mafic dyke swarms in China and other nearby cratons in Rodinia at 825 Ma (Z. X. Li et al., 2008). There appears to have been a LIP hiatus around 790 Ma with another superplume breakout at 780 Ma in western Laurentia and South China, and by 750 Ma the western half of Rodinia began to fragment above this alleged superplume.

Episodic LIP Events

Isley and Abbott (1999, 2002) and Ernst and Buchan (2003) have used the distribution of komatiites, flood basalts, mafic dyke swarms, and layered mafic intrusions in the geologic record to identify superplume events in the Precambrian. Analysis of the age distribution of giant dyke swarms indicates numerous plume-head events in the last 3 Ga, with no plume-free intervals greater than about 200 Ma (Ernst & Buchan, 2001, 2003; Prokoph et al., 2004). Although time series analyses clearly show that mantle plume activity is strongly episodic, the frequency of events depends on the database used. Using the combined database of Ernst and Buchan (2003) and Bozhko (2010), we see major mantle plume events at 2.8–2.7, 2.45, 2.2–2.1, 1.4–1.2, 0.7–0.6, and <0.2 Ga (Figure 8.19). All but the peak at 2.8–2.7 Ga correlate with supercontinent breakup (Ernst et al., 2008; Ernst & Bleeker, 2010) with concurrent development of mantle upwellings (superplumes). In contrast, the peak at 2.8–2.7 Ga corresponds to the formation of the first supercratons and with the first large production of juvenile continental crust. Notice the pronounced minimum in LIP activity during the crustal age gap at 2.4–2.2 Ga. The strongest cyclicity of superplume events reported by Prokoph et al. (2004) is at 170, 650 (730–550), 250–220, and 330 Ma, with several short cycles in the last 100 Ma.

Slab Avalanches

Some models for the origin of superplume events involve catastrophic sinking of slabs through the 660-km seismic discontinuity in the upper mantle, which upon arrival at the D″ layer above the core, initiate a superplume event (Condie, 1998). Although seismic tomographic results clearly suggest that descending slabs sink into the lower mantle today, this may not have been the case in the geologic past when Earth was hotter. Christensen and Yuen (1985) have shown that in a hotter mantle with a larger Rayleigh number, such as probably existed in the Archean, the amount of leakage across the 660-km discontinuity is considerably reduced, perhaps resulting in layered convection.

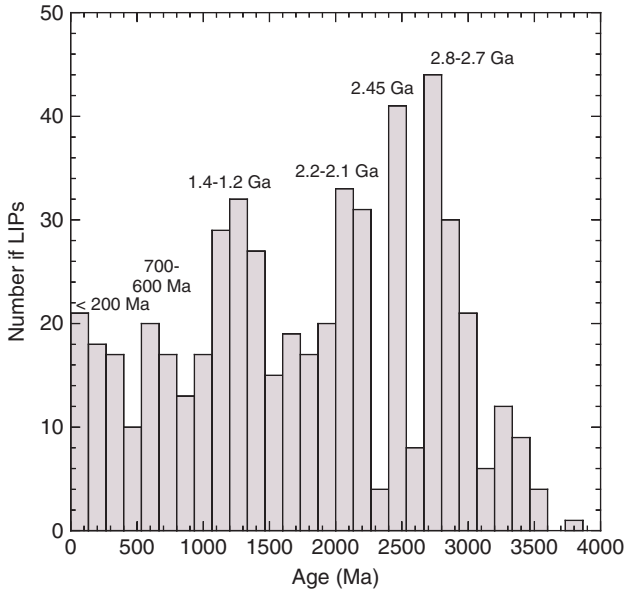

FIGURE 8.19 Secular distribution of LIPs in the last 4 Ga. Major age clusters are labeled in Ga. *Data from Ernst & Buchan (2003) plus updates.*

Numerical simulations by Yuen et al. (1993) show that at the higher temperatures that existed in the Archean, the mantle would convect more chaotically, leading to a type of convection known as hard turbulence. Their results show that during hard turbulence with a higher Raleigh number, phase transitions such as the perovskite transition at 660 km become stronger barriers and result in layered convection. This is true, however, only if the Clapeyron slope of the perovskite reaction is strongly negative. As we have seen in Chapter 4, it is likely that this reaction is at best only very slightly negative, and thus at higher mantle temperatures it should not be a serious retardant to whole-mantle convection. Hence, even in the early hotter mantle, the 660-km discontinuity should not have appreciably stalled descending slabs, and thus we lose the mechanism for slab avalanches.

SUPERCONTINENTS, SUPERPLUMES, AND THE CARBON CYCLE

One of the most exciting aspects of the supercontinent cycle and superplumes is the consequences they may have had in Earth history and especially the effect on paleoclimates and the biosphere. In this section, we review various feedbacks associated with supercontinent formation and breakup and with mantle superplume events that may affect near-surface systems in the planet.

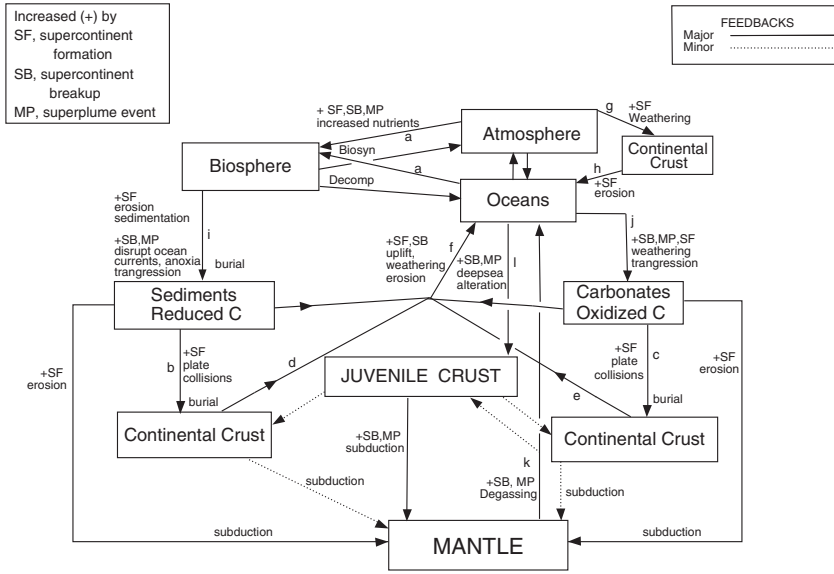

FIGURE 8.20 Carbon reservoirs in Earth showing possible effects of supercontinents and mantle superplumes. Each box represents a carbon reservoir. Juvenile crust = oceanic crust + oceanic plateaus + island arcs. Biosyn = biosynthesis; Decomp = decomposition. Numbered paths refer to text discussions. *After Condie et al. (2000).*

Supercontinent Formation

Supercontinent assembly impacts the carbon cycle in several ways (Kerr, 1998; Condie et al., 2000) (Figure 8.20). Continental collisions are initially a net source of CO_2 due to the burial and/or thermal destruction of sedimentary organic matter and carbonates within collisional zones (paths b and c, Figure 8.20) (Bickle, 1996). Continued uplift of a supercontinent accelerates erosion of sedimentary rocks and their carbon (paths d and e). Whether this carbon source changes the $\delta^{13}C$ of seawater depends on the ratio of the reduced carbon ($\delta^{13}C = -20$ to $-40‰$) to oxidized carbon ($\delta^{13}C = 0‰$) that is recycled back into the oceans (path f). For example, if both carbonate and organic carbon are recycled in approximately the same ratio as their ratio prior to supercontinent formation, the $\delta^{13}C$ of seawater will not change (Des Marais et al., 1992) (Chapter 6). As the surface area of a growing supercontinent increases, weathering of surface rocks withdraws more CO_2 from the atmosphere, transferring it to the continents (path g), where it is eventually returned to the oceans by erosion (path h). Increased erosion also releases more nutrients (e.g., phosphorus), increasing biological productivity (paths h, a). The nutrient source and CO_2 sinks can draw down atmospheric CO_2 levels, favoring cooler climates that intensify ocean circulation and, thus, increase nutrient upwelling and marine productivity. Intense drawdown of CO_2 together with increasing albedo caused

by the increasing land/ocean ratio can lead to widespread glaciation. The above factors collectively promote increased burial rates of organic carbon, relative to carbonates, and thus may raise the $\delta^{13}C$ value of seawater. However, uplift of collisional mountain belts during supercontinent formation can recycle older carbon that is depleted in ^{13}C. For instance, a dramatic drop of $\delta^{13}C$ in marine carbonates about 55 Ma coincides with initial uplift of the Himalayas in response to the India-Tibet collision and may reflect recycling of carbon depleted in ^{13}C (Beck et al., 1995). In addition, the final stages in the formation of Pangea were accompanied by compressive stresses around the margin of the supercontinent, leading to significant uplift and erosion. Faure et al. (1995) suggest that this enhanced erosion may be responsible for a pronounced minimum in seawater $\delta^{13}C$ at 250 Ma. Hence, it appears the control of $\delta^{13}C$ in seawater during supercontinent formation reflects a delicate balance between carbon burial and carbon recycling.

Two ideas have been proposed for a possible role of gas hydrates in global climate change (Kvenvolden, 1999). First is direct injection of methane, or more likely its oxidized equivalent CO_2, into the atmosphere–ocean system as gas hydrates dissolve during warm climatic regimes. This would provide a strong positive feedback for global warming. Second is that continental-margin gas hydrates release methane during falling sea level, which generally accompanies global cooling. Such cooling, for instance, could occur during glaciation or supercontinent formation. However, with the present-day reserves of gas hydrates, neither of these effects should have significant influence on climate change or on sea level (Kvenvolden, 1999; Bratton, 1999). If gas hydrates were widespread during the Precambrian, supercontinent formation could lead to gas hydrate evaporation as sea level drops, which would introduce biogenic carbon as CO_2 into the atmosphere, increasing both organic and carbonate burial rates as well as increasing greenhouse warming (Haq, 1998). Also, because gas hydrates contain carbon with very negative $\delta^{13}C$ values (averaging about –60‰), they may offset any increase in the $\delta^{13}C$ due to organic carbon burial.

As sea level falls during supercontinent formation, the ensuing regression restricts the deposition of shelf carbonates and mature clastic sediments, and the emerging shelves can accommodate deposition of extensive evaporites. Organic carbon sedimentation occurs either farther offshore or in freshwater basins within the interior of the supercontinent (Berner, 1983). Overall, supercontinent formation promotes higher rates of erosion and sedimentation (path i, Figure 8.20), which correlate with organic carbon burial rates, and platform carbonate deposition becomes more restricted. The net result is that periods of supercontinent formation favor relatively high ratios of organic versus carbonate sedimentation and burial. If this is the case, positive carbon isotope anomalies should develop in seawater during supercontinent formation. However, the fact that this is not observed indicates that other processes must obscure this effect.

Supercontinent Breakup

Supercontinent breakup creates new, narrow ocean basins having restricted circulation and hydrothermally active spreading centers (Kerr, 1998; Condie et al., 2000). These features promote anoxia in the deep ocean (path i, Figure 8.20). The actively eroding escarpments along new continental rift margins contribute sediments to the rift basins, and marine transgressions increase the rate of burial of organic and carbonate carbon on stable continental shelves. The amount of shallow marine carbonate deposition (path j), however, critically depends on redox stratification of the oceans, because reducing environments are not conducive to carbonate precipitation. Should anoxic deep-ocean water invade the shelves, it would facilitate organic carbon burial on the shelves, including the deposition of black shale and the accumulation of gas hydrates. This, in turn, should lead to enhanced growth of oxygen in the atmosphere.

The increase in length of the ocean ridge network that accompanies supercontinent fragmentation promotes increased degassing of the mantle, including CO_2 (path k). Increasing atmospheric CO_2 levels and rising sea level promote warmer climates, resulting in increased weathering rates (path g) (Berner & Berner, 1997) as well as the potential for the marine water column to become stratified and for deep water to become anoxic (path i). Increasing carbonate in the oceans together with a growing ocean ridge system would also enhance rates of removal of seawater carbonate by deep-sea alteration (path l). To the extent that these developments enhance the fraction of carbon buried as organic matter, they would also lead to an increase in the $\delta^{13}C$ of seawater because ^{12}C is preferentially incorporated into organic carbon (Melezhik et al., 1999).

Mantle Superplume Events

Most of the features described above for supercontinent breakup also apply to superplume events. In fact, superplume events can be considered as positive feedback loops for changes in the carbon cycle and paleoclimate accompanying supercontinent breakup. During a superplume event, rising sea level may trigger marine transgressions (path i, Figure 8.20). Oceanic plateaus can locally restrict ocean currents (Kerr, 1998), thus promoting local stratification of the marine water column leading to anoxia (path i). Plume volcanism and associated extensive hydrothermal activity exhale both CO_2 and reduced constituents into the atmosphere–ocean system (Caldeira & Rampino, 1991; Kerr, 1998). The increased CO_2 flux warms the climate and enhances weathering rates (path g). During superplume events when anoxia is widespread in the oceans, gas hydrates could form in large volumes, provided the oceans are not warm enough to dissolve the hydrates. Biological productivity during a superplume event is enhanced by several factors, such as increased

concentrations of CO_2, increased nutrient fluxes from both hydrothermal activity (such as CO_2, CH_4, phosphorus, iron, and trace metals [Sb, As, Se]) and enhanced weathering, and elevated temperatures due to CO_2-driven greenhouse warming (paths a).

Carbonate precipitation is enhanced by increased chemical weathering and by marine transgressions (path j). Increased hydrothermal activity on the seafloor should also increase the rate of deep-sea alteration, which in turn should increase the removal rate of carbonate from seawater (path l). Liberation of large amounts of SO_2 into the oceans by increased hydrothermal activity might decrease ocean pH, the net effect of which would be to dissolve marine carbonates, particularly those adjacent to high-temperature emanations (Kerr, 1998). However, a more acid ocean would also dissolve Na and Ca, increasing the oceanic pH again. Organic matter burial is enhanced by increased productivity, marine transgression, and the expansion of anoxic waters, in particular onto continental shelves (path i) (Larson, 1991b). In summary, phenomena associated with superplumes promote the formation and deposition of both organic and carbonate carbon.

EPILOGUE

Probably no other geologic phenomenon has left a greater imprint on Earth's history than the supercontinent cycle. The supercontinent cycle, in turn, reflects plate tectonics, and both the formation and breakup of supercontinents are driven by a cooling and convecting mantle. Orogenic mountain chains and associated climatic patterns are closely tied to continental collisions as supercontinents grow. Land bridges come and go as supercontinents form and then break up, providing ever-changing ecological niches directing the evolution of life. Long-term changes in sea level are also controlled by the comings and goings of supercontinents. Global climate changes are affected by changes in the surface area of continents and superplume-related volcanic emissions. And the episodic distribution of isotopic ages has a clear tie to supercontinent assembly. As a bottom line, it appears that any planet with plate tectonics should have a supercontinent cycle, which significantly influences planetary history including the atmosphere–ocean system and the biosphere.

FURTHER READING

Condie, K. C. (2001). *Mantle Plumes and Their Record in Earth History*. Cambridge, UK: Cambridge University Press.

Davies, G. F. (1999). *Dynamic Earth Plates, Plumes and Mantle Convection*. Cambridge, UK: Cambridge University Press.

Ernst, R. E., & Buchan, K. L. (Eds.). (2001). *Mantle Plumes: Their Identification Through Time*. Special Paper 352. Geological Society of America.

Reddy, S. M., Mazumder, R., Evans, D. A. D., & Collins, A. S. (Eds.). (2009). *Paleoproterozoic Supercontinents and Global Evolution* (272 pp). Bath, UK: Geological Society Publishing House.

Rogers, J. J. W., & Santosh, M. (2004). *Continents and Supercontinents*. Oxford, UK: Oxford University Press.

Yoshida, M., Windley, B. F., & Dasgupta, S. (2003). *Proterozoic East Gondwana: Supercontinent Assembly and Breakup*. Special Publication No. 206. Geological Society of London.

Chapter 9

Great Events in Earth History

INTRODUCTION

Although planets are often considered to evolve in a rather continuous uniformitarian-like manner, there are times in planetary history when changes occur rather rapidly—and sometimes catastrophically. During the history of Earth, many events have significantly affected the later evolution of the planet, and in some cases have had profound effects on the origin and evolution of life. Some of these events, like the onset of plate tectonics, are long lived, stretching over several hundred million years. Others, like the formation of the Moon and the Cretaceous superplume event, are of intermediate duration, 50–100 Ma. And then there are short-lived events such as asteroid impacts, whose effects are concentrated chiefly in hours to a few years. In some cases events are one-time happenings, such as the Great Oxidation Event in which, for the first time, free oxygen was liberated in significant amounts into the atmosphere. In other cases similar events have occurred many times, such as asteroid impacts and superplume events.

All of these events have one thing in common: they have influenced the evolution of Earth and in some cases have been very important in making Earth a habitable planet. If it were not for the Moon controlling our climatic regimes and plate tectonics providing continents, higher forms of life could not have developed on planet Earth, regardless of the presence of oceans and an oxygenated atmosphere. The great mass extinctions at the end of the Permian and at the end of the Cretaceous opened up new ecological niches for other organisms to evolve. If it were not for the extinction of dinosaurs at the end of the Cretaceous, it is unlikely that mammals, including humans, would have become the dominant life-forms on the planet.

In this chapter, I have selected eight events, which I call "Great Events," since they all have profound effects on the evolution of Earth. I do not claim that the events I have chosen are the only major events controlling Earth's history, but each of these has proven to be critical in some way to the origin or/and evolution of life (in fact, one event is the origin of life). We will discuss them in order of their age, beginning with the origin of the Moon at 4.5 Ga and ending the mass extinction at the end of the Cretaceous some 65 Ma.

EVENT 1: ORIGIN OF THE MOON

How Rare Is the Earth–Moon System?

The origin of the Earth–Moon system is ultimately connected with the question of "How do you make a habitable planet?" Some investigators have argued that Earth is the most diverse planet in 10 000 light years, although the great array of extrasolar planets that are being discovered seriously challenges this conclusion. One reason for thinking Earth is a rare planet type involves the question of how to make a large Moon that keeps Earth's obliquity low and thus stabilizes its climate (Williams & Pollard, 2000). Expanded modeling in the last few years calls into question the uniqueness of the Earth–Moon system, suggesting that satellites like the Moon can form over a broad range of conditions during planetary formation (Righter, 2007). In fact, Pluto's satellite Charon may have formed in a similar manner to the Moon. Although it is still not possible to resolve extrasolar planets as small as Earth, several larger extrasolar planets have been reported with a rocky component and probably have water (see Chapter 10). As the first on the list of Earth's Great Events, we will review the origin of the Moon concentrating on the giant impactor idea, which continues to be the most popular model.

Constraints on Lunar Origin

Scientific results from the *Apollo* missions have provided a voluminous amount of data on the structure, composition, and history of the Moon (Taylor, 1982, 1992). Seismic data are generally interpreted in terms of five zones within the Moon, which are, from the surface inward, a plagioclase-rich crust (dominantly gabbroic anorthosite), 60–100 km thick; an upper mantle, composed chiefly of pyroxenes and olivine, 300–400 km thick; a lower mantle of the same composition (with olivine dominating), about 500 km thick; and 200–400 km of iron core.

Among the more important constraints that any model for lunar origin must satisfy are the following:

1. The Moon does not revolve in the equatorial plane of Earth, nor in the ecliptic. The lunar orbit is inclined at 5.14° to the ecliptic, whereas the Earth's equatorial plane is inclined at 23.4° (Figure 9.1).

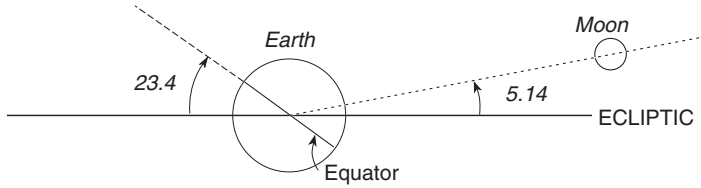

FIGURE 9.1 Orbital relations of the Earth–Moon system.

2. Tidal dissipation calculations indicate that the Moon is retreating from Earth, resulting in an increase in the length of the day of 15 s/Ma. Orbital calculations and the Roche limit indicate that the Moon has not been closer to Earth than about 24 000 km.
3. The Moon is enriched in refractory oxyphile elements and depleted in refractory siderophile and volatile elements relative to Earth (Figure 9.2). Particularly important is the low density of the Moon (3.34 g/cm^3) compared to other terrestrial planets, which indicates the Moon is significantly lower in iron than these planets.
4. The Earth–Moon system has an anomalously large amount of angular momentum (3.45×10^{41} g/cm^2/s) compared to the other planets.
5. The oxygen isotopic composition of lunar igneous rocks collected during the Apollo missions is the same as that of mantle-derived rocks from Earth, and very different from meteorites and Mars (Figure 9.3). Because oxygen isotope composition seems to vary with position in the solar system, the similarity of oxygen isotopes in lunar and terrestrial igneous rocks suggests that both bodies formed in the same part of the solar system at approximately the same distance from the Sun.
6. Attempts to date the Moon were initially focused on determining the ages of the oldest rocks and therefore providing a lower age limit (Halliday, 2003). These studies emphasized precise Sr, Nd, and Pb isotopic constraints. The ages reflect the timing of crystallization of the lunar magma ocean, the most precise values of which range from 4334 to 4003 Ma (Edmunson et al., 2009) (Figure 9.4). The oldest precise age from the

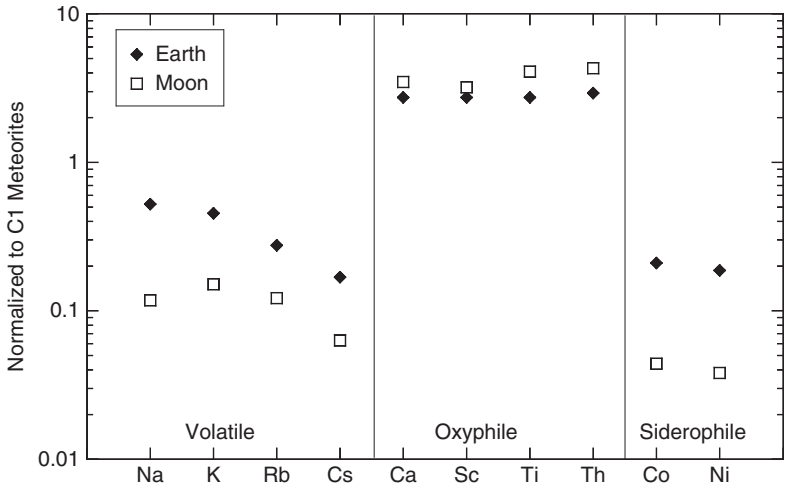

FIGURE 9.2 Volatile, oxyphile, and siderophile element distributions in Earth and Moon normalized to carbonaceous meteorites (C1, type 1).

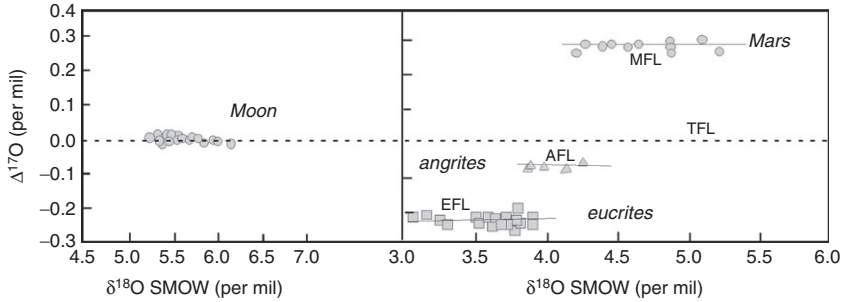

FIGURE 9.3 Comparison of oxygen isotope data for the Moon, Mars, and meteorites (angrites, eucrites). Data are normalized to Earth (TFL, terrestrial fractionation line). AFL and EFL, angrite and eucrite fractionation lines, respectively. $\delta^{18}O$ SMOW is defined as $1 - [(^{18}O/^{16}O\ (\text{sample}) - {}^{18}O/^{16}O\ (\text{standard mean ocean water or SMOW})] \times 1000$. $\Delta^{17}O = \delta\ ^{17}O - 0.5245 \times \delta^{18}O$. *After Righter (2007).*

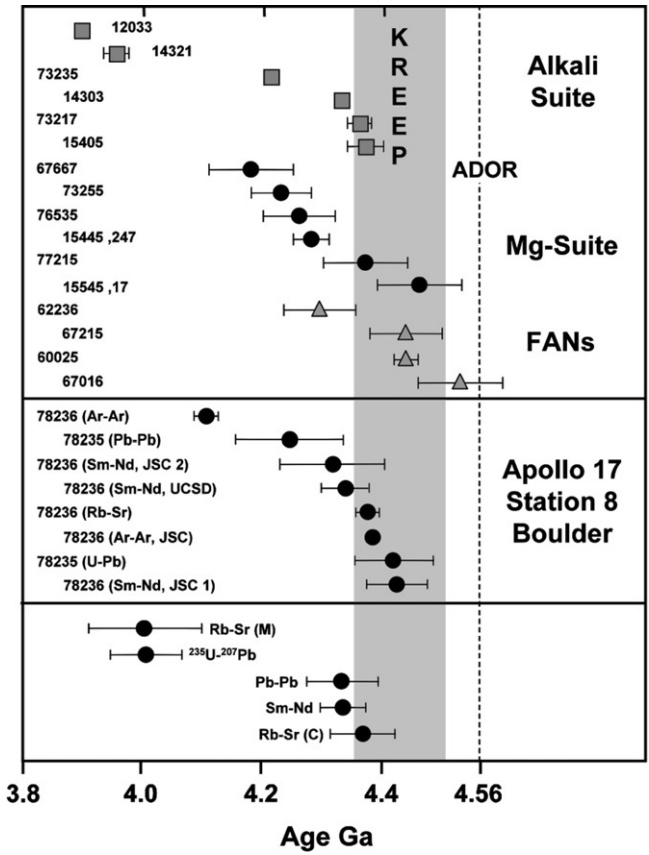

FIGURE 9.4 Summary of ages of lunar rocks. FANs, ferroan anorthosites; ADOR, Angra dos Reis, the oldest meteorite age. *Modified after Edmunson et al. (2009), courtesy of Jennifer Edmunson.*

surface is from an anorthosite clast, sample 67016, with a U/Pb age of 4562 ± 68 Ma. Hf/W isotopic data provide the most powerful current constraint on the exact age of the Moon and these ages lie in the range of 4470 to 4510 Ma. Tungsten isotopic results of Touboul et al. (2007) suggest that the Moon must form within 62 my after the formation of the solar system.

Models for the origin of the Moon generally fall into one of four categories: (1) fission from Earth, (2) the double planet scenario in which the Moon accretes from a sediment ring around Earth, (3) gravitational capture by Earth, and (4) impact on Earth's surface by a Mars-size body (Figure 9.5). Any acceptable model must account for the constraints listed above, and thus far none of these models is completely acceptable. Each of the lunar origin models will be briefly discussed, and a summary of just how well each model complies with major constraints is given in Table 9.1.

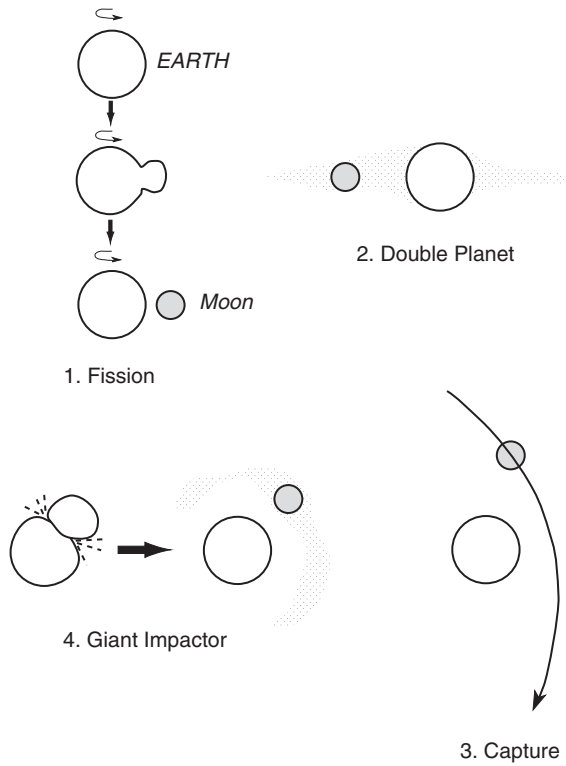

FIGURE 9.5 Models for the origin of the Moon.

TABLE 9.1 Summary of Major Constraints on Models of Lunar Origin

	Fission	Double planet	Capture	Giant impactor
1. Angular momentum	I	I	C(I)	C
2. Lunar rotation	C	C	C(C)	C
3. Orbital characteristics	I	I	C(C)	C
4. Chemical composition	I	C	I(I)	C

Note: *Values in parentheses indicate disintegrative capture. C, consistent; I, inconsistent.*

The Fission Model

The fission model involves separation of the Moon from Earth during an early stage of rapid spinning when tidal forces overcome gravitational forces. One version of the fission model (Wise, 1963) suggests that formation of Earth's core reduced the amount of inertia, increasing the rotational rate spinning off material to form the Moon. Such a model is attractive in that it accounts for the similarity in density between Earth's mantle and the Moon and for the absence of a large metallic lunar core. The hypothesis is also consistent with the fact that the Moon revolves in the same direction as Earth rotates, the circular shape of the lunar orbit, the existence of a lunar bulge facing Earth, and the similar oxygen isotope ratios of the two bodies. The model also explains the iron-poor character of the Moon if fission occurred after core formation in Earth, since the Moon would be formed largely from Earth's mantle.

Fission models, however, face several fatal obstacles (Table 9.1). For instance, they do not explain the inclination of the lunar orbit, and they require more than four times the total angular momentum than is available in the present Earth–Moon system! If the Earth–Moon system ever had this excess angular momentum, no acceptable mechanism has been proposed to lose it (Wood, 1986). Also, lunar igneous rocks are more depleted in siderophile and volatile elements than terrestrial igneous rocks (Figure 9.2), indicating that the lunar interior is not similar in composition to Earth's mantle. Although some investigators still favor a fission model (Binden, 1986), the above problems seem to render the model highly implausible.

Double Planet Models

Double planet models involve an accreting Earth with simultaneous accretion of the Moon from orbiting solid particles (Harris & Kaula, 1975). A major advantage of these models, also known as co-accretion or precipitation models,

is that they do not invoke special, low-probability events. The models assume that as Earth accreted, solid particles accumulated in orbit about the planet and accreted to form the Moon. The general scenario is as follows: Earth accretes first and its core forms during accretion; as Earth heats up, material is vaporized from the surface, forming a ring around Earth from which the Moon accretes. Because core formation extracts siderophile elements from the mantle, the material vaporized from Earth is depleted in these elements, and hence the Moon, which accretes from this material, is also depleted in these elements. Because volatile elements are largely lost by intense solar radiation from a T-Tauri wind (Chapter 10) after Earth accretes (but before the Moon accretes), the material from which the Moon accretes is depleted in volatile elements relative to Earth. This leaves material from which the Moon accretes relatively enriched in oxyphile refractory elements.

The most serious problems with the double planet models are that they do not seem capable of explaining the large amount of angular momentum in the Earth–Moon system (Wood, 1986) and they do not readily explain the inclined lunar orbit.

Capture Models

Capture models propose that the Moon and Earth formed in different parts of the solar nebula and that early in the history of the solar system the Moon or its predecessor approached Earth and was captured (Taylor, 1992). Both catastrophic and noncatastrophic models of lunar capture have been described, involving retrograde and prograde orbits for the Moon prior to capture.

Capture models fall into two categories: *intact capture*, in which a fully accreted Moon is captured by Earth, and *disintegrative capture*, in which a planetesimal comes within Earth's Roche limit, is fragmented by tidal forces with most of the debris captured in orbit about Earth, and the debris re-accretes to form the Moon (Wood & Mitler, 1974). Although intact capture models may explain the high angular momentum and inclined lunar orbit, they cannot readily account for geochemical differences between the two bodies. The similar oxygen isotopic ratios between lunar and terrestrial igneous rocks suggests that both bodies formed in the same part of the solar system, yet the capture model does not offer a ready explanation for the depletion of siderophile and volatile elements in the Moon. Also, intact lunar capture is improbable because it requires a very specific approach velocity and trajectory. Disintegrative capture models cannot account for the high angular momentum in the Earth–Moon system.

Giant Impactor Model

The first models for lunar origin involving a single giant impact proposed that the Moon was the product of a glancing blow collision with another differentiated planet (Hartmann, 1986; Cameron, 1986). A ring of debris would have

been produced from the outer silicate portions of Earth and the impactor planet. Such a model has the potential of eliminating the angular momentum and nonequatorial lunar orbit problems as well as providing a means to explain chemical differences between Earth and Moon. One of the major factors that led to the giant impactor model is the stochastic studies of Wetherill (1990), which indicate that numerous large bodies formed in the inner solar system during the early stages of planetary accretion. Results suggest the existence of at least 10 bodies larger in size than Mercury and several equal or larger than Mars. Wetherill (1994) estimates that about one-third of these objects collided with and accreted to Earth, providing 50–75% of Earth's mass. The obliquities of planets and the slow retrograde motion of Venus are also most reasonably explained by late-stage impact of large planetesimals. The impact origin of the Moon was once a controversial idea, but it has gradually been accepted for two reasons: (1) the lack of a realistic alternative and (2) the growing evidence for its compatibility with observational data.

In the giant impactor model, a Mars-size planet (named "Theia," the mother of "Selene," the goddess of the Moon) collides with Earth during the late stages of accretion (Taylor, 1993) (Figure 9.6). The giant-impact theory is supported by a number of important observations. As a starter, we know now that the Moon must have formed tens of millions of years after the start of the solar system (Halliday, 2000). This is consistent with a collision between already formed planets. Such an impact can easily account for the anomalously high angular momentum in the Earth–Moon system (Newsom & Taylor, 1989). A remarkable outcome of computer models for the collision is the short timescale: one model shows the entire collision including reaccretion of Earth finished in 24 hours (Figure 9.7)! One problem with the model is that the Moon is formed chiefly from material from the impactor, Theia, yet the Earth and the Moon are on the whole similar in composition, especially in such isotopes as oxygen (Figure 9.3). The similarity in oxygen isotopes and trace siderophile abundances between the Earth and the Moon provides evidence that Earth and Theia were neighboring planets made of an identical mix of materials with similar differentiation histories. Because iron had already segregated into Earth's core, a low iron (and other siderophile elements) content of the Moon is predicted by the model. The similarities of Earth and Theia probably relate to proximity in the early solar system, increasing the probability of collision.

The high energy of the impact results not only in complete disruption of the impacting planet, but in widespread melting of Earth, producing a magma ocean. An additional attribute of the model is that the material that escapes from the system after impact is mostly liquid or vapor, thus leaving dust enriched in refractory elements from which the Moon forms, accounting for the extreme depletion in volatile elements in the Moon (Figure 9.2). Whether the remaining material immediately accretes into the Moon or forms several small lumps that coalesce to form the Moon on timescales of the order of

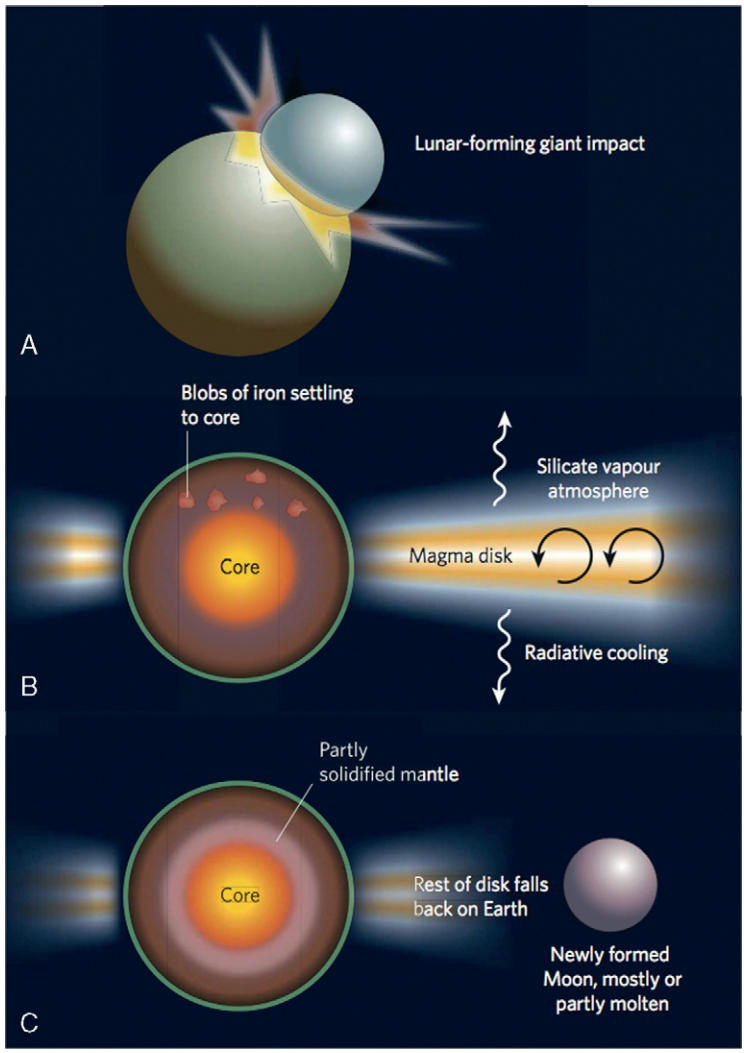

FIGURE 9.6 Three evolutionary stages in the giant impact model for the origin of the Moon. (A) Planetary embryo collides with a nearly complete Earth. (B) Formation of magma disk about the new Earth (C) Formation of the Moon from the outermost disk; inside Earth the mantle near the core is partially solidified, possibly becoming layered. *Modified after Stevenson (2008), courtesy of Dave Stevenson. Used with permission of Nature Publishing Group, permission conveyed through Copyright Clearance Center, Inc.*

100 years is unknown. In either case, the Moon heats up rapidly forming a widespread magma ocean.

Although the giant impactor model needs to be continually reevaluated, it appears to be capable of accommodating more of the constraints related to lunar origin than any of the competing models (Table 9.1).

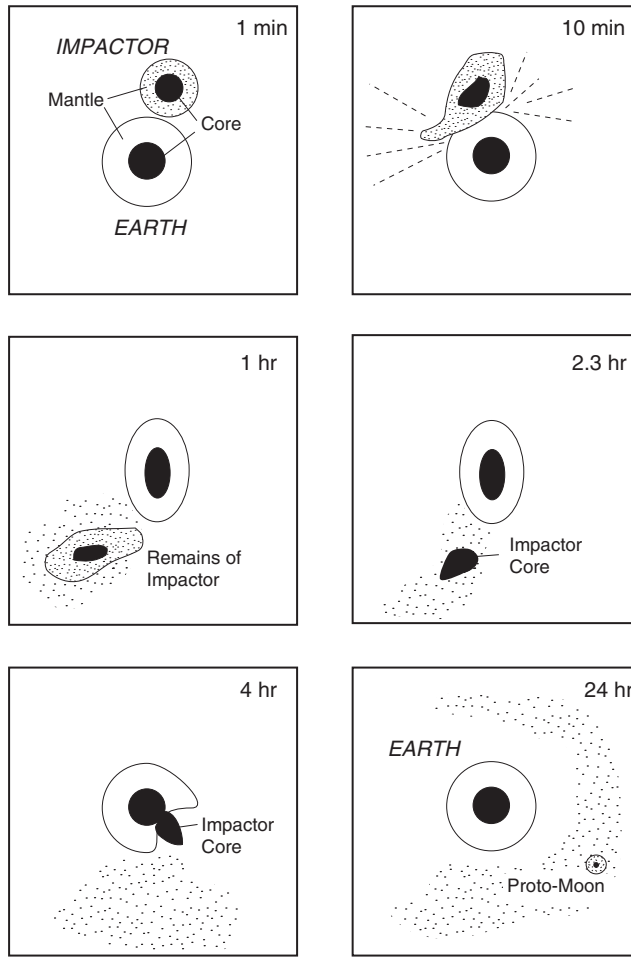

FIGURE 9.7 Computer simulation of the formation of the Moon by the giant impactor Theia. Model is for an oblique collision of Theia with Earth with Theia having 0.14 Earth mass at a velocity of 5 km/s. Time elapsed since impact is given in each box. *After Newsom and Taylor (1989).*

Early Thermal History of the Moon

Impacts previous to Theia would have heated Earth to temperatures close to or in excess of melting (Stevenson, 2008). Impact heating is uneven because various parts of Earth would be shocked to differing extents, but the immediate post–giant-impact state would relax to a very hot configuration, in which all or most of the rock and iron is in molten form and some silicate is in vapor form (Figure 9.6). In most simulations of this kind of impact, a disk forms, derived mostly from the impacting body in a period of time as short as 24 hours and no

longer than hundreds of years (Figure 9.7). During this time, most of the core of Theia merges with the core of proto-Earth, some of the preexisting Earth's atmosphere may be blown off, and a significant part of the deep, initially molten, mantle will crystallize. For the expected radiating surface area, the cooling time to remove about half of the impact energy is around 1000 years, perhaps somewhat shorter for the disk, a very short period relative to the time between major planetary collisions.

It is generally thought that the anorthositic crust on the Moon formed as a scum on a magma ocean (Breuer & Moore, 2007). Estimates of depth of this magma ocean vary considerably from whole-Moon melting to thin melt zones in the upper part of the lunar mantle. Thermal models indicate that the lunar magma ocean should cool rapidly within the first 50–100 Ma, and as crystallization proceeds, the mantle may become layered with late dense Fe-rich silicates coming to rest on less dense Mg-rich silicates (Figure 9.6c). Recent data indicate that crystallization of most of the magma ocean followed the collisional event by about only 100 Ma, with small volumes of melt continuing to crystallize for another 200–400 Ma (Nemchin et al., 2009). Also during crystallization, incompatible elements, including radioactive elements (e.g., U, K, Th), would be concentrated near the lunar surface leaving the interior very depleted in these elements. Thermal convection in the lunar mantle should lead to production of a thick lunar lithosphere (as observed, see Chapter 10), while the mantle and core cool by only a few hundred degrees centigrade, a scenario typical of a one-plate planet.

EVENT 2: ORIGIN OF LIFE

Although the distinction between living and nonliving matter is obvious for most objects, it is not so easy to draw this line between some unicellular organisms, on one hand, and large nonliving molecules such as amino acids, on the other. It is generally agreed that living matter must be able to reproduce new individuals, it must be capable of growing by using nutrients and energy from its surroundings, and it must respond in some manner to outside stimuli. Another feature of life is its chemical uniformity. Despite the great diversity of living organisms, all life is composed of a few elements (chiefly C, O, H, N, and P) that are grouped into nucleic acids, proteins, carbohydrates, fats, and a few other minor compounds. This suggests that living organisms are related and that they probably had a common origin. Reproduction is accomplished in living matter at the cellular level by two complex nucleic acids, RNA and DNA. Genes are portions of DNA molecules that carry specific hereditary information. Three components are necessary for a living system to self-replicate: RNA and DNA molecules, which provide a list of instructions for replication; proteins that promote replication; and a host organ for the RNA-DNA molecules and proteins. The smallest entities capable of replication are amino acids.

Perhaps no other subject in geology has been investigated more than that of the origin of life (Kvenvolden, 1974; Oro, 1994; Westall & Southam, 2007). It has been approached from many points of view. Geologists have searched painstakingly for fossil evidences of the earliest life, and biologists and biochemists have provided a variety of evidence from experiments and models that must be incorporated into any model for the origin of life. Although numerous models have been proposed for the origin of life, two environmental conditions are a prerequisite to all models: (1) the elements and catalysts necessary for the production of organic molecules must be present, and (2) free oxygen, which would oxidize and destroy organic molecules, must not be present. In the past, the most popular models for the origin of life involve a primordial "soup" rich in carbonaceous compounds produced by inorganic processes. Reactions in this soup promoted by catalysts such as lightning or ultraviolet radiation result in production of organic molecules. Primordial soup models, however, seem unnecessary in terms of rapid degassing of Earth prior to 4 Ga. Condensation of a steam atmosphere leading to rapid growth of the early oceans would not allow concentrated "soups" to survive except perhaps very locally in evaporite basins after 4 Ga. Because the chances of organic molecules being present in sufficient amounts, in the correct proportions, and in the proper arrangement are very remote, it would seem that the environment in which life formed would have been rare in the early Archean. Possibilities include volcanic environments and hydrothermal vents along ocean ridges.

Simple amino acids have been formed in the laboratory under a variety of conditions. The earliest experiments were those of Miller (1953), who sparked a hydrous mixture of H_2, CH_4, and NH_3 to form a variety of organic molecules including 4 of the 20 amino acids composing proteins. Similar experiments, using both sparks and ultraviolet radiation in gaseous mixtures of H_2O, CO_2, N_2, and CO (a composition more in line with that of Earth's early degassed atmosphere), also resulted in production of amino acids, HCN, and formaldehydes, the latter of which can combine to form sugars. Heat also may promote similar reactions.

The Role of Impacts

As indicated by microfossils, life was certainly in existence by 3.5 Ga, and carbon isotope data, although less definitive, suggests that life was present by 3.8 Ga. This being the case, the origin of life must have occurred during or before the last stage of heavy bombardment of planets in the inner solar system as indicated by the impact craters on the Moon and other terrestrial planets with ancient surfaces (Koeberl, 2006). As an example, the impact record on the Moon shows that crater size, and hence impact energy, falls exponentially from 4.5 Ga to about 3.0 Ga, decreasing more gradually thereafter (Sleep et al., 1989; Chyba, 1993). Similarity of crater frequency versus diameter relations for Mercury and Mars implies that planets in the inner solar system underwent a

similar early bombardment history, although Earth's history has been destroyed by plate tectonics. A decrease in impact energy with time on Earth is likely to be similar to that on the Moon, except after 3.0 Ga, energies were perhaps an order of magnitude higher on Earth. Because Earth's gravitational attraction is greater than that of the Moon, it should have been hit with many more large objects than the Moon before 3.5 Ga. The impact record on the Moon implies that Earth was subjected to cataclysmic impacts at about 3.9 Ga, known as the **Late Heavy Bombardment** (**LHB**), preceded by a comparatively quiet period from about 4.4 to 4.0 Ga (Ryder, 2002; Valley et al., 2002) (Figure 9.8). During this intense impact period, hundreds of impacts large enough to form mare basins (as found on the Moon) must have hit Earth. Single large impacts had only a small fraction of the energy necessary to evaporate Earth's oceans. Large impactors, sufficient to evaporate the entire ocean, are considered to be very rare, if any, after 4.4 Ga (Zahnle & Sleep, 1997). For instance, an impactor the size needed to make the Imbrium basin on the Moon scaled to terrestrial collisional energy would have only 1% of the energy needed to evaporate Earth's oceans. Such an impact would have vaporized only the upper few tens of meters, thus affecting only those organisms living at shallow depths. Although such large impacts mean that life could not form and survive in shallow aqueous environments, it may

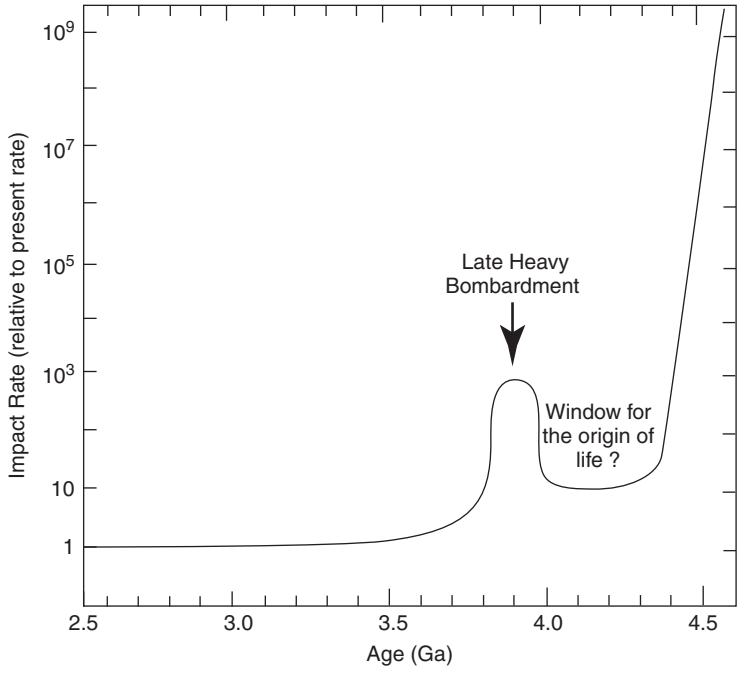

FIGURE 9.8 Estimate of asteroid impact rate for the first 2 Ga of Earth's history, showing a possible time window for the origin of life.

have survived in the deep ocean around hydrothermal vents. Life could have formed during the comparative quiet period from 4.4 to 4.3 Ga just before the LHB (Figure 9.8), and thermal models by Abramov and Mojzsis (2009) show that at least some microbes could survive the LHB. As indicated by the oldest fossils, life was verily advanced by 3.5 Ga, and thus must have had a significant evolutionary history prior to this time.

Another intriguing aspect of early impact is the possibility that relatively small impactors introduced volatile elements and small amounts of organic molecules to Earth's surface that were used in the origin of life. The idea that organic substances were brought to Earth by asteroids or comets is not new, and in fact it was first suggested in the early part of the 20th century. Lending support to the idea is the recent discovery of *in situ* organic-rich grains in comet Halley, and data suggest that up to 25% organic matter may occur in other comets. Also, many organic compounds in living organisms are also found in carbonaceous meteorites. In fact, some investigators propose that amino acids and other organic compounds important to the formation of life were carried to Earth by asteroids or comets rather than forming *in situ* on Earth (Cooper et al., 2001). Complex compounds, such as sugars, sugar alcohols, and sugar acids, have recently been reported in the Murchison and Murray carbonaceous chondrites in amounts comparable to those found in amino acids of living organisms. These compounds may have been produced by processes such as photolysis on the surfaces of asteroids or comets.

One problem with an extraterrestrial origin for organic compounds on Earth is how to get these substances to survive an impact. Even for small objects ($\sim$100 m in radius), impact should destroy organic inclusions unless the early atmosphere was very dense ($\sim$10 bar of CH_4 and CO_2) and could sufficiently slow the objects before impact. However, interplanetary dust from colliding comets or asteroids could survive impact and may have introduced significant amounts of organic molecules into the atmosphere or oceans. Whether this source of organics was important depends critically on the composition of the early atmosphere. If the atmosphere was rich in CH_4 and CO_2 as suggested in Chapter 6, the rate of production of organic molecules was probably quite small, and hence the input of organics by interplanetary dust may have been significant.

The RNA World

Although it seems relatively easy to form amino acids and other simple organic molecules, just how these molecules combined to form the first complex molecules like RNA and then evolved into living cells remains largely unknown. Studies of RNA suggest that it may have played a major role in the origin of life. RNA molecules have the ability to split and produce an enzyme that can act as a catalyst for replication (Zaug & Cech, 1986) (Figure 9.9). Necessary conditions for the production of RNA molecules in the early Archean include a supply of organic molecules, a mechanism for molecules to react to form

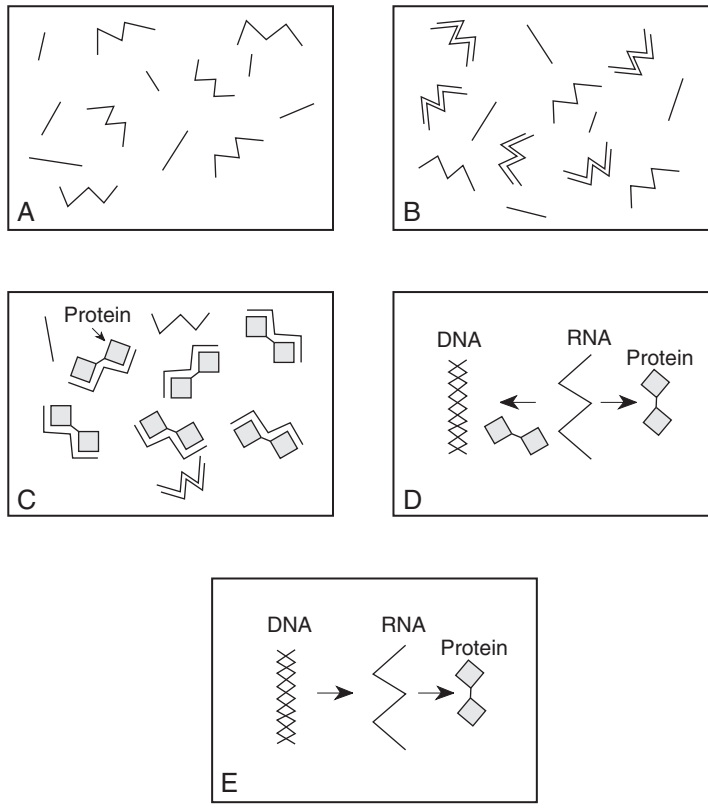

FIGURE 9.9 Diagrammatic representation of the RNA world. (A) RNA is produced from ribose and other organic compounds. (B) RNA molecules learn to copy themselves. (C) RNA molecules begin to synthesize proteins. (D) The proteins serve as catalysts for RNA replication and the synthesis of more proteins. They also enable RNA to make double-strand molecules that evolve into DNA. (E) DNA takes over and uses RNA to synthesize proteins, which in turn enables DNA to replicate itself and transfer its genetic code to RNA.

RNA, a container mineral to retain detached portions of RNA so they can aid in further replication, a mechanism by which some RNA can escape to colonize other populations, and some means of forming a membrane to surround a protocell wall (Nisbet, 1986; de Duve, 1995). During the Archean, hydrothermal systems on the seafloor may have provided these conditions (Corliss et al., 1981; Gilbert, 1986). In laboratory experiments, RNA splitting occurs at temperatures around 40°C with a pH varying from 7.5 to 9 and with Mg present in solution. The early Archean "RNA world" may have existed in clay minerals, zeolites, and in the pore spaces of altered volcanic rocks. The next stage in replication may have been the development of proteins from amino acids that were synthesized from CH_4 and NH_3. Later still, DNA must form and take over as the primary genetic library (Figure 9.9) (Gilbert, 1986).

The next stage of development, although poorly understood, seems to involve production of membranes, which allow managing of energy supply and metabolism, both of which are essential for the development of a living cell. The evolution from protometabolism to metabolism probably involved five major steps (de Duve, 1995) (Figure 9.10). In the first stage, simple organic compounds reacted to form mononucleotides, which later were converted into polynucleotides. During the second stage, RNA molecules formed and the RNA world came into existence as illustrated in Figure 9.9. This stage was followed by interaction of RNA molecules with amino acids to form peptides. It was during or before this stage that the prebiotic systems must have become encapsulated by primitive fatty membranes, producing the first primitive cells. At this stage, Darwinian competition probably began among the cells. During the fourth stage, translation and the genetic code emerged through a complex set of molecular interactions involving competition and natural selection. During the final stage, mutation of RNA genes and competition among protocells occurred and it is by this process that enzymes probably arose. As peptides emerged and assumed their functions, metabolism gradually replaced protometabolism (Figure 9.10).

Perhaps the most compelling feature of the RNA world is that a primordial molecule provided both catalytic power and the ability to propagate its chemical identity over generations. As the catalytic versatility of these primordial RNA molecules increased due to random variation and selection, metabolic complexity began to emerge. From this time onward, RNA had roles in both control of metabolism and continuity across generations, as it does today. Depending on which function one prefers to emphasize, these models have been called "Control First" or "Genetics First." In either case, the proliferation of metabolism depended on RNA being first in a line of complex molecules.

Hydrothermal Vents

Possible Site for the Origin of Life

A hydrothermal vent on the seafloor has been proposed by several investigators as a site for the origin of life (Corliss et al., 1981; Chang, 1994; Nisbet, 1995). Modern hydrothermal vents have many organisms that live in their own vent ecosystems, including a variety of unicellular types (Tunnicliffe & Fowler, 1996). Vents are attractive in that they supply the gaseous components such as CO_2, CH_4, and nitrogen species from which organic molecules can form, and they also supply nutrients for metabolism such as H_2, P, Mn, Fe, Ni, Se, Zn, and Mo (Figure 9.11). Although these elements are present in seawater, it is difficult to imagine how they could have been readily available to primitive life at such low concentrations. Early life would not have had sophisticated mechanisms capable of extracting these trace metals, thus requiring relatively high concentrations that may exist near hydrothermal vents. One objection that

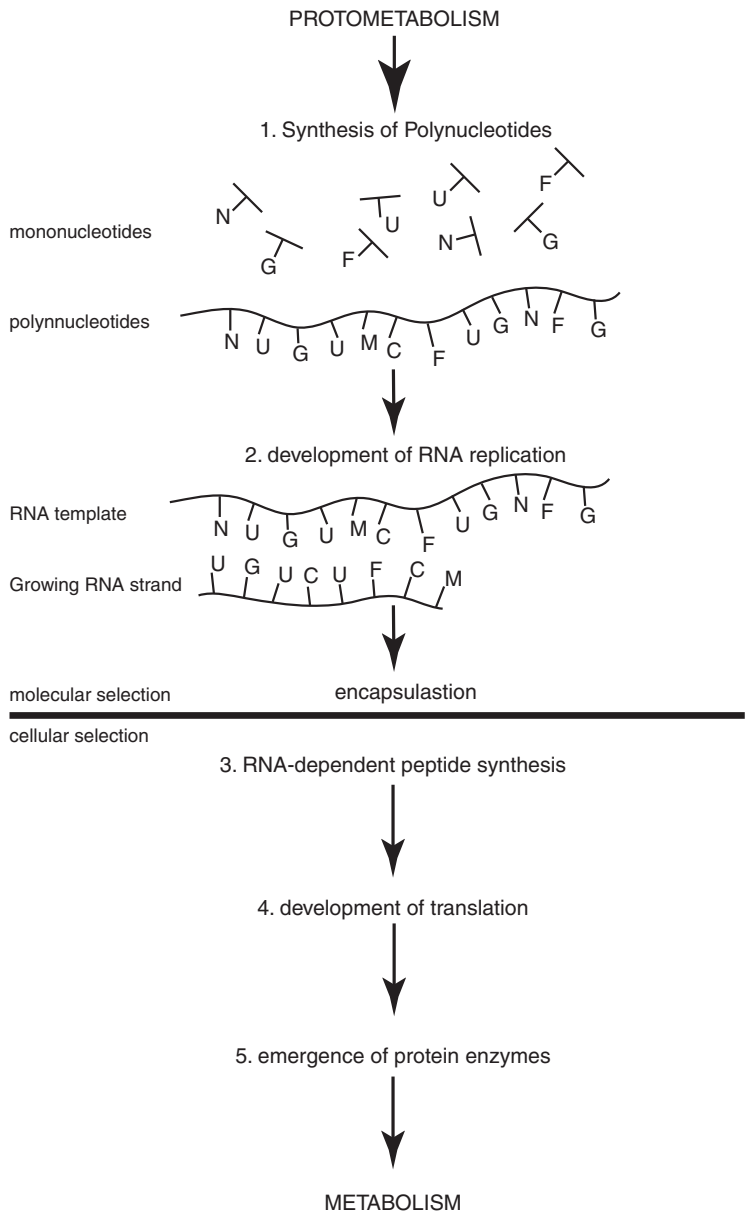

FIGURE 9.10 Diagrammatic representation of the evolution of the earliest cells and the emergence of metabolism. *Modified after de Duve (1995).*

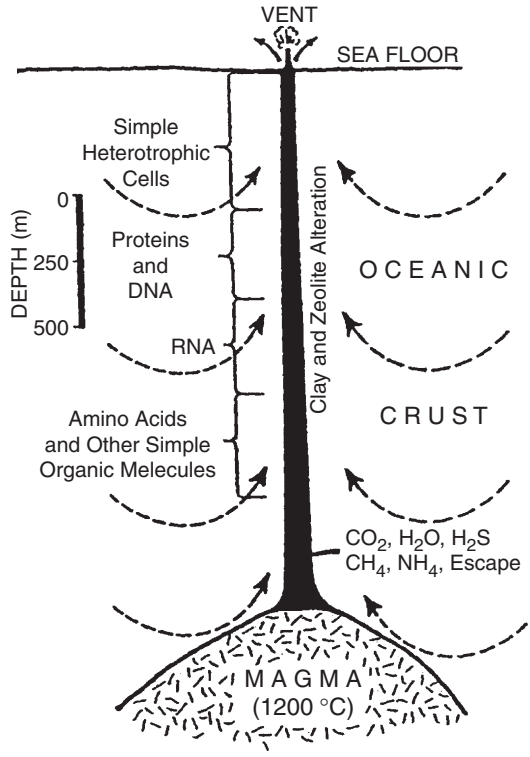

FIGURE 9.11 Idealized cross section of Archean ocean ridge hydrothermal vent showing possible conditions for the formation of life.

has been raised to a vent origin for life is the potential problem of both synthesizing and preserving organic molecules necessary for the evolution of cells. The problem is that the temperatures at many or all vents may be too high, and they would destroy, not synthesize, organic molecules (Miller & Bada, 1988). However, many of the requirements for the origin of life seem to be available at submarine hydrothermal vents and synthesis of organic molecules may occur along vent margins where the temperature is lower. Models by Shock and Schulte (1998) suggest that the oxidation state of a hydrothermal fluid, controlled in part by the composition of host rocks, may be the most important factor influencing the potential for organic synthesis. The probability of organic synthesis in the early Archean may have been much greater than at present due to the hotter and metal-rich komatiite-hosted hydrothermal systems.

A possible scenario for the origin of life at hydrothermal vents begins with CO_2 and N_2 in vent waters at high temperatures deep in the vent (Shock, 1992; Russell & Arndt, 2005). As the vent waters containing these components circulate to shallower levels and lower temperatures, they cool and thermodynamic conditions change such that CH_4 and NH_3 are the dominant gaseous species

present. Provided suitable catalysts are available, these components can then react to produce a variety of organic compounds, two of which are acetate and glycine (Russell & Arndt, 2005). It may have been from reactions between these and other organic species trapped in pockets in a hydrothermal vent that the first prokaryotic organism formed. These acetogenic precursors to bacteria diversified and migrated into the ocean floor to inaugurate the deep biosphere. Once there, they were also protected from large asteroid impact events. The widespread propagation of seafloor spreading from the late Archean onward led eventually to obduction of the deep biosphere into the photic zone along continental margins, and it may have been here that some microbes mastered the use of solar energy and photosynthesis emerged.

Experimental and Observational Evidence

Experimental results can help constrain an origin for life at hydrothermal vents. Compounds synthesized to date at conditions found at modern vents include lipids, oligonucleotides, and oligopeptides (McCollom et al., 1999). Clay minerals have been used as catalysts for the reactions. Experimental results also indicate that amino acids and mononucleotides can polymerize in hydrothermal systems, especially along the hot/cold interface of the hydrothermal fluids and cold seawater. Polymerization of amino acids to form peptides has also been reported for hydrothermal vent conditions (Ogasawara et al., 2000).

Long-chain hydrocarbons have been collected from modern hydrothermal vents along the Mid-Atlantic Ridge, indicating that organic compounds can be synthesized at these vents (Charlou et al., 1998). These compounds, which have chain lengths of 16 to 29 carbon atoms, may have formed by reactions between H_2 released during serpentinization of olivine with vent-derived CO_2 at high temperatures.

The First Life

One of the essential features of life is its ability to reproduce. It is probable that this ability was acquired long before the first cell appeared on the scene. Cairns-Smith (1982) has suggested that clays may have played an important role in the evolution of organic replication. Organic compounds absorbed in clays may have reacted to form RNA through natural selection, and RNA molecules eventually disposed of their clay hosts. Because hydrothermal systems appear to have lifetimes of the order of 10^4–10^5 years at any given location, RNA populations must have evolved rapidly into cells, or more likely they were able to colonize new vent systems. Another possible catalyst is zeolite, which possesses a wide variety of pores of different shapes and sizes that permit small organic molecules to pass through while excluding or trapping larger molecules (Nisbet, 1986). Zeolites are also characteristic secondary minerals around hydrothermal plumbing systems (Figure 9.11). The significance of variable-sized

cavities in zeolites is that a split-off RNA molecule may be trapped in such a cavity, where it can aid in replication of the parent molecule. Although the probability is small, it is possible that the first polynucleotide chain formed in the plumbing system of an early hydrothermal vent on the seafloor.

The first cells were primitive in that they had poorly developed metabolic systems and survived by absorbing a variety of nutrients from their surroundings (Kandler, 1994; Pierson, 1994). They must have obtained nutrients and energy from other organic substances by fermentation, which occurs only in anaerobic (oxygen-free) environments. **Fermentation** involves the breakdown of complex organic compounds into simpler compounds that contain less energy, and the energy liberated is used by organisms to grow and reproduce. Cells that obtain their energy and nutrients from their surroundings by fermentation or chemical reactions are known as **heterotrophs** in contrast to **autotrophs**, which are capable of manufacturing their own food. Two types of anaerobic cells evolved from DNA replication. The most primitive group, the Archaebacteria, use RNA in the synthesis of proteins, whereas the more advanced group, the eubacteria, have advanced replication processes and may have been the first photosynthesizing organisms.

Evidence of Early Life

Metabolic activity in organisms produces distinct patterns of isotopic fractionation in such elements as carbon, nitrogen, and sulfur. The geologic record of these fractionations can be obtained by analyzing organic matter of biologic origin preserved in sedimentary rocks. Enzymatic processes discriminate against ^{13}C in the fixation of atmospheric CO_2 causing up to 5% difference in the isotopic composition of biologic and nonbiologic carbon. Microbial **methanogens**, which produce methane gas during their metabolism, are responsible for isotopic fractionation to –40‰ from inorganic carbon, reaching $\delta^{13}C$ values in some forms as low as –60‰. When found in buried carbon in the geologic record, these distinct light carbon isotope signatures (–30 to –60‰) are considered diagnostic of methanogen activity at the time of burial in extreme environments, such as highly saline, high-temperature, and variable pH environments (Mojzsis & Harrison, 2000). **Methanotrophs**, which use methane in their metabolism, may also be present in these environments.

Carbon isotopic data from early Archean carbon is well known to be isotopically light, consistent with a biologic origin (Schidlowski et al., 1983; Des Marais, 1997). Carbonaceous inclusions trapped in minerals such as apatite are particularly informative, since they may have remained unchanged since burial. In the earliest known sediments from Isua in Southwest Greenland (Akilia sequence, $\leq$3.67 Ga), carbonaceous inclusions have $\delta^{13}C$ values of –30 to –40‰ (Mojzsis et al., 1996; Rosing, 1999). Although the simplest interpretation of these data is that the microorganisms in these early sediments were metabolically complex, perhaps comprising phosphate-utilizing photoautotrophs

and chemoautotrophs, later field and geochronologic studies question these results (Whitehouse et al., 2009) in that the host rocks appear to be highly deformed igneous rocks rather than sediments. When and how the carbonaceous matter entered these rocks is uncertain.

A summary of the key evidences for life, together with their first appearances in the geologic record, is given in Figure 9.12. Stromatolites, microfossils, carbon isotopes, and Raman spectroscopic features of carbonaceous matter are all considered definitive of the presence of life (Schopf, 2006). The oldest evidence comes from the Pilbara craton in Western Australia from cherts in the Dresser, Mt. Ada, and Apex Formations, all around 3.5 Ga. The paleoenvironment, carbonaceous composition, mode of preservation, and morphology of microbe-like filaments from these units, backed by new evidence of cellular structure provided by Raman imagery, clearly support a biogenetic interpretation (Schopf et al., 2007). In addition, macromolecular hydrocarbon structure, carbon bonding, functional group chemistry, and biotic element abundance of carbonaceous matter associated with filamentous structures in a chert unit associated with the Apex Basalt clearly support a biogenic origin for these structures (De Gregorio et al., 2009). Sulfur isotopic ratios ($^{34}S/^{32}S$) in Archean carbonaceous matter from the same locations are relatively low, supporting the existence of sulfate-reducing bacteria by 3.5 Ga (Shen et al., 2009).

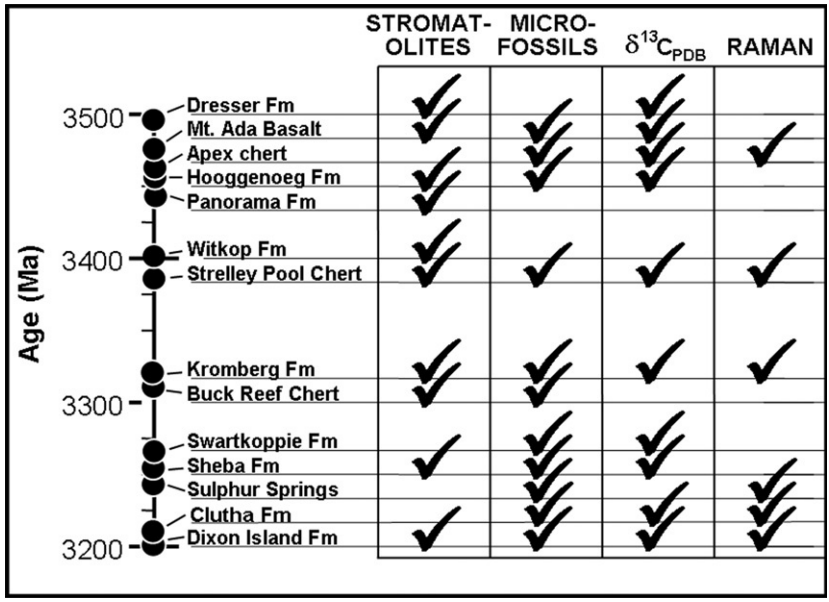

FIGURE 9.12 Early Archean evidence of life. *Courtesy of Bill Schopf.*

Biomarkers are geologically stable compounds, mostly lipids, of known biologic origin. The oldest known biomarkers come from 2.7-Ga shales from northwestern Australia (Brocks et al., 1999). These occurrences confirm the existence of photosynthetic cyanobacteria by the late Archean. Such biomarkers are widespread in the 2.5-Ga Hamersley iron formation in Western Australia and may have provided the free oxygen for precipitation of the banded iron formation. Included in the biomarkers are 2-Me-bacterioheopanepolyols, membrane lipids synthesized in large quantities only in cyanobacteria, as well as steranes, molecules derived from sterols. It is probable that at least some oxygen entered the atmosphere in the late Archean to support these forms of cyanobacteria.

The Origin of Photosynthesis

Anoxygenic Photosynthesis

Anoxygenic photosynthesis makes use of light in the longer visible and near-infrared spectrum and uses a compound other than water as the electron donor. An example is anoxygenic purple bacteria, which absorbs light at wavelengths $\geq$900 nm. Anoxygenic photosynthesis can use a wide variety of electron donors in various bacteria including hydrogen, H_2S, sulfur, iron, and various organic compounds. Again supporting the hydrothermal vent model for the origin of life, all of these substances occur in deep-sea hydrothermal systems (Nisbet, 2002).

Rapid increases in the numbers of early heterotrophs may have led to severe competition for food supplies. Selection pressures would tend to favor mutations that enabled heterotrophs to manufacture their own food and thus become autotrophs. The first autotrophs appeared by 3.5 Ga as cyanobacteria. These organisms produced their own food by photosynthesis perhaps using H_2S rather than water since free oxygen, which is liberated during normal photosynthesis, is lethal to anaerobic cells. Just how photosynthesis evolved is unknown, but perhaps the supply of organic substances and chemical reactions became less plentiful as heterotrophs increased in numbers, and selective pressures increased to develop alternative energy sources. Sunlight would be an obvious source to exploit. H_2S may have been plentiful from hydrothermal vents or decaying organic matter on the seafloor and some cells may have developed the ability to use this gas in manufacturing food. As these cells increased in numbers, the amount of H_2S would not be sufficient to meet their demands and selective pressures would be directed toward alternate substances, of which water is the obvious candidate. Thus, mutant cells able to use water may have outcompeted forms only able to use H_2S, leading to the appearance of modern photosynthesis.

Experimental results suggest that purple, nonsulfur bacteria can oxidize Fe^{2+} to brown Fe^{3+} and reduce CO_2 to cell material, implying that oxygen-dependent

biological iron oxidation was possible before the appearance of oxygenic photosynthesis (Widdel et al., 1993). This being the case, it is possible, if not probable, that bacteria were important in the deposition of banded iron formation in the Archean. Iron isotopes are also fractionated during redox changes with Fe^{2+} in solution having the lowest $^{56}Fe/^{54}Fe$ ratios relative to Fe^{3+} minerals. Microbial Fe^{3+} reduction plays the largest role in producing an isotopically distinct iron isotope signature and the positive or near-zero values of $\delta^{56}Fe$ of early Archean BIFs is supportive of such a mechanism operating in the early Archean (Johnson et al., 2008). Development of photosynthesis in the late Archean produced large quantities of Fe^{3+} and organic carbon that supported a major expansion of microbial iron reduction by about 3 Ga. However, between 2.4 and 2.2 Ga, the iron isotopic fingerprint of microbial Fe^{3+} reduction decreased, reflecting increased bacterial sulfate reduction. Thus, the temporal record of carbon, sulfur and iron isotopes reflects the interplay of changing microbial metabolisms during Earth history.

Oxygenic Photosynthesis

Oxygenic photosynthesis, in which water is the electron donor in the photosynthesis reaction, probably developed later than anoxygenic photosynthesis (Nisbet & Sleep, 2001). Unlike anoxygenic photosynthesis, oxygenic photosynthesis uses visible light in the more energetic parts of the spectrum. Green sulfur bacteria and cyanobacteria both use iron-sulfur centers as electron acceptors, whereas in purple bacteria, pigments and quinones are used as electron acceptors. The existence of both types of electron acceptors in oxygenic photosynthesis suggests an origin by genetic transfer between cooperating or closely juxtaposed cells, each using anoxygenic photosynthesis. Perhaps the key component in oxygenic photosynthesis is the O_2 that is part of a Mn complex exploiting the transition from Mn_4O_4 to Mn_4O_6. The presence of Mn is again consistent with hydrothermal systems, but the environment needs to be oxygen rich.

One of the key requirements for oxygenic photosynthesis is the presence of the catalyst ribulose bisphosphate carboxylase/oxygenase, commonly known as **Rubisco**. This species enables life to capture carbon from CO_2 in the environment to perform photosynthesis. Carbon isotopic evidence from 2.9- to 2.7-Ga stromatolites from Canada and Zimbabwe imply that reef-building autotrophs at this time included organisms using an advanced form of Rubisco (Nisbet et al., 2007). The implication of these findings is that oxygenic photosynthesis had appeared by 2.9 Ga and was probably widespread by 2.7 Ga.

The earliest cyanobacteria were probably freshwater, had small cell diameters, and lacked the traits to form thick microbial mats (Blank & Sanchez-Baracaldo, 2010). **Molecular clock studies** estimate the rate of change of gene sequences using the divergence of copies of taxa whose appearance in the fossil record is known and then use this rate to estimate the rates of older and deeper

divergences. Molecular divergence times should in principle be older than fossil dates, since fossils generally give the latest time for the appearance of a new taxon. Molecular clock studies of cyanobacteria suggest that the freshwater forms diversified into coastal brackish and marine environments around 2.4 Ga. The resultant increases in niche space and nutrient availability, and consequent burial of organic carbon in the deep oceans, should have generated large pulses of oxygen into the atmosphere, perhaps contributing to the Great Oxidation Event at 2350 Ma.

The evolution and structure of microbial mats may have paralleled the evolution of photosynthesis, with newer bacteria progressively occupying the more productive but more dangerous uppermost level in the mats, where the light is more intense. In this scenario, it is possible that the pre-photosynthetic mats were composed of hyperthermophiles (heat-loving microbes) with sulfate-processors on the top and archaea beneath that recycled redox power. This may have allowed occupation of hydrothermal vents, and eventually the open sea away from volcanic heat sources (Nisbet & Sleep, 2001). Sometime before 3.5 Ga, a new cyanobacteria component appeared, possibly from genetic exchange between coexisting purple and green bacteria living on the redox boundary of a microbial mat. This component used water, CO_2, and sunlight to photosynthesize and may have spread rapidly filling many ecological niches in the oceans. Although oxygenic photosynthesis first appeared in cyanobacteria, it was later transferred to plants (in Eukarya) through lateral gene transfer or/and symbiotic association with primitive plants.

Although microorganisms existed in the oceans from at least 3.8 Ga onward, it is still uncertain when they first came on to dry land. Two late Archean paleosols (fossil soil horizons) have been described, both of which contain evidence of biologic activity on land. Paleosols in the Schagen area of South Africa formed 2.7–2.6 Ga have very negative $\delta^{13}C$ (–30 to –35‰) suggestive of a biologic origin (Watanabe et al., 2000). Supporting an important role of cyanobacteria in the Schagen soil is a similar fractionation factor between the Archean atmosphere and the soil mat (12‰), which is similar to the fractionation value today. The existence of land-based photosynthesizing cyanobacteria by 2.7 Ga also may indicate that the ozone shield had started to develop. Organic carbon from the Mount Roe paleosol in Western Australia records strong negative $\delta^{13}C$ values (–33 to –51 ‰), suggesting in this case the presence of methanotrophs in the soil (Rye & Holland, 2000). Methanotrophs furthermore imply significant levels of methane in the Archean atmosphere as discussed in Chapter 6. Filamentous bacteria in mats from the 2.9-Ga Mozaan Group in South Africa are the oldest known occurrences of microbial mats in siliciclastic sediments (Noffke et al., 2003). Textures in these mats resemble trichomes of modern cyanobacteria, choroflexi, or sulfur-oxidizing proteobacteria. Mineralogical, isotopic, and chemical analyses of these mats are consistent with a biologic origin for the filament-like textures in the mats.

Thus, our evidence at hand suggests that cyanobacteria had moved from the oceans onto the continents by the late Archean.

The Tree of Life

We can learn about the origin and evolution of life from two sources: (1) historical information can be deduced by comparing sequences of nucleic acids contained in the genomes of living organisms by constructing family trees based on observational differences (Doolittle, 1999), and (2) we can piece together the evolutionary history of life from the fossil record. By combining the results of these two approaches, we can construct a robust framework to infer the timing of the major evolutionary events in the history of life (Bengtson, 1994; Farmer, 1998). The **Universal Phylogenetic Tree** constructed from comparisons of ribosomal RNA indicates that life can be divided into three general categories (Figure 9.13): Bacteria, Archaea, and Eukarya. Branches within the Bacteria and Archaea domains are short, suggesting relatively rapid evolution of the subgroups, with cyanobacteria, for instance, appearing by 2.7 Ga. In contrast, the branches separating the three major domains are long, indicating both greater evolutionary distances and rapid divergence. Although the placement of the root of the tree is uncertain, it likely lies somewhere near the midpoint of the Bacteria and Archaea domains. Ribosomal RNA is a slowly evolving molecule and is considered important in studying early events in biosphere evolution. Although the fossil record is poor in microbial life-forms, what we have supports the genetic relationships deduced from sequencing RNA.

The earliest branches of the Bacteria and Archaea domains include **hyperthermophiles**, which are forms that grow at temperatures >80°C (Figure 9.13). The highest temperature in which modern microbes live is 122°C. In addition to

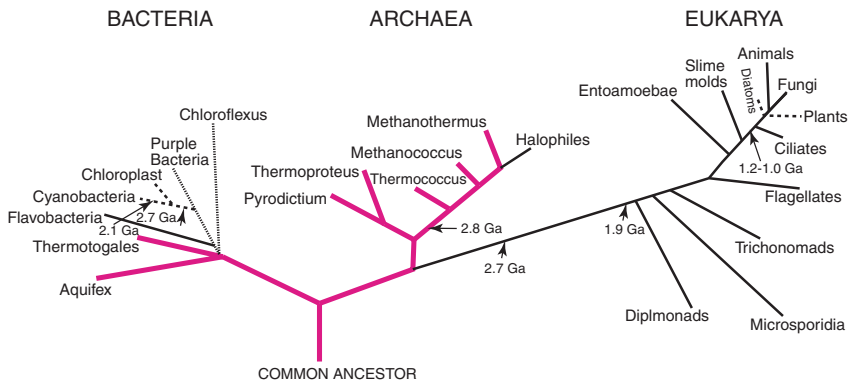

FIGURE 9.13 Phylogenetic "tree of life" based on comparison of 16S or 18S ribosomal RNA. Also shown are isotopically dated events from the fossil record. Red line, hyperthermophiles; dashed line, oxygenic photosynthetic forms; dotted line, anoxygenic photosynthetic forms.

exhibiting the highest temperature tolerances, the deepest branching organisms are **chemoautotrophs**, that is, microbes that synthesize organic molecules from inorganic materials. These combined properties of the earliest microorganisms are widely assumed to be those of the last common ancestor of living organisms. Placement of the "root of life" within the hyperthermophilic bacteria is consistent with the model for the origin of life in hydrothermal vents on the seafloor. It is also recognized that the effects of temperature on microbes leave a genetic footprint that can be uncovered from the study of modern genomes. Such genetic studies of resurrected proteins predict that bacterial ancestors were thermophilic and that bacteria later adapted to lower temperatures (Boussau et al., 2008). Combined studies of RNA and protein sequences furthermore suggest that the last universal common ancestor of the three domains of life also adapted to high-temperature environments.

The First Fossils

Two lines of evidence are available for the recognition of the former existence of living organisms in early Archean rocks: microfossils and organic geochemical evidence including carbon isotopes as described above (Figure 9.12) (Schopf, 1994). Using secondary ion mass spectrometry, it is now possible to map the distribution of carbon and other elements in suspected biogenic microstructures. Many microstructures preserved in rocks can be mistaken for cell-like objects (inclusions, bubbles, microfolds, etc.), and progressive metamorphism can produce structures that look remarkably organic and at the same time can destroy real microfossils. For these reasons caution must be exercised in accepting microstructures as totally biologic.

Microstructures in the Farrel Quartzite from Western Australia appear not only to be biogenic, but also to represent a diverse assemblage of Archean microbes, adding to the growing body of evidence that the biosphere was varied and well established on Earth by 3 Ga (Oehler et al., 2010). Some of the oldest well-described microfossil-like structures come from cherts in the 3.5-Ga Barberton greenstone belt in South Africa (Figure 9.14) and the oldest unambiguous structures of organic origin are 3.5-Ga stromatolites from the Pilbara region (Dresser Formation) of Western Australia (Walter, 1994) (Figures 9.12 and 9.15). Although older structures and biomarkers have been reported from the Akilia sequence in Southwest Greenland ($\leq$3.67 Ga) (Mojzsis et al., 1996), these rocks are not metasediments as first described, but appear to be highly deformed mafic and ultramafic igneous rocks (Whitehouse et al., 2009). Thus, they provide no unambiguous evidence that life existed by 3.7 Ga. Three types of microstructures, ranging in size from $<$1 mm to $\sim$20 mm, have been reported from the Barberton sequence. These are rod-shaped bodies, filamentous structures, and spheroidal bodies. The spheroidal bodies are similar to alga-like bodies from Proterozoic assemblages and are generally interpreted as such (Figure 9.14). Of the two types of cells, prokaryotic and eukaryotic, only prokaryotic types are

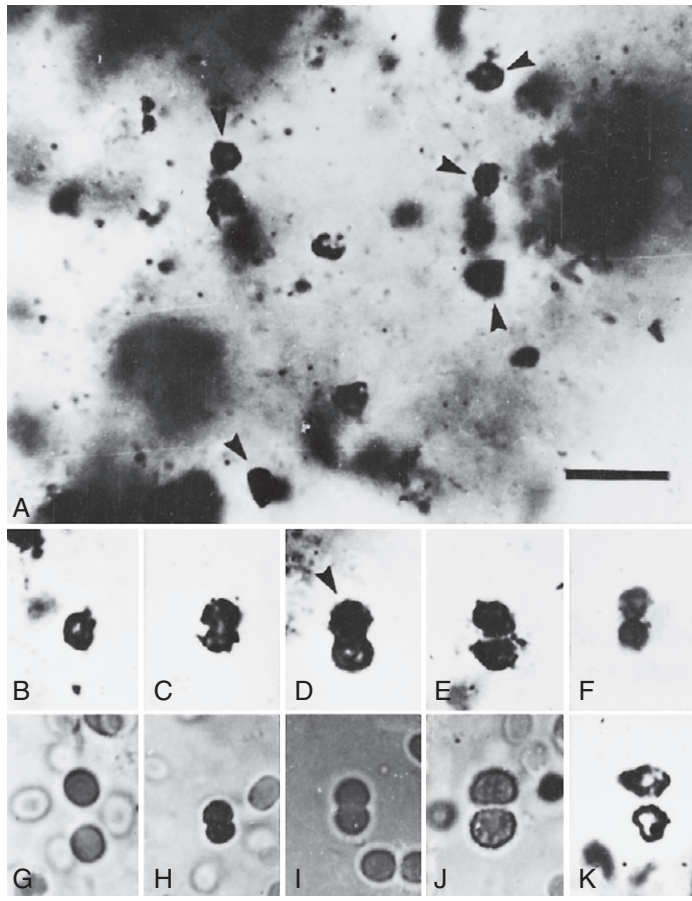

FIGURE 9.14 Photomicrograph of spheroid microstructures from the Swartkoppie Formation, Barberton greenstone, South Africa. Arrows note individual cells. Stages in cell division in the Archean samples (B) to (E) are compared to modern prokaryotes in (G) to (J). Scale bar is 10 μm. *Courtesy of Andrew Knoll.*

represented among Archean microfossils. **Prokaryotes** are primitive cells that lack a cell wall around the nucleus and are not capable of cell division; **eukaryotes** possess these features and hence are capable of transmitting genetic coding to various cells and to descendants.

Some of the earliest well-preserved structures thought to be of biogenic origin are stromatolites. Although some early Archean laminated carbonate mats appear to be of inorganic origin, by 3.2 Ga well-preserved organism-built stromatolites are widespread. The oldest relatively unambiguous stromatolite at 3.5 Ga occurs near the town of North Pole in Western Australia, and its age is constrained by U/Pb zircon dates from associated volcanics (Figure 9.15)

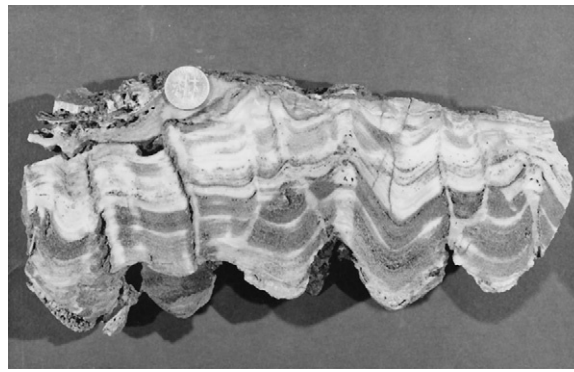

FIGURE 9.15 3.5-Ga stromatolites from the Pilbara region in Western Australia. *Courtesy of D. R. Lowe.*

(Buick et al., 1995a; Van Kranendonk et al., 2003). Early Archean stromatolites were probably built by anaerobic photoautotrophs with mucous sheaths (Walter, 1994; Hofmann et al., 1999). These microbes were able to cope with high salinities, desiccation, and high sunlight intensities as indicated by their occurrence in evaporitic cherts. Late Archean stromatolites are known from both lagoon and near-shore marine environments and some are very similar to modern stromatolites, suggesting they were constructed by cyanobacteria.

Possibility of Extraterrestrial Life

There is considerable interest today in the possibility of life on other bodies in the solar system, as well as elsewhere in the galaxy. Most astrobiologists agree that any planet or satellite on which life may exist must have a fluid medium, a source of energy, and conditions and components compatible with polymeric chemistry (Irwin & Schulze-Makuch, 2001). For carbon-based life, possible energy sources include sunlight (from central stars in other planetary systems), thermal gradients, kinetic motion, and magnetic fields. Although water is generally assumed to be the fluid medium, mixtures of water and various hydrocarbons or other organic compounds may also be suitable. With the appropriate conditions, the emergence of self-organizing systems is regarded as inevitable by many scientists (Kaufman, 1995).

Irwin and Schulze-Makuch (2001) propose a five-scale rating for the plausibility of life on other bodies as summarized for the solar system in Table 9.2. Life is most likely to exist where liquid water, organic chemistry, and one or more energy sources occur. This is category I and only Earth falls here. Category II includes bodies in which these conditions existed in the past and may still exist at present above or beneath the surface. In this category we have Mars and two satellites, Europa and Ganymede. Category III includes bodies

TABLE 9.2 Plausibility of Life Ratings

Rating	Characteristics	Examples
I	Liquid water, available energy, organic compounds	Earth
II	Evidence for past or present existence of liquid water, available energy, inference of organic compounds	Mars, Europa, Ganymede
III	Extreme conditions, evidence of energy sources and complex chemistry possibly suitable for life-forms unknown on Earth	Titan, Triton, Enceladus
IV	Past conditions possibly suitable for life	Mercury, Venus, Io
V	Conditions unfavorable for life	Sun, Moon, outer planets

Source: Modified after Irwin and Schulze-Makuch (2001).

with a nonwater liquid and energy sources, such as the Jovian satellite Triton. Category IV includes bodies where conditions for life may have existed at one time, but no longer exist, such as Venus. These bodies have such extreme conditions that water and organic molecules are unlikely to survive. Finally, in category V, conditions are so extreme that it is unlikely that life ever existed.

The most compelling factor for life on the Martian surface is the abundance of frozen water and the likelihood that Mars had running water early in its history (Carr, 1996). Although microbial life may have existed when liquid water was present on the planetary surface, it is very unlikely that life has persisted to the present on the Martian surface. However, as water began to freeze and form permafrost, life also may have retreated into the deep subsurface and continued to thrive as microbes do today in deep fractures and mines on Earth (Stevens & McKinley, 1995). Subsurface geothermal areas may provide a suitable habitat for chemoautotrophic microbes that survive by oxidizing free hydrogen to water in the presence of CO_2 from volcanic eruptions. Alternatively, or in addition, microbes might reduce CO_2 to CH_4. Solar energy has been available continuously on Mars and may still sustain life along the fringe areas of the polar icecaps. Although microstructures found in Martian meteorites (meteorites from the Martian surface) that were originally described as possible microfossils (McKay et al., 1996) are likely of inorganic origin, Mars is clearly a body that meets the requirements for life in the past, with the possible survival of some forms to the present.

An icy shell up to 200 km thick covers Europa, Jupiter's smallest major satellite, overlying a salt-bearing water ocean (Carr et al., 1998). If water

was ever liquid at the surface of Europa, theories of the origin of life on Earth could also apply to this unusual satellite. Experimental evidence allows a methanogen-driven biosphere to exist on Europa, despite the low temperatures. Oxygen may be produced in the Europan atmosphere by the Jovian magnetic field, thus permitting operation of oxidation–reduction chemical cycles (Chyba, 2000). The relatively high density and presence of a surficial electromagnetic field are consistent with a liquid core that could generate internal energy, thus providing another source of energy for microbes in the overlying ocean. Clearly, Europa needs to be explored for the possibility of microbial life-forms that may have persisted to the present.

EVENT 3: THE ONSET OF PLATE TECTONICS

As discussed in Chapter 8, the late Archean was a time of widespread preservation of continental crust, and most investigators equate this with rapid growth of one or more cratons that amalgamated into a supercraton (McCulloch & Bennett, 1994; Stein & Hofmann, 1994). However, both the tectonic regime during which this crust formed and the cause of rapid crustal growth remain controversial (Condie & Benn, 2006). From the late Archean onward, subduction zones were probably the chief sites of continental crust production. To preserve a large volume of continental crust in the late Archean, it is critical for cratons to have formed rapidly, protecting most of this new crust from recycling into the mantle. One way of accounting for numerous changes at the end of the Archean is the widespread establishment of plate tectonics. The onset of plate tectonics is certainly one of the greatest and most important events that subsequently controlled the evolution of Earth including its hydrous and atmospheric reservoirs. Herein, we review these changes and make a case for the widespread propagation of plate tectonics in the late Archean.

Plate Tectonic Indicators

Petrotectonic assemblages (Chapter 3) and other characteristics of plate tectonics make their first appearances in the late Archean although many do not become widespread until the early Paleoproterozoic (Tables 9.3 and 9.4). Geochemical and isotopic arguments require recycling of crustal material into the mantle in the early Archean, although there may be other ways to accomplish this besides plate tectonics. Apparent polar wander paths from South Africa and the Pilbara in Western Australia require differential plate motions by 3 Ga (Suganuma et al., 2006; Strik et al. 2007), and paired metamorphic belts indicative of subduction (Brown, 2007) appear in the late Archean. The earliest passive margin successions are recognized in the Pilbara craton in Western Australia by at least 2.7 Ga (Bradley, 2008). Finally, seismic images of dipping units in the lower crust of Archean cratons (such as in the Superior and Karelia cratons) are strongly suggestive of fossil subduction zones (see Figure 2.2)

TABLE 9.3 Petrotectonic Assemblages Characteristic of Plate Tectonics

Assemblage	Widespread distribution (Ga)	First appearance (Ga)
Ophiolites	≤1.0	2.0 (?)
Arc-back arc	2.7	3.1
Accretionary prisms and OPS	≤1.0	2.7 (3.8?)
Forearc basins	≤2.0	2.7 (3.25?)
Blueschists and UHP rocks	≤0.1	0.85 (1.0?)
Passive margins	≤2.0	2.7 (2.9?)
Continental rift	≤2.0	3.0
Metallic mineral deposits	≤2.7	3.5–3.4

OPS, ocean plate stratigraphy.

TABLE 9.4 Other Indicators of Plate Tectonics

Indicator	Widespread distribution (Ga)	First appearance (Ga)
UHP metamorphism	≤0.1	0.6
Paired metamorphic belts	≤2.7	3.3
Transcurrent faults and sutures	≤2.7	3.6 (?)
Collisional orogens	≤2.0	2.2
Accretionary orogens	≤2.7	3.8–3.7 (?)
Paleomagnetism	≤2.7	≥3.2 (?)
Geochemistry	≤2.7	3.1
Isotopes	≤3.0	≥4.0
Continents	≤2.7	≥3.0 (?)
Dipping reflectors in lower crust	≤2.7	(?)

UHP, ultra-high-pressure.

(Clowes et al., 2010). Taking all of the evidence together, it would appear that modern plate tectonics was operational, at least in some places on the planet, around 3 Ga and that it became widespread by 2.7 Ga (Condie & Benn, 2006; Condie & Kroner, 2008). Although some investigators have pushed the starting time of plate tectonics even further back using the 3.8-Ga Isua supracrustal rocks in Southwest Greenland as an example of a subduction-related assemblage (Nutman & Friend, 2009), the tectonic setting of these rocks is the subject of continuing debate.

However, we are faced with three indicators (ophiolites, ultra-high-pressure metamorphism, and blueschists) that suggest a much later starting date for plate tectonics around 1.0 Ga (Stern, 2005). Does this mean that the other petrotectonic assemblages and plate tectonic indicators are invalid or does it mean that the three anomalous indicators have other explanations? There are several problems with the recognition and preservation of ophiolite successions in the Archean, as discussed in Chapter 7. If Archean oceanic crust was significantly thicker than modern oceanic crust, as seems likely (Sleep & Windley, 1982; Foley et al., 2003), the deeper layers of oceanic crust that contain layered gabbros and ultramafic cumulate rocks may not have been accreted to the continents in subduction zones but, instead, were recycled into the mantle (Condie & Benn, 2006). Obduction of thick oceanic crust could have resulted in delamination of the middle to lower crustal sections and mantle lithosphere during collisional tectonics and the emplacement and preservation of only the upper, pillow-lava rich volcanic crust. One of the great challenges of the future is that of how to recognize remnants of Archean oceanic crust if they are preserved in greenstones. Perhaps many of the mafic plain–type greenstones are remnants of oceanic crust rather than of oceanic plateaus (Condie, 1994).

Stern (2005) concluded that the apparent absence of blueschists and ultra-high-pressure (UHP) metamorphic rocks before about 1 Ga is important evidence for when the modern episode of subduction began. Others think that the absence of blueschists and UHP rocks from the Archean record results from the fact that the Archean Earth was hotter, and that subduction geotherms did not pass into the blueschist stability field (Martin, 1994; Peacock, 2003; Ernst, 2003). Although earlier paleomagnetic data suggested that minimum plate velocities in the Archean were similar to average plate velocities today (Layer et al., 1989), recent paleomagnetic data suggest that Archean plate motions were significantly faster than at present (Strik et al., 2003). The most convincing evidence of steeper subduction geotherms in the Archean comes from thermobarometric studies of Archean metamorphic rocks (Komiya et al., 2002; Moyen et al., 2006). Collectively, these lines of evidence lead us to the simplest and most straightforward explanation for the apparent absence of pre–1-Ga blueschists and UHP rocks in the geologic record: most Archean subduction zones were too hot. In addition to steeper Archean subduction geotherms, the rate of uplift of UHP rocks may have been so slow in the Archean that the UHP mineral assemblages recrystallized and can no longer be recognized.

Global Changes at the End of the Archean

Decrease in Mantle Temperature

Komatiite Abundance

As summarized in Table 9.5, many global changes occurred at the end of the Archean. Komatiites, as discussed in Chapter 7, are thought to track the temperature of the mantle, and more specifically that part of the mantle from which mantle plumes arise (Arndt et al., 2008, 2009). The frequency of komatiites in greenstone belts as a function of age is given in Figure 9.16. In this figure and some of the subsequent figures there are major gaps in data, especially at 2.4–2.2 and 1.5–0.8 Ga. The gap at 2.4–2.2 Ga may reflect a global slowdown in magmatism and plate tectonics as discussed in Chapter 7. Because some types of geochemical data are available for rocks between 1.5 and 0.8 Ga, the absence of data in this time interval appears to reflect the absence of published data. The results in Figure 9.16 clearly show a major drop in the percent of komatiites after 2.5 Ga. An important feature of the graph is that it shows an abrupt rather than a gradual change in komatiite frequency at the end of the Archean. The decrease does not follow the calculated gradual cooling curve of the mantle as predicted by the decay of radiogenic heat sources (see Figure 7.25 in Chapter 7).

MgO Content of Komatiites

The average MgO content of komatiites is one way to track the average eruptive temperature of the magma and of the mantle sources, which are likely mantle plumes (Arndt et al., 2008). Each point on Figure 9.17 is the average MgO content for komatiites from a given greenstone belt. The results show a clear decrease in the average MgO content of komatiites at the end of the Archean.

TABLE 9.5 Summary of Tracers of Events in the Late Archean and Early Paleoproterozoic.

Event	Tracer
Cooling of the deep mantle	1. Decrease in frequency of komatiites 2. Decrease in komatiite MgO content 3. Decrease in Ni/Fe in banded iron formation 4. Increase in Nb/Yb and similar element ratios in nonarc oceanic basalts
Stabilization of cratons	1. Changes in incompatible element ratios in TTGs and continental crust 2. Peak in orogenic gold reserves at 2.7 Ga 3. Production of thick lithosphere at 2.7 Ga 4. Increase in $\delta^{18}O$ in granitoid zircons 5. Increase in Nb/Th and $\varepsilon_{Nd}(T)$ in nonarc oceanic basalts

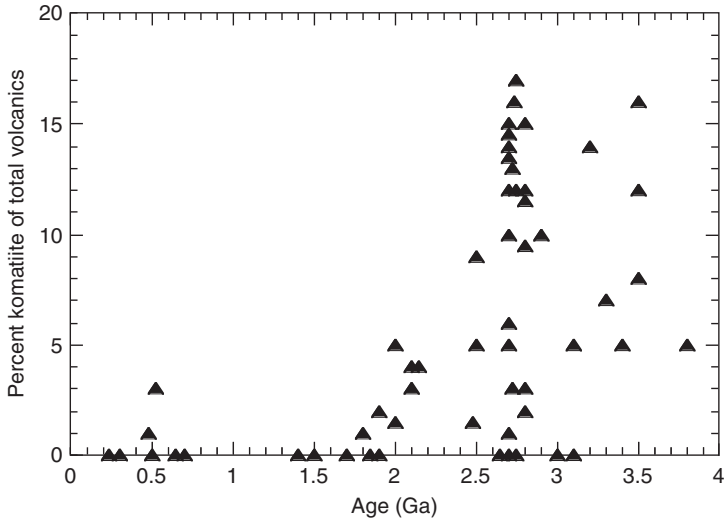

FIGURE 9.16 Percent of komatiites in greenstones versus age. *Updated after de Wit and Ashwal (1995).*

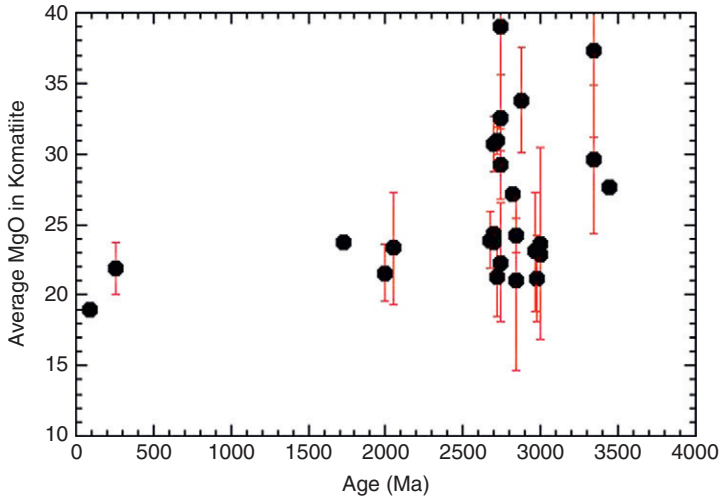

FIGURE 9.17 Average MgO content versus age for komatiites. Vertical bars are 1σ of the mean values. *Data from sources given in Arndt et al. (2008) and compiled by the author.*

It is unlikely that komatiites with >35% MgO represent pure liquids, because they may contain cumulus olivine. However, a decrease in MgO is apparent after 2500 Ma, even ignoring the sites with >35% MgO. As with komatiite frequency, the decrease in MgO at the end of the Archean also reflects a decrease in mantle temperatures at this time.

Although most data indicate that Archean komatiites crystallized from dry magmas, some investigators propose wet magmas, which do not require as high eruption temperatures as their dry counterparts (Parman et al., 2001; Arndt et al., 2008). In either case, however, the change in MgO at the end of the Archean would reflect a drop in mantle temperature, although not as large a drop as if the magmas were wet.

Ni/Fe Ratio in Banded Iron Formation

As documented by Konhauser et al. (2009), the Ni/Fe ratio in banded iron formation (BIF) also decreases rather abruptly at the end of the Archean. The authors attribute this decrease to a reduced flux of Ni into the oceans as a consequence of cooling of the mantle and a corresponding decrease in the rate of eruption of komatiites. As with changes in komatiite frequency and MgO content, the drop in Ni/Fe ratio of BIF attests to a probable drop in temperature of mantle sources near the end of the Archean.

Degree of Upper Mantle Melting

There is a noticeable increase in incompatible element ratios such as Nb/Yb, La/Yb, Zr/Y, La/Sm, and Gd/Yb in non-arc oceanic greenstone basalts at the end of the Archean (Condie, 2005). This is illustrated with the Nb/Yb ratio in Figure 9.18. Non-arc greenstones, which are identified using rock association and geochemistry, include ocean ridge, oceanic plateau, and oceanic island basalts. Because data are excluded that may reflect crustal contamination (using Nd isotopes and inherited zircons), the increase in Nb/Yb after 2.5 Ga is

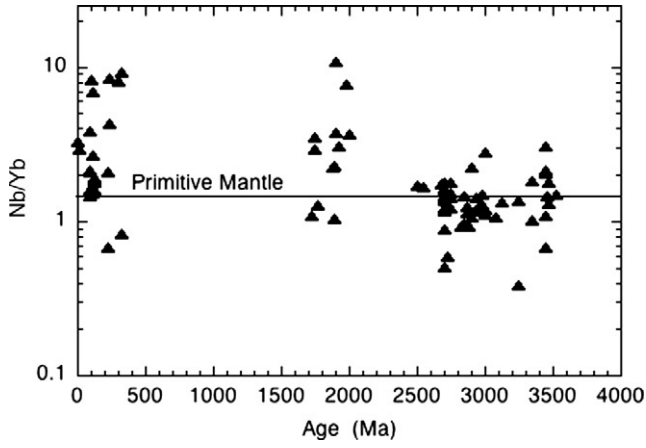

FIGURE 9.18 Nb/Yb versus age for nonarc oceanic basalts. Each data point is the average from single greenstone belts. *Updated after Condie (2003a and 2005b).*

probably caused by a decrease in the degree of melting (Condie & O'Neill, 2010) in mantle sources, which implies a decrease in mantle temperature at the end of the Archean.

The Growth of Cratons

Nb/Th Ratio and Neodymium Isotopes in Basalts

The Nb/Th ratio in non-arc oceanic basalts has been used as a proxy for the growth of continental crust, assuming that continental crust has been extracted from the mantle, leaving a depleted trace element signature in the restite (Collerson & Kamber, 1999; Condie, 2003a). The probability that at least some non-arc basalts come from mantle plume sources confirms the existence of a depleted component in plume sources since 2.7 Ga. Prior to 2.5 Ga, the Nb/Th ratio scatters around the primitive mantle value, suggesting that both slightly enriched and slightly depleted reservoirs existed in the Archean mantle (Condie, 2003a) (Figure 9.19). However, only after 2.5 Ga does the depleted mantle reservoir begin to grow in volume as reflected by the increasing Nb/Th ratios. This, in turn, may reflect the widespread onset of subduction in the late Archean. The ϵNd(T) values in non-arc type basalts and associated TTGs (tonalite-trondhjemite-granodiorite) also show an increase in maximum value after the end of the Archean (see Figure 7.12a). Bennett (2004) explains this in terms of rapid growth of continental crust in the late Archean causing a change in the Sm/Nd ratio of mantle sources.

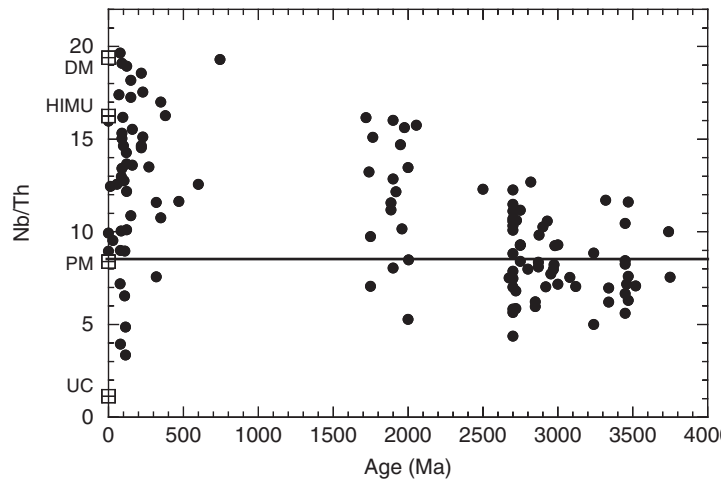

FIGURE 9.19 Nb/Th versus age for nonarc oceanic basalts. Each data point is the average from single greenstone belts. DM, depleted mantle; HIMU, high-μ source; PM, primitive mantle; UC, upper continental crust. *Updated after Condie (2003a).*

Changes in Granitoid Compositions

Significant increases in large-ion lithophile and high-field strength elements and a decrease in Sr in continental crust at the end of the Archean reflect a shift in magma series from TTG control to calc-alkaline control (Condie, 2008). The distinction between calc-alkaline and TTG suites is based on major element trends such as the K-Na-Ca graph of Martin (1993) (Figure 9.20), various silica variation diagrams, Sr content, Eu anomaly distribution, and low contents of heavy REE and Y (Condie, 2008). Decreases in $(La/Yb)_n$ and Sr/Y and possibly an increase in K_2O/Na_2O in Paleoproterozoic upper crust reflect an increasing calc-alkaline plutonic component. The drop in La/Yb reflects a decrease in garnet content of the mafic source at the end of the Archean (Figure 9.21), and the large drop in Sr/Y in the calc-alkaline component (due to restite plagioclase and/or fractional crystallization) controls the decreases in upper crustal Sr/Y with time.

These chemical changes appear to reflect chiefly a decrease in TTG magma production and a corresponding increase in calc-alkaline magma production at convergent plate margins after the end of the Archean. Furthermore, late Archean subduction zones may have differed from younger subduction zones in that they produced a thick mafic lower crust that served as a TTG magma source. One way to thicken mafic crust in the late Archean is by plate jams in subduction zones caused by the greater buoyancy of oceanic plates produced during a late Archean global thermal event. Modern subduction zones became widespread in the early Paleoproterozoic as magma production shifted from thickened crust (or/and descending slabs) to mantle wedges, where the calc-alkaline suite is produced. Large-ion lithophile element enrichment in mantle wedges reflects devolatilization of descending slabs and their associated subducted sediments.

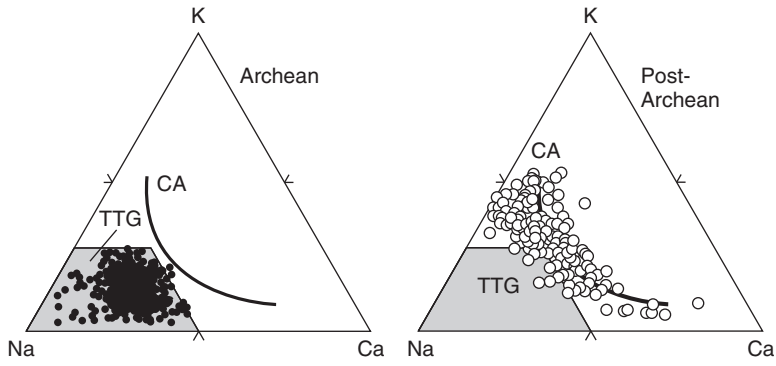

FIGURE 9.20 K-Na-Ca diagrams showing distribution of Archean and post-Archean granitoids. TTG, tonalite-trondhjemite-granodiorite field; CA, calc-alkaline trend. *Courtesy of Herve Martin.*

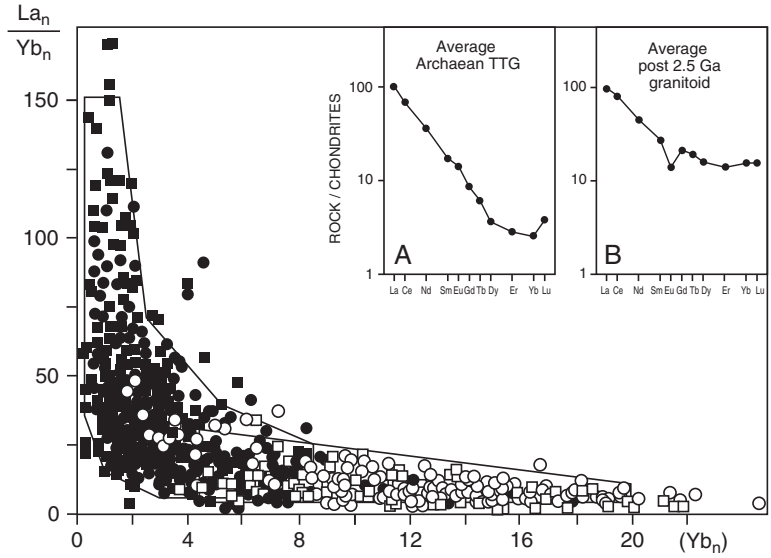

FIGURE 9.21 La_n/Yb_n ratio versus Yb_n content of granitoids. La_n and Yb_n are values normalized to chondritic meteorites. Solid symbols are Archean (mostly TTGs) and open symbols post-Archean (mostly calc-alkaline). *Courtesy of Herve Martin.*

Oxygen Isotopes in Zircons

Valley et al. (2005) have shown a prominent increase in the maximum values of $\delta^{18}O$ of zircons from granitoids after the end of the Archean (Figure 9.22). Oxygen isotopes are especially sensitive to the incorporation of source material for granitoids that have interacted with the hydrosphere, such as shales. The increase in $\delta^{18}O$ after the end of the Archean may reflect the rapid growth and stabilization of cratons in the late Archean, which provided a framework for weathering and recycling of hydrated surface rocks into magma sources of granitoids after 2.5 Ga. Prior to the end of the Archean, felsic crust may have been rapidly recycled into the mantle, thus allowing only minimal interaction with the hydrosphere.

Gold Reserves

A major peak in orogenic and volcanic-hosted massive sulfide (VHMS) gold reserves occurs at or near 2.7 Ga (see Figure 8.11 in Chapter 8) (Groves et al., 2005). As discussed by Goldfarb et al. (2001), orogenic gold deposits are produced by hydrothermal fluids in response to high thermal fluxes at convergent plate margins. Since orogenic and VHMS gold deposits are related directly to subduction and production of juvenile continental crust, it is not surprising to find major gold reserves at 2.7 Ga.

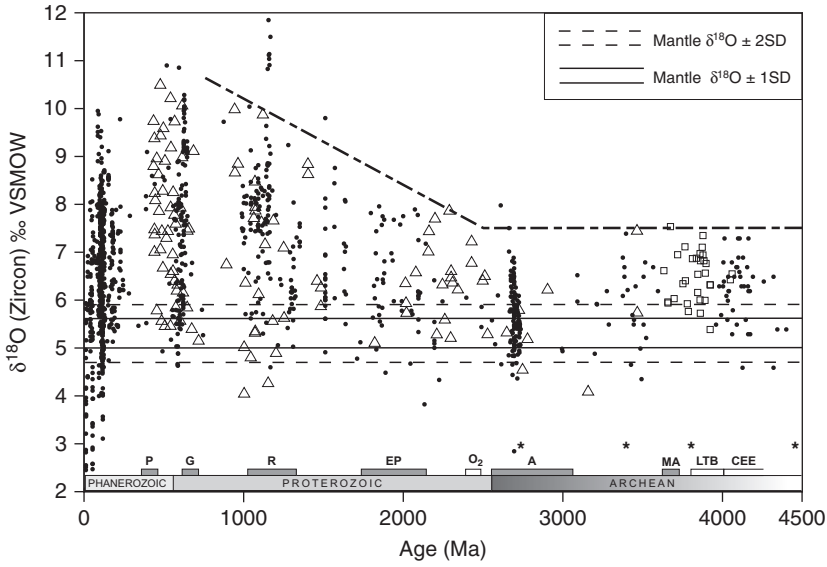

FIGURE 9.22 $\delta^{18}O$ in zircons from granitoids versus age. Dots, mostly multigrain zircons from bedrock samples; triangles/squares, single detrital zircons. *Courtesy of John Valley.*

Thickening of the Archean Lithosphere

The ^{187}Re-^{187}Os isotopic system has proved valuable in dating episodes of magma extraction from the mantle (Walker et al., 1989; Carlson et al., 2005). The key feature of the Re-Os system is that Os is compatible in the residue during mantle melting, whereas Re is moderately incompatible. Hence, the residue left after melt extraction has much lower Re, but greater Os concentration than either fertile mantle or mantle melts. The restitic lherzolite or harzburgite left in the mantle is useful in constraining the age of melt extraction, known as a **Re depletion age** ($\mathbf{T_{RD}}$).

Re-Os depletion ages from mantle xenoliths coming from beneath Archean cratons suggest that much of the thick Archean mantle lithosphere formed in the late Archean. The distribution of Archean T_{RD} ages from mantle xenoliths shows a prominent peak at 2.7 Ga consistent with widespread thickening of the continental lithosphere at this time (Figure 9.23). Although most of the data come from the Kaapvaal craton in southern Africa (which formed between 3.5 and 2.7 Ga; Pearson et al., 1995), many xenoliths from other Archean cratons also have T_{RD} ages between 2.8 and 2.65 Ga. This suggests that the thickened lithospheric roots of cratons that formed at or before 2.8 Ga were produced chiefly by a mantle event around 2.7 Ga, such as underplating with mantle plumes.

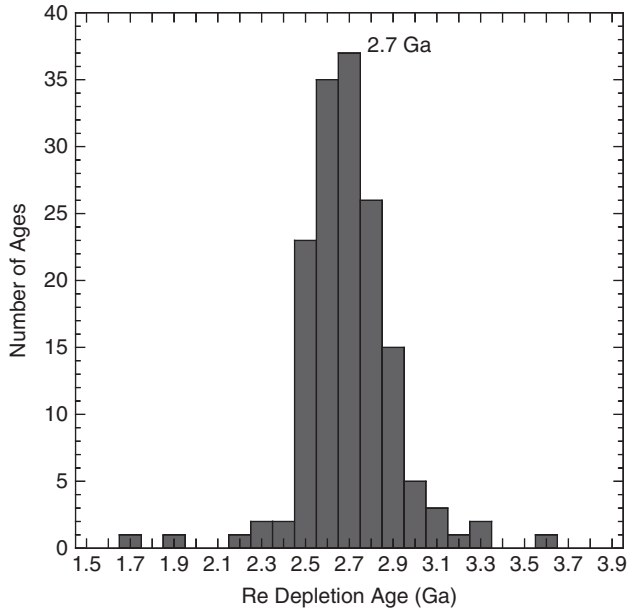

FIGURE 9.23 Histogram showing frequency of Re/Os depletion ages of xenoliths of Archean mantle lithosphere. *Data courtesy of Graham Pearson and Rick Carlson (Pearson et al., 2002; Carlson et al., 2005).*

Consistent with the thick Archean mantle lithosphere forming as a depleted plume underplate is the major element composition of mantle xenoliths coming from beneath cratons older than 2.7 Ga. Most are high in FeO and MgO, similar to the compositions of basalts derived from young depleted mantle plumes (Herzberg, 2004). However, as discussed in Chapter 7, the jury is still out on the question of whether these sources are remnants of mantle plume heads accreted to the bottom of the lithosphere or if they formed by the tectonic stacking of subducted oceanic slabs, or some combination thereof. Whatever the mechanism by which thick Archean lithosphere formed, most of it appears to have been produced over a short time interval of less than 100 Ma in the late Archean.

Numerical experiments also show that the continental lithosphere evolved through a rheological threshold at about 2.7 Ga allowing the development of significant topography (>2.5 km) on the continents (Rey & Coltice, 2008). This reflects the cooling and strengthening of the continental lithosphere, which introduced for the first time significant coupling between near-surface and deep geochemical reservoirs. This is due to felsic crust reaching the surface and being subjected to weathering and erosion and corresponding increases in the flux rate of sediments to ocean basins, which in turn, increases the rate of recycling of continental crust into the mantle.

How Did Plate Tectonics Begin: Thermal Constraints

Although it would have been possible for plates to buoyantly subduct in the Archean, they would not have been moving fast enough to remove the excess Archean heat (Davies, 1992, 1993). How then can this excess Archean heat be lost? Mantle plumes cannot be a substitute for heat loss by plate tectonics, since they bring heat into the mantle from the core and only marginally increase heat loss from the top of the mantle. In effect, plates cool the mantle while plumes cool the core. What is required is a mechanism in the lithosphere that promotes heat loss at the surface. At least three possibilities merit consideration:

1. A greater total length of the Archean ocean ridge system could help alleviate the problem (Hargraves, 1986). For instance, if Archean heat production were three times that of the present heat production, the total ocean ridge length would have to be 27 times the present length to accommodate the additional heat loss.
2. The inversion of basalt to eclogite in buoyantly subducted Archean oceanic crust may increase the density of the lithosphere sufficiently for it to subduct or delaminate. This mechanism is attractive in that thick Archean oceanic crust provides a large reserve of mafic rocks at depth that could invert to eclogite. Experimental data indicate that conditions are particularly favorable for eclogite formation and delamination at depths of 75–100 km (Rapp & Watson, 1995).
3. The oceanic mantle lithosphere may have been negatively buoyant due to latent heat loss associated with extraction of melt at ocean ridges (Davies, 1993). Two competing factors affect the density of the oceanic mantle lithosphere. The extraction of melt leaves a residue depleted in garnet and thus less dense. On the other hand, the latent heat of melting is carried away by the melt, leaving a residue colder and more dense. If the latent heat effect dominated in the Archean, the oceanic lithosphere could have become negatively buoyant.

Numerical modeling indicates that the transition to modern plate tectonic records three different styles of convection in the mantle (Figure 9.24). First is the **stagnant lid regime**, where a rigid, relatively thick immobile layer develops at the surface of the mantle. The stagnant lid is essentially decoupled from the convecting mantle, and planets in this thermal regime are often referred to as **one-plate planets**. The stagnant lid regime today characterizes Mars and the Moon. The second regime is an **episodic regime**, which begins with a stagnant lid and as it thickens it becomes mobilized and is subducted into the interior; the new hot surface cools into a new stagnant lid, which again becomes mobilized, and the cycle repeats itself (Moresi & Solomatov, 1998; O'Neill et al., 2007a,b; Sleep, 2007). Venus may be in an episodic regime today. And the final regime is the **mobile regime** or plate tectonic regime, where the surface layer is continually subducted and replaced with new lithosphere

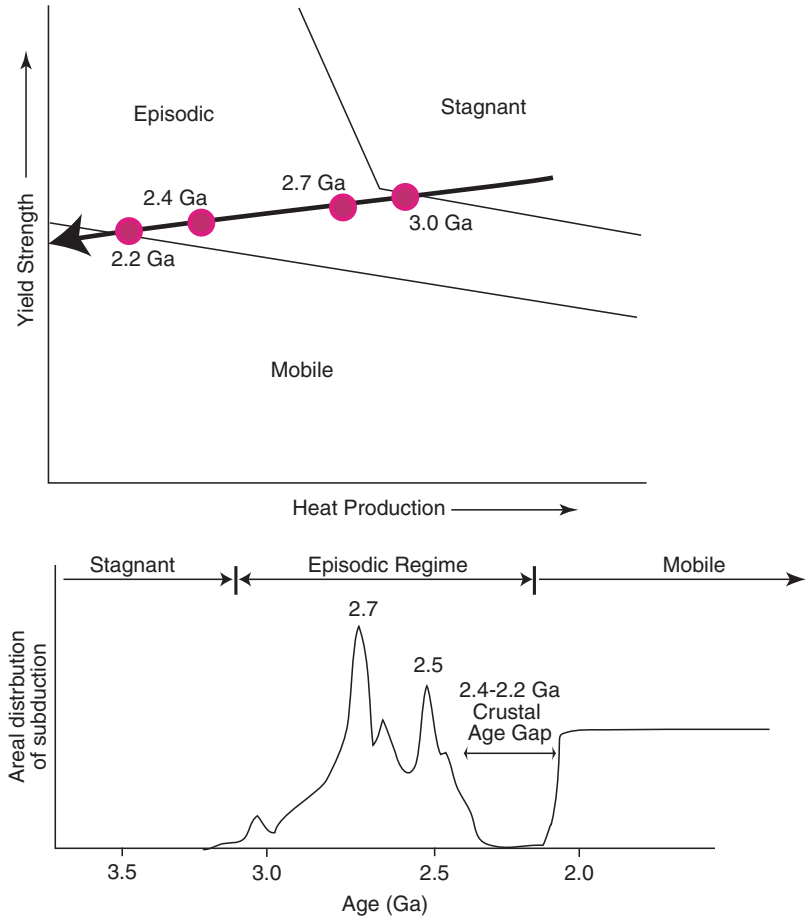

FIGURE 9.24 Yield strength versus heat production graph showing a possible evolution from stagnant lid to a mobile tectonic regime on Earth. *Modified after O'Neill et al. (2007a).*

produced at spreading centers. Earth is the only planet in the solar system today in the mobile regime. Geodynamic modeling for high mantle temperatures in the Archean Earth suggests that plate tectonics had several false starts, each followed by a return to stagnant lid tectonics (Figure 9.24). Silver and Behn (2008) have gone even farther suggesting that plate tectonics on Earth has always been intermittent, making a case for minimal subduction fluxes when supercontinents were in existence.

The hotter mantle in the Archean will have two effects: a lower viscosity and a greater degree of melting, which will produce thicker rather than thinner oceanic lithosphere. Unlike earlier models, those that consider episodic overturn find that lithospheric weakness rather than plate buoyancy is the limiting factor for

subduction (van Hunen & van den Berg, 2007; O'Neill et al., 2007b). It is very unlikely that plate tectonics began on Earth as a single global "event" at a distinct time. Rather, it is probable that a few mantle "returns" became cool enough that localized subduction became possible. As subduction zones continued to cool, more and more slabs were able to descend at steep angles, until by the late Archean modern-type subduction may have become widespread on the planet. Sizova et al. (2009) show also by thermomechanical modeling that plate tectonics evolves through three stages as the mantle cools with the transition to modern plate tectonics occurring in the late Archean.

When Did Plate Tectonics Begin?: The Ongoing Saga

Much has been written about the nature and cause of a probable global event in the late Archean (Stein & Hofmann, 1994; Condie, 1998; Condie & O'Neill, 2010). One model that has been widely discussed is a catastrophic global mantle plume event, which is triggered by collapse and sinking of oceanic slabs through the 660-km discontinuity (Tackley, 1994; Condie, 1998). As discussed in Chapter 8, this is based on the assumption that the 660-km phase transition has a large negative Clapeyron slope, and thus is a robust boundary in the hotter Archean mantle. However, experimental determinations of the Mg-perovskite reaction do not support this, and hence the catastrophic sinking slab model is no longer as attractive as an explanation for the 2.7-Ga event.

As discussed in the previous section, geodynamic modeling indicates that plate tectonics did not begin all at once, but rather went through an intermediate state (the episodic regime) during which it turned on and off several times before becoming permanently established. The last turn on may have been at about 2200 Ma, following a 200-Ma slowdown during the crustal age gap between 2.4 and 2.2 Ga (Figure 9.24). The geologic record suggests that plate tectonics may have begun, at least locally, by about 3 Ga (Condie & Kroner, 2008), but that the first really widespread plate tectonics developed in the late Archean at 2.7–2.5 Ga. Particularly relevant is a large drop in the ratio of non-arc to arc oceanic basalts from about 0.7 in the early Archean to less than 0.5 at 2.7 Ga (Figure 9.25) (Condie & O'Neill, 2010). Widespread propagation of subduction at 2.7 Ga also may be responsible for the rapid growth of cratons in the late Archean.

Any model for the late Archean must also include an explanation for a possible crustal age gap at 2.4 to 2.2 Ga (Condie et al., 2009b). Episodic mantle overturn makes a number of predictions that are of interest to this age gap. First, plate velocities should reflect rapid subduction on both sides of the gap with negligible velocities during the gap. These predicted velocities (up to 40–80 cm/y) far exceed the fastest current plate velocities (e.g., 24 cm/y), or velocities predicted by a model under steady-state plate tectonics (~10 cm/y) (O'Neill et al., 2007a). They are, however, consistent with velocities inferred for the Pilbara at ~2.7 Ga from paleomagnetic observations (~100 cm/y).

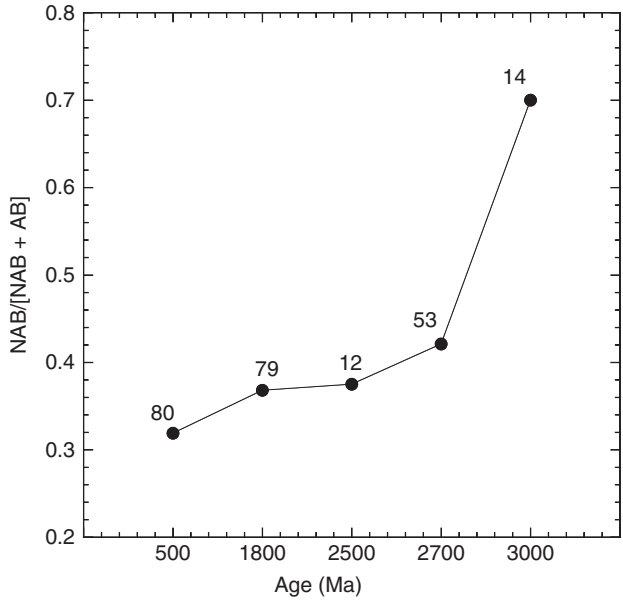

FIGURE 9.25 Ratio of oceanic nonarc (NAB) to arc (AB) type basalts versus age. Each labeled point is the number of greenstone locations. *Data updated from Condie (2003a and 2005b).*

Subducting slabs cool the upper mantle during times of subduction, whereas between subduction pulses when cooling is inefficient, the upper mantle temperature rises. With the reestablishment of plate tectonics, the mantle should be cooled and average upper mantle temperatures should drop by several hundred degrees.

One possible scenario for the onset of plate tectonics in the Archean is shown in Figure 9.26. The simplest relationship is that the onset of widespread subduction at 2.7 Ga produces continental crust in numerous arcs, which rapidly collide to form large cratons and perhaps a supercontinent. The cratons survive for two reasons: (1) they are underplated with thick lithosphere either from mantle plumes or stacking of buoyantly subducted slabs, and (2) the growth rate of continental crust exceeds the recycling rate back into the mantle, possibly reflecting buoyant subduction or colliding oceanic plateaus that produce "log jams" in subduction zones.

Oceanic slabs sinking to the D″ layer could destabilize this layer by thickening it, resulting in an enhanced production rate of mantle plumes (Figure 9.26) (Davies, 1999). Enhanced plume production should produce more oceanic plateaus and these plateaus could form the nuclei of cratons or they could collide with arcs. In either case, they would contribute to rapid production of the early cratons and one or more supercratons. A widespread large igneous province (LIP) event at 2.45 Ga (Heaman, 1997) may have been triggered by

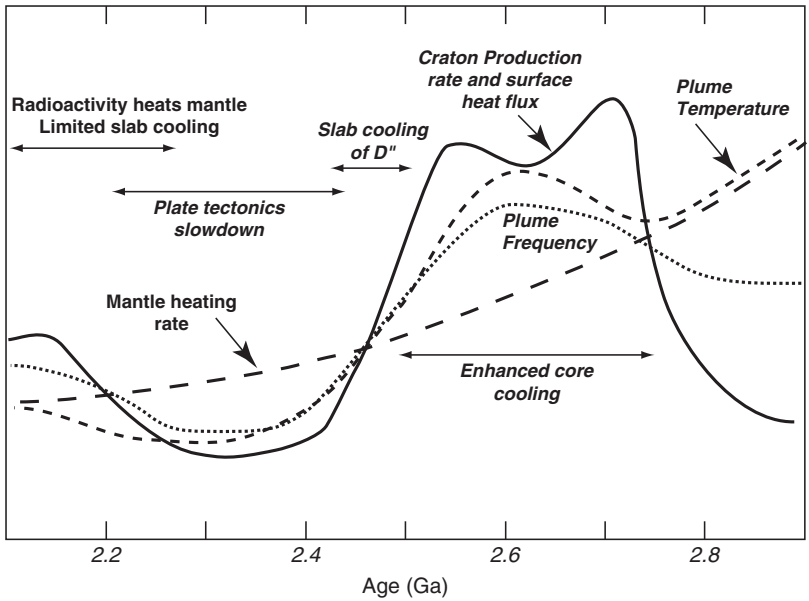

FIGURE 9.26 Thermal model for changes in the mantle near the end of the Archean and beginning of the Paleoproterozoic. *Modified after Condie and O'Neill (2010).*

the last of the slabs associated with the onset of widespread subduction at 2.7–2.5 Ga, which sank to the D″ layer. The key requirement is that all of this must happen in a 200-Ma time window between 2.7 and 2.5 Ga.

The arrival of cool, depleted slabs at the base of the mantle may also increase the heat flux from the core, which warms the newly arrived slabs (Korenaga, 2006). The cooling of the deep mantle would begin after 2.5 Ga and continue until about 2.4 Ga when a plate tectonics slowdown is initiated (Figure 9.26). This offers a possible explanation for the rapid drop in temperature of the mantle inferred from the changes in komatiite production rate and MgO levels and the increases in Nb/Yb in non-arc oceanic basalts. Also, supporting a cool lower mantle during this time window is a sparsity of LIPs between 2.4 and 2.2 Ga (Ernst & Buchan, 2001). When plate tectonics comes back on track at about 2.2 Ga, the first supercratons (or supercontinent) are formed at 2.7 Ga, break up, and are then dispersed (Bleeker, 2003). Also at this time, the temperature of plume sources is reestablished along the normal mantle heating curve of the deep mantle.

This model is not free from problems. One of the uncertainties is how fast depleted oceanic slabs sink into the deep mantle to cool plume sources. The enhanced subduction activity at 2.7 Ga would produce many sinking slabs, and if these slabs sink too fast, cooling of deep plume sources could start before 2.5 Ga. A related question is how to keep the plume sources cool for 200 Ma (2.4–2.2 Ga), when the rate of slab sinking would be greatly reduced as plate tectonics enters a global

slowdown mode. Modeling by O'Neill et al. (2007a) suggests that it may take this long for the slabs to equilibrate with the temperature in the deep mantle.

Conclusions

Important, well-documented geochemical changes in the crust–mantle system are found at the end of the Archean. Because of the lack of data between 2.4 and 2.2 Ga, it is not possible to estimate the rate at which the changes occurred. They may have taken place immediately after 2.5 Ga in a time period less than 100 Ma, or they may have extended over 100–300 Ma between 2.5 and 2.2 Ga. In either case, they may be related to one or both of two events: cooling of the deep mantle and formation of the first widespread cratons. The first major cratons, amalgamating into a supercraton or supercontinent, probably formed in the late Archean around 2.7 Ga, whereas cooling of the deep mantle began after 2.5 Ga. Both of these events could be related to a widespread onset of plate tectonics in the late Archean followed by a slowdown of plate tectonics between 2.4 and 2.2 Ga. Rapid formation of cratons at 2.7 Ga is probably tied to high production rates and relatively rapid collision of arcs, together with enhanced production rates and collision of oceanic plateaus and arcs. The cause of cooling of the deep mantle after 2.5 Ga, however, is problematical, but may be related to the arrival of large volumes of cool, depleted slabs in the lower mantle soon after an episode of widespread subduction at 2.7–2.5 Ga.

EVENT 4: THE GREAT OXIDATION EVENT

The most distinctive characteristic of Earth's atmosphere is the presence of free oxygen. It is the only planet is the solar system with enough oxygen to sustain higher life-forms. How did oxygen develop in the atmosphere and why is Earth the only planet with significant amounts? The geologic record suggests that the first major injection of oxygen into the atmosphere occurred about 2350 Ma with smaller injections in the Neoproterozoic at 800–600 Ma. In this section we review the evidence for the 2350-Ma event, known as the **Great Oxidation Event** (**GOE**), and briefly summarize the history of oxygen in the atmosphere.

Oxygen Controls in the Atmosphere

In the modern atmosphere, oxygen is produced almost entirely by **photosynthesis** (Figure 9.27) by the well-known reaction,

$$CO_2 + H_2O \rightarrow CH_2O + O_2 \qquad (9.1)$$

For oxygen to accumulate in the atmosphere, it is necessary to bury carbon (CH_2O) to keep the reaction going to the right. Burial of pyrite also frees up oxygen to enter the atmosphere, and small amounts of oxygen are liberated by reduction of carbonates and sulfates during diagenesis of sediments. A very small amount of O_2 is also produced in the upper atmosphere by photolysis

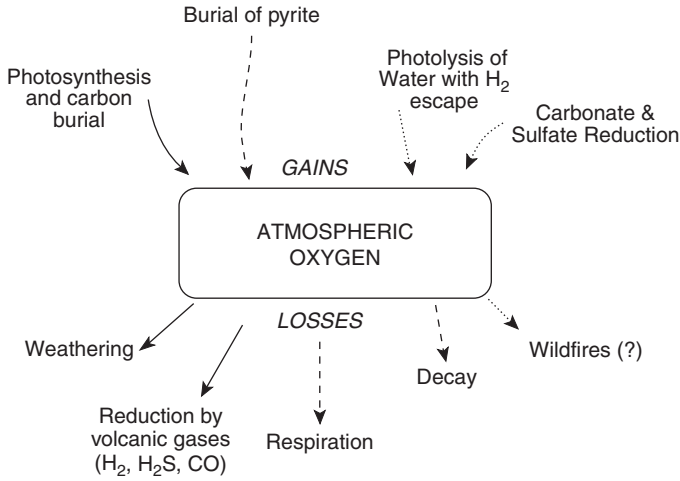

FIGURE 9.27 Gains and losses of atmospheric O_2. Solid lines, major controls; long-dash lines, intermediate controls; short-dash lines, minor controls.

of H_2O molecules. For instance, the photolysis of H_2O produces H_2 and O_2 ($H_2O \rightarrow H_2 + 0.5O_2$). Oxygen is removed from the atmosphere principally by weathering and by reduction by volcanic gases (Figure 9.27). Respiration and decay, which can be considered the reverse of the photosynthesis reaction, also remove oxygen. Virtually all of the O_2 produced by photosynthesis in a given year is lost in <50 years by oxidation of organic matter. Without oxidation of organic matter and sulfide minerals during weathering, the O_2 content of the atmosphere would double in about 10^4 years (Holland et al., 1986). It has also been suggested that wildfires may have contributed in the past to controlling the upper limit of O_2 in the atmosphere. It appears that the O_2 content of the modern atmosphere is maintained at a near constant value by various negative short-term feedback mechanisms involving primarily photosynthesis and decay. If, however, photosynthesis were to stop, respiration and decay would continue until all of the organic matter on Earth was transformed to CO_2 and H_2O. This would occur in about 20 years and involve only a minor decrease in the amount of O_2 in the atmosphere. Weathering would continue to consume O_2 and would take about 4 Ma to use up the current atmospheric supply.

Prior to the appearance of photosynthetic microorganisms, and probably for a considerable time thereafter, photosynthesis was not an important process in controlling atmospheric oxygen levels. In the primitive atmosphere, O_2 content was controlled by the rate of photolysis of water and methane, hydrogen loss from the top of the atmosphere, and weathering rates at the surface. The rate at which water is supplied by volcanic eruptions is also important because volcanism is the main source of water available for photolysis. If metallic iron were present in the mantle during the earliest stages of degassing of Earth, H_2 would have been an

important component of volcanic gases. Because H_2 rapidly reacts with O_2 to form water, significant amounts of volcanic H_2 would prevent O_2 from accumulating in the early atmosphere. As H_2O instead of H_2 became more important in volcanic gases, in response to removal of iron from the mantle as the core grew, oxygen could, in theory, begin to accumulate in the early atmosphere. Likewise, early photosynthesizing organisms and methane photolysis also may have contributed some oxygen. However, if the Archean atmosphere was rich in methane as discussed in Chapter 6, free oxygen could not survive. Not until large volumes of oxygen entered the atmosphere and destroyed the methane could free oxygen begin to accumulate. Free carbon remaining after hydrogen escapes from the upper atmosphere (from methane photolysis) reacts with oxygen to produce CO_2, which then can be used in photosynthesis to produce more oxygen (Catling et al., 2001). As photosynthesis became more widespread, recombination of H_2 and O_2 to form water could not keep pace with O_2 input and the oxygen level in the atmosphere must have increased. This assumes that the rate of weathering did not increase with time, an assumption that is supported by geologic data.

Geologic Indicators of Ancient Atmospheric Oxygen Levels

Banded Iron Formation

The distribution of banded iron formation (BIF) with geologic time provides a constraint on O_2 levels in the oceans and atmosphere (Ohmoto et al., 2006). BIFs also commonly contain layers of chert and generally have $Fe^{3+}/Fe^{2+} + Fe^{3+}$ ratios in the range of 0.3 to 0.6, reflecting an abundance of magnetite (Fe_3O_4). Most iron formations are metamorphosed and major minerals include quartz, magnetite, hematite, siderite, and various other Fe-rich carbonates, amphiboles, silicates, and sulfides (Figure 9.28). Although most abundant in the late Archean and Paleoproterozoic, BIF occurs in rocks as old as 3.8 Ga (Isua, Southwest Greenland) and as young as 0.8 Ga (Rapitan Group, northwest

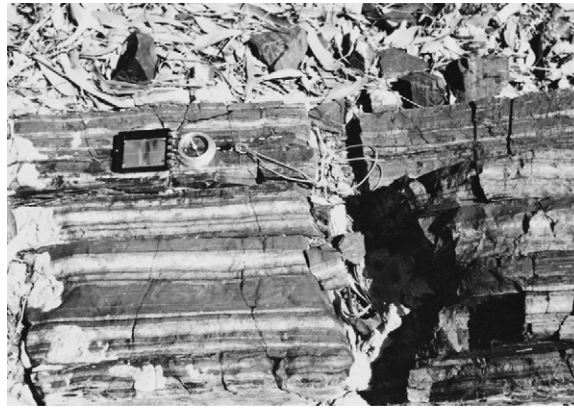

FIGURE 9.28 Early Archean banded iron formation from the Warrawoona Supergroup, Western Australia. *Courtesy of Andrew Glikson.*

Canada) (see Figure 9.32). The Hamersley Basin (2.45 Ga) in Western Australia is the single largest known single BIF depository (Klein & Beukes, 1992).

Most investigators consider the large basins of BIF to have formed on cratons or passive margins in shallow marine environments. Many BIF are characterized by thin wave-like laminations that can be correlated over hundreds of kilometers (Trendall, 1983). During the late Archean and Paleoproterozoic, enormous amounts of ferrous iron appear to have entered BIF basins with calculated Fe precipitation rates of 10^{12}–10^{15} g/y (Holland, 1984). Although some of the Fe^{2+} undoubtedly came from weathering of the continents, most appears to have entered the oceans by submarine volcanic activity (Isley, 1995). BIF is generally thought to be deposited by oxidation of Fe^{2+} in seawater as it upwells into oxidizing environments:

$$Fe^{2+} + 0.25O_2 + H_2O \rightarrow 0.5Fe_2O_3 + 2H^+ \qquad (9.2)$$

Deposition occurs as Fe reacts with dissolved O_2, probably at shallow depths forming flocculent, insoluble ferric and ferro-ferric compounds. Archean BIF may have been deposited in deep water in a stratified ocean (Klein & Beukes, 1992). Beginning at about 2.3 Ga, the stratified ocean began to break down with the deposition of shallow-water oolite-type BIF, such as those in the Lake Superior area.

Although Precambrian BIF represents a large oxygen sink, the O_2 content of the coexisting atmosphere may have been quite low. For instance, hematite (Fe_2O_3) or $Fe(OH)_3$ can be precipitated over a wide range in oxygen levels and early Archean BIF may have been deposited in reducing marine waters. The large amount of oxygen in late Archean and especially in Paleoproterozoic BIF, however, appears to require the input of photosynthetic oxygen. This agrees with paleontologic data that indicate a rapid increase in numbers of photosynthetic algae during the same period of time, and many BIF contain well-preserved fossil algae remains. Thus, it appears that the increase in abundance of BIF in the late Archean and Paleoproterozoic reflects an increase in oceanic O_2 content in response to increasing numbers of photosynthetic organisms. Only after most of the BIF was deposited and the Fe^{2+} in solution was exhausted did O_2 begin to escape from the oceans and accumulate in the atmosphere in appreciable quantities (Cloud, 1973). The drop in abundance of BIF after 1.9 Ga probably reflects the exhaustion of reduced iron in the deep oceans.

Redbeds and Sulfates

Redbeds are detrital sedimentary rocks with red ferric oxide cements. They generally form in fluvial or alluvial environments and the red cements are the result of subaerial oxidation (Folk, 1976); thus, they require the presence of O_2 in the atmosphere. The fact that redbeds do not appear in the geologic record until about 2.3 Ga (Eriksson & Cheney, 1992) suggests that oxygen levels were very low in the atmosphere prior to this time.

Sulfates, primarily gypsum and anhydrite, occur as evaporites. Although evidence of very minor gypsum deposition is found in some of the oldest

supracrustal rocks (~3.5 Ga), evaporitic sulfates do not become important in the geologic record until after 2 Ga. Since their deposition requires free O_2 in the ocean and atmosphere, their distribution supports rapid growth of oxygen in the atmosphere beginning in the Paleoproterozoic.

Detrital Uraninite Deposits

Several occurrences of late Archean to Paleoproterozoic detrital uraninite and pyrite are well documented, the best known of which are those in the Witwaterstrand Basin in South Africa (~3.0 Ga), the Pilbara craton in Western Australia (3.3–2.8 Ga), and those in the Blind River-Elliot Lake area in Canada (~2.4 Ga) (Rasmussen & Buick, 1999). Detrital siderite is also documented in the Pilbara sediments. No significant occurrences of detrital uraninite are known to be younger than Mesoproterozoic, although a few very minor occurrences are found in young sediments associated with rapidly rising mountain chains like the Himalayas (Walker et al., 1983). Both uraninite and pyrite are unstable under oxidizing conditions and are rapidly dissolved. The preservation of major late Archean and Paleoproterozoic deposits of detrital uraninite and pyrite in conglomerate and quartzite indicates that weathering did not lead to total oxidation and dissolution of uranium and iron. To preserve uraninite, the partial pressure of oxygen must have been 10^{-2} PAL (of the present atmospheric level). The few occurrences of young detrital uraninite are metastable, and the uraninite is preserved only because of extremely rapid sedimentation rates and will not survive for long.

The restriction of major detrital uraninite-pyrite deposits to >2.4 Ga again favors very low O_2 levels in the atmosphere prior to this time.

Paleosols

Paleosols are preserved ancient weathering profiles or soils that contain information about atmospheric composition (Holland, 1992). Highly oxidized paleosols retain most, if not all, of the iron in Fe^{3+} and Fe^{2+} compounds, whereas paleosols that formed in nonoxidizing or only slightly oxidizing environments show significant losses of iron in the upper horizons, especially in paleosols developed on mafic parent rocks. This is illustrated for a late Archean paleoweathering profile from Western Australia in Figure 9.29 (Yang et al., 2002). A lower atmospheric content of oxygen is necessary for the Fe to be leached from the upper paleosol horizon (Macfarlane et al., 1994). Elements such as Al, which are relatively immobile during weathering, are enriched in the upper horizons due to the loss of mobile elements such as Fe^{2+}. This indicates that by 2.7 Ga, the atmosphere contained very little if any oxygen. Also, the presence of rhabdophane (a hydrous rare earth phosphate) with Ce^{3+} in a 2.6- to 2.5-Ga paleosol from Canada provides compelling evidence for an anoxic atmosphere at 2.5 Ga (Murakami et al., 2001).

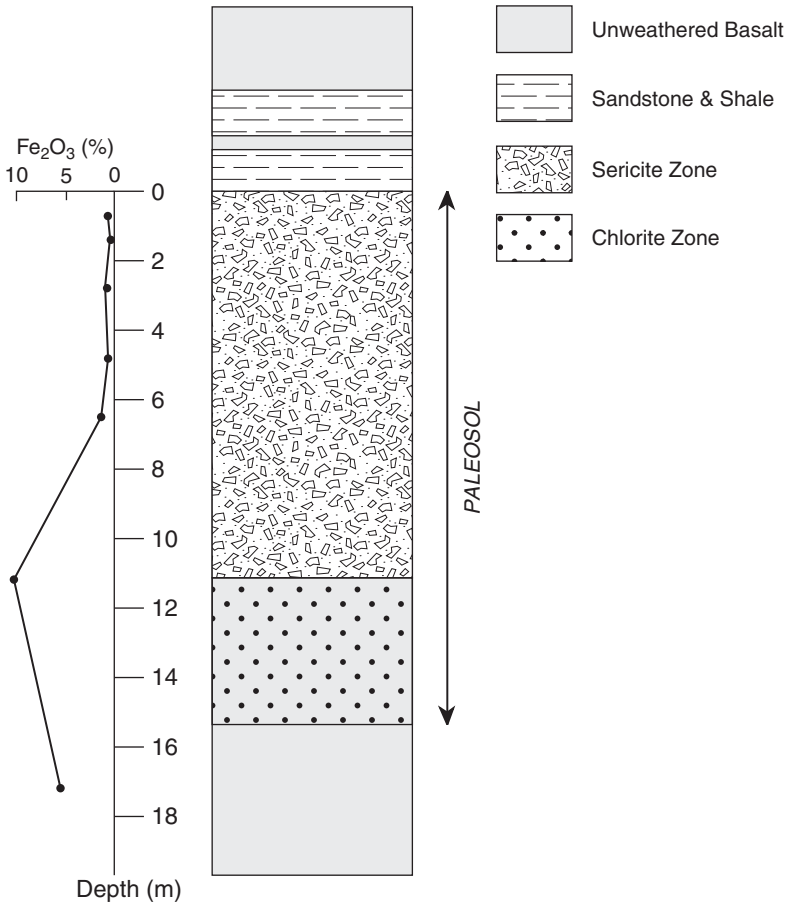

FIGURE 9.29 Stratigraphic section of the 2.7-Ga Mt. Roe paleosol, Western Australia, showing the concentration of Fe_2O_3 with depth. *After Macfarlane et al. (1994).*

Beginning in the Paleoproterozoic, paleosols do not show leaching of iron. Results suggest that the O_2 level of the atmosphere rose dramatically from about 1% PAL to >15% of this level about 2 Ga (Holland & Beukes, 1990).

Biologic Indicators

The Precambrian fossil record also provides clues to the growth of atmospheric oxygen. Archean life-forms were entirely prokaryotic organisms, the earliest examples of which evolved in anaerobic (oxygen-free) environments. Prokaryotes that produced free oxygen by photosynthesis appear to have evolved by 3.5 Ga. The timing of the transition from an anoxic to oxic atmosphere is not well constrained by microfossil remains but appears to have begun just after the Great Oxidation Event at approximately 2.35 Ga (Knoll & Carroll, 1999).

Certainly by 2.0 Ga when heterocystous cyanobacteria appear, free O_2 was present in the atmosphere in significant amounts, in agreement with the paleosol data. The first appearance of eukaryotes at about 2.4–2.3 Ga indicates atmospheric oxygen had reached 1% PAL, which is necessary for mitosis to occur. The appearance of simple metazoans at about 2 Ga requires O_2 levels high enough for oxygen to diffuse across membranes (~7% PAL).

Molybdenum in Black Shales

Molybdenum is a redox-sensitive transition element that accumulates in black shales. The small amount of accumulation prior to about 2200 Ma and extending to the late Archean is consistent with only minimal oxidative weathering on the continents prior to this time (Scott et al., 2008). An increase in Mo enrichment in black shales begins at 2150 Ma, some 200 Ma after the Great Oxidation Event. It would appear that it took this long for oxygen levels to rise high enough to promote widespread oxidative weathering of Mo and related elements.

Mass-Independent Sulfur Isotope Fractionation

Mass-independent sulfur isotope fractionation is extremely important in constraining the growth rate of oxygen in Earth's atmosphere. Farquhar et al. (2000) show that the difference in abundance between $\delta^{33}S$ and $\delta^{32}S$ is about half that between $\delta^{34}S$ and $\delta^{32}S$ in rocks older than about 2.2 Ga. These differences are thought to result solely from photolysis of SO_2 and SO in the upper atmosphere (Farquhar & Wing, 2003). In a high-O_2 atmosphere as at present, these effects are not seen in sediments because almost all sulfur gases are oxidized to sulfuric acid and accumulate in the oceans as sulfates. In a low-O_2 atmosphere, however, where sulfur can exist in a variety of oxidation states, the probability of transferring a mass-independent fractionation signature into sediments is much greater.

We can use $\Delta^{33}S$ to track the history of oxygen in the atmosphere, where

$$\Delta^{33}S = \delta^{33}S - 1000[(1 + \delta^{34}S/1000)^{0.515} - 1] \tag{9.3}$$

Three stages in atmospheric history are recognized when $\Delta^{33}S$ in marine sediments is plotted with age (Figure 9.30) (Farquhar & Wing, 2003). Stage 1 from 3.8 to about 2.35 Ga is characterized by $\Delta^{33}S$ extending to values greater than ±1‰; stage 2 from about 2.35 to 2 Ga has a much smaller range of $\Delta^{33}S$ (–0.1 to +0.5); and stage 3 from 2 Ga to the present has a very small range of $\Delta^{33}S$ of –0.1 to +0.2‰. This overall pattern supports carbon isotope data, suggesting rapid growth of oxygen in Earth's atmosphere near 2350 Ma, now known as the Great Oxidation Event or GOE. Results reported by Bekker et al. (2004) indicate that the very small range in $\Delta^{33}S$ extended at least to 2.32 Ga, suggesting rapid growth in oxygen in the atmosphere between

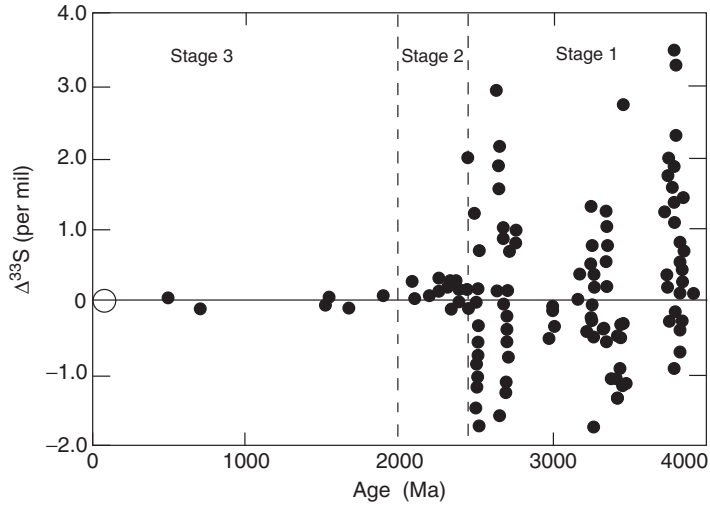

FIGURE 9.30 Variation in $\Delta^{33}S$ with time in marine sediments. Large unfilled circle represents hundreds of analyses of samples less than 2000 Ma. *Modified after Farquhar and Wing (2003).*

2.32 and 2.45 Ga. More sulfur isotope data in the age range of 2.5 to 2.0 Ga are needed to refine this estimate. Another puzzling feature of the $\Delta^{33}S$ distribution is that during stage 1, there appears to be three pulses of variability in sulfur isotopes separated by two minima. Modeling by Domagal-Goldman et al. (2008) suggests that these pulses are the result of organic haze caused by a thick CH_4 atmosphere. The sulfur isotope fractionation in the atmosphere may have been modulated by this haze layer producing the $\Delta^{33}S$ pulses. Haze filters the lower atmosphere from UV radiation responsible for the mass-independent sulfur isotope fractionation, causing the minima in $\Delta^{33}S$. The haze also would have caused and anti–greenhouse effect during these times and may have contributed to triggering the global glaciations at 2.4 Ga.

Several lines of evidence indicate that the GOE may have been the last pulse of failed attempts for free oxygen to enter the atmosphere in significant volumes. Redox-sensitive elements like molybdenum and rhenium occur in black shales that are 2.5 Ga (Anbar et al., 2007). These elements were probably supplied to the oceans by oxidative weathering of crustal sulfides, and indicate that small amounts of free oxygen existed in the atmosphere more than 50 Ma before the GOE. Also, biomarker evidence for the presence of cyanobacteria and oxygenic photosynthesis are found in sedimentary rocks of this age (Guo et al., 2009). Finally, Cr isotopes are sensitive to atmospheric oxygen levels. Oxidation of the reduced trivalent Cr on land is accompanied by an isotopic fractionation leading to an enrichment in the mobile hexavalent Cr in the heavier isotope. Cr isotope data from 2.8- to 2.6-Ga sedimentary rocks from several locations indicate that the heavier isotope must have been present in surface waters 200–400 Ma

before the GOE (Frei et al., 2009). All of these lines of geochemical evidence indicate that some free oxygen was available in the atmosphere–ocean system prior to the GOE at 2350 Ma.

The Growth of Atmospheric Oxygen

Considering all of the geologic and isotopic data, the growth of oxygen in Earth's atmosphere can be divided into three stages (Kasting, 1987, 1991; Farquhar & Wing, 2003; Holland, 2006): state I, a *reducing stage* in which free oxygen occurs in neither the oceans nor the atmosphere; state II, a rapidly *oxidizing stage* in which significant amounts of oxygen enter the atmosphere and surface ocean water, but not the deep ocean waters; and stage III, an *aerobic stage* in which free oxygen pervades the entire ocean–atmosphere system. These stages are diagrammatically illustrated in Figure 9.31 with corresponding geologic indicators.

During stage I, the ozone shield required to block out lethal ultraviolet radiation is absent. If such a shield existed on the primitive Earth, it must have been produced by a gaseous compound other than ozone. During this stage, atmospheric oxygen was probably less than a few parts per million and the oceans were anoxic, except perhaps in oxygen oases within the photic zone. Although marine cyanobacteria produced O_2 by photosynthesis during this

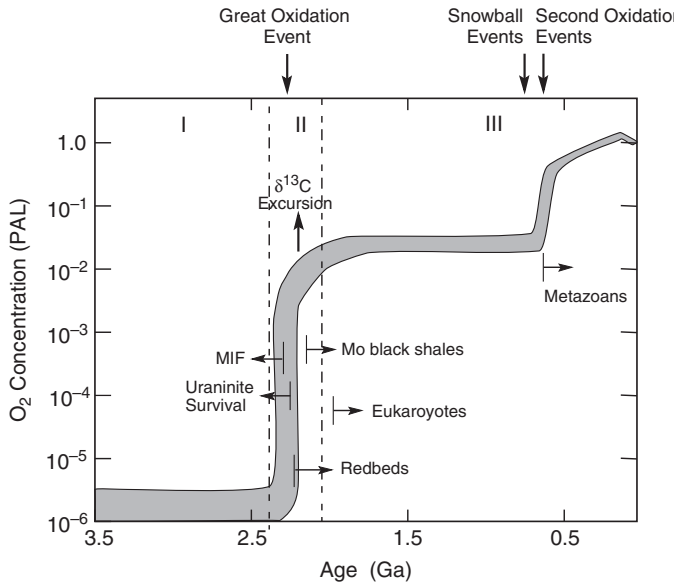

FIGURE 9.31 Growth in atmospheric oxygen with time. Shaded area is the range of O_2 concentrations permitted by geologic indicators. PAL, fraction of present atmospheric level; MIF, mass-independent sulfur isotope fractionation; Mo, molybdenum and related elements.

stage, in order for large volumes of BIF to form, this oxygen must have combined rapidly with Fe^{2+} and been deposited. The atmosphere should have remained in stage I until the amount of O_2 produced by photosynthesis followed by organic carbon burial was enough to overwhelm the input of volcanic gases.

Based on the end of mass-independent sulfur isotope fractionation, the first major increase in free oxygen in the atmosphere occurred at about 2350 Ma during the Great Oxidation Event (Figures 9.30 and 9.31) and is the basis for defining stage II (Holland, 2006). During this stage, oxygen levels rose rapidly in the atmosphere and shallow oceans, but almost certainly remained anoxic in the deep oceans. At this time, an effective ozone screen developed, which was probably responsible for the rapid diversification and increase in numbers of microorganisms in the Mesoproterozoic. Stage II is marked by the appearance of redbeds at 2.3 Ga, an increase in abundance of evaporitic sulfates, the end of major detrital uraninite-pyrite deposition, a major carbon isotope excursion, Mo enrichment in black shales, and an end to mass-independent sulfur isotope fractionation (MIF) (Figure 9.31). At this time, photosynthetic O_2 entered the atmosphere in significant amounts. The simplest explanation for the sudden appearance of oxygen is that cyanobacteria using photosystem-II evolved at this time (Holland, 2006). However, this is unlikely in that 2-α-methylhopanes occur in sedimentary rocks by 2.7 Ga, suggesting that primary producers were important long before the oxygenation event.

Just what triggered this injection of oxygen at about 2350 Ma is a subject of considerable controversy and speculation. Evidence that the lower atmosphere and surface ocean waters during this stage were weakly oxidizing, yet deep marine waters were reducing, is provided by the simultaneous deposition of oxidized surface deposits (redbeds, evaporites) and BIF in a reducing (or at least nonoxidizing) environment. Three models have been proposed for the control of atmospheric O_2 levels during stage II. One proposes that low O_2 levels are maintained by mantle-derived Fe^{2+} in the oceans, and BIF deposition and the first cessation of BIF deposition at about 2.4 Ga allowed oxygen to enter the atmosphere. A second model relies on increasing rates of photosynthetic productivity in the ocean, and the last, a newcomer to the list, proposes that the CO_2/H_2O and SO_2/H_2O ratios in volcanic gases increased rapidly at about 2.4 Ga. The third model is a complex model involving the loss of large amounts of H_2 from the upper atmosphere, which permits O_2 to accumulate in the atmosphere–ocean system (Holland, 2009). Which of these is most important is not yet clear. In any case, it would appear that the Great Oxidation Event was short lived, probably <100 Ma in duration (Figure 9.31). The change from stage II to III at about 1.8 Ga is also marked by the temporary disappearance of BIF from the geologic record and the appearance of eukaryotic organisms. During the first segment of stage III, there is little evidence for any changes in atmospheric oxygen levels (Holland, 2006). During much of this stage, the deep ocean appears to have remained anoxic, and probably euxinic as discussed in Chapter 6.

During the Snowball Earth events in the Neoproterozoic (as discussed in the next section), a considerable amount of organic carbon was buried between glaciations leading to a second rise in atmospheric oxygen between 650 and 520 Ma, sometimes referred to as the "**Second Great Oxidation Event**" (Campbell & Squire, 2010) (Figure 9.31). Banded iron formation also made a short-lived and final reappearance between 730 and 650 Ma. The deep oceans and, at least locally, the shallow oceans were anoxic and perhaps euxinic during this time. By 575 Ma, atmospheric O_2 must have risen to at least 50% PAL to permit the appearance of multicellular animal life. A controversial and yet unresolved question is what triggered the rapid growth of oxygen in the Neoproterozoic. Campbell and Squire (2010) suggest that it was the rapid uplift of high mountains in collisional orogens during the assembly of Gondwana. This led to a marked increase in the rate of erosion and hence to an increase in the flux of sediments entering the ocean. This, in turn, resulted in an increased supply of essential nutrients (especially Fe and P) for life, leading to an explosion in the unicellular plants and thus increased photosynthetic activity and O_2 production. Together with the increased burial rate of carbon due to increased erosion/sedimentation, oxygen entered the atmosphere in large amounts. This increase was required for the existence of animals, and later still increasing levels of oxygen led to the Cambrian Explosion of life.

Before leaving oxygen, a competing model of oxygen growth should be mentioned. Ohmoto (1997) and Ohmoto et al. (2006) propose a model in which the oxygen level in the atmosphere remains essentially constant for 4 Ga of Earth's history. This model questions many of the oxygen indicators and especially whether they are global in character. It also suggests that a drop in total carbon flux or decrease in the deposition rate of marine carbonates can explain the carbon isotope peak at 2.2 Ga. However, it offers no explanation for termination of the mass-independent sulfur isotope fractionation at 2350 Ma. Although this model cannot yet be dismissed, the accumulating evidence supporting a rapid rise in atmospheric oxygen at about 2350 Ma is becoming more and more compelling.

EVENT 5: THE SNOWBALL EARTH

The idea of an entirely frozen Earth has drawn the attention of both Earth scientists and the general public. It has long been recognized that glacial deposits of Neoproterozoic age are widely distributed on the continents and perhaps global in scale, but only in the last 10 years has it been possible to begin to date these deposits and tie them into the climatic record. During the period of time between about 850 and 650 Ma, the supercontinent Rodinia (Chapter 8) fragmented and dispersed, large fluctuations in stable isotopes were recorded in sedimentary rocks, and eukaryotic organisms rapidly diversified. Although we have an ever increasing database, what is still not agreed on is how many

glaciations are represented, which if any are global in extent, how the biosphere responded, and how these glaciations were triggered and what brought them to an end.

The Observational Database

There is now strong evidence for at least three global glaciations in the Neoproterozoic: the Sturtian at 717–712 Ma, the Marinoan (Vendian) at about 635 Ma, and the Gaskiers at 584 Ma (Hoffman et al., 1998). Although paleomagnetic data indicate that the Sturtian and Marinoan glaciations extended to tropical latitudes, ice was also extensive at high latitudes (Meert & van der Voo, 1994). Paleomagnetic data pin Laurentia to an equatorial location at 716.5 Ga, implying that the Sturtian glaciation was global in extent (Macdonald et al., 2010). Support for tropical glaciation also comes from carbonate debris in glacial deposits and shallow marine carbonates overlying glacial deposits known as **cap carbonates**. The Neoproterozoic also marks the reappearance of banded iron formations (BIFs). Although very minor in geographic extent, BIFs correlate in time and space with the each of the Neoproterozoic glaciations (Figure 9.32). Another constraint on the extent of freezing is found in sedimentary rocks. The fact that widespread sediments were deposited during the glacial episodes indicates that dynamic glaciers and ice streams continued to deliver sediment to the open ocean during these times (Allen & Etienne, 2008). This implies that some oceans must have remained ice free, which has important implications for the survival and diversification of life during the Neoproterozoic.

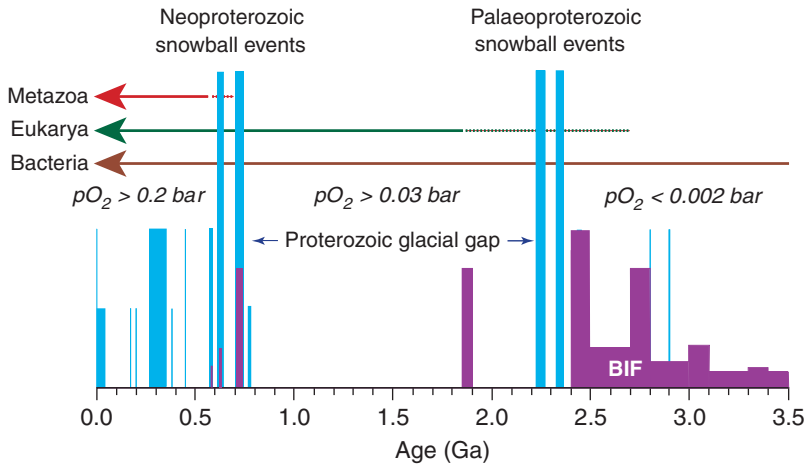

FIGURE 9.32 Age distribution of banded iron formations, major glaciations, atmospheric oxygen levels, and stages in the evolution of life. *Modified after Hoffman and Schrag (2002). Courtesy of Paul Hoffman and John Wiley & Sons Ltd.*

Another feature of both Sturtian and Marinoan glaciations is large negative carbon isotope excursions that immediately follow the glaciations as recorded in the cap carbonates (Figure 9.33). There are two competing ideas to explain these excursions: (1) a delayed effect caused by the decrease in burial rate of organic carbon during the glaciations, or (2) postglacial warming that caused methane hydrate destabilization during cap carbonate deposition (Jiang et al., 2003). The currently most popular, yet controversial, interpretation of all of these results is the **Snowball Earth model**, during which the entire Earth freezes over, or mostly freezes over, and then thaws out. Most data suggest that local areas in the tropics and areas around active volcanic centers did not freeze over, giving rise to a "slushball" rather than a hard snowball Earth.

The Snowball Model

Williams (1975) suggested that the obliquity of Earth's orbit may have changed with time and that during the Neoproterozoic the equator was tipped at a high angle to the ecliptic, resulting in a decrease in mean annual temperature. Such a condition should favor widespread glaciation even at low latitudes. However, this model does not explain the angular momentum distribution in the Earth–Moon system, the relationship between obliquity and spin rate, glaciation at mid- to high latitudes, the abrupt onsets and terminations of glaciations, nor the intimate association of glacial deposits and carbonates (Pais et al., 1999; Donnadieu et al., 2002; Hoffman & Schrag, 2002). Global glaciation has also been explained by true polar wander during which plates migrate very rapidly between high and low latitudes (Kirschvink et al., 1997). This model, however, does not account for the temporal association of glacial deposits and carbon isotope excursions, nor do we find midlatitudinal facies between diamictites (ancient glacial deposits) and their respective cap carbonates, as predicted by the model. Still another model, the ocean-overturn hypothesis (Kaufman & Knoll, 1995) predicts that the carbon isotope excursions should be short lived; however, isotopic ages indicate durations up to 9.2 Ma, thus not favoring this model (Hoffman et al., 1998).

Although still controversial, the Snowball Earth model seems to explain most of the data, including incomplete freezing of the oceans in equatorial regions, permitting the survival of multicellular life in tropical regions (Hyde et al., 2000; Hoffman & Schrag, 2002). Snowball events should begin and end abruptly and should last for millions of years because it takes a long time for volcanic degassing to overcome the ice albedo (Figure 9.33). The short-lived reappearance of banded iron formation is also predicted by the model. The ice-covered ocean should become anoxic and Fe^{2+} should accumulate and be precipitated as iron formation upon deglaciation. To produce a snowball glaciation, atmospheric CO_2 levels must be lowered rapidly. Contributing to this change may have been the fragmentation of the supercontinent Rodinia (see Chapter 8) producing new marginal basins that were repositories for

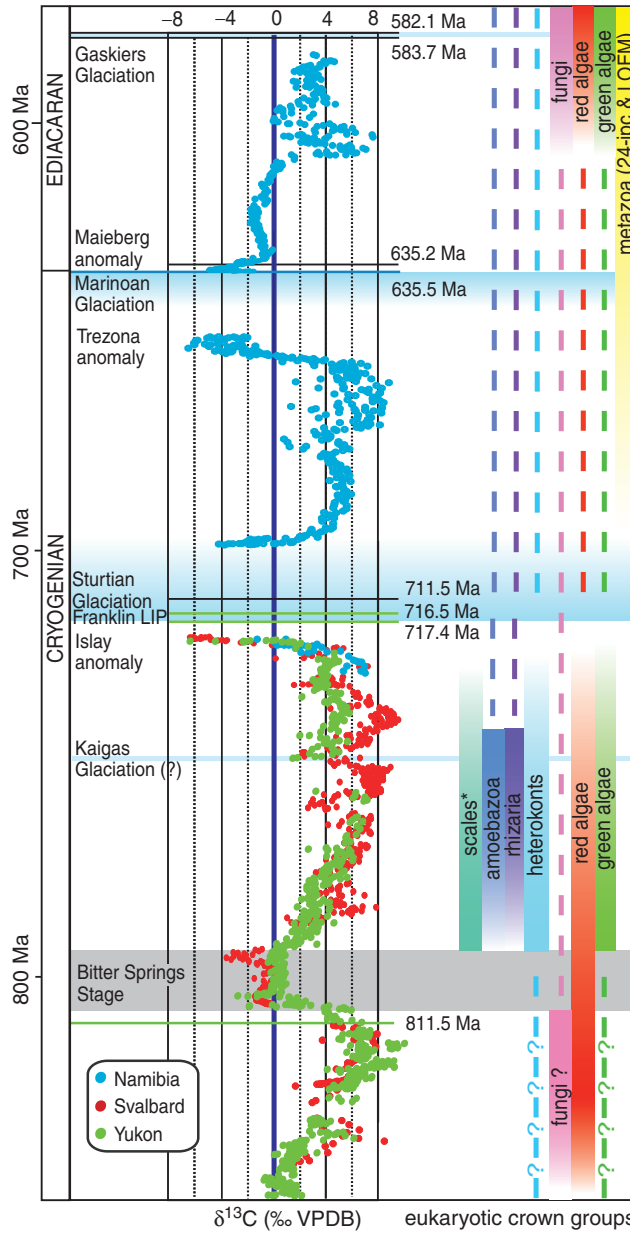

FIGURE 9.33 Neoproterozoic chemostratigraphy of carbon isotopes ($\delta^{13}C$) in cap carbonates with U/Pb zircon ages linked to the isotopic profiles. Vertical bars indicate time spans of fossil assemblages. *From Macdonald et al. (2010). Courtesy of the American Association for the Advancement of Science.*

organic carbon. Falling CO_2 led to widespread cooling and glaciation extending into equatorial regions, at least in some locations, and the high albedo of ice would give positive feedback to the glaciations. Decreases in bioproductivity and carbon burial during the glaciations led to negative carbon isotope excursions in seawater, which were recorded in the cap carbonates after glaciation.

But how do Snowball glaciations end? Volcanism continued to pump CO_2 into the atmosphere, enhanced by new ocean ridge volcanism accompanying the breakup of Rodinia, yet the continents were covered with ice, so weathering was at an all-time low. This resulted in buildup of CO_2 in the atmosphere, causing greenhouse warming, which led to warm climates globally during which the cap carbonates were deposited. The cap carbonates result from enhanced carbonate and silicate weathering during the greenhouse gas regime by increasing the alkalinity of the oceans. High rates of carbonate deposition and low rates of organic carbon deposition drive the $\delta^{13}C$ of seawater to low values as observed. Some investigators have suggested that destabilization of methane gas hydrates during warming periods may have contributed both to cap carbonate deposition and to the low $\delta^{13}C$ values of cap carbonates (Kennedy et al., 2010). Although some organisms would survive in equatorial areas and around volcanic vents, many organisms may have become extinct during the glaciations. It is difficult to evaluate such extinctions due to the lack of skeletal organisms at this time, but there are substantial changes in acritarch populations following the Sturtian glaciation.

Low latitude glaciation may also have occurred at about 2.4 Ga (Figure 9.32; also see Chapter 6). Glacial deposits of this age have been described in Laurentia, northern Europe, and South Africa. The Huronian diamictites in southern Canada have cap carbonates with negative $\delta^{13}C$ and their deposition was followed by intense lateritic weathering (Bekker et al., 2001; Hoffman & Schrag, 2002). There is no evidence, however, for glaciation between 2.4 and 0.7 Ga, a period of 1.4 billion years, known as the Proterozoic glacial gap (Figure 9.32). Is there anything unique about the beginning and the ending of the Proterozoic, and could both ends be snowball glaciations? It does not appear to be related to supercontinent breakup, since the Paleoproterozoic glaciations came before supercontinent fragmentation at 2.2–2.1 Ga, whereas the Neoproterozoic glaciations occurred during supercontinent fragmentation.

EVENT 6: MASS EXTINCTION AT THE END OF THE PERMIAN

General Features

The mass extinction that ended the Paleozoic is generally considered to be the most severe of all of the Phanerozoic mass extinctions (see Figure 6.27 in Chapter 6). Killing about 60% of all organisms on Earth is remarkably difficult, yet this is precisely what happened at the end of the Permian (McLaren & Goodfellow, 1990; Erwin, 1994, 2003; Metcalfe & Isozaki, 2009). At this time we lost 54% of marine families, 68% of genera, and up to 92% of species

(Knoll et al., 2007). Many groups of land plants and animals were also affected, thus requiring an extinction mechanism that was felt both on land and at sea. This is the closest metazoans have come to being exterminated in the past 500 Ma. Isotopic ages suggest that the extinctions occurred very rapidly in less than about 500 ka; however, the recovery was much slower lasting 4–5 Ma after the extinction (see Figure 6.26). Also at the end of the Permian, Pangea was nearly complete and sea level dropped significantly, evaporite deposition was widespread, global warming occurred, and the Siberian flood basalts were erupted (about 250 Ma).

The pattern of end-Permian extinctions is complex, with some groups disappearing well below the Permian/Triassic (P/Tr) boundary, others at the boundary, and still others after the boundary. The marine fossil record provides the most complete record of the P/Tr extinctions. In South China, where a complete marine succession across the P/Tr boundary is exposed, 91% of all invertebrate species disappeared, including 98% of amminoids, 85% of bivalves, and 75% of shallow-water fusulinids. Precise isotopic dating at the P/Tr boundary suggests that many of these extinctions occurred in <2 Ma and perhaps <1 Ma. Many groups of sessile, filter feeders disappeared at this time, as did marine invertebrates living in near-shore tropical seas. In terms of terrestrial animals, 80% of the reptile families and six of the nine amphibian families disappeared at the end of the Permian. Among the insects, 8 of the known 27 orders disappeared in the Late Permian, 4 suffered serious declines in diversity, and 3 became extinct during the Triassic. Land plants show little evidence of extinction at the P/Tr boundary, although pollens underwent significant change.

A major period of global warming is the most obvious climatic signal associated with mass extinction at the end of the Permian (Wignall, 2001). Evidence includes migration of calcareous algae to boreal latitudes, loss of high-latitude floras, and development of intermediate-latitude paleosols at high latitudes. Oxygen isotope data indicate that equatorial temperatures rose as much as 6°C at the P/Tr boundary, and Sr isotopes in marine carbonates suggest a corresponding rise in atmospheric CO_2. The inferred global warming may also have led to the widespread marine anoxia characteristic of Late Permian sediments (Isozaki, 1997). This superanoxic event first appeared in deep-water, pelagic cherts expanding in the latest Permian to oxygen-poor shallow marine seas (Knoll et al., 1996). Two effects of the warming may have been responsible for the extinctions in the oceans at the end of the Permian. First, the decrease in temperature gradient in the oceans from equator to pole led to a decrease in oceanic circulation. Second, the lower solubility of oxygen in the warmer seawater may have led to the widespread anoxia. The ultimate source of elevated CO_2 in the atmosphere, however, is unknown. Eruption of the Siberian flood basalts is one possibility and destabilization of gas hydrates is another. In fact, global warming may have led to catastrophic release of large volumes of methane from gas hydrates, which could have been directly responsible for the mass extinction (Ryskin, 2003).

One problem still not completely resolved is the precise age of the P/Tr boundary. Bowring et al. (1998) propose an age of 251 ± 0.3 Ma based on zircon ages from ash beds that bracket the boundary at Meishan in China. Recent dating of zircons from the same region by Mundil et al. (2001), however, report problems with Pb loss and inheritance in the zircons resulting in considerable scatter of the ages. Mundil et al. (2004) report a high-precision zircon age for the P/Tr boundary at 252.5 Ga, which is currently the best estimate of the age of the P/Tr boundary. However, precise $^{40}Ar/^{39}Ar$ dating of this boundary indicates that it does not precisely coincide with the major mass extinction (Reichow et al., 2009).

In evaluating possible explanations for the end-Permian mass extinction, we need to draw a clear distinction between kill and trigger mechanisms (Knoll et al., 2007). A kill mechanism actually causes death, whereas a trigger mechanism is the critical disturbance that brings one or more kill mechanisms into play. Although many triggers have been proposed for the P/Tr extinctions, only four have been seriously considered: asteroid impact, eruption of Siberian flood basalts, anoxia of the oceans, and catastrophic release of methane from seafloor hydrates.

Evidence for Impact

Unlike the Cretaceous/Tertiary (K/T) boundary, there is no evidence at the P/Tr boundary for impact fallout. No convincing Ir anomalies or shocked quartz has been found in boundary clays. New evidence for impact was proposed by Becker et al. (2001) and Poreda and Becker (2003) based on the presence of fullerenes (C_{60} and C_{70}) from boundary sections in Japan and South China. The fullerenes occur with trapped argon and helium, similar to occurrences in the K/T sections. These results, however, have not been reproduced in other laboratories, and hence are not considered definitive. Currently, the impact model has several problems in addition to the lack of critical evidence. For instance, deep-water anoxic sediments spanned large areas of the Permian ocean and there is no evidence that these sediments were disturbed during the mass extinction, as would be expected with a large impact. Also, there appear to be multiple negative peaks in $\delta^{13}C_{org}$ at the P/Tr boundary, which are difficult to reconcile with a single impact.

LIP Volcanism

Another cause considered for the Permian extinctions is the eruption of the Siberian flood basalts at 251 Ma, releasing large amounts of sulfate aerosols and CO_2, the latter causing enhanced greenhouse warming (Wignall, 2001). This LIP eruption is the largest flood basalt eruption in the Phanerozoic. Although the full lateral extent of the basalts is uncertain, because a large amount is covered with later sediments, the volume is of the order of at least 10^6 km^3, with a corresponding estimated release of CO_2 of 10^{17} to 10^{19} moles. Although other LIP eruptions also liberated noxious gases, they did not lead to

mass extinctions. What was different about the Siberian LIP? Probably adding to the erupted volatiles are volatiles from coal and carbonate that the basaltic magmas passed through on their way to the surface. The combination of greenhouse gases and toxic sulfur and halogen gases may have not only resulted in global warming but also destroyed the ozone layer due to production of such gases as methyl chloride. Global kill mechanisms related to the Siberian eruption include acid rain (both nitrate and sulfate based), poisoning from halogen and halid gases, hypercapnia (CO_2 poisoning), and immediate but transient global cooling followed by long-term global warming (Renne et al., 1995; Knoll et al., 2007).

The timing of Siberian volcanism relative to the age of the P/Tr boundary is still in a state of flux. Although the boundary is dated at 252.5 Ga (Mundil et al., 2004), it does not coincide with the main extinction. The age of the primary extinction horizon appears to correlate with a high-resolution $^{40}Ar/^{39}Ar$ age of the Siberian flood basalts at 250.3 Ga (Reichow et al., 2009). The argon age indicates that the volcanism either immediately predates or is synchronous with the end-Permian mass extinction at 250 Ma.

Shallow-Water Anoxia

The widespread distribution of black shales in the lowermost Triassic has prompted interest in global anoxia as a trigger for the end-Permian mass extinction. In addition, pelagic cherts suggest widespread deep-sea anoxia from the Late Permian to the Middle Triassic with a peak around the P/Tr boundary (Isozaki, 2009). Biomarker lipids diagnostic of anoxygenic photosynthesis also are found in Late Permian and Early Triassic sediments, and these suggest that marine continental shelves were also prone to anoxia. The trigger for shallow-water anoxia may have been global warming induced by an increased influx of CO_2 into the atmosphere–ocean system from the Siberian flood basalt eruption. Global warming of the oceans would decrease the oxygen supply in the deep oceans by increasing the rates of respiration. Kill mechanisms related to anoxia include asphyxia, hypercapnia, and H_2S poisoning (Meyer et al., 2008).

Catastrophic Methane Release

Catastrophic release of methane from destabilization of marine hydrates during global warming has been suggested to account for a pronounced negative $\delta^{13}C$ excursion near the P/Tr boundary (Figure 9.34) (Twitchett et al., 2001). Although biogenic methane provides an attractive explanation for the carbon isotope excursion (biogenic methane can have $\delta^{13}C$ values as low as –60‰), it requires a trigger that rapidly leads to global warming. The Siberian LIP eruption at 250 Ma could be such a trigger. However, both marine and terrestrial records show that the initial ecosystem stress predates the onset of the carbon isotope excursion (Wignall, 2007; Korte & Kozur, 2010), indicating that

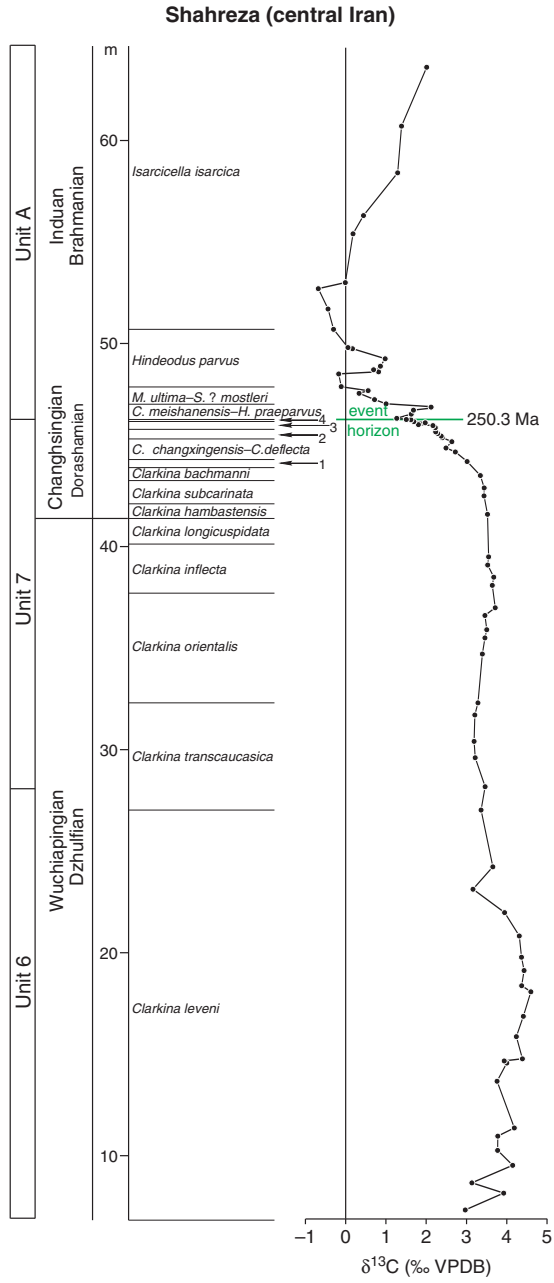

FIGURE 9.34 Permian/Triassic $\delta^{13}C$ isotope anomaly in marine sediments, central Iran. Conodont zonation: (1) Clarkinia nodosa; (2) Clarkinia zhangi; (3) Clarkinia iranica; and (4) Clarkinia hauschkei. *Modified after Korte and Kozur (2010), courtesy of Cristoph Korte*.

catastrophic methane release at the P/Tr boundary cannot be the sole killing mechanism. The excursion is probably related to the consequences of the crisis rather than the causes of it.

Conclusions

Many investigators lean toward multiple causes for the P/Tr mass extinction (Erwin, 1994, 2003). Important contributing factors may have been the following: (1) loss of shallow marine habitats in response to falling sea level; (2) completion of Pangea, resulting in increased weathering rates and drawdown of atmospheric CO_2; (3) eruption of the Siberian flood basalts, causing global warming and acid rains; and (4) rapid transgression of anoxic deep waters in the Early Triassic, destroying near-shore terrestrial habitats and perhaps liberating large volumes of methane from gas hydrates (Korte & Kozur, 2010). The long duration of the carbon isotope excursion (Figure 9.34) suggests that all short-lived events (e.g., impact, sudden release of methane) can be ruled out as major causes of this excursion. High-resolution dating of critical boundary sections shows that the mass extinction occurred in a series of stages, each with a duration of hundreds if not tens of thousands of years (Wignall, 2003). This observation tends to favor terrestrial causes rather than a single impact for the P/Tr mass extinction. Selectivity in extinction recorded by marine fossils favors hypercapnia as an important killing mechanism, and at the same time, the high CO_2 levels appear to have affected land life via global warming (Knoll et al., 2007). Clearly, the recovery was slow and appears to have lasted several million years.

EVENT 7: THE CRETACEOUS SUPERPLUME EVENT

The Mid-Cretaceous has always been recognized as a period in which Earth probably had warm climates, but it was not until Larson (1991a, b) proposed a superplume event (see Chapter 8) at this time that we began to understand why this period of time is so different. Many of the features preserved in the geologic record can be tied to a superplume event. Whatever the causes, the atmosphere, oceans, and biosphere responded to this event very rapidly mostly within a 50-Ma time window about 100 Ma. Within this time window, two carbon isotope anomalies indicate at least two subevents. As we saw in Chapter 8, superplume events are closely related to supercontinent breakups and hence both must be considered in understanding the causes of changes in paleoclimate in the Mid-Cretaceous. The question immediately appears: why was the superplume event so short lived yet the breakup of Pangea started at 185 Ma and is probably still going on?

Geologic Evidence

The effects of a Mid-Cretaceous superplume event are concentrated chiefly in an around the Pacific Basin (Larson, 1991a). The paleotemperature curve for the last 150 Ma shows a broad increase from 150 to 100 Ma, then a steady decrease to the

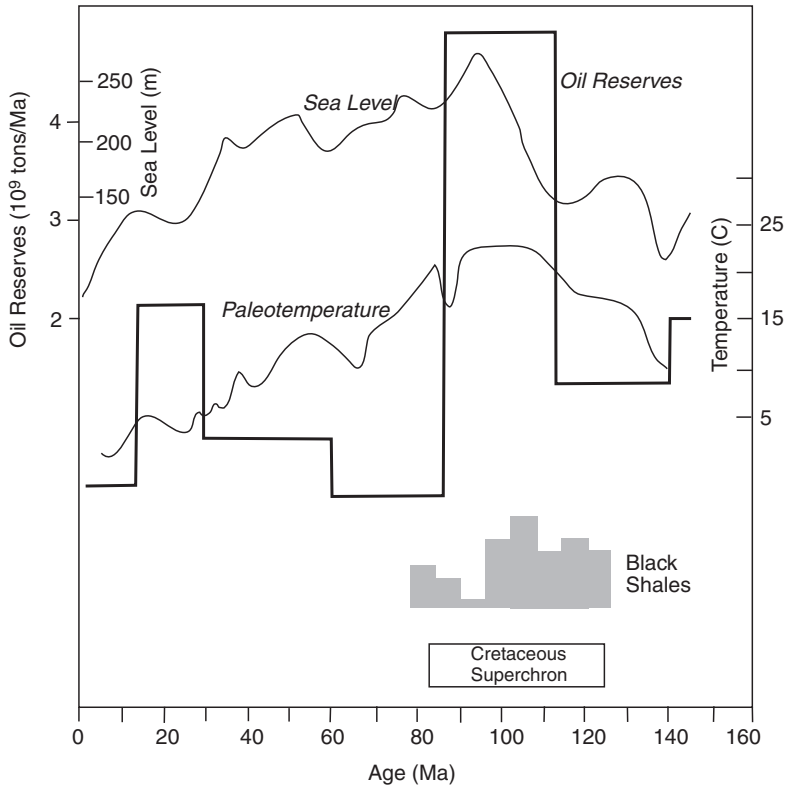

FIGURE 9.35 Distribution of paleotemperature, oil reserves, black shale, and sea level in the last 150 Ma. *Modified after Larson (1991b).*

present (Figure 9.35). The broad temperature peak at 110–90 Ma cannot be explained by supercontinent fragmentation alone, but also requires excess CO_2 in the atmosphere (Larson, 1991b; Barron et al., 1995). Approximately 2 to 6 times the present content of CO_2 is required to raise Mid-Cretaceous temperatures to the observed levels (Barron et al., 1995). LIP eruptions in the Pacific Basin may have contributed to the increase in CO_2. Models by Caldeira and Rampino (1991) show that a Mid-Cretaceous superplume event may have produced atmospheric CO_2 levels of 4 to 15 times the modern preindustrial value. This would result in global warming of 3–8°C over today's mean temperature. The continuing fragmentation of Pangea could contribute another 5°C of warming. Computer models of Barron et al. (1995) show that a combination of increased atmospheric CO_2 and an increased poleward flux of heat are necessary to explain the global distribution of warm climates in the Mid-Cretaceous. The greater poleward heat flux is necessary to prevent the tropical oceans from overheating due to the increased CO_2 content.

The approximately 125-m increase in eustatic sea level that reached a maximum at about 90 Ma (see Figures 6.11 and 9.35) may be related to increased ocean ridge activity, displacement of seawater by oceanic plateaus, or uplift of the oceanic lithosphere over mantle plumes (Larson, 1991a, b; Kerr, 1998). Although an increase in production rate of oceanic lithosphere was originally an attractive mechanism, recent studies have shown that the production rate has been relatively constant over the last 180 Ma (Rowley, 2010). In any case, it would appear that the effect of a mantle plume event is superimposed on that of supercontinent breakup. The gradual decrease in sea level after 90 Ma is not predicted by the mantle plume model, but may be related to continental collisions associated with the development of a new supercontinent (including India-Tibet, Australia-Southeast Asia, and the Mesozoic terrane collisions in the American Cordillera).

Extensive deposition of black shale is recorded worldwide from about 125 to 80 Ma and may reflect increased CO_2 related to the alleged superplume event (Jenkyns, 1980). Black shales are generally interpreted to reflect anoxic events resulting from increased organic productivity and to poor circulation in basins on continental platforms. A mantle plume event can provide both of these requirements: directly, by input of methane from destabilization of methane hydrates on the seafloor, and indirectly, by increasing sea level and the frequency of partially closed basins on the continental shelves (Kerr, 1998). The upwelling of trace metals and nutrients from the deep oceans may have increased the habitat of some marine organisms, leading to the extinction of other organisms, especially those part of a mass extinction near the Cenomanian/Turonian boundary (Wilde et al., 1990). About 60% of the world's oil reserves were generated between 110 and 88 Ma (Irving et al., 1974), consistent with the abundance of black shale at this time. There is also a broad peak in natural gas reserves at about the same time (Bois et al., 1980). A Mid-Cretaceous superplume event also may have contributed carbon and other nutrients, such as phosphorus and iron, for the expansion of phytoplankton at this time. Supporting this prediction are results from Cretaceous shales and marine carbonates, which typically have trace metal contents up to 100 times background levels (Duncan & Erba, 2003). The high stand of sea level also increased the continental shelf area covered with shallow seas providing appropriate depositional environments for hydrocarbon precursors. Also consistent with a superplume event about 100 Ma is a peak in seawater $\delta^{13}C$, consistent with extensive burial of carbon (Figure 9.36).

Finally, basalts erupted in the South Pacific have an enriched geochemical and isotopic signature indicative of an enriched mantle source, probably the Pacific superplume (Tatsumi et al., 1998). These range in age from about 150 to 90 Ma, indicating a minimal time window for superplume activity of 60 Ma.

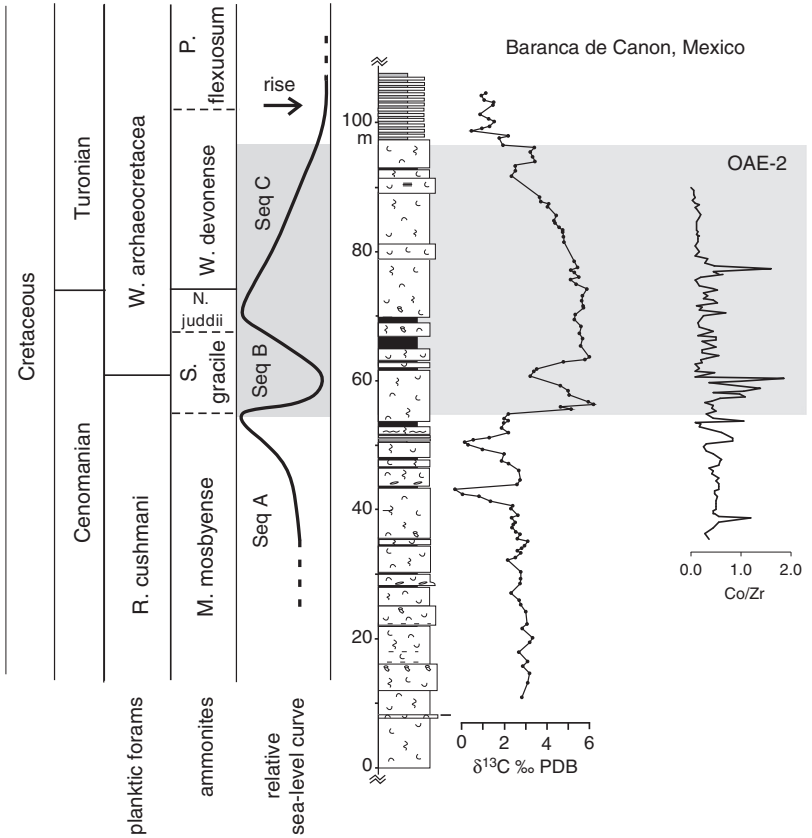

FIGURE 9.36 Variations in sea level, $\delta^{13}C$, and Co/Zr ratio in marine carbonates across the Cenomanian/Turonian boundary in a stratigraphic section from Baranca de Canon, Mexico. OAE-2, Oceanic Anoxic Event 2, shown as gray band. *Courtesy of Maya Elrick.*

The Carbon Isotope and Trace Metal Record

Another characteristic of the Mid-Cretaceous superplume event is two global positive carbon isotope anomalies in marine carbonates: one at the Cenomanian/Turonian (C/T) boundary at 93.5 Ma and another in the Aptian at about 115 Ma (Jahren, 2002; Elrick et al., 2009). The C/T anomaly characterizes the Oceanic Anoxic Event 2 (OAE2), which is one of several periods in the Cretaceous when large amounts of carbon were buried on the seafloor. The Aptian also has a large negative anomaly in $\delta^{13}C$ of organic carbon (3–5‰). The C/T anomaly begins abruptly with a 3–4‰ shift in $\delta^{13}C$, which coincides with a long-term sea level rise (Figure 9.36), although the end of OAE2 does not correspond to a change in sea level. Two peaks in trace metal contents of marine sediments (Co, V, U, and Cu; shown by the Co/Zr ratio in Figure 9.36)

correlate well with the $\delta^{13}C$ anomaly and are consistent with the idea that development of OEA2 was related to the release of reduced metals during one or more phases of eruption of the Caribbean oceanic plateau. Supporting a volcanic trigger for OEA2 is the Os isotope composition of organic-rich sediments, which changes abruptly just before the onset of OEA2, and the Os is chiefly of magmatic origin (Turgeon & Creaser, 2008). The link between the trace metals and oxygen isotopes is probably a depletion in dissolved oxygen in seawater caused by trace metal oxidation followed by rising seawater enriched in biolimiting elements that stimulate primary productivity in surface waters. The reduction in oxygen content of seawater and enhanced burial of carbon from the increased surface productivity causes the large positive shift in $\delta^{13}C$.

Seeking a Cause

The cause of a mass extinction and other environmental changes at the Cenomanian/Turonian boundary is a subject of considerable interest and disagreement. The favorable candidate is eruption of one or more oceanic plateaus, and in particular, the Caribbean and Ontong Java eruptions between 91 and 89 Ma (Kerr, 1998). However, more precise dating of the C/T boundary shows an age of 93.5 Ma, some 3 or 4 Ma before the LIP eruptions. Although the increased trace metal and Os isotopic composition of organic-rich marine sediments clearly points to a volcanic origin, no specific LIP eruption has yet been identified.

A proposed cause of the Aptian mass extinction is the release of CH_4 by destabilization of methane hydrates. Of course, the primary trigger still remains a LIP eruption. Jahren (2002) calculates that seafloor uplift associated with LIP eruptions at 115 Ma (perhaps Ontong Java at 115–122 Ma) would destabilize enormous quantities of methane hydrates over a 10-Ma period. The incorporation of the isotopically light carbon from the methane into photosynthesis via oxidation to CO_2 can explain both positive carbonate and negative organic $\delta^{13}C$ isotopic excursions at this time. It would also allow angiosperms to displace conifers at midlatitudes to high latitudes, setting the stage for the angiosperm-dominated terrestrial biosphere that would follow.

A Possible Superchron-Superplume Connection

Coincident with a Mid-Cretaceous mantle plume event at 120–80 Ma is the Cretaceous **superchron**, when very few magnetic reversals occurred for a period of 30–40 Ma (Figure 9.35). Larson and Olson (1991) show that magnetic reversal frequency correlates inversely with inferred mantle plume activity for the past 150 Ma. To explain this correlation, the authors propose a model whereby removal of large amounts of heat from the core not only fuels the plume event, but also stops, or greatly retards, the frequency of magnetic reversals generated in the outer core. They suggest that as a superplume rises from the D″ layer, this layer thins, resulting in core cooling by allowing heat to be conducted more rapidly across the core–mantle boundary. Outer core

convection then increases to restore the abnormal heat loss causing a decrease in frequency of magnetic reversals. In effect, this switches Earth's geodynamo from a reversing state to a nonreversing state. When the convective activity increases above some threshold value, a magnetic superchron is initiated. The ages of Pacific basalts that come from enriched mantle sources probably associated with the Pacific superplume range from 150 to 90 Ma (Tatsumi et al., 1998). The fact that the superplume came into existence before the superchron supports the idea that the superplume acted as a trigger for the superchron. However, Loper (1992) suggests that thermal inertia of the D″ layer may not result in rapid enough changes in the core's heat flux when mantle plumes are formed to effect reversals in the convecting core.

Although the Larson model has been widely accepted, other explanations for superchrons exist. Cox (1969) proposed a model for magnetic field reversals caused by perturbations of the outer core, which feed sufficient reverse flux into the geodynamo to overcome the main dipole. In this model, increased convective vigor generates more frequent instabilities in the fluid outer core leading to an increase in reversal rate. Courtillot and Besse (1987) suggest still a different mechanism whereby the decrease in reversal rate just before the Mid-Cretaceous superchron is caused by a decrease in core convection due to a buildup of heat at the core–mantle boundary. This excess heat is released with the plumes that rise from D″ near the end of the superchron. The loss of heat results in increased core convection, which in turn causes an increase in reversal rates. Hence, the correlation of the Mid-Cretaceous superplume event with a superchron may or may not be significant. There is also a superchron in the Permian, and perhaps in the Ordovician, neither of which is associated with geologic evidence for a superplume event.

EVENT 8: MASS EXTINCTION AT THE END OF THE CRETACEOUS

General Features

Although most or all of the dinosaurs did not survive the K/T boundary mass extinction, numerous terrestrial species, such as lizards, frogs, salamanders, fish, crocodiles, alligators, and turtles, show no significant effects across this boundary. At the generic level, the terrestrial K/T extinction was only about 15%. One of the exciting controversies today is that of whether all of the dinosaurs disappeared suddenly at the end of the Cretaceous. Teeth of 12 dinosaur genera have been described above the K/T boundary in Paleocene sediments in eastern Montana (Sloan et al., 1986). If these teeth are in place and have not been reworked from underlying Cretaceous sediments, they clearly indicate that at least some dinosaurs survived the K/T extinction. If, on the other hand, they are reworked, then the oldest *in-place* dinosaur remains are Late Cretaceous in age. Suggesting these dinosaur teeth are not reworked is the fact that reworked remains of a widespread species of Late Cretaceous mammal common in the underlying Cretaceous sediments are not found in these earliest Paleocene rocks of Montana. Also, the dinosaur teeth do not have eroded edges as they would if

they were redeposited. Other possible earliest Tertiary dinosaur remains are known from India, Argentina, and New Mexico. It would appear that debate will continue about the precise age of the final dinosaur extinctions until articulated dinosaur skeletons are found above the K/T boundary layer.

Also at the K/T boundary, selective killing agents resulted in widespread losses of swamp forests and in extinction of most of the insect-pollinated angiosperms (Sweet, 2001). The preservation of fern spores across the boundary, however, suggests that understory plants (ferns, bryophytes, etc.) survived the mass extinction event. Gymnosperm pollens in North America decrease in abundance in a northern direction in postextinction sediments, indicating widespread losses of gymnosperms.

The marine extinctions at the end of the Cretaceous are far more spectacular than the terrestrial extinctions, involving many more species and groups of animals (McLaren & Goodfellow, 1990; Erwin, 1993). At the family level, the marine extinction rate is about 15%, while at the generic and specie levels it is about 70%. Major groups to disappear at the close of the Cretaceous are the ammonites, belemnites, inoceramid clams, rudistid pelecypods, mosasaurs, and plesiosaurs. The extinction of benthic forms preferentially takes place in groups that had free-swimming larvae. Among benthic forms such as most mollusks, bryozoans, and echinoids, extinction rates were low, whereas calcareous phytoplankton and planktonic foraminifera show sharp extinctions. The abrupt disappearance of many plankton appears to have stressed marine communities by removing much of the base of the marine food chain. Particularly affected were reef-living bivalves, most oysters, clams, ammonites, many corals, most marine reptiles, and many fishes.

The K/T mass extinction coincides with a major perturbation of the global carbon cycle as indicated by a rapid drop in $\delta^{13}C$ in marine carbonates, a major decrease in calcite sedimentation in the oceans, and enrichment in platinum-group elements (such as Ir) (Schulte et al., 2010) (Figure 9.37). As shown in Figure 9.37, the mass extinction also occurs during the time at which the Deccan LIP volcanism was active 65.5 Ma.

Seeking a Cause

Evidence for Impact

Iridium Anomalies

One of the strongest pieces of evidence for impact is the enrichment of iridium (Ir) in a clay layer at the K/T boundary at many locations worldwide (Alvarez et al., 1990). The age of this clay layer has been measured at several places on the continents, and the average age is 65.5 Ma, which is precisely the age of the K/T boundary as dated from deep-sea sediments. This enrichment, known as an **iridium anomaly** (Figure 9.37), cannot be produced from crustal sources because of the exceedingly low Ir content of crustal rocks, but it could come

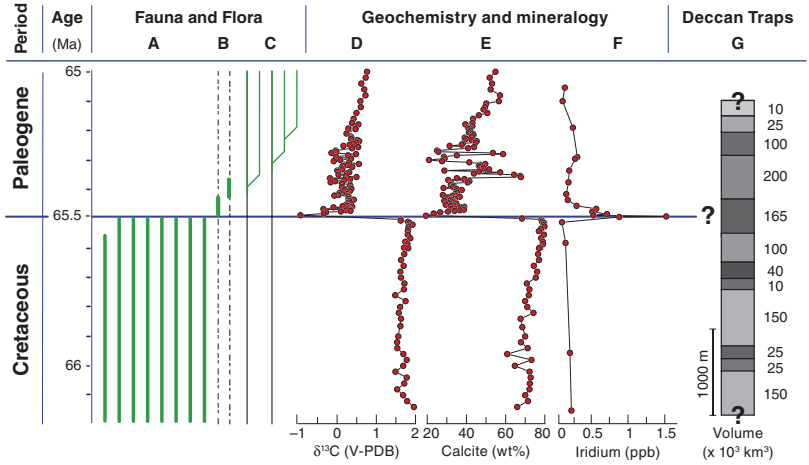

FIGURE 9.37 Schematic record of biotic events across the K/T boundary correlated with chemical and mineralogical records from North Atlantic drill cores and major eruptive units of the Deccan flood basalts in India. *From Schulte et al. (2010), courtesy of Peter Schulte and the American Association for the Advancement of Science.*

from collision of an asteroid. Following impact, Ir, which is very volatile, would have been injected into the stratosphere and spread over the globe, gradually settling out in dust particles over a few months.

Glass Spherules

Spherules are glassy droplets (a few tenths of a millimeter in diameter) of felsic composition, commonly found in K/T boundary clays (Maurrasse & Sen, 1991). By analogy with tektites, which are impact glasses with diameters up to a few centimeters found on Earth, the small spherules at the K/T boundary appear to have formed by melting of crustal rocks, followed by rapid chilling as they are thrown into the atmosphere.

Soot

Soot or small carbonaceous particles are also widespread in K/T boundary clays and may be the remains of wildfires that spread through forests following impact (Wolbach et al., 1985). The absence of charcoal in boundary-layer clays, however, means there were no global wildfires associated with the K/T impact (Belcher et al., 2003).

Shocked Quartz

One of the strongest evidences for impact is the widespread occurrence of shocked quartz in K/T boundary clays (Bohor et al., 1987; Hildebrand et al., 1991). Shock lamellae in quartz are easily identified (Figure 9.38) and are

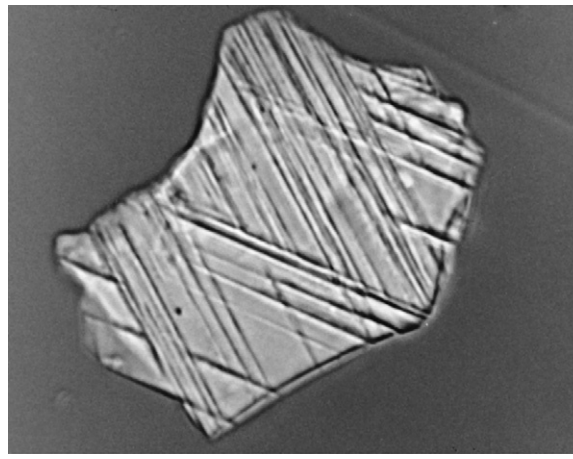

FIGURE 9.38 SEM photo of an HF-etched shocked quartz grain from the K/T boundary claystone at Teapot Dome, Wyoming. Two major sets of planar deformation features (shock lamellae) are displayed in this view. Open planar features of the two major sets originally contained a silica glass phase, which has been removed by the acid etching. Grain is 72 μm in maximum dimension. *Courtesy of Bruce Bohor.*

produced by a high-pressure shock wave passing through the rock. Such shocked quartz is common around nuclear weapon test sites and around well-documented impact sites such as Meteor Crater in Arizona.

Stishovite

Stishovite is a high-pressure polymorph of silica formed during impact and has been found in the K/T boundary layer clay (McHone et al., 1989). Like shocked quartz, it has only been reported at known impact and nuclear explosion sites.

Chromium Isotopes

The isotopic composition of Cr from K/T boundary clays in Denmark and Spain is different from the isotopic composition of terrestrial Cr, but similar to that of carbonaceous chondrites (Shukolyukov & Lugmair, 1998). This similarity strongly suggests an asteroid impact source for the Cr in the K/T boundary layer clay. Meteorite fragments have been described from K/T boundary layer clays in the North Pacific that may represent samples of a K/T asteroid impactor (Kyte, 1998).

LIP Volcanism

Evidence also exists to support a volcanic cause for the K/T mass extinction. The discovery of enriched Ir in atmospheric aerosols erupted from Kilauea in Hawaii indicates that Ir may be concentrated in oceanic plume-fed volcanic

eruptions. Although glass spherules can be formed during eruptions of basalt, their distribution is localized around eruptive centers. Isotopic dating of the Deccan traps in India indicate they were erupted 66–65 Ma near the K/T boundary and that volcanism occurred in three periods each lasting 50–100 ka (Figure 9.37). The first and most significant of these eruptions at 65.6–66.1 Ma occurred before the extinction of dinosaurs, and fossil remains of sauropods, carnosaurs, and mammals are found between the first two lava eruptions. A rapid decline in the $^{187}Os/^{186}Os$ ratio in marine sediments during this time correlates with a short period of global warming of 3–5°C (Ravizza & Peucker-Ehrenbrink, 2003). This confirms that the major pulse of Deccan volcanism occurred *before* most of the K/T extinctions and thus could not be the cause of these extinctions.

Environmental damage produced by the rapid eruption of large volumes of flood basalt is due chiefly to toxic gases (principally SO_2 and halogens) and sulfate aerosols and this requires subaerial eruption (McCartney et al., 1990). Large volcanic eruptions are capable of introducing large quantities of sulfate aerosols into the atmosphere, which could cause immense amounts of acid rain, reduce the pH of surface seawater, add both volcanic ash and carbon dioxide to the atmosphere, and perhaps deplete the ozone layer. Fluid inclusions in crystals of Deccan basalt flows contain up to 0.1% sulfur and 0.04% chlorine, which can yield huge volumes of SO_2 and HCl during eruption (Self et al., 2008). The environmental impact of even single eruptions during the Deccan activity was probably severe. Erupted ash could further reinforce a global cooling trend, and the combined effect of these events could result in widespread extinctions, spread over 1 million years or so.

Model calculations indicate that tremendous volumes of SO_2 and halogens may be introduced into the atmosphere during single large flood basalt eruptions. Also data from the eruption of Laki fissure in Iceland in 1783 document severe air pollution and plant damage in Europe related to this very small flood basalt eruption (Grattan, 2003). Hence, large flood basalt eruptions should have severe consequences on global climate and would probably produce acid rain, ozone damage, and increased reflectance of solar radiation leading to rapid cooling in the hemisphere affected (Handler, 1989). All of these may contribute to widespread extinctions. It is important to note that Deccan volcanism began at least 500 ka before the extinction event and continued for at least thousands of years thereafter (Figure 9.37). Although flood basalt eruptions may inject large volumes of toxic aerosols into the stratosphere affecting global climate, the effect of CO_2 emitted during such eruptions in warming the atmosphere may be rather minor. Calculations show that even for a relatively large eruption like the Deccan traps, the surface temperature of the planet would be raised <2°C over a period of 4×10^5 years (Caldeira & Rampino, 1990). This indicates that the K/T extinction was not caused by global warming resulting from volatiles released by eruption of the Deccan traps.

Chicxulub and the K/T Impact Site

Another question related to the asteroid impact model is where is the impact crater? If the impact was in the ocean, any crater formed on the seafloor was probably subducted in the last 65 Ma. Although the search for a crater of the right age and size (≥100 km in diameter) on the continents is still continuing, the current best candidate is the 180-km Chicxulub crater in Yucatan (Figure 9.39) (Hildebrand et al., 1991). Consistent with a location in the Caribbean for a K/T impact site is the common presence of shocked quartz and spherules in Caribbean K/T boundary clays. Both of these features require at least some continental crust and the Caribbean Basin contains both oceanic and continental crust. Impact breccia deposits also are widespread in Cuba and Haiti at the K/T boundary, also supporting a Caribbean impact site (Figure 9.40). Chicxulub crater is the only known large example of a Caribbean crater. It occurs in

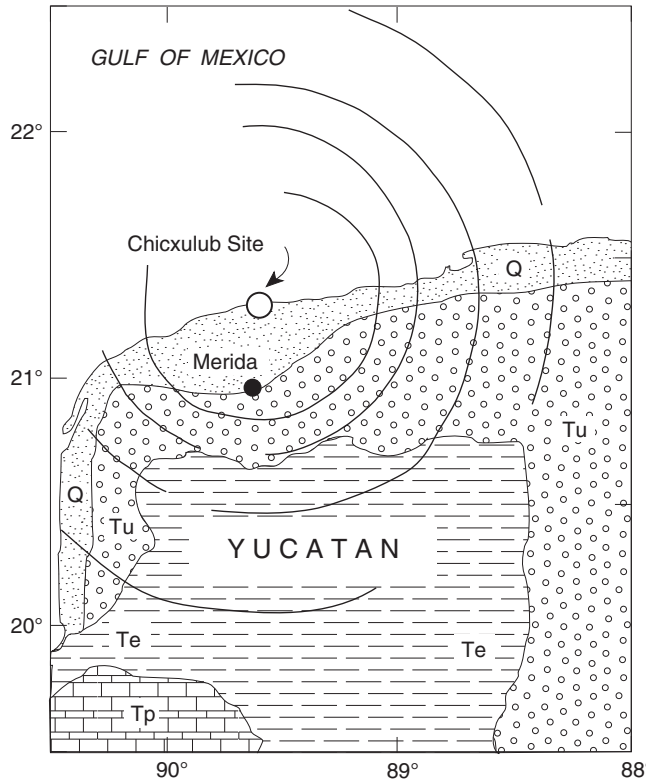

FIGURE 9.39 Simplified geologic map of the region around Merida, Mexico, showing the location of Chicxulub crater buried with Tertiary sediments. Rings are gravity anomalies related to impact. Q, Quaternary alluvium; Tu, Upper Tertiary sediments; Te, Eocene sediments; Tp, Paleocene sediments.

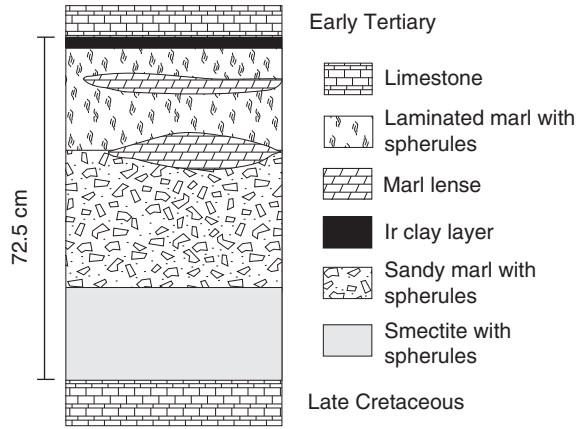

FIGURE 9.40 Section of the K/T boundary layer at Beloc, Haiti. The layer is 72.5 cm thick with Ir concentrated in the thin clay layer at the top. *After Maurrasse and Sen (1991).*

Late Cretaceous marine carbonates deposited on the Yucatan platform on continental crust (Figure 9.39). Some of the crater is now filled with impact breccias and volcanic rocks, the latter of which have chemical compositions similar to the glass spherules found in K/T boundary clays. Melted crustal rocks from the crater also have high Ir contents. Supporting Chicxulub as the K/T impact site is precise $^{40}Ar/^{39}Ar$ ages of 66–65 Ma from glassy melt rock in the crater, which, within the limit of error, is the age of the K/T boundary (Swisher et al., 1992). U-Pb isotopic ages from shocked zircons in K/T boundary-layer clays from widely spaced locations in North America yield identical ages to shocked zircons from Chicxulub crater of 65 Ma, again supporting a Chicxulub source for the fallout (Kamo & Krogh, 1995). The pattern of decreasing ejecta-layer thickness and the size of spherules and shocked quartz grains with increasing distance from the impact crater are also consistent with the Chicxulub impact as a unique source for the ejecta (Schulte et al., 2010). Also, the age distribution of the ejecta matches the ages of Chicxulub target rocks.

A major environmental consequence of asteroid impact if it occurred in the oceans is a tsunami. **Tsunamis** are rapidly traveling sea waves caused by catastrophic disturbances such as earthquakes and volcanic eruptions. Calculations indicate that the asteroid that formed Chicxulub crater should have produced successive tsunamis up to 100 m high with periods of less than 1 hour, and these would have flooded the coastlines around the Gulf of Mexico and Atlantic within a day of the impact (Matsui et al., 1999). Tsunamis should cause widespread erosion and deposit poorly sorted sediments in tidal and beach environments, and such deposits are known at the K/T boundary from the Caribbean, the Gulf of Mexico, and from the Atlantic Coast from points as far away as New Jersey and Denmark.

Possibility of Multiple K/T Impacts

Some studies of the K/T boundary in Mexico report more than one ejecta layer introducing the possibility of more than one impact at or near the K/T boundary (Adatte et al., 2003). In northeastern Mexico two to four ejecta layers occur at the K/T boundary spanning at least 300 ka. The oldest layer is dated at 65.27 ± 0.03 Ma based on sediment accumulation rates and magnetostratigraphy. The Ir anomaly occurs in only one horizon, tentatively identified as the third and final impact event at 64.9 Ma (Adatte et al., 2003; Keller et al., 2003). A multiple impact scenario is consistent with the ejecta evidence, with the first impact at 65.4–65.2 Ma correlating with a decrease in primary productivity and the onset of terminal decline in planktonic foraminifera. This impact may be the Chicxulub impact. The final K/T impact at 64.9 Ma is associated with the last pulses of Deccan volcanism and both impact and volcanism may have contributed to the major mass extinction at the end of the Cretaceous. This subject is still very controversial, but if confirmed by rigorous isotopic dating, the Chicxulub impact would appear to predate the K/T boundary by at least 300 ka. This would imply that both the Chicxulub impact and Deccan volcanism contributed to high biotic stress levels and to greenhouse warming, but not to major mass extinction. A somewhat later impact would be the killer asteroid.

Conclusions

So where do we stand in terms of understanding the K/T mass extinction today? Clearly some extinctions occur in the 10 Ma before the K/T boundary and these appear to be due to terrestrial causes such as a fall in sea level and temperature drops. However, the numerous extinctions that occurred in a short period of time 66–65 Ma seem to require a catastrophic cause. In Table 9.6 the various evidences for impact are compared to flood basalt eruption to explain the K/T extinction. Although it would appear that both impact and volcanic causes may explain the Ir anomalies, only impact can readily account for the wide distribution of glass spherules and soot, and the presence of shocked quartz and stishovite. Also, precise dating clearly indicates that the Deccan volcanism began before and lasted after the K/T extinction and cannot explain the short-lived carbon isotope anomaly and decrease in calcite at the K/T boundary (Figure 9.37). In contrast, impact would disrupt photosynthesis and acid rain would disrupt carbonate sedimentation in the oceans, thus explaining these two features. Furthermore, precise dating of K/T boundary layers and the Chicxulub crater show a clear similarity in age and composition, which supports the conclusion that the Chicxulub impact triggered the mass extinction. A very minor group favors a post-Chicxulub impact for the extinction.

TABLE 9.6 Comparison of Impact and Volcanic Models for K/T Boundary Extinctions

Observational evidence	Impact	LIP eruption
Ir anomaly	Yes; asteroid Maybe; comet	Possible, but not likely
Glass spherules	Yes; impact melts	No; of local extent only
Shocked quartz	Yes; common at impact sites	No
Stishovite	Yes; found at some impact sites	No
Soot	Yes; from widespread fires	No; fires only local
Carbon isotope anomaly/decrease in calcite	yes	no
Worldwide distribution of evidence	Yes	No
Summary	Acceptable; accounts for all observational evidence	Rejected; cannot explain shocked quartz, stishovite, or soot

Source: In part after Alvarez (1986).

FURTHER READING

Bengtson, S. (Ed.). (1994). *Early Life on Earth*. New York: Columbia University Press.

Condie, K. C., & Pease, V. (Eds.). (2008). *When Did Plate Tectonics Begin on Planet Earth?* Special Paper 440. Geological Society of America.

Courtillot, V. (1999). *Evolutionary Catastrophes: The Science of Mass Extinction* Cambridge, UK: Cambridge University Press.

Dressler, B. O., Grieve, A. F., & Sharpton, V. L. (1992). *Large Meteorite Impacts and Planetary Evolution*, Special Paper 358. Geological Society of America.

Dyson, F. (1999). *Origins of Life* (2nd ed.). Cambridge, UK: Cambridge University Press.

Hoffman, P. F., & Schrag, D. P. (2002). The snowball Earth hypothesis: testing the limits of global change. *Terra Nova*, *14*, 129–155.

Holland, H. D. (2006). The oxygenation of the atmosphere and oceans. *Philosophical Transactions of the Royal Society*, *B361*, 903–915.

Righter, K. (2007). Not so rare Earth? New developments in understanding the origin of the Earth and Moon. *Chemie der Erde*, *67*, 179–200.

Rollinson, H. (2007). When did plate tectonics begin? *Geology Today*, *23*(5), 186–191.

Westall, F., & Southam, G. (2007). *Geology, Life and Habitability,* Treastise on Geophysics (pp. 421–437). Amsterdam: Elsevier, Chap. 10.12.

Chapter 10

Comparative Planetary Evolution

INTRODUCTION

Most data favor an origin for the planets by condensation and accretion of a gaseous solar nebula in which the Sun forms at the center (Boss et al., 1989; Taylor, 1992). Considering that the age of the universe is of the order of 13.7 Ga, the formation of the solar system at about 4.6 Ga is a relatively recent event. Because it is not possible as yet to observe in detail planetary formation in other gaseous nebulae, we depend on a variety of indirect evidence to reconstruct the conditions under which the planets in the solar system formed. Geophysical and geochemical data provide the most important constraints. Also, because the interiors of planets are not accessible for sampling, we often rely on meteorites to learn more about planetary interiors. Most scientists now agree that the solar system formed from a gaseous dust cloud, known as the solar nebula.

In this, the final chapter, we look at Earth as a member of the solar system by comparing it to other planets. As we have seen in earlier chapters, much is known about the structure and history of planet Earth, and it is important to emphasize the uniqueness of Earth in comparison to the other planets. First of all, plate tectonics and continents are unique to Earth. Why should only one of the terrestrial planets have plate tectonics? Although we do not have an answer to this question yet, we shall explore some possible reasons, especially in comparison to our sister planet Venus. The oceans and the presence of free oxygen in the terrestrial atmosphere are other unique features in the solar system, as we have discussed in Chapter 6. And, of course, Earth appears to be the only member of the solar system with life, although this may not have always been so. As we review other bodies in our solar system, and especially as we discuss the origin of the solar system, let us remember these unique terrestrial features that somehow must be accommodated in any model of planetary origin and evolution.

CONDENSATION AND ACCRETION OF THE PLANETS

The Solar Nebula

The Hubble Space Telescope has provided us with images of numerous young solar mass stars forming in giant molecular clouds such as the Eagle and Orion Nebulae. It is generally thought that our Sun formed in a similar molecular cloud by collapse of the cloud, which was triggered by a shock wave from a nearby supernova (Halliday & Wood, 2007). Although many models have been proposed for the origin of the solar system, only those that begin with a gaseous dust cloud appear to be consistent with data from both astrophysics and cosmochemistry (Taylor, 1999). Consistent with such a model is the existence of daughters of many short-lived radionuclides in meteorites and terrestrial samples. The short half-lives of these nuclides (100 ka to 100 Ma) necessitate their synthesis in a star shortly before the formation of the solar system. Stars form by contraction of gaseous nebulae and planets and other bodies form by condensation and accretion as nebulae cool (Hartmann, 1983). Dust around main sequence stars, such as Vega, can be detected by excess infrared radiation above the level expected from the stellar photosphere (Weinberger, 2002). Just how the solar system formed can be considered in terms of three questions:

1. How did the Sun acquire the gaseous material from which the planets formed?
2. What is the history of condensation of the gaseous material?
3. What are the processes and history of planetary accretion?

Regarding the first question, one viewpoint is that the Sun, already in existence, attracted material into a gaseous nebula about itself. Another proposes that the pre-existing Sun captured a solar nebula of appropriate mass and angular momentum to form the solar system. Most theories, however, call on condensation and accretion of the Sun and planets from the same cloud at approximately the same time. All models have in common a gaseous nebula from which the planets form. The minimum mass of such a nebula is about 1% of a solar mass. The mechanisms by which the nebula becomes concentrated into a disk with the Sun at the center are not well understood. One possibility is that the transfer of angular momentum from the Sun to the nebula was caused either by hydromagnetic coupling during rotational instability of the Sun or by turbulent convection in the nebula. Another possibility is a nearby supernova, which probably triggered the collapse of the solar nebula. In any case, condensing matter rapidly collapses into a disk about the Sun (Boss et al., 1989; Wetherill, 1994) or into a series of Saturn-like rings, which condense and accrete into the planets (Figure 10.1). Although it is commonly assumed that the solar nebula was well mixed, differences in isotopic abundances and ages of various meteorites suggest that it was not (Wasson, 1985; Taylor, 1992). Variations in the abundance of rare gases and isotopic variations of such elements as Mg, O, Si, Ca, and Ba

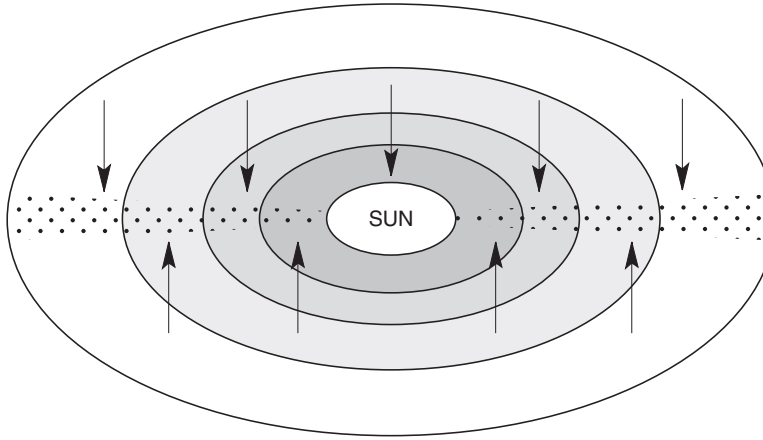

FIGURE 10.1 Schematic cross section of the primitive solar nebula. Temperatures in the nebula decrease outward from the Sun from hottest (dark gray) to coolest (white). Arrows indicate direction of gravitational sinking of solid particles into the ecliptic.

indicate large mass-dependent fractionation effects. The isotopic anomalies appear to require a sudden injection of neutrons into the early solar nebula, probably from a nearby supernova.

Emergence of Planets

Two processes are important in planet formation. **Condensation** is the production of solid dust grains as gases in the solar nebula cool, and **accretion** is the collision of the dust grains to form clumps and progressively larger bodies, some of which grow into planets (Figure 10.2). Condensation begins during collapse of the nebula into a disk, and leads to the production of silicate and oxide particles as well as to other compounds, all of which are composed chiefly of Mg, Al, Na, O, Al, Si, Fe, Ca, and Ni. In the cooler parts of the nebula, ices of C, N, O, Ne, S, Ar, and halogens form. The remaining gaseous mixture is composed chiefly of H_2 and He. The ices are especially abundant in the outer part of the disk where the giant planets form, and silicate-oxide particles are concentrated in the inner part and give rise to the terrestrial planets. Thermodynamic considerations indicate that iron should be present in the cloud initially only in an oxidized state. Type I carbonaceous chondrites (C1) may represent a sample of this primitive nebula. These meteorites contain only oxidized iron and large amounts of volatile components of the ices listed above (including organic compounds), and they have not been heated to more than 200°C to preserve their volatile constituents.

Planetary accretion models fall into two general categories. **Homogeneous accretion** involves condensation of a nebula followed by accretion of planets

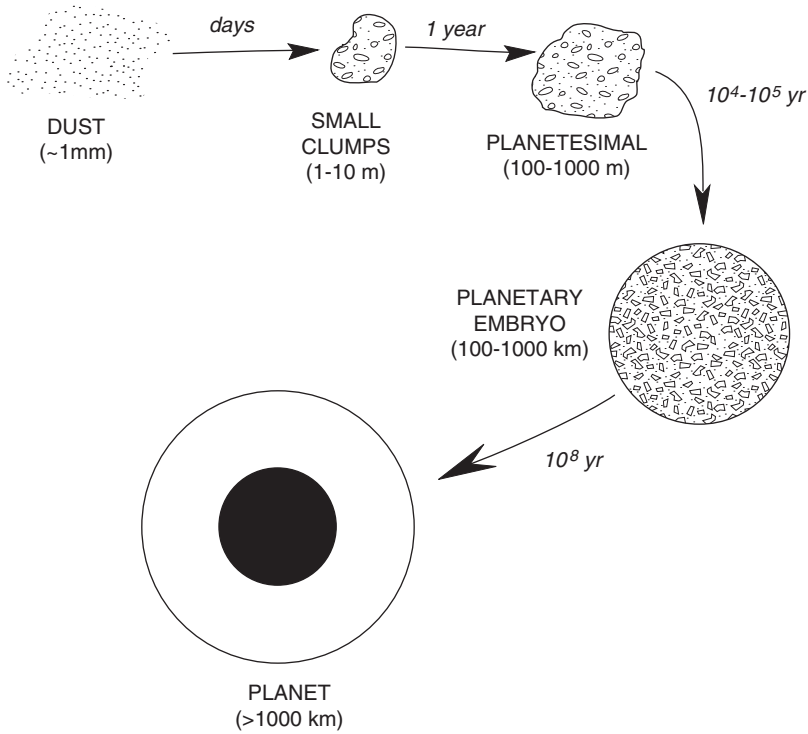

FIGURE 10.2 Diagrammatic representation of stages in planetary accretion.

and other bodies as the nebula continues to cool. In contrast, **heterogeneous accretion** occurs when condensation and accretion occur at the same time. Heterogeneous accretion is no longer considered a viable mechanism of planetary growth in that it does not explain either observational data or modern models for protracted evolution of the planets. Computer models suggest that the first generation of small planetary bodies, known as **planetesimals**, will increase in radius to the order of 100–1000 m in times of about 1 year after condensation (Figure 10.2) (Halliday, 2003). Wetherill (1986, 1994) has simulated further planetary growth by stochastic modeling using a high-speed computer. His results indicate that the planetesimals grow into planets in two distinct stages. During the first stage (10^4–10^5 years), planetesimals collide at low velocities and rapidly grow into **planetary embryos**. These embryos are commonly referred to as runaway embryos because in each local zone of the nebula, a single body grows more rapidly than its neighbors within the zone, and before it stops growing it cannibalistically consumes its neighbors. In the second stage, which lasts about 10^8 years, these embryos collide with each other to form the terrestrial planets and cores of the outer giant planets. During this stage,

there is widespread mixing of accreting materials in the inner solar system as well as "giant impacts," when one embryo collides with another. It is during this stage that a Mars-size body may have collided with Earth to form the Moon (as discussed in Chapter 9) and another body collided with Mercury, stripping it of much of its mantle. The different tilts and spins of the planets also support massive impacts during the early history of the solar system. The terrestrial planets should grow to within 50 km of their final radius in the first 25 my, and accretion should be 98% complete in 10^8 years (remember that *my* refers to time measured from the age of the solar system). These times are consistent with $^{182}W/^{182}Hf$ isotopic ages for the formation of Earth as discussed later.

Most of the gas in the nebula was swept away within a few million years by high-energy winds emanating from the Sun during a T-Tauri stage (Chapter 6). This would occur during the first few thousand to few million years when the Sun was much brighter than today. Many stars would still have disks during this stage. The gases are swept into the outer solar system where they provide building material for the gas and ice giants (Jupiter, Saturn, and the other outer planets). At about 5 AU (1 AU = Earth–Sun distance), it was cold enough that water being swept outward froze to ice, piled up, and aggregated to form the core of Jupiter. This embryo grew to about 10 times the size of Earth in as little as 500 ka, when it began to capture escaping gases and grew into a giant. Jupiter and Saturn, which consist chiefly of H_2 and He accreted onto rocky cores, also grew by planetesimal collisions. Once a planet reaches 10–50 Earth masses, it is able to attract H_2 and He from the nebula and to grow into a giant planet. Once formed, Jupiter dominated the later evolution of the solar system because of its tremendous mass and gravity. It depleted both the asteroid belt and region where Mars would later form in material, thus accounting for the small amount of mass in this region, including the small size of Mars. Uranus and Neptune accumulated late, since they are composed chiefly of ice and silicates with very little gas, the latter of which had escaped prior to their formation.

Earth and other inner planets accreted long after the outer giant planets, from volatile-poor planetesimals that were probably already differentiated into metallic cores and silicate mantles in a gas-free inner part of the nebula (Taylor, 1999). During the time of supercollisions, Earth was probably struck at high velocity many times by bodies ranging up to Mercury in size and at least once by a Mars-size body. Much of the kinetic energy associated with these collisions would have been expended in heating the interior of the planet, and calculations show that Earth should have been largely melted long before it completed its growth. Thus a widespread magma ocean would exist on the planet. It is during this stage that Earth's core formed and the planet was extensively degassed to form a primitive atmosphere as discussed in previous chapters. Core formation was the first step in producing a zoned planet.

Homogeneous Accretion

In homogeneous accretion models condensation is essentially complete before accretion begins (Taylor, 1999; Drake, 2000). Compositional zoning in the solar nebula is caused by decreasing temperature outward from the Sun (Figure 10.1) and this is reflected in planetary compositions. Refractory oxides, metals, and Mg-silicates are enriched in the inner part of the cloud where Mercury accretes, Mg-Fe silicates and metal in the region from Venus to the asteroids, and mixed silicates and ices in the outer part of the nebula where the giant planets accrete. Homogeneous accretion models produce an amazingly good match between predicted and observed planetary compositions. If, for instance, volatiles were blown outward when Mercury was accreting refractory oxides, metal, and Mg-silicates, Venus and Earth should have been enriched in volatile components compared to Mercury. The lower mean density of Venus and Earth is consistent with this prediction. Mars has a still lower density, and it is probably enriched in oxidized iron compounds relative to Earth and Venus. Likewise, the giant outer planets are composed of mixed silicates and ices, reducing their densities dramatically. If homogeneously accreted, how do the terrestrial planets become zoned? It must be by melting, which results in segregation by such processes as fractional crystallization and sinking of molten iron to the core. Where does the heat come from to melt the planets and asteroids? Some of the major known heat sources are as follows:

1. *Accretional energy*. This energy is dependent on impact velocities of accreting bodies and the amount of input energy retained by the growing planet. Accretional energy alone appears to have been sufficient, if entirely retained in the planet, to largely melt the terrestrial planets while they were accreting.
2. *Gravitational collapse*. As a planet grows, the interior is subjected to higher pressures and minerals undergo phase changes to phases with more densely packed structures. Most of these changes are exothermic as discussed in Chapter 4, and large amounts of energy are liberated into planetary interiors.
3. *Radiogenic heat sources*. Radioactive isotopes liberate significant amounts of heat during decay. Short-lived radioactive isotopes, such as ^{26}Al and ^{244}Pu may have contributed significant quantities of heat to planets during accretion. Long-lived isotopes, principally ^{40}K, ^{235}U, ^{238}U, and ^{232}Th, have been important heat producers throughout planetary history.
4. *Core formation*. Core formation is a strongly exothermic process and appears to have occurred over a relatively short period of time ($\leq$50 Ma) beginning during the late stages of planetary accretion.

Because volatiles are retained in the terrestrial planets it is unlikely that they were ever completely molten. Hence, it is necessary to remove the early heat very rapidly and convection seems the only process capable of bringing heat from planetary interiors to the surface in a short time interval ($\leq$50 Ma) to escape complete melting. During the late stages of accretion, collisions

deposited enough energy if fully retained to partly or fully melt Earth, perhaps multiple times (Drake, 2000). The result is a magma ocean, perhaps extending nearly to the center of the planet (as discussed in Chapter 7). Metal would sink through the magma ocean and accumulate at the center as the core grew (as discussed in Chapter 5). This early core was disrupted and rapidly reformed during the Moon-forming collision event. The temperature dependence of mantle viscosity appears to be the most important factor controlling planetary thermal history (Carlson, 1994; Schubert et al., 2001). Initially, when a planet is hot and viscosity is low, chaotic mantle convection rapidly cools the planet and crystallizes magma oceans (Drake, 2000). As mantle viscosity increases, beginning 50 my after accretion, convection should cool planets at reduced rates.

Chemical Composition of the Earth and the Moon

Because it is not possible to sample the interior of the Earth and the Moon, indirect methods must be used to estimate their composition (Hart, 1986; McDonough & Sun, 1995). It is generally agreed that the composition of the Sun roughly reflects the composition of the solar nebula from which the planets formed. Nucleosynthesis models for the origin of the elements also provide limiting conditions on the composition of the planets. As we saw in Chapter 4, it is possible to estimate the composition of Earth's upper mantle from analysis of mantle xenoliths and basalts, both of which transmit information about the composition of their mantle sources to the surface. Meteorite compositions and high-pressure experimental data also provide important input on the overall composition of Earth.

Shock-wave experimental results indicate a mean atomic weight for Earth of about 27 (mantle = 22.4 and core = 47.0) and show that it is composed chiefly of iron, silicon, magnesium, and oxygen. When meteorite classes are mixed in such a way as to give the correct core–mantle mass ratio (32/68) and mean atomic weight of Earth, results indicate that iron and oxygen are the most abundant elements, followed by silicon and magnesium (Table 10.1). Almost 94% of Earth is composed of these four elements. From lunar heat flow results, correlations among refractory elements, and density and moment of inertia considerations, the bulk lunar composition can be estimated. Compared to Earth, the Moon is depleted in Fe, Ni, Na, and S, and enriched in other major elements. The bulk composition of the Moon is commonly likened to the composition of Earth's mantle because of similar densities. The data indicate, however, that the Moon is enriched in refractory elements like Ti and Al compared to Earth's mantle (see Figure 9.2 in Chapter 9).

To discuss planetary formation, elements can be divided into three geochemical groups. **Volatile elements** are those elements that are volatilized from silicate melts under moderately reducing conditions at temperatures below 1400°C, whereas **refractory elements** are not volatilized under the same conditions. Refractory elements can be further subdivided into **oxyphile** and **siderophile**

TABLE 10.1 Major Element Composition of Earth and the Moon

	Earth[a,c]	Earth[b]	Moon
Fe	29.9	28.2	8.3
O	30.9	32.4	44.7
Si	17.4	17.2	20.3
Mg	15.9	15.9	19.3
Ca	1.9	1.6	3.2
Al	1.4	1.5	3.2
Ni	1.7	1.6	0.6
Na	0.9	0.25	0.06
K	0.02	0.02	0.01
Ti	0.05	0.07	0.2

Values in weight percent.
[a]Nonvolatile portion of type I carbonaceous chondrites with FeO/FeO+MgO of 0.12 and sufficient SiO_2 reduced to Si to yield a metal/silicate ratio of 32/68 (Ringwood, 1966).
[b]From Allegre et al. (1995b).
[c]Based on Ca, Al, Ti = 5 × type I carbonaceous chondrites; FeO = 12% to accommodate lunar density; and Si/Mg = chondritic ratio (after Taylor, 1982).

groups, depending on whether they follow oxygen or iron, respectively, under moderately reducing conditions. Both the Earth and the Moon differ from carbonaceous chondrites in the distribution of elements in these groups (see Figure 9.2). Compared to carbonaceous chondrites, both bodies are depleted in volatile and siderophile elements and enriched in oxyphile refractory elements.

Vertical zoning of elements has occurred in both the Earth and the Moon and is the result of element **fractionation,** which is the segregation of elements with similar geochemical properties. Fractionation results from physical and chemical processes such as condensation, melting, and fractional crystallization. Large-ion lithophile elements, such as K, Rb, Th, and U, have been strongly enriched in Earth's upper mantle and even more so in the crust in relation to the mantle and core. In contrast, siderophile refractory elements (such as Mn, Fe, Ni, and Co) are concentrated chiefly in the mantle or core, and oxyphile refractory elements (such as Ti, Zr, and La) in the mantle.

Accretion of Earth

Earth grew by the collisional accretion of many Moon- to Mars-sized planetary embryos, and the interiors of these bodies were sufficiently hot to have substantially melted, allowing segregation of molten iron to form a core and a residual

overlying silicate mantle. Models suggest that at least 60% of Earth's current size was attained in the first 10–40 my (Elliott, 2010). As the planet continued to grow, metal from the cores of accreted embryos likewise sank to the center after temporarily accumulating at the base of a silicate magma ocean. Any model for accretion of Earth must account for a depletion in volatile elements in the silicate portion of the planet (V to K, Figure 10.3) relative to the solar nebula, the composition of which is assumed to be that of type I carbonaceous chondrites (Greenberg, 1989; Wetherill, 1990; Taylor, 1992). This increasing depletion with increasing condensation temperature may reflect depletions in the nebular material in the region from which Earth accreted. Alternatively, the trend could result from mixing between two components in the nebula, one a "normal" component relatively enriched in refractory elements (Al to La, Figure 10.3), and one strongly depleted in volatiles. In this case, the earliest stage of Earth accretion would be dominated by refractory elements, followed by a second stage in which mixed refractory and volatile components accrete as the temperature of the nebula continues to decrease (partly heterogeneous accretion). Depletions in volatile elements in portions of the inner solar nebula may have been caused by an intense T-Tauri wind emitted from the Sun during its early history. This wind could have blown volatile constituents from the inner to the outer part of the solar system. What about the depletions in siderophile elements in the silicate fraction of the Earth (see Figure 9.2)? These can best be explained by core formation during which these elements (such as Co and Ni), with their strong affinities for iron, are purged from the mantle as molten iron sinks to Earth's center to form the core. Thus, it would appear

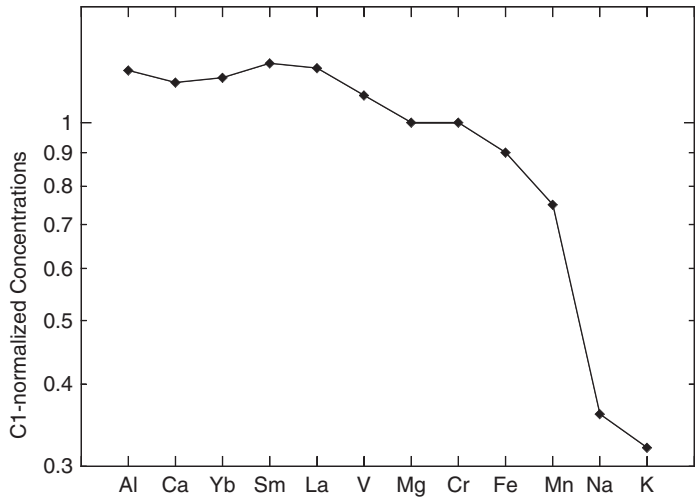

FIGURE 10.3 Element distributions in Earth normalized to type I (C1) carbonaceous chondrites.

that the volatile element depletions in Earth occurred during the early stages of planetary accretion and the siderophile element depletions during the late stages.

Volatile-depleted primitive materials have usually been assumed to represent the building blocks from which Earth was accreted. However, there are some unique compositional differences between terrestrial materials (mantle xenoliths, basalts) and any known meteorites. These include significant differences in Mg/Si, Al/Si, D/H, Ar/H_2O, and Kr/Xe ratios as well as in oxygen and osmium isotope ratios (Drake & Righter, 2002). Thus, it would appear that Earth is not made of asteroids with the common chondritic or achondritic compositions that characterize meteorites that hit the Earth. This implies that distinct compositional zones were maintained in the dust cloud from which the solar system accreted. It also means that there was no widespread mixing of the material in the inner solar system during accretion and that planets growing in the inner solar system received an overwhelming majority of their mass from narrow rings around the Sun (Drake & Righter, 2002).

A summary of the accretion of Earth is shown in Figure 10.4. Within a few million years of the birth of the solar system, T-Tauri radiation from the primitive Sun swept gaseous components from the inner to the outer solar system. Runaway growth of planetesimals produces hundreds of planetary embryos, which collide to produce the terrestrial planets within 20–30 my. One of the last of these collisions was that of Earth and a Mars-size body some 40 my after the solar system began to form, which produced the Moon (Chapter 9). It was during this time that Earth's core formed. Addition of a late veneer at about 100 my from the asteroid belt or beyond provides an explanation for the abundances of siderophile and volatile elements in the terrestrial mantle. This late veneer may also have contained water, perhaps enough to account for the origin of the early oceans (Albarede, 2009).

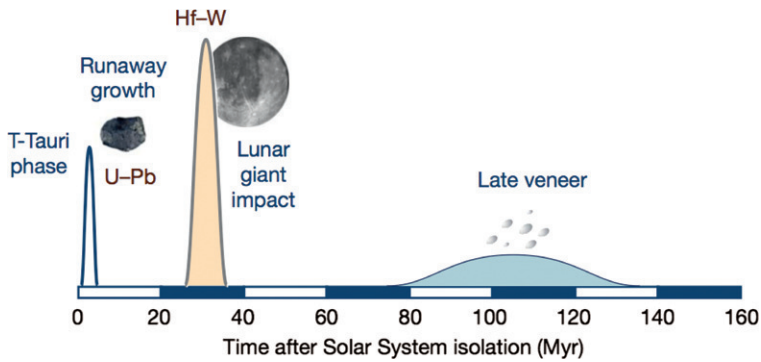

FIGURE 10.4 Summary of the early accretional history of Earth. *Modified after Albarede (2009), courtesy of Francis Albarede. Used with permission of Nature Publishing Group, permission conveyed through Copyright Clearance Center, Inc.*

The First 700 Million Years

Because Earth is mostly inaccessible to sampling and it is a continuously evolving system, it is difficult to date (Zhang, 2002). Also contributing to this difficulty is the fact that Earth accreted over some time interval, and hence if an age is obtained, what event in this time interval does it date? The first isotopic ages of Earth were model Pb ages of about 4.55 Ga obtained from sediments and oceanic basalts (Patterson et al., 1955). Until recent precise ages were obtained from meteorites, other attempts to date Earth have yielded ages in the range of 4.55 to 4.45 Ga.

Refractory inclusions enriched in Ca and Al (CAIs) found in some meteorites are the oldest dated objects in the solar system, the oldest of which comes from a meteorite in the Sahara Desert at 4568 Ma (Figure 10.5). The accretion of most chondrites began a maximum of about 3 Ma later and lasted for no more than 8 Ma. Model Pb ages from Earth probably represent the mean age of core formation, when iron was separated from the mantle and U and Pb were fractionated from each other. The fact that both meteorite and terrestrial ages are similar at 4460–4450 Ma suggests that both processes went on simultaneously during the terminal stages of planetary accretion. This being the case, the age of Earth we obtain is the age of early differentiation, and just how this age is related to the onset of planetary accretion is not well known. Recent

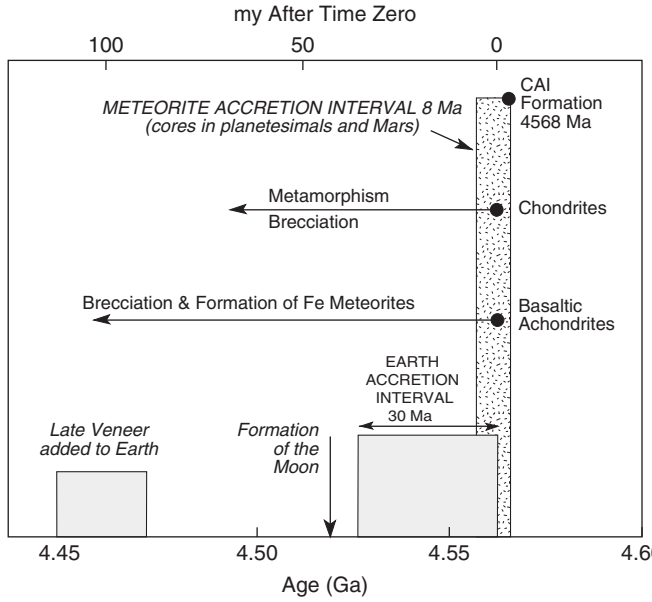

FIGURE 10.5 Isotopic timescale for the accretion of the inner solar system. CAI, Ca- and Al-rich refractory inclusions in chondrites.

high-resolution measurements using the $^{182}Hf/^{182}W$ method suggest that bodies in the inner part of the solar system all formed in the first 30 my after accretion began (Yin et al., 2002). Most of Earth's growth was in the first 10 my and it was 80–90% complete by 30 my after time zero (about 4525 Ma) (Figure 10.5).

Although the oldest ages of rocks dated from the Moon are about 4420 Ma, model ages suggest the Moon accreted 4500 to 4480 Ma. Hf isotope data, however, suggest that the Moon formed about 30 my after solar system formation, when Earth was complete or nearly complete (Yin et al., 2002). If the Moon was formed by accretion of material left over after a Mars-sized body hit the Earth, as discussed in Chapter 9, it would appear that this impact occurred at 4530–4520 Ma. If Earth began to accrete at the same time that the CAIs accreted at 4568 Ma, then the total time between accretion and the addition of a late veneer near 4450 Ma is the order of 100 Ma (Figure 10.5).

From precise isotopic ages of meteorites and Earth, a summary of the first 700 my of Earth's history is given in Figure 10.6. Most of the action preserved

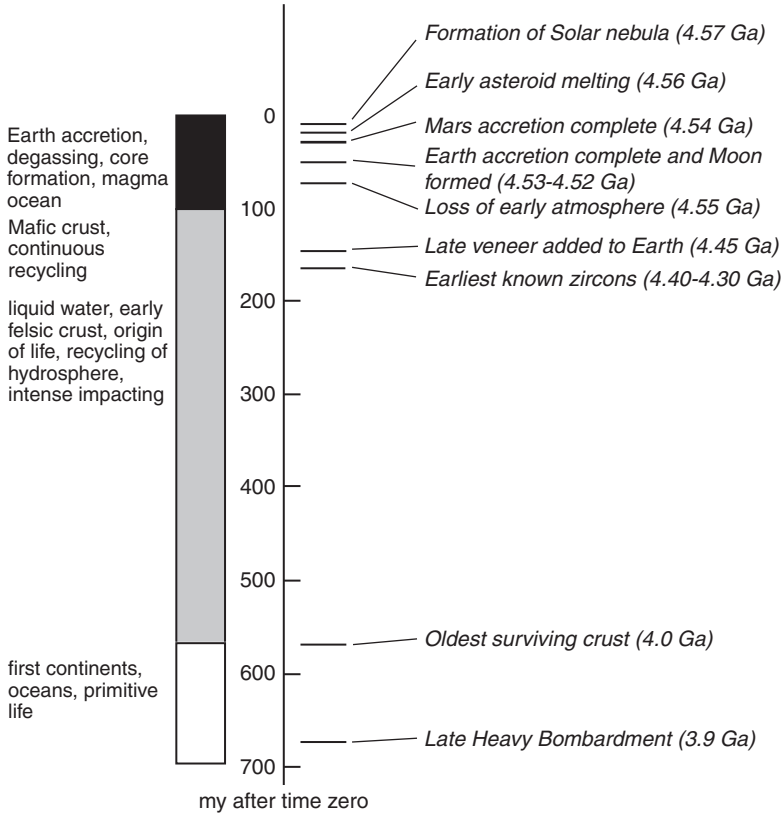

FIGURE 10.6 Summary of the first 700 my of Earth's history.

in the isotopic record is in the first 100 my, when accretion of Earth and other bodies in the inner solar system was complete and these bodies were covered with magma oceans. All or most of the early atmosphere must have been lost at or before 4550 Ma by T-Tauri events and planetary collisions. Geochemical studies of mantle xenoliths indicate that a late veneer of heavy metals was added to Earth, sometime after core formation was complete around 4450 Ma. As the terrestrial magma ocean rapidly cooled, the outer part of Earth solidified, producing the first primitive crust. The earliest known felsic crust, probably of local distribution, is recorded in the detrital zircons from Western Australia with ages as old as 4400–4300 Ma, whereas the oldest surviving felsic crust is about 4000 Ma (Chapter 7). Because of intense bombardment of the inner solar system ending with the Late Heavy Bombardment about 3900 Ma (Chapter 9), very little of this early crust survives.

MEMBERS OF THE SOLAR SYSTEM

The Planets

Basically there are three types of planets in the solar system (Sohl & Schubert, 2007). The largest distinction is the break between the inner silicate planets, known as the **terrestrial planets,** and the outer **giant planets**. The giant planets can further be divided into the gas giants, Jupiter and Saturn, and the ice giants, Uranus and Neptune. In this respect the planets reflect the three main components in the solar nebula: gas, ice, and rock. Among the terrestrial planets there are large variations. Mercury and the Moon show highly cratered surfaces indicating average crustal ages >4 Ga, with only minor volcanic activity thereafter. Mars shows a distinct dichotomy of the surface consisting of the old southern highlands with an age >4 Ga and the younger northern highlands with an average age of about 3.5 Ga (Figure 10.7) (Breuer & Moore, 2007). In contrast, the surface ages of Earth and Venus are much younger, indicating that the lithospheres of these planets are continually being recycled into their mantles. Mercury is the only planet except Earth with a measurable magnetic field, but both Mars and the Moon have remanent magnetization in parts of their crust that indicates they once had a geodynamo in action in their cores.

In this section, we review the chief characteristics of the planets, emphasizing the terrestrial planets.

Mercury

Mercury, the closest planet to the Sun, is a peculiar planet in several respects. First, the eccentricity and inclination of the orbit to the ecliptic are greater than any other planet except for Pluto (Table 10.2). Also, the high mean density (5.43 g/cm^3) of Mercury implies an Fe-Ni core that comprises about 66% of the planet's mass, thus having a core–mantle ratio greater than that of any other

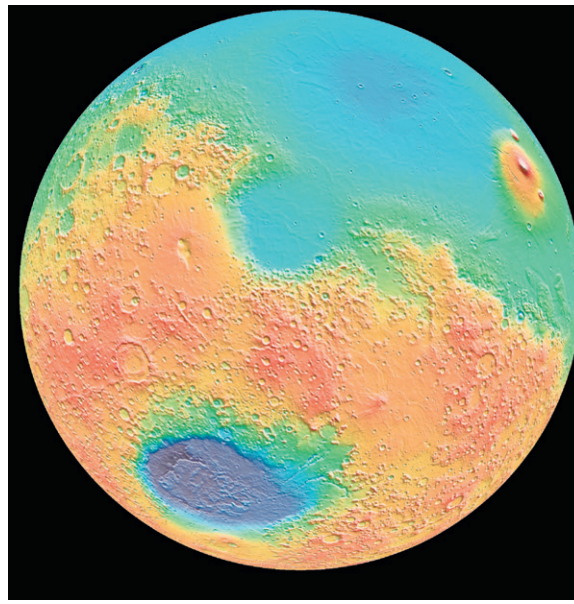

FIGURE 10.7 The Martian hemispheric dichotomy. Note the older southern highlands cratered terrane and the smooth northern highlands. Courtesy of NASA/Goddard Space Flight Center. Used with permission of Nature Publishing Group, permission conveyed through Copyright Clearance Center, Inc.

planet (Figure 10.8). Although Mercury's magnetic field is very weak, like Earth, it has a dipole field that is probably generated by an active dynamo in a liquid outer core. To maintain this magnetic field, convection in the mantle must be very weak or possibly nonexistent. Results from *Mariner 10* show that the surface of Mercury is similar to that of the Moon in terms of crater distributions and probable age. Spectral studies of the Mercurian surface are consistent with a crust rich in calcic plagioclase and low-Fe pyroxenes, much like the lunar highlands crust (Tyler et al., 1988; Solomon, 2003). The occurrence of a weak sodium cloud around the planet supports this idea. There are two types of plains on Mercury's surface: the early intercrater plains formed prior to 4 Ga and the smooth plains formed at about 3.9 Ga. These plains have been attributed to both debris sheets from large impacts and to fluid basaltic lavas, and their origin continues to be a subject of controversy (Taylor, 1992; Solomon, 2003). For instance, microwave and infrared radiation reflected from the Mercurian surface indicates a very high albedo inconsistent with the presence of basalt (Jeanloz et al., 1995). These data would seem to favor a crust on Mercury, including the plains, composed almost entirely of anorthosite.

The *Mariner 10* spacecraft returned high-resolution images of about 45% of the planet's surface. One of the major features is a global network of large lobate scarps up to 1 km in height that may be high-angle reverse faults. They indicate a contraction in planetary radius of the order of 1–3 km, probably due to rapid

TABLE 10.2 Properties of the Planets

	Mean distance to Sun (AU)	Orbital period (d, days; y, years)	Mean orbital velocity (km/s)	Mass (Earth = 1)	Equatorial radius (km)	Mean density (g/cm^3)	Zero pressure density (g/cm^3)	Area/ mass (Earth = 1)	Core–mantle (Earth = 1)
Mercury	0.387	88d	48	0.056	2439	5.43	5.3	2.5	12
Venus	0.723	225d	35	0.82	6051	5.24	3.95	1.1	0.9
Earth	1.0	365d	30	1	6378	5.52	4.0	1	1
Moon	1.0	27.3d[a]	1.0[a]	0.012	1738	3.35	3.3	6.1	0.12
Mars	1.52	687d	24	0.11	3398	3.93	3.75	2.5	0.8
Jupiter	5.2	11.9y	13	318	71 600	1.33			
Saturn	9.2	29.5y	9.7	95.2	60 000	0.69			
Uranus	19.1	84y	6.8	14.5	25 600	1.27			
Neptune	30	164y	5.4	17.2	24 760	1.64			
Pluto	39.44	248y	4.7	0.0022	1150	1.75			

[a]*Period and velocity about Earth.*

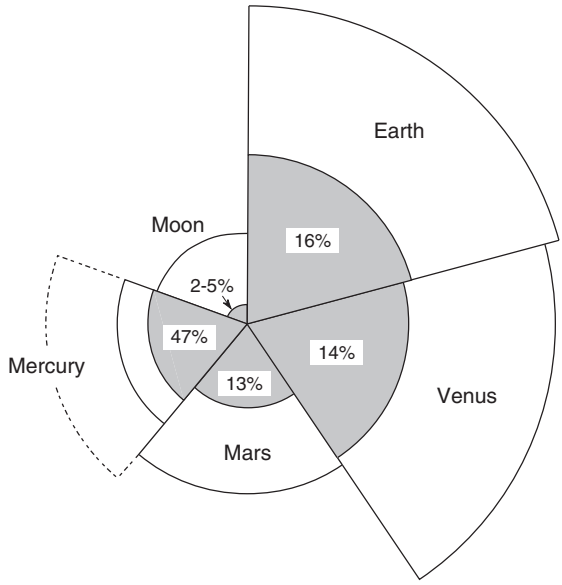

FIGURE 10.8 Comparison of the core–mantle ratios by volume in the terrestrial planets and the Moon. The dashed line for Mercury is the part of the mantle that may have been lost during collision with another planetary body.

cooling of the mantle (Watters et al., 2009). The faulting that produced the lobate scarps occurred both before and after major volcanism. The most likely source of global contraction is a combination of thermal contraction as the planet cooled and growth of an inner core (Breuer & Moore, 2007). Employing the lunar impact timescale, crater distributions indicate that the contraction occurred before massive bombardment of the planet at 3.9 Ga, and probably before 4 Ga. High-resolution images of the first *MESSENGER* flyby show evidence of volcanic vents and demonstrate that the large volcanic plains were emplaced sequentially inside and adjacent to large impact craters to depths of several kilometers (Head et al., 2008). The observations support a volcanic origin for the Mercury plains and substantiate an important role for volcanism on the planet.

Two ideas have been suggested to explain the relatively high density of Mercury: (1) high-temperature evaporation of the silicate mantle, thus enhancing the proportion of iron in the planet, and (2) removal of part of the mantle by collision with another planet during or soon after accretion of Mercury (Vilas et al., 1988). The reflectance data suggesting a plagioclase-rich crust and the presence of a sodium cloud around Mercury do not favor the evaporation theory, because volatile elements like sodium should have been removed and lost during the high-temperature evaporation event. The impactor idea has received increased support from stochastic modeling of planetary accretion in the inner solar system, which indicates that numerous potential impactors up to Mars size may have existed in the solar nebula. To give a core–mantle ratio similar to

Earth and Venus, Mercury would have to lose about half of its original mass during the collision (Figure 10.8). The fate of this fragmented material, mostly silicates and oxides, is unknown, but it may have been swept away by solar radiation, or possibly accreted to Venus or Earth if it crossed their orbits. The highly eccentric orbit of Mercury also may have developed during the alleged collision.

Mars

The *Mariner* and *Viking* missions revealed that Mars is quite different from the Moon and Mercury (Taylor, 1992; Carr et al., 1993). The Martian surface includes major shield volcanoes, fracture zones, and rifts as well as large canyons that appear to have been cut by running water. Also, much of the planet is covered with windblown dust, and more than half of the surface is covered by a variably cratered terrain similar to the surfaces of the Moon and Mercury. Large near-circular basins are similar to lunar mare basins and probably formed at 3.9 Ga during the Late Heavy Bombardment event. Much of the northern hemisphere of Mars comprises volcanic plains and large stratovolcanoes. In contrast, the southern hemisphere is covered by the Ancient Cratered Terrain >4 Ga (Figure 10.7). The Tharsis bulge, which probably formed by a large mantle upwelling, is the dominant structural feature on the Martian surface (Zuber, 2001). It is about 10 km high at the center and 8000 km across, comprising about 25% of the Martian surface. The Tharsis region includes gigantic shield volcanoes and volcanic plains, and the Valles Marineris represents an enormous rift valley that spans one-quarter of the equator. The size of Martian volcanoes implies a very thick lithosphere on Mars. The distribution and surface features of lava flows on Mars indicate low viscosities of eruption and a total volume of lavas much greater than that on Earth.

Crustal Dichotomy

A long-recognized feature of Mars is its **crustal dichotomy**: the northern and southern hemispheres are very different from each other (Figure 10.7). Topography and gravity measurements by the *Martian Global Surveyor* shows that Mars has two distinct crustal zones: the northern lowlands with uniform thin crustal thickness and the southern highlands with relatively thick crust and high topography (Zuber et al., 2000; Zuber, 2001). In addition, the northern hemisphere crust is relatively smooth and has far fewer craters than the southern hemisphere crust. On the basis of crater distributions, the dichotomy is thought to have formed >4 Ga (Kiefer, 2008). Explanations for the dichotomy include a large impact from an asteroid or comet, or large-scale mantle convection in the northern hemisphere. Although neither mechanism is fully satisfactory (Breuer & Moore, 2007), recent modeling by several different investigators clearly favors the impact idea and also shows that the northern hemisphere basin cannot result from convective mantle flow (Kiefer, 2008). Another idea that has been

around for many years is that the boundary between the two terranes is an ancient shoreline of an early ocean. Recent investigations lend support to this model in that the elevation of deltas and shoreline terraces coincides in altitude to the proposed shoreline (Achille & Hynek, 2010). Hence some 3.5 Ga, Mars may have had a large ocean in the northern hemisphere.

Surface Features

A peculiar feature of Mars in the presence of widespread windblown dust, perhaps analogous to terrestrial loess deposits. The Martian dust is the cause of the variations in albedo on the planet's surface, once thought to be canals. In Martian bright areas, dust may accumulate to more than 1 m in thickness. The movement of dust on the surface by gigantic dust storms appears to be related to seasonal changes. On the whole, erosion on the Martian surface has been very slow, consistent with the unweathered composition of rocks analyzed by the *Viking* landers. The redistribution of sediment by wind occurs at a rate much greater than that of weathering and erosion, such that much of the dusty sediment on Mars was produced early in Martian history and has been reworked ever since.

The chemical composition of the Martian crust provides a snapshot of the planet's integrated geologic history and clues to its differentiation. Spacecraft (orbiters and rovers) and SNC meteorite data now give us a glimpse of the igneous history of the crust and mantle. Chemical analyses from the Viking landing sites suggest that the dominant volcanic rocks on Mars are Fe-rich basalts and that minor weathering of the basalts occurs in a hydrous, oxidizing environment. The Russian *Phobos* mission obtained chemical analyses of a large area that is also consistent with basaltic rocks (Figure 10.9). Recent data from the NASA rovers indicate that felsic and calc-alkaline compositions are uncommon. It is also possible to learn about the composition of the Martian crust from meteorites that appear to have been ejected from the planet's surface by one or more impacts in the last 20 Ma. Chemical analysis of these meteorites shows they are picrites (Mg-rich basalts) and basalts, in agreement with the surface measurements (Zuber, 2001). The spacecraft results, however, suggest that Martian meteorites are not representative of older more voluminous crust, and may give a biased view of the planet (McSween et al., 2009). Remote sensing studies show a strong concentration of Fe^{3+} on the surface indicative of hematite, probably in windblown dust. Because Mars has an uncompressed density much less than that of Earth and Venus (Table 10.2), it must also have a distinctly different composition than these planets. If Mars has a carbonaceous chondrite (C1) composition and is completely differentiated, the core mass is about 21% of total mass and the core radius about 50% of the planetary radius. It would appear that compared to Venus and Earth, Mars is more volatile rich by at least a factor of 2, and its core probably contains a substantial amount of sulfur (Taylor, 1992).

One of the most puzzling aspects of Martian geology is the role that water has played on the planetary surface (Carr et al., 1993; Baker, 2001;

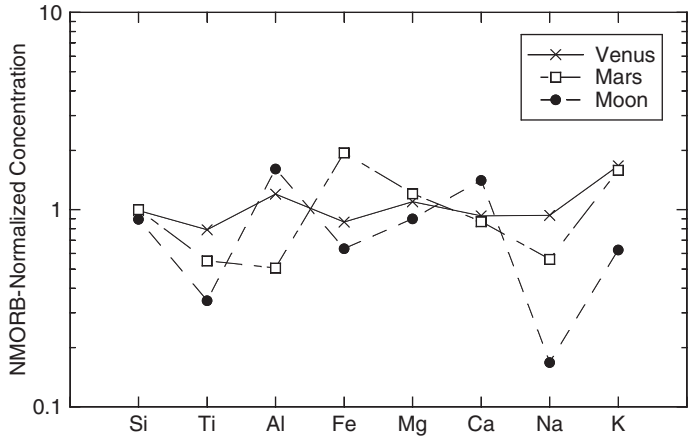

FIGURE 10.9 Major element distributions in crustal rocks from Venus, Mars, and the Moon, normalized to normal ocean ridge basalt, N-MORB.

Carr & Head, 2010). Although water is frozen on Mars today, we see evidence for running water in the past as dry valleys and canyons (Figure 10.10). Clearly climatic conditions on Mars must have been warm enough to permit running water sometime in the past (Jakosky & Phillips, 2001). The most intriguing features are the large, flat valleys up to 150 km wide, some up to 2000 km long, that have been cut by running water. These valleys are similar to Pleistocene glacial features on Earth caused by cataclysmic flooding, and by analogy, the Martian analogues are generally interpreted to have resulted from gigantic floods (Baker, 2001). The sizes of the Martian outflow channels imply immense discharges of water, much larger than any floods on Earth for which we have evidence preserved in the geologic record (Figure 10.11). Although most Martian floods appear to have occurred early (4–2 Ga), some are as recent as 10 Ma. What caused the floods remains problematic, and they may not all be of the same origin. One possible cause is volcanism, which could have melted permafrost, suddenly releasing huge volumes of water. Other Martian canyons with numerous tributaries look like terrestrial canyons and appear to have been cut more slowly by rivers or spring sapping by groundwater (Figure 10.10). Most of these canyons are in the Ancient Cratered Terrain, the oldest part of the Martian crust, indicating the presence of transient warm climates on Mars more than 4 Ga. The presence of large buried channels in the northern lowlands is consistent with northward transport of water and sediment before the end of northern hemisphere resurfacing (Zuber et al., 2000).

Martian History

Unlike Earth, Mars has no global dipole magnetic field as confirmed by the *Global Surveyor* mission. However, *Surveyor* found strong, spatially variable magnetizations in the Martian crust. These crustal magnetizations, an order

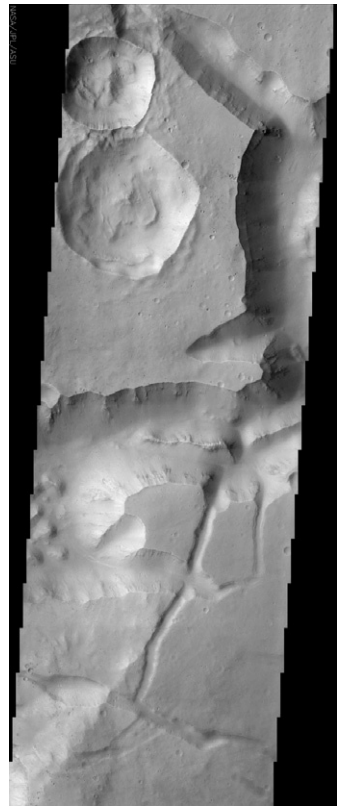

FIGURE 10.10 Part of Aureum Chaos just south of the Martian equator. The view shows canyons of various sizes and origins as well as two impact craters in the upper left. *NASA Planetary Photo, 2001 Mars Odyssey.*

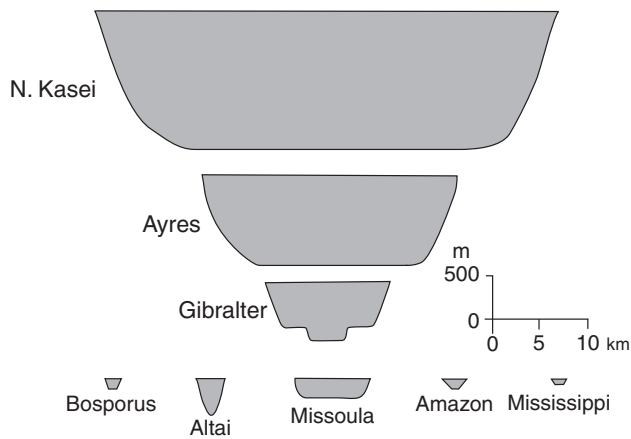

FIGURE 10.11 Comparison of channel cross sections for cataclysmic flood channels on Mars (upper two) with terrestrial straits (Gibraltar and Bosporus) and river channels on Earth. *Modified after Baker (2001).*

of magnitude larger than the strongest magnetizations found in terrestrial rocks and minerals, are probably thermal remanent magnetization. Hence, the magnetizations were produced by cooling events that occurred when a large global magnetic field was present in the planet (Stevenson, 2001). This implies that early in Martian history the planet had an active geodynamo in the core, as does Earth today. Some of the magnetizations occurred in linear bands reminiscent of the linear magnetic anomalies associated with terrestrial ocean ridges. Thermal modeling also permits an early aborted attempt at plate tectonics (O'Neill et al., 2007a).

The geologic history of Mars was probably similar to that of the Moon and Mercury for the first few hundred million years, and most subsequent activity is concentrated in the first 1.5 Ga of the planet's history (Figure 10.12) (Carr & Head, 2010). Core formation was early, probably coinciding with a transient magma ocean. Part of the early crust survived major impacting that terminated at about 3.9 Ga, and occurs as the Ancient Cratered Terrane in the southern hemisphere. After rapid crystallization of the magma ocean prior to 4.4 Ga, extensive melting in the upper mantle resulted in the formation of a thick basaltic crust. Heat loss was chiefly by mantle plumes. The Tharsis bulge developed at about 3.9–3.8 Ga, perhaps in response to a gigantic mantle plume (Mutch et al., 1976). With a drop in surface temperature, permafrost formed, which later locally and perhaps catastrophically melted and caused massive

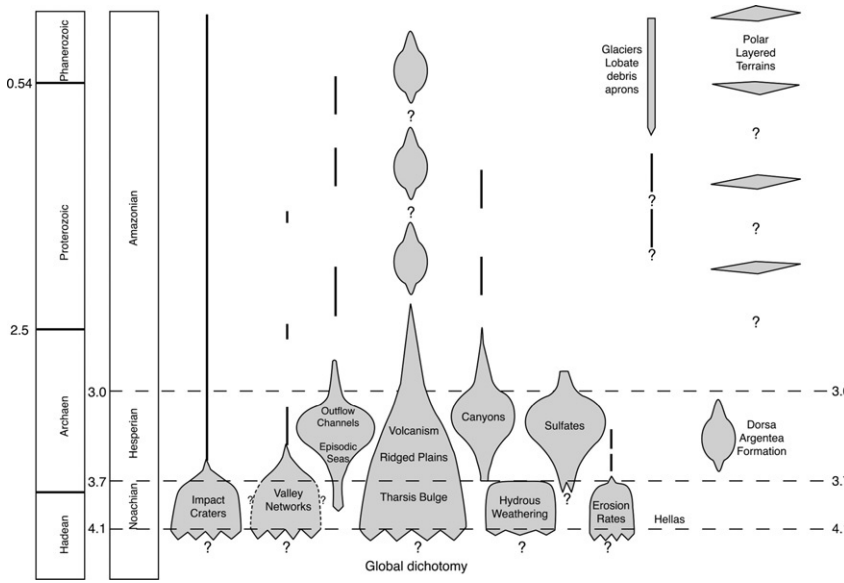

FIGURE 10.12 Summary of Martian history. Shown are the relative importances of the different processes as a function of age (in Ga on the vertical axis). *After Carr & Head (2010), courtesy of Mike Carr.*

floods that cut many of the large flat-bottom valleys. The major erosional events probably occurred during or just before the terminal large impact events between 4.1 and 3.7 Ga (Figure 10.12). In fact, by the end of the Noachian period some 3.7 Ga, the cratering rate had fallen and the rates of erosion, weathering, and cutting of gigantic canyons dropped precipitously. Volcanism continued, however, until about 3 Ga and between 3.7 and 3.0 Ga at least 30% of the planet was resurfaced with magmas and sulfates widely deposited on the surface (Carr 7 Head, 2010). Also, significant canyon cutting and episodic flooding continued until about 3 Ga. After 3 Ga, the pace of geologic activity again decreased, with volcanism largely restricted to the Tharsis and Elysium centers. Continued fracturing and volcanism on Mars extended to at least 1000 Ma and perhaps 100 Ma. However, most characteristic of the last 3 Ga and especially the last 1 Ga are features that have been attributed to ice including polar layered deposits, ice-rich veneers at high latitudes, glacial deposits, and a variety of landforms attributed to ice and glacial flow and glacial fluvial deposits.

Venus

In Comparison to Earth

Unlike the other terrestrial planets, Venus is similar to Earth both in size and mean density (5.24 and 5.52 g/cm^3, respectively) (Table 10.2). After correcting for pressure differences, the uncompressed density of Venus is within 1% of that of Earth, indicating that both planets are similar in composition, with Venus having a somewhat smaller core–mantle ratio. Although both planets also have similar amounts of N_2 and CO_2, most of Earth's CO_2 is not in the atmosphere but in carbonates. Venus also differs from Earth by the near absence of water and by the high density and temperature of its atmosphere (Chapter 6). As discussed later, Venus may at one time may have lost massive amounts of water by the loss of hydrogen from the upper atmosphere. Unlike Earth, Venus lacks a satellite, has a slow retrograde rotation (225 Earth days for one rotation), and does not have a measurable magnetic field. The absence of a magnetic field in Venus may be due the absence of a solid inner core, since as discussed in Chapter 5, crystallization of an inner core may be required for a dynamo to operate in the outer core of a planet. Of the total Venusian surface, 84% is flat rolling plains, some of which are over 1 km above the average plain elevation (Figure 10.13). Only 8% of the surface is true highlands, and the remainder (16%) lies below the average radius, forming broad shallow basins. This is very much unlike the topographic distribution on Earth, which is bimodal due to plate tectonics (Figure 10.14). The unimodal distribution of elevation on Venus does not support the existence of plate tectonics on Venus today.

The spectacular *Magellan* imagery indicates that unlike Earth, deformation on Venus is distributed over thousands of kilometers rather than occurring in rather narrow orogenic belts (Solomon et al., 1992). Numerous examples of

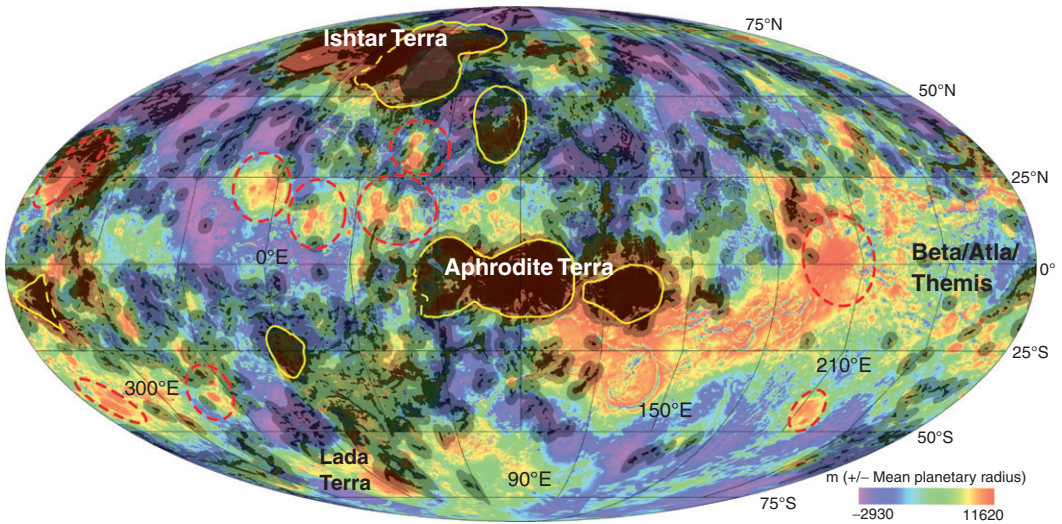

FIGURE 10.13 The surface of Venus with altimetry from Magellan. Tessera terrains in black with yellow outlines showing isostatically supported crustal plateaus; dashed red lines around volcanic rises. Modified from Hansen and Lopez (2010), courtesy of Vicki Hansen and the Geological Society of America.

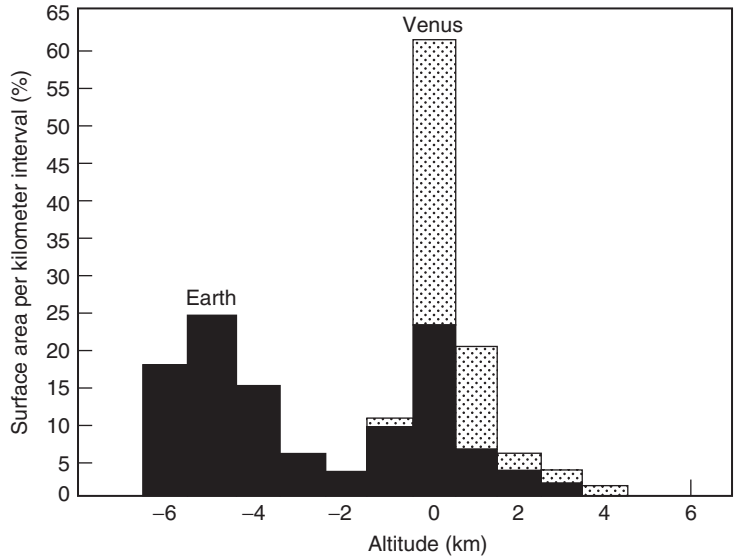

FIGURE 10.14 Comparison of relief on Venus and Earth. Surface height is plotted in 1-km intervals as a function of surface area. Height is measured from a sphere of average planetary radius for Venus and from sea level for Earth. *After Pettengill et al. (1980).*

compressional tectonic features are found on Venus, such as the Maxwell Montes deformational belt in the western part of Ishtar Terra. Ishtar Terra is a crustal plateau about 3 km above mean planetary radius (Figure 10.13) surrounded by compressional features that are suggestive of tectonic convergence resulting in crustal thickening. Maxwell Montes stands 11 km above the surrounding plains and shows a wrinkle-like pattern suggestive of compressional deformation (Kreep & Hansen, 1994). The deformation in this belt appears to have occurred passively in response to horizontal stresses from below.

Coronae are large circular features (60–2600 km in diameter, with most 100–300 km) with a great diversity of morphologies (Stofan et al., 2001). Almost all coronae occur between 80 °N and 80 °S latitude and show a high concentration in equatorial areas. Venus is the only planet known to have coronae. An approximately inverse correlation between crater and corona density suggests that the volcanic-tectonic process that forms coronae may be the same process that destroys craters (Stefanick & Jurdy, 1996). The most widely accepted models for the origin of coronae are those involving mantle plumes or thermals (Figure 10.15). A rising plume creates a region of uplift accompanied by radial deformation and dyke emplacement and a large stratovolcano such as Beta Regio (Figure 10.15) (Copp et al., 1998). Volcanism may also accompany this stage. As the plume head spreads at the base of the lithosphere, it elevates the surface, producing annuli in some coronae. This is generally followed by collapse as the plume head cools.

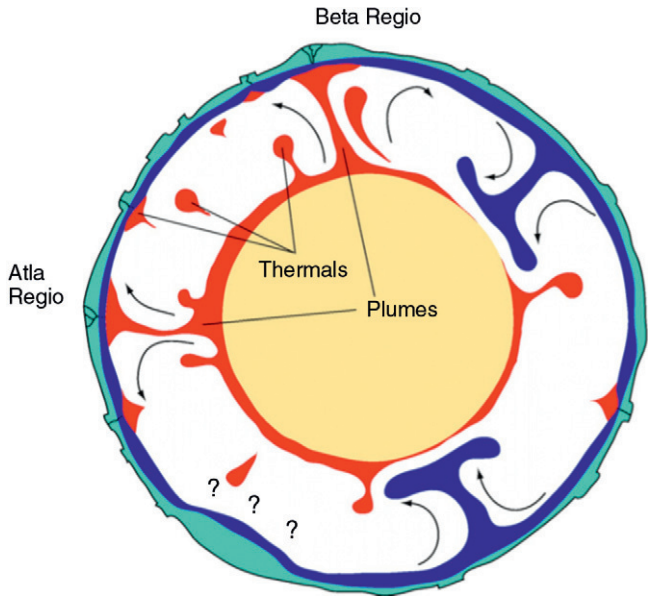

FIGURE 10.15 Model for the internal dynamics of Venus with mixed-mode convection, which explains the dynamically supported coronae and the plateau-like highlands. *Modified after Johnson & Richards (2003), courtesy of Catherine Johnson. Reproduced with permission of American Geophysical Union.*

Perhaps the most important data from the *Magellan* mission are those related to impact craters (Kaula, 1995). Unlike the Moon, Mars, and Mercury, Venus does not preserve a record of heavy bombardment from the early history of the solar system (Price & Suppe, 1994). In fact, crater size and age distributions imply an average age for the Venusian surface of only 800–300 Ma, indicating extensive resurfacing of the planetary surface at this time. Most of this resurfacing is with low-viscosity lavas, mostly basalts as inferred from the *Venera* geochemical data. Crater distribution also indicates a rapid decline in the resurfacing rate within the last few tens of millions of years. However, results suggest that some large volcanoes (72 Ma), some basalt flows (128 Ma) and rifts (130 Ma), and many of the coronae (120 Ma) are much younger than the average age of the resurfaced plains and probably represent ongoing volcanic and tectonic activity (Price et al., 1996).

The differences between Venus and Earth, together with the lower bulk density of Venus, affect the nature and rates of surface processes (weathering, erosion, deposition) as well as tectonic and volcanic processes. Because a planet's thermal and tectonic history is dependent on its size and area/mass ratio as described later, Venus and Earth are expected to have similar histories. However, the surface features of Venus are quite different from those of Earth, raising questions about how Venus transfers heat to the surface and whether

plate tectonics has ever been active. The chief differences between Earth and Venus appear to have two underlying causes: (1) small differences in planetary mass leading to different cooling, degassing, and tectonic histories, and (2) differences in distance from the Sun, resulting in different atmospheric histories.

Volcanism

Volcanism is still active on Venus with notable hotspots that deliver heat, magma, and atmospheric H_2O and SO_2 (Smrekar et al., 2010). Estimates of the eruption age of many surface flows range from a few thousand years to at most 2.5 Ma. Together with gravity and topography measurements, the existence of recently active volcanism supports evidence for active plumes in the mantle. The estimated number of large mantle plumes of about nine (Figure 10.15) is similar to the number believed to come from the D″ layer in Earth in the last 100 Ma. Furthermore the scale of flows on the Venusian surface is most consistent with ongoing rather than catastrophic resurfacing models.

Much has been learned about the surface of Venus from scientific missions by the United States and Russia. The Russian *Venera* landings on the Venusian surface have provided a large amount of data on the structure and composition of the volcanic crust. Results suggest that the majority of the Venusian surface is composed of blocky bedrock surfaces and less than one-fourth contains porous, soil-like material (McGill et al., 1983). The *Venera* landers have also revealed the presence of abundant volcanic features, complex tectonic deformation, and unusual ovoidal features of probable volcanic-tectonic origin. Reflectance studies of the Venusian surface suggest that iron oxides may be important components. Partial chemical analyses made by the *Venera* landers indicate that basalt is the most important rock type. The high K_2O recorded by *Venera* 8 and 13 are suggestive of alkali basalt, while the results from the other *Venera* landings clearly indicate tholeiitic basalt, perhaps with geochemical affinities to terrestrial ocean ridge tholeiites (Figure 10.9). A Venusian crust composed chiefly of tholeiitic basalt is consistent with the presence of thousands of small shield volcanoes that occur on the volcanic plains, typically 1–10 km in diameter and with slopes of about 5°. The size and distribution of these volcanoes resemble terrestrial ocean-island and seamount volcanoes.

The Venusian Core

Venus has no global magnetic field, although it is likely to have a molten outer core, with or without an inner core (Stevenson, 2003). The absence of a dynamo in the outer core probably reflects the lack of convection caused either by the absence of an inner core or because the outer core is not cooling. If the inside of Venus is hotter than the corresponding depth in Earth, which seems likely, an inner core is not expected. Alternatively, or in addition, the Venusian core may not be cooling at present because it is still recovering from heat loss associated with a resurfacing event some 800–300 Ma. Recent thermal models suggest that Venus had a magnetic field for the first 3 Ga, of the same order of strength as

Earth's field (Breuer & Moore, 2007). During this time, thermal convection drove the geodynamo until stopped by continued cooling, but the core was still too hot for an inner core to develop.

Crustal Plateaus

Another unique and peculiar feature of the Venusian surface is the closely packed sets of grooves and ridges known as **tessera**, which cover most of the highland areas and crustal plateaus (Figures 10.13 and 10.16). Global observations of the Venusian surface suggest that the tessera terrains record a prolonged geologic history that predated the formation of most rises and basins (Hansen & Lopez, 2010). Surface patterns of tesserae suggest that crustal plateaus formed individually and that both the tesserae and plateaus formed by the same process. Furthermore, cross-cutting relationships indicate that at least some crustal plateaus are younger than suites of tesserae in adjacent lowlands (Figure 10.16).

Different models for crustal plateau formation have been proposed, but no consensus has yet emerged. The two principal models consider the Venusian plateaus as either the surface expression of downwelling or upwelling mantle flows. The downwelling models usually involve crustal thickening due to compression caused by subsolidus flow on an ancient lithosphere over a downwelling (Bindschadler et al., 1992). In contrast, the upwelling models accomplish lithospheric thickening by magmatic underplating associated with large mantle plumes (Hansen et al., 1999).

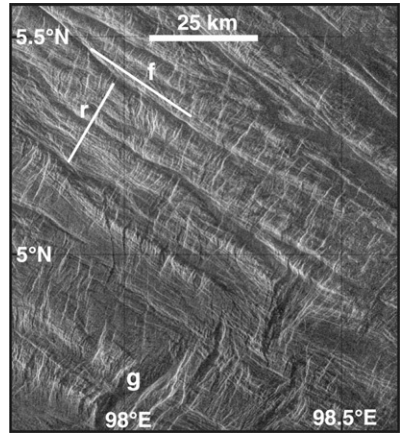

FIGURE 10.16 *Magellan* synthetic-aperture radar image of Venus showing the major tessera terrain fabric. Ribbons 20–100 km long parallel the r line defining alternating flat-topped ridges and narrow steep-sided, flat-bottomed troughs. Folds (parallel to the f line) with wavelengths of <1 km up to 50 km; g is a typical graben. *From Hansen & Lopez (2010), courtesy of Vicki Hansen and the Geological Society of America.*

As an example of a downwelling model, Romeo and Turcotte (2008) suggest that tessera terrains on Venus represent continental crust that does not participate in the periodic recycling of the lithosphere through global detachment events. In their model, the ratio between the crustal and lithospheric mantle thicknesses controls the force balance. If the crust thickness is less than about two-fifths of the lithospheric mantle thickness, the continental area will be compressed, but for higher values the continental area will spread out and collapse. Hence, if the lithospheric mantle beneath a continental region is detached during a global resurfacing event, the continent will collapse, generating tessera inliers dominated by extensional tectonics. But if a significant portion of lithospheric mantle remains, then the continental area will be compressed, generating a plateau by crustal shortening. One advantage of the model is that the observed plateau heights can be explained. Also during the compressional stage concentric fold and thrust belts are generated in the plateau, erasing any impact craters that were present. The pulsating continent model links for the first time the generation of crustal plateaus and the origin of the volcanic plains predicting the observed effective crater density for both terrains.

Thermal History

To understand the tectonic and volcanic processes on Venus, it is first necessary to understand how heat is lost from the mantle. Four sources of information are important in this regard: the amount of ^{40}Ar in the Venusian atmosphere, lithosphere thickness, topography, and gravity anomalies. The amount of ^{40}Ar in planetary atmospheres can be used as a rough index of past tectonic and volcanic activity, because it is produced in planetary interiors by radioactive decay and requires tectonic-volcanic processes to escape. Venus has about one-third as much ^{40}Ar in its atmosphere as does Earth, which implies less tectonic and volcanic activity for comparable ^{40}K contents.

In contrast to Earth, where at least 90% of the heat is lost by the production and subduction of oceanic lithosphere, there is no evidence for plate tectonics on Venus. The difficulty of initiating and sustaining subduction on Venus is probably due to a combination of high mantle viscosity, high fault strength, and thick, relatively buoyant basaltic crust. Thus, it would appear that Venus, like the Moon, Mercury, and Mars, must lose its heat through conduction from the lithosphere, perhaps transmitted upward chiefly by mantle plumes. The base of the thermal lithosphere in terrestrial ocean basins is about 150 km deep, where the average geotherm intersects the wet mantle solidus. On Venus, however, where it is likely that the mantle is dry, an average geotherm does not intersect the dry solidus, indicating the absence of a distinct boundary between the lithosphere and mantle (Figure 10.17). The base of the elastic lithosphere in ocean basins is at the 500°C isotherm or about 50 km deep. Because 500°C is near the average surface temperature of Venus, there is no elastic lithosphere on Venus. Another important difference between Venus and

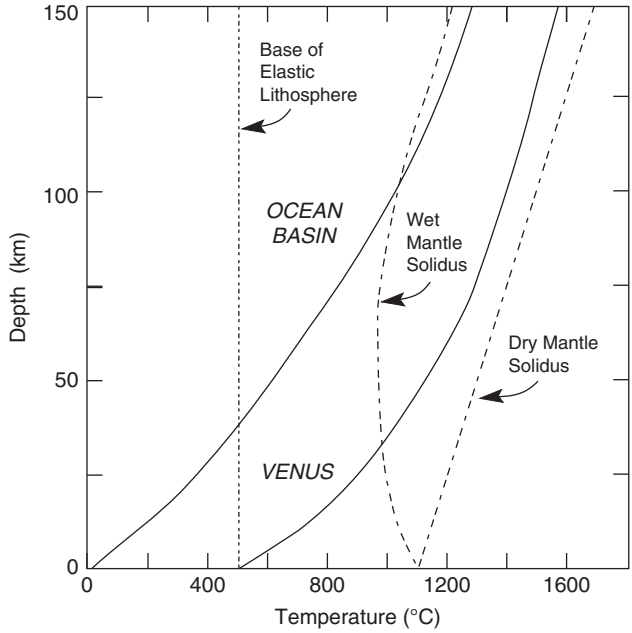

FIGURE 10.17 Comparison of geotherms from an average terrestrial ocean basin and Venus. Conduction is assumed to be the only mode of lithospheric heat transfer on Venus. Also shown are wet (0.1% H_2O) and dry mantle solidi.

Earth is the strong positive correlation between gravity and topography on Venus, implying compensation depths in the Venusian mantle of 100–1000 km. This requires strong coupling of the mantle and lithosphere, and hence the absence of an asthenosphere, agreeing with the thermal arguments above. This situation may have arisen from a lack of water in Venus. One of the important consequences of a stiff mantle is the inability to recycle lithosphere through the mantle, again showing that plate tectonics cannot operate on Venus. The deformed plateaus and the lack of features characteristic of brittle deformation, such as long faults, suggest that the Venusian lithosphere behaves more like a viscous fluid than a brittle solid. The very steep-sided high-elevation plateaus on Venus, however, attest to the high strength of the Venusian lithosphere.

Two thermal-tectonic models, both in the stagnant lid thermal regime, have been proposed for Venus: the conduction model and the mantle plume model (Bindschadler et al., 1992). In the conduction model, Venus loses heat by simple conduction through the lithosphere, and tectonics is a result of compression and tension in the lithosphere in response to the changing thermal state of the planet. It is likely that such a model describes the Moon, Mercury, and Mars at present. Not favoring a conduction model for Venus, however, is the implication that the topography is young, since it cannot be supported for long with a warm, thin lithosphere.

Supporting the mantle plume models for Venus are laboratory experiments on free and forced thermal convection at high Rayleigh numbers ($Ra \sim 10^7$) in a variable-viscosity fluid following a major mantle overturn event (Johnson & Richards, 2003; Robin et al., 2007). Much like the results of Moresi and Solomatov (1998) and O'Neill et al. (2007b), results show an evolution from a stagnant lid regime through an episodic regime ending in a mobile regime (see Figure 9.24). Mantle plumes and isoviscous thermals rise from the thermal boundary layer. Results support the hypothesis that the contemporaneous coexistence of the Atla and Beta highland regions with interspersed uncompensated coronae is consistent with a transient thermal regime following a lithospheric overturn. Thus, thermals (small mantle plumes) dynamically support the coronae, and continuous mantle upwellings (larger plumes) support the highland plateaus (Figure 10.15).

In the plume models, Venus is assumed to lose heat from large mantle plumes coupled with some sort of detachment and sinking of the lithosphere (Turcotte, 1995, 1996). Also consistent with plumes are the deep levels of isostatic gravity compensation beneath large topographic features, suggesting the existence of plumes beneath these features. Unlike Earth, most of the topographic and structural features on Venus can be accounted for by mantle plumes, with compressional forces over mantle downwellings responsible for the compressional features on the surface. On the whole, the geophysical observations from Venus support the idea that mantle downwelling is the dominant driving force for deformation of the surface of Venus. The return flow in the mantle would also occur in downwellings and undoubtedly involve detachment and sinking of significant volumes of the lithosphere (blue regions in Figure 10.15).

Although the Venusian surface ranges from about 800 to 300 Ma in average age (Breuer & Moore, 2007), studies of crater distributions indicate that >80% of the surface had most of its craters removed in a short interval of time, probably between 10 and 100 Ma (Nimmo & McKenzie, 1998). It is still debated whether the resurfacing of the planet was caused by a catastrophic planet-wide mantle plume event or short-lived plate tectonic event (episodic regime) that is the waning stages today, or simply ongoing resurfacing of which the mean age is 800–300 Ma (Strom et al., 1994; Nimmo & McKenzie, 1998).

The Giant Planets

Jupiter and Saturn, the two largest planets, have densities indicating that they are composed chiefly of hydrogen and helium (Table 10.2). In the outer parts of the planets, these elements occur as ices and gases and at greater depths as fluids. The cores of the giant planets include a mixture of high-density ices and silicates. Relative to the Sun, the giant planets are enriched in elements heavier than He. The magnetic fields of these planets vary significantly in orientation or

magnitude, and the origin of these fields is poorly understood. They are not, however, produced by dynamo action in a liquid Fe core, as is the case in Earth. Unlike Jupiter and Saturn, the densities of Uranus and Neptune require a greater silicate fraction in their interiors. Models for Uranus, for instance, suggest a silicate core and icy inner mantle composed chiefly of H_2O, CH_4, and NH_3, and a gaseous and icy outer mantle composed chiefly of H_2 and He. Neptune must have an even greater proportion of silicate and ice. Except for Jupiter, with a 3° inclination to the ecliptic, the outer planets are highly tilted in their orbits (Saturn, 26.7°; Uranus, 98°; Neptune, 29°). Such large tilts probably result from collisions with other planets early in the history of the solar system. Whatever hit Uranus to knock it completely over must have had a mass similar to that of Earth.

Satellites and Planetary Rings

General Features

The solar system has about 60 satellites system. Although there is great diversity in the satellites and no two are truly alike, three general classes of planetary satellites are recognized:

1. *Regular satellites*, which include most of the larger satellites and many of the smaller ones, are those that revolve in or near the plane of the planetary equator and revolve in the same direction as the parent planet moves about the Sun.
2. *Irregular satellites* have highly inclined, often retrograde and eccentric orbits, and some are far from the planet. Many of Jupiter's satellites belong to this category, as do the outermost satellites of Saturn and Neptune (Phoebe and Nereid, respectively). Most, if not all, of these satellites were captured by the parent planet.
3. *Collisional shards* are small, often irregular-shaped satellites that appear to have been continually eroded by ongoing collisions with smaller bodies. Many of the satellites of Saturn and Uranus are of this type. Phobos and Deimos, the tiny satellites of Mars, may be captured asteroids.

There are regularities in satellite systems that are important in constraining satellite origin. For instance, the large regular satellites of Jupiter, Saturn, and Uranus have low-inclination, prograde orbits indicative of formation from an equatorial disk (Stevenson, 1990). Although regular satellites extend to 20–50 planet radii, they do not form a scale model of the solar system. While the large satellites are mostly rocky or rock-ice mixtures, small satellites tend to be more ice rich, suggesting that some of the larger satellites may have lost ice or accreted rock. Very volatile ices, such as CH_4 and N_2, appear only on satellites distant from both the Sun and the parent planet, reflecting the cold temperatures necessary for their formation. One thing that emerges from an attempt to classify satellites is that no general theory of satellite formation is possible.

Planetary Rings

Since the *Voyager* photos of planetary rings in the outer planets, the origin of planetary rings has taken on new significance. Some have suggested that the rings of Saturn can be used as an analogue for the solar nebula from which the solar system formed. Although Jupiter, Saturn, Uranus, and Neptune are now all known to have ring systems, they are all different, and no common theory can explain all of them. Although the rings of Saturn are large in diameter, the thickness of the rings in probably less than 50 m. The average particle size in the rings is only a few meters and single particles orbit the planet in about 1 day. Three models have attracted most attention for the origin of planetary rings. In the first two models, rings are formed with the parent planet as remnants of an accretionary disk or of broken pieces of satellites. Neither of these origins is likely, however, in that the rings should not have survived beyond a few million years and, as discussed below, the rings should have accreted into satellites. Alternatively, the rings may be the debris resulting from the disruption of captured comets such as Charon. In this model the small particles become rings and the larger fragments may become satellites. If the rings around the giant planets are the remains of captured comets, they are latecomers to the solar system, since as we shall see below, comets are among the youngest members of the solar system.

The Moon

As a planetary satellite, the Moon has many unique features. Among the more important are the following, all of which must be accommodated by any acceptable model for lunar origin as discussed in Chapter 9:

1. The orbit of the Moon about the Earth is neither in the equatorial plane of the Earth, nor in the ecliptic, but it is inclined at 5.14° to the ecliptic (Figure 9.1).
2. Except for the Pluto–Charon pair, the Moon has the largest mass of any planet–satellite system.
3. The Moon has a low density compared to the terrestrial planets (Table 10.2), implying a relatively low iron content.
4. The Moon is strongly depleted in volatile elements and enriched in some refractory elements such as Ti, Al, and U (see Figure 9.2).
5. The angular momentum of the Earth–Moon system is anomalously high compared to other planet–satellite systems.
6. The Moon rotates in the same direction as does Earth.

A great deal has been learned about the geochemistry and geophysics of the Moon from the *Apollo* landings (Taylor, 1982, 1992). Although average lunar density is much less than average Earth density (Table 10.2), its uncompressed density is about the same as Earth's mantle, implying that the Moon is composed largely of Fe and Mg silicates. Unlike most other satellites, which are mixtures of silicates and water ice, the Moon must have formed in the inner part of the solar system. Although the Moon is generally considered to be a dry planetary body with

virtually no water, geochemical evidence for water both on the surface and in the interior of the Moon has recently been described (McCubbin et al., 2010). Hydroxyl is reported in lunar apatite, which suggests that hundreds of parts per million of water are present in apatite in the Moon's interior.

From seismometers placed on the Moon by astronauts, we can deduce the broad structure of the lunar interior. The Moon has a thick crust (60–100 km) comprising about 12% of the lunar volume, and it appears to have formed very soon after planetary accretion at 4530–4520 Ma (Figure 10.5). From our limited sampling of the lunar crust by the astronauts, it is composed chiefly of anorthosites and gabbroic anorthosites as represented by exposures in the lunar highlands. These rocks typically have cumulus igneous textures, although modified by impact brecciation. Isotopic dating indicates that this plagioclase-rich crust formed at about 4.5 Ga just after the Moon-forming collision (Figure 10.5). Also characteristic of the lunar surface are the mare basins, large impact basins formed prior to 3.9 Ga, covering about 17% of the lunar surface (Figure 10.18). These basins are flooded with basalt flows that are collectively only 1–2 km thick, and were probably erupted chiefly from fissures.

Isotopically dated mare basalts range from 3.9 to 2.5 Ga. The impacts that formed the mare basins did not initiate the melting that produced the basalts, which were erupted up to hundreds of millions of years later and, thus, represent a secondary crust on the Moon. The youngest basaltic eruptions may be as

FIGURE 10.18 *Mariner 10* photo of the lunar surface showing cratered anorthositic primary crust, and mare basins filled with basalts. Mare Crisium is near the lower right. *NASA Planetary Photo,* Mariner 10*, 1973*.

young as 1 Ga. The lunar crust overlies a mantle comprised of two layers. The upper layer or lithosphere extends to a depth of 400–500 km and is probably composed of cumulate ultramafic rocks. The second layer extends to about 1100 km, where a sharp break in seismic velocity occurs. Although evidence is still not definitive, it appears that the Moon has a small metallic core (300–500 km in diameter), comprising 2–5% of the lunar volume (Figure 10.8).

Although the Moon does not have a magnetic field, remanent magnetization in lunar rocks suggests a lunar-wide magnetic field at least between 3.9 and 3.6 Ga (Fuller & Cisowski, 1987). The maximum strength of this field was probably only about one-half that of the present Earth's field. It is likely this field was generated by fluid motions in the lunar core, much like the present Earth's field is produced. A steady decrease in the magnetic field after 3.9 Ga reflects cooling and complete solidification of the lunar core by no later than 3 Ga.

The most popular model for lunar evolution involves the production of an ultramafic magma ocean that covers the entire Moon to depth of 500 km or more and crystallizes in $<$100 Ma beginning at about 4.45 Ga soon after the Moon-forming collision (Figure 10.19). Plagioclase floats, producing an anorthositic crust, and pyroxenes and olivine largely sink, producing an incompatible-element depleted upper mantle. Later partial melting of this mantle produces the mare basalts. Detailed models for crystallization of the magma ocean indicate the process was complex, involving floating "rockbergs" and cycles of assimilation, mixing, and trapping of residual liquids. The quenched surface and anorthositic rafts were also continually broken up by impact.

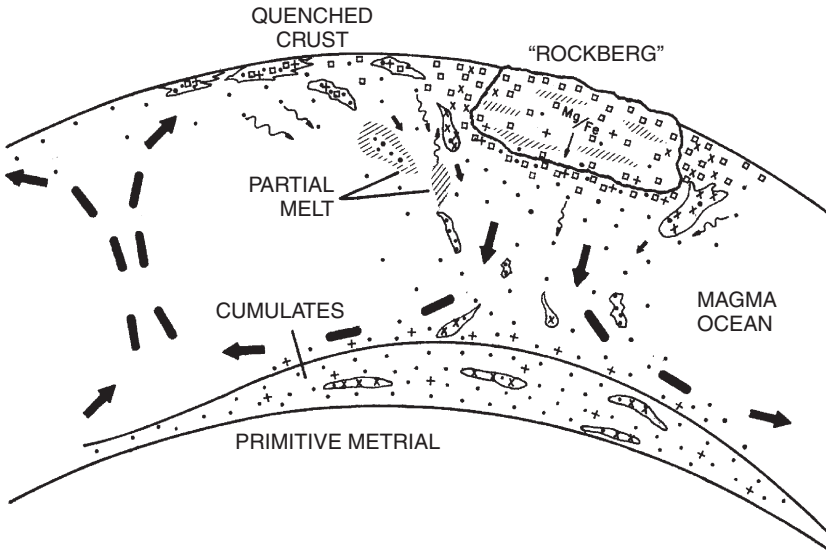

FIGURE 10.19 Schematic diagram of a lunar magma ocean about 4.5 Ga. Arrows are flow patterns and rockbergs are principally anorthosites. *After Longhi (1978).*

Rotational History of the Earth–Moon System

Integration of equations of motion of the Moon indicate that there has been a minimum in the Earth–Moon distance in the geologic past, that the inclination of the lunar orbit has decreased with time, and that the eccentricity of the lunar orbit has increased with time as the Earth–Moon distance has increased (Lambeck, 1980). It has long been known that angular momentum is being transferred from Earth's spin to lunar orbital motion, which results in the Moon moving away from the Earth. The current rate of this retreat is about 5 cm/y. The corresponding rotational rate of Earth has been decreasing at a rate of about 5×10^{-22} rad/s. Tidal torques cause the inclination of the Moon's orbit to vary slowly with time as a function of the Earth–Moon distance. When this distance is greater than ~10 Earth radii, the lunar orbital plane moves toward the ecliptic, and when it is <10 Earth radii, it moves toward Earth's equatorial plane. For an initially eccentric orbit, the transfer of angular momentum is greater at perigee than apogee, and hence the degree of eccentricity increases with time. These evolutionary changes in angular momentum of the Earth–Moon system result in changes in the length of the terrestrial day and month.

Many groups of organisms secrete sequential layers that are related to cyclical astronomical phenomena. Such organisms, which are known as **biological rhythmites** (Pannella, 1972), provide a means of independently evaluating the calculated orbital retreat of the Moon. The most important groups are corals and bivalves. Daily increments in these organisms are controlled by successive alternation of daylight and darkness. Seasonal increments reflect changes in the length of sunlight per day, seasonal changes in food supply, and in some instances, tidal changes. Actual growth patterns are complex, and local environmental factors may cause difficulties in identifying periodic growth patterns. Results from Phanerozoic bivalves and corals, however, are consistent and suggest a decreasing rotational rate of Earth of about 5.3×10^{-22} rad/s (Figure 10.20), which is in good agreement with the astronomical value above. This corresponds to 420–430 days/y at 500–400 Ma. Stromatolites also deposit regular bands, although a quantitative relationship of banding to astronomical rhythm has not yet been established (Cao, 1991). The interpretation of stromatolite bands from the Biwabik Iron Formation in Minnesota is that at 2000 Ma there were 800–900 days/y (Figure 10.20) (Mohr, 1975). Another type of geochronometer has been recognized in laminated fine-grained sediments, known as **sedimentological rhythmites**. Cyclically laminated Neoproterozoic (750–650 Ma) tidal sediments from Australia have been interpreted to record paleotidal periods as well as paleorotation of Earth (Williams, 1989). Results suggest that 650 Ma, there were 13 months/y and 450 days/y. When both biologic and sedimentary rhythmite data are plotted with time, results suggest a sublinear relationship with the number of days per year decreasing at about 0.2 day/Ma, in good agreement with the extrapolation of astronomical calculations. However, determination of absolute Earth–Moon distances from

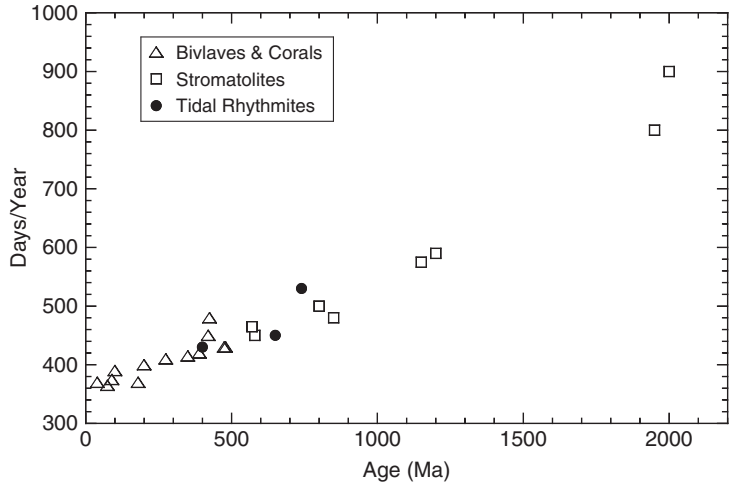

FIGURE 10.20 Terrestrial days per year as inferred from biological and sedimentological rhythmites.

biological and sedimentary rhythmites remains ambiguous because of the difficulties in determining the absolute length of the ancient lunar sidereal month (Mazumder & Arima, 2005).

If the Moon came within the Roche limit of Earth (~2.9 Earth radii) after it formed some 4.5 Ga, a record of such a close encounter should be preserved. The **Roche limit** is the distance at which tidal forces of the planet fragment a satellite and disrupt the surface of the planet. Even if the Moon survived this encounter without disintegrating, the energy dissipated in the two bodies would largely melt both bodies and completely disrupt and recycle any crust. The preservation of 4.5-Ga crust on the Moon strongly indicates that the Moon has not been within Earth's Roche limit since it formed about 4.5 Ga, and thus the relationship in Figure 10.20 cannot be extrapolated much before 2 Ga.

Satellite Origin

Regular satellites in the outer solar system are commonly thought to form in disks around their parent planets. The disks may have formed directly from the solar nebula as the planets accreted, and the satellites grew by collision of small bodies within the disks. Alternatively, the disks could form by the breakup of planetesimals when they came within the Roche limit**.** Still other possible origins for planetary disks include spin-off due to contraction of a planet and outward transfer of angular momentum, and massive collisions between accreting planets. The collisional scenario is discussed for the origin of the Moon in Chapter 9. Regardless of the way it originates, once a disk is formed, computer modeling indicates that satellites will accrete in very short periods of time of the order of 1 Ma. The irregular satellites and collisional shards, however, cannot be

readily explained by the disk accretion model. This has led to the idea that many satellites have been captured by the gravity field of their parent planet, during a near collision of the two bodies. As dictated by their compositions, some of the rocky satellites in the outer solar system may have accreted in the inner solar system, and their orbits were perturbed in such a manner to take them into the outer solar system where they were captured by one of the Jovian planets.

Comets and Other Icy Bodies

Comets are important probes of the early history of the solar system, since compared to other bodies in the solar system, they appear to have been least affected by thermal and collisional events (Wyckoff, 1991). Comet heads are small (radii of 1–10 km) and have a low density (0.1–1 g/cm^3). Because of their highly elliptical orbits, comets reside in a "dormant state" most of the time in the outer reaches of the solar system at temperatures $\leq$180°C, in what is known as the Edgeworth-Kuiper belt (30–1000 AU from the Sun) and the Oort cloud (1000–50 000 AU) (Stern, 2003). Perturbations of cometary orbits by passing stars have randomized them, making it difficult to determine where comets originally formed in the solar nebula. However, the presence of CO_2 and sulfur in comets suggests that they formed in the outer cold regions of the nebula. Only for a few months do most comets come close enough to the Sun (0.5–1.5 AU) to form vaporized tails. Short-period comets, which orbit the Sun in less than 200 years, appear to come from just beyond Neptune at 35–50 AU in the Edgeworth-Kuiper belt. Closely related to comets are Pluto and Triton (a large satellite of Neptune) and related icy bodies in the outer solar system. Pluto, which is about 0.2 the mass of the Moon, has a highly inclined and eccentric orbit (Table 10.2). It has one satellite, Charon, whose orbit is inclined 90° to the ecliptic. Charon is much less dense than Pluto and contains a large volume of ice, whereas Pluto has a greater silicate content. It is generally thought that Charon was produced by a collision with Pluto, stripping some of the ice from Pluto, which re-accreted into the satellite. We now realize that Pluto is really not a planet, but is more closely related to comets. However, it has too great a density to be a typical comet, perhaps increasing in density during the collision that formed Charon.

Our knowledge of cometary composition was greatly increased by the *Giotto* mission in 1986 during a close approach to comet Halley (Jessberger & Kissel, 1989). The nucleus of comet Halley is very irregular in shape and its surface is covered with craters, as well as with a layer of dark dust up to 1 m thick. How much dust (silicates, oxides) resides inside this or other comets is still unknown. Model calculations, however, indicate that the dust/ice ratio in comets is of the order of 0.5–0.9. Data show that the gaseous component in Halley is composed chiefly of water vapor with only traces of CO_2, CO, CH_4, and NH_3 (Nuth, 2001). Because the ratios of these gases are dissimilar from the Sun, it appears that the material composing Halley is not primitive, but has been fractionated. Also compared to solar abundances, hydrogen is strongly depleted in Halley. So what is the origin

of the great clouds of comets in the solar system? Because the original solar nebula probably did not have enough mass to extend to the Oort cloud, comets must have been added later to form this cloud. The giant planets appear to have ejected icy bodies out of the inner solar system to >50 AU and in this manner the outer part of the solar system became populated with great clouds of comets. In this respect, comets are some of the youngest members of the solar system.

Asteroids

Asteroids are small planetary bodies, most of which revolve about the Sun in an orbit between Mars and Jupiter (Lebofsky et al., 1989; Taylor, 1992). Of the 10000 or so known asteroids, most occur between 2 and 3 AU from the Sun (Figure 10.21). The total mass of the asteroid belt is only about 5% of that of the Moon. Only a few large asteroids are recognized, the largest of which is Ceres with a diameter of 933 km. Most asteroids are <100 km in diameter and many of them have diameters of 20–30 km. Three main groups of asteroids are recognized: (1) the Near-Earth asteroids (Apollo, Aten, and Amor classes), some of which have orbits that cross that of Earth; (2) the main belt asteroids; and (3) the Trojans, revolving in the orbit of Jupiter (Figure 10.21). Most meteorites arriving on Earth are coming from the Apollo asteroids. The orbital gaps where no asteroids occur in the asteroid belt (for instance, at 3.8 and 2.1 AU, Figure 10.21), appear to reflect orbital perturbations caused by resonances in the gravity field of Jupiter. In terms of spectral studies, asteroids vary significantly in composition (Table 10.3), and some can be matched to meteorite groups. Within the asteroid belt, there is a zonal arrangement that reflects chemical composition. S, C, P, and D asteroid classes

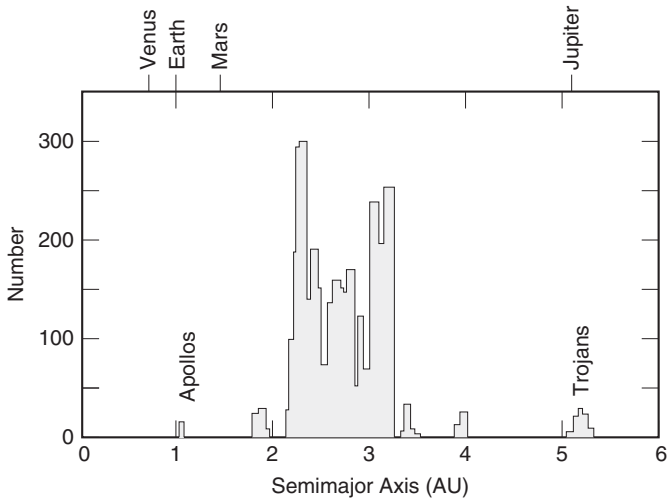

FIGURE 10.21 Histogram of frequency of asteroid distances from the Sun. Distance from Sun is in astronomical units (1 AU = Earth–Sun distance).

TABLE 10.3 Characteristics of Major Asteroid Classes

Low-Albedo Classes	
C	Common in the outer part of the asteroid belt at 3 AU; perhaps parental to carbonaceous chondrites
D	Found close to the orbit of Jupiter (5 AU); no meteorite analogues
P	Common near 4 AU; no meteorite analogues
Moderate-Albedo Classes	
M	Common in main asteroid belt (3 AU); similar to Fe meteorites
Q	Apollo and related asteroids that cross Earth's orbit; parental to major chondrite meteorite groups
S	Common in inner parts of asteroid belt (2 AU); some in Earth-crossing orbits; may be parental to pallasites and some Fe meteorites

occupy successive rings outward in the belt, whereas M types dominate near the middle, and B and F types near the outer edge. The broad pattern is that fractionated asteroids dominate in the inner part of the belt, and the low-albedo primitive types (class C) occur only in the outer portions of the belt. Thus, asteroids inward of 2 AU are igneous asteroids, and the proportion of igneous to primitive asteroids decreases outward such that by 3.5 AU, no igneous types are represented. Although asteroids are continually colliding with each other as indicated by the angular and irregular shapes of most, the remarkable compositional zonation in the asteroid belt indicates that mixing and stirring in the belt must be relatively minor.

The existence of the asteroid belt raises some interesting questions about the origin of the solar system. Why is there such a depletion in mass in this belt in comparison to that predicted by interpolation of planetary masses? Was there ever a single small planet in the asteroid belt and if not, why? Cooling rate data from iron meteorites that come from the asteroids, as well as an estimate of the tidal forces of Jupiter, indicate that a single planet never existed in the asteroid belt. The tidal forces of Jupiter would fragment the planet before it grew to planetary size. Hence, it appears that the asteroids accreted directly from the solar nebula as small bodies, and they have subsequently been broken into even smaller fragments by continuing collisions. The depletion of mass in the asteroid belt may also be due to Jupiter. Because of its large gravitation field, it is likely that Jupiter swept up most of the mass in this part of the solar system. Asteroid growth stopped in most bodies when they reached about 100 km in diameter, as the belt ran out of material. Furthermore, the preservation of what appears to be basaltic crust on some asteroids suggests that they have survived for 4.55 Ga, when melting occurred in many asteroids as determined by dating fragments of these bodies that arrived on Earth as meteorites.

Meteorites

Meteorites are small extraterrestrial bodies that have fallen on Earth. Most meteorites fall as showers of many fragments, and more than 3000 individual meteorites have been described. Meteorites range in size from dust particles to bodies hundreds of meters across. Those with masses of more than 500 g fall on Earth at a rate of about one per $10^6 km^2$ per year. Meteorites have also been found on the Moon's surface and presumably occur also on other planetary surfaces. One of the best preserved and largest suites of meteorites is found within the ice sheets of Antarctica. To avoid contamination, when they are chopped out of the ice, they are given special care and documentation similar to the samples collected on the Moon's surface. Trajectories of meteorites entering Earth's atmosphere have been measured and indicate that most come from the asteroid belt. Others are fragments ejected off the lunar surface or other planetary surfaces by impact. Most appear to have been produced during collisions between asteroids. Meteorites date to 4.56–4.55 Ga, supporting an origin as fragments of asteroids formed during the early stages of accretion in the solar nebula. Many meteorites are breccias in that they are composed of an amalgamation of angular rock fragments tightly welded together. These breccias formed during collisions on the surfaces of asteroids, and in some cases, melting occurred around fragment boundaries as reflected by the presence of glass.

Meteorites are classified as **stones**, including chondrites and achondrites, **stony-irons**, and **irons** depending on the relative amounts of silicates and Fe-Ni metal phases present. **Chondrites**, the most widespread meteorites, are composed in part of small silicate spheroids known as **chondrules** (Figure 10.22),

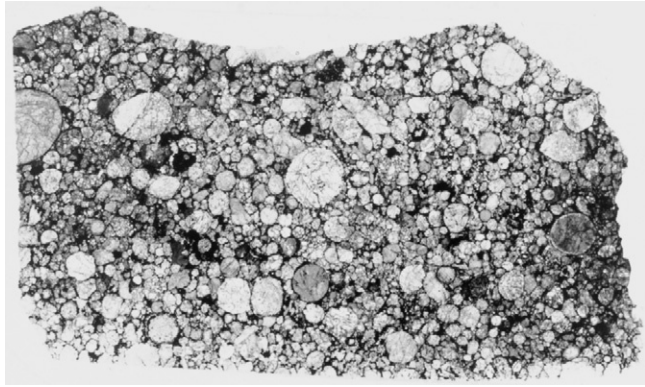

FIGURE 10.22 Thin section of the Inman chondrite. Photomicrograph shows chondrules (circular bodies), which are about 1 mm in diameter. The chondrules, which formed by rapid cooling of liquid droplets, are composed of olivine and pyroxene crystals surrounded by metallic iron (black). Long dimension about 2.5 cm. *Courtesy of Rhian Jones.*

and have chemical compositions similar to that of the Sun. **Achondrites**, which lack chondrules, commonly have igneous textures and appear to have crystallized from magmas, and thus preserve the earliest record of magmatism in the solar system. Many achondritic meteorites come from fractionated asteroid parent bodies, and at least some of these must have been covered with magma oceans (Greenwood et al., 2005). Some achondrites are breccias that probably formed on asteroid surfaces by impact. Stony-irons and irons have textures and chemical compositions that suggest they formed in asteroid interiors by fractionation and segregation of melts. The metal in meteorites is composed of two phases of Fe-Ni, which are intergrown producing the Widmanstätten structure visible on polished surfaces of iron meteorites.

Chondrites

Chondrites are the most common meteorite and are composed of two components: chondrules and matrix (Figure 10.22). Chondrules have a restricted size range of 0.2–4 mm in diameter, with most <1 mm. Despite considerable diversity in the composition of individual chondrules, mean compositions of chondrules from various groups of chondrites are very similar suggesting they were well mixed before accreting into parent bodies. One group of chondrites, the **carbonaceous chondrites** are of special interest. These meteorites are hydrated, contain carbonaceous matter, and have not been subjected to temperatures $>200°C$ for carbonaceous compounds to survive. They consist of a matrix of hydrated Mg silicates (principally chlorite and serpentine) enclosing chondrules of olivine and pyroxene. An important chemical feature of carbonaceous chondrites is that they contain elements in approximately solar ratios, suggesting they are primitive, and many investigators think one class of carbonaceous chondrites (type I or C1) is a sample of the primitive solar nebula from which the solar system formed. Matrices typically show wide variations in chemical and mineralogical composition that are thought to reflect differences in chemical composition within the solar nebula.

Although it is clear that chondrules are the products of rapid cooling of liquid droplets, it is not yet agreed how and just where in the solar nebula this occurred. Relative to primitive carbonaceous chondrites, chondrules are enriched in lithophile elements and depleted in siderophile and chalcophile elements. This provides an important boundary condition for chondrule origin, in that the material from which they formed must have undergone earlier melting to fractionate elements prior to chondrule formation. This would seem to eliminate an origin for chondrules by direct condensation from the solar nebula. An alternative to nebular condensation is that chondrules formed by melting of preexisting solids in the solar nebula, which is the only mechanism that can explain all of the physical and chemical constraints. It would appear that metal, sulfide, and silicate phases must have been present in the nebula before chondrule formation, and that chondrules formed by rapid melting and cooling of these substances. What caused the melting? Perhaps there were nebular flares,

analogous to modern solar flares, that released sudden bursts of energy into the nebular cloud that instantly melted local clumps of dust, which chilled, forming chondrules, and these chondrules were later accreted into asteroids.

SNC Meteorites

The **SNC meteorites** (named after Shergotty, Nakhla, and Chassigny meteorites) have distinct chemical compositions requiring that they come from a rather evolved planet, probably Mars (Marti et al., 1995). SNC meteorites are fine-grained igneous cumulates of mafic or komatiitic composition. The most convincing evidence that they have come from Mars is the presence of a trapped atmospheric component similar to the composition of the Martian atmosphere as determined from spectral studies. Also, the major element composition of shergottites is very similar to the compositions measured by the *Viking* lander on the Martian surface. Because of the problems of ejecting material from the Martian surface, it is possible that SNC meteorites were all derived from a single large impact that occurred about 200 Ma. Sm/Nd isotopic ages suggest that some of these meteorites crystallized from magmas about 1.3 Ga, at shallow depths. One Martian meteorite from Antarctica (ALH84001), however, yields a Lu/Hf age of about 4091 ± 30 Ma, and appears to represent a fragment of the Martian Ancient Cratered Terrane, possibly some of the oldest crust preserved in the solar system.

Refractory Inclusions

Meteorite breccias contain a great variety of components, which have been subjected to detailed chemical studies. Among these are inclusions rich in refractory elements (such as Ca, Al, Ti, and Zr) known as **CAIs** (Ca- and Al-rich inclusions), which range in size from dust to a few centimeters across. Stable isotope compositions of these inclusions indicate that they are foreign to our solar system (Taylor, 1992). Because the sequence of mineral appearance in CAIs does not follow that predicted by condensation in a progressively cooling solar nebula, and differs from inclusion to inclusion, it is probable that local rather than widespread heating occurred in their nebular sources. Some appear to be direct condensates from a nebular cloud, while others show evidence favoring an origin as a residue from evaporation. The ages of CAIs indicate they became incorporated in our solar nebula during the early stages of condensation and accretion. Just where they came from and how they became incorporated in the solar nebula, however, remains a mystery, although they may be inherited from a nearby supernova.

Iron Meteorites and Parent Body Cooling Rates

It is likely that most iron meteorites come from the cores of asteroids. For such cores to form, the parent bodies must have melted soon after or during accretion, with molten Fe-Ni settling to the center. It is possible to constrain the cooling rates of iron meteorites from the thickness and Ni content of kamacite bands. This, in turn, provides a means of estimating the size of the parent body, since

smaller parent bodies cool faster than larger ones. Calculated cooling rates are generally in the range of 1 to 10°C/Ma, which indicates an upper limit for the radius of parent bodies of 300 km with most lying between 100 and 200 km. Such results clearly eliminate the possibility that a single planet was the parent body for meteorites and asteroids. This conclusion is consistent with that deduced from estimates of Jupiter's tidal forces, which also indicate that a single planet could not form in the asteroid belt.

Asteroid Sources

From a combination of mineralogical and spectral studies of meteorites and from spectral studies of asteroids, it is possible to assign likely parent bodies of some meteorites to specific asteroid groups (Lebofsky et al., 1989). The most remarkable spectral match is between the visible spectrum of the third largest asteroid, 4 Vesta, and a group of meteorites known as basaltic achondrites (Figure 10.23). Supporting this source is the fact that Vesta occurs in an orbit with a 3:1 resonance, which is an "escape hatch" for material knocked off Vesta to enter the inner solar system. Most groups of meteorites do not seem to have

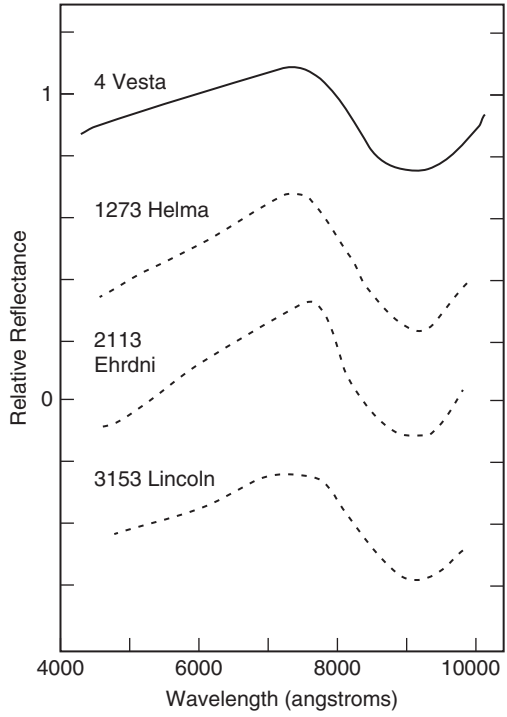

FIGURE 10.23 Comparison of the visible reflectance of asteroid 4 Vesta with three basaltic achondrite meteorites that may have been derived from Vesta.

spectral matches among the asteroids, including the most common meteorites, the chondrites. This may be due to what is generally referred to as "space weathering" of asteroid surfaces changing their spectral characteristics (Pieters & McFadden, 1994). However, no evidence to support this idea has yet been recovered. Another possibility is that the asteroid parents of most chondrites are smaller than we can resolve with our remote sensing on Earth.

Meteorite Chronology

Sm/Nd, Rb/Sr, Hf/W, and Re/Os isotopic ages record the times of accretion and partial melting in meteorite parent bodies. As discussed earlier in the chapter, the ^{182}Hf-^{182}W isotopic system provides the most precise chronology of accretion and earliest evolution of the asteroids prior to their breakup (Kleine et al., 2009). The ages cluster between 4.56 and 4.53 Ga, which is currently the best estimate for the age of the solar system (Figure 10.24).

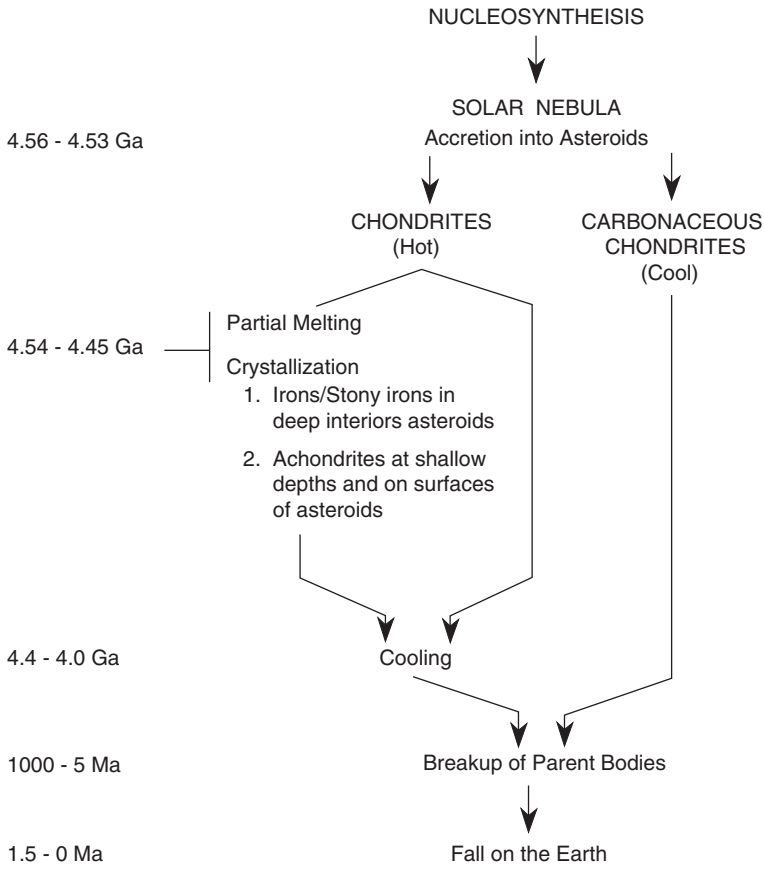

FIGURE 10.24 Summary of the history of meteorites and asteroids.

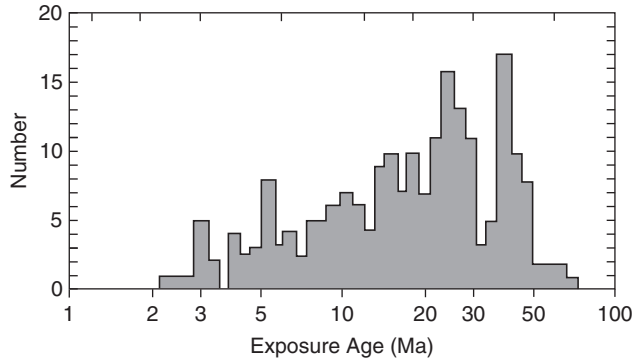

FIGURE 10.25 Histogram of cosmic-ray exposure ages of L-chondrites. *After Marti & Graf (1992).*

The oldest reliably dated objects in the solar system are the CAIs in Allende meteorite at 4568 Ma. The oldest Sm/Nd ages that reflect melting of asteroids are from basaltic achondrites at 4539 ±4 Ma. Iron meteorite ages range from 4.56 to 4.46 Ga, with some of them forming in <1 Ma after the CAIs. K/Ar dates from meteorites reflect the cooling ages of the parent bodies and generally fall in the range of 4.4 to 4.0 Ga.

Fragmentation of asteroids by continual collisions exposes new surfaces to bombardment with cosmic rays. Interactions of cosmic rays with elements in the outer meter of meteorites produces radioactive isotopes that can be used to date major times of parent-body breakup (Marti & Graf, 1992). Stone meteorites have cosmic-ray exposure ages of 100–5 Ma, as illustrated by L-chondrites (Figure 10.25), while irons are chiefly 1000–200 Ma. The peak at about 40 Ma in the L-chondrite exposure ages is interpreted as a major collisional event between asteroids at this time. The differences in exposure ages between stones and irons reflect chiefly the fact that irons are more resistant to collisional destruction than stones. After a meteorite falls on Earth, it is shielded from cosmic rays and the amount of parent isotope remaining can be used to calculate a so-called **terrestrial age**, which is the time at which the meteorite fell on Earth's surface and became effectively cut off from a high cosmic-ray flux. Although most terrestrial ages are less than 100 years, some as old as 1.5 Ma have been reported (Figure 10.24).

IMPACT CHRONOLOGY OF THE INNER SOLAR SYSTEM

We have long known that impacts on planetary surfaces play an important role in planetary evolution. Impact effects are known on varying scales from dust size to planetary size, and have occurred throughout the history of the solar system. A considerable amount of effort has gone into studying the impact record of the inner solar system as recorded on the lunar surface, and this record

is now used to estimate the ages of craters on other planets. The sequence of events (volcanism, rifting, erosion, etc.) on a planetary or satellite surface can be deduced from cross-cutting relationships of craters, and if we can date important events, we can then tie this relative history to absolute ages (Price et al., 1996). This, of course, assumes that we can estimate the impact flux rate with time. It is well known that most of the large impacts on the lunar surface were early, terminating about 3.9 Ga, with the large Imbrium impact (Figure 10.18). Although the termination of major impacts in the inner solar system was likely very early, it may not have been synchronous throughout. However, the striking similarity of age/crater density curves on the Moon, Mercury, Venus, Mars, and asteroids strongly suggests a similar impact history for the inner part of the solar system, and hence it is probably valid to use the lunar timescale throughout this region. All of these bodies appear to have been "resurfaced" by the Late Heavy Bombardment (LHB) at about 3.9 Ga (Kring & Cohen, 2002; Koeberl, 2006). The source of the impacting debris still remains problematic. Favoring a cometary source is the extremely high Ir content of some sedimentary rocks from the 3.8-Ga Isua greenstone belt in Southwest Greenland (Jorgensen et al., 2009). If these sediments were deposited during the LHB, their Ir contents indicate that an equivalent depth of at least 1 km of water was delivered by the colliding comets.

In addition, the early impact history of Earth is at least partially preserved in Early Archean sediments in South Africa and Western Australia (Glikson, 2008). At least 10 thin layers of sand-size spherules, interpreted as impact spherules, were deposited in both regions within two relatively narrow time windows: 3.47–3.23 and 2.64–2.49 Ga (Simonson & Harnik, 2000). Each layer is thought to be the product of a large asteroid-size impactor. The oldest recognized impact, as dated by precise U/Pb isotopic ages from impact-produced zircons in the ejecta, occurs in both South Africa and Western Australia at 3470 $\pm$ 2 Ma (Byerly et al., 2002). The spherule beds are extremely enriched in platinum-group elements, unlike modern volcanic ejecta. Confirming the presence of asteroid material in late Archean impact layers are anomalous Cr isotopic compositions and large Ir anomalies in some of the spherule beds (Kyte et al., 2003). Both platinum-group elements and Cr isotopes indicate that most, if not all, late Archean impactors were chondritic in composition (Simonson et al., 2009); in contrast, the early Archean impact layers have geochemical signatures of carbonaceous chondrites.

VOLCANISM IN THE SOLAR SYSTEM

Although volcanism is widespread on the terrestrial planets and many planetary satellites, it is highly variable in terms of types of eruptions (Wilson, 2009). In a Plinian eruption on a planet with a significant atmosphere, the jet of gas and pyroclastic material emerging from the vent will entrain atmospheric gases.

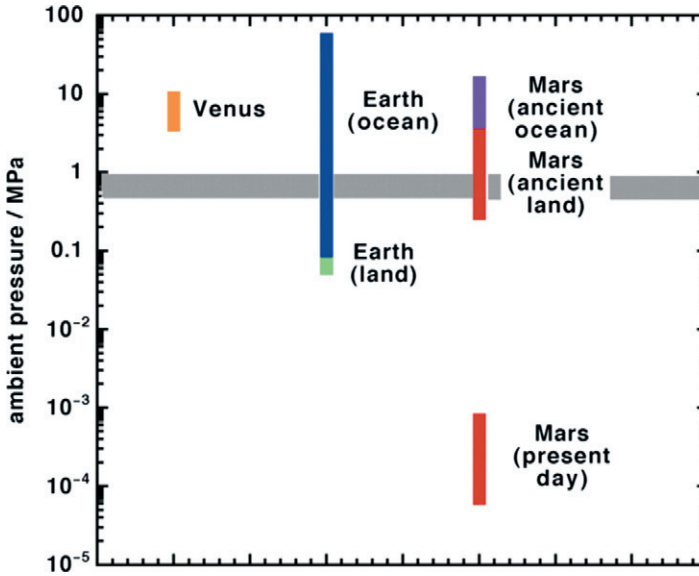

FIGURE 10.26 Relationship of fluid pressure to explosive volcanic eruptions. Vertical bars represent eruption types. The horizontal gray band divides fragmental eruptions (below) from lava eruptions (above). All bodies lacking atmospheres (e.g., Moon, Mercury, Io, asteroids) lie off the bottom of the diagram. *Used with permission of Nature Publishing Group, permission conveyed through Copyright Clearance Center, Inc.*

This slows the gas jet down, but heating of the entrained gas initiates convection and makes the gas more buoyant and pyroclasts settle and are dispersed by the wind. The atmospheric pressure on Venus ranges from ~9 MPa in the lowlands to ~4 MPa over the highest mountains (Figure 10.26). Elevation differences above sea level on Earth produce a range of pressures from ~0.1 to 0.06 MPa, but pressures up to ~50 MPa apply for eruptions on the seafloor. The current atmospheric pressure range for volcanoes on Mars is ~700 to ~70 Pa, but the early atmosphere on Mars may have had a pressure greater than that of present-day Earth, perhaps ~0.3 MPa, and eruptions on the floor of a putative 3-km-deep early northern hemisphere ocean would then have experienced pressures of ~12 MPa. The atmospheric pressure is now, and almost certainly always has been, close to zero on Mercury, our Moon, Io, and Triton.

The gray-shaded band in Figure 10.26 is a typical range of pressures over which the conversion of magma from a liquid containing gas bubbles to a continuous gas stream entraining pyroclasts takes place. This suggests that Plinian eruptions should be impossible on Venus unless magmas contain a very unusually large content of volatiles. On Earth, most steady eruptions on land and in shallow water should be explosive, whereas deep submarine eruptions should not. On Mars, all steady eruptions under present-day conditions should be

explosive. Finally all eruptions on bodies lacking an atmosphere should be extremely explosive unless magmas have minuscule volatile contents (Wilson, 2009).

PLANETARY CRUSTS

Planetary crusts are of three types (Breuer & Moore, 2007; Taylor & McLennan, 2009). **Primary crust** forms during or immediately after planetary accretion by cooling at the surface of a magma ocean. By analogy with the preserved primary crust on the Moon and probably on Mercury, primary crusts on the terrestrial planets may have been anorthositic in composition, produced by flotation of plagioclase during rapid crystallization of magma oceans. If a crust formed on Earth's magma oceans, it also would be an example of a primary crust. Primary crust can be strongly enriched in incompatible elements and may have significantly depleted the mantle during its formation. **Secondary crust** arises later from partial melting of recycled primary crust, or from partial melting of planetary interiors. Secondary crusts are typically basaltic in composition, and their formation further depletes the mantle in incompatible elements. They are produced by partial melting of ultramafic rocks in planetary mantles and in mantle plumes. Examples include the lunar maria basalts, Earth's oceanic crust, and perhaps most of the crust preserved on Mars and Venus. Mechanisms of production of secondary crust may vary: on Earth most secondary crust is produced at ocean ridges as part of the plate tectonic cooling regime, whereas on Venus secondary crust may be chiefly produced at hotspots associated with mantle plumes. Both primary and secondary crust may also be produced on satellites. **Tertiary crust** is formed by partial melting and further processing of secondary crust in subduction zones, and Earth's continents may be the only example of tertiary crust in the solar system.

In the absence of crustal recycling by plate tectonics or some other mechanism, crustal growth on planets is essentially irreversible, leading to a stagnant lid tectonic regime (as discussed in Chapter 9).

PLATE TECTONICS

Plate tectonics on Earth is driven by the subduction of cool, dense lithospheric slabs into the underlying mantle. For such a regime to exist on any planet, stresses associated with mantle convection must exceed the strength of the lithosphere (O'Neill et al., 2007a). At present, this condition is sufficiently restrictive that plate tectonics operates only on Earth, and mantle convection in most terrestrial planets and the Moon is probably in a stagnant lid regime. Convective stresses at the base of the lithosphere depend on the viscosity contrast and velocity of underlying cold downwellings. The lithospheric yield stress is controlled by its friction coefficient and elastic thickness (the depth to the brittle–ductile transition). Both convective stresses and a plate's yield strength depend critically on the size, thermal state, and cooling history of a planet. O'Neill et al. (2007a) use numerical simulations

and scaling theory to identify conditions in which mantle convection leads to lithospheric failure for a range of conditions relevant to the terrestrial planets. Whereas Earth is expected to have been in a plate tectonic regime at least for the last 3 Ga (see Figure 9.24), the Moon and Mercury are expected to have always remained in a stagnant lid regime. Venus, Io, and Europa currently fall in the episodic regime, which is consistent with episodic resurfacing of Venus, and suggests such resurfacing for Io and Europa. These results allow but do not necessitate that Venus may have been in a plate tectonic regime in the past. While currently in the stagnant lid regime, it is possible that Mars may have also been in the mobile or episodic regime in the past, depending on whether there was liquid water on the surface.

MINERAL EVOLUTION

The mineralogy of terrestrial planets evolves as a consequence of a range of physical, chemical, and biological processes (Hazen et al., 2008). In prestellar molecular clouds, widely dispersed microscopic dust particles contain approximately a dozen refractory minerals that represent the starting point of planetary mineral evolution. Protoplanetary disk formation, star formation, and the resultant heating in the stellar nebula produce the refractory constituents of chondritic meteorites, including chondrules and CAIs, with ~60 different mineral phases. Later aqueous and thermal alteration of chondrites, asteroidal differentiation, and the formation of igneous achondrites adds ~250 more minerals that we find in unweathered meteorites. With the onset of plate tectonics and associated convergent magmatism, 1500 new minerals were added to the list by such processes as fractional crystallization, crystal settling, metamorphism, large-scale fluid–rock interactions, evaporite deposition, and surface weathering. Biological processes began to affect Earth's surface mineralogy by about 3.8 Ga when banded iron formation was deposited under the influence of changing atmospheric and ocean composition. The Great Oxidation Event at 2350 Ma (Chapter 6) and the Neoproterozoic oxidation events, together with several major glaciations, ultimately gave rise to multicellular life. The increasing oxygen content of the atmosphere together with skeletal biomineralization irreversibly transformed Earth's surface mineralogy by the end of the Precambrian. In fact, biochemical processes may be responsible, directly or indirectly, for most of Earth's 4300 known mineral species.

The stages of mineral evolution arise from three primary mechanisms: (1) the progressive separation and concentration of the elements from their original relatively uniform distribution in the presolar nebula; (2) an increase in range of intensive variables such as pressure, temperature, and the activities of H_2O, CO_2, and O_2; and (3) the generation of disequilibrium conditions by living organisms. The sequential evolution of Earth's mineralogy from chondritic simplicity to Phanerozoic complexity introduces the dimension of geologic time to mineralogy and provides a dynamic alternative approach to studying mineral and rock evolution.

EVOLUTION OF THE ATMOSPHERES OF EARTH, VENUS, AND MARS

The only three terrestrial planets that have retained atmospheres are Earth, Venus, and Mars, yet the compositions and densities of their atmospheres differ significantly from each other (see Table 6.1 in Chapter 6). The greenhouse effect, the distance from the Sun, and planetary mass all played a role in giving rise to such different atmospheres (Prinn & Fegley, 1987; Hunten, 1993; Fegley, 2003). Planetary surface temperature is controlled largely by the greenhouse effect and hence only when significant amounts of CO_2, H_2O, or CH_4 accumulate in the atmosphere will the surface temperature begin to rise. This can be illustrated by the effect of progressively increasing water pressure in an early planetary atmosphere (Walker, 1977) (the same sequence of events can be shown for either CH_4 or CO_2). Beginning with estimated surface temperatures as dictated by the distance from the Sun, water vapor will increase in each atmosphere in response to planetary degassing until intersecting the water vapor saturation curve (Figure 10.27). For Earth, this occurs at about 0.01 atm where H_2O begins to condense and precipitate on the surface. Further degassing does not increase the H_2O content of the atmosphere or the surface temperature, but rains out and begins to form the oceans, a process that occurred on Earth probably between

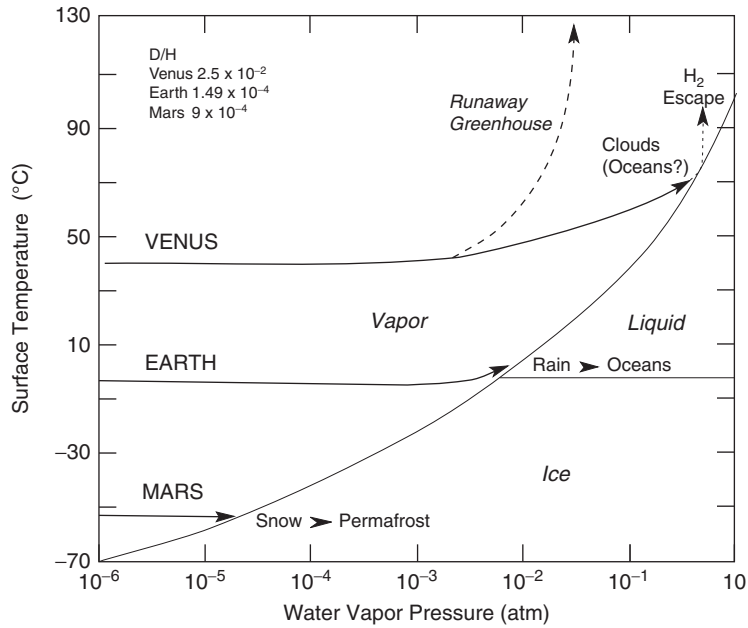

FIGURE 10.27 Idealized trajectories for increasing atmospheric water vapor pressure on Venus, Earth, and Mars. *Modified after Walker (1977).*

4.53 and 4.50 Ga. The growing oceans also stabilize the CO_2 content of the atmosphere via the carbon cycle as discussed in Chapter 6. Because Venus is closer to the Sun, it had a higher initial surface temperature than Earth. This results in the greenhouse effect raising the surface temperature before the vapor saturation curve is intersected. As degassing continues, H_2O, CH_4, and CO_2 may rapidly accumulate in the atmosphere producing a **runaway greenhouse** in which atmospheric temperature continues to rise indefinitely (Figure 10.27). The reason water is virtually absent in the Venusian atmosphere today is due to photolysis in the upper atmosphere producing H_2, which readily escapes. The remaining O_2 may be incorporated into weathered rocks on the surface and perhaps returned to the Venusian mantle by tectonic processes. It is noteworthy that the amount of CO_2 in the Venusian atmosphere is approximately equivalent to the amount in near-surface reservoirs on Earth (most of it in marine carbonates). Hence, if it were not for the oceans that provide a vital link in the carbon cycle, Earth would probably have an uninhabitable atmosphere like Venus.

Mars is farther from the Sun than Earth and has a colder initial surface temperature. Hence, as water increases in the atmosphere and intersects the vapor saturation curve, snow rather than liquid water precipitates (Figure 10.27). As with Earth, neither surface temperature nor atmospheric water vapor pressure increase with further degassing. Upon further cooling (due to lack of a greenhouse effect), CO_2 would also freeze, forming the Martian polar ice caps. The sparsity of light gases like H_2 and N_2 on Mars probably reflects the relatively small mass of the planet and its inability to retain light gases, which escape from its gravitational field.

Although this model accounts for the general features of the evolution of the atmospheres of Earth, Venus, and Mars, some aspects require modification. For instance, the model assumes that Mars was cold and frozen from the beginning, an assumption that is unlikely in terms of the large canyons on the surface that were almost certainly cut by running water before 4 Ga as previously discussed (Carr, 1987). For this reason, it is probable that an early CH_4 or CO_2 greenhouse effect existed on Mars and this necessitates some kind of tectonic recycling of these gases. Because Mars is too small to retain oceans and it is unlikely that plate tectonics ever operated, it is unlikely that an Earth-like carbon cycle controlled CH_4 or CO_2 levels in the early atmosphere. Although the nature of the Martian early recycling system is unknown, the planet must have cooled more rapidly than Earth, perhaps trapping most of the CH_4 or CO_2 and at least some of the water in its interior. Due to insufficient greenhouse heating, the surface cooled and most of the remaining CO_2 condensed as ice on the surface. It is probable that today most of the degassed water and some of the CO_2 on Mars occur as permafrost near the surface.

The runaway greenhouse model for Venus assumes that Venus never had oceans, another assumption that is questionable in terms of the high D/H (deuterium/hydrogen) ratio in trace amounts of water in the Venusian atmosphere. This ratio, which is 100 times higher than that in Earth's water (Figure 10.27),

may have developed during preferential loss of H_2 from the Venusian atmosphere enriching the residual water in the heavier deuterium isotope, which has a much smaller escape probability than hydrogen (Gurwell, 1995). Although this observation does not prove the existence of early oceans on Venus, the planet at one time must have had at least 10^3 times more water than at present, either in oceans or as water vapor in the atmosphere. An alternative and preferred evolutionary path for Venus leads to condensation of water at 4.5–4.4 Ga, formation of water vapor clouds, and possibly of oceans (Figure 10.27). On Earth, water is blocked from entering the stratosphere by a cold trap (a temperature minimum) at 10–15 km above the surface (Figure 6.1), and most water vapor condenses when it reaches the cold trap. However, if water vapor in the lower atmosphere exceeds 20%, as it must have on Venus, it produces greenhouse warming. This results in movement of the cold trap to a high altitude ($\sim$100 km) where it no longer is effective in preventing water vapor from rising into the upper atmosphere, and thus, water can undergo photolysis and hydrogen escape. On Venus hydrogen escape could have eliminated an oceanic volume of water in $<$30 Ma. Some of the missing water also may be housed in hydrous minerals in the interior of Venus (Lecuyer et al., 2000). Following the early loss of water, the Venusian atmosphere would rapidly evolve into a runaway greenhouse caused by the remaining CO_2, and this is the situation that exists today on Venus.

THE CONTINUOUSLY HABITABLE ZONE

Life in the solar system requires a very narrow range in surface temperature and hence a narrow range in the content of greenhouse gases. From a knowledge of temperature and gas distributions in the inner solar system, the width of this zone, known as the **Continuously Habitable Zone** (**CHZ**), can be estimated. If Earth, for instance, had accreted in an orbit 5% closer to the Sun, the atmosphere would continue to rise in temperature and the oceans would evaporate, leading to a runaway greenhouse as just described. The outer extreme of the CHZ is less certain, but appears to extend somewhat beyond the orbit of Mars, and thus the CHZ would extend from 0.95 to 1.5 AU (Kasting et al., 1993b). This observation is important in that the CHZ is wide enough that habitable planets may exist in other planetary systems. Although in any planetary system most life, and all higher forms of life, would be limited to the CHZ, some microbes that can withstand extreme conditions as discussed in Chapter 9 may survive outside of this zone, and in particular, they may survive on some satellites of the Jovian planets.

COMPARATIVE PLANETARY EVOLUTION

The terrestrial planets all have low masses, small radii, and large densities compared to the giant planets in the outer solar system (Table 10.2). This is also true for the Moon and many of the satellites of the outer planets. Rotational,

gravitational, and magnetic field observations indicate that the interiors of these "rocky" bodies are differentiated and layered into iron-rich cores, silicate mantles, and crusts, the latter derived from partial melting of the mantles. Furthermore, geodetic observations suggest that the interiors are hot enough to maintain partially to completely liquid iron cores. For Mars, Venus, and Earth, mantle pressures are sufficient for mineral phase transitions from olivine, pyroxenes, and garnet at low pressures to perovskite and post-perovskite phases at high pressures.

From our survey of the solar system, it seems clear that no two bodies in the solar system have identical histories. Although the terrestrial planets have many features in common, as do the outer giant planets, each planet has its own unique history. At least from our perspective, Earth seems to be most peculiar. Not only is it the only planet with oceans, an oxygen-bearing atmosphere, and living organisms, but it is the only planet in which plate tectonic processes are known to be active. As a final topic in this chapter, let us compare the evolutionary histories of the terrestrial planets, and in doing so identify some of the important variables that control and direct the paths of planetary evolution.

As we have seen, the terrestrial planets and the Moon have similar densities (Table 10.2) and thus, on the whole, similar bulk compositions. Each of them is evolving toward a stage of thermal and tectonic stability and quiescence as they cool. The rate at which a planet approaches this final stage is dependent on a variety of factors, which directly or indirectly control the loss of heat (Carlson, 1994; Taylor, 1992, 1999). First of all, the position of a planet in the solar system is important because, as we have seen, it reflects the condensation sequence of elements from the cooling solar nebula. Also important are the abundances of radiogenic isotopes that contribute to heating planetary bodies. The Moon, for instance, contains considerably smaller amounts of U, Th, and K than Earth, and as such will not produce as much radiogenic heat. Analyses of fine-grained materials from the *Viking* landing sites suggest that Mars is also depleted in radiogenic isotopes compared to the Earth. Planetary mass is important in that the amount of accretional and gravitational energy is directly dependent on mass. Planetary size is also important, in that greater area/mass ratios result in more rapid heat loss from planetary surfaces. For instance, the Moon, Mars, and Mercury should cool much faster than Venus and Earth because of their higher area/mass ratios (Table 10.2). Also important is the size of the iron core, in that much of initial planetary heat is produced during core formation. Except for Mercury, Earth has the highest core–mantle ratio, followed by slightly lower values for Venus and Mars. As discussed previously, the very high core–mantle ratio for Mercury is probably a result of loss of some of the Mercurian mantle by an early giant impact, and thus is not indicative of a large contribution of heat from core formation. The volatile contents and especially the water content of planetary mantles and the rate of volatile release are important in controlling atmosphere development, the amount of melting, fractional crystallization trends, and the viscosity of planetary interiors, which, in turn, affects the rate

of cooling. Convection and/or mantle plume activity are the primary mechanisms by which heat is lost from the terrestrial planets. Only Earth, however, requires mantle convection at present and supports plate tectonics.

Although every planet has its own unique history, the primary differences in planetary thermal history are controlled chiefly by heat productivities, volatile-element contents, and cooling rates. Distance from the Sun is also an important variable, especially in terms of planetary composition and atmosphere evolution. A qualitative portrayal of planetary thermal histories is illustrated in Figure 10.28. The temperature scale is schematic. All terrestrial planets underwent rapid heating during late stages of accretion, reaching maximum temperatures between 4.55 and 4.50 Ga, at which time widespread magma oceans were produced. Just prior to or coincident with this time, molten iron descended to planetary centers, forming metal cores, and planetary mantles rapidly degassed. Rapid, chaotic convection in the magma oceans resulted in rapid cooling and crystallization producing a transient primary crust, probably of anorthositic composition. Partial melting of recycled crust or/and mantle ultramafic rocks gave rise to widespread secondary basaltic crusts on all of the terrestrial planets, a process that is still occurring on Earth as ocean ridge basalts and oceanic plateaus are produced. At least on Earth and Venus, where substantial heat was available, early crust and lithosphere were rapidly recycled into the mantle, aided by intense giant impacts, which continued to about 3.9 Ga with the LHB (Figure 10.28).

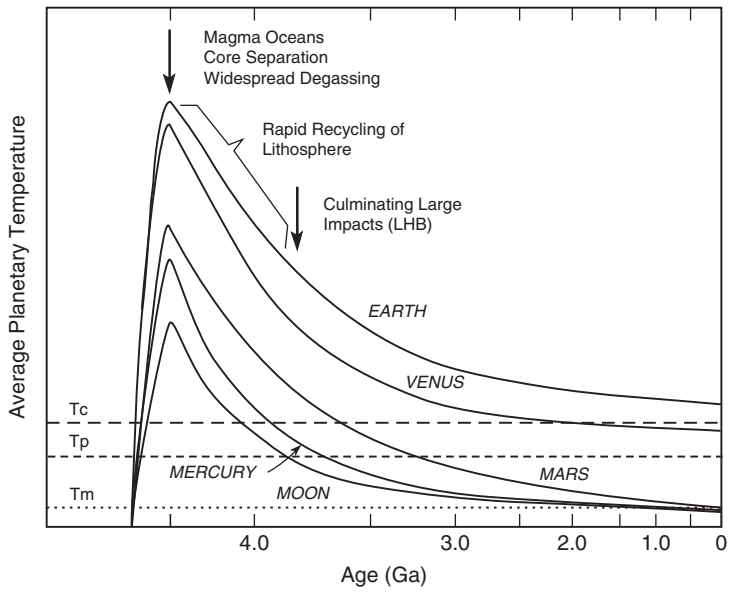

FIGURE 10.28 Schematic thermal evolution of the terrestrial planets and the Moon. Lower threshold temperatures for planetary processes: Tc, convection; Tp, mantle plume generation at the core–mantle boundary; Tm, magmatism.

Although continental crust is not preserved on Earth until 4 Ga, it may have been produced and rapidly recycled into the mantle before this time (Chapter 4). Rapid cooling of the smaller planets, including Mercury and probably Mars, led to thickened and strong lithospheres by 4.5 Ga. These planets, as well as the Moon, are known as **one-plate planets**, because their thick, strong planet-wide lithosphere is basically all one plate. Most of the magmatic activity on these planets resulted from mantle plume activity and occurred before 3.9 Ga. The Moon formed by accretion of material blasted from Earth by a giant impact about 4.53 Ga, and it rapidly heated and melted, forming a magma ocean, which crystallized by 4.5 Ga and produced the anorthositic lunar highlands crust. The youngest volcanism on the Moon appears to have been about 2.5 Ga, perhaps 1.5 Ga on Mercury, and maybe as recent as 200 Ma on Mars.

Because of their greater initial heat, Venus and Earth cooled more slowly than the other terrestrial planets. Venus may have passed through the minimum temperature for convection some 2 Ga, while Earth has not yet reached that point in its cooling history (Figure 10.28). If the resurfacing of Venus at 800–300 Ma was caused by a catastrophic mantle plume event, it may have been the last such event, as suggested by the intersection of the Venus cooling curve with Tp, the lower temperature limit for plume production at the core–mantle interface. Volcanism is probably still active on Venus, however. The most intriguing question—that of why Venus and Earth followed such different cooling paths, even though both planets are similar in mass and density—remains problematic. One possibility is that while Earth cooled chiefly by convection and plate tectonics, Venus cooled by mantle plumes and conduction through the lithosphere. If this is the case, we are still left with the question of why different cooling mechanisms dominated in each planet. Some investigators suggest it has to do with the absence of water on Venus. They argue that in a dry planet the lithosphere is as thick and strong as it is on Venus, and there is no melting to produce a low velocity zone, and thus plates cannot move about or subduct. Taking this one step further, we might ask why is Venus dry, yet Earth is wet? As suggested previously, Venus may have rapidly lost its water as hydrogen escaped from the atmosphere soon after or during planetary accretion, because the surface of the planet was too hot for oceans to survive. And why was the surface too hot? Perhaps because Venus is closer to the Sun than Earth. If this line of reasoning is correct, it may be that the position that a planet accretes in a gaseous nebula is one of the most important variables controlling its evolution. The reason Mars did not sustain plate tectonics or accumulate an ocean may be due to its small mass and rapid cooling, resulting in a lithosphere that was too thick and strong to subduct. If there was enough water to form Martian oceans, it either escaped by hydrogen loss or is trapped in the interior of the planet.

If the above scenario bears any resemblance to what really happened, it would appear that two important features led to a unique history for Earth: (1) its position in the solar system and (2) its relatively large mass. Without both of these, Earth may have evolved into quite a different planet than the one we live on.

EXTRASOLAR PLANETS

As our ability to detect planets around stars increases with improved instrumentation and data reduction techniques, many new planets have been discovered (more than 1500 in 2011) (Bodenheimer & Lin, 2002). The chief method of planet detection is a radial-velocity survey. As a planet orbits a star, its gravity causes the star to wobble, producing a periodic change in the spectrum of light emitted by the star, which can be used to infer the planet's presence. Also, the star's wobble can be measured by tracking its position. Planets can also be detected as they pass in front of the star. The most unexpected feature of the new planets is their peculiar properties (Taylor, 1999). Most extrasolar planets have masses of 0.75 to 3 Jovian masses, but masses less than 0.5 of a Jovian mass are difficult to detect. Some of the most exciting finds in the last few years have been planets with rocky compositions and the probable existence of water. One "super-Earth" appears to be composed primarily of water surrounded by an atmosphere of hydrogen-helium that is only 0.05% of the mass of the planet (Charbonneau et al., 2009). Unlike planets in the solar system, most extrasolar planets are much closer to their parent star than Mercury is to the Sun and they have orbital periods of only a few days. Most also have anomalous eccentricities (>0.1) compared to Jupiter (0.048) and Saturn (0.055). One multiple system, however, resembles a scaled version of our solar system with the mass ratio, separation ratio, and temperatures of the planets similar to those of Jupiter and Saturn (Gaudi et al., 2008). These properties are difficult to explain with current models for the origin of planetary systems, which work for the solar system. Clearly, the conditions that existed to make our solar system are not easily reproduced in other planetary systems.

FURTHER READING

Beatty, J. K., Petersen, C. C., & Chaikin, A. L. (1999). *The New Solar System* (4th ed.). Cambridge, UK: Cambridge University Press.

Carr, M. H., & Head, J. W., III (2010). Geologic history of Mars. *Earth and Planetary Science Letters*, *294*, 185–203.

de Pater, I., & Lissauer, J. (2001). *Planetary Sciences.* Cambridge, UK: Cambridge University Press.

Fegley, B. (2003). *Venus,* Treatise on Geochemistry (Vol. 1.19, pp. 487–507). Amsterdam: Elsevier.

Halliday, A. N., & Wood, B. J. (2007). *The Composition and Major Reservoirs of the Earth around the Time of the Moon-Forming Giant Impact,* Treatise on Geophysics (Vol. 9.02, pp. 13–50) Amsterdam: Elsevier.

Lewis, J. S. (2004). *Physics and Chemistry of the Solar System* (2nd ed.). San Diego, CA: Academic Press.

McSween, H. Y. (1999). *Meteorites and Their Parent Bodies.* Cambridge, UK: Cambridge University Press.

Taylor, S. R., & McLennan, S. M. (2009). *Planetary Crusts: Their Composition, Origin and Evolution.* Cambridge, UK: Cambridge University Press.

References

Abbott, D. (1996). Plumes and hotspots as sources of greenstone belts. *Lithos*, *37*, 113–127.

Abbott, D. H., & Hoffman, S. E. (1984). Archean plate tectonics revisited 1. *Tectonics*, *3*, 429–448.

Abbott, D., & Isley, A. E. (2002). Extraterrestrial influences on mantle plume activity. *Earth and Planetary Science Letters*, *205*, 53–62.

Abbott, D. H., & Mooney, W. (1995). The structural and geochemical evolution of the continental crust: support for the oceanic plateau model of continental growth. *Review of Geophysics*, (Suppl.), 231–242.

Abbott, D., Burgess, L., Longhi, J., & Smith, W. H. F. (1994). An empirical thermal history of the Earth's upper mantle. *Journal of Geophysical Research*, *99*, 13,835–13,850.

Abramov, O., & Mojzsis, S. J. (2009). Microbial habitability of the Hadean Earth during the late heavy bombardment. *Nature*, 459. doi:10.1038/nature08015.

Achille, G. D., & Hynek, B. M. (2010). Ancient ocean on Mars supported by global distribution of deltas and valleys. *Nature Geoscience*, *3*, 459–463.

Adatte, T., Keller, G., Harting, M., Stueben, D., Kramar, U., & Stinnesbeck, W. (2003). Cretaceous-Tertiary events: a multi-causal scenario. In *Mantle Plumes: Physical Processes, Chemical Signatures and Biological Effects* (Abstract Vol., p. 1). Cardiff, UK: Cardiff University, September 2003.

Ahall, K. I., Persson, P.-O., & Skiold, T. (1995). Westward accretion of the Baltic Shield: implications from the 1.6 Ga Amal-Horred belt, SW Sweden. *Nature Geoscience*, *70*, 235–251.

Aharon, P. (2005). Redox stratification and anoxia of the early Precambrian oceans: implications for carbon isotope excursions and oxidation events. *Precambrian Research*, *137*, 207–222.

Ahrens, T. J., Holland, K. G., & Chen, G. Q. (2002). Phase diagram of iron, revised-core temperatures. *Geophysical Research Letters*, *29*. doi:10.1029/2001GL014350.

Alabaster, T., Pearce, J. A., & Malpas, J. (1982). The volcanic stratigraphy and petrogenesis of the Oman ophiolitic complex. *Contributions to Mineralogy and Petrology*, *81*, 168–183.

Albarede, F. (1998). Time-dependent models of U-Th-He and K-Ar evolution and the layering of mantle convection. *Chemical Geology*, *145*, 413–429.

Albarede, F. (2009). Volatile accretion history of the terrestrial planets and dynamic implications. *Nature*, *461*, 1227–1233.

Albarede, F., & van der Hilst, R. D. (1999). New mantle convection model may reconcile conflicting evidence. *Eos*, *80*, 535–539.

Alfe, D., Gillan, M. J., & Price, G. D. (2002). Composition and temperature of the Earth's core constrained by combining *ab initio* calculations and seismic data. *Earth and Planetary Science Letters*, *195*, 91–98.

Algeo, T. J., & Seslavinsky, K. B. (1995). The Paleozoic world: continental flooding, hypsometry, and sea level. *American Journal of Science*, *295*, 787–822.

Allegre, C. J. (1982). Chemical geodynamics. *Tectonics*, *81*, 109–132.

Allegre, C. J., & Minster, J. F. (1978). Quantitative models of trace element behavior in magmatic processes. *Earth and Planetary Science Letters*, *38*, 1–25.

Allegre, C. J., Brevart, O., Dupre, B., & Minster, J. F. (1980). Isotopic and chemical effects produced in a continuously differentiating convecting earth mantle. *Philosophical Transactions of the Royal Society of London*, *297A*, 447–477.

Allegre, C. J., Moreira, M., & Staudacher, T. (1995a). $^{4}He/^{3}He$ dispersion and mantle convection. *Geophysical Research Letters*, *22*, 2325–2328.

Allegre, C. J., Poirier, J. P., Humler, E., & Hofmann, A. W. (1995b). The chemical composition of the Earth. *Earth and Planetary Science Letters*, *134*, 515–526.

Allen, P. A., & Etienne, J. L. (2008). Sedimentary challenge to Snowball Earth. *Nature Geoscience*, *1*, 817–825.

Allen, P. A., & Homewood, P. (Eds.). (1986). *Foreland Basins* (453 pp). Oxford: Blackwell Scientific.

Alvarez, W. L. (1986). Toward a theory of impact crises. *Eos*, September 1986, 649–655.

Alvarez, W. L., Alvarez, L. W., Asaro, F., & Michel, H. V. (1982). Extraterrestrial cause for the K/T extinction. *Science*, *208*, 1095–1108.

Alvaraex, W., Asaro, F., & Montanari, A. (1990). Iridium profile for 10 million years across the Cretaceous–Tertiary boundary at Gubbio (Italy). *Science*, *250*, 1700–1702.

Amelin, Y., Lee, D. C., Halliday, A. N., & Pidgeon, R. T. (1999). Nature of the Earth's earliest crust from hafnium isotopes in single detrital zircons. *Nature*, *399*, 252–255.

Anbar, A. D. (2008). Elements and evolution. *Science*, *322*, 1481–1482.

Anbar, A. D., & Knoll, A. H. (2002). Proterozoic ocean chemistry and evolution: a bioinorganic bridge? *Science*, *297*, 1137–1142.

Anbar, A. D., Duan, Y., Lyons, T. W., Arnold, G. L., Kendall, B., Creaser, R. A., et al. (2007). A whiff of oxygen before the Great Oxidation Event? *Science*, *317*, 1903–1906.

Anderson, D. L. (1982). Hotspots, polar wander, Mesozoic convection and the geoid. *Nature*, *297*, 391–393.

Anderson, D. L. (2003). The plume hypothesis. *Geoscientist*, *13*, 16–17.

Anderson, D. L., & Natland, J. H. (2005). *A brief history of the plume hypothesis and its competitors: concept and controversy* (pp. 119–145). Boulder, CO: Geological Society of America, Special Paper 388.

Anderson, D. L., Sammis, C., & Jordan, T. (1971). Composition and evolution of the mantle and core. *Science*, *171*, 1103–1112.

Anderson, J. L. (1983). *Proterozoic anorogenic plutonism of North America* (pp. 133–154). Boulder, CO: Geological Society of America, Memoir 161.

Anderson, J. L., & Morrison, J. (1992). The role of anorogenic granites in the Proterozoic crustal development of North America. In K. C. Condie (Ed.), *Proterozoic Crustal Evolution* (pp. 263–300). Amsterdam: Elsevier.

Antonangeli, D., Siebert, J., Badro, J., Farber, D. L., Fiquet, G., Morard, G., et al. (2010). Composition of the Earth's inner core from high-pressure sound velocity measurments in Fe-Ni-Si alloys. *Earth and Planetary Science Letters*, *295*, 292–296.

Arculus, R. J., & Johnson, R. W. (1978). Criticism of generalized models for the magmatic evolution of arc-trench systems. *Earth and Planetary Science Letters*, *39*, 118–126.

Argus, D. F., & Heflin, M. B. (1995). Plate motion and crustal deformation estimated with geodetic data from the GPS. *Geophysical Research Letters*, *22*, 1973–1976.

Armstrong, R. L. (1981). Radiogenic isotopes: the case for curstal recycling on a near-steady-state no-continental-growth Earth. *Philosophical Transactions of the Royal Society of London*, *A301*, 443–472.

Armstrong, R. L. (1991). The persistent myth of crust growth. *Australian Journal of Earth Sciences*, *38*, 613–630.

Arndt, N. T. (1983). Role of a thin, komatiite-rich oceanic crust in the Archean plate-tectonic process. *Geology*, *11*, 372–375.

Arndt, N. T. (1991). High Ni in Archean tholeiites. *Tectonophysics*, *187*, 411–420.

Arndt, N. T. (1994). Archean komatiites. In K. C. Condie (Ed.), *Archean Crustal Evolution* (pp. 11–44). Amsterdam: Elsevier.

Arndt, N. (1999). Why was flood volcanism on submerged continental platforms so common in the Precambrian? *Precambrian Research*, *97*, 155–164.

Arndt, N. T., & Goldstein, S. L. (1987). Use and abuse of crust formation ages. *Geology*, *15*, 893–895.

Arndt, N., Ginibre, C., Chauvel, C., Albarede, F., Cheadle, M., Herzberg, C., et al. (1998). Were komatiites wet? *Geology*, *26*, 739–742.

Arndt, N. T., Lesher, C. M., & Barnes, S. J. (2008). *Komatiite*. Cambridge, UK: Cambridge University Press.

Arndt, N. T., Coltice, N., Helmstaedt, H., & Gregoire, M. (2009). Origin of Archean subcontinental lithospheric mantle: some petrological constraints. *Lithos*, *109*, 61–71.

Artemieva, I. M. (2006). Global thermal model TC1 for the continental lithosphere: implications for lithosphere secular evolution. *Tectonophysics*, *416*, 245–277.

Artemieva, I. M. (2009). The continental lithosphere: reconciling thermal, seismic, and petrologic data. *Lithos*, *109*, 23–46.

Artemieva, I. M., & Mooney, W. D. (2001). Thermal thickness and evolution of Precambrian lithosphere: a global study. *Journal of Geophysical Research*, *106*, 16,387–16,414.

Asahara, Y., Ohtani, E., & Suzuki, A. (1998). Melting relations of hydrous and dry mantle compositions and the genesis of komatiites. *Geophysical Research Letters*, *25*, 2201–2204.

Aspler, L. B., & Chiarenzelli, J. R. (1998). Two Neoarchean supercontinents? Evidence from the Paleoproterozoic. *Sedimentology Geol*, *120*, 75–104.

Ayers, L. D., & Thurston, P. C. (1985). *Archean supracrustal sequences in the Canadian Shield: an overview* (pp. 343–380). Geological Association of Canada, Special Paper 28.

BABEL Working Group. (1990). Evidence for Early Proterozoic plate tectonics from seismic reflection profiles in the Baltic shield. *Nature*, *348*, 34–38.

Badro, J., Fiquet, G., Guyot, F., Grewgoryanz, E., Occelli, F., Antonangeli, D., et al. (2007). Effect of light elements on the sound velocities in solid iron: implication for the composition of Earth' core. *Earth and Planetary Science Letters*, *254*, 233–238.

Bahlburg, H., Vervoort, J. D., Du Frane, S. A., Bock, B., Augustsson, C., & Reimann, C. (2009). Timing of crust formation and crecycling in accretionary orogens: insights learned from the western margin of South America. *Earth-Science Reviews*, *97*, 215–241.

Baier, J., Audetat, A., & Keppler, H. (2008). The origin of the negative niobium tantalum anomaly in subduction zone magmas. *Earth and Planetary Science Letters*, *267*, 290–300.

Baker, V. R. (2001). Water and the martian landscape. *Nature*, *412*, 228–236.

Bambach, R. K. (2006). Phanerozoic biodiversity mass extinctions. *Annual Review of Earth and Planetary Sciences*, *34*, 127–155.

Baragar, W. R. A., Lamber, M. B., Baglow, N., & Gibson, I. L. (1990). The sheeted dyke zone in the Troodos ophiolite. In J. Malpas, et al. (Ed.), *Ophiolites: Oceanic Crustal Analogues* (pp. 37–51). Cyprus Geolological Survey.

Baragar, W. R. A., Ernst, R. E., Hulbert, L., & Peterson, T. (1996). Longitudinal petrochemical variation in the Mackenzie dyke swarm, NW Canadian shield. *J Petrol*, *37*, 317–359.

Barley, M. E. (1993). Volcanic, sedimentary and tectonostratigraphic environments of the 3.46 Ga Warrawoona Megasequence: a review. *Precambrian Research*, *60*, 47–67.

Barley, M. E., Pickard, A. L., & Sylvester, P. J. (1997). Emplacement of a large igneous province as a possible cause of BIF 2.45 Ga. *Nature*, *385*, 55–58.

Barley, M. E., Krapez, B., Groves, D. I., & Kerrich, R. (1998). The Late Archean bonanza: metallogenic and environmental consequences of the interaction between mantle plumes, lithospheric tectonics and global cyclicity. *Precambrian Research*, *91*, 65–90.

Barnes, C. R. (1999). Paleoceanography and Paleoclimatology: an Earth system perspective. *Chemical Geol*, *161*, 17–35.

Barron, E. J., Fawcett, P. J., Peterson, W. H., Pollard, D., & Thompson, S. L. (1995). A "simulation" of mid-Cretaceous climate. *Paleoceanography*, *10*, 953–962.

Bartley, J. K., et al. (2001). Global events across the Mesoproterozoic-Neoproterozoic boundary: Ca and Sr isotopic evidence from Siberia. *Precambrian Research*, *111*, 165–202.

Barton, J. M., Jr., et al. (1994). Discrete metamorphic events in the Limpopo belt, southern Africa: implications for the application of P-T paths in complex metamorphic terrains. *Geology*, *22*, 1035–1038.

Beck, R. A., Burbank, D. W., Sercombe, W. J., Olson, T. L., & Khan, A. M. (1995). Organic carbon exhumation and global warming during the early Himalayan collision. *Geology*, *23*, 387–390.

Becker, L., Poreda, R. J., Hunt, A. G., Bunch, T. E., & Rampino, M. (2001). Impact event at the Permian-Triassic boundary: evidence from extraterrestrial noble gases in fullerenes. *Science*, *291*, 1530–1533.

Bedard, J. H. (2006). A catalytic delamination-driven model for coupled genesis of Archean crust and sub-continental lithospheric mantle. *Geochimica et Cosmochimica Acta*, *70*, 1188–1214.

Bednarz, U., & Schmincke, H. (1994). Petrological and chemical evolution of the NE Troodos extrusive series. *Cyprus: Journal of Petrology*, *35*, 489–523.

Be'eri-Shlevin, Y., Katzir, Y., & Valley, J. W. (2009). Crustal evolution and recycling in a juvenile continent: oxygen isotope ratio of zircon in the northern Arabian Nubian shield. *Lithos*, *107*, 169–184.

Bekker, A., Kaufman, A. J., Karhu, J. A., Beukes, N. J., Swart, Q. D., Coetzee, L. L., et al. (2001). Chemostratigraphy of the Paleoproterozoic Duitschland Formation South Africa: implications for coupled climate change and carbon cycling. *American Journal of Science*, *301*, 261–285.

Bekker, A., Holland, H. D., Wang, P. L., Rumble, D., Stein, H. J., Hannah, J. L., et al. (2004). Dating the rise of atmospheric oxygen. *Nature*, *427*, 117–120.

Belcher, C. M., Collinson, M. R., Sweet, A. R., Hildebrand, A. R., & Scott, A. C. (2003). Fireball passes and nothing burns—the rolde of thermal radiation in the Cretaceous-Tertiary event: evidence from the charcoal record of North America. *Geology*, *31*, 1061–1064.

Belonoshko, A. B., Ahuja, R., & Johansson, B. (2003). Stability of the body-centered-cubic phase of iron in the Earth's inner core. *Nature*, *424*, 1032–1034.

Belousova, E. A., Kostitsyn, Y. A., Griffin, W. L., Begg, G. C., O'Reilly, S. Y., & Pearson, N. J. (2010). The growth of the continental crust: constraints from zircon Hf-isotope data. *Lithos*, *119*, 457–466.

Bengtson, S. (Ed.). (1994). *Early Life on Earth* (630 pp). New York: Columbia University Press.

Bennett, V. C. (2004). *Compositional Evolution of the Mantle*. *Treatise on Geochemistry* (Chap. 2.13, pp. 493–519). Amsterdam: Elsevier.

Bennett, V. C., Brandon, A. D., & Nutman, A. F. (2007). Coupled ^{142}Nd-^{143}Nd isotopic evidence for Hadean mantle dynamics. *Science*, *318*, 1907–1910.

Benoit, T., Degayle, E., & Wittlinger, G. (2010). Seismic evidence for a global low-velocity layer within the Earth's upper mantle. *Nature Geoscience*, *3*, 718–721.

Benton, M. J. (1995). Diversification and extinction in the history of life. *Science*, *268*, 52–58.

Benz, W., & Cameron, A. G. W. (1990). Terrestrial effects of the giant impact. In H. E. Newsom & J. H. Jones (Eds.), *Origin of the Earth* (pp. 61–67). New York: Oxford University Press.

Bercovici, D., & Karato, S. (2003). Whole-mantle convection and the transition zone water filter. *Nature*, *425*, 39–44.

Berger, W. H., et al. (1992). The record of Ontong Java Plateau: main results of ODP Leg 130. *Geological Society of America Bulletin*, *104*, 954–972.

Berger, W. H., Bickert, T., Schmidt, H., & Wefer, G. (1993). Quaternary oxygen isotope record of pelagic foraminifers: Site 806, Ontong Java plateau. *Proceedings of the Ocean Drilling Program, Scientific Results*, *130*, 381–395.

Bergman, M. I. (1997). Measurements of elastic anisotropy due to solidification texturing and the implications for the Earth's inner core. *Nature*, *489*, 60–63.

Berner, R. A. (1983). Burial of organic carbon and pyrite sulfur in sediments over Phanerozoic time: a new theory. *Geochimica et Cosmochimica Acta*, *47*, 855–862.

Berner, R. A. (1987). Models for carbon and sulfur cycles and atmospheric oxygen: application to Paleozoic history. *American Journal of Science*, *287*, 177–196.

Berner, R. A. (1994). 3Geocarb II: a revised model of atmospheric CO_2 over Phanerozoic time. *American Journal of Science*, *294*, 56–91.

Berner, R. A. (1999). A new look at the long-term carbon cycle. *GSA Today*, *9*(11), 1–6.

Berner, R. A. (2001). Modeling atmospheric O_2 over Phaerozoic time. *Geochimica et Cosmochimica Acta*, *65*, 685–694.

Berner, R. A., & Berner, E. K. (1997). Silicate weathering and climate. In W. F. Ruddiman (Ed.), *Tectonic Uplift and Climate Change* (pp. 354–365). New York: Plenum Press.

Berner, R. A., & Canfield, D. E. (1989). A new model for atmospheric oxygen over Phanerozoic time. *American Journal of Science*, *289*, 333–361.

Berner, R. A., VandenBrooks, J. M., & Ward, P. D. (2007). Oxygen and evolution. *Science*, *316*, 557–558.

Berry, A. J., Danyushevsky, L. V., O'Neill, H. C., St., Newville, M., & Sutton, S. R. (2008). Oxidation state of iron in komatiitic melt inclusions indicates hot Archean mantle. *Nature*, *455*, 960–964.

Beukes, J. J., Klein, C., Kaufman, A. J., & Hayes, J. M. (1990). Carbonate petrography, kerogen distribution, and carbon and oxygen isotope variations in an early Proterozoic transition from limestone to iron-formation deposition, Transvaal Supergroup, South Africa. *Bull Soc Econ Geol*, *85*, 663–690.

Bickle, M. J. (1986). Implications of melting for stabilization of the lithosphere and heat loss in the Archean. *Earth and Planetary Science Letters*, *80*, 314–324.

Bickle, M. J. (1996). Metamorphic decarbonation, silicate weathering and the long-term carbon cycle. *Terra Nova*, *8*, 270–276.

Bickle, M. J., Nisbet, E. G., & Martin, A. (1994). Archean greenstone belts are not oceanic crust. *Journal of Geology*, *102*, 121–137.

Binden, A. B. (1986). The binary fission origin of the moon. In W. K. Hartmann, R. J. Phillips & G. J. Taylor (Eds.), *Origin of the Moon* (pp. 519–550). Houston, TX: Lunar & Planetary Institute.

Bindschadler, D. L., Schubert, G., & Kaula, W. M. (1992). Coldspots and hotspots: global tectonics and mantle dynamics of Venus. *Journal of Geophysical Research*, *97*, 13,495–13,532.

Blackman, D. K., Kendall, J. M., Dawson, P. R., Wenk, H. R., Boyce, D., & Morgan, J. P. (2007). Telseismic imaging of subaxial flow a mid-ocean ridges: travel time effects of anisotropic mineral texture in the mantle. *Geophysical Journal International*, *127*, 415–426.

Blackwell, D. D. (1971). *The thermal structure of the continental crust* (pp. 169–191). American Geophysical Union, Monograph 14.

Blank, C. E., & Sanchez-Baracaldo, P. (2010). Timing of morphological and ecological innovations in the cyanbacteria-akey to understanding the rise in atmospheric oxygen. *Geobiology*, *8*, 1–23.

Bleeker, W. (2002). *Archean tectonics: a review, with illustrations from the Slave craton* (pp. 151–181). Geological Society of London, Special Publication 199.

Bleeker, W. (2003). The Late Archean record: a puzzle in ca. 35 pieces. *Lithos*, *71*, 99–134.

Bleeker, W., & Ernst, R. (2006). Short-lived mantle generated magmatic events and their dyke swarms: the key to unlocking Earth's paleogeographic record by to 2.6 Ga. In E. Hanski, S. Mertanen, T. Ramo & J. Vullo (Eds.), *Dyke Swarms—Time Markers of Crustal Evolution* (pp. 3–26). Rotterdam: Balkema Publishers.

Blichert-Toft, J., & Albarede, F. (1994). Short-lived chemical heterogeneities in the Archean mantle with implications for mantle convection. *Science*, *263*, 1593–1596.

Blichert-Toft, J., Frey, F. A., & Albarede, F. (1999). Hf isotope evidence for pelagic sediments in the source of Hawaiian basalts. *Science*, *285*, 879–882.

Bloxham, J. (1992). The steady part of the secular variation of Earth's magnetic field. *Journal of Geophysical Research*, *97*, 19,565–19,579.

Blum, J. (2000). Laboratory experiments on preplanetary dust aggregation. *Space Science Review*, *92*, 265–278.

Bodenheimer, P., & Lin, D. N. C. (2002). Implications of extrasolar planets for understanding planet formation. *Annual Review of Earth and Planetary Sciences*, *30*, 113–148.

Boehler, R. (1996). Experimental constraints on melting conditions relevant to core formation. *Geochimica et Cosmochimica Acta*, *60*, 1109–1112.

Bogue, S. W., & Merrill, R. T. (1992). The character of the field during geomagnetic reversals. *Annual Review of Earth and Planetary Sciences*, *20*, 181–219.

Boher, M., Abouchami, W., Michard, A., Albarede, F., & Arndt, N. T. (1992). Crustal growth in West Africa at 2.1 Ga. *Journal of Geophysical Research*, *97*, 345–369.

Bohlen, S. R. (1991). On the formation of granulites. *Journal of Metamorphic Geology*, *9*, 223–229.

Bohor, B. F., Modreski, P. J., & Foord, E. E. (1987). Shocked quartz in the K/T boundary clays: evidence for a global distribution. *Science*, *236*, 705–709.

Bois, C., Bouche, P., & Pelet, R. (1980). Historie geologique et repartition des reserves d'hydrocarbures dans le Monde. *Inst Fracais du Petrole Rev*, *35*, 237–298.

Bonatti, E. (1967). Mechanisms of deepsea volcanism in the South Pacific. In P. H. Abelson (Ed.), *Researches in Geochemistry* (pp. 453–491). New York: Wiley.

Bortolotti, V., Marroni, M., Pandolfi, L., Principi, G., & Saccani, E. (2002). Interaction between mid-ocean ridge and subduction magmatism in Albanian ophiolites. *Journal of Geology*, *110*, 561–576.

Boryta, M., & Condie, K. C. (1990). Geochemistry and origin of the Archean Beit Bridge complex, Limpopo belt, South Africa. *Journal of the Geological Society of London*, *147*, 229–239.

Boschi, L., & Dziewonski, A. M. (1999). High- and low-resolution images of the Earth's mantle: implicaitons of different approaches to tomographic modeling. *Journal of Geophysical Research*, *104*, 25567–25594.

Boschi, L., Becker, T. W., & Steinberger, B. (2007). Mantle plumes: dynamic models and seismic images. *Geochem. Geophys. Geosyst*, *8*(10), Q10006. doi:10.1029/2007GC001733.

Boss, A. P., Morfill, G. E., & Tscharnuter, W. M. (1989). Models of the formation and evolution of the solar nebula. In S. K. Atreya, J. B. Pollack, & M. S. Matthews (Eds.), *Origin and Evolution of Planetary and Satellite Atmospheres* (pp. 35–77). Tucson: University of Arizona Press.

Bott, M. H. P. (1979). Subsidence mechanisms at passive continental margins. *Am Assoc Petrol Geol, Mem*, *29*, 3–9.

Bottinga, Y., & Allegre, C. J. (1973). Thermal aspects of sea-floor spreading and the nature of the oceanic crust. *Tectonophysics*, *18*, 1–17.

Bottinga, Y., & Allegre, C. J. (1978). Partial melting under spreading ridges. *Philosophical Transactions of the Royal Society of London*, *288A*, 501–525.

Boussau, B., Blanquart, S., Necsulea, A., Lartillot, N., & Gouy, M. (2008). Parallel adaptations to high temperatures in the Archean eon. *Nature*, 456. doi:10.1038/nature07393.

Bowring, S. A. (1990). The Acasta gneisses: remnant of Earth's early crust. In H. E. Newsom & J.H. Jones (Eds.), *Origin of the Earth* (pp. 319–343). Oxford: Oxford University Press.

Bowring, S. A., & Housh, T. (1995). The Earth's early evolution. *Science*, *269*, 1535–1540.

Bowring, S. A., Williams, I. S., & Compston, W. (1989). 3.96 Ga gneisses from the Slave province, NW territories, Canada. *Geology*, *17*, 971–975.

Bowring, S. A., et al. (1993). Calibrating rates of Early Cambrian evolution. *Science*, *261*, 1293–1298.

Bowring, S. A., Erwin, D. H., Jin, Y. G., Martin, M. W., Davidek, K., & Wang, W. (1998). U/Pb zircon geochronology and tempo of the end-Permian mass extinction. *Science*, *280*, 1039–1045.

Boyd, F. R. (1989). Compositional distinction between oceanic and cratonic lithosphere. *Earth and Planetary Science Letters*, *96*, 15–26.

Bozhko, N. A. (2010). Intraplate basic-ultrabasic magmatism through time in terms of supercontinental cyclicity. *Moscow Univ Bull*, *65*, 161–176.

Bradley, D. C. (2008). Passive margins through earth history. *Earth-Science Reviews*, *91*, 1–26.

Bradshaw, T. K., Hawkesworth, C. J., & Gallagher, K. (1993). Basaltic volcanism in the southern Basin and Range: no role for a mantle plume. *Earth and Planetary Science Letters*, *116*, 45–62.

Brady, P. V. (1991). The effect of silicate weathering on global temperature and atmospheric CO_2. *Journal of Geophysical Research*, *96*, 18,101–18,106.

Brasier, M. D., & Lindsey, J. F. (1998). A billion years of environmental stability and emergence of eukaryotes: new data from northern Australia. *Geology*, *26*, 555–558.

Bratton, J. F. (1999). Clathrate eustasy: methane hydrate melting as a mechanism for geologically rapid sea-level fall. *Geology*, *27*, 915–918.

Breuer, D., & Moore, W. B. (2007). *Dynamics and Thermal History of the Terrestrial Planets, the Moon, and Io*. *Treatise on Geophysics* (Chap. 10.09, pp. 299–348). Amsterdam: Elsevier.

Breuer, D., & Spohn, T. (1995). Possible flush instability in mantle convection at the Archean-Proterozoic transition. *Nature*, *378*, 608–610.

Brocks, J. J., Logan, G. A., Buick, R., & Summons, R. E. (1999). Archean molecular fossils and the early rise of eukaryotes. *Science*, *285*, 1033–1036.

Brooks, C., Hart, S. R., Hofman, A., & Jarnes, D. E. (1976). Rb-Sr mantle isochrons from oceanic areas. *Earth and Planetary Science Letters*, *32*, 51–61.

Brown, M. (1993). P-T-t evolution of orogenic belts and the causes of regional metamorphism. *Journal of the Geological Society of London*, *150*, 227–241.

Brown, M. (2006). A duality of thermal regimes is the hallmark of plate tectonics since the Neoarchean. *Geology*, *34*, 961–964.

Brown, M. (2007). Metamorphic conditions in orogenic belts: a record of secular change. *International Geology Review*, *49*, 193–234.

Brown, M. (2010). Melting of the continental crust during orogenesis: the thermal, rheological, and compositional consequences of melt transport from lower to upper continental crust. *Canadian Journal of Earth Sciences*, *47*, 655–694.

Brown, M., Rushmer, T., & Sawyer, E. W. (1995). Introduction to special section: mechanisms and consequences of melt segregation from crustal protoliths. *Journal of Geophysical Research*, *100*, 15,551–15,563.

Brueckner, H. K., Carswell, D. A., Griffin, W. L., Medaris, L. G., Van Roermund, H. L. M., & Cuthbert, S. J. (2010). The mantle and crustal evolution of two garnet peridotite suites from the Western Gneiss region, Norwegian Caledonides: an isotopic investigation. *Lithos*, *117*, 1–19.

Bruhn, D., Groebner, N., & Kohlstedt, D. L. (2000). An interconnected network of core-forming melts produced by shear deformation. *Nature*, *403*, 883–886.

Bryan, S. E., & Ernst, R. E. (2008). Revised definition of Large Igneous Provinces (LIPs). *Earth-Science Reviews*, *86*, 175–202.

Bryan, P., & Gordon, R. G. (1986). Errors in minimum plate velocity determined from paleomagnetic data. *Journal of Geophysical Research*, *91*, 462–470.

Buchan, K. L., Halls, H. C., & Mortensen, J. K. (1996). Paleomagnetism, U-Pb geochronology, and geochemistry of Marathon dykes, Superior Province, and comparison with the Fort Frances swarm. *Canadian Journal of Earth Sciences*, *33*, 1583–1595.

Buffett, B. A. (2000). Earth's core and the geodynamo. *Science*, *288*, 2007–2012.

Buffett, B. A., et al. (1996). On the thermal evolution of the Earth's core. *Journal of Geophysical Research*, *101*, 7989–8006.

Buick, R., & Dunlop, J. S. R. (1990). Evaporitic sediments of Early Archean age from the Warrawoona Group, Western Australia. *Sedimentology*, *37*, 247–278.

Buick, R., Groves, D. I., & Dunlop, J. S. R. (1995a). Geological origin of described stromatolites older the 3.2 Ga: comment & reply. *Geology*, *23*, 191–192.

Buick, R., et al. (1995b). Record of emergent continental crust 3.5 Ga in the Pilbara craton of Australia. *Nature*, *375*, 574–577.

Burke, K., Dewey, J. F., & Kidd, W. S. F. (1976). Precambrian paleomagnetic results compatible with contemporary operation of the Wilson cycle. *Tectonophysics*, *33*, 287–299.

Burke, K., Steinberger, B., Torsvik, T. H., & Smethurst, M. A. (2008). Plume generation zones at the margins of large low shear velocity provinces on the core–mantle boundary. *Earth and Planetary Science Letters*, *265*, 49–60.

Byerly, G. R., Lowe, D. R., Wooden, J. L., & Xie, X. (2002). An Archean impact layer from the Pilbara and Kaapvaal cratons. *Science*, *297*, 1325–1327.

Cairns-Smith, A. G. (1982). *Genetic Takeover and Mineral Origins of Life* (477 pp). Cambridge: Cambridge University Press.

Caldeira, K., & Rampino, M. R. (1990). The Mid-Cretaceous superplume, carbon dioxide, and global warming. *Geophysical Research Letters*, *18*, 987–990.

Calvert, A. J., Sawyer, E. W., Davis, W. J., & Ludden, J. N. (1995). Archean subduction inferred from seismic images of a mantle suture in the Superior province. *Nature*, *375*, 670–674.

Campbell, I. H. (2002). Implications of Nb/U, Th/U and Sm/Nd in plume magmas for the relationship between continental and oceanic crust formation and the development of the depleted mantle. *Geochimica et Cosmochimica Acta*, *66*, 1651–1661.

Campbell, I. H., & Allen, C. M. (2008). Formation of supercontinents linked to increases in atmospheric oxygen. *Nature Geoscience*, *1*, 554–558.

Campbell, I. H., & Griffiths, R. W. (1992a). The changing nature of mantle hotspots through time: implications for the chemical evolution of the mantle. *Journal of Geology*, *92*, 497–523.

Campbell, I. H., & Griffiths, R. W. (1992b). The evolution of the mantle's chemical structure. *Lithos*, *30*, 389–399.

Campbell, I. H., & Squire, R. J. (2010). The mountains that triggered the Late Neoproterozoic increase in oxygen: the Second Great Oxidation Event. *Geochimica et Cosmochimica Acta*, *74*, 4187–4206.

Campbell, I. H., Griffiths, R. W., & Hill, R. I. (1989). Melting in an Archean mantle plume: heads it's basalts, tails it's komatiites. *Nature*, *339*, 697–699.

Cameron, A. G. W. (1973). Accumulation processes in the primitive solar nebula. *Icarus*, *18*, 407–450.

Cameron, A. G. W. (1986). The impact theory for origin of the Moon. In W. K. Hartmann, R. J. Phillips & G. J. Taylor (Eds.), *Origin of the Moon* (pp. 609–616). Houston, TX: Lunar & Planetary Institute.

Cande, S. C., Leslie, R. B., Parra, J. C., & Hobart, M. (1987). Interaction between the Chile ridge and the Chile trench: geophysical and geothermal evidence. *Journal of Geophysical Research*, *92*, 495–520.

Canfield, D. E. (1998). A new model for Proterozoic ocean chemistry. *Nature*, *396*, 450–453.

Canfield, D. E., & Teske, A. (1996). Late Proterozoic rise in atmospheric oxygen from phylogenetic and stable isotopic studies. *Nature*, *382*, 127–132.

Canfield, D. E., Habicht, K. S., & Thamdrup, B. (2000). The Archean sulfur cycle and the early history of atmospheric oxygen. *Science*, *288*, 658–661.

Canup, R. M. (2004). Simulations of a late lunar-forming impact. *Icarus*, *168*, 433–456.

Cao, R. (1991). Origin and order of cyclic growth patterns in mat-ministromatolite bioherms from the Proterozoic Wumishan formation, North China. *Precambrian Research*, *52*, 167–178.

Caputo, M. V., & Crowell, J. C. (1985). Migration of glacial centers across Gondwana during Paleozoic era. *Geological Society of America Bulletin*, *96*, 1020–1036.

Card, K. D., & Ciesielski, A. (1986). Subdivisions of the Superior Province of the Canadian Shield. *Geoscience Canada*, *13*, 5–13.

Carey, S., & Sigurdsson, H. A. (1984). *A model of volcanigenic sedimentation in marginal basins* (pp. 37–58). Geological Society of London, Special Publication 16.

Carlson, R. L. (1995). A plate cooling model relating rates of plate motion to the age of the lithosphere at trenches. *Geophysical Research Letters*, *22*, 1977–1980.

Carlson, R. W. (1994). Mechanisms of Earth differentiation: consequences for the chemical structure of the mantle. *Review of Geophysics*, *32*, 337–361.

Carlson, R. W. (1995). Physical and chemical evidence on the cause and source characteristics of flood basalt volcanism. *Australian Journal of Earth Sciences*, *38*, 525–544.

Carlson, R. W., Shirey, S. B., Pearson, D. G., & Boyd, F. R. (1994). *The mantle beneath continents* (pp. 109–117). Carnegie Institution of Washington, Year Book 93.

Carlson, R. W., Pearson, D. G., & James, D. E. (2005). Physical, chemical and chronological characteristics of continental mantle. *Review of Geophysics*, *43*(1). doi:10.1029/2004RG000156.

Caro, G., & Bourdon, B. (2010). Non-chondritic Sm/Nd ratio in the terrestrial planets: consequences for the geochemical evolution of the mantle-crust system. *Geochimica et Cosmochimica Acta*, *74*, 3333–3349.

Carr, M. H. (1987). Water on Mars. *Nature*, *326*, 30–35.

Carr, M. H. (1996). *Water on Mars.* Oxford: Oxford University Press.

Carr, M. H., & Head, J. W., III (2010). Geologic history of Mars. *Earth and Planetary Science Letters*, *294*, 185–203.

Carr, M. H., Kuzmin, R. O., & Masson, P. L. (1993). Geology of Mars. *Episodes*, *16*, 307–315.

Carr, M. H., et al. (1998). Evidence for a sub-surface ocean on Europa. *Nature*, *391*, 363–365.

Catling, D. C., & Claire, M. W. (2005). How Earth's atmosphere evolved to an oxic state: a status report. *Earth and Planetary Science Letters*, *237*, 1–20.

Catling, D. C., Zahnle, K. J., & McKay, C. P. (2001). Biogenic methane, hydrogen escape, and the irreversible oxidation of early Earth. *Science*, *293*, 839–843.

Cavalier-Smith, T. (1987). The simultaneous symbiotic origin of mitochondria, chloroplasts and microbodies. *Annals of the New York Academy of Sciences*, *503*, 55–71.

Cawood, P. A., & Suhr, G. (1992). Generation and obduction of ophiolites: constraints from the Bay of Islands Complex, Western Newfoundland. *Tectonics*, *11*, 884–897.

Cawood, P. A., & Buchan, C. (2007). Linking accretionary orogenesis with supercontinent assembly. *Earth-Science Reviews*, *82*, 217–256.

Cawood, P. A., Kroener, A., Collins, W. J., Kusky, T. M., Mooney, W. D., & Windley, B. F. (2009). Accretionary orogens through Earth history. *Geological Society, London, Special Publications*, *318*, *1–36*.

Chandler, F. W. (1988). Quartz arenites: review and interpretation. *Sed Geol*, *58*, 105–126.

Chang, S. (1994). The planetary setting of prebiotic evolution. In S. Bengtson (Ed.), *Early Life on Earth* (pp. 10–23). New York: Columbia University Press.

Chapman, D. S. (1986). Thermal gradients in the continental crust. In J. B. Dawson, D. A. Carswell, J. Hall, & K. H. Wedepohl (Eds.), *The Nature of the Lower Continental Crust* (pp. 63–70). Geological Society of London, Special Publication 24.

Chapman, D. S., & Furlong, K. P. (1992). Thermal state of the continental lower crust. In D. M. Fountain, R. Arculus, & R. W. Kay (Eds.), *Continental Lower Crust* (pp. 179–199). Amsterdam: Elsevier.

Charbonneau, D., et al. (2009). A super-Earth transiting a nearby low-mass star. *Nature*, *462*, 891–894.

Charlou, J. L., Fouquet, Y., bougalt, H., Donval, J. P., Etoubleau, J., Jean-Baptiste, P., et al. (1998). Intense CH_4 plumes generated by serpentinization of ultramafic rocks at the intersection of the 15°20′ N fracture zone and the Mid-Atlantic Ridge. *Geochimica et Cosmochimica Acta*, *62*, 2323–2333.

Christensen, N. I. (1966). Elasticity of ultrabasic rocks. *Journal of Geophysical Research*, *71*, 5921–5931.

Christensen, N. I., & Mooney, W. D. (1995). Seismic velocity structure and composition of the continental crust: a global view. *Journal of Geophysical Research*, *100*, 9761–9788.

Christensen, U. R. (1995). Effects of phase transitions on mantle convection. *Annual Review of Earth and Planetary Sciences*, *23*, 65–87.

Christensen, U. R., & Yuen, D. A. (1985). Layered convection induced by phase transitions. *Journal of Geophysical Research*, *90*, 10,291–10,300.

Chyba, C. F. (1993). The violent environment of the origin of life: progress and uncertainties. *Geochimica et Cosmochimica Acta*, *57*, 3351–3358.

Chyba, C. F. (2000). Energy for microbial life on Europa. *Nature*, *403*, 381–382.

Clift, P. D., & Hartley, A. J. (2007). Slow rates of subduction erosion and coastal underplating along the Andean margin of Chile and Peru. *Geology*, *35*, 503–506.

Clift, P., & Vannucchi, P. (2004). Controls on tectonic accretion versus erosion in subduction zones: implications for the origin and recycling of the continental crust. *Review of Geophysics*, *42*, RG2001. doi:10.1029/2003RG000127.

Clift, P. D., Vannucchi, P., & Morgan, J. P. (2009). Crustal redistribution, crust-mantle recycling and Phanerozoic evolution of the continental crust. *Earth-Science Reviews*, *97*, 80–104.

Cloos, M. (1993). Lithospheric buoyancy and collisional orogenesis: subduction of oceanic plateaus, continental margins, island arcs, spreading ridges, and seamounts. *Geological Society of America Bulletin*, *105*, 715–737.

Cloud, P. (1968a). Atmospheric and hydrospheric evolution on the primitive Earth. *Science*, *160*, 729–736.

Cloud, P. (1968b). Pre-metazoan evolution and the origins of the metazoa. In E. T. Drake (Ed.), *Evolution and Environment* (pp. 1–72). New Haven, CT: Yale University Press.

Cloud, P. (1973). Paleoecological significance of the banded iron formation. *Economic Geology*, *68*, 1135–1143.

Clowes, R. M., et al. (1992). Lithoprobe: New perspectives on crustal evolution. *Canadian Journal of Earth Sciences*, *29*, 1813–1864.

Clowes, R. M., White, D. J., & Hajnal, Z. (2010). Mantle heterogeneities and their significance: results from Lithoprobe seismic reflection and refraction—wide-angle reflection studies. *Canadian Journal of Earth Sciences*, *47*, 409–443.

Coffin, M. F., & Eldholm, O. (1994). Large igneous provinces: crustal structure, dimensions, and external consequences. *Review of Geophysics*, *32*, 1–36.

Coffin, M. F., Duncan, R. A., Eldholm, O., Fitton, J. G., Frey, F. A., Larsen, H. C., et al. (2006). Large igneous provinces and scientific ocean drilling. *Oceanography*, *19*, 150–160.

Cogley, J. G. (1984). Continental margins and the extent and number of continents. *Review of Geophysics*, *22*, 101–122.

Cogne, J. P., Humler, E., & Courtillot, V. (2006). Mean age of ocanic lithospshere drives eustatic sea level change since Pangea breakup. *Earth and Planetary Science Letter*, *245*, 115–122.

Coleman, R. G. (1977). *Ophiolites* (229 pp). Berlin: Springer-Verlag.

Collerson, K. D., & Kamber, B. S. (1999). Evolution of the continents and the atmosphere inferred from Th-U-Nb systematics of the depleted mantle. *Science*, *283*, 1519–1522.

Collins, W. J. (2002). Hot orogens, tectonic switching, and creation of continental crust. *Geology*, *30*, 535–538.

Coltice, N., Phillips, B. R., Bertrand, H., Ricard, Y., & Rey, P. (2007). Global warming of the mantle at the origin of flood basalts over supercontinents. *Geology*, *35*, 391–394.

Condie, K. C. (1981). *Archean Greenstone Belts* (434 pp). Amsterdam: Elsevier.

Condie, K. C. (1986). Origin and early growth rate of continents. *Precamh Res*, *32*, 261–278.

Condie, K. C. (1989). Geochemical changes in basalts and andesites across the Archean-Proterozoic boundary: identification and significance. *Lithos*, *23*, 1–18.

Condie, K. C. (1990a). Geochemical characteristics of Precambrian basaltic greenstones. In R. P. Hall & D. J. Hughes (Eds.), *Early Precambrian Basic Magmatism* (pp. 40–55). Glasgow, UK: Blackie & Son.

Condie, K. C. (1990b). Growth and accretion of continental crust: inferences based on Laurentia. *Chemical Geology*, *83*, 183–194.

Condie, K. C. (1992a). Evolutionary changes at the Archean-Proterozoic boundary. In J. E. Glover & S. E. Ho (Eds.), *The Archean: Terrains, Processes and Metallogeny. Proceedings Volume of the Third International Archean Symposium 1990* (pp. 177–189). Perth, Australia: University of Western Australia, Publication No. 22.

Condie, K. C. (1992b). Proterozoic terranes and continental accretion in SW North America. In K. C. Condie (Ed.), *Proterozoic Crustal Evolution* (pp. 447–480). Amsterdam: Elsevier.

Condie, K. C. (1993). Chemical composition and evolution of the upper continental crust: contrasting results from surface samples and shales. *Chemical Geology*, *104*, 1–37.

Condie, K. C. (1994). Greenstones through time. In K. C. Condie (Ed.), *Archean Crustal Evolution* (pp. 85–120). Amsterdam: Elsevier.

Condie, K. C. (1995). Episodic ages of greenstones: a key to mantle dynamics. *Geophysical Research Letters*, *22*, 2215–2218.

Condie, K. C. (1997). Contrasting sources for upper and lower continental crust: the greenstone connection. *Journal of Geology*, *105*, 729–736.

Condie, K. C. (1998). Episodic continental growth and supercontinents: a mantle avalanche connection? *Earth and Planetary Science Letters*, *163*, 97–108.

Condie, K. C. (1999). Mafic crustal xenoliths and the origin of the lower continental crust. *Lithos*, *46*, 95–101.

Condie, K. C. (2000). Episodic continental growth models: afterthoughts and extensions. *Tectonophysics*, *322*, 153–162.

Condie, K. C. (2001). *Mantle Plumes and Their Record in Earth History* (306 pp). Cambridge, UK: Cambridge University Press.

Condie, K. C. (2002a). The supercontinent cycle: are there two patterns of cyclicity? *Journal of African Earth Sciences*, *35*(2), 179–183.

Condie, K. C. (2002b). Breakup of a Paleoproterozoic supercontinent. *Gondwana Research*, *5*(1), 41–43.

Condie, K. C. (2003a). Incompatible element ratios in oceanic basalts and komatiites: tracking deep mantle sources and continental growth rates with time. *Geochemistry Geophysics Geosystems*, *4*(1). doi:10.1029/2002GC000333.

Condie, K. C. (2003b). *Supercontinents, superplumes and continental growth: the Neoproterozoic record* (pp. 1–21). Geological Society of London, Special Publication 206.

Condie, K. C. (2004). High field strength element ratios in Archean basalts: a window to evolving sources of mantle plumes. *Lithos*, *79*, 491–504.

Condie, K. C. (2005). High field strength element ratios in Archean basalts: a window to evolving sources of mantle plumes. *Lithos*, *79*, 491–504.

Condie, K. C. (2007). *Accretionary orogens in space and time* (pp. 1–14). Boulder, CO: Geological Society of America, Memoir 200.

Condie, K. C. (2008). Did the character of subduction change at the end of the Archean? Constraints from convergent-margin granitoids. *Geology*, *36*(8), 611–614.

Condie, K. C., & Aster, R. C. (2010). Episodic zircon age spectra of orogenic granitoids: the supercontinent connection and continental growth. *Precambrian Research*, *180*, 227–236.

Condie, K. C., & Benn, K. (2006). *Archean geodynamics: similar to or different from modern geodynamics?* (pp. 47–59). American Geophysical Union, Monograph 164.

Condie, K. C., & Chomiak, B. (1996). Continental accretion: contrasting Mesozoic and Early Proterozoic tectonic regimes in the North America. *Tectonophysics*, *265*, 101–126.

Condie, K. C., & Kroner, A. (2008). *When did plate tectonics begin? Evidence from the geologic record* (pp. 281–295). Boulder, CO: Geological Society of America, Special Paper 440.

Condie, K. C., & O'Neill, C. (2010). The Archean-Proterozoic boundary: 500 My of tectonic transition in Earth history. *American Journal of Science*, *310*, 775–790.

Condie, K. C., & Rosen, O. M. (1994). Laurentia-Siberia connection revisited. *Geology*, *22*, 168–170.

Condie, K. C., & Wronkiewicz, D. J. (1990). The Cr/Th ratio in Precambrian pelites from the Kaapvaal craton as an index of craton evolution. *Earth and Planetary Science Letters*, *97*, 256–267.

Condie, K. C., Des Marais, D. J., & Abbott, D. (2000). Geologic evidence for a mantle superplume event at 1.9 Ga. *Geochemistry Geophysics Geosystems*, 1: Paper no. 2000GC000095.

Condie, K. C., Belousova, E., Griffin, W. L., & Sircombe, K. N. (2009a). Granitoid events in space and time: constraints from igneous and detrital zircon age spectra. *Gondwana Research*, *15*, 228–242.

Condie, K. C., O'Neill, C., & Aster, R. (2009b). Evidence and Implications for a widespread magmatic shutdown for 250 My on Earth. *Earth and Planetary Science Letters*, *282*, 294–298.

Condie, K. C., Bickford, M. E., Aster, R. C., Belousova, E., & Scholl, D. W. (2011). Episodic zircon ages, Hf isotopic composition, and the preservation rate of continental crust. *Geological Society of America Bulletin*, *123*, 951–957.

Conrad, C. P., & Lithgow-Bertelloni, C. (2002). How mantle slabs drive plate tectonics. *Science*, *298*, 207–209.

Cook, F. A., Brown, L. D., Kaufman, S., Oliver, J. E., & Petersen, J. (1981). COCORP seismic profiling of the Appalachian orogen beneath the coastal plain of Georgia. *Geological Society of America Bulletin*, *92*, 738–748.

Cook, F. A., White, D. J., Jones, A. G., Eaton, D. W. S., Hall, J., & Clowes, R. M. (2010). How the crust meets the mantle: lithoprobe perspectives on the Mohorocic discontinuity and crust-mantle transition. *Canadian Journal of Earth Sciences*, *47*, 315–351.

Cook, P. J. (1992). Phosphogenesis around the Proterozoic-Phanerozoic transition. *Journal of the Geological Society of London*, *149*, 615–620.

Cook, P. J., & McElhinny, M. W. (1979). A reevaluation of the spatial and temporal distribution of sedimentary phosphate deposits in the light of plate tectonics. *Economic Geology*, *74*, 315–330.

Cooper, G., Klimmich, N., Belisle, W., Sarinana, J., Brabham, K., & Garrel, L. (2001). Carbonaceous meteorites as a source of sugar-related organic compounds for the early Earth. *Nature*, *414*, 879–883.

Cooper, K. M., Eiler, J. M., Sims, K. W. W., & Languir, C. H. (2009). Distribution of recycled crust within the upper mantle: insights from the oxygen isotope composition of MORB from the Autralian-Antarctic discordance. *Geochemistry Geophysics Geosystems*, *10*(12), Q12004. doi:10.1029/2009GC002728.

Copp, D. L., Guest, J. E., & Stofan, E. R. (1998). New insights into coronae evolutionj: mapping on Venus. *Journal of Geophysical Research*, *103*, 19401–19417.

Corliss, J. B., Baross, J. A., & Hoffman, S. E. (1981). *An hypothesis concerning the relationship between submarine hot springs and the origin of life on Earth* (pp. 59–69). Oceanologica Acta Special Publication No. SP.

Coulton, A. J., Harper, G. D., & O'Hanley, D. S. (1995). Oceanic versus emplacement age serpentinization in the Josephine ophiolite: implications for the nature of the Moho at intermediate and slow spreading ridges. *Journal of Geophysical Research*, *100*, 22,245–22,260.

Courtillot, V., & Besse, J. (1987). Magnetic field reversal, polar wander, and core-mantle coupling. *Science*, *237*, 1140–1147.

Courtillot, V. E., & Cisowski, S. (1987). The K/T boundary events: external or internal causes? *Eos*, *68*, 193.

Courtillot, V., & Olson, P. (2007). Mantle plumes link magnetic superchrons to Phanerozoic mass depletion events. *Earth and Planetary Science Letters*, *260*, 495–504.

Courtillot, V., Jaupart, C., Manighetti, I., Tapponnier, P., & Besse, J. (1999). On causal links between flood basalts and continental breakup. *Earth and Planetary Science Letters*, *166*, 177–195.

Cowan, D. S. (1986). The origin of some common types of melange in the western Cordillera of North America. In N. Nasu, K. Kobayashi, S. Nyeda, I. Kushiro & H. Kagami (Eds.), *Formation of Active Ocean Margins* (pp. 257–272). Dordrecht: D. Reidel Publishers.

Coward, M. P., Jan, M. Q., Rex, O., Tarney, J., Thirwall, M., & Windley, B. F. (1982). Geotectonic framework of the Himalaya of N. Pakistan. *Journal of the Geological Society of London*, *139*, 299–308.

Coward, M. P., Broughton, R. D., Luff, I. W., Peterson, M. G., Pudsey, C. J., Rex, D. C., et al. (1986). *Collision tectonics in the NW Himalayas* (pp. 203–220). Geological Society of London, Special Publication 19.

Cox, A. (1969). Geomagnetic reversals. *Science*, *163*, 237–245.

Cronin, V. S. (1991). The cycloid relative-motion model and the kinematics of transform faulting. *Tectonophysics*, *187*, 215–249.

Crough, S. T. (1983). Hotspot swells. *Annual Review of Earth and Planetary Sciences*, *11*, 165–193.

Crowell, J. C. (1999). *Pre-Mesozoic ice ages: their bearing on understanding the climate system.* Boulder, CO: Geological Society of America, Memoir 192.

Crowhurst, J. C., Brown, J. M., Goncharov, A. F., & Jacobsen, S. D. (2008). Elasticity of (Mg,Fe)O through the spin transition of iron in the lower mantle. *Science*, *319*, 451. doi:10.1126/science.1149606.

Crowley, K. D., & Kuhlman, S. L. (1988). Apatite thermchronometry of Western Canadian shield: implications for origin of the Williston basin. *Geophysical Research Letters*, *15*, 221–224.

Crowley, T. J. (1983). The geologic record of climatic change. *Reviews of geophysics and space physics*, *21*, 828–877.

Crowley, T. J., & Berner, R. A. (2001). CO_2 and climate change. *Science*, *292*, 870–872.

Culotta, R. C., Pratt, T., & Oliver, J. (1990). A tale of two sutures: COCORP's deep seismic surveys of the Grenville province in the eastern U. S. midcontinent. *Geology*, *18*, 646–649.

Dahlen, F. A., & Suppe, J. (1988). *Mechanics, growth and erosion of mountain belts* (pp. 161–178). Boulder, CO: Geological Society of America, Special Paper 218.

Dallmeyer, R. D. & Brown, M. (1992). Rapid Variscan exhumation of Eo-Variscan metamorphic rocks from S. Brittany, France. *Geol Soc Am Progs with Abstracts*, *24*, A236.

Dalziel, I. W. D. (1997). Neoproterozoic-Paleozoic geography and tectonics: review, hypothesis, environmental speculation. *Geological Society of America Bulletin*, *109*, 16–42.

Dalziel, I. W. D., Dalla Salda, L. H., & Gahagan, L. M. (1994). Paleozoic Laurentia-Gondwana interaction and the origin of the Appalachian-Andean mountain system. *Geological Society of America Bulletin*, *106*, 243–252.

Dalziel, I. W. D., Lawver, L. A., & Murphy, J. B. (2000). Plumes, orogenesis, and supercontinental fragmentation. *Earth and Planetary Science Letters*, *178*, 1–11.

Danielson, A., Moller, P., & Dulski, P. (1992). The Eu anomalies in BIFs and the thermal history of the oceanic crust. *Chemical Geology*, *97*, 89–100.

Dauphas, N. (2003). The dual origin of the terrestrial atmosphere. *Icarus*, *165*, 326–339.

Davaille, A. (1999). Simultaneous generation of hotspots and superswells by convection in a heterogeneous planetary mantle. *Nature*, *402*, 756–760.

Davies, G. F. (1980). Review of oceanic and global heat flow estimates. *Review of Geophysics*, *18*, 718–722.

Davies, G. F. (1992). On the emergence of plate tectonics. *Geology*, *20*, 963–966.

Davies, G. F. (1993). Conjectures on the thermal and tectonic evolution of the Earth. *Lithos*, *30*, 281–289.

Davies, G. F. (1995). Penetration of plates and plumes trough the mantle transition zone. *Earth and Planetary Science Letters*, *133*, 507–516.

Davies, G. F. (1996). Punctuated tectonic evolution of the Earth. *Earth and Planetary Science Letters*, *136*, 363–379.

Davies, G. F. (1999). *Dynamic Earth Plates, Plumes and Mantle Convection* (458 pp). Cambridge, UK: Cambridge University Press.

Davies, G. F. (2002). Stirring geochemistry in mantle convection mdels with stiff plates and slabs. *Geochimica et Cosmochimica Acta*, *66*, 3125–3142.

de Duve, C. (1995). The beginnings of life on Earth. *Am Scient*, *83*, 428–437.

De Gregorio, B. T., Sharp, T. G., Flynn, G. J., Wirick, S., & Hevig, R. L. (2009). Biogenic origin for Earth's oldest putative microfossils. *Geology*, *37*, 631–634.

de Kock, M. O., Evans, D. A. D., & Beukes, N. J. (2009). Validating the existence of Vaalbara in the Neoarchean. *Precambrian Research*, *174*, 145–154.

de Wit, M. J. (1998). On Archean granites, greenstones, cratons and tectonics: does the evidence demand a verdict? *Precambrian Research*, *91*, 181–226.

de Wit, M. J. (2004). Archean greenstone belts do contain fragments of ophiolites. In T. M. Kusky (Ed.), *Precambrian Ophiolites and Related Rocks* (pp. 599–614). Amsterdam: Elsevier.

de Wit, M. J., & Ashwal, L. D. (1995). Greenstone belts: what are they? *South African Journal of Geology*, *98*, 505–520.

deWit, M. J., Hart, R. A., & Hart, R. J. (1987). The Jamestown ophiolite complex, Barberton mountain belt: a section through 3.5 Ga oceanic crust. *Journal of African Earth Sciences*, *6*, 681–730.

de Wit, M. J., et al. (1992). Formation of an Archean continent. *Nature*, *357*, 553–562.

DeBari, S. M., & Sleep, N. H. High-Mg, (1991). Low-Al bulk composition of the Talkeetna island arc, Alaska: implications for primary magmas and the nature of the arc crust. *Geological Society of America Bulletin*, *103*, 37–47.

Deenen, M. H. L., Ruhl, M., Bonis, N. R., Krijgsman, W., Kuerschner, W. M., Reitsma, M., et al. (2010). A new chronology for the end-Triassic extinction. *Earth and Planetary Science Letters*, *291*, 113–125.

Deguen, R., & Cardin, P. (2009). Tectonic history of the Earth's inner core preserved in its seismic structure. *Nature Geoscience*, *2*, 419–422.

DeLong, S. E., & Fox, P. J. (1977). Geological consequence of ridge subduction. In M. Talwani & W. C. Pittman (Eds.), *Island Arcs, Deep-Sea Trenches, and Back Arc Basins. Maurice Ewing Series 1* (pp. 221–228). American Geophysical Union.

DeMets, C., Gordon, R. G., Stein, S., & Argus, D. F. (1990). Current plate motions. *Geophysical Research Letters*, *14*, 911–914.

Deming, D. (1999). On the possible influence of extraterrestrial volaties on Earth's climate and the origin of the oceans. *Palaeogeography, Palaeoclimatology, Palaeoecology*, *146*, 33–51.

Derry, L. A., & Jacobsen, S. R. (1990). The chemical evolution of Precambrian seawater: evidence from REEs in BIF. *Geochimica et Cosmochimica Acta*, *54*, 2965–2977.

Derry, L. A., Kaufman, A. J., & Jacobsen, S. B. (1992). Sedimentary cycling and environmental change in the Late Proterozoic: evidence from stable and radiogenic isotopes. *Geochimica et Cosmochimica Acta*, *56*, 1317–1329.

Des Marais, D. J. (1994). The Archean atmosphere: its composition and fate. In K. C. Condie (Ed.), *Archean Crustal Evolution* (pp. 505–523). Amsterdam: Elsevier.

Des Marais, D. J. (1997). Long-term evolution of the bio-geochemical carbon cycle. In J. F. Banfield & K. H. Nielsen. (Eds.), *Geomicrobiology: interactions between microbes and minerals. Rev. Mineral* (Vol. 35, pp. 429–448).

Des Marais, D. J., Strauss, H., Summons, R. E., & Hayes, J. M. (1992). Carbon isotope evidence for the stepwise oxidation of the Proterozoic environment. *Nature*, *359*, 605–609.

Desrochers, J.-P., Hubert, C., Ludden, J. N., & Pilote, P. (1993). Accretion of Archean oceanic plateau fragments in the Abitibi greenstone belt, Canada. *Geology*, *21*, 451–454.

Deuss, A., Irvina, J. D. E., & Woodhouse, J. H. (2010). Regional variation of inner core anisotropy from seismic normal mode observations. *Science*, *328*, 1018–1020.

Dewey, J. F. (1988). Extensional collapse of orogens. *Tectonics*, *7*, 1123–1139.

Dewey, J. F., & Kidd, W. S. F. (1977). Geometry of plate accretion. *Geological Society of America Bulletin*, *88*, 960–968.

Dewey, J. F., Hempton, M. R., Kidd, W. S. F., Saroglu, F., & Sengor, A. M. C. (1986). *Shortening of continental lithosphere: the neotectonics of eastern Anatolia—a young collision zone* (pp. 3–36). Geological Society of London, Special Publication 19.

Dick, H. J. B., Lin, J., & Schouten, H. (2003). An ultraslow spreading class of ocean ridge. *Nature*, *426*, 405–412.

Dickinson, W. R. (1970). Relations of andesites, granites, and derivative sandstones to arc-trench tectonics. *Review of Geophysics*, *8*, 813–860.

Dickinson, W. R. (1973). Widths of modern arc-trench gaps proportional to past duration of igneous activity in associated magmatic arcs. *Journal of Geophysical Research*, *78*, 3376–3389.

Dickinson, W. R., & Seely, D. R. (1986). Structure and stratigraphy of forearc regions. *American Association of Petroleum Geologists Bulletin*, *63*, 2–31.

Dilek, Y., & Eddy, E. A. (1992). The Troodos and Kizaldag ophiolites as structural models for slow-spreading ridge segments. *Journal of Geology*, *100*, 305–322.

Dilek, Y., & Robinson, P. T. (2003). *Ophiolites in Earth History* (717 pp). Geological Society London, Special Publication 218.

Domagal-Goldman, S. D., Kasting, J. F., Johnston, D. T., & Farquhar, J. (2008). Organic haze, glaciations and multiple sulfur isotopes in the mid-Archean era. *Earth and Planetary Science Letters*, *269*, 29–40.

Donnadieu, Y., Ramstein, G., Fluteau, F., Besse, J., & Meert, J. (2002). Is high obliquity a plausible cause for Neoproterozoic glaciations? *Geophysical Research Letters*, 29. doi:10.1029/2002GL015902.

Doolittle, W. F. (1999). Phylogenetic classification and the universal tree. *Science*, *284*, 2124–2128.

Dott, R. H., Jr. (2003). The importance of eolian abrasion in supermature quartz sandstones and the paradox of weathering on vegetation-free landscapes. *Journal of Geology*, *111*, 387–405.

Douglass, J., Schilling, J. G., & Fontignie, D. (1999). Plume-ridge interactions of the Discovery and Shona mantle plumes with the southern Mid-Atlantic Ridge (40–55°S). *Journal of Geophysical Research*, *104*, 2941–2962.

Downes, H. (1993). The nature of the lower continental crust of Europe: petrological and geochemical evidence from xenoliths. *Physics of the Earth and Planetary Interiors*, *79*, 195–218.

Drake, M. J. (2000). Accretion and primary differentiation of the Earth: a personal journey. *Geochimica et Cosmochimica Acta*, *64*, 2363–2370.

Drake, M. J., & Righter, K. (2002). Determining the composition of the Earth. *Nature*, *416*, 39–44.

Duba, A. (1992). Earth's core not so hot. *Nature*, *359*, 197–198.

Dubrovinsky, L., et al. (2003). Iron-silica interaction at extreme conditions and the electrically conducting layer at the base of Earth's mantle. *Nature*, *422*, 58–61.

Duffy, T. S. (2008). Mineralogy at the extremes. *Nature*, *451*, 269–270.

Duffy, T. S., Zha, C., Downs, R. T., Mao, H., & Hemley, R. J. (1995). Elasticity of forsterite to 16 GPa and the composition of the upper mantle. *Nature*, *378*, 170–173.

Dumberry, M., & Bloxham, J. (2003). Torque balance, Taylor's constraint and torsional oscillations in the numerical model of the geodynamo. *Physics of the Earth and Planetary Interiors*, *140*, 29–51.

Duncan, R. A. (1991). Ocean drilling and the volcanic record of hotspots. *GSA Today*, *1*(10), October, 1991.

Duncan, R. A., & Erba, E. (2003). Thermal and compositional effects of oceanic LIPSs: consequences for Cretaceous ocean anoxic events. In *Mantle Plumes: Physical Processes, Chemical Signatures and Biological Effects* (Abstract Vol., p. 10). Cardiff, UK: Cardiff University, September 2003.

Duncan, R. A., & Richards, M. A. (1991). Hotspots, mantle plumes, flood basalts, and true polar wander. *Review of Geophysics*, *29*, 31–50.

Dunlop, D. J. (1995). Magnetism in rocks. *Journal of Geophysical Research*, *100*, 2161–2174.

Durrheim, R. J., & Mooney, W. D. (1991). Archean and Proterozoic crustal evolution: evidence from crustal seismology. *Geology*, *19*, 606–609.

Durrheim, R. J., & Mooney, W. D. (1994). Evolution of the Precambrian lithosphere: seismological and geochemical constraints. *Journal of Geophysical Research*, *99*, 15,359–15,374.

DuToit, A. (1937). *Our Wandering Continents* (366 pp). London: Oliver and Boyd.

Eaton, D. W., Darbyshire, F., Evans, R. L., Grutter, H., Jones, A. G., & Yuan, X. (2009). The elusive lithosphere-asthenosphere boundary (LAB) beneath cratons. *Lithos*, *109*, 1–22.

Edmunson, J., Borg, L. E., Nyquist, L. E., & Asmerom, Y. (2009). A combined Sm-Nd, Rb-Sr, and U-Pb isotopic study of Mg-suite norite 78238: further evidence for early differentiation of the Moon. *Geochimica et Cosmochimica Acta*, *73*, 514–527.

El Albani, A., et al. Large colonial organisms with coordinated growth in oxygenated environments 2.1 Ga ago. *Nature*, *466*, 100–104.

Elliott, T. (2010). Hard core contstraints on accretion. *Nature Geoscience*, *3*, 382–383.

Elrick, M., Molina-Garza, R., Duncan, R., & Snow, L. (2009). C-isotope stratigraphy and paleoenvironmental changes across OAE2 from shallow-water platform carbonates of southern Mexico. *Earth and Planetary Science Letters*, *277*, 295–306.

Elthon, D., & Scarfe, C. M. (1984). High pressure phase equilibria of a high-MgO basalt and the genesis of primary oceanic basalts. *American Mineralogist*, *69*, 1–15.

Emslie, R. F. (1978). Anorthosite massifs, rapakivi granites, and Late Proterozoic rifting of North America. *Precamb Res*, *7*, 61–98.

Engel, A. E. J., Itson, S. P., Engel, C. G., Stickney, D. M., & Cray, D. J. (1974). Crustal evolution and global tectonics: a petrogenetic view. *Geological Society of America Bulletin*, *85*, 843–858.

England, P. C., & Richardson, S. W. (1977). The influence of erosion upon the mineral facies of rocks from different metamorphic environments. *Journal of the Geological Society of London*, *134*, 201–213.

Eriksson, K. A., & Fedo, C. M. (1994). Archean synrift and stable-shelf sedimentary successions. In K. C. Condie (Ed.), *Archean Crustal Evolution* (pp. 171–203). Amsterdam: Elsevier.

Eriksson, P. G. (1999). Sea level changes and the continental freeboard concept: general principles and application to the Precambrian. *Precambrian Research*, *97*, 143–154.

Eriksson, P. G., & Cheney, E. S. (1992). Evidence for the transition to an oxygen-rich atmosphere during the evolution of redbeds in the Lower Proterozoic sequences of southern Africa. *Precambrian Research*, *54*, 257–269.

Eriksson, P. G., Mazumder, R., Sarkar, S., Bose, P. K., Altermann, W., & van der Merwe, R. (1999). The 2.7–2.0 Ga volcano-sedimentary record of Africa, India, and Australia: evidence for global and local changes in sea level and continental freeboard. *Precambrian Res*, *97*, 269–302.

Eriksson, P. B., et al. (2002). Late Archean superplume events: a Kaapvaal-Pilbara perspective. *Journal of Geodynamics*, *34*, 207–247.

Ernst, R., & Bleeker, W. (2010). Large igneous provinces (LIPs), giant dyke swarms, and mantle plumes: significance for breakup events within Canada and adjacent regions from 2.5 Ga to the present. *Canadian Journal of Earth Sciences*, *47*, 695–739.

Ernst, R. E., & Buchan, K. L. (2001). *The use of mafic dike swarms in identifying and locating mantle plumes* (pp. 247–266). Boulder, CO: Geological Society of America, Special Paper 352.

Ernst, R. E., & Buchan, K. L. (2003). Recognizing mantle plumes in the geological record. *Annual Review of Earth and Planetary Sciences*, *31*, 469–523.

Ernst, R. E., Head, J. W., Parfitt, E., Grosfils, E., & Wilson, L. (1995). Giant radiating dyke swarms on Earth and Venus. *Earth-Science Reviews*, *39*, 1–58.

Ernst, R. E., Wingate, M. T. D., Buchan, K. L., & Li, Z. X. (2008). Global record of 1600–700 Ma large igneous provinces (LIPs): implications for the recontruction of the proposed Nuna (Columbia) and Rodinia supercontinents. *Precambrian Research*, *160*, 159–178.

Ernst, W. G. (1972). Occurrence and mineralogic evolution of blueschist belts with time. *American Journal of Science*, *272*, 657–668.

Ernst, W. G. (Ed.). (2000). *Earth Systems: Processes and Issues* (566 pp). Cambridge, UK: Cambridge University Press.

Ernst, W. G. (2003). High-pressure and ultrahigh-pressure metamorphic belts - Subduction, recrystallization, exhumation, and significance for ophiolite studies. In Y. Dilek & S. Newcombe (Eds.), *Ophiolite Concept and Evolution of Geological Thought* (pp. 365–384). Boulder, CO: Geological Society of America, Special Paper 373.

Erwin, D. H. (1993). *The Great Paleozoic Crisis.* NY: Columbia University Press.

Erwin, D. H. (1994). The Permo-Triassic extinction. *Nature*, *367*, 231–235.

Erwin, D. H. (2003). Impact at the Permo-Triassic boundary: a critical evaluation. *Astrobiology*, *3*, 67–74.

Estey, L. H., & Douglas, B. J. (1986). Upper mantle anisotropy: a preliminary model. *Journal of Geophysical Research*, *91*, 11393–11406.

Evans, A. D., & Pisarevsky, S. A. (2008). *Plate tectonics on early Earth? Weighing the paleomagnetic evidence* (pp. 249–263). Boulder, CO: Geological Society of America, Special Paper 440.

Evans, D. A. D., Li, Z. X., Kirschvinik, J. L., & Wingate, M. T. D. (2000). A high-quality mid-Neoproterozoic paleomagnetic pole from South China, with implications for ice ages and the breakup configuration of Rodinia. *Precambrian Research*, *100*, 313–334.

Eyles, N. (1993). Earth's glacial record and its tectonic setting. *Earth-Science Reviews*, *35*, 1–248.

Ernst, W. G. (2003). High-pressure and ultrahigh-pressure metamorphic belts—subduction, recrystallization, exhumation, and significance for ophiolite studies. In Y. Dilek & S. Newcombe (Eds.), *Ophiolite Concept and Evolution of Geological Thought* (pp. 365–384). Boulder, CO: Geological Society of America, Special Paper 373.

Fahrig, W. F. (1987). *The tectonic settings of continental mafic dyke swarms: failed arm and early passive margin* (pp. 331–348). Geological Association of Canada, Special Paper 34.

Fanale, F. P. (1971). A case for catastrophic early degassing of the Earth. *Chemical Geology*, *8*, 79–105.

Farmer, J. (1998). Thermophiles, early biosphere evolution, and the origin of life on Earth: implications for the exobiological exploration of Mars. *Journal of Geophysical Research*, *103*, 28457–28461.

Farquhar, J., & Wing, B. A. (2003). Multiple sulfur isotopes and the evolution of the atmosphere. *Earth and Planetary Science Letters*, *213*, 1–13.

Farquhar, J., Bao, H. M., & Thiemens, M. (2000). Atmospheric influence of Earth's earliest sulfur cycle. *Science*, *289*, 756–758.

Faure, K., de Wit, M. J., & Willis, J. P. (1995). Late Permian global coal hiatus linked to ^{13}C-depleted CO_2 flux into the atmosphere during the final consolidation of Pangea. *Geology*, *23*, 507–510.

Fedo, C. M., Myers, J. S., & Appel, P. W. U. (2001). Depositional setting and paleogeographic implications of Earth's oldest supracrustal rocks, the >3.7 Ga Isua greenstone belt, West Greenland. *Sedimentol Geol*, *141–142*, 61–77.

Fegley, B. (2003). *Venus. Treatise on Geochemistry* (Chap. 1.19, pp. 487–507). Amsterdam: Elsevier.

Fei, Y., Van Orman, J., van Westrenen, W., Sanloup, C., Minarik, W., Hirose, K., et al. (2004). Experimentally determined postspine transformation boundary in Mg2SiO4 uing MgO as an internal pressure standard and its geophysical implications. *Journal of Geophysical Research*, *108*, B02305. doi:10.1029/2003JB002562.

Fischer, A. G. (1984). Biological innovations and the sedimentary record. In H. D. Holland & A. F. Trendall (Eds.), *Patterns of Change in Earth Evolution* (pp. 145–157). Berlin: Springer-Verlag.

Fischer, K. M., Ford, H. A., Abt, D. L., & Rychert, C. A. (2010). The lithosphere-asthenosphere boundary. *Annual Review of Earth and Planetary Sciences*, *38*, 551–575.

Fisher, D. E. (1985). Radiogenic rare gases and the evolutionary history of the depleted mantle. *Journal of Geophysical Research*, *90*, 1801–1807.

Fisher, R. V. (1984). *Submarine volcaniclastic rocks* (pp. 5–28). Geological Society of London, Special Publication 16.

Fitton, J. G., Saunders, A. D., Larsen, L. M., Hardarson, B. S., & Norry, M. J. (1998). Volcanic rocks from the SE Greenland margin at 63° N: composition, petrogenesis, and mantle sources. *Proceedings of the Ocean Drilling Program, Scientific Results*, *152*, 331–350.

Foley, S. F., Buhre, S., & Jacob, D. E. (2003). Evolution of the Archean crust by shallow subduction and recycling. *Nature*, *421*, 249–252.

Follmi, K. B. (1996). The phosphorus cycle, phosphogenesis and marine phosphate-rich deposits. *Earth-Science Reviews*, *40*, 55–124.

Folk, R. L. (1976). Reddening of desert sands: Simpson Desert, N.T. *Australia Journal of Sedimentary Petrology*, *46*, 604–615.

Foote, M. (2003). Origination and extinction through the Phanerozoic: a new approach. *Journal of Geology*, *111*, 125–148.

Forsyth, D. W. (1996). Partial melting beneath a Mid-Atlantic segment detected by teleseismic PKP delays. *Geophysical Research Letters*, *23*, 463–466.

Fouch, D. E., Vandecar, J. C., van der Lee, S., & Kaapvaal Seismic Group. (2004). Mantle seismic structure beneath the Kaapvaal and Zimbabwe cratons. *South African Journal of Geology*, *107*, 33–44.

Foulger, G. R., & Natland, J. H. (2003). Is "hotspot" volcanism a consequence of plate tectonics? *Science*, *300*, 921–922.

Fountain, D. M., & Salisbury, M. H. (1981). Exposed crustal-sections through the continental crust: implications for crustal structure, petrology and evolution. *Earth and Planetary Science Letters*, *56*, 263–277.

Fountain, D. M., Furlong, K. P., & Salisbury, M. H. (1987). A heat production model of a shield area and its implications for the heat flow-heat production relationship. *Geophysical Research Letters*, *14*, 283–286.

Frakes, L. A. (1979). *Climates throughout Geologic Time* (310 pp). Amsterdam: Elsevier.

Frakes, L. A., Francis, J. E., & Syktus, J. L. (1992). *Climate Modes of the Phanerozoic* (274 pp). New York: Cambridge University Press.

Frei, R., Gaucher, C., Poulton, S. W., & Canfield, D. E. (2009). Fluctuations in Precambrian atmospheric oxygenation recorded by chromium isotopes. *Nature*, 461. doi:10.1038/nature08266.

Friend, C. R. L., Nutman, A. P., & McGregor, V. R. (1988). Late Archean terrane accretion in the Godthab region, southern West Greenland. *Nature*, *335*, 535–538.

Frost, C. D., & Frost, B. R. (1997). Reduced rapakivi-type granites: the tholeiite connection. *Geology*, *25*, 647–650.

Froude, D. O., Ireland, T. R., Kinny, P. O., Williams, I. S., & Compston, W. (1983). Ion microprobe identification of 4100–4200 Ma-old terrestrial zircons. *Nature*, *304*, 616–618.

Fryer, P. (1996). Evolution of the Mariana convergent plate margin system. *Review of Geophysics*, *34*, 89–125.

Fukao, Y., Obayashi, M., Nakakuki, T., & Deep Slab Project Group, (2009). Stagnant slab: a review. *Annual Review of Earth and Planetary Sciences*, *37*, 19–46.

Fuller, M., & Cisowski, S. M. (1987). Review of lunar magnetism. In J. A. Jacobs (Ed.), *Geomagnetism*. New York: Academic Press.

Furnes, H., de Wit, M., Staudigel, H., Rosing, M., & Muehlenbachs, K. (2007). A vestige of Earth's oldest ophiolite. *Science*, *315*, 1704–1707.

Fyfe, W. S. (1978). The evolution of the Earth's crust: modern plate tectonics to ancient hot spot tectonics? *Chemical Geology*, *23*, 89–114.

Gaffin, S. (1987). Ridge volume dependence on seafloor generation rate and inversion using long term sea level change. *American Journal of Science*, *287*, 596–611.

Gaherty, J. B., & Jordan, T. H. (1995). Lehmann discontinuity as the base of an anisotropic layer beneath continents. *Science*, *268*, 1468–1471.

Galer, S. J. G. (1991). Interrelationships between continental freeboard, tectonics and mantle temperature. *Earth and Planetary Science Letters*, *105*, 214–228.

Galer, S. J. G., & Mezger, K. (1998). Metamorphism, denudation and sea level in the Archean and cooling of the Earth. *Precambrian Research*, *92*, 389–412.

Ganguly, J., Freed, A. M., & Saxena, S. K. (2009). Density profiles of oceanic slabs and surrounding mantle: integrated thermodynamic and thermal modeling, and implications for the fate of slabs at the 660 km discontinuity. *Physics of the Earth and Planetary Interiors*, *172*, 257–267.

Gao, S., & Wedepohl, K. H. (1995). The negative Eu anomaly in Archean sedimentary rocks: implications for decomposition, age and importance of their granitic sources. *Earth and Planetary Science Letters*, *133*, 81–94.

Garfunkel, Z. (1986). Review of oceanic transform activity and development. *Journal of the Geological Society of London*, *143*, 775–784.

Garfunkel, Z., Anderson, C. A., & Schubert, G. (1986). Mantle circulation and the lateral migration of subducted slabs. *Geophys Res*, *91*, 7205–7223.

Gastil, G. (1960). The distribution of mineral dates in time and space. *American Journal of Science*, *258*, 1–35.

Gaudi, B. S., et al. (2008). Discovery of a Jupiter/Sturn analog with gravitiational micorlensing. *Science*, *319*, 927–930.

Genda, H., & Abe, Y. (2003). Survival of a proto-atmosphere through the stage of giant impacts: the mechanical aspect. *Icarus*, *164*, 149–162.

Genda, H., & Ikoma, M. (2007). Origin of the ocean on the Earth: early evolution of water D/H in a hydrogen-rich atmosphere. *Icarus*, *194*, 42–52.

Gibbs, A. K., Montgomery, C. W., O'Day, P. A., & Erslev, E. A. (1986). The Archean/Proterozoic transition: evidence form the geochemistry of metasedimentary rocks of Guyana and Montana. *Geochimica et Cosmochimica Acta*, *50*, 2125–2141.

Gilbert, W. (1986). The RNA world. *Nature*, *319*, 618.

Glatzmaier, G. A. (2002). Geodynamo simulations—how realistic are they? *Annual Review of Earth and Planetary Sciences*, *30*, 237–257.

Glikson, A. Y. (2008). Field evidence of Eros-scale asteroids and impact-forcing of Predcambrian geohynamic episodes, Kaapvaal and Pilbara cratons. *Earth and Planetary Science Letters*, *267*, 558–570.

Glodny, J., Echtler, H., Figueroa, O., Franz, G., Grafe, K., Kemnitz, H., et al. (2006). Long-term geological evolution and mass-flow balance of the South-Central Andes. In *The Andes, Frontiers in Earth Sciences* (2006, Part III, pp. 401–428). DOI: 10.1007/978-3-540-48684-8_19.

Goff, J. A., Holliger, K., & Levander, A. (1994). Modal fields: a new method for characterization of random velocity heterogeneity. *Geophysical Research Letters*, *21*, 493–496.

Goldblatt, C., Claire, M. W., Lenton, T. M., Matthews, A. J., Watson, A. J., & Zahnle, K. J. (2009). Nitrogen-enhanced greenhouse warming on early Earth. *Nature Geoscience*, *2*, 891–896.

Goldfarb, R. J., Groves, D. I., & Gardoll, S. (2001). Orogenic gold and geologic time: a global synthesis. *Ore Geology Reviews*, *18*, 1–75.

Goldfarb, R. J., Bradley, D., & Leach, D. L. (2010). Secular variation in economic geology. *Economic Geology*, *105*, 459–465.

Goldstein, S. J., & Jacobsen, S. B. (1988). Nd and Sr isotopic systematics of river water suspended material: implications for crustal evolution. *Earth and Planetary Science Letters*, *87*, 249–265.

Gordon, R. G., & Stein, S. (1992). Global tectonics and space geodesy. *Science*, *256*, 333–342.

Gostin, V. A., McKirdy, D. M., Webster, L. J., & Williams, G. E. (2010). Ediacaran ice-rafting and coeval asteroid impact, South Australia: insights into the terminal Proterozoic environment. *Australian Journal of Earth Sciences*, *57*, 859–869.

Goto, K., Hamaguchi, H., & Suzuki, Z. (1985). Earthquake generating stresses in a descending slab. *Tectonophysics*, *112*, 111–128.

Graham, J. B., Dudley, R., Aguilar, N. M., & Gans, C. (1995). Implications of the late Paleozoic oxygen pulse for physiology and evolution. *Nature*, *375*, 117–120.

Graham, S. A., et al. (1986). Provenance modeling as a technique for analyzing source terrane evolution and controls on foreland sedimentation. In A. Allen & P. Homewood (Eds.), *Foreland Basins* (pp. 425–436). Oxford: Blackwell Scientific.

Grand, S. P. (1987). Tomographic inversion for shear velocity beneath the North American plate. *Journal of Geophysical Research*, *92*, 14,065–14,090.

Grand, S. P., van der Hilst, R. D., & Widiyantoro, S. (1997). Global seismic tomography: a snapshot of convection in the Earth. *GSA Today*, *7*(4), 1–7.

Grattan, J. (2003). Pollution and paradigms: lessons from the Laki fissure eruption. In *Mantle Plumes: Physical Processes, Chemical Signatures and Biological Effects* (19 pp). Cardiff, UK: Abstract Volume, Cardiff University, September 2003.

Greenberg, R. (1989). Planetary accretion. In S. K. Atreya, J. B. Pollack, & M. S. Matthews (Eds.), *Origin and Evolution of Planetary and Satellite Atmospheres* (pp. 137–165). Tucson: University of Arizona Press.

Greene, A. R., Scoates, J. S., & Weis, D. (2008). Wrangellia flood basalts in Alaska: a record of plume-lithosphere interaction in a Late Triassic accreted oceanic plateau. *Geochemistry Geophysics Geosystems*, *9*(12). doi:10.1029/2008GC002092.

Greenwood, R. C., Franchi, I. A., Jambon, A., & Buchanan, P. C. (2005). Widespread magma oceans on asteroidal bodies in the early solar system. *Nature*, *435*, 916–918.

Gregory, R. T. (1991). Oxygen isotope history of seawater revisited: time scales for boundary event changes in the oxygen isotope composition of seawater. In H. P. Taylor Jr., et al. (Eds.), *Stable Isotope Geochemistry* (pp. 65–76). Geochemical Society Special Publication No. 3.

Grey, K., Walter, M. R., & Calver, C. R. (2003). Neoproterozoic biotic diversification: snowball Earth or aftermath of the Acraman impact? *Geology*, *31*, 459–462.

Grieve, R. A. F. (1980). Impact bombardment and its role in protocontinental growth on the early Earth. *Precambrian Research*, *10*, 217–247.

Griffin, W. L., & O'Reilly, S. Y. (1987). Is the continental Moho the crust-mantle boundary? *Geology*, *15*, 241–244.

Griffin, W. L., O'Reilly, S. Y., Ryan, C. G., Gaul, O., & Ionov, D. A. (1998). *Secular variation in the composition of subcontinental lithospheric mantle: geophysical and geodynamic implications. Geodynamic Series Monograph 26* (25 pp). American Geophysical Union.

Griffin, W. L., O'Reilly, S. Y., & Ryan, C. G. (1999). The composition and origin of subcontinental lithospheric mantle. In Y. Fei, C. M. Berka, & B. O. Mysen (Eds.), *Mantle Petrology: Field Observations and High Pressure Experimentation* (pp. 13–45). Geochemical Society, Special Publication 6.

Griffin, W. L., O'Reilly, S. Y., Abe, N., Aulbach, S., Davies, R. M., Pearson, N. J., et al. (2003). The origin and evolution of Archean lithospheric mantle. *Precambrian Research*, *127*, 19–41.

Griffiths, R. W., & Campbell, I. H. (1990). Stirring and structure in mantle plumes. *Earth and Planetary Science Letters*, *99*, 66–78.

Grossman, L. (1972). Condensation in the primitive solar nebula. *Geochimica et Cosmochimica Acta*, *36*, 597–619.

Grotzinger, J. P. (1990). Geochemical model for Proterozoic stromatolite decline. *American Journal of Science*, *290–A*, 80–103.

Grotzinger, J. P., & Kasting, J. F. (1993). New constraints on Precambrian ocean composition. *Journal of Geology*, *101*, 235–243.

Grotzinger, J. P., & Knoll, A. H. (1999). Stomatolites in Precambrian carbonates: evolutionary mileposts or environmental dipsticks? *Annual Review of Earth and Planetary Sciences*, *27*, 313–358.

Grotzinger, J. P., Bowring, S. A., Saylor, B. Z., & Kaufman, A. J. (1995). Biostratigraphic and geochronologic constraints on early animal evolution. *Science*, *270*, 589–604.

Grove, T. L., & Parman, S. W. (2004). Thermal evolution of the Earth recorded by komatiites. *Earth and Planetary Science Letters*, *219*, 173–187.

Grove, T. L., Till, C. B., Lev, E., Chatterjee, N., & Medard, E. (2009). Kinematic variables and water transport control the formation and leation of arc volcanoes. *Nature*, *459*(4), 694–697.

Groves, D. I., & Barley, M. E. (1994). Archean Mineralization. In K. C. Condie (Ed.), *Archean Crustal Evolution* (pp. 461–504). Amsterdam: Elsevier.

Groves, D. I., Vielreicher, R. M., Goldfarb, R. J., & Condie, K. C. (2005). *Controls on the heterogeneous distribution of mineral deposits through time* (pp. 71–101). Geological Society of London, Special Publication 248.

Gubbins, D. (1994). Geomagnetic polarity reversals: a connection with secular variation and core-mantle interaction? *Review of Geophysics*, *32*, 61–83.

Gubbins, D. (2008). Geomagnetic reversals. *Nature*, *452*, 165–167.

Guillou, L., & Jaupart, C. (1995). On the effect of continents on mantle convection. *Journal of Geophysical Research*, *100*, 24,217–24,238.

Guo, Q., Strauss, H., Kaufman, A. J., Schroder, S., Gutzmer, J., Wing, B., et al. (2009). Reconstructing Earth's surface oxidation across the Archean-Proterozoic transition. *Geology*, *37*, 399–402.

Gurnis, M. (1988). Large-scale mantle convection and the aggregation and dispersal of supercontinents. *Nature*, *332*, 695–699.

Gurnis, M. (1993). Phanerozoic marine inundation of continents driven by dynamic topography above subductiing slabs. *Nature*, *364*, 589–593.

Gurnis, M., & Davies, G. F. (1986). Apparent episodic crustal growth arising from a smoothly evolving mantle. *Geology*, *14*, 396–399.

Gurwell, M. A. (1995). Evolution of deuterium on Venus. *Nature*, *378*, 22–23.

Haapala, I., & Ramo, T. (1990). *Petrogenesis of the Proterozoic rapakivi granites of Finland* (pp. 275–286). Boulder, CO: Geological Society of America, Special Paper 246.

Hager, B. H., & Clayton, R. W. (1988). Constraints on the structure of mantle convection using seismic observations, flow models, and the geoid. In W. R. Peltier (Ed.), *Mantle Convection* (pp. 657–763). New York: Gordon & Breach.

Hager, B. H., & Clayton, R. W. (1989). Constraints on the structure of mantle convection using seismic observations, flow models, and the geoid. In W. R. Peltier (Ed.), *Mantle Convection* (pp. 657–763). New York: Gordon & Breach.

Hager, B. H., Clayton, R. W., Richards, M. A., Comer, R. P., & Dziewonski, A. M. (1985). Lower mantle heterogeneity, dynamic topography, and the geoid. *Nature*, *313*, 541–545.

Haggerty, S. E., & Sautter, V. (1990). Ultradeep ultramafic upper mantle xenoliths. *Science*, *248*, 993–996.

Hale, C. J. (1987). Paleomagnetic data suggest link between the Archean/Proterozoic boundary and inner core nucleation. *Nature*, *329*, 233–236.

Hallam, A. (1973). Provinciality, diversity, and extinction of Mesozoic marine invertebrates in relation to plate movements. In D. H. Tarling & S. K. Runcorn (Eds.), *Implications of Continental Drift to the Earth Sciences* (Vol. 1, pp. 287–294). London: Academic Press.

Hallam, A. (1974). Changing patterns of provinciality and diversity of fossil animals in relation to plate tectonics. *Journal of Biogeography*, *1*, 213–225.

Hallam, A. (1987). End-Cretaceous mass extinction event: argument for terrestrial causation. *Science*, *29*, 1237–1242.

Hallam, A., & Wignall, P. B. (1999). Mass extinctions and sea-level changes. *Earth-Science Reviews*, *48*, 217–250.

Halliday, A. N. (2000). Terrestrial accretion rates and the origin of the Moon. *Earth and Planetary Science Letters*, *176*, 17–30.

Halliday, A. N. (2003). *The Origin and Earliest History of the Earth. Treatise on Geochemistry* (Vol. 1, pp. 508–557). Amsterdam: Elsevier.

Halliday, A. N., & Wood, B. J. (2007). *The Composition and Major Reservoirs of the Earth around the Time of the Moon-Forming Giant Impact. Treatise on Geophysics* (Chap. 9.02, pp. 13–50). Amsterdam: Elsevier.

Hamilton, W. B. (1988). Plate tectonics and island arcs. *Geological Society of America Bulletin*, *100*, 1503–1527.

Hamilton, W. B. (1998). Archean magmatism and deformation were not products of plate tectonics. *Precambrian Research*, *91*, 143–179.

Hammond, W. C., & Toomey, D. R. (2003). Seismic velocity anisotropy and heterogeneity beneath the mantle electromagnetic and tomography experiment (MELT) region of the East Pacific Rise from analysis of P and S body waves. *Journal of Geophysical Research*, *108*(B4), 2176. doi:10.1029/2002JB001789.

Hanan, B. B., & Graham, D. W. (1996). Lead and helium isotope evidence from oceanic basalts for a common deep source of mantle plumes. *Science*, *272*, 991–995.

Handler, P. (1989). The effect of volcanic aerosols on global climate. *Journal of Volcanology and Geothermal Research*, *37*, 233–249.

Hansen, V. L., & Lopez, I. (2010). Venus records a rich early history. *Geology*, *38*, 311–314.

Hansen, V. L., Banks, B. K., & Ghent, R. R. (1999). Tessera terrain and crustal plateaus, Venus. *Geology*, *27*, 1071–1074.

Haq, B. U. (1998). Gas hydrates: greenhouse nightmare? Energy panacea or pipe dream? *GSA Today*, *8*(11), 1–6.

Hardebeck, J., & Anderson, D. L. (1996). Eustasy as a test of a Cretaceous superplume hypothesis. *Earth and Planetary Science Letters*, *137*, 101–108.

Hardie, L. A. (1996). Secular variation in seawater chemistry: an explanation for the coupled secular variation in the mineralogies of marine limestones and potash evaporites over the past 600 My. *Geology*, *24*, 279–283.

Hardie, L. A. (2003). Secular variations in Precambrian seawater chemistry and the timing of Precambrian aragonite seas and calcite seas. *Geology*, *31*, 785–788.

Hargraves, R. B. (1986). Faster spreading or greater ridge length in the Archean? *Geology*, *14*, 750–752.

Harley, S. L., & Black, L. P. (1987). The Archean geological evolution of Enderby Land, Antarctica. *Geological Society, London, Special Publications*, *27*, 285–296.

Harper, C. L., & Jacobsen, S. B. (1996). Evidence for 182Hf in the early Solar System and constraints on the timescale of terrestrial accretion and core formation. *Geochimica et Cosmochimica Acta*, *60*, 1131–1153.

Harris, A. W., & Kaula, W. M. (1975). A co-accretional model of satellite formation. *Icarus*, *24*, 516–524.

Harris, N. B. W. (1995). Significance of weathering Himalayan metasedimentary rocks and leucogranites for the Sr isotope evolution of seawater during the Early Miocene. *Geology*, *23*, 795–798.

Harris, N. B. W., Pearce, J. A., & Tindle, A. G. (1986). Geochemical characteristics of collision-zone magmatism. In M. P. Coward & A. C. Ries (Eds.), *Collision Tectonics* (pp. 67–81). Geological Society of London, Special Publication 19.

Harrison, C. G. A. (1987). Marine magnetic anomalies—the origin of the stripes. *Annual Review of Earth and Planetary Sciences*, *15*, 505–534.

Harrison, T. M. (2009). The Hadean crust: evidence from > 4 Ga zircons. *Annual Review of Earth and Planetary Sciences*, *37*, 479–505.

Harrison, T. M., Copeland, P., Kidd, W. S. F., & Yin, A. (1992). Raising Tibet. *Science*, *255*, 1663–1670.

Harrison, T. M., Schmitt, A. K., McCulloch, M. T., & Lovera, O. M. (2008). Early formation of terrestrial crust: Lu-Hf, d18O and Ti thermometry results for Hadan zircons. *Earth and Planetary Science Letters*, *268*, 476–486.

Hart, S. R. (1986). In search of a bulk-Earth composition. *Chemical Geology*, *57*, 247–267.

Hart, S. R. (1988). Heterogeneous mantle domains: signatures, genesis and mixing chronologies. *Earth and Planetary Science Letters*, *90*, 273–296.

Hart, S. R., Hauri, E. H., Oschmann, L. A., & Whitehead, J. A. (1992). Mantle plumes and entrainment: isotopic evidence. *Science*, *256*, 517–519.

Hartlaub, R. P., Heaman, L. M., Chacko, T., & Ashton, K. E. (2007). Circ2.3–Ga magmatism of the Arrowsmith orogeny, Uranium City Region, Western Churchill craton, Canada. *Journal of Geology*, *115*, 181–195.

Hartmann, W. K. (1983). *Moons and Planets* (509 pp). Belmont, CA: Wadsworth.

Hartmann, W. K. (1986). Moon origin: the impact-trigger hypothesis. In W. K. Hartmann, R. J. Phillips, & G. J. Taylor (Eds.), *Origin of the Moon* (pp. 579–608). Houston, TX: Lunar & Planetary Institute.

Hartnady, C. J. H. (1991). About turn for supercontinents. *Nature*, *352*, 476–478.

Hartnady, C. J. H., & leRoex, A. P. (1985). Southern ocean hotspot tracks and the Cenozoic absolute motion of the African, Antarctic and South American plates. *Earth and Planetary Science Letters*, *75*, 245–257.

Hastie, A. R., Kerr, A. C., McDonald, I., Mitchell, S. F., Pearce, J. A., Wolstencroft, M., et al. (2010). Do Cenozoic analogues support a plate tectonic origin for Earth's earliest continental crust? *Geology*, *38*, 495–498.

Hauri, E. H., & Hart, S. R. (1993). Re-Os isotope systematics of HIMU and EMII oceanic island basalts from the south Pacific Ocean. *Earth and Planetary Science Letters*, *114*, 353–371.

Hauri, E. H., Whitehead, J. A., & Hart, S. R. (1994). Fluid dynamic and geochemical aspects of entrainment in mantle plumes. *Journal of Geophysical Research*, *99*, 24,275–24,300.

Hawkesworth, C. J., Erlank, A. J., Kempton, P. D., & Waters, F. G. (1990). Mantle metasomatism: isotope and trace-element trends in xenoliths from Kimberley, South Africa. *Chemical Geology*, *85*, 19–34.

Hawkesworth, C. J., Gallahger, K., Hergt, J. M., & McDermott, F. (1994). Destructive plate margin magmatism: geochemistry and melt generation. *Lithos*, *33*, 169–188.

Hayes, J. M., & Waldbauer, J. R. (2006). The carbon cycle and associated redox processes through time. *Philosophical Transactions of the Royal Society*, *B361*, 931–950.

Hazen, R. M., et al. (2008). Mineral evolution. *American Mineralogist*, *93*, 1693–1720.

Head, J. W., et al. (2008). Volcanism on Mercury: evidence from the first MESSENGER flyby. *Science*, *321*, 69–72.

Heaman, L. M. (1997). Global mafic magmatism at 2.45 Ga: remnants of an ancient large igneous province? *Geology*, *25*, 299–302.

Hedges, S. B., Parker, P. H., Sibley, C. G., & Kumar, S. (1996). Continental breakup and the ordinal diversification of birds and mammals. *Nature*, *381*, 226–229.

Heirtzler, J. R., et al. (1968). Marine magnetic anomalies, geomagnetic field reversals, and motions of the ocean floor and continents. *Journal of Geophysical Research*, *73*, 2119–2135.

Heizler, M. T. (1993). *Thermal history of the continental lithosphere using multiple diffusion domain thermochronometry* (295 pp). PhD thesis. University of California–Los Angeles.

Helffrich, G. R., & Wood, B. J. (2001). The Earth's mantle. *Nature*, *412*, 501–507.

Heller, P. L., & Angevine, C. L. (1985). Sea level cycles during the growth of Atlantic-type oceans. *Earth and Planetary Science Letters*, *75*, 417–426.

Helmstaedt, H. H., & Scott, D. J. (1992). The Proterozoic ophiolite problem. In K. C. Condie (Ed.), *Proterozoic Crustal Evolution* (pp. 55–95). Amsterdam: Elsevier.

Helmstaedt, H., Padgham, W. A., & Brophy, J. A. (1986). Multiple dykes in lower Kam Group, Yellowknife greenstone belt: evidence for Archean seafloor spreading? *Geology*, *14*, 562–566.

Hernlund, J. W., Thomas, C., & Tackley, P. J. (2005). A doubling of the post-perovskite phase boundary and structure of the Earth's lowermost mantle. *Nature*, *434*, 882–886.

Herzberg, C. (1995). Generation of plume magmas through time: an experimental perspective. *Chemical Geology*, *126*, 1–16.

Herzberg, C. (2004). Geodynamic information in peridotite petrology. *J Petrol*, *45*, 2507–2530.

Herzberg, C., & Asimow, P. D. (2008). Petrology of some oceanic island basalts: PRIMEL T2.XLS software for primary magma calculation. *Geochemistry Geophysics Geosystems*, 8. doi:10.1029GC002057.

Herzberg, C., Condie, K., & Korenaga, J. (2010). Thermal history of the Earth and its petrological expression. *Earth and Planetary Science Letters*, *292*, 79–88.

Hey, R., Duennebier, F. K., & Morgan, W. J. (1980). Propagating rifts on mid-ocean ridges. *Journal of Geophysical Research*, *85*, 3647–3658.

Hildebrand, A. R., et al. (1991). Chicxulub crater: a possible K/T boundary impact crater on the Yucatan Peninsula, Mexico. *Geology*, *19*, 867–871.

Hilde, T. W. C. (1983). Sediment subduction versus accretion around the Pacific. *Tectonophysics*, *99*, 381–397.

Hirn, A., Nercessian, A., Sapin, M., Jobert, G., & Xu, Z. X. (1984). Lhasa block and bordering sutures—a continuation of the 500-km Moho traverse through Tibet. *Nature*, *307*, 25–27.

Hirose, K. (2002). Phase transitions in pyrolitic mantle around 670–km depth: implications for upwelling of plumes from the lower mantle. *Journal of Geophysical Research*, *107*(B4). doi:10.1029/2001JB000597.

Hirose, K., Fei, Y., Ma, Y., & Mao, H. K. (1999). The fate of subducted basaltic crust in the Earth's lower mantle. *Nature*, *397*, 53–56.

Hirschmann, M. M. (2006). Water, melting, and the deep Earth H_2O cycle. *Annual Review of Earth and Planetary Sciences*, *34*, 629–653.

Hoffman, P. F. (1988). United plates of America, the birth of a craton. *Annual Review of Earth and Planetary Sciences*, *16*, 543–603.

Hoffman, P. F. (1989). Speculations on Laurentia's first gigayear. *Geology*, *17*, 135–138.

Hoffman, P. F. (1990). Geological constraints on the origin of the mantle root beneath the Canadian shield. *Philosophical Transactions of the Royal Society of London*, *331A*, 523–532.

Hoffman, P. F. (1991). Did the breakout of Laurentia turn Gondwanaland inside-out? *Science*, *252*, 1409–1412.

Hoffman, P. F., & Schrag, D. P. (2002). The snowball Earth hypothesis: testing the limits of global change. *Terra Nova*, *14*, 129–155.

Hoffman, P. F., Kaufman, A. J., Halverson, G. P., & Schrag, D. P. (1998). A Neoproterozoic snowball Earth. *Science*, *281*, 1342–1346.

Hoffman, S. E., Wilson, M., & Stakes, D. S. (1986). Inferred oxygen isotope profile of Archean oceanic crust, Onverwacht Group, South Africa. *Nature*, *321*, 55–58.

Hofmann, A. W. (1988). Chemical differentiation of the Earth: the relationship between mantle, continental crust, and oceanic crust. *Earth and Planetary Science Letters*, *90*, 297–314.

Hofmann, A. W. (1997). Mantle geochemistry: the message from oceanic volcanism. *Nature*, *385*, 219–229.

Hofmann, A. W. (2003). *Sampling Mangle Heterogeneity through Oceanic Basalts: Isotopes and Trace Elements. Treatise on Geochemistry* (Vol. 2, pp. 61–101). Elsevier.

Hofmann, A. W., Jochum, K. P., Seufert, M., & White, W. M. (1986). Nb and Pb in oceanic basalts: new constraints on mantle evolution. *Earth and Planetary Science Letters*, *79*, 33–45.

Hofmann, H. J., Grey, K., Hickman, A. H., & Thorpe, R. I. (1999). Origin of 3.45 Ga coniform stromatolites in Warrawoona Group, Western Australia. *Geological Society of America Bulletin*, *111*, 1256–1262.

Holbrook, W. S., & Kelemen, P. B. (1993). Large igneous province on the US Altlantic margin and implications for magmatism during continental breakup. *Nature*, *364*, 433–436.

Holbrook, W. S., Mooney, W. D., & Christensen, N. J. (1992). The seismic velocity structure of the deep continental crust. In D. M. Fountain, R. Arculus, & R. W. Kay (Eds.), *Continental Lower Crust* (pp. 1–43). Amsterdam: Elsevier.

Holland, H. D. (1984). *The Chemical Evolution of the Atmosphere and Oceans* (582 pp). Princeton, NJ: Princeton University Press.

Holland, H. D. (1992). Distribution and paleoenvironmental interpretation of Proterozoic paleosols. In J. W. Schopf & C. Klein (Eds.), *The Proterozoic Bisophere, A Multidisciplinary Study* (pp. 153–155). New York: Cambridge University Press.

Holland, H. D. (1994). Early Proterozoic atmospheric change. In S. Bergtson (Ed.), *Early Life on Earth* (pp. 237–244). New York: Columbia University Press.

Holland, H. D. (2002). Volcanic gases, black smokers and the Great Oxidation Event. *Geochimica et Cosmochimica Acta*, *66*, 3811–3826.

Holland, H. D. (2006). The oxygenation of the atmosphere and oceans. *Philosophical Transactions of the Royal Society*, *B361*, 903–915.

Holland, H. D. (2009). Why the atmosphere became oxygenated: a proposal. *Geochimica et Cosmochimica Acta*, *73*, 5241–5255.

Holland, H. D., & Beukes, N. J. (1990). A paleoweathering profile from Griqualand West, South Africa: evidence for a dramatic rise in atmospheric oxygen between 2.2 and 1.9 Ga. *American Journal of Science*, *290–A*, 1–34.

Holland, H. D., & Zimmermann, H. (2000). The dolomite problem revisted. *International Geology Review*, *42*, 481–490.

Holland, H. D., Lazar, B., & McGaffrey, M. (1986). Evolution of the atmosphere and oceans. *Nature*, *320*, 27–33.

Hollerbach, R., & Jones, C. A. (1993). Influence of the Earth's inner core on geomagnetic fluctuations and reversals. *Nature*, *365*, 541–543.

Holliger, K., Levander, A. R., & Goff, J. A. (1993). Stochastic modeling of the reflective lower crust: petrophysical and geological evidence from the Ivrea zone. *Journal of Geophysical Research*, *98*, 11,967–11,980.

Holmden, C., & Muehlenbachs, K. (1993). The 18/16O ratio of 2–Ga seawater inferred from ancient oceanic crust. *Science*, *259*, 1733–1736.

Holser, W. T. (1984). Gradual and abrupt shifts in ocean chemistry during Phanerozoic time. In H. D. Holland & A. F. Trendall (Eds.), *Patterns of Change in Earth Evolution* (pp. 123–143). Berlin: Springer-Verlag.

Holser, W. T., Schidlowski, M., Mackenzie, F. T., & Maynard, J. B. (1988). Geochemical cycles of carbon and sulfur. In C. B. Gregor, R. M. Garrels, F. T. Mackenzie & J. B. Maynard (Eds.), *Chemical Cycles in the Evolution of the Earth* (pp. 105–173). New York: John Wiley.

Homewood, P., Allen, P. A., & Williams, G. D. (1986). Dynamics of the Molasse basin of western Switzerland. In A. Allen & P. Homewood (Eds.), *Foreland Basins* (pp. 199–218). Oxford: Blackwell Scientific.

Horita, J., Zimmermann, H., & Holland, H. D. (2002). Chemical evolution of seawater during the Phanerozoic: implications from the record of marine evaporites. *Geochimica et Cosmochimica Acta*, *66*, 3733–3756.

Hou, G., Santosh, M., Qian, X., Lister, G. S., & Li, J. (2008). Tectonic constraints on 1.3–1.2 Ga final breakup of Columbia supecontient from a giat radiating dyke swarm. *Gondwana Research*, *14*, 561–566.

Hren, M. T., Tice, M. M., & Chamberlain, C. P. (2009). Oxygen and hydrogen isotopce evidence for a termperate climate 3.42 billion years ago. *Nature*, 462. doi:10.1038/nature08518.

Humphris, S. E., et al. (1995). The internal structure of an active sea floor massive sulphide deposit. *Nature*, *377*, 713–716.

Hunten, D. M. (1993). Atmospheric evolution of the terrestrial planets. *Science*, *259*, 915–920.

Hunter, D. R. (1975). *The regional geological setting of the Bushveld Complex* (18 pp). Johannesburg: University Witwatersrand, Econ. Geol. Research Unit.

Hurley, P. M., & Rand, J. R. (1969). Predrift continental nuclei. *Science*, *164*, 1229–1242.

Hut, P., et al. (1987). Comet showers as a cause of mass extinctions. *Nature*, *329*, 118–125.

Hyde, W. T., Crowley, T. J., Baum, S. K., & Peltier, R. (2000). Neoproterozoic 'snowball Earth' simulations with a coupled climate/ice-sheet model. *Nature*, *405*, 425–429.

Iizuka, T., Komiya, T., Ueno, Y., Katayama, I., Uehara, Y., Maruyama, S., et al. (2007). Geology and zircon geochronology of the Acasta Gneiss Complex, Northwestern Canada: new constraints on its tectonothermal history. *Precambrian Research*, *153*, 179–208.

Iizuka, T., Komiya, T., Rino, S., Maruyama, S., & Hirata, T. (2010). Detrital zircon evidence for Hf isotopic evolution of granitic crust and continental growth. *Geochimica et Cosmochimica Acta*, *74*, 2450–2472.

Ildefonse, B., Blackman, D. K., John, B. E., Ohara, Y., Miller, D. J., & MacLeod, C. J. (2007). *Geology*, *35*(7), 623–626.

Imbrie, J. (1985). A theoretical framework for the Pleistocene ice ages. *Quart. J Geol Lond*, *142*, 417–432.

Ingersoll, R. V. (1988). Tectonics of sedimentary basins. *Geological Society of America Bulletin*, *100*, 1704–1719.

Ingram, B. L., Coccioni, R., Montana, A., & Richter, F. M. (1994). Sr isotopic composition of mid-Cretaceous seawater. *Science*, *264*, 546–549.

Irifune, T., & Ringwood, A. E. (1993). Phase transformations in subducted oceanic crust and buoyancy relationships at depths of 600–800 km in the mantle. *Earth and Planetary Science Letters*, *117*, 101–110.

Irving, E., North, F. K., & Couillard, R. (1974). Oil, climate and tectonics. *Canadian Journal of Earth Sciences*, *11*, 1–17.

Irwin, L. N., & Schulze-Makuch, D. (2001). Assessing the plausibility of life on other worlds. *Astrobiology*, *1*, 143–160.

Ishii, M., & Dziewonski, A. M. (2003). Distinct seismic anisotropy at the center of the Earth. *Physics of the Earth and Planetary Interiors*, *140*, 203–217.

Isley, A. E. (1995). Hydrothermal plumes and the delivery of iron to BIF. *Journal of Geology*, *103*, 169–185.

Isley, A. E., & Abbott, D. H. (1999). Plume-related mafic volcanism and the deposition of banded iron formation. *Journal of Geophysical Research*, *104*, 15,461–15,477.

Isley, A. E., & Abbott, D. H. (2002). Implication for the temporal distribution of high-Mg magmas for mantle plume volcanism through time. *Journal of Geology*, *110*, 141–158.

Isozaki, Y. (1997). Permo-Triassic boundary superanoxia and stratified superocean: records from lost deep sea. *Science*, *276*, 235–238.

Isozaki, Y. (2009). Integrated "plume winter" scenario for the double-phased extinction during the Paleozoic-Mesozoic transition: the G-LB and P-TB events from a Panthalassan perspective. *Journal of Asian Earth Science*, *36*, 459–480.

Ita, J., & Stixrude, L. (1992). Petrology, elasticity, and composition of the mantle transition zone. *Journal of Geophysical Research*, *97*, 6849–6866.

Ito, E., Morooka, K., Ujike, O., & Katsura, T. (1995). Reactions between molten iron and silicate melts a high pressure: implications for the chemical evolution of Earth's core. *Journal of Geophysical Research*, *100*, 5901–5910.

Jackson, J., McKenzie, D., Priestley, K., & Emmerson, B. (2008). New views on the structure and rheology of the lithosphere. *Journal of the Geological Society of London*, *165*, 453–465.

Jackson, M. G., Carlson, R. W., Kurz, M. D., Kempton, P. D., Francis, D., & Blusztajn, J. (2010). Evidence for the survival of the oldest terrestrial mantle reservoir. *Nature*, *466*, 853–858.

Jacobs, J. A. (1992). *Deep Interior of the Earth* (167 pp). New York: Chapman & Hill.

Jacobs, J. A. (1995). The Earth's inner core and the geodynamo: determining their roles in the Earth's history. *Eos*, *76*(25), 249.

Jacobsen, S. B., & Pimentel-Klose, M. (1988). Nd isotopic variations in Precambrian BIF. *Geophysical Research Letters*, *15*, 393–396.

Jaffres, J. B. D., Shields, G. A., & Wallmann, K. (2007). The oxygen isotope evolution of seawater: a critical review of the long-standing controversy and an improved geological water cycle model for the past 3.4 billion years. *Earth-Science Reviews*, *83*, 83–122.

Jahren, A. H. (2002). The biogeochemical consequences of the mid-Cretaceous superplume. *Journal of Geodynamics*, *34*, 177–191.

Jakosky, B. M., & Phillips, R. J. (2001). Mars' volatile and climate history. *Nature*, *412*, 237–244.

James, D. E., Niu, F., & Rokosky, J. (2003). Crustal structure of the Kaapvaal craton and its significance for early crustal evolution. *Lithos*, *71*, 423–429.

Jarchow, C. M., & Thompson, G. A. (1989). The nature of the Mohorovicic discontinuity. *Annual Review of Earth and Planetary Sciences*, *17*, 475–506.

Jaupart, C., & Mareschal, J. C. (1999). The thermal structure and thickness of continental roots. *Lithos*, *48*, 93–114.

Jaupart, C., Mareschal, J. C., Guillou-Frottier, L., & Davaille, A. (1998). Heat flow and thickness of the lithosphere in the Canadian shield. *Journal of Geophysical Research*, *103*, 15269–15286.

Jeanloz, R. (1990). The nature of the Earth's core. *Annual Review of Earth and Planetary Sciences*, *18*, 357–386.

Jeanloz, R., Mitchell, D. L., Sprague, A. L., & de Pater, I. (1995). Evidence for a basalt-free surface on Mercury and implications for internal heat. *Science*, *268*, 1455–1457.

Jellinek, A., & Manga, M. (2004). Links between long-lived hotspots, mantle plumes, D″, and plate tectonics. *Review of Geophysics*, *42*, RG3002. doi:10.1029/2003RG000144.

Jenkins, G. S. (1995). Early Earth's climate: cloud feedback from reduced land fraction and ozone concentrations. *Geophysical Research Letters*, *22*, 1513–1516.

Jenkins, G. S., Marshall, H. G., & Kuhn, W. R. (1993). Precambrian climate: the effects of land area and Earth's rotation rate. *Journal of Geophysical Research*, *98*, 8785–8791.

Jenkyns, H. C. (1980). Cretaceous anoxic events: from continents to oceans. *Journal of the Geological Society of London*, *137*, 171–188.

Jephcoat, A., & Olson, P. (1987). Is the inner core of the Earth pure iron? *Nature*, *325*, 332.

Jessberger, E. K., & Kissel, J. (1989). The composition of comets. In S. K. Atreya, J. B. Pollack, & M. S. Matthews (Eds.), *Origin and Evolution of Planetary and Satellite Atmospheres* (pp. 167–191). Tucson: University of Arizona Press.

Jessop, A. M., & Lewis, T. (1978). Heat flow and heat generation in the Superior province of the Canadian shield. *Tectonophysics*, *50*, 55–77.

Ji, S., Wang, Q., & Salisbury, M. H. (2008). Composition and tectonic evolution of the Chinese continental crust constrained by Poisson's ratio. *Tectonophysics*, *463*, 15–30.

Jiang, G., Kennedy, M. J., & Christie-Blick, N. (2003). Stable isotopic evidence for methane seeps in Neoproterozoic postglacial cap carbonates. *Nature*, *426*, 822–826.

Johansson, A. (2009). Baltica, Amazonia and the SAMBA connection—1000 million years of neighbourhood during the Proterozoic? *Precambrian Res*, *175*, 221–234.

Johnson, C. L., & Richards, M. A. (2003). A conceptual model for the relationship between coronae and large-scale mantle dynamics on Venus. *Journal of Geophysical Research*, *108*, 5058. doi:10.1029/2002/JE001962, 2003.

Johnson, C. M., Beard, B. L., & Roden, E. E. (2008). The iron isotope fingerprints of redox and biogeochemical cycling in modern and ancient Earth. *Annual Review of Earth and Planetary Sciences*, *36*, 457–493.

Johnson, D. M. (1993). Mesozoic and Cenozoic contributions to crustal growth in the SW United States. *Earth and Planetary Science Letters*, *118*, 75–89.

Jolivet, L., Huchon, P., & Ranguin, C. (1989). Tectonic setting of Western Pacific marginal basins. *Tectonophysics*, *160*, 23–47.

Jorgensen, U. G., Appel, P. W. U., Hatsukawa, Y., Frei, R., Oshima, M., Toh, Y., et al. (2009). The Earth-Moon system during the late heavy bombardment period – geochemical support for impacts dominated by comets. *Icarus*, *204*, 368–380.

Jurdy, D. M., Stefanick, M., & Scotese, C. R. (1995). Paleozoic plate dynamics. *Journal of Geophysical Research*, *100*, 17,965–17,975.

Kah, L. C., Lyons, T. W., & Chesley, J. T. (2001). Geochemistry of a 1.2–Ga carbonate-evaporite succession, northern Baffin and Bylot Islands: implications for Mesoproterozoic marine evolution. *Precambrian Research*, *111*, 203–234.

Kamber, B. S., & Collerson, K. D. (1999). Origin of ocean island basalts: a new model based on lead and helium isotope systematics. *Journal of Geophysical Research*, *104*, 15,479–15,491.

Kamber, B. S., Greig, A., Schoenberg, R., & Collerson, K. D. (2003). A refined solution to Earth's hidden niobium: implications for evolution of continental crust and mode of core formation. *Precambrian Research*, *126*, 289–308.

Kamo, S. L., & Davis, D. W. (1994). Reassessment of Archean crust development in the Barberton Mountain Land, South Africa, base on U-Pb dating. *Tectonics*, *13*, 167–192.

Kamo, S. L., & Krogh, T. E. (1995). Chicxulub crater source for shocked zircon crystals from the Cretaceous/Tertiary boundary layer, Saskatchewan: evidence from new U-Pb data. *Geology*, *23*, 281–284.

Kandler, O. (1994). The early diversification of life. In S. Bengtson (Ed.), *Early Life on Earth* (pp. 152–160). New York: Columbia University Press.

Kaneshima, S., & Helffrich, G. (1999). Dipping low-velocity layer in the mid-lower mantle: evidence for geochemical heterogeneity. *Science*, *283*, 1888–1891.

Kárason, H., & Van der Hilst, R. D. (2000). Constraints on mantle convection from seismic tomography. In M. R. Richards, R. Gordon & R. D. Van der Hilst (Eds.), *The History and Dynamics of Global Plate Motion* (pp. 277–288). Washington, DC: American Geophysical Union, Geophysical Monograph 121.

Karato, S. I. (1999). Seismic anisotropy of the Earth's inner core resulting from flow induced my Maxwell stresses. *Nature*, *402*, 871–873.

Karhu, J. A., & Holland, H. D. (1996). Carbon isotopes and the rise of atmospheric oxygen. *Geology*, *24*, 867–870.

Karlstrom, K. E., & Houston, R. S. (1984). The Cheyenne Belt: analysis of a Proterozoic suture in southern Wyoming. *Precambrian Res*, *25*, 415–446.

Karlstrom, K. E., Ahall, K. I., Harlan, S. S., Williams, M. L., McLelland, J., & Geissman, J. W. (2001). Long-lived convergent orogen in southern Laurentia, its extensions to Australia and Baltica, and implications for refining Rodinia. *Precambrian Research*, *111*, 5–30.

Karsten, J. L., Klein, E. M., & Sherman, S. B. (1996). Subduction zone geochemical characteristics in ocean ridge basalts from the southern Chile ridge: implications of modern ridge subduction systems for the Archean. *Lithos*, *37*, 143–161.

Kasting, J. F. (1987). Theoretical constraints on oxygen and carbon dioxide concentrations in the Precambrian atmosphere. *Precambrian Research*, *34*, 205–229.

Kasting, J. F. (1991). Box models for the evolution of atmospheric oxygen: an update. *Palaeogeography, Palaeoclimatology, Palaeoecology*, *97*, 125–131.

Kasting, J. F. (1993). Earth's early atmosphere. *Science*, *259*, 920–926.

Kasting, J. F. (2010). Faint young Sun redux. *Nature*, *464*, 687–689.

Kasting, J. F., & Howard, M. T. (2006). Atmospheric composition and climate on the early Earth. *Philosophical Transactions of the Royal Society*, *B361*, 1733–1742.

Kasting, J. F., & Ono, S. (2006). Palaeoclimates: the first two billion years. *Philosophical Transactions of the Royal Society*, *B361*, 917–929.

Kasting, J. F., Eggler, D. H., & Raeburn, S. P. (1993a). Mantle redox evolution and the oxidation state of the Archean atmosphere. *Journal of Geology*, *101*, 245–257.

Kasting, J. F., Whitmire, D. P., & Reynolds, R. T. (1993b). Habitable zones around main sequence stars. *Icarus*, *101*, 1460–1464.

Kato, T., & Ringwood, A. E. (1989). Melting relationships in the system Fe-FeO at high pressures: implications for the composition and formation of the Earth's core. *Physics and Chemistry of Minerals*, *16*, 524–538.

Kato, Y., Yamaguchi, K. E., & Ohmoto, H. (2006). *Rare earth elements in Precambrian banded iron formations: secular changes of Ce and Eu anomalies and evolutuon of atmospheric oxygen* (pp. 269–289). Boulder, CO: Geological Society of America, Memoir 198.

Katsura, T., Yamada, H., Shinmei, T., Kubo, A., Ono, S., Kanzaki, M., et al. (2003). Post-spinel transition in Mg_2SiO_4 determined by high_P-T in situ X-ray diffractometry. *Physics of the Earth and Planetary Interiors*, *136*, 11–24.

Kaufman, A. J. (1995). *At Home in the Universe: The Search for Laws of Self-Organization and Complexity*. New York: Oxford University Press.

Kaufman, A. J. (1997). An ice age in the tropics. *Nature*, *386*, 227–228.

Kaufman, A. J., & Knoll, A. H. (1995). Neoproterozoic variations in the C-isotopic composition of seawater: stratigraphic and biogeochemical implications. *Precambrian Research*, *73*, 27–49.

Kaula, W. M. (1995). Venus reconsidered. *Science*, *270*, 1460–1464.

Kawai, K., & Tsuchiya, T. (2009). Temperature profile in the lowermost mantle from seismological and mineral physics joint modeling. *Proceedings of the National Academy of Sciences of the United States of America*, *106*, 22,119–22,123.

Kawakatsu, H., Kumar, P., Takei, Y., Shinohara, M., Kanazawa, T., Araki, E., et al. (2009). Seismic evidence for sharp lithosphere-asthenosphere boundaries of oceanic plates. *Science*, *324*, 499–502.

Kay, R. W., & Kay, S. M. (1981). The nature of the lower continental crust: inferences from geophysics, surface geology and crustal xenoliths. *Review of Geophysics Space Phys*, *19*, 271–297.

Kay, S. M., & Kay, R. W. (1985). Role of crystal cumulates and the oceanic crust in the formation of the lower crust of the Aleutian arc. *Geology*, *13*, 461–464.

Kay, S. M., Ramos, V. A., Mpodozis, C., & Sruoga, P. (1989). Late Paleozoic to Jurassic silicic magmatism at the Gondwana margin: analogy to the Middle Proterozoic in North America? *Geology*, *17*, 324–328.

Keller, G., Meudt, M., Adatte, T., Berner, Z., Stueben, D., & Tantawy, A. A. (2003). Biotic effects of impacts and volcanism. In *Mantle Plumes: Physical Processes, Chemical Signatures and Biological Effects* (Abstract Vol., p. 25). Cardiff, UK: Cardiff University, September 2003.

Kelley, S. (2007). The geochronology of large igneous provinces, terrestrial impact craters, and their relationship to mass extinctions on Earth. *Journal of the Geological Society of London*, *164*, 923–936.

Kellogg, L. H. (1992). Mixing in the mantle. *Annual Review of Earth and Planetary Sciences*, *20*, 365–388.

Kellogg, L. H., Hager, B. H., & van der Hilst, R. D. (1999). Compositional stratification in the deep mantle. *Science*, *283*, 1881–1884.

Kemp, A. I. S., Hawkesworth, C. J., Paterson, B. A., & Kinny, P. D. (2006). Episodic growth of the Gondwana supercontinent from hafnium and oxygen isotopes in zircon. *Nature*, *439*, 581–583.

Kemp, A. I. S., Wilde, S. A., Hawkesworth, C. J., Coath, C. D., Pidgeon, R. T., Vervoort, J. D., et al. (2010). Hadean crustal evolution revisited: new constraints from Pb-Hf isotope systematics of the Jack Hills zircons. *Earth and Planetary Science Letters*, *296*, 45–56.

Kempton, P. D., et al. (2000). The Iceland plume in space and time: a Sr-Nd-Pb-Hf study of the North Atlantic rifted margin. *Earth and Planetary Science Letters*, *177*, 255–271.

Kendall, J. M., & Silver, P. G. (1996). Constraints from seismic anisotropy on the nature of the lowermost mantle. *Nature*, *381*, 409–412.

Kennedy, M. J., Christie-Blick, N., & Sohl, L. E. (2010). Are Proterozoic cap carbonates and isotopic excursion a record of gas hydrate destabilization following Earth's coldest intervals? *Geology*, *29*, 443–446.

Keppler, H. (1996). Constraints from partitioning experiments of the composition of subduction-zone fluids. *Nature*, *380*, 237–240.

Kerr, A. C. (1994). Lithospheric thinning during the evolution of continental large igneous provinces. *Geology*, *22*, 1027–1030.

Kerr, A. C. (1998). Oceanic plateau formation: a cause of mass extinction and black shale deposition around the Cenomanian-Turonian boundary. *Journal of the Geological Society of London*, *155*, 619–626.

Kershaw, S. (1990). Evolution of the Earth's atmosphere and its geological impact. *Geol Today*, March/April, pp. 55–57.

Kiefer, W. S. (2008). Forming the Martian great divide. *Nature*, *453*, 1191–1192.

Kilburn, M. R., & Wood, B. J. (1997). Metal-silicate partitioning and the incompatibility of S and Si during core formation. *Earth and Planetary Science Letters*, *152*, 139–148.

Kimura, H., & Watanabe, Y. (2001). Oceanic anoxia at the Precambrian-Cambrian boundary. *Geology*, *29*, 995–998.

Kingma, K. J., Cohen, R. E., Hemley, R. J., & Mao, H. K. (1995). Transformation of stishovite to a denser phase at lower mantle pressures. *Nature*, *374*, 243–245.

Kirschvink, J. L., Ripperdan, R. L., & Evans, D. A. (1997). Evidence for a large-scale reorganization of Early Cambrian continental masses by inertial interchange true polar wander. *Science*, *277*, 541–545.

Klein, C., & Beukes, N. J. (1992). Proterozoic iron-formations. In K. C. Condie (Ed.), *Proterozoic Crustal Evolution* (pp. 383–417). Amsterdam: Elsevier.

Klein, G. deVries (1982). Probable sequential arrangement of depositional systems on cratons. *Geology*, *10*, 17–22.

Klein, G. deVries (1986). Sedimentation patterns in relation to rifting, arc volcanism and tectonic uplift in back-arc basins of the western Pacific Ocean. In N. Nasu, K. Kobayashi, S. Uyeda, I. Kushiro, & H. Kagami (Eds.), *Formation of Active Continental Margins* (pp. 517–550). Dordrecht: D. Reidel Publishers.

Kleine, T., Munker, C., Mezger, K., & Palme, H. (2002). Rapid accretion and early core formation on asteroids and the terrestrial planets from Hf-W chronometry. *Nature*, *418*, 952–955.

Kleine, T., Palme, H., Mezger, M., & Halliday, A. N. (2005). Hf-W chronometry of lunar metals and the age and early differentiation of the Moon. *Science*, *310*, 1671–1673.

Kleine, T., et al. (2009). Hf-W chronology of the accretion and early evolution of asteroids and terrestrial planets. *Geochimica et Cosmochimica Acta*, *73*, 5150–5188.

Klemperer, S. L. (1987). A relation between continental heat flow and the seismic reflectivity of the lower crust. *J Geophys*, *61*, 1–11.

Knauth, L. P. (2005). Temperature and salinity history of the Precambrian ocean: implications for the course of microbial evolution. *Palaeogeography, Palaeoclimatology, Palaeoecology*, *219*, 53–69.

Knauth, L. P., & Lowe, D. R. (1978). Oxygen isotope geochemistry of cherts from the Onverwacht Group, South Africa. *Earth and Planetary Science Letters*, *41*, 209–222.

Knauth, L. P., & Lowe, D. R. (2003). High Archean climatic temperature inferred from oxygen isotope geochemistry of cherts in the 3.5 Ga Swaziland Supergroup, South Africa. *Geological Society of America Bulletin*, *115*, 566–580.

Knittle, E., & Jeanloz, R. (1991). Earth's core-mantle boundary: results of experiments at high pressures and high temperatures. *Science*, *251*, 1438–1443.

Knoll, A. H. (2003). The geological consequences of evolution. *Geobiology*, *1*, 3–14.

Knoll, A. H., & Carroll, S. B. (1999). Early animal evolution: emerging views from comparative biology and geology. *Science*, *284*, 2129–2136.

Knoll, A. H., Bambach, R. K., Canfield, D. E., & Grotzinger, J. P. (1996). Comparative Earth history and Late Permian mass extinction. *Science*, *273*, 452–457.

Knoll, A. H., Bambach, R. K., Payne, J. L., Pruss, S., & Fischer, W. W. (2007). Paleophysiology and end-Permian mass extinction. *Earth and Planetary Science Letters*, *256*, 295–313.

Koeberl, C. (2006). *The record of impact processes on the early Earth: a review of the 2.5 billion years* (pp. 1–22). Geological Society of America, Boulder, CO, Special Paper, 405.

Kokelaar, P. (1986). Magma-water interactions in subaqueous and emergent basaltic volcanism. *Bull Volcanol*, *48*, 275–289.

Kominz, M. A., & Bond, G. C. (1991). Unusually large subsidence and sea level events during middle Paleozoic time: new evidence supporting mantle convection models for supercontinent assembly. *Geology*, *19*, 56–60.

Komiya, T., Hayashi, M., Maruyama, S., & Yurimoto, H. (2002). Intermediate-*P/T* type Archean metamorphism of the Isua supracrustal belt: implications for secular change of geothermal gradients at subduction zones and for Archean plate tectonics. *American Journal of Science*, *302*, 806–826.

Konhauser, K. O., Pecoits, E., Lalonde, S. V., Papineau, D., Nisbet, E. G., Barley, M. E., et al. (2009). Oceanic nickel depletion and a methanogen famine before the great oxidation event. *Nature*, *458*, 750–754.

Kontak, D. J., & Reynolds, P. H. (1994). $^{40}Ar/^{39}Ar$ dating of metamorphic and igneous rocks of the Liscomb Complex, Meguma terrane, S Nova Scotia, Canada. *Canadian Journal of Earth Sciences*, *31*, 1643–1653.

Korenaga, J. (2006). *Archean geodynamics and the thermal evolution of Earth. Monograph Series 164* (pp. 7–32). American Geophysical Union.

Korenaga, J. (2008a). Urey ratio and the structure and evolution of Earth's mantle. *Review of Geophysics*, *46*, RG2007. doi:10.1029/2007RG000241.

Korenaga, J. (2008b). Plate tectonics, flood basalts and the evolution of Earth's oceans. *Terra Nova*, *20*, 419–439.

Korte, C., & Kozur, H. W. (2010). Carbon-isotope stratigraphy across the Permian-Triassic boundary: a review. *Journal of Asian Earth Science*, *39*, 215–235.

Kramers, J. D. (2003). Volatile element abundance patterns and an early liquid water ocean on Earth. *Precambrian Research*, *126*, 379–394.

Kramers, J. D. (2007). Hierarchiacal Earth accretion and the Hadean eon. *Journal of the Geological Society of London*, *164*, 3–17.

Krapez, B. (1993). Sequence stratigraphy of the Archean supracrustal belts of the Pilbara block, Western Australia. *Precambrian Research*, *60*, 1–45.

Kreep, M., & Hansen, V. L. (1994). Structural history of Maxwell Montes, Venus: implications for venusian mountain belt formation. *Journal of Geophysical Research*, *99*, 26015–26028.

Kring, D. A., & Cohen, B. A. (2002). Cataclysmic bombardment throughout the inner solar system 3.9–4.0 Ga. *Journal of Geophysical Research*, *107*(E2). doi:10.1029/2001JE001529.

Kroner, A., & Cordani, U. (2003). African, southern Indian and South American cratons were not part of the Rodinia supercontinent: evidence from field relationships and geochronology. *Tectonophysics*, *375*, 325–352.

Kroner, A., & Layer, P. W. (1992). Crust formation and plate motion in the Early Archean. *Science*, *256*, 1405–1411.

Kroner, A., Compston, W., & Williams, I. S. (1989). Growth of Early Archean crust in the Ancient Gneiss Complex of Swaziland as revealed by single zircon dating. *Tectonophysics*, *161*, 271–298.

Kroner, A., Hegner, E., Wendt, J. I., & Byerly, G. R. (1996). The oldest part of the Barberton granitoid-greenstone terrain, South Africa: evidence for crust formation between 3.5 and 3.7 Ga. *Precambrian Research*, *78*, 105–124.

Kuang, W., & Bloxham, J. (1997). An Earth-like numerical dynamo model. *Nature*, *389*, 371–374.

Kumagai, I., Davaille, A., Kurita, K., & Stutzmann, E. (2008). Mantle plumes: thin, fat, successful or failing? Constraints to explain hotspot volcanism through time and space. *Geophysical Research Letters*, *35*, L16301. doi:10.1029/2008GL035079.

Kump, L. R., Kasting, J. F., & Crane, R. G. (1999). *The Earth System* (351 pp). Upper Saddle River, NJ: Prentice Hall.

Kushiro, I. (2001). Partial melting experiments on peridotite and origin of mid-ocean ridge basalt. *Annual Review of Earth and Planetary Sciences*, *29*, 71–107.

Kusky, T. M. (Ed.), (2004). Precambrian ophiolites and related rocks. In *Developments in Precambrian Geology* (Vol. 13, pp. 748). Amsterdam: Elsevier.

Kusky, T. M., & Kidd, W. S. F. (1992). Remnants of an Archean oceanic plateau, Belingwe greenstone belt, Zimbabwe. *Geology*, *20*, 43–46.

Kusky, T. M., & Polat, A. (1999). Growth of granite-greenstone terranes a convergent margins and stabilizaion of Archean cratons. *Tectonophysics*, *305*, 43–73.

Kutzner, C., & Christensen, U. (2000). Effects of driving mechanisms in geodynamo models. *Geophysical Research Letters*, *27*, 29–32.

Kvenvolden, K. A. (1974). Natural evidence for chemical and early biologic evolution. *Origins of Life*, *5*, 71–86.

Kvenvolden, K. A. (1999). Potential effects of gas hydrate on human welfare. *Proceedings of the National Academy of Sciences of the United States of America*, *96*, 3420–3426.

Kyte, F. T. (1998). A meteorite from the Cretaceous/Tertiary boundary. *Nature*, *396*, 237–239.

Kyte, F. T., Shukolyukov, A., Lugmair, G. W., Lowe, D. R., & Byerly, G. R. (2003). Early Archean spherule beds: chromium isotopes confirm origin through multiple impacts of projectiles of carbonaceous chondrite type. *Geology*, *31*, 283–286.

Labrosse, S. (2003). Thermal and magnetic evolution of the Earth's core. *Physics of the Earth and Planetary Interiors*, *140*, 127–143.

Labrosse, S., & Jaupart, C. (2007). Thermal evolution of the Earth: secular changes and fluctuations of plate characteristics. *Earth and Planetary Science Letters*, *260*, 465–481.

Labrosse, S., Poirier, J. P., & Le Mouel, J. L. (2001). The age of the inner core. *Earth and Planetary Science Letters*, *190*, 111–123.

Lambeck, K. (1980). *The Earth's Rotation: Geophysical Cause and Consequences* (449 pp). Cambridge: Cambridge University Press.

Larsen, H. C., & Saunders, A. D. (1998). Tectonism and volcanism at the SE Greenland rifted margin: a record of plume impact and later continental rupture. *Proceedings of the Ocean Drilling Program, Scientific Results*, *152*, 503–533.

Larsen, T. B., & Yuen, D. A. (1997). Fast plumeheads: temperature-dependent versus non-Newtonian rheology. *Geophysical Research Letters*, *24*, 1995–1998.

Larson, R. L. (1991a). Latest pulse of Earth: evidence for a Mid-Cretaceous superplume. *Geology*, *19*, 547–550.

Larson, R. L. (1991b). Geological consequences of superplumes. *Geology*, *19*, 963–966.

Larson, R. L., & Kincaid, C. (1996). Onset of mid-Cretaceous volcanism by elevation of the 670 km thermal boundary layer. *Geology*, *24*, 551–554.

Larson, R. L., & Olson, P. (1991). Mantle plumes control magnetic reversal frequency. *Earth and Planetary Science Letters*, *107*, 437–447.

Lash, G. G. (1987). Diverse melanges of an ancient subduction complex. *Geology*, *15*, 652–655.

Laske, G., & Masters, G. (1999). Limits on differential rotation of the inner core from an analysis of the Earth's free oscillations. *Nature*, *402*, 66–69.

Lassak, T. M., McNamara, A. K., & Zhong, S. (2007). Influence of thermochemical piles on topography at Earth's core-mantle boundary. *Earth and Planetary Science Letters*, *261*, 443–455.

Lawton, T. F. (1986). Compositional trends within a clastic wedge adjacent to a fold-thrust belt: Indianola Group, central Utah, Utah, USA. In A. Allen & P. Homewood (Eds.), *Foreland Basins* (pp. 411–424). Oxford: Blackwell Scientific.

Lay, T., Hernlund, J., & Buffett, B. A. (2008). Core–mantle boundary heat flow. *Nature Geoscience*, *1*, 25–32.

Layer, P. W., Kroner, A., McWilliams, M., & York, D. (1989). Elements of the Archean thermal history and apparent polar wander of the eastern Kaapvaal Craton, Swaziland, from single grain dating and paleomagnetism. *Earth and Planetary Science Letters*, *93*, 23–34.

Leahy, G. M., & Bercovici, D. (2010). Reactive infiltration of hydrous melt avove the mantle transition zone. *Journal of Geophysical Research*, *115*, B08406. doi:10.1029/2009/JB006757.

Lebofsky, L. A., Jones, T. D., & Herbert, F. (1989). Asteroid volatile inventories. In S. K. Atreya, J. B. Pollack & M. S. Matthews (Eds.), *Origin and Evolution of Planetary and Satellite Atmospheres* (pp. 192–229). Tucson: University of Arizona Press.

Lecuyer, C., Gruau, G., Fruh-Green, G. L., & Picard, C. (1996). Hydrogen isotope composition of Early Proterozoic seawater. *Geology*, *24*, 291–294.

Lecuyer, C., Simon, L., & Guyot, F. (2000). Comparison of carbon, nitrogen and water budgets on Venus and the Earth. *Earth and Planetary Science Letters*, *181*, 33–40.

Lee, C. T. (2006). *Geochemical/Petrologic constraints on the origin of cratonic mantle*. *American Geophysical Union, Monograph Series* (Vol. 164, pp. 89–114).

Lee, C. T., Morton, D. M., Kistler, R. W., & Baird, A. K. (2007). Petrology and tectonics of Phanerozoic continent formation: from island arcs to accretion and continental arc magmatism. *Earth and Planetary Science Letters*, *263*, 370–387.

Lee, D. C., & Halliday, A. N. (1995). Hf-W chonometry and the timing of terrestrial core formation. *Nature*, *378*, 771–774.

Leitch, E. C. (1984). *Marginal basins of the SW Pacific and the preservation and recognition of their ancient analogues: a review* (pp. 97–108). Geological Society of London, Special Publication 16.

Lenardic, A. (1997). On the heat flow variation from Archean cratons to Proterozoic mobile belts. *Journal of Geophysical Research*, *102*, 709–721.

Lenardic, A., & Kaula, W. M. (1996). Near-surface thermal/chemical boundary layer convection at infinite Prandtl number: two-dimensional numerical experiments. *Geophysical Journal International*, *126*, 689–711.

Li, Z.-X., & Zhong, S. (2009). Supercontinent-superplume coupling, true polar wander and plume mobility: plate dominance in whole-mantle tectonics. *Physics of the Earth and Planetary Interiors*, *17*, 143–156.

Li, C., van der Hilst, R. D., Engdahl, E. R., & Burdick, S. (2008). A new global model for P wave speed variations in Earth's mantle. *Geochemistry Geophysics Geosystems*, *9*(5), Q05018. doi:10.1029/2007GC001806.

Li, J., & Agee, C. B. (2001). Element partitioning constraints on the light element composition of the Earth's core. *Geophysical Research Letters*, *28*, 81–84.

Li, J. P., O'Neil, H. C., St., & Seifert, F. (1995). Subsolidus phase relations in the system MgO–SiO_2–Gr–O in equilibrium with metallic Cr, and their significance for the petrochemistry of chromium. *J Petrol*, *36*, 107–132.

Li, X., & Yuan, X. (2003). Receiver functions in NE China—implications for slab penetration into the lower mantle in NW Pacific subduction zone. *Earth and Planetary Science Letters*, *216*, 679–691.

Li, X., Kind, R., Priestley, K., Sobolev, S. V., Tilmann, F., Yuan, X., et al. (2000). Mapping the Hawaiian plume conduit with converted seismic waves. *Nature*, *405*, 938–941.

Li, Z. X., & Powell, C. Mc A. (2001). An outline of the paleogeographic evolution of the Australasian region since the beginning of the Neoproterozoic. *Earth-Science Reviews*, *53*, 237–277.

Li, Z. X., et al. (2008). Assembly, confirguration, and break-up history of Rodinia: a synthesis. *Precambrian Research*, *160*, 179–210.

Lin, J. F., Struzhkin, V. V., Jacobsen, S. D., Hu, M. Y., Chow, P., Kung, J., et al. (2005). Spin transition of iron in magnesiowustite in the Earth's lower mantle. *Nature*, *436*. doi:10.1038/nature03825.

Litak, R. K., & Brown, L. D. (1989). A modern perspective on the Conrad discontinuity. American Geophysical Union. *Eos*, *70*(29).

Litasov, K., Ohtani, E., Langenhorst, F., Yurimoto, H., Kubo, T., & Kondo, T. (2003). Water solubility in Mg-perovskites and water storage capacity in the lower mantle. *Earth and Planetary Science Letters, 211*, 189–203.

Litasov, K. D., Ohtani, E., Sano, A., Suzuki, A., & Funakoshi, K. (2005). In situ X-ray diffraction study of postspinel transformation in a periodotite mantle: implication for the 660–km discontinuity. *Earth and Planetary Science Letters*, *238*, 311–328.

Lithgow-Bertelloni, C., & Richards, M. A. (1995). Cenozoic plate driving forces. *Geophysical Research Letters*, *22*, 1317–1320.

Lithgow-Bertelloni, C., & Silver, P. G. (1998). Dynamic topography, plate driving forces and the African superswell. *Nature*, *395*, 269–272.

Liu, C. Z., Snow, J. E., Hellebrand, E., Brugmann, G., von der Handt, A., Buchl, A., et al. (2008). Ancient, highly heterogeneous mantle beneath Gakkel ridge, Arctic Ocean. *Nature*, *452*, 311–316.

Liu, M. (1994). Asymmetric phase effects and mantle convection patterns. *Science*, *264*, 1904–1907.

Long, M. D., & Silver, P. G. (2009). Mantle flow in subduction systems: the subslab flow field and implications for mantle dynamics. *Journal of Geophysical Research*, 114. doi:10.1029/2008JB006200.

Longhi, J. (1978). Pyroxene stability and composition of the lunar magma ocean. In *Proc. 9th Lunar Planet. Sci. Conf.* (pp. 285–306). Houston, TX: Lunar and Planetary Science Institute.

Lovell, B. (2010). Pulse in the planet: regional control of high-frequency changes in relative sea level by mantle convection. *Journal of the Geological Society of London*, *167*, 637–648.

Lowman, J. P., & Gable, C. W. (1999). Thermal evolution of the mantle following continental aggregation in 3D convection models. *Geophysical Research Letters*, *26*, 2649–2652.

Lowman, J. P., & Jarvis, G. T. (1996). Continental collisions in wide aspect ratio and high Rayleigh number two-dimensional mantle convection models. *Journal of Geophysical Research*, *101*, 25,485–25,497.

Lowman, J. P., & Jarvis, G. T. (1999). Effects on mantle heat source distribution on supercontinent stability. *Journal of Geophysical Research*, *104*(12), 733–746.

Loper, D. E. (1992). On the correlation between mantle plume flux and the frequency of reversals of the geomagnetic field. *Geophysical Research Letters*, *19*, 25–28.

Loper, D. E., & Lay, T. (1995). The core-mantle boundary region. *Journal of Geophysical Research*, *100*, 6397–6420.

Lowe, D. R. (1994a). Accretionary history of the Archean Barberton greenstone belt, southern Africa. *Geology*, *22*, 1099–1102.

Lowe, D. R. (1994b). Archean greenstone-related sedimentary rocks. In K. C. Condie (Ed.), *Archean Crustal Evolution* (pp. 121–170). Amsterdam: Elsevier.

Lucas, S. B., et al. (1993). Deep seismic profile across a Proterozoic collision zone: surprises at depth. *Nature*, *363*, 339–342.

Lyons, T. W., Anbar, A. D., Severmann, S., Scott, C., & Gill, B. C. (2009). Tracking euxinia in the ancient ocean: a multiproxy perspective and Proterozoic case study. *Annual Review of Earth and Planetary Sciences*, *37*, 507–534.

Macdonald, F. A., Schmitz, M. D., Crowley, J. L., Roots, C. F., Jones, D. S., Maloof, A. C., et al. (2010). Calibrating the Cryogenian. *Science*, *327*, 1241–1243.

MacDonald, K. C. (1982). Mid-ocean ridges: fine scale tectonic, volcanic and hydrothermal processes within the plate boundary zone. *Annual Review of Earth and Planetary Sciences*, *10*, 155–190.

Macfarlane, A. W., Danielson, A., & Holland, H. D. (1994). Geology and major and trace element chemistry of Late Archean weathering profiles in the Fortescue Group, Western Australia: implications for atmospheric PO_2. *Precambrian Research*, *65*, 297–317.

Maggi, A., Jackson, J. A., McKenzie, D., & Priestley, K. (2000). Earthquake focal depths, effective elastic thickness, and the strength of the continental lithosphere. *Geology*, *28*, 495–498.

Mahoney, J. J., Jones, W. B., Frey, F. A., Salters, V. J., Pyle, D. G., & Davies, H. L. (1995). Geochemical characteristics of lavas from Broken ridge, the Naturaliste plateau and southernmost Kerguelen plateau: Cretaceous plateau volcanism in the SE Indian Ocean. *Chemical Geology*, *120*, 315–345.

Mambole, A., & Fleitout, L. (2002). Petrological layering induced by an endothermic phase transition in the Earth's mantle. *Geophysical Research Letters*, *29*(22). doi:10.1029/2002GL014674.

Mann, P., & Taira, A. (2004). Global tectonic significance of the Solomon Islands and Ontong Java plateau convergent zone. *Tectonophysics*, *389*, 137–190.

Manning, C. E., Mojzsis, S. J., & Harrison, T. M. (2006). Geology, age and origin of supracrustal rocks at Akilia, West Greenland. *American Journal of Science*, *306*, 303–366.

Marakami, T., Utsunomiya, S., Imazu, Y., & Prasad, N. (2001). Direct evidence of late Archean to early Proterozoic anoxic atmosphere from a product of 2.5 Ga ole weathering. *Earth and Planetary Science Letters*, *184*, 523–528.

Mareschal, J. C., Jaupart, C., Cheng, L. Z., Rolandone, F., Gariepy, C., Bienfait, G., et al. (1999). Heat flow in the Trans-Hudson orogen of the Canadian shield: implications for Proterozoic continental growth. *Journal of Geophysical Research*, *104*, 29007–29024.

Margulis, L. (1970). *Origin of Eukaryotic Cells*. New Haven, CT: Yale University Press.

Marin, J., Chaussidon, M., & Robert, F. (2010). Microscale oxygen isotope variations in 1.9 Ga Gunflint cherts: assessments of diagensis effects and implications for oceanic paleotemperature reconstructions. *Geochimica et Cosmochimica Acta*, *74*, 116–130.

Marko, G. M. (1980). Velocity and attenuation in partially molten rocks. *Journal of Geophysical Research*, *85*, 5173–5189.

Marone, F., & Romanowicz, B. (2007). The depth distribution of azimuthal anisotropy in the continental upper mantle. *Nature*, 447. doi:10.1038/nature0574.

Marshall, C. R. (2006). Explaining the Cambrian "explosion" of animals. *Annual Review of Earth and Planetary Sciences*, *34*, 355–384.

Marti, K., & Graf, T. (1992). Cosmic-ray exposure history of ordinary chondrites. *Annual Review of Earth and Planetary Sciences*, *20*, 221–243.

Marti, K., Kim, J. S., Thakur, A. N., McCoy, T. J., & Keil, K. (1995). Signatures of the martian atmosphere in glass of the Zagami meteorite. *Science*, *267*, 1981–1984.

Martignole, J. (1992). Exhumation of high-grade terranes-a review. *Canadian Journal of Earth Sciences*, *29*, 737–745.

Martin, H. (1993). The mechanisms of petrogenesis of the Archean continental crust-comparison with modern processes. *Lithos*, *30*, 373–388.

Martin, H. (1994). Archean grey gneisses and the genesis of continental crust. In K. C. Condie (Ed.), *Archean Crustal Evolution* (pp. 205–260). Amsterdam: Elsevier.

Marty, B., & Dauphas, N. (2002). Formation and early evolution of the atmosphere. Geological Society of London. *Special Publication*, *199*, pp. 213–229.

Maruyama, S. (1994). Plume tectonics. *Journal of the Geological Society of Japan*, *100*, 24–49.

Maruyama, S. (1997). Pacific-type orogen revisited: Miyashiro-type orogen proposed. *Island Arc*, *6*, 91–120.

Maruyama, S., Santosh, M., & Zhao, D. (2007). Superplume, supercontinent, and post-perovskite: mantle dynamics and anti-plate tectonics on the core-mantle boundary. *Gondwana Research*, *11*, 7–37.

Massey, N. W. D. (1986). Metchosin igneous complex, southern Vancouver Island: ophiolite stratigraphy developed in an emergent island setting. *Geology*, *14*, 602–605.

Matsui, T., Imamura, F., Tajika, E., Nakano, Y., & Fujisawa, Y. (1999). *K-T impact tsunami* (Abstract Vol. XXX). Houston, TX: Lunar & Planetary Institute, Abstract No. 1527, CD-ROM.

Mattesini, M., Belonoshko, A. B., Buforn, E., Ramierez, M., Simak, S. I., Udias, A., et al. (2010). Hemispherical anisotropic patterns of the Earth's inner core. *Proceedings of the National Academy of Sciences of the United States of America*, *107*(21), 9507–9512.

Mattie, P. D., Condie, K. C., Selverstone, J., & Kyle, P. R. (1997). Composition of the lower continental crust in the Colorado Plateau: geochemical evidence from mafic xenoliths from the Navajo Volcanic Field, SW United States. *Geochimica et Cosmochimica Acta*, *61*, 2007–2021.

Maurrasse, F. J. M., & Sen, G. (1991). Impacts, tsunamis, and the Haitian K/T boundary layer. *Science*, *252*, 1690–1693.

Mazumder, R., & Arima, M. (2005). Tidal rhythmites and their implications. *Earth-Science Reviews*, *69*, 79–95.

McBirney, A. R. (1976). Some geologic constraints on models for magma generation in orogenic environments. *Can Mineral*, *14*, 245–254.

McCabe, R. (1984). Implications of paleomagnetic data on the collision related bending of island arcs. *Tectonics*, *3*, 409–428.

McCartney, K. M., Huffman, A. R., & Tredoux, M. (1990). *A paradigm for endogenous causation of mass extinctions* (pp. 125–138). Boulder, CO: Geological Society of America, Special Paper 247.

McClain, J. S., & Atallah, C. A. (1986). Thickening of the oceanic crust with age. *Geology*, *14*, 574–576.

McCollom, T. M., Ritter, G., & Simoneit, B. R. T. (1999). Lipid synthesis under hydrothermal conditions by Fischer-Tropsch-type reactions. *Origins of Life and Evolution of the Biosphere*, *29*, 153–166.

McCubbin, F. M., Steele, A., Hauri, E. H., Nekvasil, H., Yamashita, S., & Hemley, R. J. (2010). Nominally hydrous magmatism on the Moon. *Proceedings of the National Academy of Sciences of the United States of America*, *107*, 11223–11228.

McCulloch, M. T., & Bennett, V. C. (1994). Progressive growth of the Earth's continental crust and depleted mantle: geochemical constraints. *Geochimica et Cosmochimica Acta*, *58*, 4717–4738.

McCulloch, M. T., & Gamble, J. A. (1991). Geochemical and geodynamical constraints on subduction zone magmatism. *Earth and Planetary Science Letters*, *102*, 358–374.

McDonough, W. F. (1990). Constraints on the composition of the continental lithospheric mantle. *Earth and Planetary Science Letters*, *101*, 1–18.

McDonough, W. F., & Sun, S. S. (1995). The composition of the Earth. *Chemical Geology*, *120*, 223–253.

McDougall, I., & Harrison, T. M. (1988). *Geochronology and Thermochronology by the $^{40}Ar/^{39}Ar$ Method* (212 pp). New York: Oxford University Press.

McGeary, S., Nur, A., & Ben-Avraham, Z. (1985). Spatial gaps in arc volcanism: the effect of collision or subduction of oceanic plateaus. *Tectonophysics*, *119*, 195–221.

McGill, G. E., Warner, J. L., Malin, M. C., Arvidson, R. E., Eliason, E., Nozette, S., et al. (1983). Topography, surface properties and tectonic evolution of Venus. In D. M. Hunter, L. Colin, T. M. Donahue & V. I. Moroz (Eds.), *Venus* (pp. 69–130). Tucson: University of Arizona Press.

McGovern, P. J., & Schubert, G. (1989). Thermal evolution of the Earth: effects of volatile exchange between atmosphere and interior. *Earth and Planetary Science Letters*, *96*, 27–37.

McHone, J. F., Niema, R. A., Lewis, C. F., & Yates, A. M. (1989). Stishovite at the K/T boundary, Raton, New Mexico. *Science*, *243*, 1182–1184.

McKay, D. S., et al. (1996). Search for past life on Mars: possible relic biogenic activity in Martian meteorite ALH84001. *Science*, *273*, 924–930.

McKenzie, D. P., & Bickle, M. J. (1988). The volume and composition of melt generated by extension of the lithosphere. *J Petrol*, *29*, 625–679.

McKenzie, D. P., & Morgan, W. J. (1969). Evolution of triple junctions. *Nature*, *224*, 125–133.

McLaren, D. J., & Goodfellow, W. D. (1990). Geological and biological consequences of giant impacts. *Annual Review of Earth and Planetary Sciences*, *18*, 123–171.

McLennan, S. M. (1988). Recycling of the continental crust. *Pure & Applied Geophysics*, *128*, 683–898.

McLennan, S. M., & Hemming, S. (1992). Sm/Nd elemental and isotopic systematics in sedimentary rocks. *Geochimica et Cosmochimica Acta*, *56*, 887–898.

McNamara, A. K., & van Keken, P. E. (2000). Cooling of the Earth: a parameterized convection study of whole versus layered modes. *Geochemistry Geophysics Geosystems*, *1*, 2000GC000045.

McNamara, A. K., & Zhong, S. (2005). Thermochemical structures beneath Africa and the Pacific Ocean. *Nature*, *437*, 1136–1139.

McSween, H. Y., Taylor, G., & Wyatt, M. B. (2009). Elemental composition of the Martian crust. *Nature*, *324*, 736–739.

Meert, J. G. (2002). Paleomagnetic evidence for a Paleo-Mesoproterozoic supercontinent Columbia. *Gondwana Research*, *5*, 207–215.

Meert, J. G., & Lieberman, B. S. (2008). The Neoproterozoic assembly of Gondwana and its relationship to the Ediacaran-Cambrian radiation. *Gondwana Research*, *14*, 5–21.

Meert, J. G., & Torsvik, T. H. (2003). The making and unmaking of a supercontinent: Rodinia revisited. *Tectonophysics*, *375*, 261–288.

Meert, J. G., & van der Voo, R. (1994). The Neoproterozoic glacial intervals: no more snowball Earth? *Earth and Planetary Science Letters*, *123*, 1–13.

Meissner, R., & Mooney, W. (1998). Weakness of the lower continental crust: a condition for delamination, uplift, and escape. *Tectonophysics*, *296*, 47–60.

Melezhik, V. A., Fallick, A. E., Medvedev, P. V., & Makarikhin, V. V. (1999). Extreme $^{13}C_{carb}$ enrichment in ca. 2.0 Ga magnesite-stromatolite-dolomite-'red beds' association in a global context: a case for the world-wide signal enhanced by a local environment. *Earth-Science Reviews*, *48*, 71–120.

Melezhik, V. A., Huhma, H., Condon, D. J., Fallick, A. E., & Whitehouse, M. J. (2007). Temporal constraints on the Paleoproterozoic Lomagundi-Jatuli carbon isotopic event. *Geology*, *35*(7), 655–658.

Melville, R. (1973). Continental drift and plant distribution. In D. H. Tarling & S. K. Runcorn (Eds.), *Implications of Continental Drift to the Earth Sciences* (Vol. 1, pp. 439–446). London: Academic Press.

Menard, H. W. (1967). Transitional types of crust under small ocean basins. *Journal of Geophysical Research*, *72*, 3061–3073.

Menzies, M. A. (1990). Archean, Proterozoic, and Phanerozoic lithospheres. In M. A. Menzies (Ed.), *Continental Mantle* (pp. 67–85). Oxford: Clarendon Press.

Menzies, M. A., Klemperer, S. L., Ebinger, C. J., & Baker, J. (2002). *Characteristics of volcanic rifted margins* (pp. 1–14). Geological Society of America, Boulder, CO, Special Paper, 363.

Metcalfe, I., & Isozaki, Y. (2009). Current perspectives on the Permian-Triassic boundary and end-Permian mass extinction: preface. *Journal of Asian Earth Science*, *36*, 407–412.

Meyer, K. M., Kump, L. R., & Ridgwell, A. (2008). Biogeochemical controls on photic-zone euxinia during the end-Permian mass extinction. *Geology*, *36*, 747–750.

Mezger, K., Rawnsley, C. M., Bohlen, S. R., & Hanson, G. N. (1991). U-Pb garnet, sphene, monazite, and rutile ages: implications for the duration of high-grade metamorphism and cooling histories, Adirondack Mts, NY. *Journal of Geology*, *99*, 415–428.

Michaut, C., Jaupart, C., & Bell, D. R. (2007). Transient geotherms in Archean continental lithosphere: new constraints on thickness and heat production of the subcontinental lithospheric mantle. *Journal of Geophysical Research*, *112*, B04408. doi:10.1029/2006JB004464.

Miller, K. G., Kominz, M. A., Browning, J. V., Wright, J. D., Mountain, G. S., Katz, M. E., et al. (2005). The Phanerozoic record of global sea level change. *Science*, *310*, 1293–1298.

Miller, S. L. (1953). A production of amino acids under possible primitive Earth conditions. *Science*, *117*, 528–529.

Miller, S. L., & Bada, J. L. (1988). Submarine hot springs and the origin of life. *Nature*, *334*, 609–611.

Mirota, M. D., & Veizer, J. (1994). Geochemistry of Precambrian carbonates: VI. Aphebian Albanel formations, Quebec, Canada. *Geochimica et Cosmochimica Acta*, *58*, 1735–1745.

Mo, X., Niu, Y., Dong, G., Zhao, Z., Hou, Z., Zhou, S., et al. (2008). Contribution of sycollisional felsic magmatism to continental crust growth: a case study of the Paleogene Linzizong volcanic succession in southern Tibet. *Chemical Geology*, *250*, 49–67.

Mohr, P. (1982). *Musings on continental rifts*. *Geodynamic Series 8* (pp. 293–309). American Geophysical Union/Geological Society of America.

Mohr, R. E. (1975). Measured periodicities of the Biwabik stromatolites and their geophysical significance. In G. D. Rosenberg & S. K. Runcorn (Eds.), *Growth Rhythms and the History of the Earth's Rotation* (pp. 43–55). New York: J Wiley.

Mojzsis, S. J., & Harrison, T. M. (2000). Vestiges of a Beginning: clues to the emergent bidsphee recorded in the oldest known sedimentary rocks. *GSA Today*, *10*(4), 1–6.

Mojzsis, S. J., Arrhenius, G., McKeegan, K. D., Harrison, T. M., Nutman, A. P., & Friend, C. R. L. (1996). Evidence for life on Earth before 3800 million years ago. *Nature*, *384*, 55–59.

Mojzsis, S. J., Harrison, T. M., & Pidgeon, R. T. (2001). Oxygen-isotope evidence from ancient zircons for liquid water at the Earth's surface 4300 Myr ago. *Nature*, *409*, 178–180.

Molnar, P., & Stock, J. (1987). Relative motions of hotspots in the Pacific, Atlantic and Indian Oceans since late Cretaceous time. *Nature*, *327*, 587–591.

Monnereau, M., & Yuen, D. A. (2010). Seismic imaging of the D″ and constraints on the core heat flux. *Physics of the Earth and Planetary Interiors*, *180*, 258–270.

Montelli, R., Nolet, G., Dahlen, F. A., & Masters, G. (2006). A catalogue of deep mantle plumes: new results from finite-frequency tomography. *Geochemistry Geophysics Geosystems*, *7*(11), Q11007. doi:10.1029/2006GC001248.

Mookherjee, M., Stixrude, L., & Karki, B. (2008). Hydrous silicate melt at high pressure. *Nature*, *452*, 983–986.

Mooney, W. D., & Meissner, R. (1992). Milti-genetic origin of crustal reflectivity: a review of seismic reflection profiling of the continental lower crust and Moho. In D. M. Fountain, R. Arculus & R. W. Kay (Eds.), *Continental Lower Crust* (pp. 45–79). Amsterdam: Elsevier.

Mooney, W. D., Laske, G., & Masters, T. G. (1998). CRUST 5.1: a global crustal model at 5° × 5°. *Journal of Geophysical Research*, *103*, 727–747.

Moore, G. F., Curray, J. R., & Emmel, F. J. (1982). *Sedimentation in the Sunda trends and forearc region* (pp. 245–258). Geological Society of London, Special Publication 10.

Moores, E. M. (1982). Origin and emplacement of ophiolites. *Review of Geophysics*, *20*, 735–760.

Moores, E. M. (1991). SW US-East Antarctic (SWEAT) connection: a hypothesis. *Geology*, *19*, 425–428.

Moores, E. M. (2002). Pre-1 Ga ophiolites: their tectonic and environmental implications. *Geological Society of America Bulletin*, *114*, 80–95.

Moores, E. M., Kellogg, L. H., & Dilek, Y. (2000). *Tethyan ophiolites, mantle convection, and tectonic historical contingency: a resolution of the ophiolite conundrum* (pp. 3–12). Boulder, CO: Geological Society of America, Special Paper 349.

Moresi, L., & Solomatov, V. S. (1998). Mantle convection with a brittle lithosphere: thoughts on the global tectonic styles of the Earth and Venus. *Geophysical Journal International*, *133*, 669–682.

Morgan, J. P., Parmentier, E. M., & Lin, J. (1987). Mechanisms for the origin of mid-ocean ridge axial topography: implications for the thermal and mechanical structure of accreting plate boundaries. *Journal of Geophysical Research*, *92*, 12,823–12,836.

Morgan, P. (1985). Crustal radiogenic heat production and the selective survival of ancient continental crust. *Journal of Geophysical Research*, *90*, C561–C570.

Moucha, R., Forte, A. M., Mitrova, J. X., Rowley, D. B., Quere, S., Simmons, N. A., et al. (2008). Dynamic topography and long-term sea-level variations: there is no such thing as astable continental platform. *Earth and Planetary Science Letters*, *271*, 101–108.

Moyen, F., Stevens, G., & Kisters, A. (2006). Record of mid-Archean subduction from metamorphism in the Barberton terrain, South Africa. *Nature*, *442*, 559–562.

Moyes, A. B., Barton, J. M., & Groenewald, P. B. (1993). Late Proterozoic to Early Paleozoic tectonism in Dronning Maud Land, Antarctica: supercontinental fragmentation and amalgamation. *Journal of the Geological Society of London*, *150*, 833–842.

Moynier, F., Yin, Q. Z., Irisawa, K., Boyet, M., Jacobsen, B., & Rosing, M. T. (2010). Coupled 182W-142Nd constraint for early Earth differentiation. *Proceedings of the National Academy of Sciences of the United States of America*, *107*(24), 10,810–10,814.

Muehlenbachs, K., & Clayton, R. N. (1976). Oxygen isotope composition of oceanic crust and its bearing on seawater. *Journal of Geophysical Research*, *81*, 4365–4369.

Mueller, S., & Phillips, R. J. (1991). On the initiation of subduction. *Journal of Geophysical Research*, *96*, 651–665.

Mueller, W. (1991). Volcanism and related slope to shallow-marine volcaniclastic sedimentation: an Archean example near Chibougamau, Quebec, Canada. *Precambrian Research*, *49*, 1–22.

Mundil, R., Ludwig, K. R., Metcalfe, K. R., & Renne, I. (2004). Age and timing of the Permian mass extinctions: U/Pb geochronology on closed-system zircons. *Science*, *305*, 1760–1763.

Mundil, R., Ludwig, K. R., Metcalfe, K. R., & Renne, I. (2004). Age and timing of the Permian mass extinctions: U/Pb geochronology on closed-system zircons. *Science*, *305*, 1760–1763.

Mundil, R., Metcalfe, I., Ludwig, K. R., Renne, P. R., Oberli, F., & Nicol, R. S. (2001). Timing of the Permian-Triassic biotic crisis: implications from new zircon U/Pb age data. *Earth and Planetary Science Letters*, *187*, 131–145.

Murakami, T., Utsunomiya, S., Imazu, Y., & Prasad, N. (2001). Direct evidence of late Archean to Early Proterozoic anoxic atmosphere from a product of 2.5 GA old weathering. *Earth and Planetary Science Letters*, *184*, 523–528.

Murthy, V. R. (1991). Early differentiation of the Earth and the problem of mantle siderophile elements: a new approach. *Science*, *253*, 303–306.

Mutch, T., Amdson, R. E., Head, J. W., Jones, K. L., & Saunders, R. S. (1976). A summary of Martian geologic history. In T. Mutch, et al. (Eds.), *The Geology of Mars* (pp. 316–319). New Jersey: Princeton University Press.

Nadeau, L., & van Breemen, O. (1994). Do the 1.45–1.39 Ga Montauban Group and the La Bostonnais Complex constitute a Grenvillian accreted terrane? *Geological Association of Canada, Program with Abstracts*, *19*, A81.

Nance, R. D., Worsley, T. R., & Moody, J. B. (1986). Post Archean biogeochemical cycles and long-term episodicity in tectonic processes. *Geology*, *14*, 524–1518.

Narbonne, G. M. (1998). The Ediacara biota: a terminal Neoproterozoic experiment in the evolution of life. *GSA Today*, *8*(2), 1–6.

Nebel-Jacobsen, Y., Munker, C., Nebel, O., Gerdes, A., Mezger, K., & Nelson, D. R. (2010). Reworking of Earth's first crust: constraints from Hf isotopes in Archean zircons from Mt. Narryer, Australia. *Precamb Res*, *182*, 175–186.

Nelson, B. K., & DePaolo, D. J. (1985). Rapid production of continental crust 1.7 to 1.9 by ago: Nd isotopic evidence from the basement of the North American mid-continent. *Geological Society of America Bulletin*, *96*, 746–754.

Nelson, K. D. (1991). A unified view of craton evolution motivated by recent deep seismic reflection and refraction results. *Geophysical Journal International*, *105*, 25–35.

Nemchin, A., Timms, N., Pidgeon, R., Geisler, T., Reddy, S., & Meyer, C. (2009). Timing of crystallization of the lunar magma ocean constrained by the oldest zircon. *Nature Geoscience*, *2*, 133–136.

Nesbitt, H. W., & Young, G. M. (1982). Early Proterozoic climates and plate motions inferred from major element chemistry of lutites. *Nature*, *299*, 715–717.

Newsom, H. E., & Sims, K. W. W. (1991). Core formation during early accretion of the Earth. *Science*, *252*, 926–933.

Newsom, H. E., & Taylor, S. R. (1989). Geochemical implications of the formation of the Moon by a single giant impact. *Nature*, *338*, 29–34.

Ni, S., & Helmberger, D. V. (2003). Further constraints on the African superlpume structure. *Physics of the Earth and Planetary Interiors*, *140*, 243–251.

Nicholas, A. (1986). Structure and petrology of peridotites: clues to their geodynamic environment. *Journal of Geophysical Research, Space Physics*, *24*, 875–895.

Nicolas, A. (1986). Structure and petrology of peridotites: clues to their geodynamic environment. *Review of Geophysics*, *24*, 875–895.

Nimmo, F. (2007). *Thermal and Compositional Evolution of the Core*. *Treatise on Geophysics* (Chap. 9.09, pp. 217–241). Amsterdam: Elsevier.

Nimmo, F., & McKenzie, D. (1998). Volcanism and tectonics on Venus. *Annual Review of Earth and Planetary Sciences*, *26*, 23–51.

Nisbet, E. G. (1986). RNA, hydrothermal systems, zeolites and the origin of life. *Episodes*, *9*, 83–90.

Nisbet, E. G. (1995). Archean ecology: a review of evidence for the early development of bacterail biomes, and speculations on the development of a global-scale biosphere. In M. P. Coward & A. C. Ries (Eds.), *Early Precambrian Processes* (pp. 27–51). Geological Society of London, Special Publication 95.

Nisbet, E. G. (2002). *Fermor lecture: the influence of life on the face of the Earth: garnets and moving continents* (pp. 275–307). Geological Society of London, Special Publication 199.

Nisbet, E. G., & Sleep, N. H. (2001). The habitat and nature of early life. *Nature*, *409*, 1083–1091.

Nisbet, E. G., Cheadle, M. J., Arndt, N. T., & Bickle, M. J. (1993). Constraining the potential temperature of the Archean mantle: a review of the evidence from komatiites. *Lithos*, *30*, 291–307.

Nisbet, E. G., Grassineau, N. V., Howe, C. J., Abel, P. I., Regelous, M., & Nisbet, R. E. R. (2007). The age of Rubisco: the evolution of osygenic photosynthesis. *Geobiology*, *5*, 311–335.

Nishi, M., Kubo, T., Kato, T., Tominaga, A., Shimojuku, A., Doi, N., et al. (2010). Survival of majoritic garnet in diamond by direct kimberlite ascent from deep mantle. *Geophysical Research Letters*, *37*, L09305. doi:10.1029/2010GL042706.

Nixon, P. H., Rogers, N. W., Gibson, I. L., & Grey, A. (1981). Depleted and fertile mantle xenoliths from southern African kimberlites. *Annual Review of Earth and Planetary Sciences*, *9*, 285–309.

Noffke, N., Hazen, R., & Nhleko, N. (2003). Earth's earliest microbial mats in a siliciclastic marine environment 2.9 Ga mozaan Group, South Africa. *Geology*, *31*, 673–676.

Nuth, J. A. (2001). How were the comets made? *American Scientist*, *89*, 228–235.

Nutman, A. P. (2001). On the scarcity of >3900 Ma detrital zircons in ≥3500 Ma metasediments. *Precambrian Research*, *105*, 93–114.

Nutman, A. P., & Friend, C. R. L. (2009). New 1:20,000 scale geological maps, synthesis and history of investgation of the Isua supracrustal belt and adjacent orthogneisses, souther West Greenland: a glimpse of Eoarchean crust formation and orogeny. *Precambrian Research*, *172*, 189–211.

Nutman, A. P., McGregor, V. R., Friend, C. R. L., Bennett, V. C., & Kinny, P. D. (1996). The Itsaq gneiss complex of southern West Greenland; the world's most extensive record of early crustal evolution. *Precambrian Research*, *78*, 1–39.

Nutman, A. P., Friend, C. R. L., & Bennett, V. C. (2002). Evidence for 3650–3600 Ma assembly of the northern end of the Itsaq Gneiss complex, Greenland: implicationm for early Archean tectonics. *Tectonics*, *21*(1). doi:10.1029/2000TC001203.

Nyblade, A. A., & Pollack, H. N. (1993). A global analysis of heat flow from Precambrian terrains: implications for the thermal structure of Archean and Proterozoic lithosphere. *Journal of Geophysical Research*, *98*, 12,207–12,218.

Oberbeck, V. R., Marshall, J. R., & Aggarwal, H. (1993). Impacts, tillites, and the breakup of Gondwanaland. *Journal of Geology*, *101*, 1–19.

O'Connor, J. M., & Duncan, R. A. (1990). Evolution of the Walvis ridge and Rio Grande rise hotspot system: implications for African and South American plate motions over plumes. *Journal of Geophysical Research*, *95*, 17475–17502.

Oehler, D. Z., Robert, F., Walter, M. R., Sugitani, K., Meibom, A., Mostefaoui, S., et al. (2010). Diversity in the Archean biosphere: new insights from NanoSIMS. *Astrobiology*, *10*(4). doi:10.1089/ast.2009.0426.

Officer, C. B., Hallam, A., Drake, C. L., & Devine, J. D. (1987). Late Cretaceous and paroxysmal Cretaceous/Tertiary extinctions. *Nature*, *326*, 143–149.

Oganov, A. R., & Ono, S. (2004). Theoretical and experimental evidence for a post-perovskite phase of $MgSiO_3$ in Earth's D″ layer. *Nature*, *430*, 445–458.

Ogasawara, H., Yoshida, A., Imai, E. I., Honda, H., Hatori, K., & Matsuno, K. (2000). Synthesizing oligomers from monomeric nucleotides in simulated hydrothermal environments. *Origins of Life and Evolution of the Biosphere*, *30*, 519–526.

Ogawa, M. (2003). Chemical stratification in a two-dimensional convecting mantle with magmatism and moving plates. *Journal of Geophysical Research*, *108*(B12), 2561. doi:10.1029/2002JB002205.

Ohmoto, H. (1997). When did the Earth's atmosphere become anoxic? *The Geochemical News*, *93*, 12.

Ohmoto, H., & Felder, R. P. (1987). Bacterial activity in the warmer, sulphate-bearing Archean oceans. *Nature*, *328*, 244–246.

Ohmoto, H., Kadegawa, T., & Lowe, D. R. (1993). 3.4-Ga biogenic pyrites from Barberton, South Africa: sulfur isotope evidence. *Science*, *262*, 555–557.

Ohmoto, H., Watanabe, Y., Yamaguchi, K. E., Naraoka, H., Haruna, M., Kakegawa, T., et al. (2006). *Chemical and biological evolution of early Earth: constraints from banded iron formations* (pp. 1–41). Boulder, CO: Geological Society of America, Memoir 198.

Ohta, K., Hirose, K., Lay, T., Sata, N., & Ohishi, Y. (2008). Phase transitions in pyrolite and MORB at lowermost mantle conditions: implications for a MORB-rich pile above the core-mantle boundary. *Earth and Planetary Science Letters*, *267*, 107–117.

Ohtani, E., & Sakai, T. (2008). Recent advances in the study of mantle transitions. *Physics of the Earth and Planetary Interiors*, *170*, 240–247.

Ohtani, E., Shibata, T., Kubo, T., & Katao, T. (1995). Stability of hydrous phases in the transition zone and the upper most part of the lower mantle. *Geophysical Research Letters*, *22*, 2553–2556.

Olivarez, A. M., & Owen, R. M. (1991). The Eu anomaly of seawater: implications for fluvial versus hydrothermal REE inputs to the oceans. *Chemical Geology*, *92*, 317–328.

Olson, P. (1997). Probing Earth's dynamo. *Nature*, *389*, 337–338.

Olson, P., & Aurnou, J. (1999). A polar vortex in the Earth's core. *Nature*, *402*, 170–173.

Olson, P., Schuber, G., & Anderson, C. (1987). Plume formation in the D″ layer and the roughness of the core-mantle boundary. *Nature*, *327*, 409–413.

Omar, G. I., & Steckler, M. S. (1995). Fission track evidence on the initial rifting of the Red Sea: two pulses, no propagation. *Science*, *270*, 1341–1344.

O'Neill, C., Jellinek, A. M., & Lenardic, A. (2007a). Conditions for the onset of plate tectonics on terrestrial planets and moons. *Earth and Planetary Science Letters*, *261*, 20–32.

O'Neill, C., Lenardic, A., Moresi, L., Torsvik, T. H., & Lee, C. T. A. (2007b). Episodic Precambrian subduction. *Earth and Planetary Science Letters*, *262*, 552–562.

O'Nions, R. K. (1987). Relationships between chemical and convective layering in the Earth. *Journal of the Geological Society of London*, *144*, 259–274.

O'Reilly, S. Y., & Griffin, W. L. (1985). A xenolith-derived geotherm for SE Australia and its geophysical implications. *Tectonophysics*, *111*, 41–63.

O'Reilly, S. Y., Griffin, W. L., & Gaul, O. (1997). Paleogeotherms in Australia: basis for 4–D lithosphere mapping. *Australian Geological Survey Organisation. Journal*, *17*, 63–72.

O'Reilly, S. Y., Griffin, W. L., Djomani, Y. H. P., & Morgan, P. (2001). Are lithospheres forever? *GSA Today*, April 2001, 4–9.

Oro, J. (1994). Early chemical stages in the origin of life. In S. Bengtson (Ed.), *Early Life on Earth* (pp. 48–59). New York: Columbia University Press.

Orth, C. J., Gilmore, J. S., & Knight, J. D. (1987). Ir anomaly at the K/T boundary in the Raton basin. In *New Mexico Geological Society Guidebook, 38th Field Conference* (pp. 265–269).

Ozima, M., & Podosek, F. A. (1999). Formation of Earth from $^{129}I/^{127}I$ and $^{244}Pu/^{238}U$ systematics and the missing Xe. *Journal of Geophysical Research*, *104*, 25493–25499.

Pais, M. A., Le Mouel, J. L., Lambeck, K., & Poirier, J. P. (1999). Late Precambrian paradoxical glaciation and obliquity of the Earth – a discussion of dynamical constraints. *Earth and Planetary Science Letters*, *174*, 155–171.

Pannella, G. (1972). Paleontologic evidence of the Earth's rotational history since early Precambrian. *Astrophys Space Sci*, *16*, 212–237.

Papineau, D. (2010). Global biogeochemical changes at both ends of the Proterozoic: insights from phosphorites. *Astrobiology*, *10*.

Papuc, A. M., & Davies, G. F. (2008). The internal activity and thermal evolution of Earth-like planets. *Icarus*, *195*, 447–458.

Parman, S., Grove, T. L., & Dann, J. (2001). The production of Barberton komatiites in an Archean subduction zone. *Geophysical Research Letters*, *28*, 2513–2516.

Pasteris, J. D. (1984). Kimberlites: complex mantle melts. *Annual Review of Earth and Planetary Sciences*, *12*, 133–153.

Patchett, J. P., & Arndt, N. T. (1986). Nd isotopes and tectonics of 1.9–1.7 Ga crusta genesis. *Earth and Planetary Science Letters*, *78*, 329–338.

Patchett, J. P., & Gehrels, G. E. (1998). Continental influence on Canadian Cordilleran terranes from Nd isotopic study, and significance for crustal growth processes. *Journal of Geology*, *106*, 269–280.

Patterson, C. C., Tilton, G. R., & Inghram, M. G. (1955). Age of the Earth. *Science*, *121*, 69–75.

Paulick, H., Munker, C., & Schuth, S. (2010). The influence of small-scale mantle heterogeneities on mid-ocean ridge volcanis: evidence from the southern mid-Atlantic ridge and Ascension Island. *Earth and Planetary Science Letters*, *296*, 299–310.

Pavlov, A. A., Kasting, J. F., Brown, L. L., Rages, K. A., & Freedman, R. (2000). Greenhouse warming by CH_4 in the atmosphere of early Earth. *Journal of Geophysical Research*, *105*, 11981–11990.

Pavlov, A. A., Hurtgen, M. T., Kasting, J. F., & Arthur, M. A. (2003). Methane-rich Proterozoic atmosphere? *Geology*, *31*, 87–90.

Pavoni, N. (1997). Geotectonic bipolarity—evidence of bicellular convection in the Earth' mantle. *South African Journal of Geology*, *100*(4), 291–299.

Payne, J. L., et al. (2009). Two-phase increase in the maximum size of life over 3.5 billion years reflects biological innovation and environmental opportunity. *Proceedings of the National Academy of Sciences of the United States of America*, *106*, 24–27.

Peacock, S. M. (1990). Fluid processes in subduction zones. *Science*, *248*, 329–337.

Peacock, S. M. (2003). Thermal structure and metamorphic evolution of subducting slabs. In J. Eiler & M. Hirschman (Eds.), *Subduction Factory* (pp. 7–22). American Geophysical Union, Monograph 138.

Pearce, J. A., & Peate, D. W. (1995). Tectonic implications of the composition of volcanic arc magmas. *Annual Review of Earth and Planetary Sciences*, *23*, 251–285.

Pearce, J. A., Harris, N. B. W., & Tindle, A. G. (1984). Trace element discrimination diagrams for the tectonic interpretation of granitic rocks. *J Petrol*, *25*, 956–983.

Pearson, D. G., et al. (1995). Re-Os, Sm-Nd and Rb-Sr isotope evidence for thick Archean lithospheric mantle beneath the Siberian craton modified by multistage metasomatism. *Geochimica et Cosmochimica Acta*, *59*, 959–977.

Pearson, N. J., Alard, O., Griffin, W. L., Jackson, S. E., & O'Reilly, S. Y. (2002). In situ measurement of Re-Os isotopes in mantle sulfides by laser ablation multicollector-inductively coupled plasma mass spectrometry: analytical methods and preliminary results. *Geochimica et Cosmochimica Acta*, *66*, 1037–1050.

Peate, D. W. (1997). *The Parana-Etendeka province* (pp. 217–245). American Geophysical Union Monograph 100.

Pepin, R. O. (1997). Evolution of Earth's noble gases: consequences of assuming hydrodynamic loss driven by giant impact. *Icarus*, *126*, 148–156.

Percival, J. A., & West, G. F. (1994). The Kapuskasing uplift: a geological and geophysical synthesis. *Canadian Journal of Earth Sciences*, *31*, 1256–1286.

Percival, J. A., & Williams, H. R. (1989). Late Archean Quetico accretionary complex, Superior province, Canada. *Geology*, *17*, 23–25.

Percival, J. A., Green, A. G., Milkereit, B., Cook, F. A., Geis, W., & West, G. F. (1989). Seismic reflection profiles across deep continental crust exposed in the Kapuskasing uplift structure. *Nature*, *342*, 416–419.

Percival, J. A., Fountain, D. M., & Salisbury, M. H. (1992). Exposed crustal cross sections as windows on the lower crust. In D. M. Fountain, R. Arculus & R. W. Kay (Eds.), *Continental Lower Crust* (pp. 317–362). Amsterdam: Elsevier.

Perry, E. C., Jr., Ahmad, S. N., & Swulius, T. M. (1978). The oxygen isotope composition of 3800–Ma metamorphosed chert and iron formation from Isukasia, W Greenland. *Journal of Geology*, *86*, 223–239.

Pesonen, L. J., et al. (2003). Paleomagnetic configuration of continents during the Proterozoic. *Tectonophysics*, *375*, 289–324.

Pettengill, G. H., Campbell, D. B., & Masursky, H. (1980). The surface of Venus. *Scientific American*, *243*, 54–65.

Pfiffner, A. (1992). Alpine orogeny. In D. Blundell, R. Freeman & S. Mueller (Eds.), *A Continent Revealed: The European Geotraverse* (pp. 180–190). Cambridge: Cambridge University Press.

Phillips, B. R., Bunge, H. P., & Schaber, K. (2009). Trupolar wander in mantle convection models with multiple, mobile continents. *Gondwana Research*, *15*, 254–266.

Pierson, B. K. (1994). The emergence, diversification, and role of photosynthetic eubacteria. In S. Bengtson (Ed.), *Early Life on Earth* (pp. 161–180). New York: Columbia University Press.

Pieters, C. M., & McFadden, L. A. (1994). Meteorite and asteroid reflectance spectroscopy: clues to early Solar System processes. *Annual Review of Earth and Planetary Sciences*, *22*, 457–497.

Pietranik, A. B., Hawkesworth, C. J., Storey, C. D., Kemp, A. I. S., Sircombe, K. N., Whitehouse, M. J., et al. (2008). Episodic mafic crust formation from 45. To 2.8 Ga: new evidence from detrital zircons, Slave craton, Canada. *Geology*, *36*, 875–878.

Piper, J. D. A. (1987). *Paleomagnetism and the Continental Crust* (434 pp). New York: J. Wiley & Sons.

Pisarevsky, S. A., Wingate, M. T. D., Powell, C. M. c. A., Johnson, S., & Evans, D. A. D. (2003). *Models of Rodinia assembly and fragmentation* (pp. 35–55). Geolological Society of London, Special Publication, 206.

Pitman, W. C., & Talwani, M. (1972). Seafloor spreading in the North Atlantic. *Geological Society of America Bulletin*, *83*, 619–646.

Plint, H. E., & McDonough, M. R. (1995). 40Ar/39Ar age constraints on shear zone evolution, southern Taltson magmatic zone, northeastern Alberta. *Canadian Journal of Earth Sciences*, *32*, 281–291.

Plotnick, R. E. (1980). Relationship between biological extinctions and geomagnetic reversals. *Geology*, *8*, 578–581.

Polet, J., & Anderson, D. L. (1995). Depth extent of cratons as inferred from tomographic studies. *Geology*, *23*, 205–208.

Poli, S., & Schmidt, M. W. (1995). H2O transport and release in subduction zones: experimental constraints on basaltic and andesitic systems. *Journal of Geophysical Research*, *100*, 22,299–22,314.

Pollack, J. B., & Bodenheimer, P. (1989). theories of the origin and evolution of the giant planets. In S. K. Atreya, J. B. Pollack & M. S. Matthews (Eds.), *Origin and Evolution of Planetary and Satellite Atmospheres* (pp. 564–602). Tucson: University of Arizona Press.

Porcelli, D., & Elliott, T. (2008). The evolution of He isotopes in the convecting mantle and the preservation of high $^{3}He/^{4}He$ ratios. *Earth and Planetary Science Letters*, *269*, 175–185.

Poreda, R. J., & Becker, L. (2003). Fullerenes and interplanetary dust at the Permian-Triassic boundary. *Astrobiology*, *3*, 75–90.

Poudjom Djomani, Y. H. P., O'Reilly, S. Y., Griffin, W. L., & Morgan, P. (2001). The density structure of subcontinental lithosphere through time. *Earth and Planetary Science Letters*, *184*, 605–621.

Poulton, S. W., Fralick, P. W., & Canfield, D. E. (2010). Spatial variability in ocdanic redox structure 1.8 billion years ago. *Nature Geoscience*, *3*, 486–490.

Poupinet, G., & Shapiro, N. M. (2009). Worldwide distribution of ages of the continental lithosphere derived from a global seismic tomographic model. *Lithos*, *109*, 125–130.

Powell, C. Mc A., et al. (1993). Paleomagnetic constraints on timing of the Neoproterozoic breakup of Rodinia and the Cambrian formation of Gondwana. *Geology*, *21*, 889–892.

Pretorius, D. A. (1976). The nature of the Witwatersrand gold-uranium deposits. In K. H. Wolfe (Ed.), *Handbook of Stratabound Ore Deposits* (pp. 29–88). Amsterdam: Elsevier.

Prevot, M., Mankineu, E. A., Gromme, C. S., & Coe, R. S. (1985). How geomagnetic field vector reverses polarity. *Nature*, *316*, 230–234.

Price, M. H., & Suppe, J. (1994). Mean age of rifting and volcanism on Venus deduced from impact crater densities. *Nature*, *372*, 756–759.

Price, M. H., Watson, G., Suppe, J., & Brankman, C. (1996). Dating volcanism and rifting on Venus using impact crater densities. *Journal of Geophysical Research*, *101*(E2), 4657–4671.

Prinn, R. G., & Fegley, B. (1987). The atmosphere of Venus, Earth and Mars: a critical comparison. *Annual Review of Earth and Planetary Sciences*, *15*, 171–212.

Prokoph, A., Ernst, R. E., & Buchan, K. L. (2004). Time-series analysis of large igneous provinces: 3500 Ma to present. *Journal of Geology*, *112*, 1–22.

Quinteros, J., Sobolev, S. V., & Popov, A. A. (2010). Viscosity in transition zone and lower mantle: implications for slab penetration. *Geophysical Research Letters*, *37*, L09307. doi:10.1029/2010GL043140.

Rampino, M. R. (1994). Tillites, diamictites, and ballistic ejecta of large impacts. *Journal of Geology*, *102*, 439–456.

Rampino, M. R., & Caldeira, K. (1994). The Goldilocks problem: climatic evolution and long-term habitability of terrestrial planets. *Annual Review of Astronomy and Astrophysics*, *32*, 83–114.

Ranalli, G. (1991). Regional variations in lithosphere rheology from heat flow observations. In V. Cermak & L. Rybach (Eds.), *Exploration of the Deep Continental Crust* (pp. 1–22). Berlin: Springer-Verlag.

Rapp, R. P., & Watson, E. B. (1995). Dehydration melting of metabasalt at 8–32kb: implications for continental growth and crust-mantle recycling. *J Petrol*, *36*, 891–931.

Rasmussen, B., & Buick, R. (1999). Redox state of the Archean atmosphere: evidence from detrital heavy minerals in ca. 3250–2750 Ma sandstones from the Pilbara craton, Australia. *Geology*, *27*, 115–118.

Ravizza, G., & Peucker-Ehrenbrink, B. (2003). Chemostratigraphic evidence of Deccan volcanism from the marine osmium isotope record. *Science*, *302*, 1392–1395.

Reichow, M. K., Pringle, M. S., Al'Mukhamedov, A. I., Allen, M. B., Andreichev, V. L., Buslov, M. M., et al. (2009). *Earth and Planetary Science Letters*, *277*, 9–20.

Renne, P. R., Zichao, Z., Richards, M. A., Black, M. T., & Basu, A. R. (1995). Syncrony and causal relations between Permian-Triassic boundary crises and Siberian volcanism. *Science*, *269*, 1413–1416.

Reston, T. J. (2009). The structure, evolution and symmetry of the magma-poor rifted margins of the North and Cdtral Atlantic: a synthesis. *Tectonophysics*, *468*, 6–27.

Rey, P. F., & Coltice, N. (2008). Neoarchean lithospheric strengthening and the coupling of Earth's geochemical reservoirs. *Geology*, *36*, 636–638.

Reymer, A., & Schubert, G. (1984). Phanerozoic addition rates to the continental crust and crustal growth. *Tectonics*, *3*, 63–77.

Rhodes, M., & Davies, J. H. (2001). Tomographic imaging of multiple mantle plumes in the uppermost lower mantle. *Geophysical Journal International*, *147*, 88–92.

Ribe, N. M., & de Valpine, D. P. (1994). The global hotspot distribution and instability of D″. *Geophysical Research Letters*, *21*, 1507–1510.

Richard, G., Monnereau, M., & Ingrin, J. (2002). Is the transition zone an empty water reservoir? Inferences from numerical model of mantle dynamics. *Earth and Planetary Science Letters*, *205*, 37–51.

Richards, M. A., Duncan, R. A., & Courtillot, V. E. (1989). Flood basalts and hotspot tracks: plume heads and tails. *Science*, *246*, 103–107.

Richardson, S. H. (1990). Age and early evolution of the continental mantel. In M. A. Menzies (Ed.), *Continental Mantle* (pp. 55–65). Oxford: Clarendon Press.

Richardson, S. H., Harris, J. W., & Gurney, J. J. (1993). Three generations of diamonds from old continental mantle. *Nature*, *366*, 256–258.

Richter, F. M. (1988). A major change in the thermal state of the Earth at the Archean-Proterozoic boundary: consequences for the nature and preservation of continental lithosphere [Special lithosphere issue]. *J Petrol*, 39–52.

Richter, F. M., Rowley, D. B., & DePaolo, D. J. (1992). Sr isotope evolution of seawater: the role of tectonics. *Earth and Planetary Science Letters*, *109*, 11–23.

Ridley, V. A., & Richards, M. A. (2010). Deep crustal structure beneath large igneous provinces and the petrologic evolution of flood basalts. *Geochemistry Geophysics Geosystems*, *11*(9), Q09006. doi:10.1029/2009GC002935.

Righter, K. (2003). Metal-silicate partitioning of siderophile elements and core formation in the early Earth. *Annual Review of Earth and Planetary Sciences*, *31*, 135–174.

Righter, K. (2007). Not so rare Earth? New developments in understanding the origin of the Earth and Moon. *Chemie der Erde*, *67*, 179–200.

Ringwood, A. E. (1966). The chemical composition and origin of the earth. In P. M. Hurley (Ed.), *Advances in Earth Sciences* (pp. 287–326). Cambridge: Massachusetts Institute of Technology Press.

Ringwood, A. E. (1979). *Origin of the Earth and Moon* (295 pp). New York: Springer-Verlag.

Rino, S., Kon, Y., Sato, W., Maruyama, S., Santosh, M., & Zhao, D. (2008). The Grenvillian and Pan-African orogens: world's largest orogenies through geologic time, and their implications on the origin of superplume. *Gondwana Research*, *14*, 51–72.

Ritsema, J., & Allen, R. M. (2003). The elusive mantle plume. *Earth and Planetary Science Letters*, *207*, 1–12.

Rivers, T. (1997). Lithotectonic elements of the Grenville province: review and tectonic implications. *Precambrian Research*, *86*, 117–154.

Robert, F. (2001). The origin of water on Earth. *Science*, *293*, 1056–1058.

Robert, F., & Chaussidon, M. (2006). A palaeotemperature curve for the Precambrian oceans based on silicon isotopes in cherts. *Nature*, *443*, 969–972.

Robertson, D. S. (1991). Geophysical applications of very-long-baseline interferometry. *Review of Modern Physics*, *63*, 899–918.

Robin, C. M. I., Jellinek, A. M., Thayalan, V., & Lenardic, A. (2007). Transient mantle convection on Venus: the paradoxical coexistence of highlands and coronae in the BAT region. *Earth and Planetary Science Letters*, *256*, 100–119.

Robinson, P. I. (1973). Paleoclimatology and continental drift. In D. H. Tarling & S. K. Runcorn (Eds.), *Implications of Continental Drift to the Earth Sciences* (Vol. 1, pp. 451–476). London: Academic Press.

Roering, C., et al. (1992). Tectonic model for the evolution of the Limpopo belt. *Precambrian Research*, *55*, 539–552.

Rogers, J. J. W. (1996). A history of continents in the past three billion years. *Journal of Geology*, *104*, 91–107.

Rollinson, H. (2008). Ophiolitic trondhjemites: a possible analogue for Hadean felsic crust. *Terra Nova*, *20*, 364–369.

Romeo, I., & Turcotte, D. L. (2008). Pulsating continents on Venus: an explanation for crustal plateaus and tessera terrains. *Earth and Planetary Science Letters*, *276*, 85–97.

Rona, P. A. (1977). Plate tectonics, energy and mineral resources: basic research leading tom payoff. *Eos*, *58*, 629–639.

Rona, P. A., Klinkhammer, G., Nelson, T. A., Trefry, H., & Elderfield, H. (1986). Black smokers, massive sulfides and vent biota at the Mid-Atlantic Ridge. *Nature*, *321*, 33–37.

Ronov, A. B., & Yaroshevsky, A. A. (1969). *Chemical Composition of the Earth's Crust* (pp. 37–57). American Geophysical Union, Monograph 13.

Ronov, A. B., Bredanova, N. V., & Migdisov, A. A. (1992). General trends in the evolution of the chemical composition of sedimentary and magmatic rocks of the continental Earth crust. *Sov Sci Riev G Geol*, *1*, 1–37.

Rosing, M. T. (1999). ^{13}C-depleted carbon microparticles in >3700–Ma seafloor sedimentary rocks from West Greenland. *Science*, *283*, 674–676.

Rosing, M. T., Rose, N. R., Bridgwater, D., & Thomsen, H. S. (1996). Earliest part of Earth's stratigraphic record: a reappraisal of the >3.7 Ga Isua supracrust sequence. *Geology*, *24*, 43–46.

Rosing, M. T., Bird, D. K., Sleep, N. H., & Bjerrum, D. J. (2010). No climate paradox under the faint early Sun. *Nature*, *464*, 744–747.

Rothschild, L. J., & Mancinellli, R. L. (1990). Model of carbon fixation in microbial mats from 3500 Myr ago to the present. *Nature*, *345*, 710–712.

Ross, M. I., & Scotese, C. R. (1988). A hierarchical tectonic model of the Gulf of Mexico and Caribbean region. *Tectonophysics*, *155*, 139–168.

Rowley, D. B. (2002). Rate of plate creation and destruction: 180 Ma to present. *Geological Society of America Bulletin*, *114*, 927–933.

Rowley, D. B. (2010). Rate of plate creation and destruction: 180 Ma to present. *Geological Society of America Bulletin*, *114*, 927–933.

Royden, L. H. (1993). Evolution of retreating subduction boundaries formed during continental collision. *Tectonics*, *12*, 629–638.

Rubey, W. W. (1951). Geologic history of sea water. *Geological Society of America Bulletin*, *62*, 1111–1148.

Rubie, D. C., Nimmo, F., & Melosh, H. J. (2007). *Formation of Earth's Core*. *Treatise of Geophysics* (Chap. 9.03, pp. 51–90). Amsterdam: Elsevier.

Rudge, J. F. (2006). Mantle pseudo-isochrons revisited. *Earth and Planetary Science Letters*, *249*, 494–513.

Rudnick, R. L. (1992). Xenoliths-samples of the lower continental crust. In D. M. Fountain, R. Arculus & R. W. Kay (Eds.), *Continental Lower Crust* (pp. 269–316). Amsterdam: Elsevier.

Rudnick, R. L. (1995). Making continental crust. *Nature*, *378*, 571–578.

Rudnick, R. L., & Fountain, D. M. (1995). Nature and composition of the continental crust: a lower crustal perspective. *Review of Geophysics*, *33*, 267–309.

Rudnick, R. L., & Gao, S. (2004). *Composition of Continental Crust*. *Treatise on Geochemistry* (Chap. 3.01, pp. 1–64). Amsterdam: Elsevier.

Rudnick, R. L., & Taylor, S. R. (1987). The composition and petrogenesis of the lower crust: A xenolith study. *Journal of Geophysical Research*, *92*, 13,981–14,005.

Rudnick, R. L., McDonough, W. F., & O'Connell, R. J. (1998). Thermal structure, thickness and composition of continental lithosphere. *Chemical Geology*, *145*, 395–411.

Runnegar, B. (1995). Proterozoic eukaryotes: evidence form biology and geology. In S. Bengtson (Ed.), *Early Life on Earth* (pp. 287–297). New York: Columbia University Press.

Ruppel, C. (1995). Extensional processes in continental lithosphere. *Journal of Geophysical Research*, *100*, 24,187–24,215.

Russell, M. J., & Arndt, N. T. (2005). Geodynamic and metabolic cycles in the Hadean. *Biogeosciences*, *2*, 97–111.

Rutter, E. H., & Brodie, K. H. (1992). Rheology of the lower crust. In D. M. Fountain, R. Arculus, & R. W. Kay (Eds.), *Continental Lower Crust* (pp. 201–267). Amsterdam: Elsevier.

Rutter, E. H., & Neumann, D. (1995). Experimental deformation of partially molten Westerly granite under fluid-absent condition, with implications for the extraction of granitic magmas. *Journal of Geophysical Research*, *100*, 15,679–15,716.

Ryan, C. G., Griffin, W. L., & Pearson, N. J. (1996). Garnet geotherms: a technique for derivation of P-T data from Cr-pyrope garnets. *Journal of Geophysical Research*, *101*, 5611–5625.

Rychert, C. A., & Shearer, P. M. (2009). A global view of the lithosphere–asthenosphere boundary. *Science*, *324*, 495–498.

Rye, R., & Holland, H. D. (2000). Life associated with a 2.76 ga ephemeral pond? Evidence from Moutn Roe #2 paleosol. *Geology*, *28*, 483–486.

Rye, R., Kuo, P. H., & Holland, H. D. (1995). Atmospheric CO2 concentrations before 2.2 Ga. *Nature*, *378*, 603–605.

Ryder, G. (2002). Mass flux in the ancient Earth-Moon system and benign implications for the origin of life on Earth. *Journal of Geophysical Research*, *107*. doi:10.1029/2001JE001583.

Ryskin, G. (2003). Methane-driven oceanic eruptions and mass extinctions. *Geology*, *31*, 741–744.

Sacks, I. S. (1983). The subduction of young lithosphere. *Journal of Geophysical Research*, *88*, 3355–3366.

Saikia, A., Frost, D. J., & Rubie, D. C. (2008). Splitting of the 520–km seismic discontinuity and chemical heterogeneity in the mantle. *Science*, *319*, 1515–1518.

Sakamaki, T., Suzuki, A., & Ohtani, E. (2006). Stability of hydrous melt at the base of the Earth's upper mantle. *Nature*, 439. doi:10.1038/nature04352.

Sakuyama, M., & Nesbitt, R. W. (1986). Geochemistry of the Quaternary volcanic rocks of the northeast Japan arc. *Journal of Volcanology and Geothermal Research*, *29*, 413–450.

Sample, J. C., & Fisher, D. M. (1986). Duplex accretion and underthrusting in an ancient accretionary complex, Kodiak Islands, Alaska. *Geology*, *14*, 160–163.

Samson, S. D., & Patchett, P. J. (1991). The Canadian Cordillera as a modern analogue of Proterozoic crustal growth. *Australian Journal of Earth Sciences*, *38*, 595–611.

Sanford, A. R., & Einarsson, P. (1982). *Magma chambers in rifts*. *American Geophysical Union/ Geological Society of America, Geodynamic Series* (Vol. 8. pp. 147–168).

Sarda, P., Staudacher, T., & Allegre, C. J. (1985). 40Ar/39Ar in MORB glasses: constraints on atmosphere and mantle evolution. *Earth and Planetary Science Letters*, *72*, 357–375.

Sarda, P., Moreira, M., Staudacher, T., Schilling, J. G., & Allegre, C. J. (2000). Rare gas systematics on the southernmost Mid-Atlantic ridge: constraints on the lower mantle and the Dupal source. *Journal of Geophysical Research*, *105*, 5973–5996.

Saunders, A. D., Tarney, J., & Weaver, S. D. (1980). Transverse geochemical variations across the Antarctic Peninsula: implications for the genesis of calc-alkaline magmas. *Earth and Planetary Science Letters*, *46*, 344–360.

Saunders, A. D., Tarney, J., Kerr, A. C., & Kent, R. W. (1996). The formation and fate of large igneous provinces. *Lithos*, *37*, 81–95.

Sawkins, F. J. (1990). *Metal Deposits in Relation to Plate Tectonics.* Berlin: Springer-Verlag.

Schermer, E. R., Howell, D. G., & Jones, D. L. (1984). The origin of allochthonous terranes. *Annual Review of Earth and Planetary Sciences*, *12*, 107–131.

Schersten, A., Elliot, T., Hawkesworth, C., & Norman, M. (2004). Tungsten isotope evidence that mantle plumes contain no contribution from the Earth's core. *Nature*, *427*, 234–237.

Schidlowski, M., Hayes, J. M., & Kaplan, I. R. (1983). Isotopic inferences of ancient biochemistries: carbon, sulfur, hydrogen and nitrogen. In J. W. Schopf (Ed.), *The Earth's Earliest Biosphere: Its Origin and Evolution* (pp. 149–186). Princeton, NJ: Princeton University Press.

Schlanger, S. O., & Jenkyns, H. C. (1976). Cretaceous oceanic anoxic events: causes and consequences. *Geol. Mijnbouw*, *55*, 179–184.

Schmerr, N., & Garnero, E. (2007). Upper mantle discontinuity topography from thermal and chemical heterogeneity. *Science*, *318*, 623–626.

Schneider, D. A., Heizler, M. T., Bickford, M. E., Wortman, G. L., Condie, K. C., & Perilli, S. (2007). Timing constraints of orogeny to cratonization: thermochronology of the Paleoproterozoic Trans-Hudson orogen, Manitoba and Saskatchewan, Canada. *Precambrian Research*, *153*, 65–95.

Scholl, D. W., & von Huene, R. (2007). Crustal recycling at modern subduction zones applied to the past—issues of growth and preservation of continental basement, mantle geochemistry, and supercontinent reconstruc-tion. In R. D. Hatcher Jr., M. P. Carlson, J. H. McBride & J. R. Martínez Catalán (Eds.), *The 4–D Framework of Continental Crust* (pp. 9–32). Boulder, CO: Geological Society of America, Memoir 200.

Scholl, D. W., & von Huene, R. (2009). *Implictions of estimated magmatic additions and recycling losses at the subduction zoens of accretionary (non-collisional) and collisional (suturing) orogens* (pp. 105–125). Geological Society of London, Special Publication 318.

Scholl, D. W., von Huene, R., Vallier, T. L., & Howell, D. G. (1980). Sedimentary masses and concepts about tectonic processes at underthrust ocean margins. *Geology*, *8*, 564–568.

Schopf, J. W. (1994). The oldest known records of life: early Archean stromatolites, microfossils, and organic matter. In S. Bengtson (Ed.), *Early Life on Earth* (pp. 193–206). New York: Columbia University Press.

Schopf, J. W. (2006). Fossil evidence of Archean life. *Philosophical transactions of the Royal Society of London. Series B*, *361*, 869–885.

Schopf, J. W., Kudryavtsev, A. B., Czaja, A. D., & Tripathi, A. B. (2007). Evidence of Archean life: stomatolites and microfossils. *Precambrian Research*, *158*, 141–155.

Schott, B., & Schmeling, H. (1998). Delamination and detachment of a lithospheric root. *Tectonophysics*, *296*, 225–247.

Schreyer, W. (1995). Ultradeep metamorphic rocks: the retrospective viewpoint. *Journal of Geophysical Research*, *100*, 8353–8366.

Schubert, G., Turcotte, D. L., & Olson, P. (2001). *Mantle Convection in the Earth and Planets*. Cambridge, UK: Cambridge University Press.

Schulte, P., et al. (2010). The Chicxulub asteroid impact and mass extinction at the Cretaceous-Paleogene boundary. *Science*, *327*, 1214–1218.

Schwab, F. L. (1978). Secular trends in the composition of sedimentary rocks assemblages-Archean through Pherozoic time. *Geology*, *6*, 532–536.

Sclater, J. G., Jaupart, C., & Galson, D. (1980). The heat flow through oceanic and continental crust and the heat loss of the Earth. *Review of Geophysics*, *18*, 269–311.

Scotese, C. R. (1991). Jurassic and Cretaceous plate tectonic reconstructions. *Palaeogeog Palaeoclimat Palaeoecol*, *87*, 493–501.

Scott, C., Lyons, T. W., Bekker, A., Shen, Y., Poulton, S. W., Chu, X., et al. (2008). Tracing the stepwise oxygenation of the Proterozoic ocean. *Nature*, *452*, 456–459.

Scott, D. J., Helmstaedt, H., & Bickle, M. J. (1992). Purtuniq ophiolite, Cape Smith belt, northern Quebec, Canada: a reconstructed section of Early Proterozoic oceanic crust. *Geology*, *20*, 173–176.

Searle, M. P., et al. (1987). The closing of Tethys and the tectonics of the Himalaya. *Geological Society of America Bulletin*, *98*, 678–701.

Seber, D., Barazangi, M., Ibenbrahim, A., & Demnati, A. (1996). Geophysical evidence for llithosphereic delamination beneath the Alboran Sea and Rit-Betic Mountains. *Nature*, *379*, 785–790.

Seilacher, A. (1994). Early multicellular life: late Proterozoic fossils and the Cambrian explosion. In S. Bengtson (Ed.), *Early Life on Earth* (pp. 389–400). New York: Columbia University Press.

Self, S., Blake, S., Sharma, K., Widdowson, M., & Sephton, S. (2008). Sulfur and chlorine in Late Cretaceous Deccan magmas and eruptive gas release. *Science*, *319*, 1654–1657.

Sengor, A. M. C., & Burke, K. (1978). Relative timing of rifting and volcanism on Earth and its tectonic implications. *Geophysical Research Letters*, *5*, 419–421.

Sengor, A. M. C., Natal'in, B. A., & Burtman, V. S. (1993). Evolution of the Altaid tectonic collage and Paleozoic crustal growth in Eurasia. *Nature*, *364*, 299–307.

Sepkoski, J. J. (1989). Periodicity in extinction and the problem of catastrophism in the history of life. *Journal of the Geological Society of London*, *146*, 7–19.

Sepkoski, J. J. (1996). Patterns of Pohanerozoic extinction: a perspective from global data bases. In O. H. Walliser (Ed.), *Global Events and Event Stratigraphy in the Phanerozoic* (pp. 35–51). Berlin: Springer-Verlag.

Shaviv, N. J., & Veizer, J. (2003). Celestial driver of Phanerozoic climate? *GSA Today*, July 2003, 4–10.

Shaw, D. M. (1976). Development of the early continental crust. Part 2. In B. F. Windley (Ed.), *The Early History of the Earth* (pp. 33–54). New York: J. Wiley.

Shaw, D. M., Cramer, J. J., Higgins, M. D., & Truscott, M. G. (1986). *Composition of the Canadian Precambrian shield and the continental crust of the Earth* (pp. 275–282). Geological Society London, Special Publication 24.

Shaw, G. H. (2008). Earth's atmosphere-Hadean to early Proterozoic. *Chemie der Erde*, *68*, 235–264.

Sheehan, P. M. (2001). The Late Ordovician mass extinction event. *Annual Review of Earth and Planetary Sciences*, *29*, 331–364.

Sheldon, N. D. (2006). Precambrian paleosols and atmospheric CO_2 levels. *Precambrian Research*, *147*, 148–155.

Shen, Y., Farquhar, J., Msterson, A., Kaufman, A. J., & Buick, R. (2009). Evaluating the role of microbial sulfate reduction in the early Archean using quadruple isotpe systematics. *Earth and Planetary Science Letters*, *279*, 383–391.

Sherman, D. M. (1995). Stability of possible Fe-FeS and Fe-FeO alloy phases at high pressure and the composition of the Earth's core. *Earth and Planetary Science Letters*, *132*, 87–98.

Sherman, D. M. (1997). The composition of the Earth's core: constraints on S and Si vs. temperature. *Earth and Planetary Science Letters*, *153*, 149–155.

Sheth, H. C. (2007). Large igneous provinces (LIPs): definition, recommended terminology, and a hierarchical classification. *Earth-Science Reviews*, *85*, 117–124.

Shimamoto, T. (1985). The origin of large or great thrust-type earthquakes along subducting plate boundaries. *Tectonophysics*, *119*, 37–65.

Shixing, Z., & Huineng, C. (1995). Megascopic multicellular organisms form the 1700-My-old Tuanshanzi Formation in the Jixian area, North China. *Science*, *270*, 620–622.

Shock, E. L. (1992). Chemical environment of submarine hydrothermal systems. *Origin Life Evol. Biosphere*, *22*, 67–108.

Shock, E. L., & Schulte, M. D. (1998). Organic synthesis during fluid mixing in hydrothermal systems. *Journal of Geophysical Research*, *103*, 28513–28527.

Shukolyukov, A., & Lugmair, G. W. (1998). Isotopic evidence for the Cretaceous-Tertiary impactor and its type. *Science*, *282*, 927–929.

Sidorin, I., Gurnis, M., & Helmberger, D. V. (1999). Evidence for a ubiquitious seismic discontinuity at the base of the mantle. *Science*, *286*, 1326–1331.

Sillitoe, R. H. (1976). *Andean mineralization: a model for the metallogeny of convergent plate margins* (pp. 59–100). Geological Association of Canada, Special Paper 14.

Silver, P. G., & Behn, M. D. (2008). Intermittent plate tectonics? *Science*, *319*, 85–88.

Silver, P. G., & Chan, W. W. (1991). Shear wave splitting and subcontinental mantle deformation. *Journal of Geophysical Research*, *96*, 16,429–16,454.

Simon, N. S. C., Carlson, R. W., Pearson, D. G., & Davies, G. R. (2007). The origin and evolution of thre Kaapvaal cratonic lithospheric mantle. *J Petrol*, *48*, 589–625.

Simonson, B. M., & Harnik, P. (2000). Have distal impact ejecta changed through geologic time? *Geology*, *28*, 975–978.

Simonson, B. M., McDonald, I., Shkolyukov, A., Koeberl, C., Remold, W. U., & Lugmair, G. W. (2009). Geochemistry of 2.63–2.49 Ga impact spherule layers and implications for stratigraphic correlatins and impact processes. *Precambrian Research*, *175*, 51–76.

Sims, K. W. W., Newsom, H. E., & Gladney, E. S. (1990). Chemical fractionation during formation of the Earth's core and continental crust: clues from As, Sb, W, and Mo. In H. E. Newsom & J. H. Jones (Eds.), *Origin of the Earth* (pp. 291–317). New York: Oxford University Press.

Sinigoi, S., et al. (1994). Chemical evolution of a large mafic intrusion in the lower crust, Ivrea-Verbano zone, N Italy. *Journal of Geophysical Research*, *99*, 21,575–21,590.

Sizova, E., Gerya, T., Brown, M., & Perchuk, L. L. (2009). Subduction styles in the Precambrian: insight from numerical experiments. *Lithos*, *116*, 209–229.

Sleep, N. H. (1990). Hotspots and mantle plumes: some phenomenology. *Journal of Geophysical Research*, *95*, 6715–6736.

Sleep, N. H. (1992). Archean plate tectonics: what can be learned from continental geology? *Canadian Journal of Earth Sciences*, *29*, 2066–2071.

Sleep, N. H. (2007). *Plate Tectonics through Time*. *Treatise on Geophysics* (Chap. 9.06, pp. 145–169). Amsterdam: Elsevier.

Sleep, N. H., & Windley, B. F. (1982). Archean plate tectonics: constraints and inferences. *Journal of Geology*, *90*, 363–379.

Sleep, N. H., & Zahnle, K. (2001). Carbon dioxide cycling and implications for climate on ancient Earth. *Journal of Geophysical Research*, *106*(E1), 1373–1399.

Sleep, N. H., Nunn, J. A., & Chou, L. (1980). Platform basins. *Annual Review of Earth and Planetary Sciences*, *8*, 17–34.

Sleep, N. H., Zahnle, K. J., Kasting, J. F., & Morowitz, H. J. (1989). Annihilation of ecosystems by large asteroid impacts on the early Earth. *Nature*, *342*, 139–142.

Sleep, N. H., Zahnle, K., & Neuhoff, P. S. (2001). Initiation of clement surface conditions on the earliest Earth. *Proceedings of the National Academy of Sciences of the United States of America*, *98*, 3666–3672.

Sloan, R. E., Rigby, J. K., Jr., Van Valen, L. M., & Gabriel, D. (1986). Gradual dinosaur extinction and simultaneous ungulate radiation in the Hell Creek Formation. *Science*, *232*, 629–633.

Small, C. (1995). Observations of ridge-hotspot interactions in the southern Ocean. *Journal of Geophysical Research*, *100*, 17931–17946.

Smith, A. G., & Woodcock, N. H. (1982). *Tectonic synthesis of the Alpine-Mediterranean region: a review*. *Geodynamic Series* (Vol. 7, pp. 15–38). American Geophysical Union/Geological Society of America.

Smith, D. E., et al. (1994). Contemporary global horizontal crustal motion. *Geophysical Journal International*, *119*, 511–520.

Smith, R. B., & Braile, L. W. (1994). The Yellowstone hotspot. *Journal of Volcanology and Geothermal Research*, *61*, 121–187.

Smithies, R. H., Champion, D. C., Van Kranendonk, M. J., Howard, H. M., & Hickman, A. H. (2005). Modern-style subduction processes in the Mesoarchean: geochemical evidence from the 3.12 Ga Whundo intra-oceanic arc. *Earth and Planetary Science Letters*, *231*, 221–237.

Smrekar, S. E., et al. (2010). Recent hotspot vocanism on Venus frm VIRTIS emissivity data. *Science*, *328*, 605–608.

Sohl, F., & Schubert, G. (2007). *Interior Structure, Compostion, and Mineralogy of the Terrestrial Planets. Treatise on Geophysics* (Chap. 10.02, pp. 27–68). Amsterdam: Elsevier.

Solomatov, V. (2007). *Magma Oceans and Primordial Mantle Differentiation. Treatise on Geophysics* (Chap. 9.04, pp. 92–119). Amsterdam: Elsevier.

Solomon, S. C. (2003). Mercury: the enigmatic innermost planet. *Earth and Planetary Science Letters*, *216*, 441–455.

Solomon, S. C., & Toomey, D. R. (1992). The structure of mid-ocean ridges. *Annual Review of Earth and Planetary Sciences*, *20*, 329–364.

Solomon, S. C., et al. (1992). Venus tectonics: an overview of Magellan observations. *Journal of Geophysical Research*, *97*, 13,199–13,255.

Song, X., & Helmberger, D. V. (1998). Seismic evidence for an inner core transition zone. *Science*, *282*, 924–927.

Spain, M., & Hirn, A. (1997). Seismic structure and evidence for eclogitization during the Himalayan convergence. *Tectonophysics*, *273*, 1–16.

Spence, W. (1987). Slab pull and the seismotectonics of subducting lithosphere. *Review of Geophysics*, *25*, 55–69.

Spray, J. G. (1984). *Possible causes and consequences of upper mantle decoupling and ophiolite displacement* (pp. 255–267). Geological Society of London, Special Publication 13.

Steckler, M. (1984). Changes in sea level. In H. D. Holland & A. F. Trendall (Eds.), *Patterns of Change in Earth Evolution* (pp. 103–121). Berlin: Springer-Verlag.

Stefanick, M., & Jurdy, D. M. (1984). The distribution of hotspots. *Journal of Geophysical Research*, *89*, 9919–9925.

Stefanick, M., & Jurdy, D. M. (1996). Venus coronae, craters, and chasmata. *Journal of Geophysical Research*, *101*, 4637–4643.

Stein, M., & Hofmann, A. W. (1994). Mantle plumes and episodic crustal growth. *Nature*, *372*, 63–68.

Steinberger, B., & O'Connell, R. J. (1998). Advection of plumes in mantle flow: implications for hotspot motion, mantle viscosity and plume distribution. *Geophysical Journal International*, *132*, 412–434.

Stephen, R. A. (1985). Seismic anisotrophy in the upper oceanic crust. *Journal of Geophysical Research*, *90*(11), 383–396.

Stern, R. J. (2002). Subduction zones. *Review of Geophysics*, *40*(4), 3–1 to 3–38.

Stern, R. J. (2005). Evidence from ophiolites, blueschists, and ultrahigh-pressure metamorphic terranes that the modern episode of subduction tectonics began in Neoproterozoic time. *Geology*, *33*, 557–560.

Stern, R. J. (2008). Modern-style plate tectonics began in Neoproterozoic time: an alternative interpretation of Earth's tectonic history. In K. Condie & V. Pease (Eds.), *When Did Plate Tectonics Begin?* (pp. 265–280). Boulder, CO: Geological Society of America, Special Paper 440.

Stern, R. J., & Scholl, D. W. (2010). Yin and yang of continental crust creation and destruction by plate tectonic processes. *International Geology Review*, *52*, 1–31.

Stern, S. A. (2003). The evolution of comets in the Oort cloud and Kuiper belt. *Nature*, *424*, 639–642.

Steuber, T., & Veizer, J. (2002). Phanerozoic record of plate tectonic control of seawater chemistry and carbonate sedimentation. *Geology*, *30*, 1123–1126.

Stevens, T. O., & McKinley, J. P. (1995). Lithoautotrophic microbial ecosystems in deep basalt aquifers. *Science*, *270*, 450–454.

Stevenson, D. J. (1990a). Chemical heterogeneity and imperfect mixing in the solar nebula. *Astrophysical Journal*, *348*, 730–737.

Stevenson, D. J. (1990b). Fluid dynamics of core formation. In H. E. Newsom & J. H. Jones (Eds.), *Origin of the Earth* (pp. 231–249). Oxford, UK: Oxford University Press.

Stevenson, D. J. (2001). Mars' core and magnetism. *Nature*, *412*, 214–219.

Stevenson, D. J. (2003). Planetary magnetic fields. *Earth and Planetary Science Letters*, *208*, 1–11.

Stevenson, D. J. (2008). A planetary perspective on the deep Earth. *Nature*, *451*, 261–265.

Stixrude, L., & Brown, J. M. (1998). The Earth's core. In R. J. Hemley (Ed.), *Ultrahigh-Pressure Mineralogy: Physics and Chemistry of the Earth's Deep Interior* (Vol. 37, pp. 261–282). Washington, DC: Mineralogical Society of America.

Stockmal, G. S., Beaumont, C., & Boutilier, R. (1986). Geodynamic models of convergent margin tectonics: transition from rifted margin to overthrust belt and consequences fro foreland-basin development. *Bulletin of the American Association of Petroleum Geologists*, *70*, 181–190.

Stockwell, C. H. (1965). Structural trends in the Canadian shield. *Bull Am Assoc Petrol Geol*, *49*, 887–893.

Stockwell, G. S., Beaumont, C., & Boutilier, R. (1986). Geodynamic models of convergent margin tectonics: the transition from rifted margin to overthrust belt and the consequences for foreland basin development. *Bull Am Assoc Petrol Geol*, *70*, 181–190.

Stoddard, P. R., & Abbott, D. (1996). Influence of the tectosphere upon plate motion. *Journal of Geophysical Research*, *101*, 5425–5433.

Stofan, E. R., Smrekar, S. E., Tapper, S. W., Guest, J. E., & Grindrod, P. M. (2001). Preliminary analysis of an expanded database for Venus. *Geophysical Research Letters*, *28*, 4267–4270.

Stone, W. E., Deloule, E., Larson, M. S., & Lesher, M. (1997). Evidence for hydrous high-MgO melts in the Precambrian. *Geology*, *25*, 143–146.

Storey, B. C. (1995). The role of mantle plumes in continental breakup: case histories from Gondwanaland. *Nature*, *377*, 301–308.

Strik, G., Blake, T. S., Zergers, T. E., White, S. H., & Langereis, C. G. (2003). Paleomagnetism of flood basalts in the Pilbara craton, Western Australia: Late Archean contiental drift and the oldest known reversal of the geomagnetic field. *Journal of Geophysical Research*, 108. doi:10.1029/2003JB002475.

Strik, G., de Wit, M. J., & Langereis, C. G. (2007). Paleomagnetism of the Neoarchean Pongola and Ventersdorp Supergroups and an appraisal of the 3.0–1.9 Ga apparent polar wander path of the Kaapvaal craton, Southern Africa. *Precambrian Research*, *153*, 96–115.

Strom, R. G., Schaber, G. G., & Dawson, D. D. (1994). The global resurfacing of Venus. *Journal of Geophysical Research*, *99*, 10,899–10,926.

Suetsugu, D., Isse, T., Tanaka, S., Obayashi, M., Shiobara, H., Sugioka, H., et al. (2009). South Pacific mantle plumes imaged by seismic observation on island and seafloor. *Geochemistry Geophysics Geosystems*, *10*(11), Q11014. doi:10.1029/2009GC002533.

Suganuma, Y., et al. (2006). Paleomagnetism of the Marble Bar Chert Member, Western Australia: implications for apparent polar wander path for Pilbara craton during Archean time. *Earth and Planetary Science Letters*, *252*, 360–371.

Sun, S. Q. (1994). A reappraisal of dolomite abundance and occurrence in the Phanerozoic. *J Sed Res*, *A64*, 396–404.

Sun, S., & McDonough, W. F. (1989). Chemical and isotopic systematics of oceanic basalts: implications for mantle composition and processes. In A. D. Saunder & J. J. Norry (Eds.), *Magmatism in the Ocean Basins* (pp. 313–345). Geological Soceity of London, Special Publication 42.

Sweet, A. R. (2001). Plants, a yardstick for measuring the environmental consequences of the Cretaceous-Tertiary boundary event. *Geoscience Canada*, *28*, 127–138.

Swisher, C. C., et al. (1992). Coeval 40Ar/39Ar ages of 65 Ma from Chicxulub crater melt rock and K/T boundary tektites. *Science*, *257*, 954–958.

Sylvester, P. J. (1994). Archean granite plutons. In K. C. Condie (Ed.), *Archean Crustal Evolution* (pp. 261–314). Amsterdam: Elsevier.

Sylvester, P. J., Campbell, I. H., & Bowyer, D. A. (1997). Nb/U evidence for early formation of the continental crust. *Science*, *275*, 521–523.

Tackley, P. J. (1997a). Effects of phase transitions on three-dimensional mantle convection. In D. Crossley (Ed.), *The Fluid Mechanics of Astrophysics and Geophysics Volume 5: The Doornbos Volume* (pp. 273–336). New York: Gordon and Breach.

Tackley, P. J., Stevenson, D. J., Glatzmaier, G. A., & Schubert, G. (1994). Effects of multiple phase transitions in a three-dimensional spherical model of convection in the Earth's mantle. *Journal of Geophysical Research*, *99*, 15,877–15,901.

Takafuji, N., Hirose, K., Mitome, M., & Bando, Y. (2005). Solubilities of O and Si in liquid iron in equilibrium with (Mg,Fe)SiO3 perovskite and the light elements in the core. *Geophysical Research Letters*, *32*, L06313. doi:10.1029/2005GL022773.

Takashima, R., Nishi, H., & Yoshida, T. (2002). Geology, petrology and tectonic setting of the Late Jurassic ophiolite in Hokkaido, Japan. *Journal of Asian Earth Science*, *21*, 197–215.

Tanner, L. H., Lucas, S. G., & Chapman, M. G. (2004). Assessing the record and causes of Late Triassic extinctions. *Earth-Science Reviews*, *65*, 103–139.

Tapponnier, P., Peltzer, G., & Armijo, R. (1986). *On the mechanics of the collision between India and Asia* (pp. 115–158). Geological Society of London, Special Publication 19.

Tarduno, J. A., & Gee, J. (1995). Large-scale motion between Pacific and Atlantic hotspots. *Nature*, *378*, 477–479.

Tarduno, J. A., et al. (2003). The Emperor seamounts: southward motion of the Hawaiian hotspot plume in Earth's mantle. *Science*, *301*, 1064–1069.

Tarduno, J. A., Cottrell, R. D., Watkeys, M. K., & Bauch, D. (2007). Geomagnetic field strength 3.2 billion years ago recorded by single silicate crystals. *Nature*, 446. doi:10.1038/nature05667.

Tarduno, J. A., Buge, H. P., Sleep, N., & Hansen, U. (2009). The bent Hawaiiam-Emperor hotspot track: inheriting the mantle wind. *Science*, *324*, 50–53.

Tarney, J. (1992). Geochemistry and significance of mafic dyke swarms in the Proterozoic. In K. C. Condie (Ed.), *Proterozoic Crustal Evolution* (pp. 151–179). Amsterdam: Elsevier.

Tamey, J., Wood, D. A., Varet, J., Saunders, A. D., & Cann, J. R. (1979). *Nature of mantle heterogeneity in the North Atlantic: evidence from Leg 49 basalts*. *Maurice Ewing Series* (Vol. 2, pp. 285–301). American Geophysics Union.

Tarney, J., Pickering, K. T., Knipe, R. J., & Dewey, J. F. (Eds.), (1991). *The Behaviour and Influence of Fluids in Subduction Zones*. Royal Society of London, Special Publication A335.

Tatsumi, Y., Shinjoe, H., Ishizuka, H., Sager, W. W., & Klaus, A. (1998). Geochemical evidence for a Mid-Cretacous superplume. *Geology*, *26*, 151–154.

Tatsumi, Y., Kani, T., Ishizuka, H., Maruyama, S., & Nishimura, Y. (2000). Activation of Pacific mantle plumes during the Carboniferous: evidence from accretionary complexes in SW Japan. *Geology*, *28*, 580–582.

Taylor, S. R. (1982). *Planetary Science: A Lunar Perspective* (481 pp). Houston, TX: Lunar & Planetary Institute.

Taylor, S. R. (1987). The unique lunar composition and its bearing on the origin of the Moon. *Geochimica et Cosmochimica Acta*, *51*, 1297–1309.

Taylor, S. R. (1992). *Solar System Evolution* (307 pp). Cambridge: Cambridge University Press.

Taylor, S. R. (1993). Early accretional history of the Earth and the Moon-forming event. *Lithos*, *30*, 207–221.

Taylor, S. R. (1999). On the difficulties of making Earth-like planets. *Meteoritics and Planetary Science*, *34*, 317–329.

Taylor, S. R., & McLennan, S. M. (1985). *The Continental Crust: Its Composition and Evolution* (312 pp). Oxford: Blackwell Scientific.

Taylor, S. R., & McLennan, S. M. (1995). The geochemical evolution of the continental crust. *Review of Geophysics*, *33*, 241–265.

Taylor, S. R., & McLennan, S. M. (2009). *Planetary Crusts: Their Composition, Origin and Evolution* (400 pp). Cambridge, UK: Cambridge University Press.

Thompson, A. B., & Ridley, J. R. (1987). P-T-t histories of orogenic belts. *Philosophical Transactions of the Royal Society of London*, *A321*, 27–45.

Thompson, R. N., & Gibson, S. A. (1994). Magmatic expression of lithospheric thinning across continental rifts. *Tectonophysics*, *233*, 41–68.

Thurston, P. C. (1994). Archean volcanic patterns. In K. C. Condie (Ed.), *Archean Crustal Evolution* (pp. 45–84). Amsterdam: Elsevier.

Thurston, P. C., & Chivers, K. M. (1990). Secular variation in greenstone sequence development emphasizing Superior province, Canada. *Precambrian Research*, *46*, 21–58.

Thybo, H., Ross, A. R., & Egorkin, A. V. (2003). Explosion seismic reflections from the Earth's core. *Earth and Planetary Science Letters*, *216*, 693–702.

Tkalcic, H., & Kennett, B. L. N. (2008). Core structure and heterogeneity: a seismological perspective. *Australian Journal of Earth Sciences*, *55*, 419–431.

Tohver, E., van der Pluijm, B. A., van der Voo, R., Rizzotto, G., & Scandolara, J. E. (2002). Paleogeography of the Amazon craton at 1.2 Ga: early Grenvillian collision with the Llano segment of Laurentia. *Earth and Planetary Science Letters*, *199*, 185–200.

Toksoz, N. M., Minear, J. W., & Julian, B. R. (1971). Temperature field and geophysical effects of the downgoing slab. *Journal of Geophysical Research*, *76*, 1113–1137.

Tolstikhin, I. N., & Hofmann, A. (2005). Early crust on top of the Earth's core. *Physics of the Earth and Planetary Interiors*, *148*, 109–130.

Tomlinson, K. Y., & Condie, K. C. (2001). *Archean Mantle Plumes: Evidence from Greenstone Belt Geochemistry* (pp. 341–357). Boulder, CO: Geological Society of America, Memoir 352.

Tomlinson, K. Y., Hughes, D. J., Thurston, P. C., & Hall, R. P. (1999). Plume magmatism and crustal growth at 2.9 to 3.0 Ga in the Steep Rock and Lumby Lake area, western Superior Province. *Lithos*, *46*, 103–136.

Tonegawa, T., Hirahara, K., Shibutani, T., Iwamori, H., Kanamori, H., & Shiomi, K. (2008). Water flow to the matle transition zone inferred from a receiver function image of the Pacific slab. *Earth and Planetary Science Letters*, *274*, 346–354.

Toon, O. B. (1984). Sudden changes in atmospheric composition and climate. In H. D. Holland & A. F. Trendall (Eds.), *Patterns of Change in Earth Evolution* (pp. 41–61). Berlin: Springer-Verlag.

Toon, O. B., Turco, R. P., & Covey, C. (1997). Environmental perturbations caused by the impacts of asteroids and comets. *Review of Geophysics*, *35*, 41–78.

Touboul, M., Kleine, T., Bourdon, B., Palme, H., & Wieler, R. (2007). Late formation and prolonged differentiation of the Moon inferred from W isotopes in lunar metals. *Nature*, *450*, 1206–1209.

Trampert, J., Deschamps, F., Resovsky, J., & Yuen, D. (2004). Probabilistic tomography maps chemical heterogeneities throught the lower mantle. *Science*, *306*, 853–856.

Trendall, A. F. (1983). Precambrian iron formation of Australia. *Economic Geology*, *68*, 1023–1034.

Tromp, J. (2001). Inner-core anisotropy and rotation. *Annual Review of Earth and Planetary Sciences*, *29*, 47–69.

Tunnicliffe, V., & Fowler, M. R. (1996). Influence of seafloor spreading on the global hydrothermal vent fauna. *Nature*, *379*, 531–533.

Turcotte, D. L. (1995). How does Venus lose heat? *Journal of Geophysical Research*, *100*, 16,931–16,940.

Turcotte, D. L. (1996). Magellan and comparative planetology. *Journal of Geophysical Research*, *101*, 4765–4773.

Turcotte, D. L., & White, W. M. (2001). Thorium-uranium systematics requires layered mantle convection. *Journal of Geophysical Research*, *106*, 4265–4276.

Turgeon, S. C., & Creaser, R. A. (2008). Cretaceous oceanic anoxic event 2 triggered by a massive magmatic episode. *Nature*, *454*, 323–326.

Twitchett, R. J., Looy, C. V., Morante, R., Visscher, H., & Wignall, P. B. (2001). Rapid and synchronous collapse of marine and terrestrial ecosystems during the end-Permian biotic crisis. *Geology*, *29*, 351–354.

Tyler, A. L., Kozlowski, R. W. H., & Lebofsky, L. A. (1988). Determination of rock type on Mercury and the Moon through remote sensing in the thermal infrared. *Geophysical Research Letters*, *15*, 808–811.

Ueno, Y., Johnson, M. S., Danielache, S. O., Eskebjerg, C., Pandey, A., & Yoshida, N. (2009). Geological sulfur isotopes indicate elevated OCS in the Archean atmoslphere, solving faint young Sun paradox. *Proceedings of the National Academy of Sciences of the United States of America*, *106*, 14784–14789.

Unrug, R. (1993). The supercontinent cycle and Gondwanaland assembly: composition of cratons and the timing of suturing events. *Journal of Geodynamics*, *16*, 215–240.

Usui, Y., Tarduno, J. A., Watkeys, M., Hofmann, A., & Cottrell, R. D. (2009). Evidence for a 3.45-billion-year-old magnetic remanence: hints of an ancient geodynamo from conglomerates of South Africa. *Geochemistry Geophysics Geosystems*, *10*(9), Q09Z07. doi:10.1029/2009GC002496.

Uyeda, S., & Miyashiro, A. (1974). Plate tectonics and the Japanese islands: a synthesis. *Geological Society of America Bulletin*, *85*, 1159–1170.

Vail, P. R., & Mitchum, R. M. (1979). Global cycles of relative changes of sea level from seismic stratigraphy. *Am Assoc Petrol Geol Mem*, *29*, 469–472.

Valet, J. P., & Meynadier, L. (1993). Geomagnetic field intensity and reversals during the past 4 My. *Nature*, *366*, 234–238.

Valet, J. P., Laj, C., & Tucholka, P. (1986). High resolution sedimentary record of a geomagnetic reversal. *Nature*, *322*, 27–32.

Valley, J. W., Peck, W. H., King, E. M., & Wilde, S. A. (2002). A cool early Earth. *Geology*, *30*, 351–354.

Valley, J. W., Lackey, J. S., Cavosie, A. J., Clechenko, C. C., Spicuzza, J. J., Basei, M. A. S., et al. (2005). 4.4 billion years of crustal maturation: oxygen isotopes in magmatic zircon. *Contributions to Mineralogy and Petrology*, *150*, 561–580.

van der Hilst, R. D. (1995). Complex morphology of subducted lithosphere in the mantle beneath the Tonga trench. *Nature*, *374*, 154–157.

van der Hilst, R. D., & Karason, H. (1999). Compositional heterogeneity in the bottom 1000 kilometers of Earth's mantle: toward a hybrid convection model. *Science*, *283*, 1885–1888.

van der Hilst, R. D., Engdahl, R., Spakman, W., & Nolet, G. (1991). Tomographic imaging of subducted lithosphere below NW Pacific island arcs. *Nature*, *353*, 37–43.

van der Hilst, R. D., Widiyantoro, S., & Engdahl, E. R. (1997). Evidence for deep mantle circulation from global tomography. *Nature*, *386*, 578–584.

van der Meijde, M., Marone, F., Giardini, D., & van der Lee, S. (2003). Seismic evidence for water deep in Earth's upper mantle. *Science*, *300*, 1556–1558.

Van der Voo, R., Spakman, W., & Bijwaard, H. (1999). Mesozoic subducted slabs under Siberia. *Nature*, *397*, 246–249.

Van Fossen, M. C., & Kent, D. V. (1992). Paleomagnetism of 122 Ma plutons in New England and the Mid-Cretaceous paleomagnetic field in North America: true polar wander or large-scale differential mantle motion? *Journal of Geophysical Research*, *97*, 19651–19661.

van Gerven, L., Deschamps, F., & van der Hilst, R. D. (2004). Geophysical evidence for chemical variations in the Australian continental mantle. *Geophysical Research Letters*, *31*, L17607. doi:10.1029/2004GL020307.

van Hunen, J., & van den Berg, A. P. (2007). Plate tectonics on the early Earth: limitations imposed by strength and buoyancy of subducted lithosphere. *Lithos*, *103*, 217–235.

Van Kranendonk, M. J., Hickman, A. H., Smithies, R. H., & Nelson, D. R. (2002). Geology and tectonic evolution of the Archean North Pilbara terrain, Pilbara craton, Western Australia. *Economic Geology*, *97*, 695–732.

Van Kranendonk, M. J., Webb, G. E., & Kamber, B. S. (2003). Geological and trace element evidence for a marine sedimentary environment of deposition and biogenicity of 3.45 Ga strromatolitic carbonates in the Pilbara craton, and support for a reducing Archean ocean. *Geobiology*, *1*, 91–108.

Varsek, J. L., et al. (1993). Lithoprobe crustal reflection structure of the southern Canadian Cordillera 2: Coast Mountains transect. *Tectonics*, *12*, 334–360.

Vaughan, A. P., & Storey, B. C. (2007). A new supercontinent self-destruct mechanism: evidence from the Late Triassic-/early Jurassic. *Journal of the Geological Society of London*, *164*, 382–392.

Veevers, J. J. (1990). Tectonic-climatic supercycle in the billion-year plate-tectonic eon: Permian Pangean icehouse alternates with Cretaceous dispersed-continents greenhouse. *Sed Geol*, *68*, 1–16.

Veizer, J. (1979). Secular variations in chemical composition of sediments: a review. *Physics and Chemistry of the Earth*, *11*, 269–278.

Veizer, J. (1989). Strontium isotopes in seawater through time. *Annual Review of Earth and Planetary Sciences*, *17*, 141–187.

Veizer, J., & Compston, W. (1976). $^{87}Sr/^{86}Sr$ in Precambrian carbonates as an index of crustal evolution. *Geochimica et Cosmochimica Acta*, *40*, 905–914.

Veizer, J., & Jansen, S. L. (1985). Basement and sedimentary recycling -2: time dimension to global tectonics. *Journal of Geology*, *93*, 625–643.

Veizer, J., & Mackenzie, F. T. (2003). *Evolution of Sedimentary Rocks*. *Treatise on Geochemistry* (Chap. 7.15, pp. 369–407). Amsterdam: Elsevier.

Veizer, J., Bell, K., & Jansen, S. L. (1992). Temporal distribution of carbonatites. *Geology*, *20*, 1147–1149.

Veizer, J., Compston, W., Clauer, N., & Schidlowski, M. (1983). $^{87}Sr/^{86}Sr$ in Late Proterozoic carbonates: evidence for a mantle event at 900 Ma. *Geochimica et Cosmochimica Acta*, *47*, 295–302.

Veizer, J., Hoefs, J., Lowe, D. R., & Thurston, P. C. (1989). Geochemistry of Precambrian carbonates: II. Archean greenstone belts and Archean seawater. *Geochimica et Cosmochimica Acta*, *53*, 859–871.

Veizer, J., et al. (1999). $^{87}Sr/^{86}Sr$, $d^{13}C$ and $d^{18}O$ evolution of Phanerozoic seawater. *Chemical Geology*, *161*, 59–88.

Veizer, J., Godderis, Y., & Francois, L. M. (2000). Evidence for decoupling of atmospheric CO_2 and global climate during the Phanerozoic eon. *Nature*, *408*, 698–701.

Vidal, P. h., Bernard-Griffiths, J., Cocheric, A., LeFort, P., Peucat, J. J., & Sheppard, S. M. (1984). Geochemical comparison between Himalayan and Hercynian leucogranites. *Physics of the Earth and Planetary Interiors*, *35*, 179–190.

Vidale, J. E., Ding, X. Y., & Grand, S. P. (1995). The 410–km-depth discontinuity: a sharpness estimate from near-critical reflections. *Geophysical Research Letters*, *22*, 2557–2560.

Vidale, J. E., Dodge, D. A., & Earle, P. S. (2000). Slow differential rotation of the Earth's inner core indicated by temporal changes in scattering. *Nature*, *405*, 445–447.

Vielzeuf, D., Clemens, J. D., Pin, C., & Moinet, E. (1990). Granites, granulites, and crustal differentiation. In D. Vielzeuf & P. H. Vidal (Eds.), *Granulites and Crustal Evolution* (pp. 59–85). Norwell, MA: Kluwer Academic Press.

Vigny, C., Ricard, Y., & Froidevaux, C. (1991). The driving mechanism of plate tectonics. *Tectonophysics*, *187*, 345–360.

Vilas, F., et al. (1988). *Mercury*. Tucson: University Arizona Press.

Vine, F. (1966). Spreading of the ocean floor: evidence. *Science*, *154*, 1405–1415.

Vine, F., & Matthews, D. H. (1963). Magnetic anomalies over oceanic ridges. *Nature*, *199*, 947–949.

Vinnik, L. P., Green, R. W. E., & Nicolaysen, L. O. (1995). Recent deformations of the deep continental root beneath southern Africa. *Nature*, *375*, 50–52.

Vitorello, I., & Pollack, H. N. (1980). On the variation of continental heat flow with age and the thermal evolution of continents. *Journal of Geophysical Research*, *85*, 983–995.

Vlastelic, L., Aslanian, D., Dosso, L., Bougault, H., Olivet, J. L., & Geli, L. (1999). Large-scale chemical and thermal division of the Pacific mantle. *Nature*, *399*, 345–350.

Vocadlo, L., Alfe, D., Gillan, M. J., Wood, I. G., Brodholt, J. P., & Price, G. D. (2003). Possible thermal and chemical stabilization of body-centered-cubic iron in the Earth's core. *Nature*, *424*, 536–539.

von Brunn, V., & Gold, D. J. D. (1993). Diamictite in the Archean Pongola sequence of southern Africa. *Journal of African Earth Sciences*, *16*, 367–374.

Von Damm, K. L. (1990). Seafloor hydrothermal activity: black smoker chemistry and chimneys. *Annual Review of Earth and Planetary Sciences*, *18*, 173–204.

von Huene, R., & Scholl, D. W. (1991). Observations at convergent margins concerning sediment subduction, subduction erosion, and the growth of continental crust. *Review of Geophysics*, *29*, 279–316.

von Raumer, J. F., Stampfli, G. M., & Bussy, F. (2003). Gondwana-derived microcontinents – the constituents of the Variscan and Alpine collisional orogens. *Tectonophysics*, *365*, 7–22.

Walck, M. C. (1985). The upper mantle beneath the northeast Pacific rim: a comparison with the Gulf of California. *Geophysical Journal of the Royal Astronomical Society*, *81*, 243–276.

Walker, J. C. G. (1977). *Evolution of the Atmosphere* (318 pp). New York: Macmillan.

Walker, J. C. G. (1990). Precambrian evolution of the climate system. *Palaeogeog Palaeoclimat Palaeoecol*, *82*, 261–289.

Walker, J. C. G., Klein, C., Schidlowski, M., Schopf, J. W., Stevenson, D. J., & Walter, M. R. (1983). Environmental evolution of the Archean-Early Proterozoic Earth. In J. W. Schopf (Ed.), *The Earth's Earliest Biosphere: Its Origin and Evolution* (pp. 260–290). Princeton, NJ: Princeton University Press.

Walker, R. J., Morgan, J. W., & Horan, M. F. (1995). Osmium-187 enrichment in some plumes: evidence for core-mantle interaction? *Science*, *269*, 819–821.

Walker, R. J., Carlson, R. W., Shirey, S. B., & Boyd, F. R. (1989). Os, Sr, Nd and Pb isotope systematics of southern African peridotite xenoliths: implications for chemical evolution of subcontinental mantle. *Geochimica et Cosmochimica Acta*, *53*, 1583–1595.

Walter, M. R. (1994). Stromatolites: the main geological source of information on the evolution of the early benthos. In S. Bengtson (Ed.), *Early Life on Earth* (pp. 270–286). New York: Columbia University Press.

Walter, M. R., Veevers, J. J., Claver, C. R., Gorjan, P., & Hill, A. C. (2000). Dating the 840–544 Ma Neoproterozoic interval by isotopes of Sr, C, and S in seawater, and some interpretative models. *Precambrian Research*, *100*, 371–433.

Wang, T., Jahn, B. M., Kovach, V. P., Tong, Y., Hong, D. W., & Han, B. F. (2009). Nd-Sr isotopic mapping of the Chinese Altai and implications for continental growth in the Central Asian Orogenic Belt. *Lithos*, *110*, 359–372.

Wang, Y., Weidner, D. J., Liebermann, R. C., & Zhao, Y. (1994). P-V-T equation of state of perovskite: constraints on composition of the lower mantle. *Physics of the Earth and Planetary Interiors*, *83*, 13–40.

Warner, M., et al. (1996). Seismic reflections from the mantle represent relict subduction zones within the continental lithosphere. *Geology*, *24*, 39–42.

Wasson, J. T. (1985). *Meteorites* (276 pp). New York: W. H. Freedman.

Watanabe, Y., Martini, J. E. J., & Ohmoto, H. (2000). Geochemical evidence for terrestrial ecosystems 2.6 billion years ago. *Nature*, *408*, 574–577.

Waters, F. G., & Erlank, A. J. (1988). Assessment of the vertical extent and distribution of mantle metasomatism below Kimberley, South Africa [Special lithosphere Issue]. *J Petrol*, 185–204.

Watters, T. R., Solomon, S. C., Roinson, M. S., Head, J. W., Andre, S. L., Hauck, S. A., et al. (2009). The tectonics of Mercury: the view after *MESSENGER*'s first flyby. *Earth and Planetary Science Letters*, *285*, 283–296.

Weaver, B. L., Wood, D. A., Tarney, J., & Joron, J. L. (1987). *Geochemistry of ocean island basalts from the South Atlantic: Ascension, Bouvet, St. Helena, Gough and Trista da Cunha* (pp. 253–267). Geological Society of London, Special Publication 30.

Wedepohl, K. H. (1995). The composition of the continental crust. *Geochimica et Cosmochimica Acta*, *59*, 1217–1232.

Wegener, A. (1912). Die Entstehung der Kontinente. *Geol Rund*, *3*, 276–292.

Weiguo, S. (1994). Early multicellular fossils. In S. Bengtson (Ed.), *Early Life on Earth* (pp. 358–369). New York: Columbia University Press.

Weinberger, A. J. (2002). A dusty business. *Science*, *295*, 2027–2028.

Wendlandt, E., DePaolo, D. J., & Baldridge, W. S. (1993). Nd and Sr isotope chronostratigraphy of Colorado Plateau lithosphere: implications for magmatic and tectonic underplating of the continental crust. *Earth and Planetary Science Letters*, *116*, 23–43.

Wernicke, B., Davis, J. L., Niemi, N. A., Luffi, P., & Bisnath, S. (2008). Active megadetachment beneath the western United States. *Journal of Geophysical Research*, *113*, B11409. doi:10.1029/2007JB005375.

Westall, F., & Southam, G. (2007). *Geology, Life and Habitability. Treastise on Geophysics* (Chap. 10.12, pp. 421–437). Amsterdam: Elsevier.

Wetherill, G. W. (1986). Accumulation of the terrestrial planets and implications concerning lunar origina. In W. K. Hartmann, R. J. Phillips & G. J. Taylor (Eds.), *Origin of the Moon* (pp. 519–550). Houston, TX: Lunar & Planetary Institute.

Wetherill, G. W. (1990). Formation of the Earth. *Annual Review of Earth and Planetary Sciences*, *18*, 205–256.

Wetherill, G. W. (1994). Provenance of the terrestrial planets. *Geochimica et Cosmochimica Acta*, *58*, 4513–4520.

White, R. S. (1988). The Earth's crust and lithosphere [Special lithosphere issue]. *J Petrol*, 1–10.

White, R. S., & McKenzie, D. (1995). Mantle plumes and flood basalts. *Journal of Geophysical Research*, *100*, 17,543–17,585.

White, R. S., et al. (1987). Magmatism at rifted continental margins. *Nature*, *330*, 439–444.

White, W. M. (2010). Oceanic island basalts and mantle plumes: the geochemical perspective. *Annual Review of Earth and Planetary Sciences*, *38*, 133–160.

Whitehead, J. A., & Clift, P. D. (2009). Continent elevation, mountains, and erosion: freeboard implications. *Journal of Geophysical Research*, *114*, B05410. doi:10.1029/2008JB006176.

Whitehouse, M. J., Myers, J. S., & Fedo, C. M. (2009). The Akilia controversy: field, structural and geochronological evidence questions interpretations of >3.8 Ga life in SW Greenland. *Journal of the Geological Society of London*, *166*, 335–348.

Whiteside, J. H., Olsen, P. E., Eglinton, T., Brookfield, M. E., & Sambrotto, R. N. (2010). *Proceedings of the National Academy of Sciences*, *107*, 6721–6725.

Wickham, S. M. (1992). Fluids in the deep crust—petrological and isotopic evidence. In D. M. Fountain, R. Arculus & R. W. Kay (Eds.), *Continental Lower Crust* (pp. 391–421). Amsterdam: Elsevier.

Widdel, F., Schnell, S., Heising, S., Ehrenreich, A., Assmus, B., & Schink, B. (1993). Ferrous iron oxidation by anoxygenic phototrophic bacteria. *Nature*, *362*, 834–836.

Wiens, D. A., & Stein, S. (1985). Implications of oceanic intraplate seismicity for plate stresses, driving forces and rheology. *Tectonophysics*, *116*, 143–162.

Wignall, P. (2001). Large igneous provinces and mass extinctions. *Earth-Science Reviews*, *53*, 1–33.

Wignall, P. (2003). The nature of the end-Permian mass extinction and its bearing on volcanic extinction mechanisms. In *Mantle Plumes: Physical Processes, Chemical Signatures and Biological Effects* (Abstract Vol., p. 45). Cardiff, UK: Cardiff University, September 2003.

Wignall, P. (2007). The End-Permian mass extinction – how bad did it get? *Geobiology*, *5*, 303–309.

Wilde, P., Quinby-Hunt, M. S., & Berry, B. N. (1990). Vertical advection from oxic or anoxic water from the pycnocline as a cause of rapid extinction or rapid radiations. In E. G. Kauffman & O. H. Walliser (Eds.), *Extinction Events in Earth History* (Vol. 30, pp. 85–97). Lecture Notes on Earth Science, Heidelberg: Springer.

Wilde, S. A., Valley, J. W., Peck, W. H., & Graham, C. M. (2001). Evidence from detrital zircon from the existence of continental crust and oceans on the Earth 4.4 Ga. *Nature*, *409*, 175–178.

Willbold, M., & Stracke, A. (2006). Trace element composition of mantle end-members: implications for recycling of oceanic and upper and lower continental crust. *Geochemistry Geophysics Geosystems*, *7*(4), Q044004. doi:10.1029/2005GC001005.

Willbold, M., & Stracke, A. (2010). Formation of enriched mantle components by recycling of upper and lower continental crust. *Chemical Geology*, *276*, 188–197.

Willbold, M., Hegner, E., Stracke, A., & Rocholl, A. (2009). Continental geochemical signatures in dacites from Iceland and implications for models of early Archean crust formation. *Earth and Planetary Science Letters*, *279*, 44–52.

Williams, D. M., & Pollard, D. (2000). Earth-Moon interactions: implications for terrestrial climate and life. In R. M. Canup & R. M. Righter (Eds.), *Origin of the Earth and Moon* (pp. 513–525). Tucson, AZ: University of Arizona Press.

Williams, G. E. (1975). Late Precambrian glacial climate and the Earth's obliquity. *Geological Magazine*, *112*, 441–465.

Williams, G. E. (1989). Precambrian tidal sedimentary cycles and Earth's paleorotation. *Eos*, *70*, 40–41.

Williams, L. A. J. (1982). *Physical aspects of magmatism in continental rifts. Geodynamic Series* (Vol. 8, pp. 193–219). American Geophysical Union/Geological Society of America.

Williams, Q. (2007). *Water, the Solid Earth, and the Atmosphere: The Genesis and Effects of a Wet Surface on a Mostly Dry Planet. Treatise of Geophysics* (Chap. 9.05, pp. 121–142). Amsterdam: Elsevier.

Wilson, J. T. (1963). Evidence from islands on the spreading of the ocean floor. *Nature*, *197*, 536–538.

Wilson, J. T. (1965). Transform faults, oceanic ridges and magnetic anomalies SW of Vancouver Island. *Science*, *150*, 482–485.

Wilson, L. (2009). Volcanism in the solar system. *Nature Geoscience*, *2*, 389–397.

Wilson, M. (1993). Magmatism and the geodynamics of basin formation. *Sedimentol Geol*, *86*, 5–29.

Wilson, P. A., & Norris, R. D. (2001). Warm tropical ocean surface and global anoxia during the mid-Cretaceous period. *Nature*, *412*, 425–428.

Windley, B. F. (1992). Proterozoic collision and accretionary orogens. In K. C. Condie (Ed.), *Proterozoic Crustal Evolution* (pp. 419–446). Amsterdam: Elsevier.

Windley, B. F. (1993). Proterozoic anorogenic magmatism and its orogenic connections. *Journal of the Geological Society of London*, *150*, 39–50.

Windley, B. F. (1995). *The Evolving Continents* (3rd., 526 pp). New York: J. Wiley.

Windley, B. F., & Garde, A. A. (2009). Arc-generated blocks with crustal sections in the North Atlantic craton of West Greenland: crustal growth in the Archean with modern analogues. *Earth-Science Reviews*, *93*, 1–30.

Wingate, M. T. D., Pisarevsky, S. A., Gladkochub, D. P., Donskaya, T. V., Konstantinov, K. M., Mazukabzov, A. M., et al. (2009). Geochronology and paleomagnetism of mafic igneous rocks in the Olenek uplift, northern Siberia: implications for Mesoproterozoic supercontients and paleogeography. *Precambrian Research*, *170*, 256–266.

Wise, D. U. (1963). An origin of the Moon by rotational fission during formation of the Earth's core. *Journal of Geophysical Research*, *68*, 1547–1554.

Wise, D. U. (1973). *Freeboard of continents through time* (pp. 87–100). Boulder, CO: Geological Society of America, Memoir 132.

Wolbach, W. S., Lewis, R. S., & Anders, E. (1985). Cretaceous extinctions: evidence for wildfires and search for meteoric material. *Science*, *230*, 167–170.

Wood, B. J. (1995). The effect of water on the 410–km seismic discontinuity. *Science*, *268*, 74–76.

Wood, D. A. (1979). A variably veined suboceanic upper mantle-genetic significance for mid-ocean ridge basalts from geochemical evidence. *Geology*, *7*, 499–503.

Wood, D. A., Tarney, J., Varet, J., Saunders, A. D., Bougault, H., Joron, J. L., et al. (1979). Geochemistry of basalts drilled in the North Atlantic by IPOD Leg 49: Implications for mantle heterogeneity. *Earth and Planetary Science Letters*, *42*, 77–97.

Wood, J. A. (1986). Moon over Mauna Loa: a review of hypotheses of formation of the Earth's moon. In W. K. Hartmann, R. J. Phillips & G. J. Taylor (Eds.), *Origin of the Moon* (pp. 17–56). Houston, TX: Lunar & Planetary Institute.

Wood, J. A., & Mitler, H. E. (1974). Origin of the Moon by a modified capture mechanism, or half a loaf is better than a whole one. *Lunar Sci*, *5*, 851–853.

Woollard, G. P. (1968). *The interrelationship of the crust, upper mantle, and isostatic gravity anomalies in the United States* (pp. 312–341). American Geophysical Union, Monograh 12.

Workman, R. K., Hart, S. R., Blusztajn, J., Jackson, M., Kurz, M., & Staudigel, H. (2003). Enriched mantle II: a new view from the Samoan hotspot. *Geophysical Research Abstracts*, *5*, 13656.

Workman, R. K., Eiler, J. M., Hart, S. R., & Jackson, M. G. (2008). Oxygen isotopes in Samoan lavas: confirmation of continent recycling. *Geology*, *36*, 551–554.

Worsley, T. R., & Nance, R. D. (1989). Carbon redox and climate control through Earth history: a speculative reconstruction. *Palaeogeog Palaeoclimat Palaeoecol*, *75*, 259–282.

Worsley, T. R., Nance, R. D., & Moody, J. B. (1984). Global tectonics and eustasy for the past 2 billion years. *Marine Geology*, *58*, 373–400.

Worsley, T. R., Nance, R. D., & Moody, J. B. (1986). Tectonic cycles and the history of the Earth's biogeochemical and paleoceanographic record. *Paleoceanography*, *1*, 233–263.

Wronkiewicz, D. J., & Condie, K. C. (1989). Geochemistry and provenance of sediments from the Pongola Supergroup South Africa: evidence for a 3.0-Ga-old continental craton. *Geochimica et Cosmochimica Acta*, *53*, 1537–1549.

Wu, Y., Fei, Y., Jin, Z., & Liu, X. (2009). The fate of subducted upper continental crust: an experimental study. *Earth and Planetary Science Letters*, *282*, 275–284.

Wyckoff, S. (1991). Comets: clues to the early history of the Solar System. *Earth-Science Reviews*, *30*, 125–174.

Wyllie, P. J. (1971). The role of water in magma generation and initiation of diapiric uprise in the mantle. *Journal of Geophysical Research*, *76*, 1328–1338.

Wyman, D. A., & Kerrich, R. (2002). Formation of Archean continental lithospheric roots: the role of mantle plumes. *Geology*, *30*, 543–546.

Xiao, W. J., Windley, B. F., Huang, B. C., Han, C. M., Yuan, C., Chen, H. L., et al. (2009). End-Permian to mid-=Triassic termination of the accretionary processes of the southern Altaids: implications for the geodynamic evolution, Phanerozoic continental growth, and metallogeny of central Asia. *The International Journal of Earth Sciences*, doi:10/1007s00531–008–0407–z.

Xie, Q., & Kerrich, R. (1994). Silicate-perovskite and majorite signature komatiites from the Archean Abitibi greenstone belt: implications for early mantle differentiation and stratification. *Journal of Geophysical Research*, *99*, 15,799–15,812.

Xie, Q., Kerrich, R., & Fan, J. (1993). HFSE/REE fractionations recorded in three komatiite-basalt sequences, Archean Abitibi greenstone belt: implications for multiple plume sources and depths. *Geochimica et Cosmochimica Acta*, *57*, 4111–4118.

Xie, Q., McCuaig, T. C., & Kerrich, R. (1995). Secular trends in the melting depths of mantle plumes: evidence from HFSE/REE systematics of Archean high-Mg lavas and modern oceanic basalts. *Chemical Geology*, *126*, 29–42.

Yang, J. H., Wu, F. Y., Wilde, S. A., Belousova, E., & Griffin, W. L. (2008). Mesozoic decratonization of the North China block. *Geology*, *36*, 467–470.

Yang, W., Holland, H. D., & Rye, R. (2002). Evidence for low or no oxygen in the late Archean atmosphere from the 2.76 Ga Mt Roe #2 paleosol, Western Australia: Part 3. *Geochimica et Cosmochimica Acta*, *66*, 3707–3718.

Yardley, B. W. D. (2009). Role of water in the evolution of the continental crust. *Journal of the Geological Society of London*, *166*, 585–600.

Yin, Q., Jacobsen, S. B., Yamashita, K., Blichert-Toft, J., Telouk, P., & Albarede, F. (2002). A short timescale for terrestrial planet formation from Hf-W chronometry of meteorites. *Nature*, *418*, 949–952.

Yoshida, S. I., Sumita, I., & Kumazawa, M. (1996). Growth model of the inner core coupled with the outer core dynamics and the resulting elastic anisotropy. *Journal of Geophysical Research*, *101*, 28085–28103.

Young, C. J., & Lay, T. (1987). The core-mantle boundary. *Annual Review of Earth and Planetary Sciences*, *15*, 25–46.

Young, G. M. (1991). The geologic record of glaciation: relevance to the climatic history of Earth. *Geoscience Canada*, *18*, 100–108.

Yuan, H., & Romanowicz, B. (2010). Lithospheric layering in the North American craton. *Nature*, *466*, 1063–1068.

Yuen, D. A., Hansen, U., Zhao, W., Vincent, A. P., & Malevsky, A. V. (1993). Hard turbulent thermal convection and thermal evolution of the mantle. *Journal of Geophysical Research*, *98*, 5355–5373.

Yukutake, T. (1998). Implausibility of thermal convection in the Earth's solid inner core. *Physics of the Earth and Planetary Interiors*, *108*, 1–13.

Zahnle, K. J., & Sleep, N. H. (1997). Impacts and the early evolution of life. In P. J. Thomas, C. F. Chyba, & C. P. McKay (Eds.), *Comets and the Origin and Evolution of Life* (pp. 175–208). New York: Springer.

Zaug, A. J., & Cech, T. R. (1986). The interviewing sequence RNA of Tetrahymena is an enzyme. *Science*, *231*, 47–475.

Zandt, G., & Ammon, C. J. (1995). Continental crust composition constrained by measurements of crustal Poisson's ratio. *Nature*, *374*, 152–154.

Zegers, T. E., & van Keken, P. E. (2001). Middle Archean continent formation by crustal delamination. *Geology*, *29*, 1083–1086.

Zeh, A., Gerdes, A., Klemd, R., & Barton, J. M., Jr. (2007). Archean to Proterozoic crustal evolution in the central zone of the Limpopo belt (South Africa–Botswana): constraints from combined U-Pb and Lu-Hf iso- tope analyses of zircon. *J Petrol*, *48*, 1605–1639.

Zhai, Y., & Halls, H. C. (1994). Multiple episodes of dike emplacement along the NW margin of the Superior province, Manitoba. *Journal of Geophysical Research*, *99*, 21,717–21,732.

Zhang, Y. (2002). The age and accretion of the Earth. *Earth-Science Reviews*, *59*, 235–263.

Zhang, Y. S., & Tanimoto, T. (1992). Ridges, hotspots and their interaction as observed in seismic velocity maps. *Nature*, *355*, 45–49.

Zhang, Y. S., & Tanimoto, T. (1993). High-resolution global upper mantle structure and plate tectonics. *Journal of Geophysical Research*, *98*, 9793–9823.

Zhao, D. (2007). Seismic images under 60 hotspots: search for mantle plumes. *Gondwana Research*, *12*, 335–355.

Zhao, D., Akira, H., & Horiuchi, S. (1992). Tomographic imaging of P and S wave velocity structure beneath NE Japan. *Journal of Geophysical Research*, *97*, 19,909–19,928.

Zhao, G., Cawood, P. A., Wilde, S. A., & Sun, M. (2002). Review of global 2.1–1.8 Ga orogens: implications for a pre-Rodinia supercontiennt. *Earth-Science Reviews*, *59*, 125–162.

Zheng, Y. (2008). A perspective view on ultrahigh-pressure metamorphism and continental collision in the Dabie-Sulu orogenic belt. *Chinese Science Bulletin*, *53*, 3081–3104.

Zhong, S., & Gurnis, M. (1994). Role of plates and temperature-dependent viscosity in phase change dynamics. *Journal of Geophysical Research*, *99*, 903–917.

Zhong, S., & Gurnis, M. (1995). Mantle convection with plates and mobile, faulted plate margins. *Science*, *267*, 838–843.

Zhong, S., Zhang, N., Li, Z. X., & Roberts, J. H. (2007). Supercontinent cycles, true polar wander, and very long-wavelength mantle convection. *Earth and Planetary Science Letters*, *261*, 551–564.

Zimmer, C. (2009). On the origin of eukaryotes. *Science*, *325*, 666–667.

Zindler, A., & Hart, S. R. (1986). Chemical geodynamics. *Annual Review of Earth and Planetary Sciences*, *14*, 493–571.

Zoback, M. L., & Zoback, M. (1980). State of stress in the coterminous United States. *Journal of Geophysical Research*, *85*, 6113–6145.

Zuber, M. T. (2001). The crust and mantle of Mars. *Nature*, *412*, 220–227.

Zuber, M. T., et al. (2000). Internal structure and early thermal evolution of Mars from Mars Global Surveyor togography and gravity. *Science*, *287*, 1788–1793.

Index

Note: Page numbers followed by *f* indicate figures and *t* indicate tables.

B

C

D

E

R

S

T